The Resilient and Plastic Characteristics of Michigan Subgrade Soils and Their Soil Support Values

August 1981

Final Report

Prepared for

Michigan Department of Transportation

P.O. Box 30050

Lansing, MI. 48909

TE
208
.E34
1981

LIBRARY
RESEARCH
TESTING &
MICH. DEPT. OF STATE HWYS.

NOTICE

This document is disseminated under the sponsorship of Michigan Department of Transportation in the interest of research and development. The Government of the State of Michigan assumes no liability for its contents or use thereof.

The contents of this report reflect the views of the contracting organization, which is responsible for the facts and the accuracy of the data presented herein. The contents do not necessarily reflect the official views or policy of the Michigan Department of Transportation. This report does not constitute a standard, specification, or regulation.

Technical Report Documentation Page

1. Report No.	2. Government Accession No.	3. Recipient's Catalog No.
FHWA-MI-RD-81-02		

4. Title and Subtitle	5. Report Date
The Resilient and Plastic Characteristics of Michigan Subgrade Soils and Their Soil Support Values	August, 1981
	6. Performing Organization Code
	8. Performing Organization Report No.

7. Author(s)	
Gilbert Y. Baladi, Tesfai Goitom	

9. Performing Organization Name and Address	10. Work Unit No. (TRAIS)
Michigan State University Department of Civil and Sanitary Engineering East Lansing, Michigan 48824	11. Contract or Grant No. HPR-0010 (3)
	13. Type of Report and Period Covered Final Report
12. Sponsoring Agency Name and Address Michigan Department of Transportation 425 W. Ottawa P.O. Box 30050 Lansing, Michigan 48909	14. Sponsoring Agency Code

15. Supplementary Notes

MDOT Contract Manager, James Burge
In cooperation with U. S. DOT-FHWA

16. Abstract

In this study, the plastic and elastic characteristics of Michigan cohesive subgrade soils are evaluated using repeated load triaxial tests on undisturbed samples. The results of the investigation led to the development of a normalized predictive model of the plastic strain. The model has demonstrated its ability to evaluate and predict the plastic behavior of several materials subjected to cyclic loadings. The input parameters of the model consist of the static strength and the corresponding total strain of the material in question. The model was tested and evaluated using five different materials ranging from gravel, sand, clay and clayey silt.

The developed normalized predictive model neutralizes the effects of several sample and test variables. The model was found to be unqiue for each class of soil and independent of compaction, density, water content and stress-level. Further, the model was used to develop a new approach and understanding of the soil support value of the AASHTO INTERIM GUIDE FOR THE DESIGN OF FLEXIBLE PAVEMENT.

17. Key Words	18. Distribution Statement
Flexible Pavement Design Soil Support Value Elastic and Plastic Strain Pavement Rehabilitation Pavement Management	No restrictions. This document is available to the public through the National Technical Information Service, Springfield, Virginia 22151

19. Security Classif. (of this report)	20. Security Classif. (of this page)	21. No. of Pages	22. Price
unclassified	unclassified	352	

Form DOT F 1700.7 (8-72) Reproduction of completed page authorized

TABLE OF CONTENTS

LIST OF TABLES

LIST OF FIGURES

LIST OF SYMBOLS

A_1, A_{100}, a_1, a_{100}	Permanent strain at N=1 and N=100 respectively.
a_n, b_n, a_m, b_m	Regression constants.
A_v	Coefficient of compressibility.
B_1, B_{100}, b_1, b_{100}	Slope of the straight lines.
C	Crack index (in Chapter 2 only).
C	Consolidated.
c_1 and c_2	Cohesion.
C_c	Slope of the field compression curve.
C_d	Average coefficient of secondary compression.
C_v	Coefficient of consolidation.
CCT	Conventional consolidation test.
CTT	Cyclic triaxial tests.
1_o	Initial calculated void ratio.
F	Fall sample.
G_s	Specific gravity.
ICT	Incremental creep test.
LL	Liquid limit.
M_R	Resilient modulus.
m and n	Normalized model's parameters or regression constants.
N	Number of axle load repetitions.
P	Patched area.
P_o	Effective overburden pressure.
P_p	Preconsolidation pressure.
PSI	Present serviceability index.
PL	Plastic limit.
P_t	Terminal serviceability index.

R	Regional factor.
r	Radius of the sample.
r^2, r_1^2, r_{100}^2	Coefficient of correlation.
R_1	Moment arm from the hinge to the middle of the plate.
R_2	Radius of the brackets holding the horizontal LVDT(s).
$\overline{RD}$	Average rut depth.
RT	Ramp test.
S	Spring sample.
Sd	Principal stress difference.
SSV	Soil support value.
SV	Slope variance.
Sl-LP	Site number - Lower Peninsula.
Sl-UP	Site number - Upper Peninsula.
U	Unconsolidated.
W_i	Initial natural water content.
W_f	Final water content.
$W_{t_{18}}$	Number of equivalent 18-kip single axle load
σ_i and μ_i	Permanent deformation response parameters.
Δ_t	Total deformation.
ε_e	Axial elastic strain.
ε_R	Radial elastic or permanent strain.
ε_T	Total axial vertical strain.
$\varepsilon_{0.95Sd}$	Axial strain at 95% of the sample strength.
γ_d	Initial dry density.
ϕ_1 and ϕ_2	Angle of internal frictions.

σ_1 and σ_3	Principal stresses.
$(\sigma_1-\sigma_3)_d$	Cyclic principal stress.

CHAPTER I

INTRODUCTION

The complexity and variability of pavement subgrade materials and their interactive mechanisms make the design of flexible pavements a major task. Present design procedures call for material characterization techniques whereby several parameters and/or scaling factors are measured or estimated. These factors and/or parameters are then used in pre-established relationships to correlate performance, structural thickness and traffic loadings and frequency. Further, it is generally recognized that any material characterization technique should take cognizance of the fact that pavement materials are subjected to continuous series of rapidly applied and released stresses of varying magnitudes and frequencies [1,2*]. The duration** of these stresses depends upon the speed of the moving vehicles; the interval between two consequent applications depends on the frequency of traffic and gear configurations [3], and their magnitudes depend on the vehicle weight, gear configurations and tire pressure [4,5,6]. A laboratory test that closely simulates the traffic action in the field is the repeated-load triaxial test [2,7,8]. In this test, samples of paving materials are placed in a chamber and subjected to radial and axial stresses, just as in the conventional triaxial test. The difference, however, is that the application of stresses to the sample in the cell is cycled or repeated. The sample responses, from the repeated-load triaxial tests, are measured and characterized under different parameters and

* Figures in brackets indicate reference number in the bibliography.

** Also see references [56, 92 and 93).

moduli and then used in a related design method.

Recently, several design procedures adopted a design criterion whereby the magnitude of the vertical strain at the surface of the subgrade material is limited to some tolerable amount associated with a specific number of load repetitions [9,10,11,12,13]. The use of this limiting strain criterion has been based on empirical and theoretical considerations of the magnitude of soil deformation and stress intensity which are related to vehicle speeds, traffic frequency and tire pressure [5,6]. An important factor in any overall pavement design system, whether it be empirical or rational, is the consideration and limitation of permanent deformation of the subgrade material [14,15,16]. Consequently, the general practice is to design pavement layers of such thickness and strength that the stresses transmitted to the subgrade are low enough relative to the strength of the soil so that permanent deformation in the subgrade materials are minimized or eliminated [13]. Furthermore, the strength and the plastic behavior of the subgrade should be evaluated and characterized prior to design. Different design methods call for different strength-scaling factor using several evaluation techniques such as California bearing ratio (CBR), soil support value (SSV), resilient modulus (M_R), elastic modulus (E),...etc. The AASHO design method in particular uses a subgrade strength factor called soil support value (SSV). This factor was assigned a scale of 3 to 10 depending on the type of subgrade. The values of this scale, however, are limited by the condition under which it was assigned [17]. Consequently, the AASHO interim guide for design of pavement structures points out that it is the responsibility of local highway departments to establish a correlation between soil support values and the subgrade materials that are suitable for the partic-

ular location and environmental conditions. Thus, it is necessary to develop soil support values for each of the soil textures encountered in the State of Michigan prior to the application of the AASHO design method.

This research project deals with characterization of subgrade cohesive soils found under Michigan highway pavements through the use of repeated load triaxial testing. The objectives of this study include: 1) establishment of relationships between material characteristics of cohesive soils and the soil support value scale using the repeated load triaxial tests under different test and sample conditions; 2) establishment of a limiting stress and/or strain criterion that could be used in different design methods such as: the AASHO design method, the VESYS structural subsystem for a predictive design procedure [18] and the elastic layers design method. This limiting criterion will be based upon the buildup of the different components of the vertical compressive strain in the subgrade layer as measured in the repeated load test.

The scope of the study presented in this report includes a brief description of the cyclic triaxial test system and the experimental techniques employed to evaluate dynamic properties of subgrade cohesive soil. Also included is a discussion of the experimental results and comparison of results of the present study to those reported by other investigators.

CHAPTER II

REVIEW OF LITERATURE

2.1 General

The principal objective of any pavement design procedure is to provide a structural system which will be suitable in a specific regional area and be able to sustain the anticipated traffic loading and frequency [13, 8,14]. It is generally accepted that pavement deteriorates or looses serviceability with time due to load repetitions and environmental conditions. Existing design methods attempt to control or limit this loss in serviceability by minimizing the factors contributing to the different distress modes such as fatigue, rutting, excessive deflection, temporary excessive rebound in the subgrade and base materials and lack of stability in the wearing course [20,24]. Thus, the design of a pavement-section is not simply a matter of guessing or estimating the thickness of the surface, base, subbase and subgrade of the pavement structure. Rather it embraces a more detailed study of each pavement component through the investigation of their physical properties and interaction mechanism. These properties are looked at, in general, through three different aspects. The first of these is the stress-strain characteristics (mechanistic model) of the different materials used in the various layers of the pavement structure. The second, is the most likely failure mode of the various pavement components. Finally the third aspect is the interaction between the different materials and their integrated behavior under traffic loadings and environmental conditions. Current pavement-design procedures use different design criteria and call for different

material characterization techniques using one or more of these three aspects. Consequently, it may be beneficial at this time to look briefly at several different design methods.

2.2 Design Methodologies

The strength of a flexible pavement is the result of building up thick layers and thereby distributing the load over the subgrade rather than by the bending action of the slab [6]. Historically, pavement design has been approached from two broad differing points of view. First, the practicing engineer often approaches the problem solely from the standpoint of pavement performance. In contrast researchers and educators approach the problem largely from theoretical concepts. Neither of the above approaches is satisfactory within itself. Complete reliance upon pavement performance represents a lengthy process. Thus, one must wait a relatively long period of time before new concepts can be proven. On the other hand, theoretical equations are generally based upon simplified assumptions and many times do not apply to conditions as they exist in the field. For comprehensive and ideal pavement design, both approaches must be integrated and used properly [19]. For any pavement design procedure to be completely rational, total consideration must be given to three elements. These elements are:

01. the theory used to predict the failure or distress parameter,
02. the determination of the relationship between the magnitude of the parameter in question to the failure or performance level desired, and
03. the evaluation of the pertinent material properties necessary for the theory selected.

A great deal of research and analysis has been devoted toward development of a fundamental rational design system for flexible pavement based on the above stated elements. Even though all of the design elements have been

recognized by many pavement engineers, differences exist among them in adapting these design factors. Therefore, the design methods that they adopt for a given set of conditions are also different.

The design of flexible pavement has changed rather significantly in the past several years. Generally speaking, flexible pavements were classified as pavement structures having a relatively thin asphalt-wearing course with layers of granular base and subbase used to protect the subgrade from being overstressed. This type of pavement design was primarily based upon empiricism or experience, with theory playing only a subordinate role in the procedure. Presently, highway engineers are faced with the need to provide remedial measures to upgrade existing pavements to meet today's traffic loadings and frequencies. Also, they have recognized that various independent distress modes, such as rutting, shoving, cracking, etc..., contribute to pavement structural and/or functional failure. These needs and knowledge have brought about several changes in pavement design and have led many investigators to search for a more comprehensive pavement design analyses based on theroetical and experimental considerations. Today, there is no one fundamental or rational design procedure that is widely accepted in the pavement design industry. Yoder and Witczak [13,19] described two broad categorical approaches to the problem of pavement design based upon the limitation of subgrade overstress. The first category is based on empirical correlations of excessive deformations related to some predefined failure condition of the pavement. The second category is based on the prediction of the cumulative deformations (cumulative damage) of the pavement system under consideration. These two categories will be discussed further below.

2.2.1 Deformation-failure approach:

This category is further subdivided into two procedures:

2.2.1.a Laboratory or field index test procedure:

In this design procedure, laboratory or field index tests (CBR, stabilometer...) are used to categorize the strength of the subgrade materials. It is one of the most widely accepted design procedures for control of repetitive shear deformations used to date [19,18,22]. Generally the fundamental approach is to control pavement layer thickness and material quality based upon some of the above mentioned index tests. It is inherently assumed that the primary source of deformation occurs in the subgrade provided that the thickness and material quality controls are met [19,3,14]. Consequently, allowable deformations are controlled by adjustment of the pavement thickness to reduce the stresses on the subgrade to a level such that actual deformation will not exceed the allowable deformation within the design life of the pavement [19,8]. One such design method is presented in the AASHO interim guide for design of pavement structures [14]. A brief review of this method is presented below.

In the early 1950's, the highway engineers were confronted with the need to predict the performance of pavement systems subjected to greater wheel loads and frequencies than they had ever before experienced [19] and to establish an equitable policy for vehicle sizes and weights. This need has led the American Association of State Highway and Transportation officials (AASHTO) to develop the AASHO-Interim Guide design procedure to alleviate the above-mentioned problem. The procedure is based on an extensive road test that was conducted in Ottawa, Illinois. The test site consisted of six loops (two small loops and four large ones). The first AASHO Interim Guide [14] was published in 1961 and all recommendations for the design procedure were based on the result obtained through a period of 25 months of testing. The primary objectives of the AASHO Road tests were:

a. To establish relationships between the number of load repetitions and the performance of different pavement systems of known subgrade soil characteristics.

b. To determine the effect of different loadings, represented by the magnitude and frequency of axle loads.

c. To establish instrumentation, test procedures, data charts, graphs and formulas which would be helpful in future highway design, for both rigid and flexible pavements of conventional design.

In general, the AASHO interim guide is used to determine the total thickness of the pavement structure, as well as the thickness of the individual pavement components. It should be noted that the main assumption of the procedure is that most subgrade soils can be adequately represented, for pavement design purposes, by means of their soil support value (SSV) for flexible pavements or by their modulus of subgrade reaction (K) for rigid pavements. In special cases when poorer soils (frost susceptible, highly organic, etc.) are encountered, adequate pavement performance is achieved by increasing the thickness of the pavement structure, or by using special precautions. The term "pavement performance" is defined in the AASHO interim guide as follows: "a pavement which maintains a high level of ability to serve traffic over a period of time is superior in performance to one whose riding quality and general conditions deteriorate at a more rapid rate under the same traffic conditions." The term pavement serviceability was adopted to represent the ability of a pavement to perform under the given traffic. Thus, pavement performance is assigned a value from zero to five and it is called pavement serviceability index. Prediction of the present serviceability index of a pavement system can be achieved by using a combination of different physical measurements and is given by the following relationships (14).

$$PSI = 5.03-1.91 \log (1+SV)-1.38 \overline{RD}^2 -0.01 (C+P)^{1/2} \quad (2.1)$$

where

SV = slope variance, a measure of longitudinal roughness

$\overline{RD}$ = average rut depth

C+P = area of class 2 and 3 cracking plus patching per 1000 ft^2 (92.9 m^2)

This serviceability-performance concept is the basic philosophy of the AASHO interim guide. Thus, a pavement section may be designed for the level of serviceability desired at the end of the selected traffic analysis or after exposure to a specific total traffic volume. The basic flexible pavement design equation, developed from the results of the AASHO Road test, uses a traffic equivalency criterion which convert mixed-traffic to 18-kip equivalent single-axle load.

$$\log W_{t18} = 9,36 \log (\overline{SN}+1)-0.20+ \frac{\log[4.2-P_t)/(4.2-1.5)]}{0.40+[1094/(\overline{SN}+1)^{5.19}]} + \log (\frac{1}{R}) + 0.372 (SSV-3.0) \quad (2.2)$$

where

W_{t18} = number of equivalent 18-log single axle loads expected in time t

$\overline{SN}$ = structural number of the pavement system

P_t = the terminal serviceability index or the serviceability index at time t

R = regional factor

SSV = soil support value

The soil support value (SSV) of any given soil ranged from 3.0 for A-6 materials to 10.0 for A-1 materials. The objectives of this research project include a study of the (SSV) scale as related to some physical characteristics of the subgrade soil in question.

2.2.1.b Limiting subgrade strain procedure

This design approach as described by Yoder and Witczak [13] uses the elastic layered theory to limit the vertical subgrade strain. Concepts for designing flexible

pavements using multilayer elastic analysis were presented by Dorman and Metcalf in 1965 [9]. The principles outlined by these investigators were based upon limiting strains in the asphalt surface and permanent deformation in the subgrade. The use of multilayered elastic theory in conjunction with a limiting strain criteria for design involves the consideration of three factors: the theory used, the material characterization technique, and the development of failure criterion for each mode of distress. In the development of the procedure, use was made of computer solutions to solve stresses, strains and displacements within a multilayered (elastic) pavement system [24,25,26]. Most elastic layered design procedures, considers both permanent deformation (rutting) of subgrade as well as fatigue cracking of the asphalt-bound layer as the two most significant failure mechanisms.

Dissatisfaction has been expressed by many highway agencies concerning the use of these conventional procedures, because both design procedures are based on empirical relationships derived from experience and observations. Furthermore they are applicable only to a defined range of pavement materials, traffic loads and environmental conditions for which experience is available [19,8,18, 27,16]. Also both procedures failed to predict the amount of anticipated deformation after a given number of load applications.

2.2.2 Prediction of cumulative deformation approach

Yoder and Witczak [19] described this category as representative of procedures that are based upon the prediction of accumulated deformations in pavement systems using quasi-elastic or viscoelastic approaches. These approaches, however, are not presently refined to the point where this can be accomplished with a level of confidence needed for adequate design methods [19,8,28,29]. Despite this disadvantage, the methodology is the most preferred for use in a more advanced or rational design

method due to its capability of obtaining cumulative deformations of any pavement system [19,28,29,18,27,30, 31,3]. Many investigators have suggested that research should be directed towards developing better material characterization techniques for use in such rational design methods [19,8,18,27,30,3,32,33]. A comprehensive literature review of the quasi-elastic and viscoelastic approaches may be found in reference [23], a part of which is repeated here for the benefit of the reader.

2.2.2.a Quasi-elastic approach

The quasi-elastic approach as described by Yoder and Witczak [19] is based upon the use of elastic theory and the results of plastic strains determined by repeated load laboratory tests on pavement materials. This approach was initially introduced by Heuklom and Klomp [34]. Since then, research has been conducted by others such as Monismith [35] and Barksdale [29] for soils, granular materials and asphalt concrete. The fundamental concept of the analysis is the assumption that the plastic strain [ε_p] is functionally proportional to the elastic state of stress (or strain) and number of load repetitions. This constitutive deformation law is considered applicable for any material type and at any point within the pavement system. The response of any material must be experimentally determined from laboratory tests for conditions (time, temperature, stress state, density, moisture, etc.) expected to occur in situ. The elastic theory (either linear or nonlinear) is then used to determine the expected stress state within the pavement provided that the plastic deformation is known. Subdividing each layer into convenient thicknesses (ΔZ_j) and determining the average stress state at each layer increment, the permanent deformation of the pavement may be computed using [13,10,14]

$$\Delta_t = \sum_{j=1}^{n} \varepsilon_{p_j} (\Delta Z_j) \qquad (2.3)$$

where

Δ_t = total deformation

n = number of layers

ϵ_p = permanent strain

Δz = thickness

j = the layer in question

2.2.2.b Viscoelastic Approaches

A pavement design method employing the visco-elastic approach has been developed under the direction of the Office of Research, Federal Highway Administration, (FHWA) [18]. The procedure is based on a mechanistic structural subsystem known as VESYS IIM computer program. This computer program predicts the performance of a pavement in terms of its present serviceability index, PSI, derived from the American Association of State Highway Officials (AASHO) Road Test analysis [19,18]. Inputs to the program must be in the form of statistical distributions describing material properties, geometry of the pavement section being analyzed, traffic and environment. Program outputs are presented in terms of means and variances of the damage indicators - cracking, rutting, roughness and serviceability. The VESYS IIM computer program consists of three models shown diagramatically in Figure 2.1. These models are:

2.2.2.b.1 Primary Response Model

The Primary Response Model represents the pavement system by a three layer semi-infinite continuum such that the upper two layers are finite in thickness while the third layer is infinite in extent. Each layer is infinite in the horizontal directions and may have elastic or viscoelastic behavior. The model constitutes a closed form probabilistic solution to the three layers linear viscoelastic boundary value problem. It is valid for a

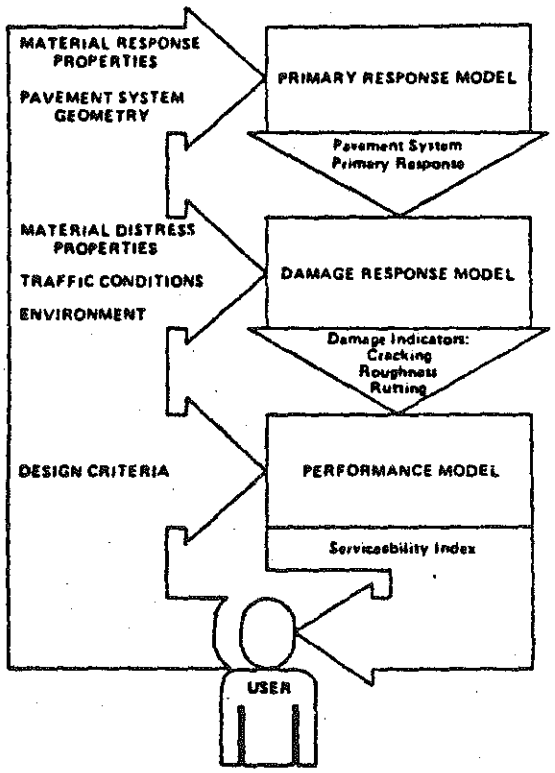

FIGURE 2.1 Modular Structure of VESYS IIM (18).

single stationary circular loading at the pavement surface. Stochastic inputs to the model are in terms of the means and variances of the creep compliances for viscoelastic materials, and elastic or resilient moduli for elastic materials. The output from the Primary Response Model, in the form of statistical estimates of stresses, strains and deflections, is used as input to the Damage Model.

2.2.2.b.2 Damage Model

The Damage Model consists of three separate models each designed to predict distress accumulation in the pavement.

01. The Rut Depth Model uses the results from the Primary Response model along with laboratory determined permanent deformation characteristics of the pavement and subgrade materials to compute the mean and variance of the rut depth accumulated over any incremental analysis period.

02. The Roughness Model uses the rut depth output from the Rut Depth Model, along with the assumption that rut depth at any time along the wheel path will vary due to material variability and non-uniform construction practices, to compute the roughness in terms of slope variance as defined by AASHO [14].

03. The Fatigue Cracking Model is a phenomenological model which predicts the extent of cracking of the asphalt layer based on Miner's hypothesis. This cracking is due to fatigue resulting from tensile strain at the bottom of the asphalt concrete layer. A crack index is computed after any number of load applications using the viscoelastic radial strain amplitude at the bottom of the asphalt concrete layer along with laboratory determined fatigue properties of the asphalt concrete. The radial strain amplitude is found at the peak of a haversine load pulse of specified duration applied to the pavement surface. From this crack index the expected area of cracking is computed in square yards per 1000 square yards.

The output from the above three parts of the Damage Model, i.e., rut depth, slope variance, and crack index, is used as input to the Performance Model.

2.2.2.b.3 Performance Model

The Performance Model computes a Serviceability Index, Pavement Reliability and Expected Life of the Pavement. The serviceability index, PSI, is defined according to the AASHO Interim Guide 1972 [14] as

$$PSI = a + b \log_{10} (1 + SV) + c\sqrt{C + P} + dR^2 \qquad (2.4)$$

where

a = 5.03, b = 0.01, c = 1.91, d = 1.38 are multiple regressions constants

SV = Slope Variance (Roughness)

C = Crack Index

R = Rut depth

P = Patched area

The expected value and variance of the PSI is then calculated at any time. The reliability of the serviceability index at any time is defined as the probability that the PSI is above some unacceptable level, PSI_f, which has been established beforehand. The distribution of PSI's is obtained assuming a Gaussian distribution. The expected life of the pavement is the time for the Serviceability Index to reach the unacceptable level, PSI_f.

Two categories of mechanical properties are required for the VESYS IIM structural analysis, primary response properties, and distress properties. The primary response properties define the response of layer materials to the given loads and environments. These properties are in the form of elastic or viscoelastic characteristics which may exhibit non-linear behavior because of previous load histories, plastic effects, and stress dependencies. The distress properties are those properties defining the capability of the materials to withstand the imposed loads. The Rut Depth Model in the current version of VESYS IIM [18] assumes a permanent deformation accumulative

damage law of the form

$$F(N) = \mu_i N^{\alpha i} \qquad (2.5)$$

where

N = Number of axle load repetitions

α_i and μ_i = Permanent deformation response parameters for material in layer i.

One method for determining α_i μ_i for equation 2.5 is to use the results of the Dynamic Series of an "Incremental Static-Dynamic" test described by the load program shown in Figure 2.2. For more detailed information the reader is referred to reference [11].

A sensitivity analysis of the VESYS IIM structural model [29] determined that calculated responses of the system were: a) insensitive to variations of the parameter μ for base and subgrade; b) insensitive to variations of parameter α for base materials; c) sensitive to variations of α for subgrade material.

Researchers have indicated that one of the most urgent research needs in material characterization is the development of simplified tests which decrease the total number of tests, shorten the amount of time required for each test, and simplify the test methods and instrumentation requirements [30,27,18,3,32].

2.3 Cyclic Loadings

Timoshenko [36] credits Poncelet as being the first to consider the strength of materials under repeated loadings and to introduce the term "fatigue" to describe the resulting strength-deterioration characteristics. Timoshenko also credits Wohter for conducting the most extensive and the earliest experimental repeated load tests, Wohter found that the number of load cycles to failure increased as the cyclic stress intensity increased. Other investigators [37,38,39] concerned themselves with fundamental aspects of fatigue and developed hypotheses to

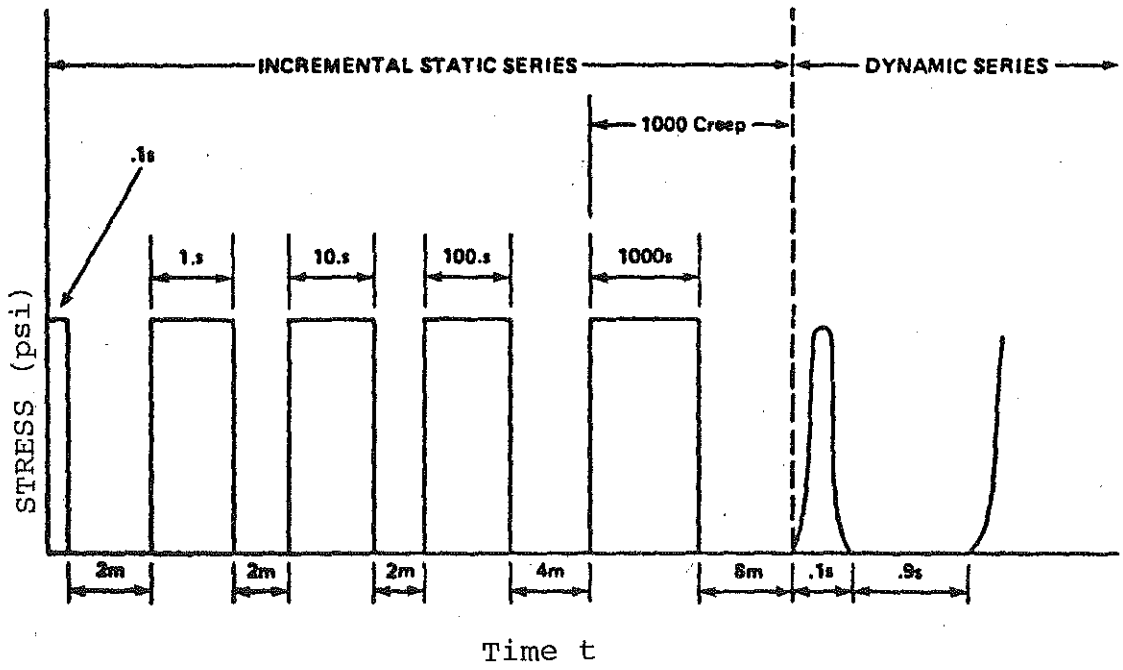

FIGURE 2.2 Load History Used in "Incremental Static-Dynamic" Test (18).

explain their experimental data. They postulated the formation of crystalline or intergranular structure during cyclic loading. These studies are still continuing with many theories proposed each satisfying one or more aspects of the fatigue phenomenons and yet none being adequate for all cases. In general, all materials including soils lose strength or stiffness, or both, with increasing number of cyclic stress [40] as shown in Figure 2.3. Most of the early studies, and indeed most of the more recent studies have used uniform repeated load intensity rather than irregular one to study the effects of traffic loading on the pavement system in question. This is so because a uniform repeated load intensity test machine is easier and cheaper to build and operate than an irregular loading apparatus. Generally, the loading patterns are likely to vary from vehicle to vehicle or from case to case even within the same problem area. Thus, irregular or variable cyclic loading tests will better simulate the traffic action. However, this requires the evaluation of each possible load pattern to be expected throughout the lifetime of the pavement structure [41,42]. A review of literature concerning the behavior of cohesive soils subjected to cyclic loading is presented in the next paragraph. The background information for cohesionless soils, on the other hand, may be found in Reference [1].

2.3.1 Behavior of Cohesive Soils Subjected to Cyclic Loadings

A qualitative measure of the behavior of soils subjected to cyclic loadings, such as that induced by earthquakes, has been widely recognized since they were examined by Casagrande in 1936 [43]. Over the past several years, considerable advances have been made in our understanding of soil behavior during cyclic loading and in our ability to reasonably predict this behavior. According to Idriss and Ricardo [27], the stress-strain characteristics of soils subjected to cyclic loadings is nonlinear and

Material (1)	Reference Stress Conditions (2)	Cyclic Stress Conditions (3)
Metals	Static tensile strength	Reversing compression/ extension
Clays	Static Compressive strength	Reversing compression/ extension
Sands	Cyclic stress to fail in N = 1 cycle	Reversing compression/ extension
Asphalt and Treated Soil	Cyclic stress to fail in N = 1 cycle	One-directional beam bending

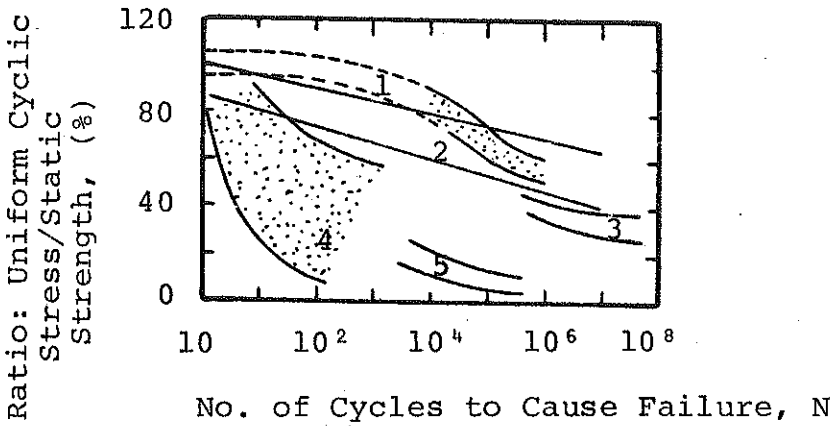

1) 5% Cr-MO V Steel
2) Cement and Lime Treated Soils
3) Ferrous and Non-Ferrous Materials
4) Saturated Sands and Clays
5) Asphalt

FIGURE 2.3 No. of Load Applications versus Ratio of Cyclic Stress to Static Strength (40).

hysteretic in nature. Figure 2.4 shows an idealized stress-strain loop obtained for a soil specimen subjected to a symmetrical cyclic shear load along a plane free of initial shear stress [44,45]. Seed [46] reported that the method of cyclic load application to a soil has an important effect on the magnitude of soil deformation. For example, a specimen subjected to repeated loading has been found to deform many times more than an identical specimen subjected to a sustained load of equal magnitude. This difference in soil behavior under different types of loading raises the question whether tests performed under conditions of slowly increasing stresses can satisfactorily indicate the performance of a soil under the repetitive type loading to which it is subjected to under a pavement structure [46,47]. Further, a pavement may be considered to have failed when the deformation of the soil below the wearing surface is of such a magnitude as to cause an uneven riding surface or to cause cracking of the surfacing material. One of the objectives of pavement design procedures is to determine the thickness of pavement and base which must be placed over a subgrade in order that the deformation of the subgrade will not be excessive. Thus, for a satisfactory method of pavement design, it is necessary to devise some means of evaluating the resistance to deformation of the subgrade soils when it is subjected to a series of repeated loads of different magnitudes, durations and frequencies [8,32,47]. Recent research [31], however, has shown that it is not sufficient to evaluate only the resistance to permanent or plastic deformation of the subgrade, but also the elastic or resilient properties of the subgrade soils. A number of investigations conducted by the California Division of Highways have shown that there is a close correlation between observations of cracking and fatigue-type failures in bituminous pavements and the measured deflections of these pavements due to passing wheel loads. It appears, therefore, that large elastic deformations in

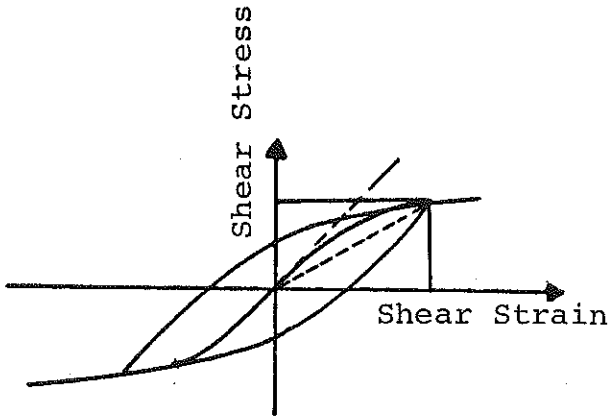

FIGURE 2.4 Shear Stress vs Shear Strain for Cyclic Loading (27).

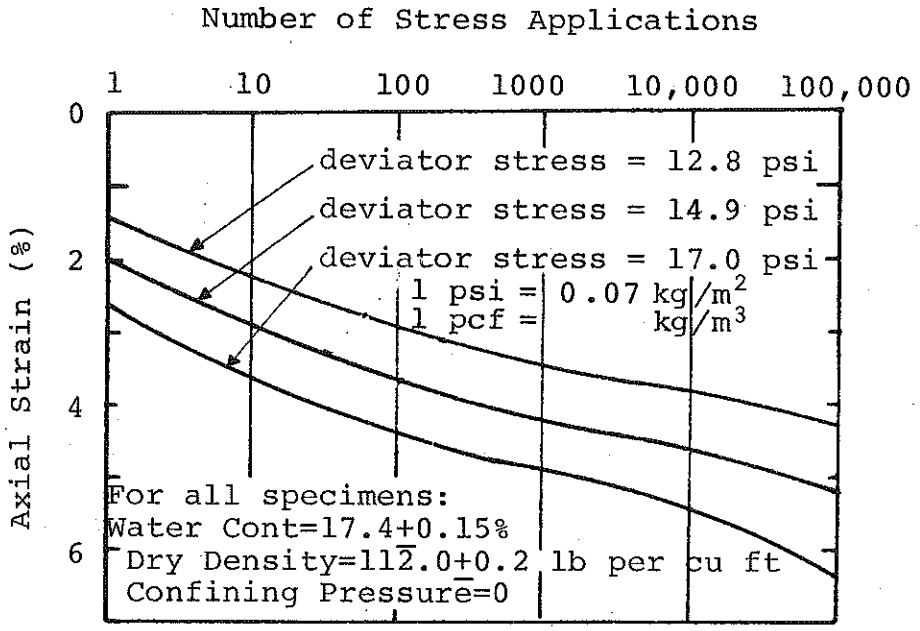

FIGURE 2.5 Permanent Strain vs Number of Load Repetitions for Silt Clay (46).

a soil are a primary cause of pavement failure. Several cases were reported where soils having low resistance to plastic deformation exhibited high resilient deformations. Also, it is likely that some soils may exhibit extremely small plastic deformations and yet show high elastic deformations. Such soils would probably cause more fatigue failure in the surfacing materials than would a soil exhibiting a larger plastic deformation and much smaller elastic movement. Therefore, it is necessary to evaluate the soil resistance to elastic and plastic deformations separately prior to the design of pavement structure [48,49].

Soils are often subjected to vibratory loadings as a result of natural forces (earthquakes, wind, waves) or human activities (trains, pile driving, blasting, traffic, etc.). Variations in the soil responses due to these forces are to be expected since the response depends on the load and soil parameters. These parameters include: 1) number of load applications (N), 2) frequency, 3) magnitude of loadings, 4) load duration, 5) relaxation period, 6) density and moisture content of the soils, 7) thixotropy and 8) stress history (2,3,7,56). The effects of some of these factors on the plastic and elastic response of cohesive soils will be reviewed next.

2.3.1.1 Factors Affecting the Plastic Deformations of Cohesive Soils

2.3.1.1.a Number of Load Applications

Several investigators [50,51,52] stated that, in general, silt and clay subgrade materials exhibit a stiffening behavior with an increasing number of stress applications (N). The permanent deformation of cohesive soils subjected to repeated load applications is large during the first few cycles. Each subsequent load application results in a smaller increment of permanent deformation. After a large number of load applications the rate of change in permanent deformation becomes very small.

The total permanent deformation of test specimens, however, increases with increasing number of stress applications [19,53,54,55,56]. Seed [55] studied the effects of the number of load applications on the plastic behavior of soils by testing several samples up to 100,000 load repetitions using triaxial cyclic apparatus. He reported that the cumulative plastic strain increased with increasing number of stress applications. Seed concluded that the relationship between the total permanent strain and the logarithm of the number of load cycles could be expressed by a linear function as shown in Figure 2.5. Yoder [13] on the other hand reported a linear relationship between the logarithm of the accumulated plastic strain and the logarithm of the number of load applications.

2.3.1.1.b Magnitude of Loadings

Most researchers agree that the loading magnitude (confining pressure and cyclic principal stress difference) is the most important test parameter controlling the plastic soil behavior. However, the magnitude of this load in the highway subgrade materials is very difficult to determine [57]. This is so because the locked in radial stresses during compaction are highly variable and may be as high as 50 or 100 psi (345 or 689 KN/m^2). Hicks and Monismith [58] reported that the range of radial stress encountered in the subgrade materials as a consequence of the passage of a load vehicle varied from zero to ten psi (0 to 68.9 KN/m^2). Thus, when evaluating the resilient and permanent characteristics of subgrade materials it is desirable to do so under wide range of confining pressure and cyclic stress difference. Researchers unanimously agree that for the same number of load applications and for the same confining pressure, the higher the stress ratio (principal stress difference to confining pressure) the higher the permanent strain, as shown in Figure 2.6 [22,59]. Also, for the same stress

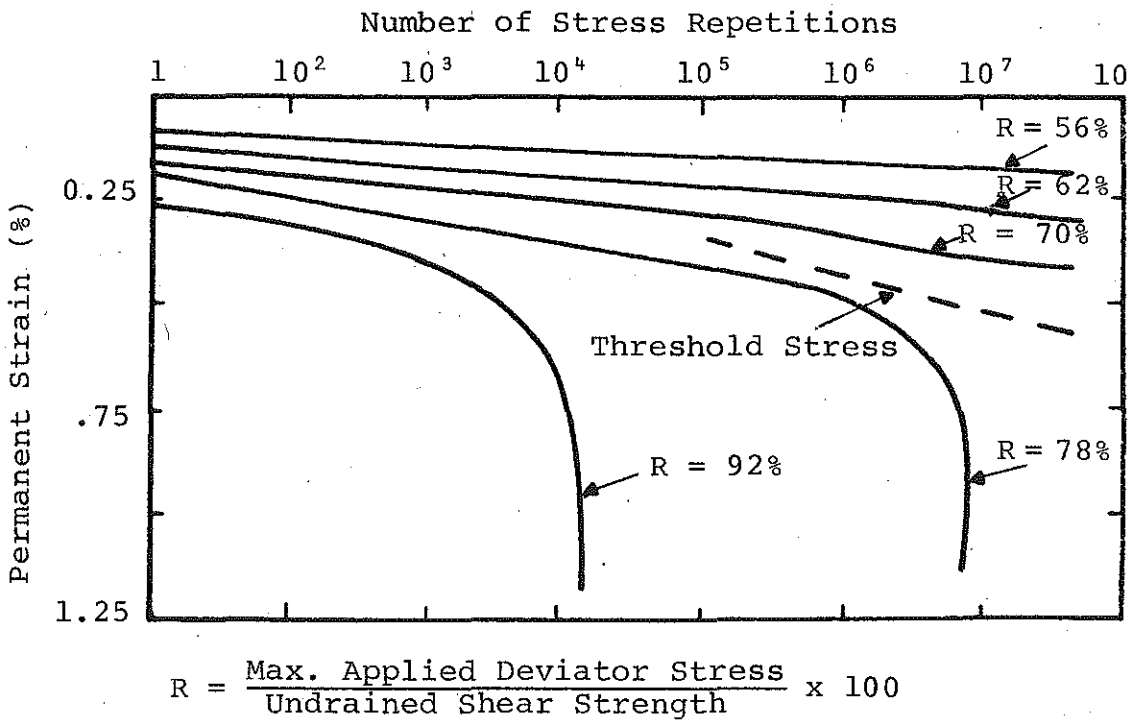

$$R = \frac{\text{Max. Applied Deviator Stress}}{\text{Undrained Shear Strength}} \times 100$$

FIGURE 2.6 Effect of Deviatoric Stress on Deformation of Silty Clay under Repeated Loading (22).

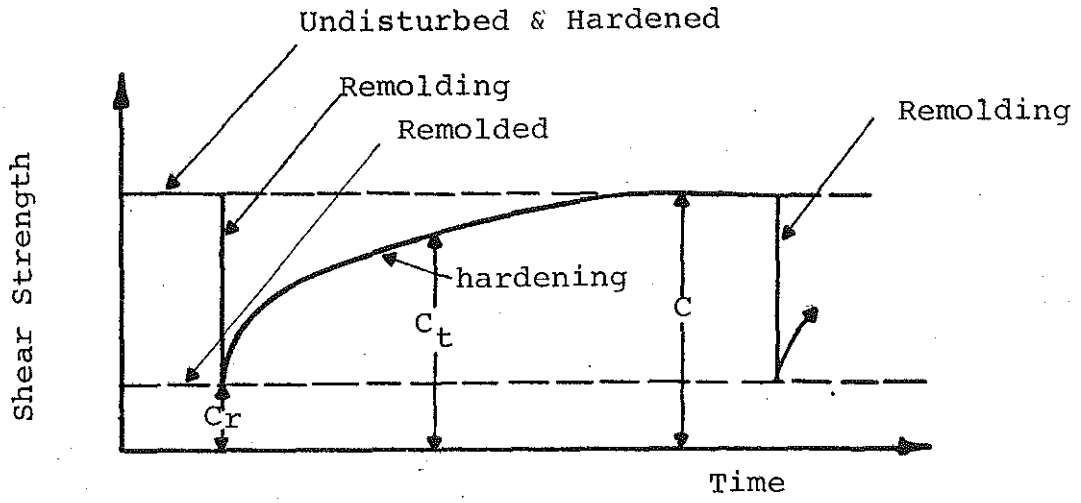

FIGURE 2.7 Strength Regain in a Thixotropic Material (24).

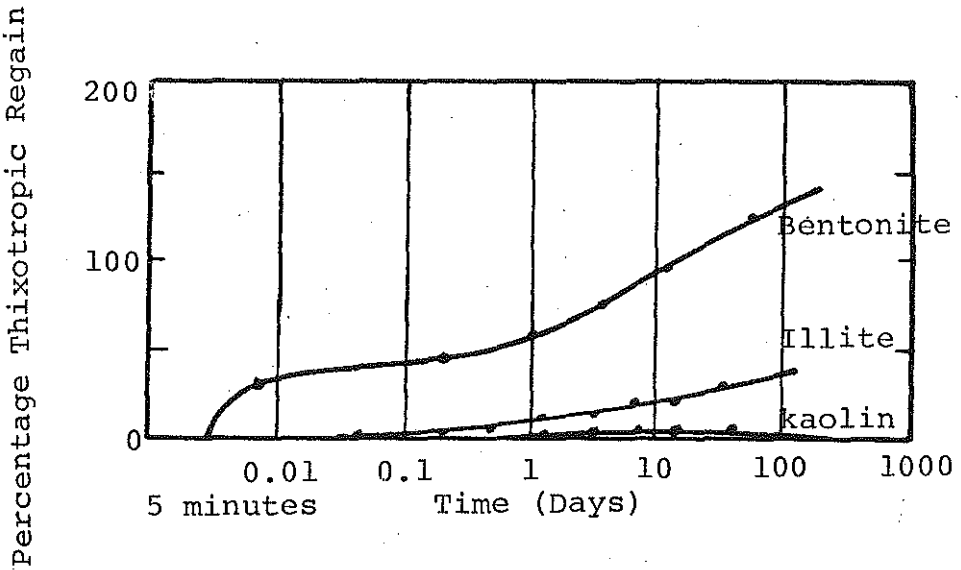

FIGURE 2.8 Effect of Thixotropic in Three Clay Minerals (24).

ratio, the higher the confining pressure the higher the permanent strain.

2.3.1.1.c Effect of Thixotropy

The response of cohesive soils to cyclic loadings is greatly influenced by the length of time between sample preparation and testing. Generally, the sample strength increases as the time between preparation and testing (storage time) increases. However, this effect tends to diminish as the number of load applications increases [59]. Several investigations have been conducted to determine the extent to which the sensitivity of natural deposits of saturated clays is attributable to thixotropy [60,61]. The properties of a purely thixotropic material have been illustrated by Skempton and Northey [24] as shown in Figure 2.7. The shear strength of the material assumes a value of C in the undisturbed state as shown in the figure. This value drops to C_r immediately after remolding. If the material is then allowed to remain under constant external conditions and without any change in composition, the strength will gradually increase and after a sufficient length of time the original strength C will be regained. Figure 2.8 shows the thixotropic strength increase for three clay minerals as measured by Skempton and Northey. They reported that Kaolin shows almost no thixotropy and illite shows only a small effect. In contrast, the bentonite shows a remarkable strength regain at very short time interval.

2.3.1.1.d Effect of Stress History

Stress history has a significant effect on permanent strain of soils [55,56,62,63]. It has long been recognized that stress history has an important effect in determining the consolidation and strength characteristics of saturated clays. Recently, it has been shown that changes in the sequence of pressure application can

also affect the swelling characteristic of clays [55,63]. Lentz [23,8] concluded that subjecting soil samples to a low stress level increases their resistance to permanent strain under subsequent higher loads.

2.3.1.1.e Effect of Frequency and Duration

The duration of the stress pulse applied to a subgrade soil by a moving wheel load lasts about 0.01 to 0.1 second under actual field conditions (64). This duration time is primarily dependent upon the speed of the vehicle and the position of the element under consideration within the pavement structure. Hence, the vehicle speed is inversely related to the load duration. As vehicle speed increases, the duration of loading decreases and visa versa [43]. Barksdale [64] found that the load duration time increases with depth by a factor of about 2.7 from the pavement surface to the subgrade. This is shown in Figures 2.9 and 2.10. Barksdale recommended the use of the appropriate magnitude of the principal stress and its time pulse for investigation of the resilient and permanent characteristics of the soil materials in question.

2.3.1.2 Factors Affecting the Resilient or Elastic Characteristics of Cohesive Soils

Unlike cohesionless soils, cohesive subgrade materials cannot be accurately characterized without great attention being given to the sample preparation. In determining the resilient parameters for clay, the laboratory samples should be identical in composition to the field. This means that water content, density and the structural arrangement of the particles (which is controlled by the method of compaction used in preparing the sample) must be identical. The importance of this may be recognized by knowing that the resilient deformation of a flexible pavement structure is a major contributor to fatigue failure in the asphaltic concrete surface course. Recognition of the importance of the resilient behavior of

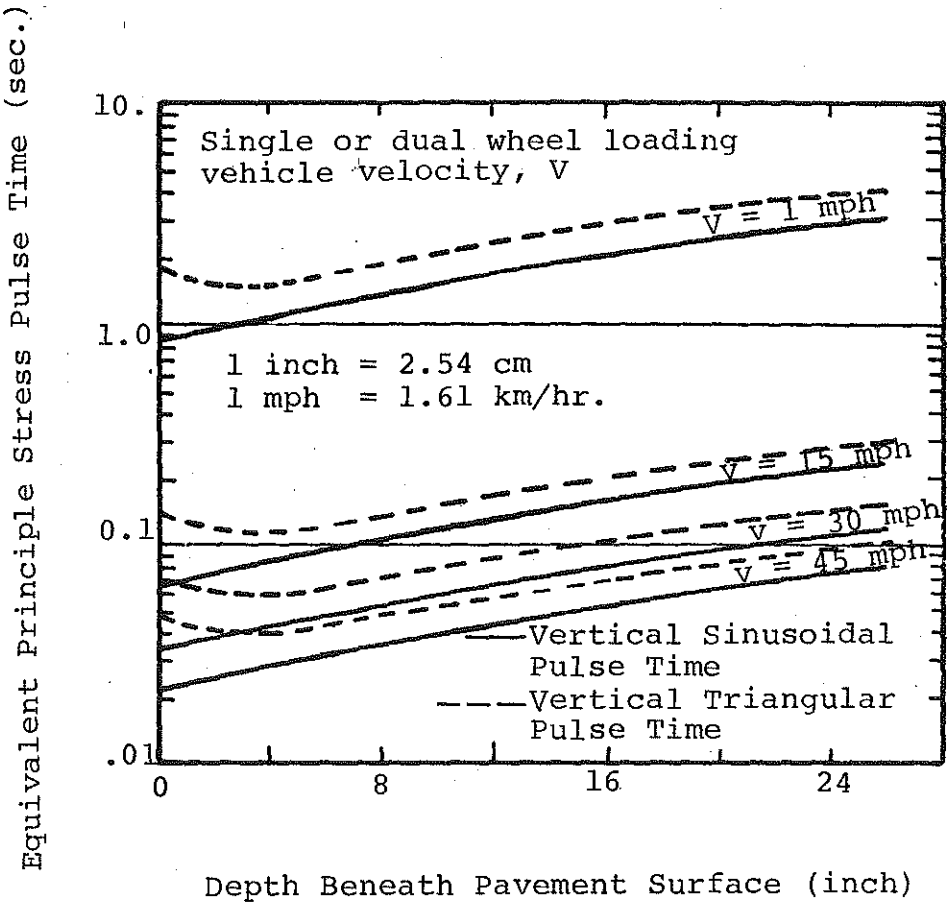

FIGURE 2.9 Variation of Equivalent Vertical Stress Pulse Time with Vehicle Velocity and Depth (64).

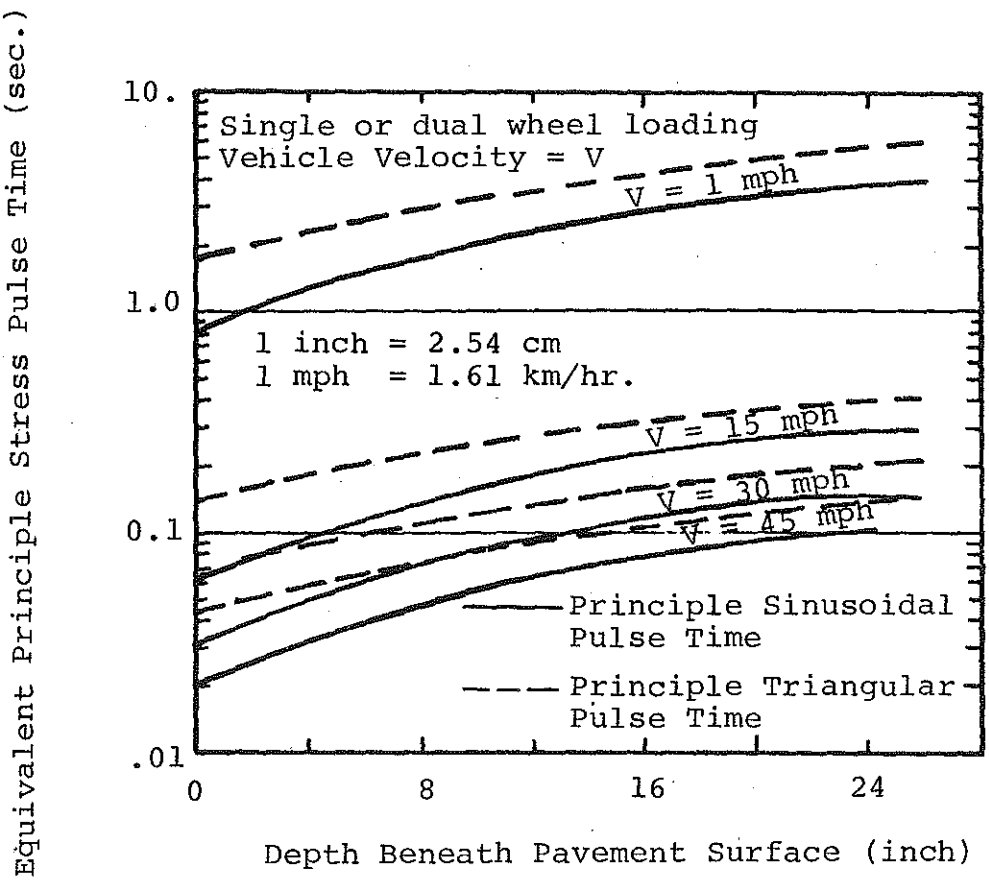

FIGURE 2.10 Variation of Equivalent Principle Stress Pulse Time with Vehicle Velocity and Depth (64).

flexible pavements is reflected by the fact that many current flexible pavement thickness design philosophies incorporate limiting deflection criterion [65,66]. Generally, the factors that influence the resilient characteristics of cohesive soils include:

2.3.1.2.a Number of Load Applications

Resilient deformation generally decreases as the number of load repetition increases. Thus, deformations that determined under a relatively small number of stress applications may present a misleading picture of the resilient characteristics of the subgrade soil [59,67]. In tests on stiff clays, Dehlen [68] found that 1000 stress repetitions were sufficient to condition the sample for testing without significantly altering the specimen response. He found that once the sample was conditioned, the response obtained at a relatively low number of stress applications was representative. Tanimoto and Nishi [69] also emphasized the importance of selecting the proper number of stress applications to determine the resilient properties. Seed et al. [50] found that the response of clay samples was dependent on the number of stress applications (N). In general, they reported that compacted clays develop their greatest resilient deformation when N is less than 5000.

2.3.1.2.b Confining Pressure

The resilient response of cohesive soils is relatively unaffected by changes in cell pressure during the repeated load triaxial test [43,52,53,54].

2.3.1.2.c Stress-Level

In all investigations, the relationship between the resilient modulus and the principal stress difference is similar. At low stress levels, the resilient modulus decreases and the principal stress difference increases. This is true up to a value of about 10 psi where the

resilient modulus is found to be unaffected or increases only slightly with further increase in principal stress difference. Because of this dependence on the principal stress difference, it is important that laboratory tests be conducted at stresses which are expected in the field. Figure 2.11 shows the decrease in the resilient modulus M_R as the principal stress difference increases from 2 to 10 psi (.1406 to .703 Kg/cm^2) under a constant radial pressure. It also shows that Poisson's ratio is only slightly affected by changes in the applied stress. For tests on silty clays Mitchell et al. (58), using 24,000 load applications, found that the resilient modulus decreased with increasing applied stress up to 25 psi (0.176 Kg/cm^2), above which the resilient modulus increased slightly. Seed et al. [50] had also found that the resilient modulus decreased rapidly with a variation of 300 to 400 percent as the principal stress difference increased from 3 to 15 psi (0.21 to 1.05 Kg/cm^2). Above this range the resilient modulus was observed to increase slightly, as shown in Figure 2.12.

2.3.1.2.d Load Duration and Frequency

Most researchers agree that the effect of stress duration on the resilient response of cohesive soils is negligible. In general, the resilient modulus tends to increase slightly as the time of load duration decreases, this effect is considered insignificant for the range of load durations encountered in pavement structures [59].

Conflicting findings concerning the effects of frequency on the resilient response are reported in the literature. Coffman [71] stated that the resilient modulus increases as the load frequency increases. This increase was on the order of 50 to 400 percent depending on the water content and density of the sample. Tanimoto and Nishi [69], on the other hand, reported a decrease in resilient modulus with an increase in load frequency.

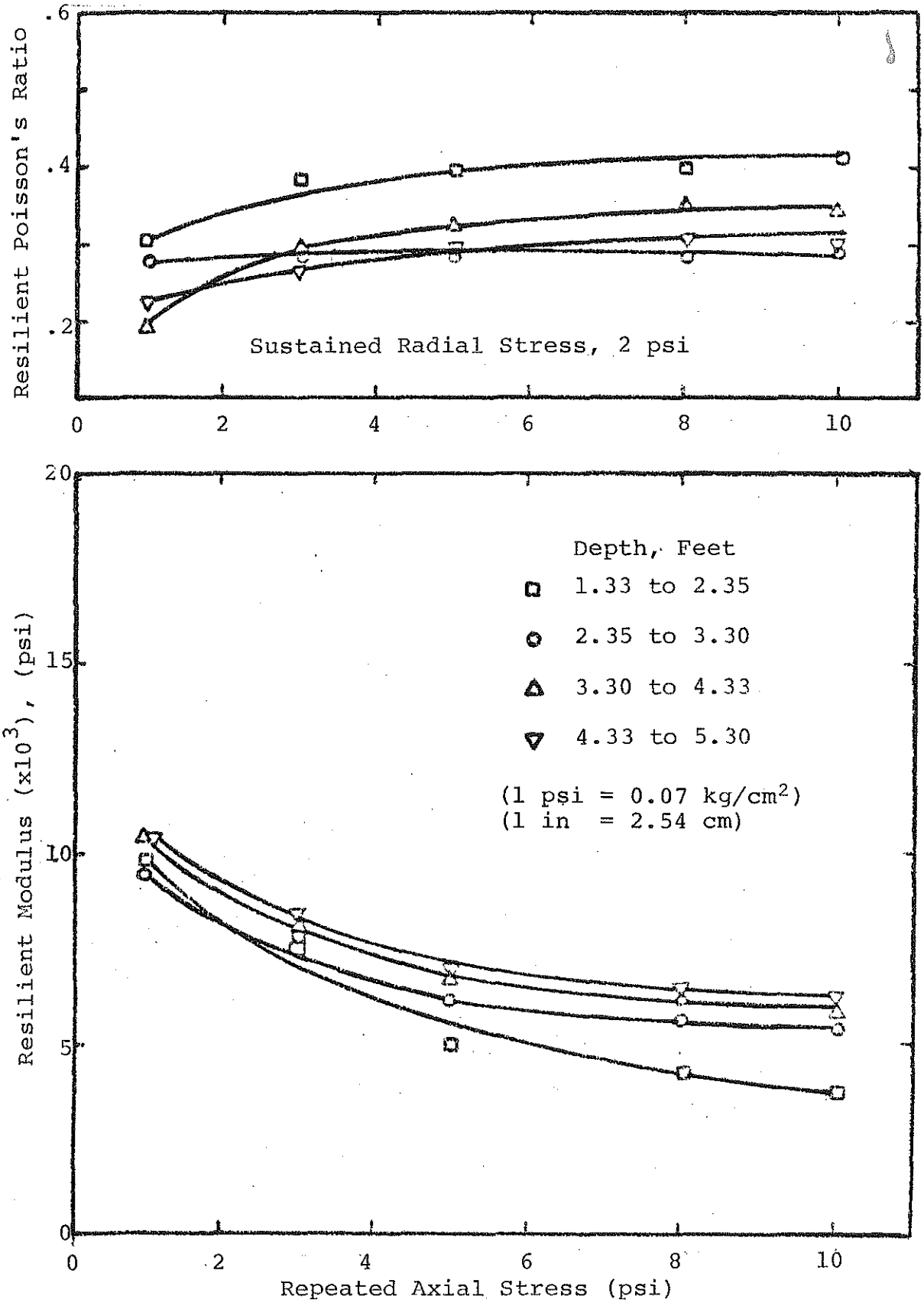

FIGURE 2.11 Secant Modulus and Poisson's Ratio of Clay Subgrade as a Function of Repeated Axial Stress and Depth Beneath Pavement Surface (58)

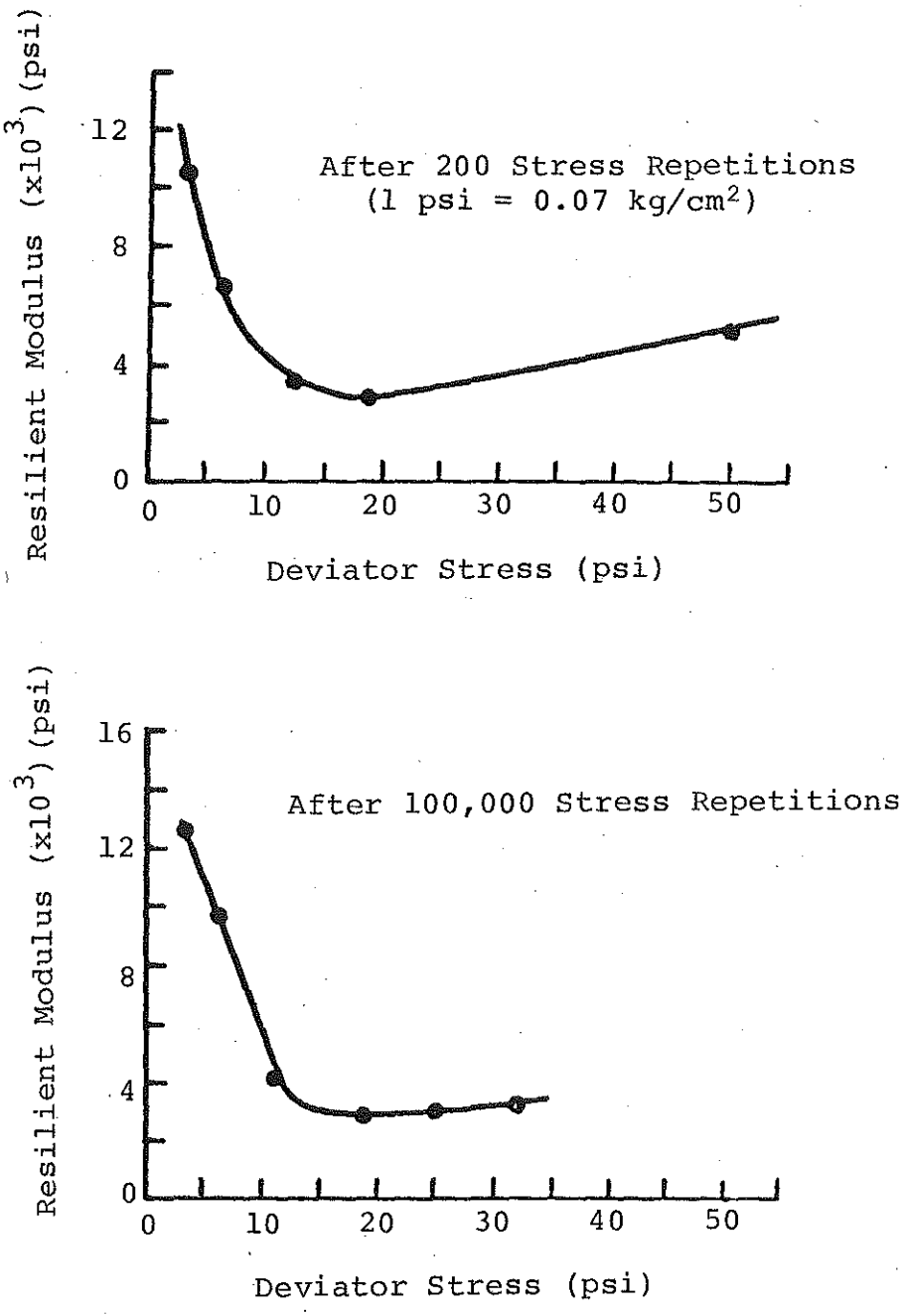

FIGURE 2.12 Effect of Stress Intensity on Resilient Characteristics for AASHO Road Test Subgrade Soil (50).

Further, Kalcheff and Hicks [67] found that frequency changes had no effect on the resilient modulus.

2.3.1.2.e Compaction Density and Water Content

All investigators have found that increasing water content at compaction leads to an increase in resilient deformation, and a decrease in strength and resilient modulus. For a given compactive effort, the resilient deformation is relatively low at water contents dry of optimum, but it increases rapidly as the water content at compaction exceeds the optimum. Several researchers [70,69,72] found that for a given dry density, the resilient modulus decreased as the water content at compaction increased. Consequently, the resilient deformations increased with the water content. Seed et al. [50] and Tanimoto and Nishi [61] reported similar results. Figure 2.13 from Finn et al. [73], relates the resilient modulus to water content and dry density. It shows the decrease of M_R with increasing water content. It also shows that for a given water content at compaction, as the dry density increases, the resilient modulus also increases, until it levels off at the optimum condition, then M_R begins to decrease slightly.

At high degrees of saturation, minor changes in dry density or water content have significant effects on the resilient behavior. Seed [50] suggested that this is attributable to the marked change which can take place in the soil structure at this range. He feels that it is desirable to compact samples at 80 percent saturation to avoid this and minimize the effects of resilient deformation. One further caution is also made that under field conditions, traffic loading of the subgrade soil may tend to densify it and reduce the water content. Both of these conditions, along with the large number of repeated loadings, will lead to higher strength and resilient modulus than expected. This is an important consideration in pavement deflection predictions.

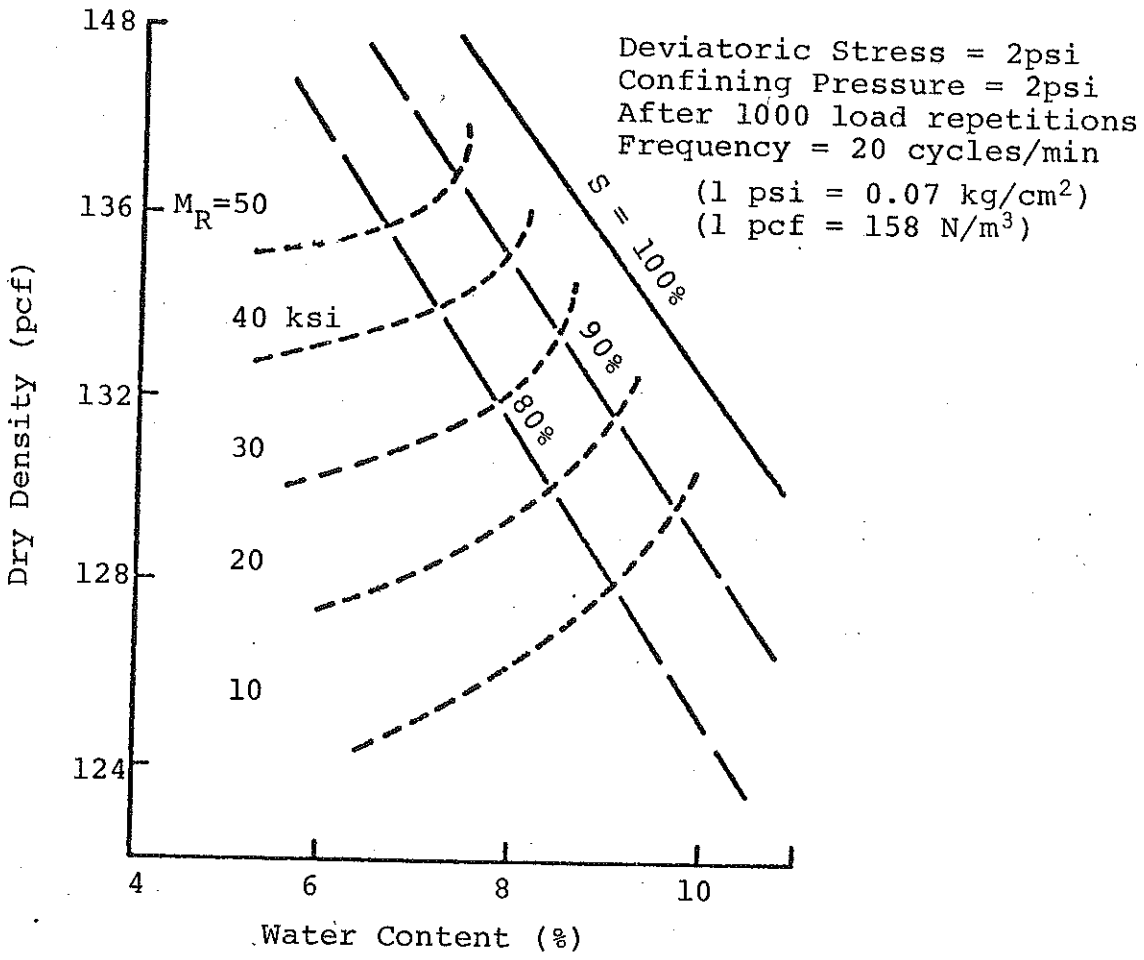

FIGURE 2.13 Water Content - Dry Density - Resilient Modulus Relationship for Subgrade Soil(73).

During construction, a subgrade will most often be compacted to a degree of saturation of approximately 75 percent. This would correspond to a flocculated particle structure as stated previously. After a long period of time, the subgrade may absorb water with no volume change, raising its degree of saturation to about 90 or 95 percent. It is virtually impossible to reproduce this condition by soaking, because the degree of saturation will not be uniform throughout the sample. The exterior portions may be saturated 100 percent, while the center may still be only at about 80 percent saturation. This is the reason static compaction is used for tests on samples with degrees of saturation greater than 85 percent.

2.3.1.2.f Thixotropy

As stated before, investigators have found that the response of cohesive soils can be greatly influenced by the length of time between preparation and testing. The strength increases as the time between preparation and testing (storage time) increased. However, this effect tends to diminish as the number of load applications increased [59].

Seed et al. [50] found the resilient deformation decreases (the resilient modulus increased) as the time between compaction and testing increases. This effect could be seen from Figure 2.14 if the number of load applications (N) is less than 40,000. For N greater than 40,000, samples of all different ages exhibit the same behavior. For a number of load applications of the order of 10, the resilient modulus for 1 day and 50 days storage time may differ by as much as 300 or 400 percent. Figure 2.14 also shows the effect of different storage times on the resilient modulus for a range of number of stress applications. For large value of N, the effects of aging are reduced and the same results are obtained for samples tested immediately after compaction as those tested after a period of time.

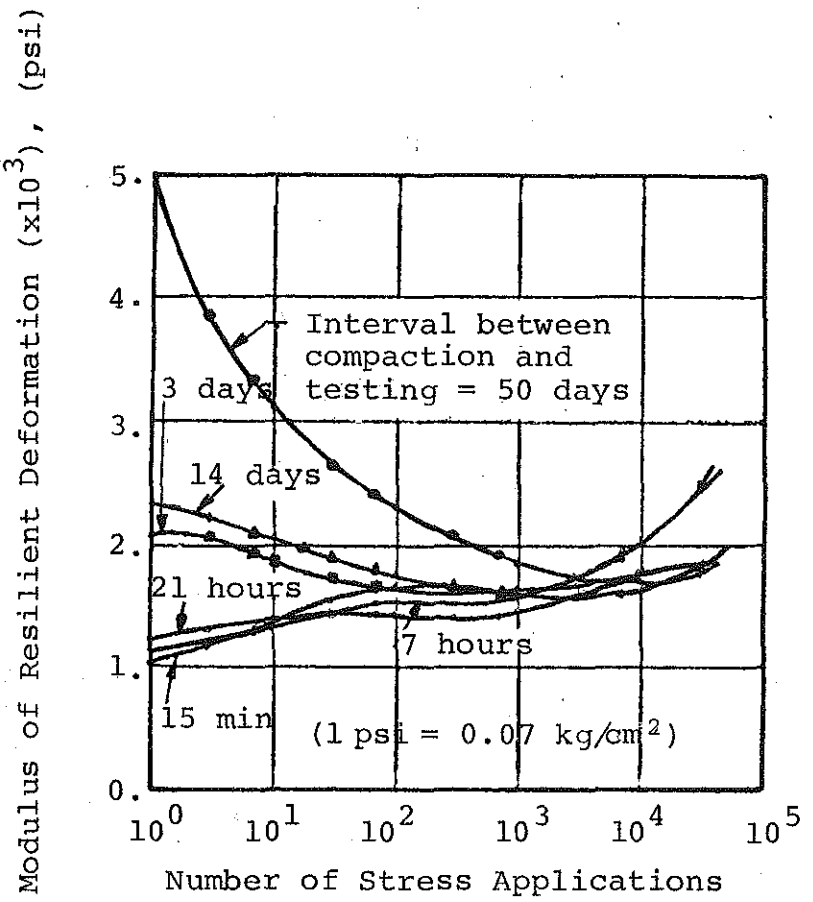

FIGURE 2.14 Effect of Thixotropy on Resilience Characteristics, AASHO Roadtest Subgrade Soil (61).

Tanimoto and Nishi [69] also found this to be the case, but water content appeared to affect the thixotropic strength gain. At water contents far below or well above the optimum, they found that storage time had little effect on the specimem response. However, at water contents just above optimum this effect is much more pronounced. Again, these effects were minimum at high number of stress applications. Figure 2.15 illustrates this point for a silty clay with an optimum water content of about 18 percent.

The effect of storage time on strength is still uncertain. The number of stress applications used in the laboratory can be developed usually within one day, whereas the number of stress applications under in-service conditions may take many years to develop. Once again, it appears that the laboratory estimates of strength are conservative due to the much shorter times involved.

2.4 Correlations of Soil Support Values (SSV) to Material Characterization

The basic design equation, developed from the results of the AASHO road test, is valid for one soil support value (SSV) representing the roadbed soils at the test site under conditions existed at the time of testing. Thus, it was necessary to assume a soil support value scale to accommodate the variety of soils which could be encountered at other sites [74,75].

This assumed soil support scale, however, has no defined relationship to any of the physical parameters of the roadbed soils. Several correlations relating the SSV to different tests and test results were developed by local agencies and highway departments [75]. These correlations are discussed next.

2.4.1 Correlations Between California Bearing Ratio (CBR) and Soil Support Values (SSV)

The Utah State Department of Highways conducted several CBR tests on compacted samples of the AASHO Road

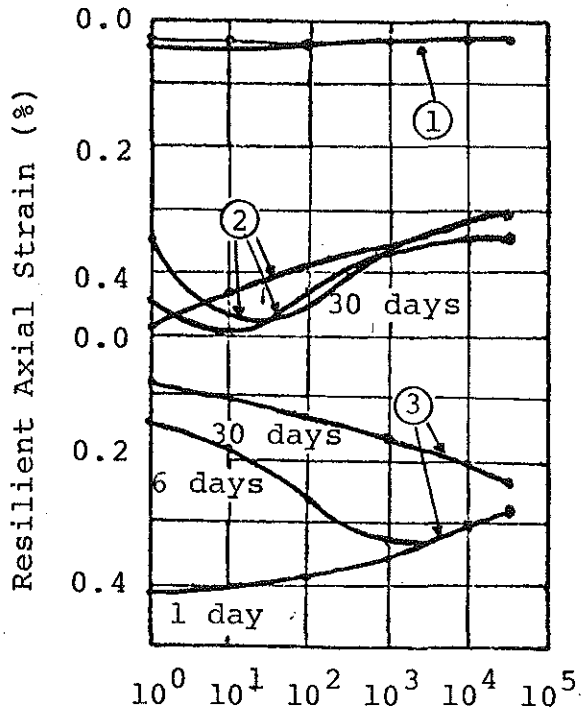

LEGEND	1	2	3
Water Content (%)	13.1%	22.2%	19.9%
Dry Density (pcf)	107.0	106.3	111.0
Deviatoric Stress (psi)	5.69	5.69	5.69

(1 psi = 0.0703 kg/cm^2)

(1 pcf = 0.0624 kg/cm^3)

FIGURE 2.15 Effect of Storage Period on Resilience Characteristics of Compacted Subgrade Material (69)

Test roadbed soils, the crushed stone base materials, and other soil types. An empirical logarithmic scale, shown in Figure 2.16 was then assumed to relate the CBR and the estimated SSV of these materials. Also, in the figure the same correlation plotted on arithmetic scales is shown.

2.4.2 Correlation Between Modulus of Deformation and SSV

Chou et al. [57] presented a procedure for subgrade evaluation to estimate the SSV. They conducted triaxial tests on subgrade soil samples at field densities and moisture contents. The modulus of deformations were then calculated and correlated to an assumed SSV scale as shown in Figure 2.17.

2.4.3 Correlation Between SSV and Resilient Modulus

Van Til et al. [22] were among the first researchers to establish a correlation between the soil support value and the resilient modulus of the subgrade soil at the AASHO road test. They used 40,000 psi (2812 Kg/cm^2) (a maximum value) as the resilient modulus of the crushed stone materials and 3,000 psi (211 Kg/cm^2) (a minimum value) as the resilient modulus of the AASHO A-6 subgrade soils. These two values were the limiting resilient modulus values on their scale, as shown in Figure 2.18. Van Til et al. recommended that effort should be made to strengthen the validity of the soil support scale as new analytical tools and methods of characterizing material properties become available. Based on this, Baladi and Boker developed a relationship between SSV and the resilient modulus of Michigan cohesionless soil. This relationship was dependent on the stress intensity and is given in the following equation:

$$SSV = 1.96 \log M_R + \frac{M_R}{19750} - 3.98 \qquad (2.6)$$

Figures 2.19, 2.20 and 2.21 show this relationship for recompacted and undisturbed Michigan cohensionless subgrade soil tested under first stress invariants (θ) of 15, 20, and 30 psi, respectively.

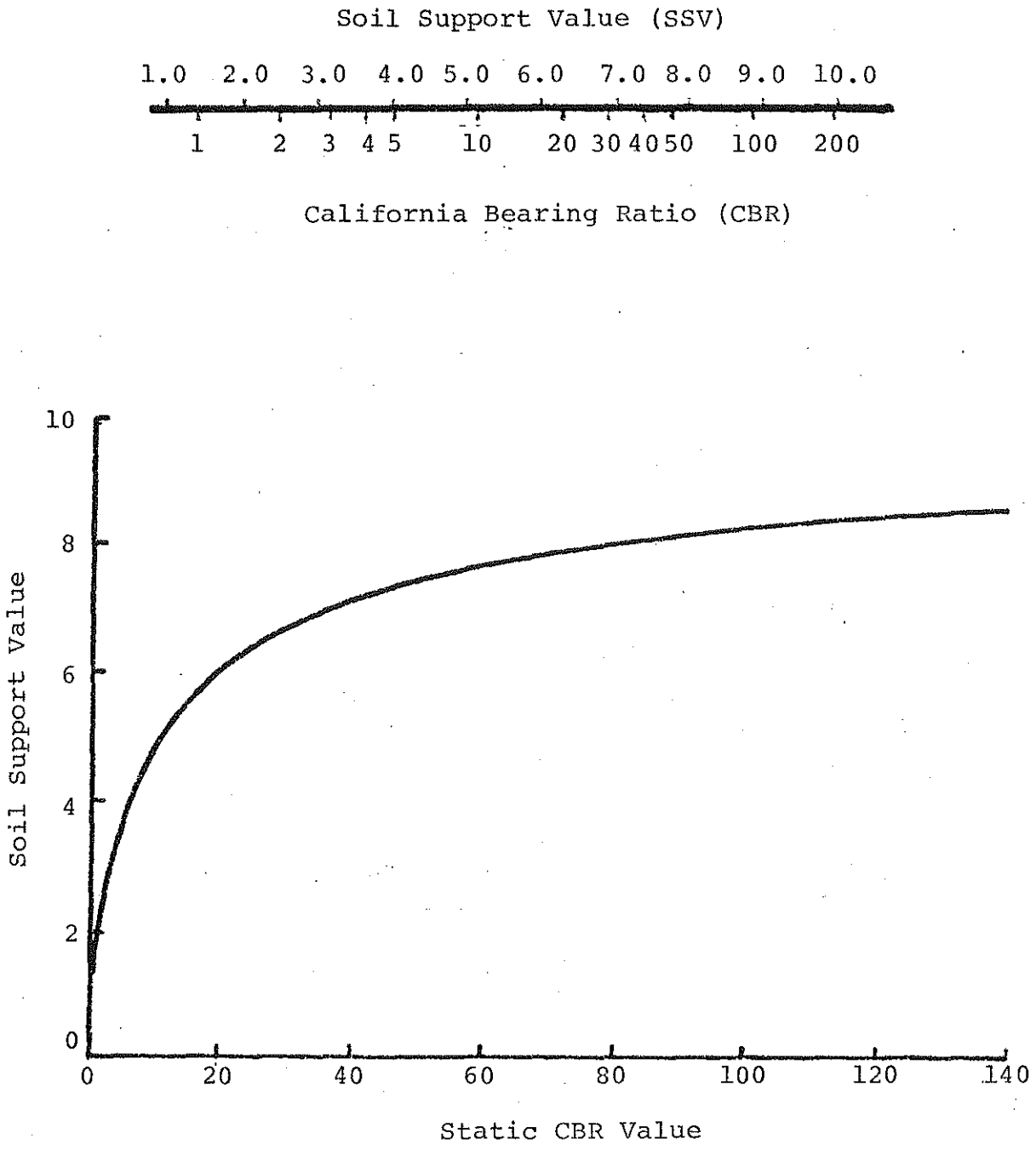

FIGURE 2.16 Correlation between Soil Support Value (SSV) and California Bearing Ratio (CBR) (57).

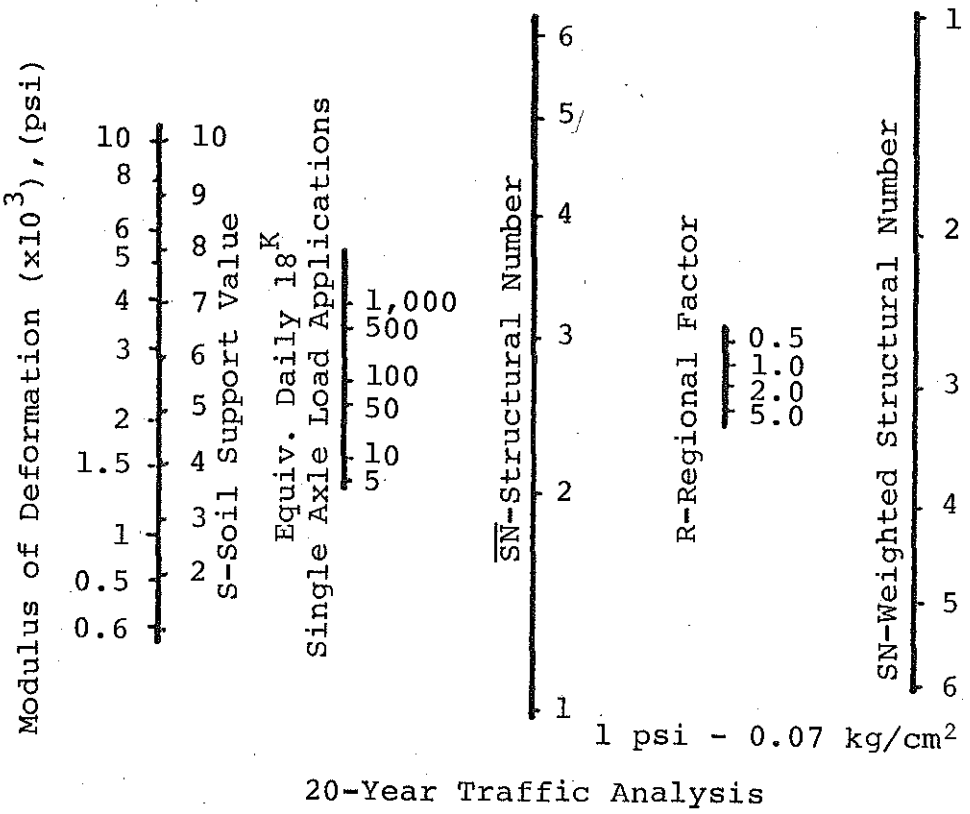

FIGURE 2.17 Design Chart for Terminal Serviceability Index of 2.5 (Based on AASHO Interim Guide Except for Addition of Modulus of Deformation Scale) (57).

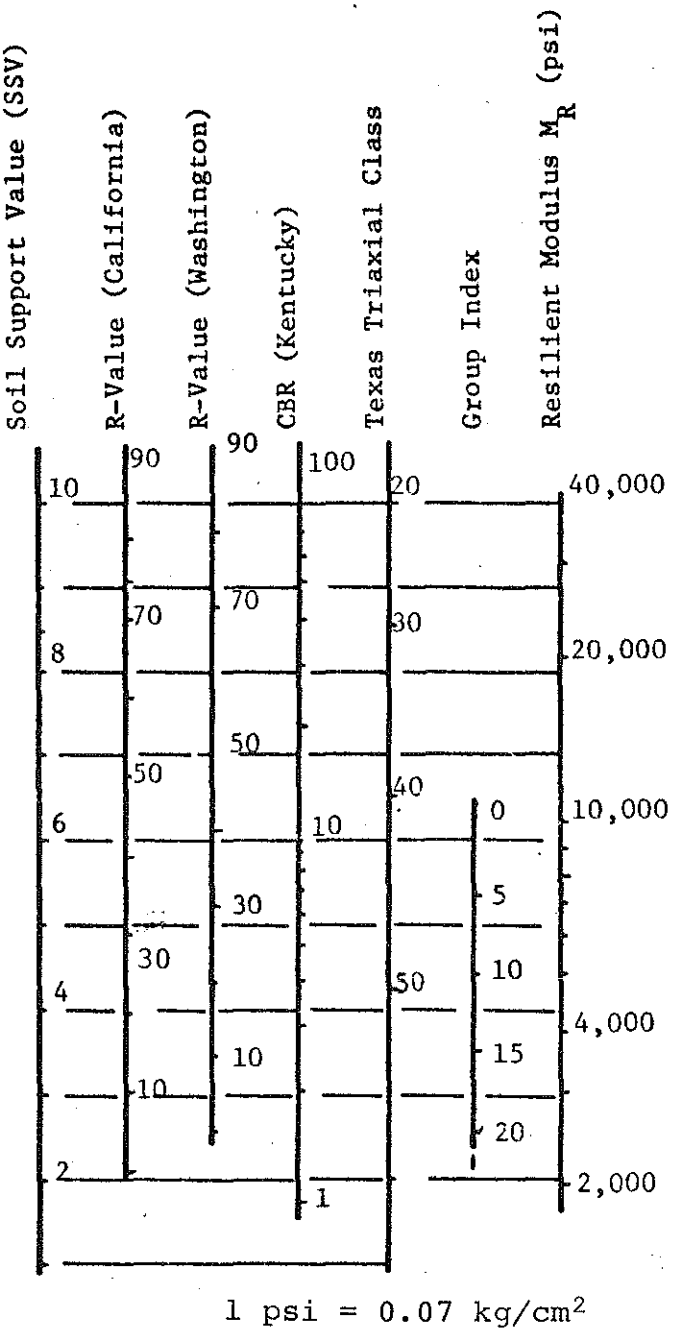

FIGURE 2.18 Correlation Chart for Estimating Soil Support Value (SSV) (22).

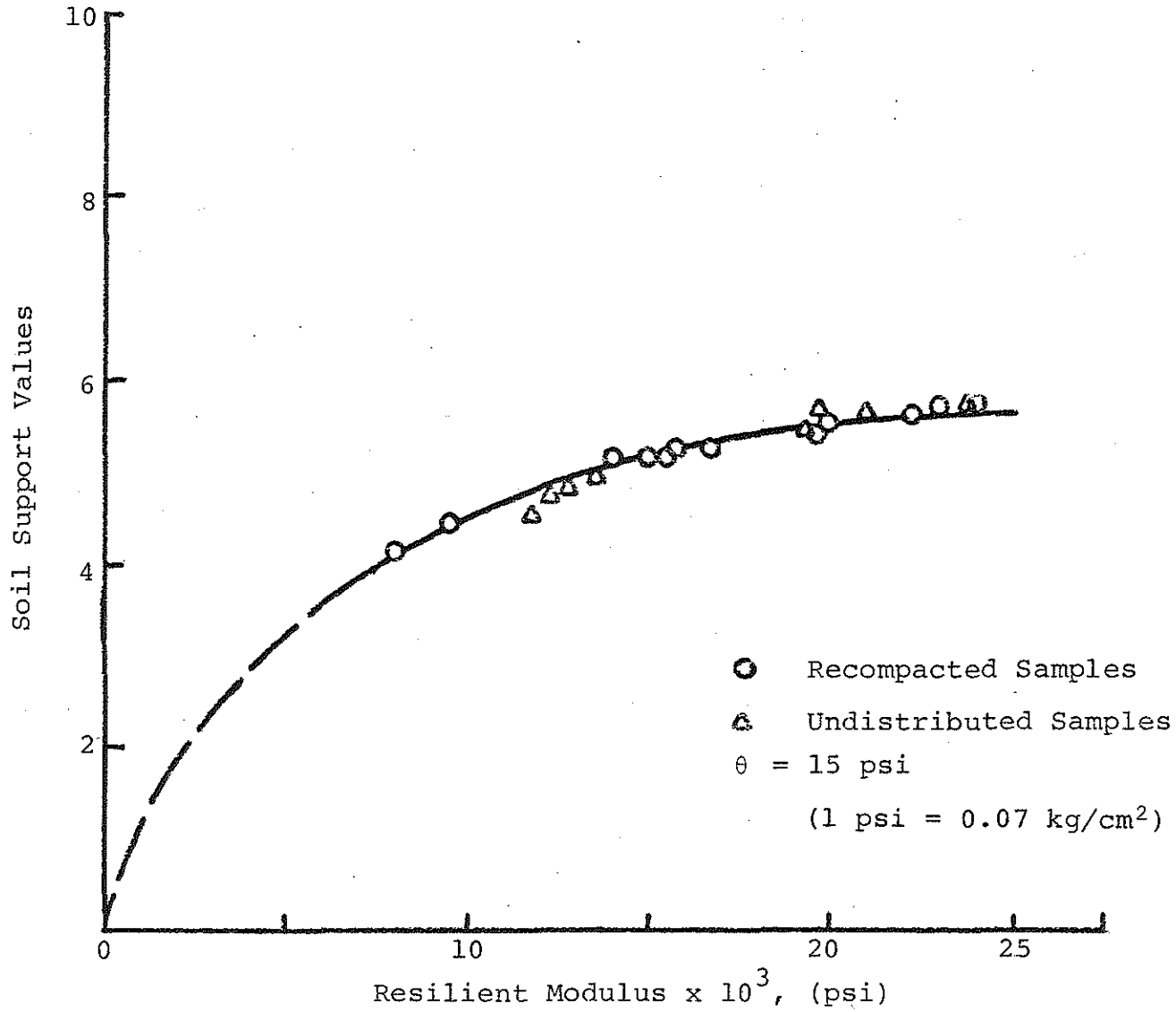

FIGURE 2.19 Resilient Modulus vs SSV for Recompacted and Undisturbed Cohesionless Soils for First Stress Invariant. θ = 15 psi (7).

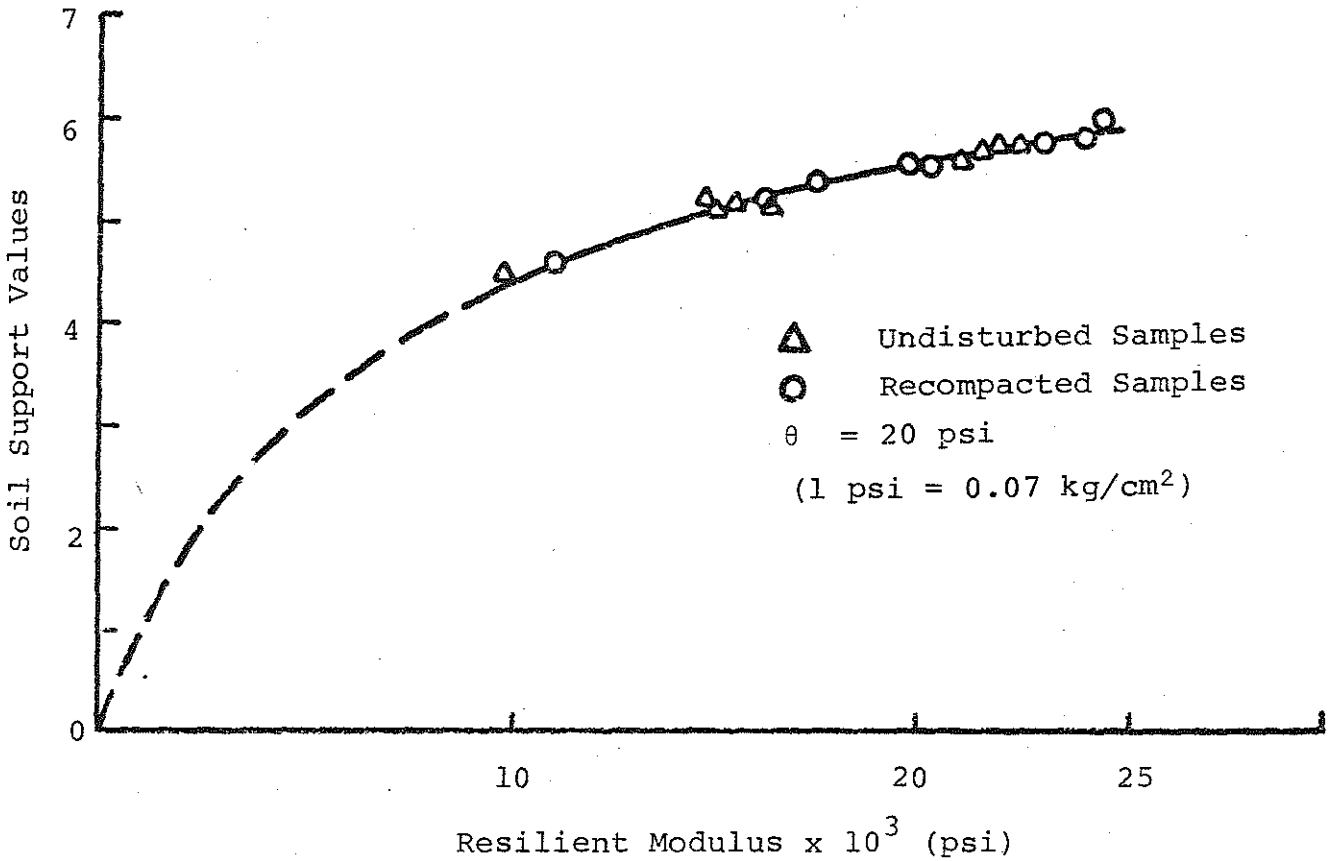

FIGURE 2.20 Resilient Modulus Vs SSV for Recompacted and Undisturbed Cohesionless Soils for First Stress Invariant θ = 20 psi (7).

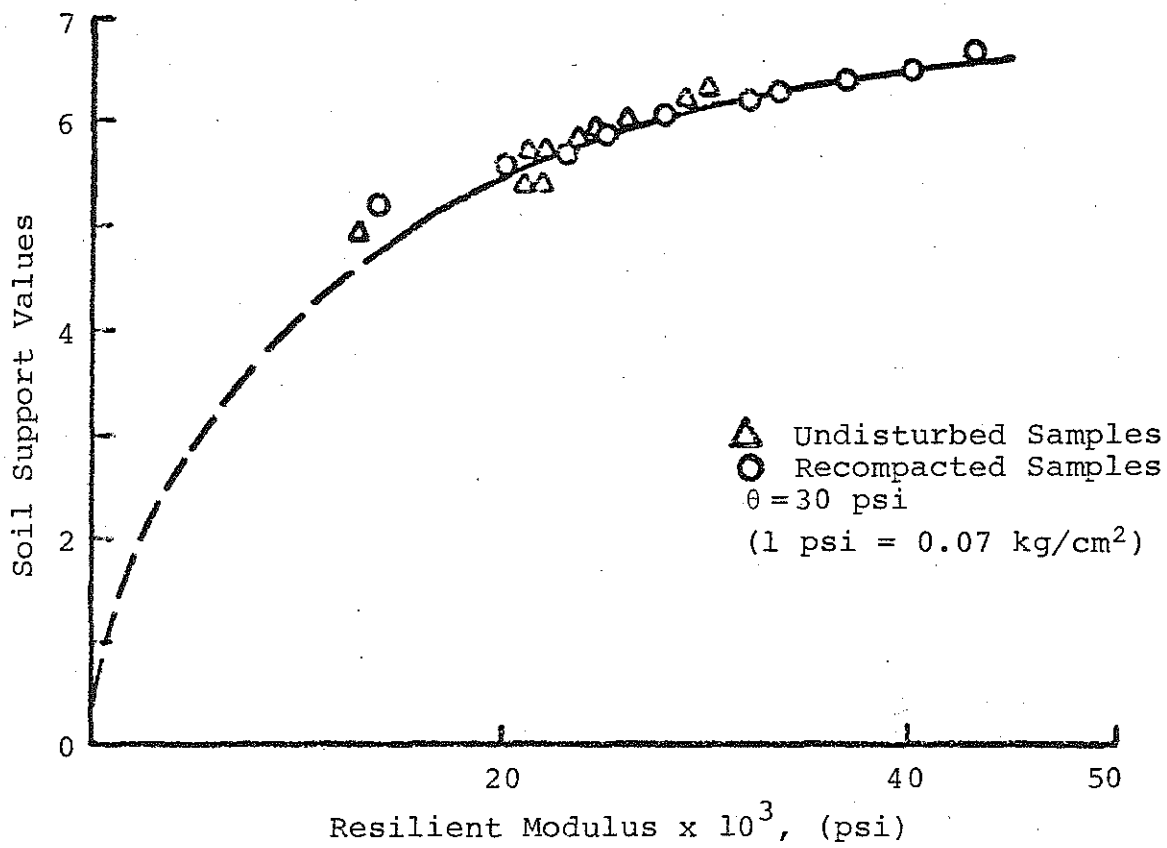

FIGURE 2.21 Resilient Modulus vs SSV for Recompacted and Undisturbed Cohesionless Soils for First Stress Invariant θ = 30 psi (7).

CHAPTER III

FIELD AND LABORATORY INVESTIGATIONS

3.1 Field Investigations

3.1.1 Site Selection

The field phase of this study had as its objectives the selection of several test sites; where the highway pavements showed different signs of distress and the subgrade materials were of different compositions. The investigations were conducted at eight different sites. Four sites were located in the lower Peninsula of the State of Michigan and four sites in the upper Peninsula as shown in Figure 3.1. Tables 3.1 and 3.2 provide general information concerning location, topography and pavement conditions at the test sites, while Figures 3.2 and 3.3 show their cross-sections. The subgrade materials of the lower Peninsula sites were Brookston and Blount clays (pedological soil classifications) [79] with different composition, gradation and properties. All the upper Peninsula test sites had Ontanagon Rudyard or Ontonagon Bergland varved clay as subgrade materials.

3.1.2 Scope of Sampling Techniques

Generally, for all the test sites, the investigations were designed and samples were obtained to accomplish several objectives. These include:

01. The determination of the resilient and permanent characteristics of the subgrade materials,
02. the determination of the grain size distribution curves, Atterberg limits and specific gravities of the subgrade soils, and
03. the reconstruction of the pavement cross-sections.

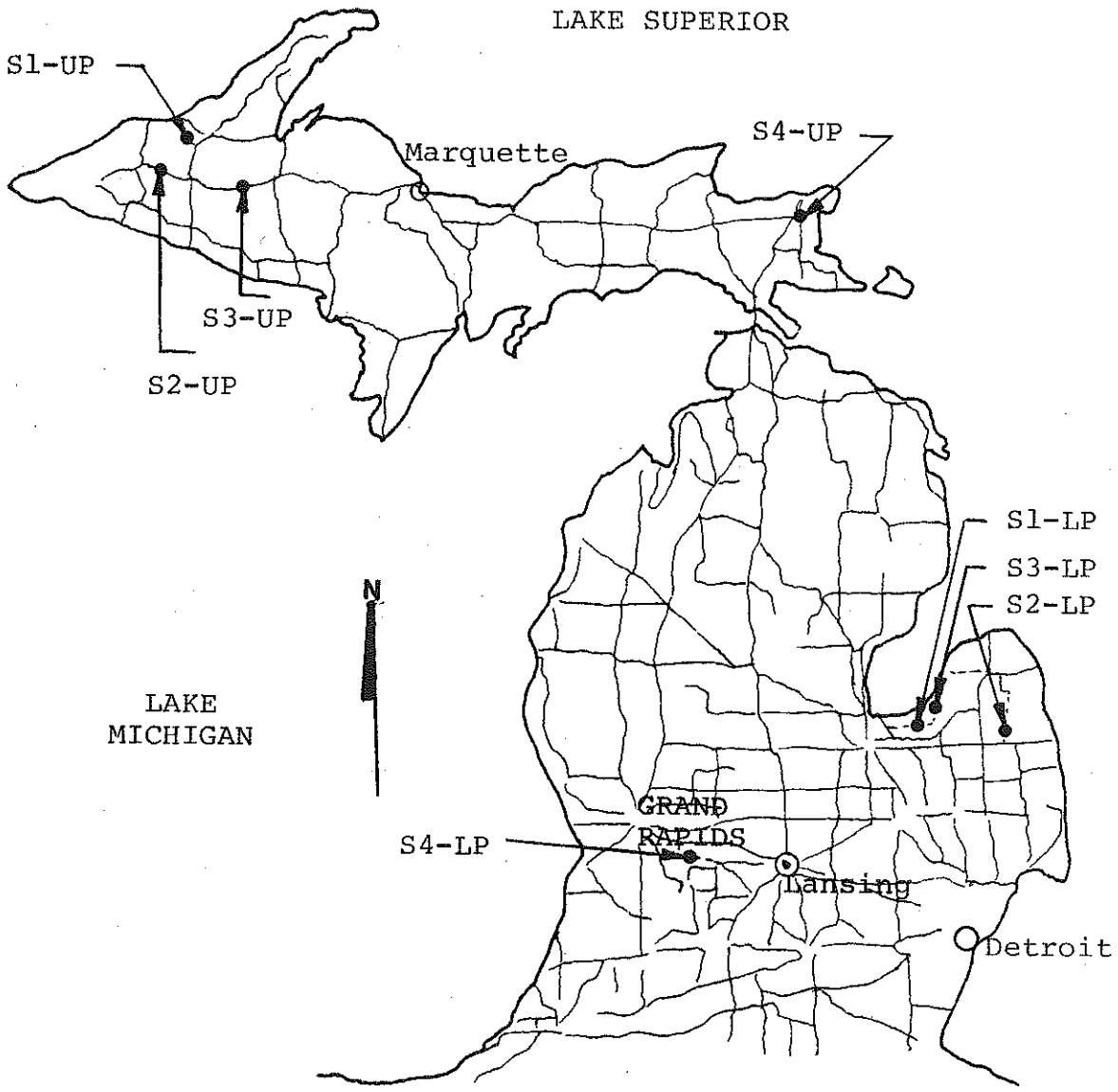

FIGURE 3.1 General location of test sites.

TABLE 3.1 General information concerning the test sites, upper peninsula.

Test-Sites	General - Description	Pavement - Conditions	General Location
S1-UP	Gently undulating glacial deposits of boulder and ontonagon clay. Surfaces are generally rough and broken	Predominantly transverse with some longitudinal cracks. With 0.025 "to 0.050" rut depth	North bound, about 8 miles on US-45 south of Ontanogon City
S2-UP	Level to gently undulating ontonagon clay	Discrete longitudinal and transverse cracks. Some longitudinal cracks in outer wheel path. With 0.05" - 0.1" rut depth	West bound, about 3 miles on M-28 west of Ewen
S3-UP	Hilly deposits of boulder and varved clay, surfaces rough and broken. Ontonagon clay	Same as S2-UP except the rut depth is in between 0.025" to 0.40"	East bound, about 6/10 of a mile on M-28 east of Kenton City
S4-UP	Level to gently undulating Esabella clay	Newly resurfaced, no major distresses, with the rut depth varies from 0100 to 0.05"	South bound, near Saulte Ste. Marie on M-129

TABLE 3.2 General information concerning the test sites, lower peninsula.

Designation of Test Site	General - Description	Pavement - Conditions	Approximate Location
S1 - LP	Level to nearly level till plain, mainly deposits of Brookston clay soils	Discrete longitudinal and transverse cracks	West bound, about 1.5 miles from the county line of Tuscona County on M-138
S2 - LP	Level to gently undulating Brookston clay soils	Predominantly transverse but not as severe as S1-LP	North bound, about 1-2 miles from Elmer Village on M-19
S3 - LP	Same as S1-LP	Same as S1-LP	South bound, about 5 miles from Unionville on M-138
S4 - LP	Hilly deposits of Blount clay soils	No major distresses	West bound, about 3.5 miles from Lake Odessa City on M-50

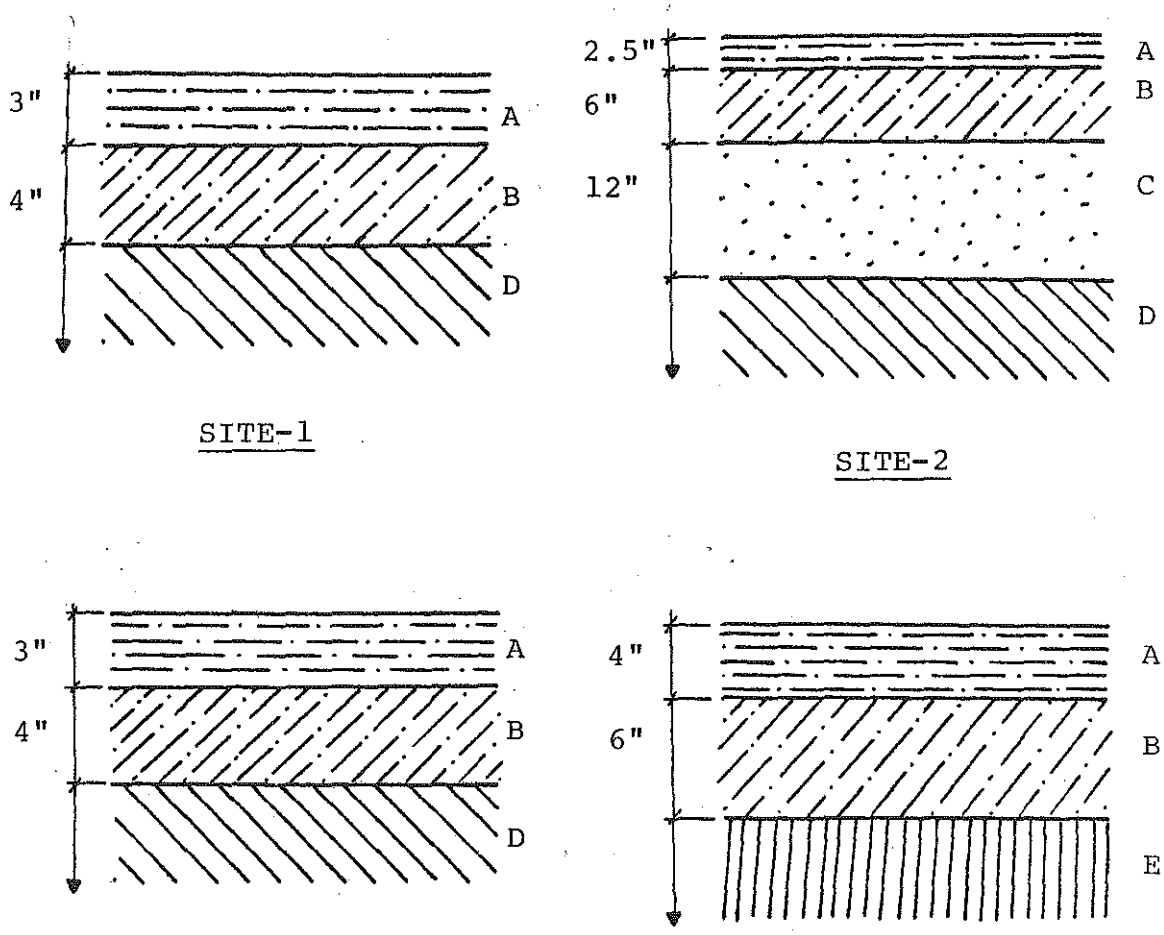

LEGEND

(1 inch = 2.54 cm)

A = Asphalt-Bituminous Concrete

B = Gravel Base

C = Sand Subbase

D = Brookston Subgrade Soil

E = Blount Subgrade Soil

FIGURE 3.2 Pavement cross-sections at the test sites, Lower Peninsula.

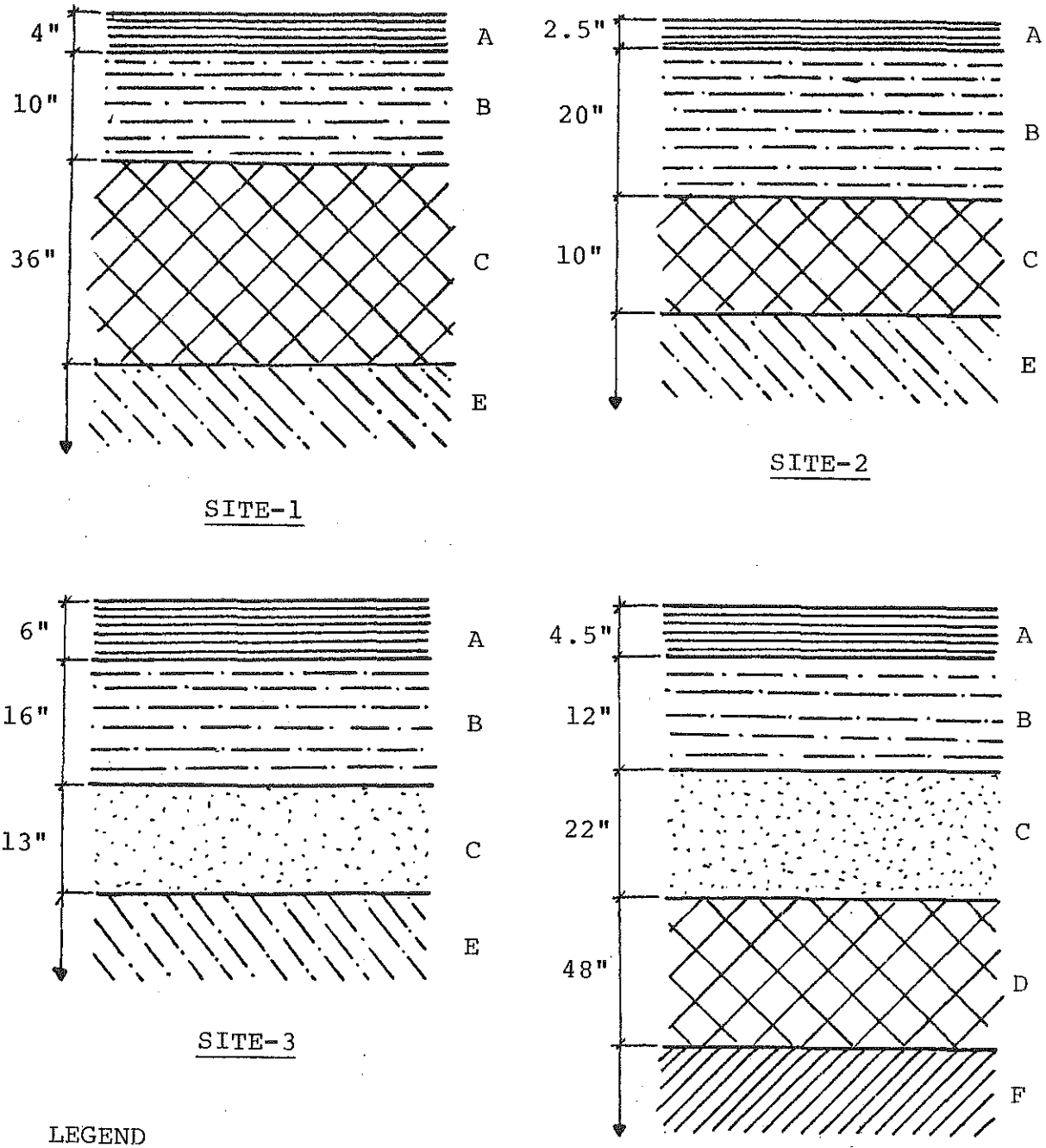

LEGEND

A = Asphalt-Bituminous Concrete

B = Gravel Base

C = Sand Subbase

D = Rock Fill

E = Ontonagon Rudyard

F = Ontonagon Bergland

(1 inch = 2.54 cm)

FIGURE 3.3 Pavement cross-section at the test sites Upper Peninsula.

To accomplish these objectives, the following sampling techniques were used.

01. A circular section, of the pavement surface, approximately six inches (15.3 cm) in diameter was cut and removed from the existing pavement (along the outer traffic wheel path) and a hole through the pavement structure was drilled using an auger. The base and subbase materials were collected in separate bags and the thickness of each pavement structure (pavement surface, base and subbase) was measured. This information was used to reconstruct the pavement cross-section of the upper Peninsula test sites that are shown in Figure 3.3. The cross-sections of the lower Peninsula test sites shown in Figure 3.2 were drawn using information supplied by Michigan Department of Transportation (MDOT). After collection of the base and subbase materials, the hole was then cleared and shelby tubes were driven to obtain subgrade samples.

02. A test pit along the ditch of the road was excavated and prepared as shown in Figure 3.4(a) and an undisturbed box samples were obtained using the same sampling techniques that was previously used by Boker [74]. Shelby tubes were then driven through the bottom of the test pit to obtain more representative subgrade samples. The numbering technique of the shelby tubes and of the samples obtained from these tubes is shown in Figure 3.4.

It should be noted that part a of the sampling technique and the box samples were used for the upper Peninsula test sites only.

3.2 Laboratory Investigation

3.2.1 Test Material

The test materials of these investigations consisted of four different subgrade soil deposits encountered in some parts of the State of Michigan [79,91]. These deposits are:

01. Brookston soils at test sites S1-LP, S2-LP and S3-LP
02. Blount soils at test site S4-LP
03. Ontonagon Rudyard soils at test sites S1-UP, S2-UP and S3-UP
04. Ontonagon Bergland soils at test site S4-UP

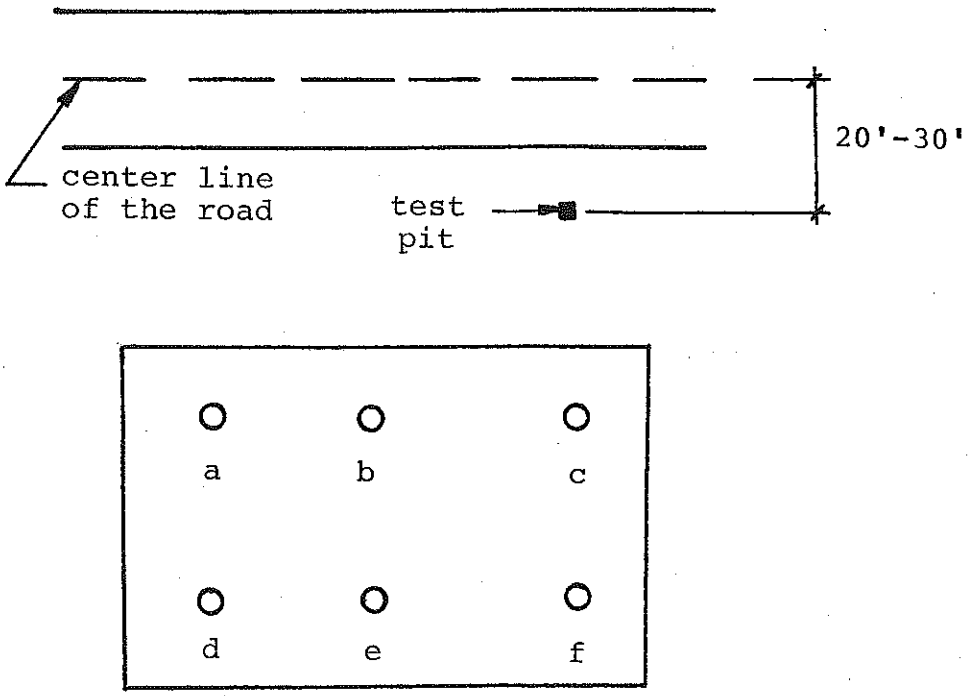

a) Numbering of Shelby Tubes in the Test Pit

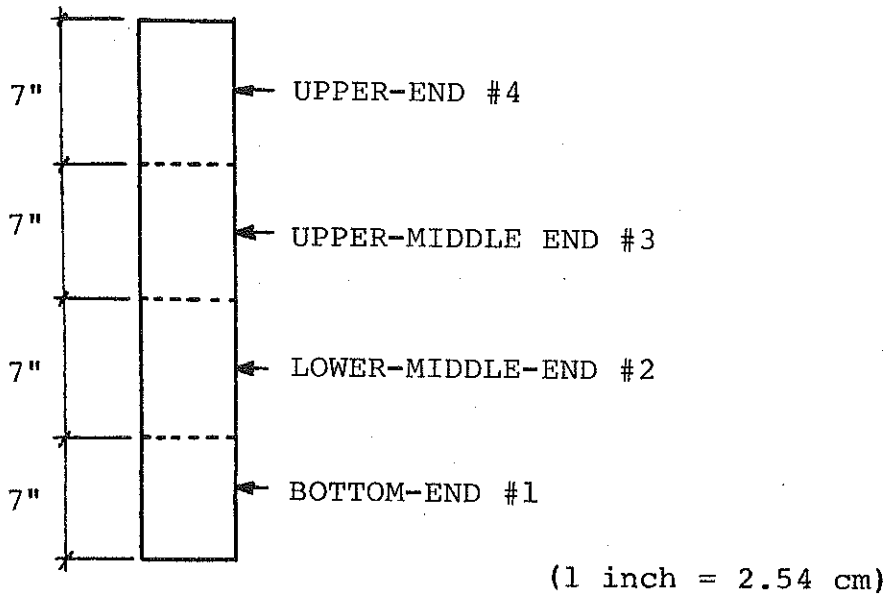

b) Numbering of Samples in the Shelby Tube

FIGURE 3.4 Samples and Shelby tubes numbering technique.

The grain size distribution curves of these materials are shown in Figures 3.5 through 3.8. Their specific gravities, atterberg limits and average natural moisture contents are listed in Table 3.3.

In general, Michigan cohesive soils are the result of glaciofluvial and glacial-lake deposits. The glaciofluvial soils are generally unstratified and primarily composed of silt, clay, sand and gravel. Such cohesive soils in the lower peninsula of the State of Michigan are Brookston and Blount soil desposits. Construction and/or excavation in these materials is not generally difficult. In wet periods, however, the materials are slippery and difficult to haul over. The surface will crust and become hard in periods of prolonged hot dry weather. Seepage may be encountered but not extensive enough to be a serious construction problem [79]. The glacial-lake deposits on the other hand exhibit silt and clay stratification which are the characteristics of varved clay [80,81,82,84,85,86]. The subgrade of the upper peninsula test sites (ontanagon soil deposits) exhibit such characteristics. Figure 3.9 shows a cross section through a varved clay specimen. These materials have very low permeability and because of high moisture content excavation by means of scraper equipment is generally difficult [79]. Hauling over this material is difficult due to its slippery and soft conditions and to its adhesion characteristics. Also, compaction of this material for embankments or any other purpose is often difficult due to its high moisture content. Further, it was reported [80] that glacial-lake deposits often exist as normally consolidated clays. Such clays with low shear strength and high compressibility often are not suitable for use as subgrade material. Near the ground surface, however, desiccation due to seasonal fluctuations in the water table has

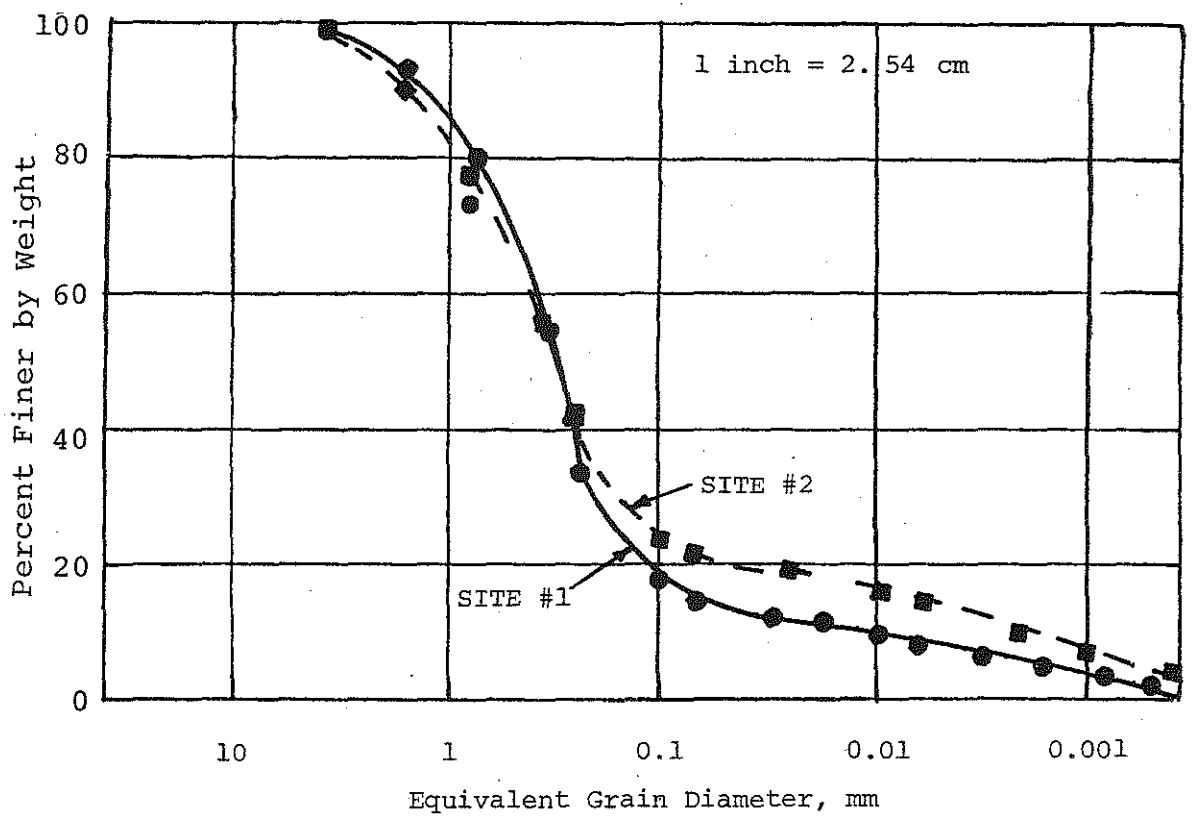

FIGURE 3.5 Grain size distribution curves for site 1 and site 2, Lower Peninsula.

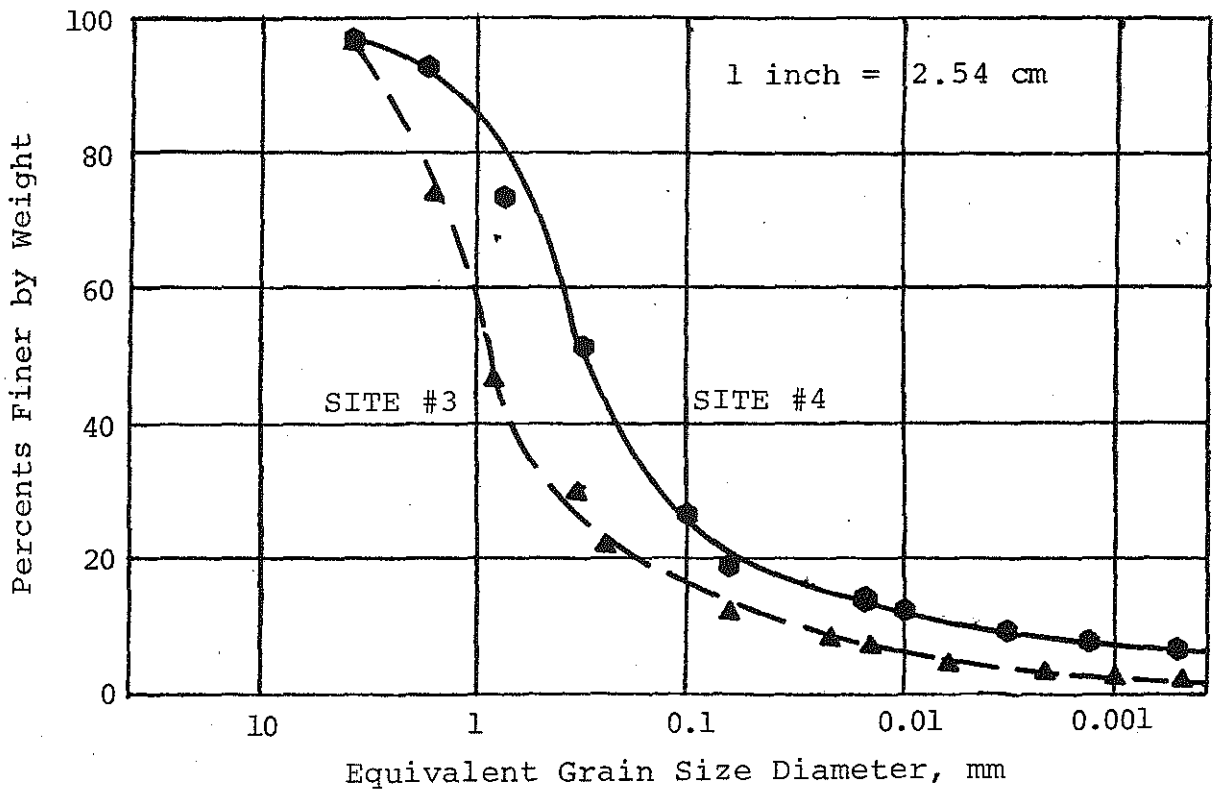

FIGURE 3.6 Grain size distribution curves for site 3 and site 4, Lower Peninsula.

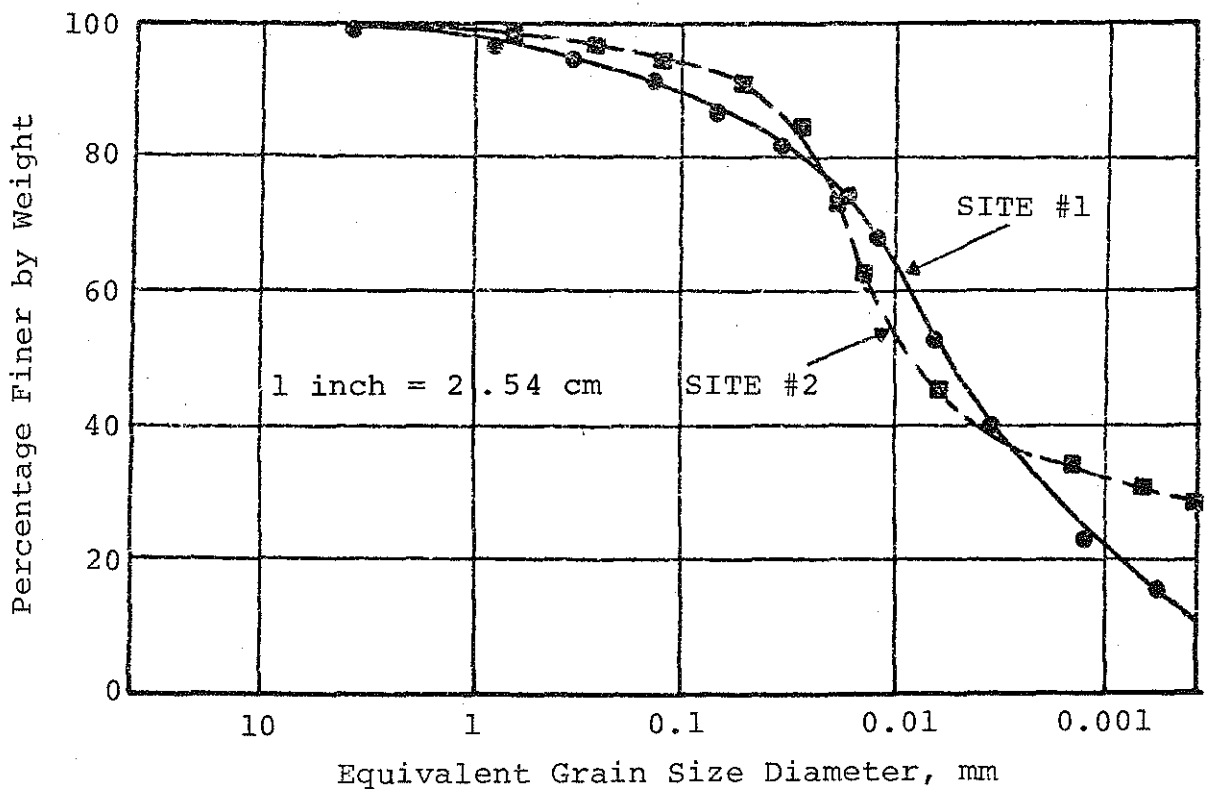

FIGURE 3.7 Grain size distribution curves for site 1 and site 2, Upper Peninsula.

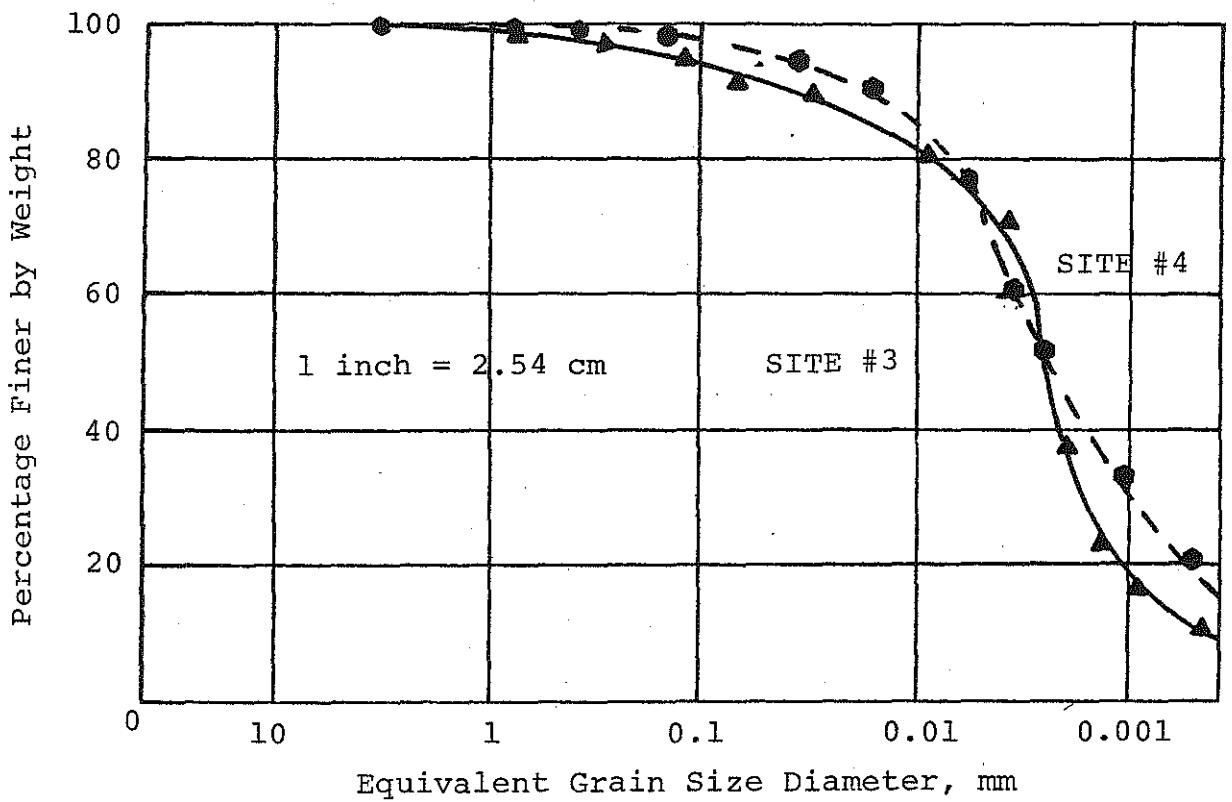

FIGURE 3.8 Grain Size Distribution curves for site 3 and site 4, Upper Peninsula.

TABLE 3.3 Specific gravity, Atterberg limits and average natural moisture content of the subgrade materials at the test sites.

Sites	Water Content (%)	G_s	LL (%)	PL (%)
S1-LP	17.56	2.700	30.75	15.05
S2-LP	20.51	2.716	33.0	19.56
Se-LP	15.35	2.720	25.0	16.28
S4-LP	20.83	2.700	23.5	16.39
S1-UP	20.12	2.694	26.4	16.12
S2-UP	21.83	2.700	23.2	16.52
S3-UP	22.45	2.689	28.1	15.74
S4-UP	18.23	2.705	29.4	15.02

Legend:

LP = Lower peninsula

UP = Upper peninsula

G_s = Specific gravity

LL = Liquid limit

PL = Plastic limit

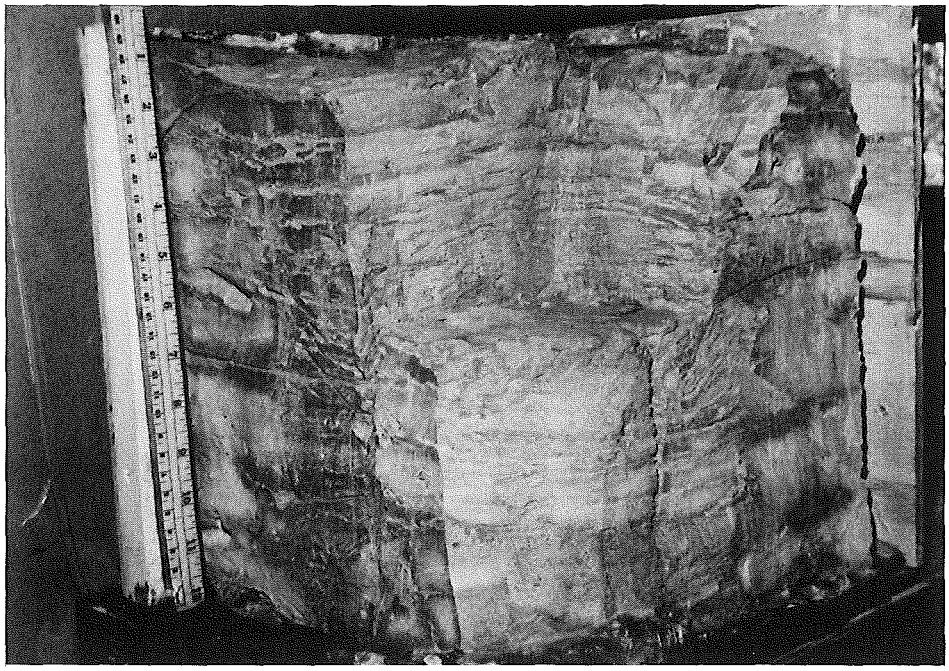

FIGURE 3.9 Typical varved clay cross section.

resulted in a slightly overconsolidated condition. The subgrade samples of the upper peninsula test sites are normally consolidated to slightly overconsolidated varved clay deposits as shown in the next section.

3.2.2 Laboratory Tests

3.2.2.1 Static Creep Tests

Conventional triaxial test equipment (ASTM specification D-2850) which utilizes the same size specimens as that used in the repeated load triaxial tests were not available to this project. Thus, to provide the best possible correspondence between static and dynamic test conditions, the static tests were performed in the dynamic triaxial cell. This equipment and the way they were setup (stress control mode) precluded loading the sample at a constant deformation rate as is usually done in the conventional triaxial test. Rather, the axial load was applied incrementally and consequently the test is called incremental creep test (ICT), or it was applied at a constant rate for the ramp test (RT). A brief discussion of both tests is presented in the following subsections:

3.2.2.1.a Incremental Creep Test (ICT)

The axial load for the ICT was applied gradually in small increments using the load control mode of the MTS system (for more information, the reader is referred to reference number 13 in the bibliography). The size of the load increment at the beginning of the test was approximately ten percent of the estimated sample strength as suggested by Bishop and Henkel [87]. The size of the load increment however, was reduced as the failure stress was approached to allow for a reliable determination of strength. Each load increment was maintained on the sample until the rate of strain decreased to a value less than 0.02 percent per minute. At that time, the sample

deformation and the magnitude of the load were recorded. Using these data, stress strain curves were plotted and the strength parameters were determined as explained in Chapter 4. It should be noted that only the peak sample strength could be determined from these tests. This is so because the load control mode of the MTS system did not allow the load to decrease to the ultimate strength level as the sample deformed.

3.2.2.1.b Ramp Test (R.T.)

The axial load for the ramp test was applied on the sample at a constant rate. This was accomplished using the triangular loading pattern of the MTS system at a frequency of 0.01 Hertz. The maximum principal stress difference which corresponds to the peak of this triangular loading was set at a value higher than the estimated sample strength by 25 percent. This high principal stress difference value insured that failure will occur before the end of the first loading cycle.

3.2.2.2 Cyclic Triaxial Tests (CTT)

Cyclic triaxial tests were performed to study the elastic and plastic characteristics of clay soils subjected to repeated loadings under different test and sample parameters. These parameters include:

a. number of load repetitions (N),
b. Confining pressure (σ_3),
c. cyclic principal stress difference $(\sigma_1-\sigma_3)d$,
d. stress history,
e. moisture content, and
f. density

All samples were tested up to thirty thousand load repetitions (unless failure occurred) under constant confining pressure and maximum cyclic principal stress difference. Several tests, however, were conducted up to

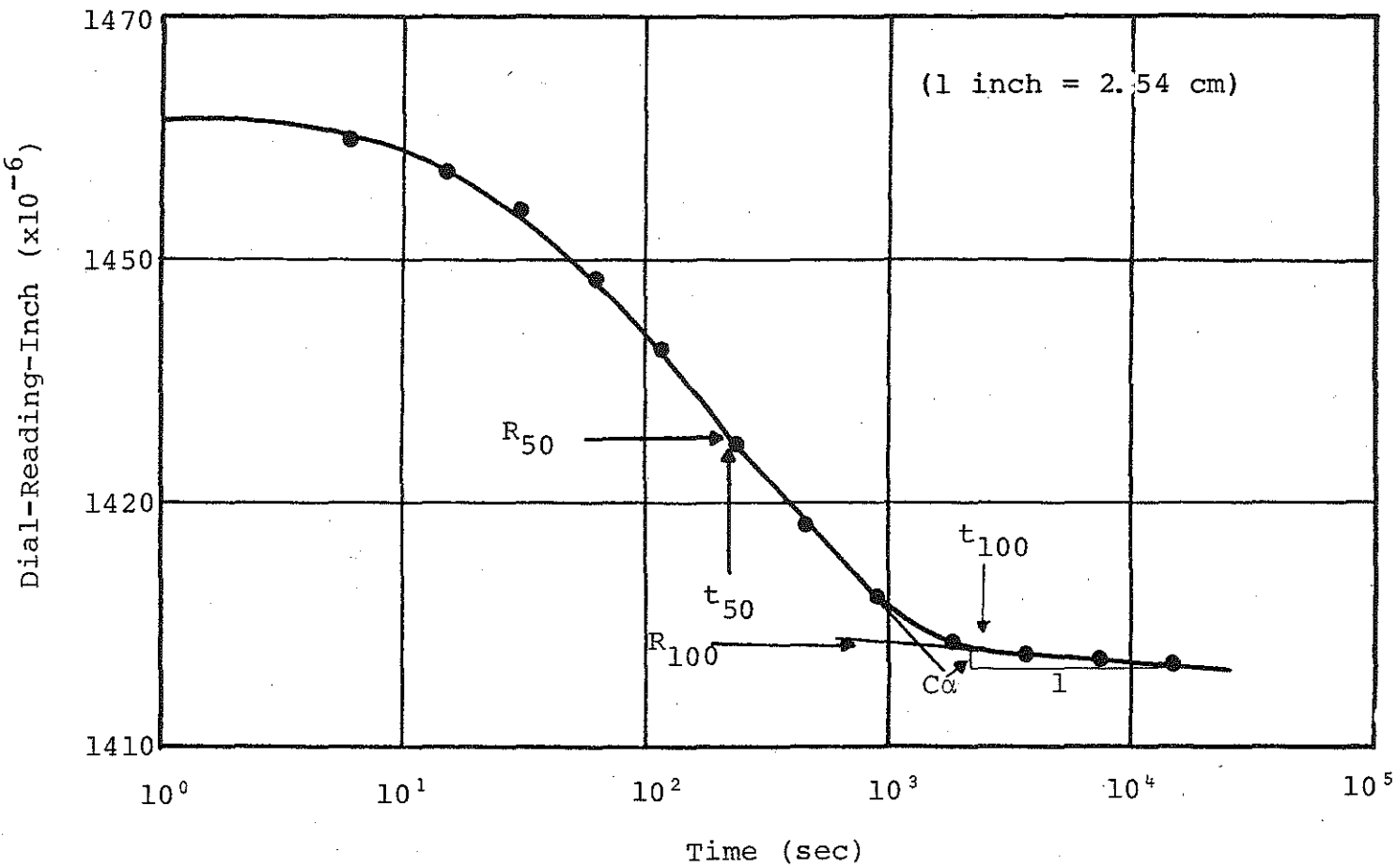

FIGURE 3.10 Typical Dial-Reading versus Logarithm of Time Curve for One Load Increment, Site 3.

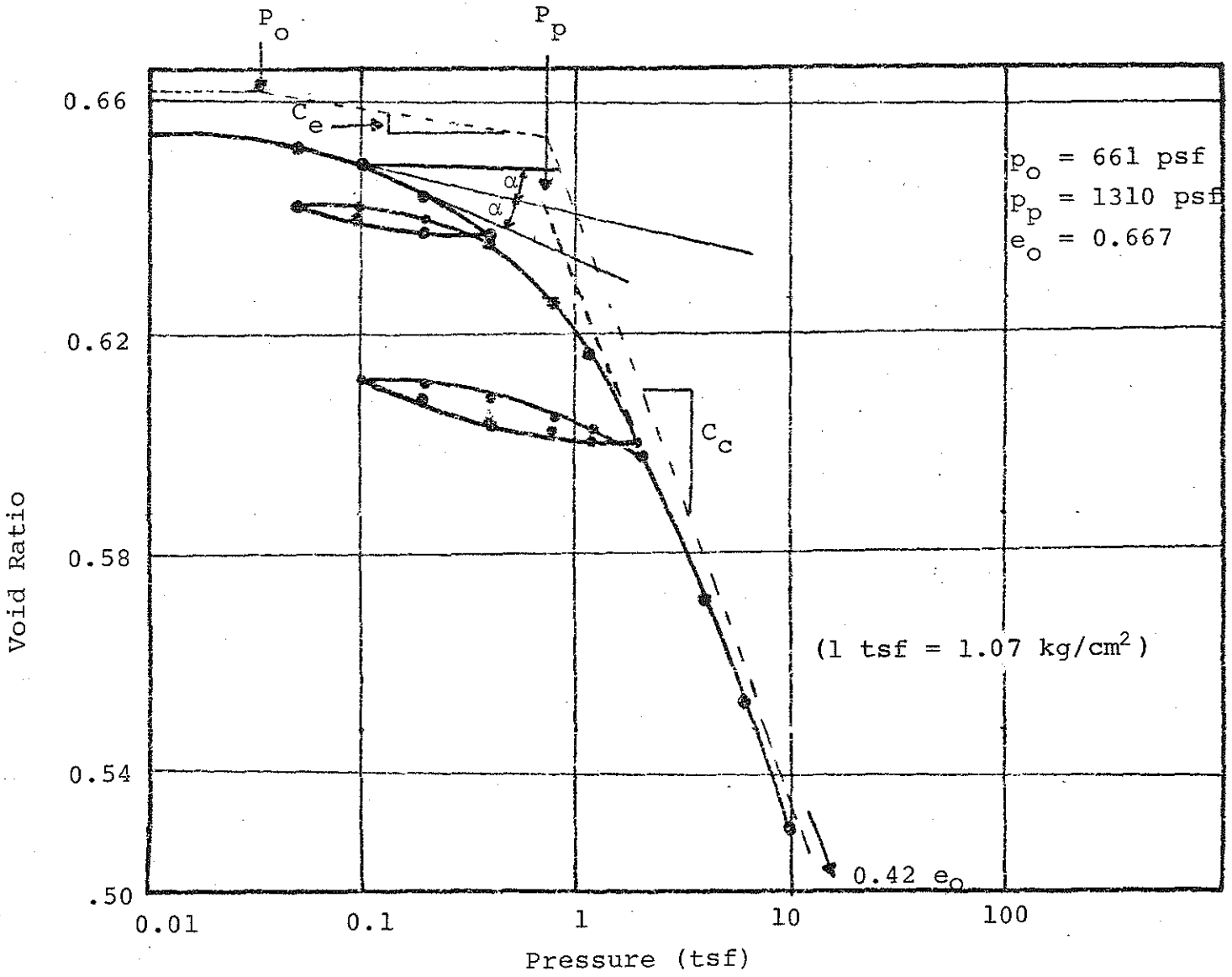

FIGURE 3.11 Typical Consolidation Curve, Void Ratio vs Logarithm of Pressure, Site 2.

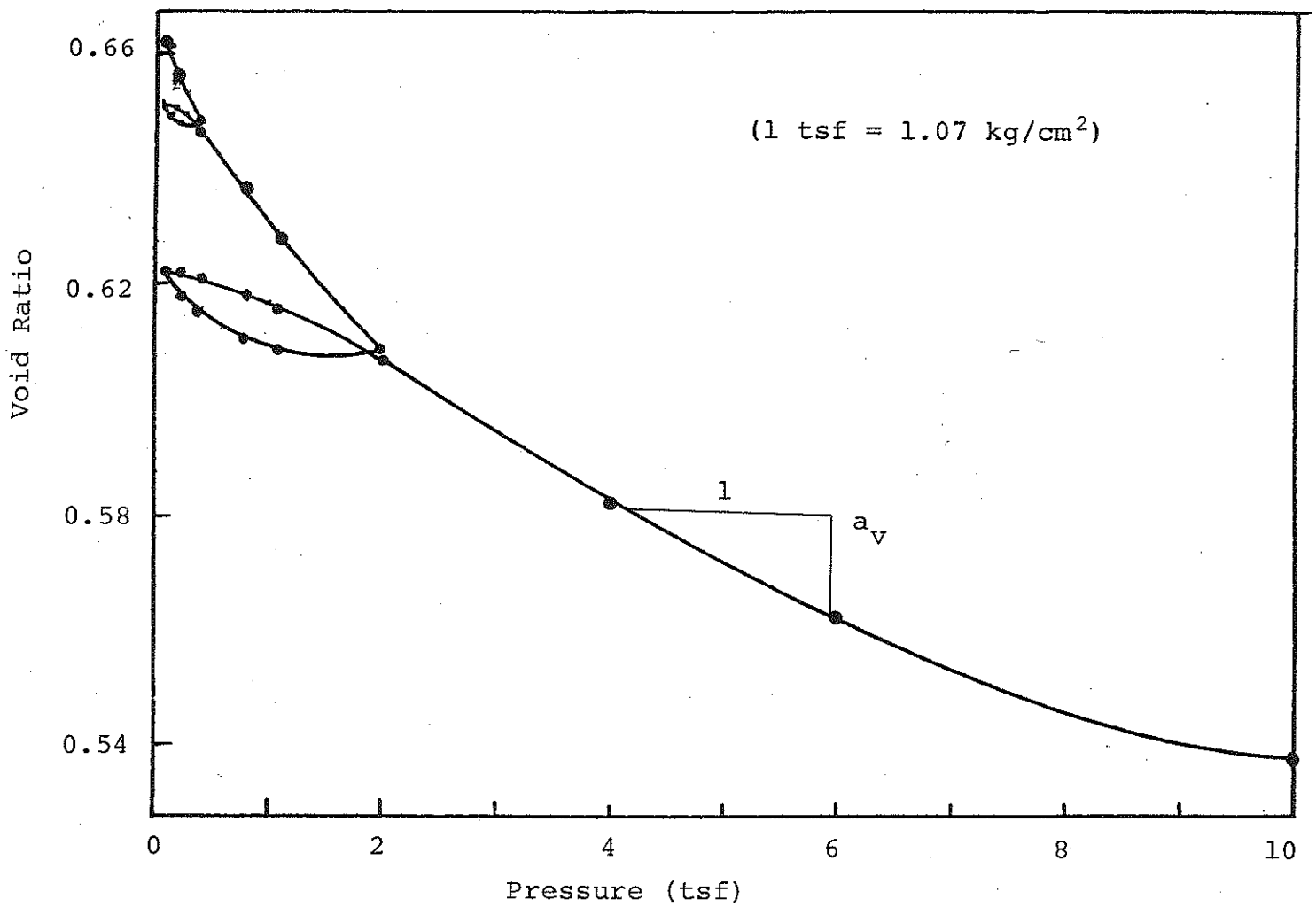

FIGURE 3.12 Typical Void Ratio vs Pressure Curve, Site 3.

TABLE 3.4 Consolidation Data of the Test Sites

Test-Sites and Location	P_o (psf)	P_p (psf)	C_α	C_c	C_v (in^2/sec)	A_v (in^2/lb)
S1-LP	491	1375	0.00101	0.181	0.00049	0.0023
S2-LP	859	1187	0.00083	0.139	0.00050	0.00156
S3-LP	661	1310	0.00092	0.231	0.00044	0.00218
S4-LP	559	896	0.00110	0.193	0.00036	0.00127
S1-UP	960	2149	0.00098	0.283	0.00053	0.00227
S2-UP	860	2005	0.00072	0.198	0.00067	0.00210
S3-UP	737	1494	0.00088	0.201	0.00059	0.00212
S4-UP	986	1166	0.00078	0.300	0.00056	0.0020

LEGEND

P_o = Effective Overburden Pressure

P_p = Preconsolidation Pressure

C_α = Average Coefficient of Secondary Compression

C_c = Slope of the Field Compression Curve

C_v = Average Coefficient of Consolidation

A_v = Coefficient of Compressibility

1 inch = 2.54 cm

1 psi = 0.07 kg/cm^2

1 psf = 1 kg/cm^2

ninety thousand load repetitions. The results of these tests helped to verify the validity of the developed relationship beyond thirty thousand cycles and to study the effects of stress history on the sample behavior. The cyclic triaxial tests were conducted using two different procedures. In the first, the samples were consolidated under the confining pressure prior to the application of cyclic loading. In the second procedure, the samples were confined and then subjected to cyclic loading without allowing any time for consolidation.

3.2.2.3 Conventional Consolidation Test (CCT)

One consolidation test (ASTM-designated D-2435) was conducted for each test site to study the compression characteristics of the test materials. Typical test results plotted as dial reading versus the logarithm of time for one single increment of load is shown in Figure 3.10. From this curve the time to 100 percent consolidation (t_{100}) and the dial reading at this time (R_{100}) and the coefficient of consolidation (C_v) were determined for the load increment in question. Figure 3.11 shows a typical consolidation curve, void ratio versus logarithm of pressure for site 2. The characteristics of this curve (the preconsolidation pressure (σ_p) and the slope of the estimated field virgin compression curve (C_c) were obtained. The coefficient of compressibility (a_v) of the sample was obtained using Figure 3.12. The consolidation data of the test sites are listed in Table 3.4. It should be noted that the test materials at the test sites are covered with varying thicknesses of overburden material and, in general, they were subjected in the past to pressure higher than the existing overburden pressure [88,89]. Consequently, the soils are said to be overconsolidated. The overconsolidation ratio (OCR) of the materials at the test sites are listed in Table 3.4.

3.2.3 Test Procedures

The following tests and testing procedures were used to provide information pertaining to the test materials studied in this investigation.

3.2.3.1 Cyclic Triaxial Test

a. The MTS hydraulic pump, the minicomputer and the signal monitoring and recording equipment were turned on at the beginning of sample preparation to allow enough time to warm up.

b. The minicomputer was programmed and left on the stop position until testing (see Appendix A).

c. The stylus of the load channel of the strip chart recorder was adjusted to the zero position before loading the sample.

d. The loading plate of the triaxial cell was put in place and carefully adjusted so that it was exactly parallel to the top of the sample cap. The loading plate was then secured in place.

e. The triaxial cell was assembled around the sample and the desired confining pressure was then applied.

f. The stylus of the deformation channel of the strip chart recorder was then adjusted to the zero position.

g. The required initial axial sustained stress (one psi) was applied to the sample by moving the actuator of the MTS system (using the set point dial as described in Appendix A). This sustained stress was carefully controlled through its read-out signal on a voltmeter.

h. The span dial of the MTS system was then adjusted to the proper setting for the desired principal stress difference.

i. The function generator was set to the desired frequency (one hertz for all tests in these investigations) and the cycle counter was set to zero.

j. The run button on the minicomputer was engaged to conduct the cyclic test.

k. The load and deformation output were recorded on a strip chart recorder for the desired number of cycles. All cycles from cycle number one to cycle number two hundred were recorded continuously, after which only segments of about ten cycles before and after the desired cycle number were recorded. Recordings were stopped between readings for economical reasons.

l. At the end of test, all final values pertaining to diameter, length, deformation and load were recorded and the cell was then dismantled. A part of the sample was then used to determine its final moisture content.

3.2.3.2 Ramp Triaxial Test

The testing procedure for the ramp tests was the same as steps a through h for the cyclic triaxial tests. After setting the spin dial of the MTS system at a principal stress difference value of 25 percent higher than the estimated sample strength at the particular confining pressure, the following steps were taken:

i. The function generator was set to the minimum frequency of 0.01 hertz.

j. The run button on the minicomputer was engaged to conduct the cyclic test.

k. The output was continuously recorded on a strip chart recorded until the sample failed.

l. Same as step l of the cyclic triaxial test procedure.

3.2.3.3 Incremental Creep Test

The test procedure for the incremental creep test was the same as steps a through f for the cyclic triaxial tests. After positioning the stylus of the strip chart recorder, the following steps were then taken:

g. The first increment of load which is equivalent to about ten percent of the estimated sample strength was then applied by adjusting the span dial set of the MTS system. This increment of load was maintained on the sample until the rate of strain of the sample decreased to less than 0.02 percent per minute. At this time a second increment of load was then applied. It should be noted at this time that the size of the load increment was decreased as the failure stress was approached to allow more accurate determination of the sample strength.

h. Same as step l of the cyclic triaxial test procedure.

3.2.4 Test Parameters

3.2.4.1 Number of Load Repetitions

A reasonable estimate of the number of eighteen thousand pounds equivalent single axle load, that traffic

a highway pavement throughout its life cycle, is not possible. However, it is believed that a typical pavement section may be subjected to about one hundred thousand to ten million load repetitions of eighteen thousand pounds equivalent single axle load [90]. The application of ten million or even one hundred thousand load repetitions on soil samples, at a frequency of one hertz, in the laboratory would require a constant data monitoring of up to 28 hours per test. This is impractical due to lack of automatic monitoring devices. Further, other researchers such as Brown [57] reported that both elastic and plastic characteristics of soil samples changed very little after ten thousand cycles. Consequently, it was decided that for the purpose of this study, most soil samples be tested up to thirty thousand load cycles and few to ninety thousand cycles for verification and study of stress history purposes.

3.2.4.2 Confining Pressure

The determination of lateral stress in highway subgrade materials is not an easy task. Several researchers [76,79,74] indicated that the value of this stress may vary from as low as a fraction of the applied axial stress (corresponding to at rest conditions) to as high as a fraction of the compaction stresses. Boker [79] used the existing Chevron computer program and calculated the lateral stress in the subgrade in the vicinity of four to six pounds per square inch (psi) (0.28 to 42 Kg/cm^2) depending on the pavement thickness. Others estimated this stress at sixty to seventy psi (4.2 to 4.9 Kg/cm^2) due to locked stress during compaction. In these investigations, it was decided to use different values of confining pressures (five, twenty-five and fifty psi) (0.35, 1.76 and 3.5 Kg/cm^2) to study its effects on the sample behavior.

3.2.4.3 Cyclic Principal Stress Difference

The elastic and plastic characteristics of soil samples are dependent on the level of cyclic principal stress difference [74]. Consequently, it was decided that for each confining pressure samples be tested at several values of principal stress differences $(\sigma_1-\sigma_3)_d$. These values ranged from 0.25 to 0.90 of the soil strength.

3.2.5 Sample Preparation

Throughout the course of these investigations, the soil samples, for all tests, were prepared using the following procedure:

01. Shelby-tubes were cut to a length of approximately seven inches and the soil was extracted using a hydraulic jack.

02. The sample was placed on a trimmer and trimmed to a diameter close to that of the trimmer head (about 5.40 cm), using a wire cutter.

03. The sample was then removed and placed in a specially designed steel sleeve for end trimming. After end trimming the following measurements were taken.

    a. Four sample height measurements were taken at approximately 90° apart. The average value of these readings was used as the initial specimen height.

    b. Two diameter readings 90° apart were taken at each of the following locations: top (dt), midheight (dm) and bottom (db) of the sample. The average diameter of the sample at these locations was computed. The sample's average diameter was computed using equation 3.1.

$$d_{av} = \frac{dt_{av} + 2dm_{av} + db_{av}}{4} \qquad (3.1)$$

where

dt_{av} = average diameter at the top of the sample

dm_{av} = diameter at the middle height of the sample

db_{av} = average diameter at the bottom of the sample.

04. The sample was then placed on the sample base of the MTS system and the sample cap was positioned on top of the sample.

05. The sample cap and base were then seated in place using membrane (two membranes were used to avoid leakage), rubber strips and O-rings.

06. The sample with the cap and base was then attached to the loading frame of the triaxial equipment.

3.3 Data Reduction

In all triaxial cyclic tests, a sustained stress of one psi was applied on the samples at the beginning of the test. This was felt to be a large enough stress to have seated the top cap firmly on the top of the sample without causing significant deformation in the sample. The cyclic principal stress difference $(\sigma_1-\sigma_3)_d$ was applied in a wave form shown in Figure 3.13. This was thought to closely duplicate the stress applied to the subgrade in the field due to a moving tandum axle truck. The wave form shown in Figure 3.13 was obtained using the sinusoidal wave form of the MTS modified by coupling a minicomputer and a function generator. Also, this coupling insured that the sample was at rest (under the confining pressure and sustained stress) prior to the application of the cyclic stress. The LVTD's output corresponding to rest condition was selected as the datum for deformations.

The axial permanent and elastic strains of the sample were calculated as the permanent or elastic change in distance between the sample cap and sample base divided by the original sample length, respectively. This change in distance was calculated as the average reading of two vertical LVDT(s) mounted on the sample at 180° from each other, multiplied by the appropriate calibration factors (see Appendix B). The radial permanent and elastic strains on the other hand were calculated using the following formula:

$$\varepsilon_R = \frac{\Delta}{2r} \left(\frac{R_2}{R_1}\right) \qquad (3.2)$$

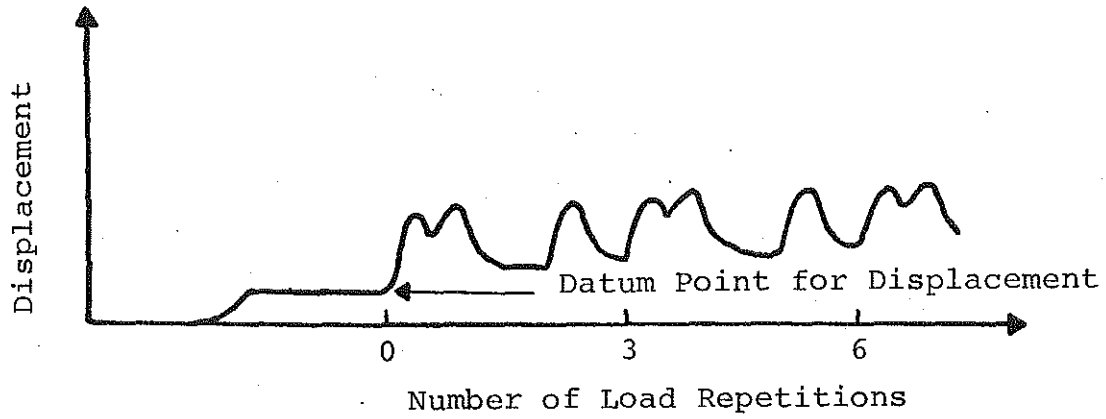

a) Displacement-Record

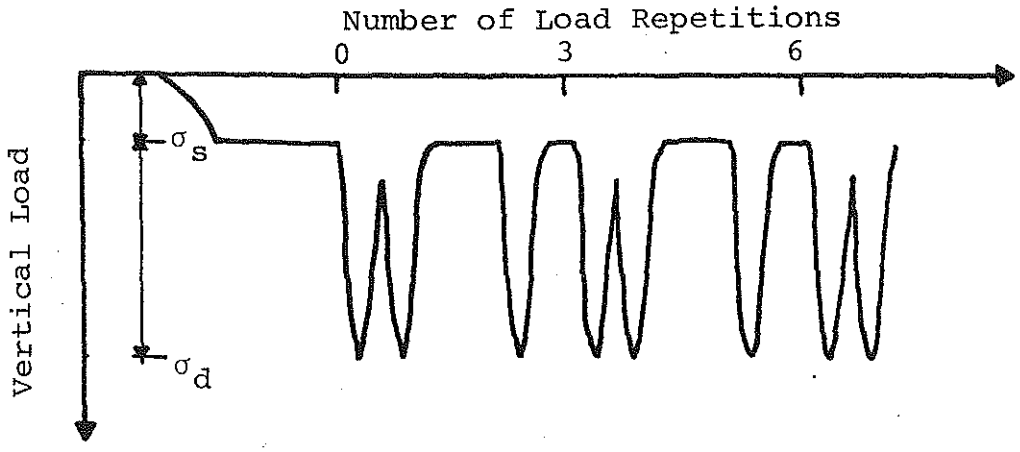

σ_s = Sustained Loading

σ_d = Principal Stress Difference

b) Load-Record

FIGURE 3.13 Typical Displacement and Load Records

where

ε_R = elastic or permanent strain of the sample

R_1 = moment arm from the hinge to the middle of the plate as shown in Figure 3.14

R_2 = the average radius of the brakets holding the horizontal LVDT(s) as shown in Figure 3.14

r = radius of the sample, and

Δ = the elastic or permanent deflection of the sample

Throughout this investigation, the resilient modulus was calculated using the following formula

$$M_R = \frac{(\sigma_1-\sigma_3)_d}{\varepsilon_e} \qquad (3.3)$$

where

M_R = resilient modulus

$(\sigma_1-\sigma_3)_d$ = cyclic principal stress difference

ε_e = elastic strain corresponding to a particular number of stress repetition

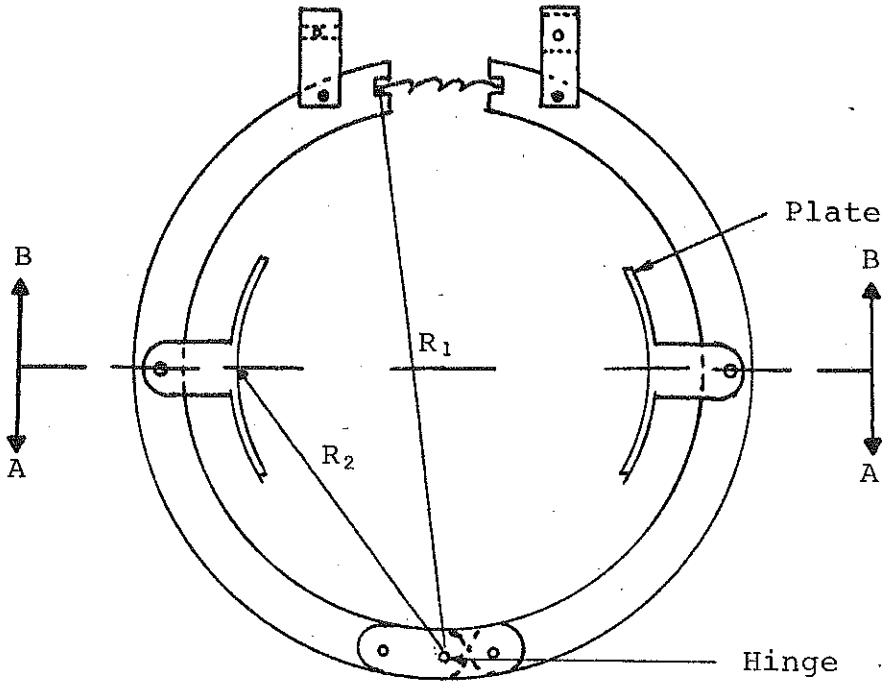

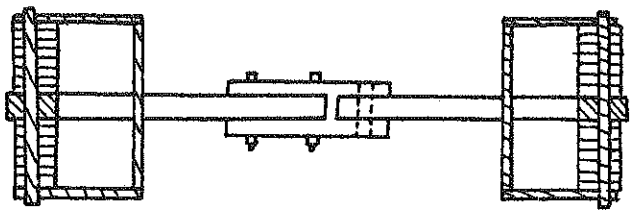

Section A-A

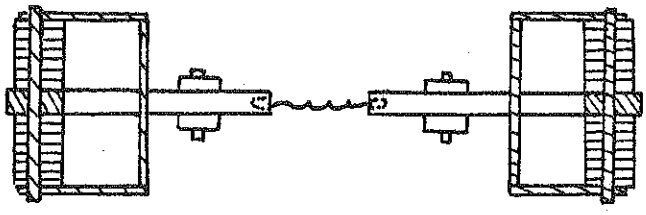

Section B-B

Scale 1:1

FIGURE 3.14 Brackets used to hold the horizontal LVDT's.

CHAPTER IV

TEST RESULTS

4.1 General

The laboratory phase of this study was designed and tests were conducted so that the collected data would provide most, if not all, the information needed to accomplish the objectives of this investigation. As described in Chapter III, several different tests were conducted on identical soil samples. Information pertaining to these tests along with sample numbers and several of its parameters are summarized in Table 4.1 for the lower peninsula test sites and Table 4.2 for the upper peninsula test sites. These tables include the following information:

01. test-site designation and location,
02. sample number,
03. initial natural water content of the sample before testing (w_i),
04. final water content of the sample after testing (w_f),
05. initial calculated void ratio (e_o),
06. initial dry density (γ_d),
07. test confining pressure (σ_3),
08. ratio of principal stress difference to the confining pressure, and
09. the kind of test that was conducted on the indicated sample.

Typical measured data have been summarized in the proper figures in this chapter. All other data were plotted and the figures may be found in Appendix C.

TABLE 4.1 Information Pertaining to the Test Samples of the Lower Peninsula Test Sites.

Site-Number Location	Sample Number	Wi (%)	Wf (%)	e_o	γ_d (pcf)	σ_3 (psi)	$\frac{(\sigma_1-\sigma_3)_d}{\sigma_3}$	TEST MODE			
								CCT	ICT	RT	CT
S1-LP	1a-F	19.12	16.68	0.3807	122.0	5	--		C		
S1-LP	2a-F	19.42	16.81	0.4115	119.0	5	2.0				C
S1-LP	4a-S	19.70	17.67	0.4362	117.31	50	0.5				C
S1-LP	2b-F	12.31	12.10	0.4274	118.03	5	1.0				C
S1-LP	3b-S	19.1	17.7	0.7188	98.02	50	--				
S1-LP	4b-F	14.42	18.62	0.6718	100.78	--	--	X			
S1-LP	1c-F	16.41	14.74	0.4869	113.31	5	3.0				C
S1-LP	2c-F	16.40	14.0	0.3674	123.21	50	--		C		
S1-LP	1d-F	16.8	14.20	0.3435	125.4	25	--		C		
S1-LP	2d-F	16.5	15.33	0.5215	110.73	25	1.0				C
S1-LP	3d-F	16.80	15.00	0.9770	85.22	5	1.0				U
S1-LP	4d-F	17.9	16.81	0.4379	117.17	25	2.0				C
S1-LP	1e-F	12.09	11.98	0.3435	125.4	5	3.0				U
S1-LP	2e-S	17.66	15.90	0.4032	120.07	25	1.5				U

TABLE 4.1 (Continued).

Site-Number Location	Sample Number	Wi (%)	Wf (%)	e_o	γ_d (pcf)	σ_3 (psi)	$\frac{(\sigma_1-\sigma_3)_d}{\sigma_3}$	TEST MODE			
								CCT	ICT	RT	CT
S1-LP	4e-F	19.40	17.35	0.4339	117.50	--	--				
S1-LP	1f-F	21.43	16.92	0.3457	125.2	5	2.0				U
S1-LP	2f-S	24.0	22.90	0.3500	124.80	25	1.5				C
S1-LP	3f-S	17.04	16.21	0.3863	121.53	25	1.0				U
S1-LP	4f-s	16.79	16.76	0.6527	101.94	5	--			U	
S1-LP	3a-s	18.98	18.42	0.4716	114.49	25	--			U	
S2-LP	1a-F	17.10	16.84	0.5526	109.16	25	2.0				U
S2-LP	2a-F	19.16	18.08	0.4763	114.80	5	--			C	
S2-LP	3a-S	19.83	18.13	0.5189	111.58	25	0.6				U
S2-LP	4a-F	22.94	20.4	0.6627	101.93	25	--			C	
S2-LP	1b-S	21.40	20.91	0.4813	114.41	5	1.0				C
S2-LP	2b-S	19.22	18.68	0.6195	104.64	25	--				
S2-LP	2b-F	21.36	19.84	0.4536	116.59	25	--		C		

TABLE 4.1 (Continued).

Site-Number Location	Sample Number	Wi (%)	Wf (%)	E_o	γ_d (pcf)	σ_3 (psi)	$\frac{(\sigma_1-\sigma_3)_d}{\sigma_3}$	TEST MODE			
								CCT	ICT	RT	CT
S2-LP	3b-S	18.48	18.02	0.4265	118.81	25	1.0				C
S2-LP	4b-S	21.40	20.91	0.5666	108.18	5	1.0				C
S2-LP	4b-F	17.90	17.0	0.4123	120.0	25	1.0				C
S2-LP	1c-F	22.0	19.2	0.4494	116.93	5	3.0				U
S2-LP	2c-S	15.0	13.79	0.4431	117.44	50	0.5				C
S2-LP	3c-F	20.90	19.20	0.4580	116.24	25	1.0				U
S2-LP	4c-S	21.48	20.18	0.5666	108.18	50	0.75				C
S2-LP	4c-F	21.73	20.3	0.6415	103.25	5	--		C		
S2-LP	2d-S	21.25	19.40	0.5779	107.41	5	2.0				C
S2-LP	3d-S	22.37	21.0	0.6617	101.99	50	--		C		
S2-LP	4d-S	22.80	20.8	0.5674	108.13	50				C	
S2-LP	1e-F	18.52	18.35	0.4912	113.65	5	2.0				U
S2-LP	2e-F	19.39	18.73	0.4583	116.22	5	1.0				U
S2-LP	3e-F	18.10	17.40	0.4283	118.66	25	2.0				C

TABLE 4.1 (Continued).

Site-Number Location	Sample Number	Wi (%)	Wf (%)	e_o	γ_d (pcf)	σ_3 (psi)	$\frac{(\sigma_1-\sigma_3)_d}{\sigma_3}$	TEST MODE			
								CCT	ICT	RT	CT
S2-LP	4e-F	21.20	25.29	0.6904	100.26	--	--	X			
S2-LP	1f-F	21.56	20.45	0.6406	103.30	5	1.0				C
S2-LP	2f-F	21.75	21.15	0.6064	105.50	5	2.0				C
S2-LP	3f-F	19.14	18.72	0.4757	114.85	25	1.5				C
S2-LP	4f-F	22.55	19.80	0.6486	102.80	5	3.0				C
S2-LP	4f-S	23.9	22.72	0.5506	103.90	5	--			U	
S2-LP	2f-S	22.80	21.31	0.4603	116.06	25	--			U	
S3-LP	1a-F	14.90	14.40	0.6578	102.38	5	3.0				C
S3-LP	2a-F	14.00	12.69	0.2783	132.78	25	1.5				C
S3-LP	3a-F	14.40	13.80	0.2734	133.29	25	2.0				C
S3-LP	2b-F	12.94	12.67	0.6508	102.82	5	2.0				C
S3-LP	3b-F	13.60	12.74	0.3086	129.70	25	--		C		
S3-LP	4b-F	13.64	13.01	0.2844	132.14	25	1.0				C

TABLE 4.1 (Continued).

Site-Number Location	Sample Number	Wi (%)	Wf (%)	e_o	γ_d (pcf)	σ_3 (psi)	$\frac{(\sigma_1-\sigma_3)_d}{\sigma_3}$	TEST MODE			
								CCT	ICT	RT	CT
S3-LP	1c-S	13.40	15.54	0.6730	101.45	--	--	X			
S3-LP	2c-F	20.18	10.12	0.6661	101.87	5	1.0				C
S3-LP	3c-F	19.12	16.68	0.3301	127.61	5	--		C		
S3-LP	4c-S	14.0	13.8	0.6738	101.40	5	stress history				U
S3-LP	2e-S	14.04	14.20	0.6692	101.68	5	2.0				U
S3-LP	3e-S	13.70	12.02	0.3219	128.40	25	1.5				U
S3-LP	4e-S	13.68	12.24	0.2706	133.58	50	--		C		
S3-LP	1f-S	12.91	11.80	0.2293	138.07	5	--			U	
S3-LP	2f-S	15.64	14.92	0.3038	130.18	25	--			U	
S4-LP	1a-F	19.30	14.00	0.6359	102.99	5	1.0				C
S4-LP	2a-F	22.94	20.00	0.6392	102.78	5	--		C		
S4-LP	3a-F	19.40	23.0	0.5800	106.63	--	--	X			
S4-LP	4a-F	23.0	21.80	0.6508	102.06	5	0.70				C
S4-LP	2d-F	21.0	19.0	0.5015	112.21	25	0.50				C
S4-LP	2e-F	18.0	17.0	0.507	111.75	25	1.0				C

TABLE 4.1 (Continued).

Site-Number Location	Sample Number	Wi (%)	Wf (%)	e_o	γ_d (pcf)	σ_3 (psi)	$\frac{(\sigma_1-\sigma_3)_d}{\sigma_3}$	TEST MODE			
								CCT	ICT	RT	CT
S4-LP	3e-F	22.0	20.80	0.6146	104.35	5	2.0				C
S4-LP	4e-F	19.56	15.70	0.6165	104.23	25	--		C		

LEGEND:

W_i = Initial Water Content

W_f = Final Water Content

e_o = Initial Void Ratio

γ_d = Initial Dry Density

σ_3 = Confining Pressure

CCT = Conventional Consolidation Test

ICT = Incremental Creep Test

RT = Ramp Test

C = Consolidated Sample

U = Unconsolidated Sample

S = Spring Samples

F = Fall Samples

1 psi = 0.07 kg/cm^2

1 pcf = .0624 kg/cm^3

TABLE 4.2 Information Pertaining to the Test Samples of the Upper Peninsula Test Sites.

Site-Number Location	Sample Number	Wi* (%)	Wf* (%)	e_o*	γd* (pcf)	$\sigma 3$* (psi)	$\frac{(\sigma 1-\sigma 3)d^*}{\sigma 3}$	TEST MODE*			
								CCT	ICT	RT	CT
S1-UP	1b-F	26.42	24.31	0.9177	87.66	10	1.0				C
S1-UP	2b-F	26.81	25.12	0.6076	104.57	25	--		C		
S1-UP	3b-S	20.66	19.12	0.469	114.43	10	1.0				U
S1-UP	1c-S	23.64	21.38	0.6556	101.54	10				U	
S1-UP	2c-S	21.9	20.80	0.5226	110.41	25				U	
S1-UP	3c-S	26.88	24.81	0.5234	110.35	0				U	
S1-UP	4c-S	25.42	23.92	0.5234	110.35	--		X			
S2-UP	1a-F	26.4	25.61	0.8691	90.14	10	1				C
S2-UP	2a-F	27.0	25.84	0.9191	87.79	10	2				C
S2-UP	3a-F	32.0	28.0	0.9062	88.19	10	3				C
S2-UP	1b-F	27.0	25.7	0.7268	97.35	0				U	
S2-UP	2b-F	27.0	25.7	0.7268	97.35	--	--	X			
S2-UP	3b-F	27.0	25.7	0.7268	97.35	5				U	
S2-UP	4b-F	27.0	25.7	0.7268	97.35	25				U	
S2-UP	1c-f	26.81	25.90	0.6130	104.30	10				C	

* See Table 4.1

TABLE 4.2 (Continued).

Site-Number Location	Sample Number	Wi* (%)	Wf* (%)	e_o*	γd* (pcf)	$\sigma 3$* (psi)	$\frac{(\sigma 1-\sigma e)d}{\sigma 3}$*	TEST MODE*			
								CCT	ICT	RT	CT
S3-UP	1a-F	29.3	28.12	0.7881	93.84	10	1.0				C
S3-UP	2a-F	28.0	27.28	0.7692	94.84	10	2.0				C
S3-UP	3a-F	28.24	27.62	0.7049	98.42	--	--	X			
S3-UP	1b-S	26.42	25.18	0.7241	97.32	10				U	
S3-UP	2b-S	27.24	26.03	0.8725	89.61	25				U	
S3-UP	3b-S	27.18	25.14	0.7756	94.50	0				U	
S4-UP	4a-F	26.82	25.08	0.6544	101.42	--	--	X			
S4-UP	2c-S**	26.20	24.71	0.6864	100.09	25	--			U	
S4-UP	3c-S**	26.70	24.98	0.6959	98.94	50				U	
S4-UP	1a-S	27.10	26.75	0.5885	105.63	5	--			U	
S4-UP	2a-S	28.45	27.5	0.7480	95.99	25	--			U	
S4-UP	3a-S	25.60	25.39	0.9137	87.68	50	--			U	
S4-UP	1b-S	40.0	36.6	0.8248	91.95	5	1.0				U
S4-UP	2b-S	27.3	24.2	0.5791	106.26	5	2.0				U
S4-UP	4c-S	27.88	26.05	0.7104	98.10	0	--			U	

** Inclined samples

4.2 Lower Peninsula Test Sites

4.2.1 Static Triaxial Tests

At least three static triaxial tests were performed on three different samples from each test site using confining pressures of 5, 25, and 50 psi (0.35, 1.76 and 3.5 Kg/cm^2) (identical to the confining pressures used in the triaxial cyclic test program). As explained in Chapter III, the static triaxial tests were performed using the MTS hydraulic system and consequently it is called incremental creep test or ramp test. Generally, the incremental creep tests were performed on isotropically consolidated samples. Unconsolidated samples were used for the ramp test. Figure 4.1 displays typical time dependent consolidation curves for samples from site 2, consolidated in the cyclic triaxial cell under the designated confining pressure. For each sample, the incremental creep test was commenced after one hundred percent consolidation is reached. Figure 4.2 shows plots of the stress strain curves of the same samples obtained from the incremental creep tests. The data for the other sites are shown in Appendix C. The stress conditions at failure from the ICT were used to construct Mohr circle diagrams that are shown in Figures 4.3 through 4.6 for all the test sites of the lower peninsula. The failure envelopes and the resulting strength parameters for confining pressures of 5, 25, and 50 psi (0.35, 1.76 and 3.5 Kg/cm^2) are shown in the figures. The strength parameters c_1 and ϕ_1 were obtained using test data at confining pressures of 5 and 25 psi (0.35 and 1.76 Kg/cm^2). Mohr circles at confining pressures of 25 and 50 psi (1.76 and 3.5 Kg/cm^2) were used to obtain the second failure envelope with strength parameters of c_2 and ϕ_2. The data for the upper peninsula test sites were plotted and the figures are shown in Appendix C.

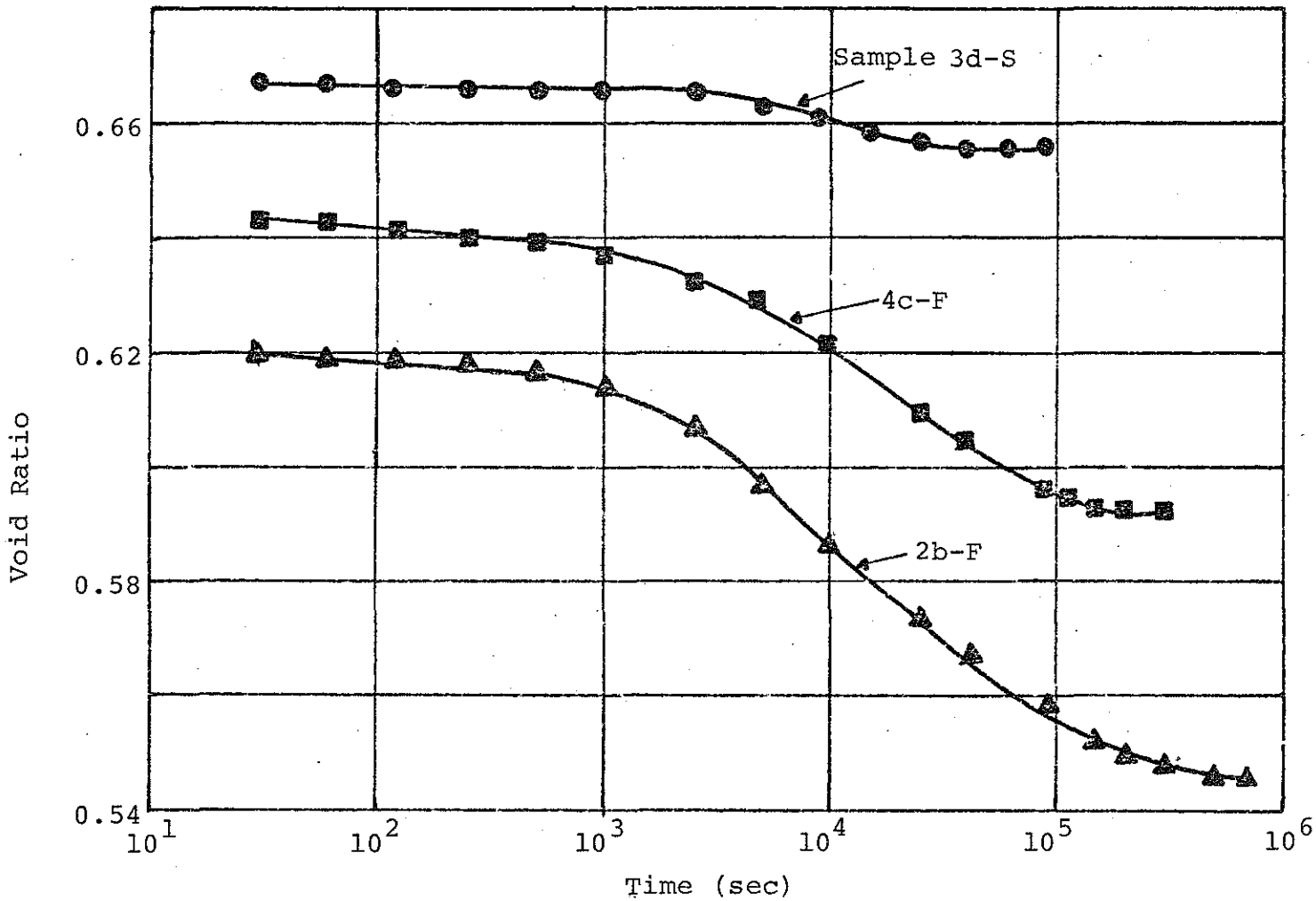

FIGURE 4.1 Void Ratio versus the Logarithm of Time for Samples Consolidated under the Designated Confining Pressure Prior to the Commencement of the Incremental Creep Tests, Site 2, Lower Peninsula.

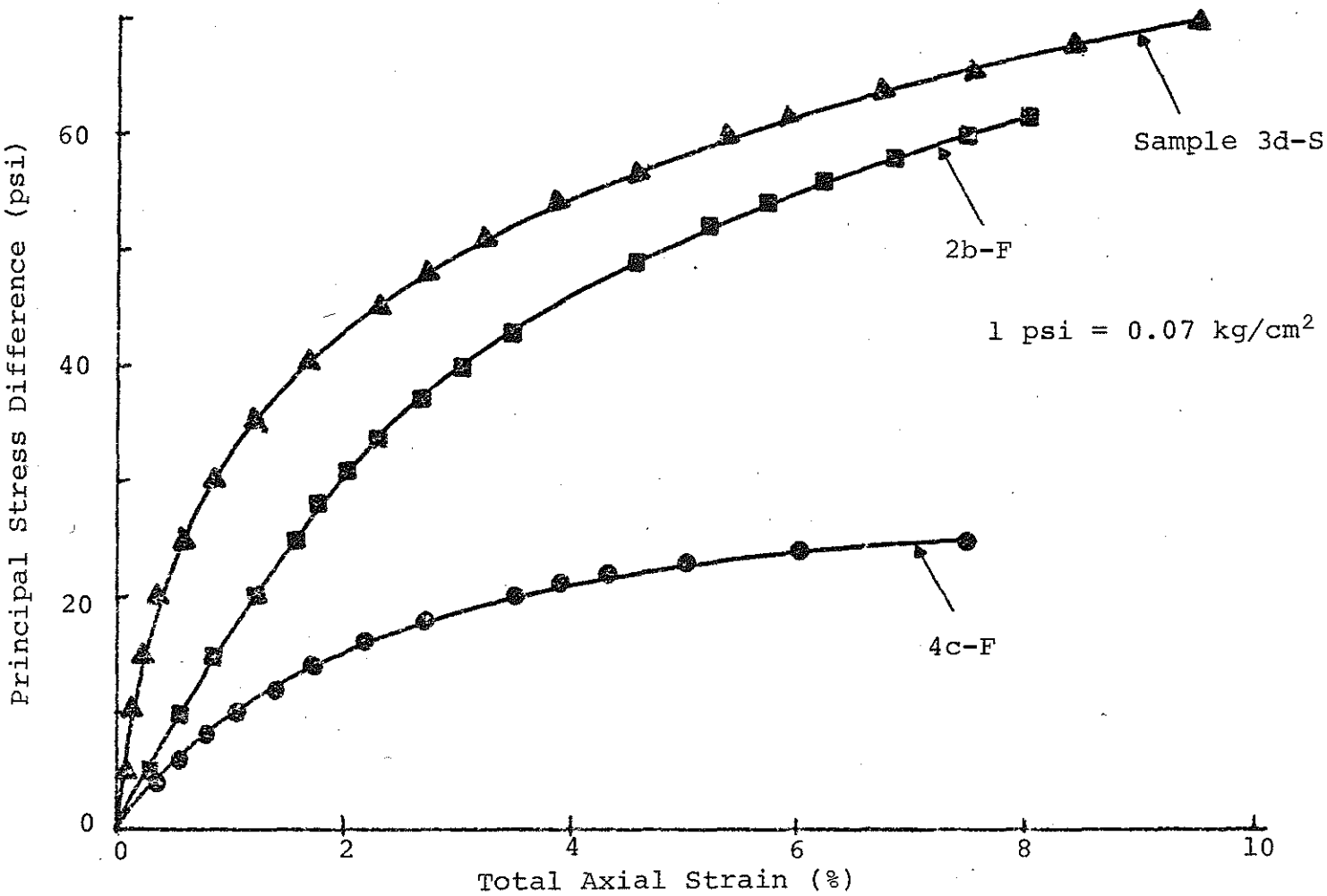

FIGURE 4.2 Principal Stress Difference versus Total Axial Strain from Incremental Creep Tests, Site 2, Lower Peninsula.

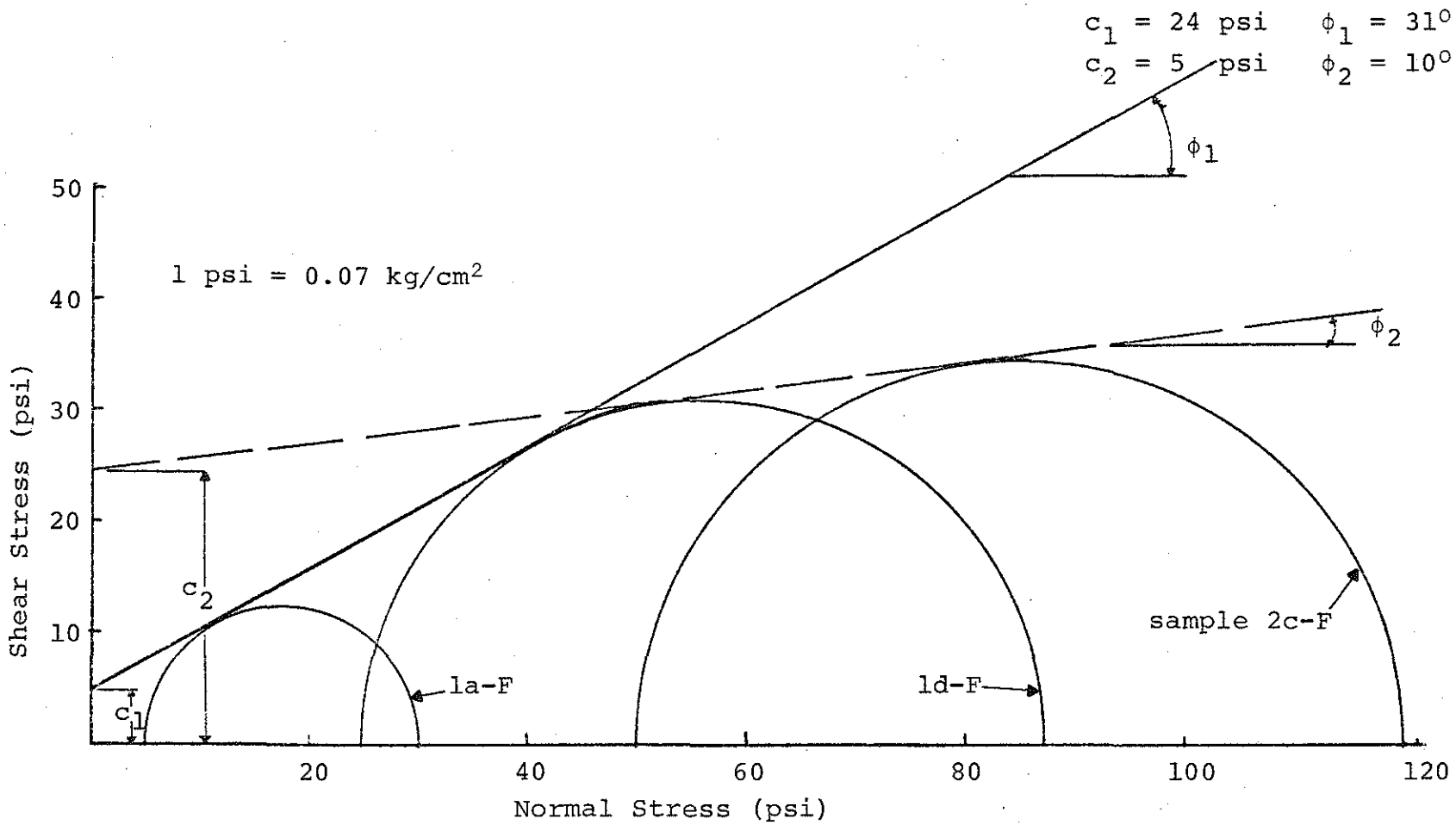

FIGURE 4.3 Mohr Circles and Failure Envelopes from Incremental Creep Tests, Site 1, Lower Peninsula.

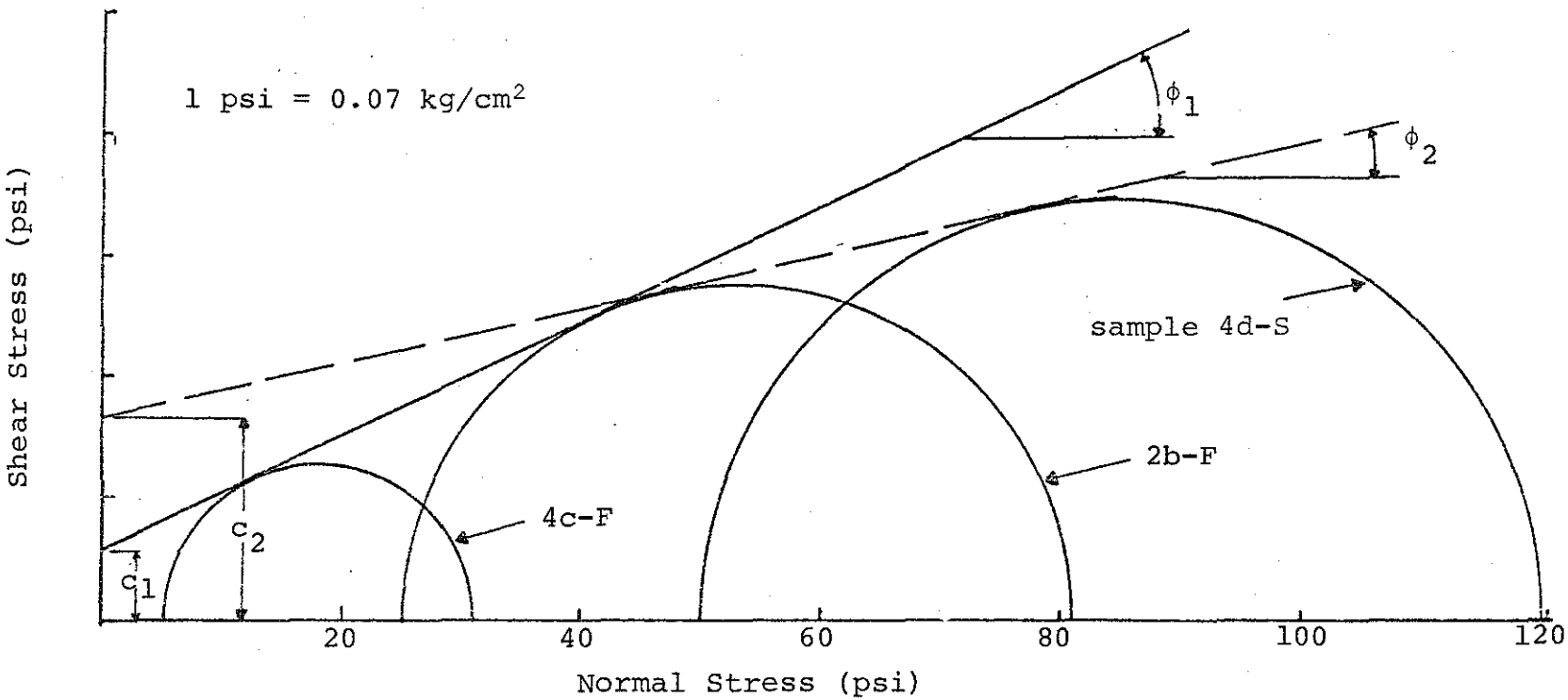

FIGURE 4.4 Mohr Circles and Failure Envelopes from Incremental Creep Tests, Site 2, Lower Peninsula.

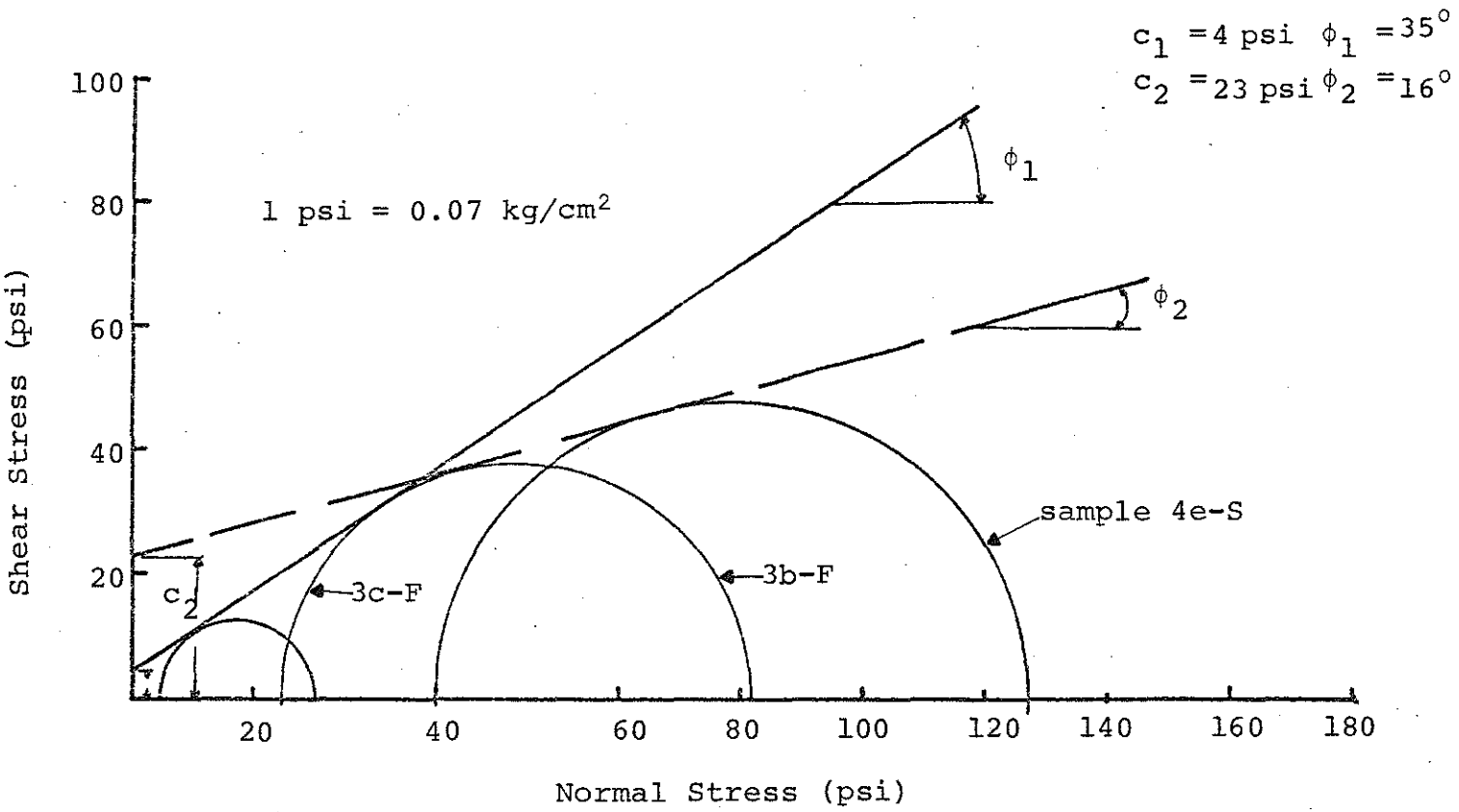

FIGURE 4.5 Mohr Circles and Failure Envelopes from Incremental Creep Tests, Site 3, Lower Peninsula.

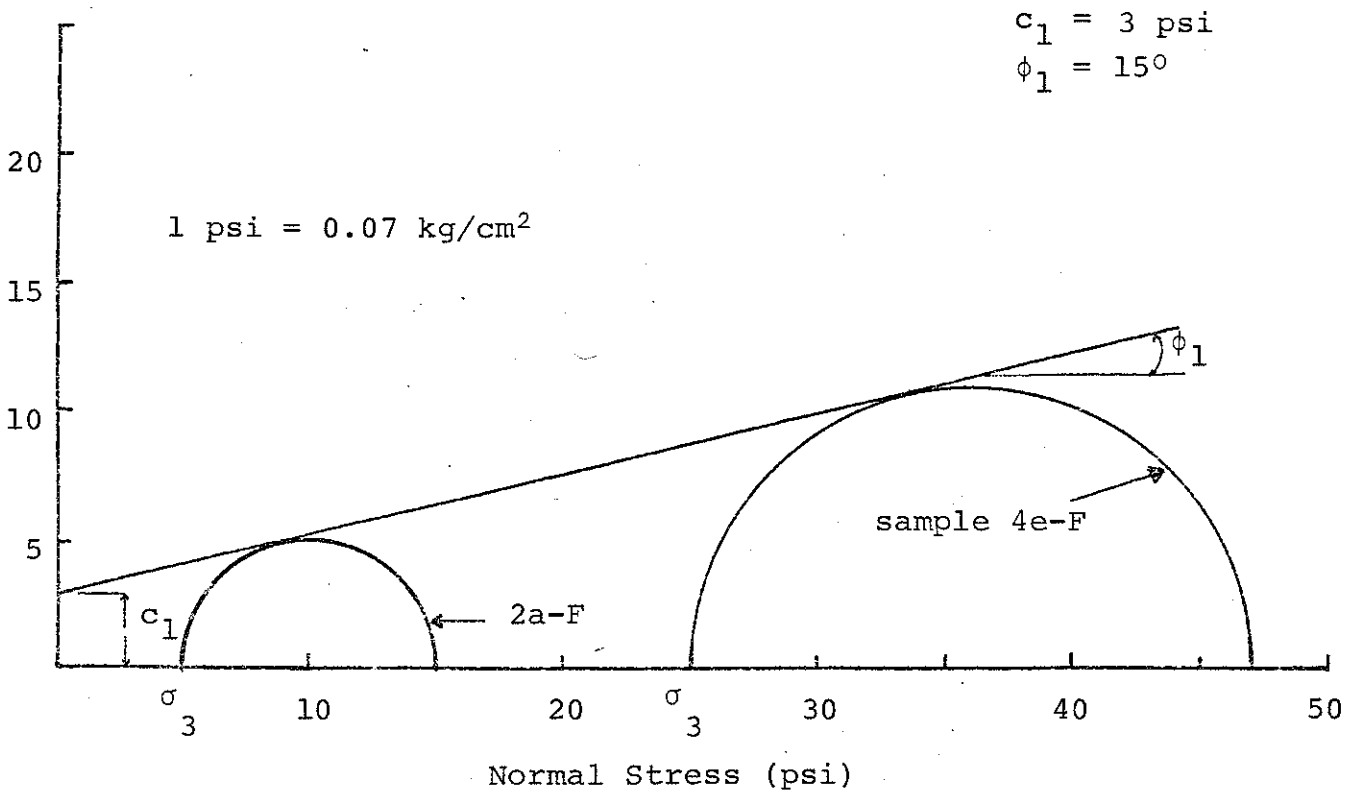

FIGURE 4.6 Mohr Circles and Failure Envelope from Incremental Creep Tests, Site 4, Lower Peninsula.

4.2.2 Cyclic Triaxial Tests

Cyclic triaxial tests were performed on consolidated and unconsolidated samples to study the elastic and plastic characteristics of the test materials. All tests were conducted up to thirty thousand load repetitions unless failure occurred. The maximum cyclic principal stress difference and the cell pressure were kept constant throughout each test.

4.2.2.1 Consolidated Cyclic Triaxial Tests

The samples were isotropically consolidated under the confining pressure. Plots of typical time dependent consolidation curves for site 2, are shown in Figure 4.7. A sustained deviatoric stress of one psi (0.07 Kg/cm^2) was applied to the samples after one hundred percent consolidation was reached. The cyclic triaxial test was then commenced and the output was recorded. Typical plots of the logarithm of accumulated axial permanent strain as a function of the logarithm of number of load cycles for site 2, lower peninsula are shown in Figures 4.8 through 4.10. The confining pressure and the sample number (see Table 4.1) are indicated in the figures. Plots of the logarithm of resilient modulus versus the logarithm of number of load cycles for the same samples are shown in Figures 4.11 through 4.13. Finally, the radial permanent strain versus the logarithm of number of load repetitions of the same samples are shown in Figures 4.14 through 4.18. It should be noted that the straight lines in Figures 4.8 through 4.18 were obtained using a least squares fitting technique. The intercepts, slopes and the correlation coefficients (r^2) of these lines are listed in Table 5.3.

4.2.2.2 Unconsolidated Cyclic Triaxial Tests

The unconsolidated soil samples were subjected to the confining pressure first after which, an additional

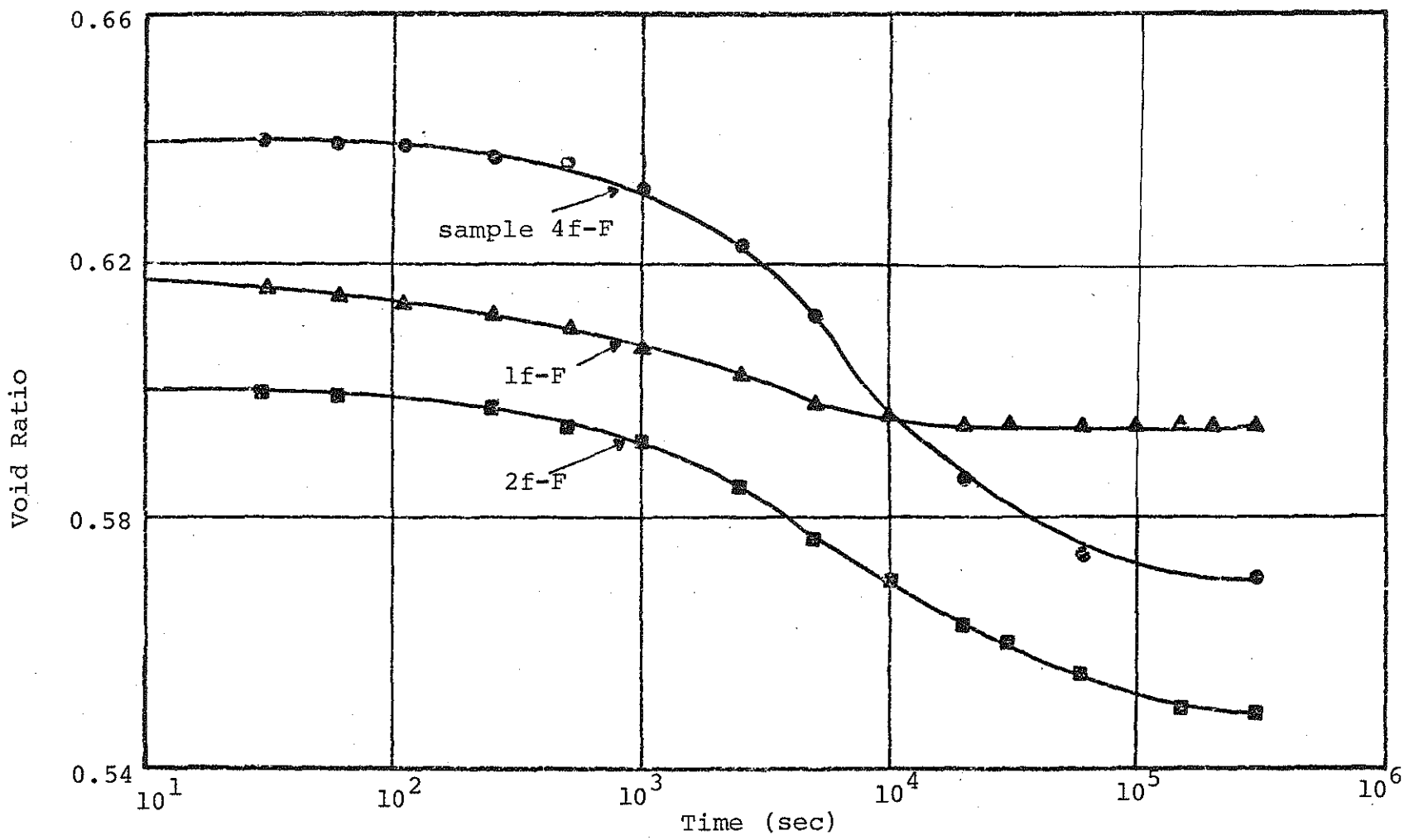

FIGURE 4.7 Typical Void Ratio versus the Logarithm of Time for Three Samples Consolidated Under a Confining Pressure of 5 psi Prior to the Commencement of the Triaxial Cyclic Load, Site 2, Lower Peninsula.

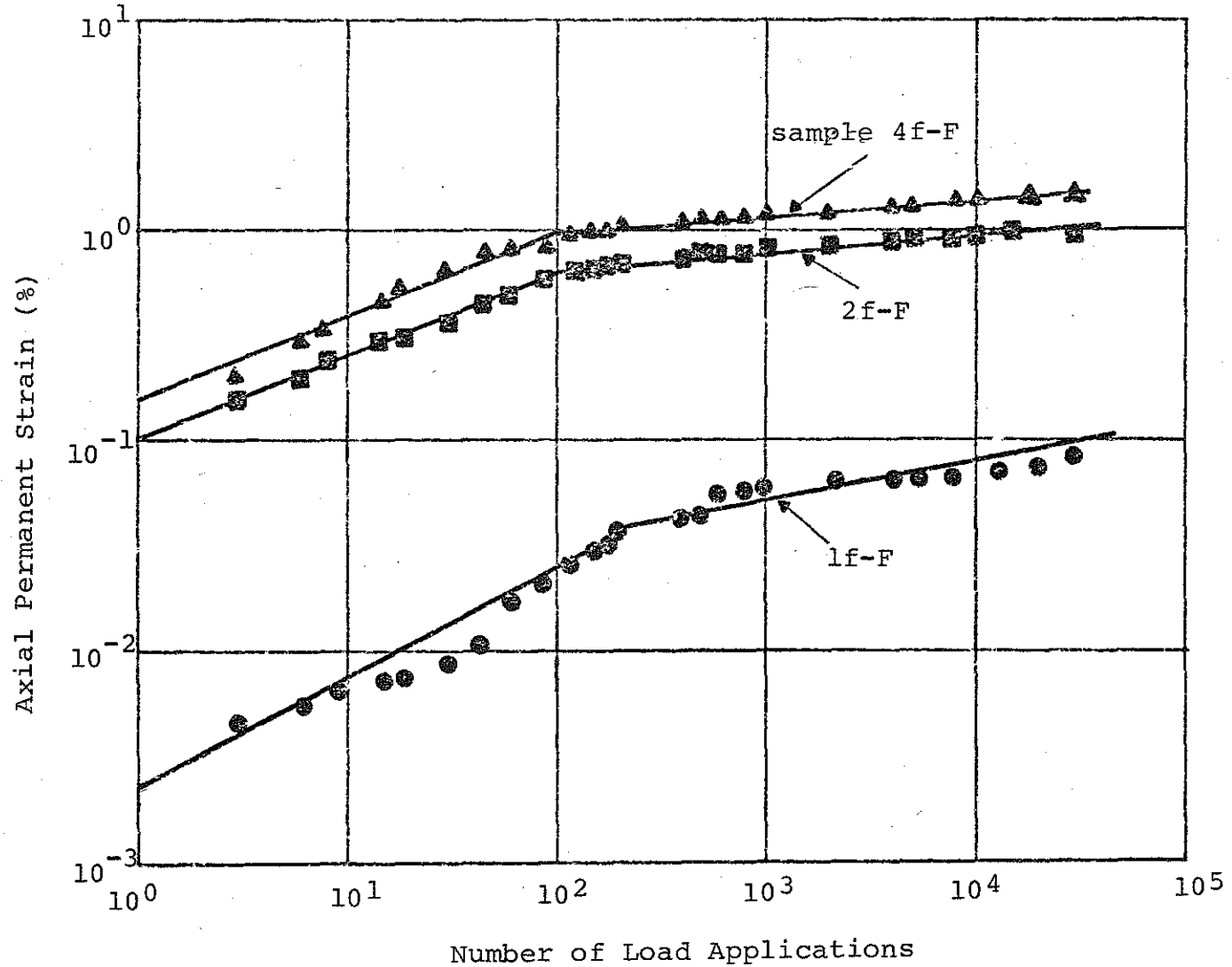

FIGURE 4.8 Typical Axial Permanent Strain versus Number of Load Applications for Samples Consolidated Under a Confining Pressure of 5 psi and Tested Using Different Cyclic Stress Ratio, Site 2, Lower Peninsula.

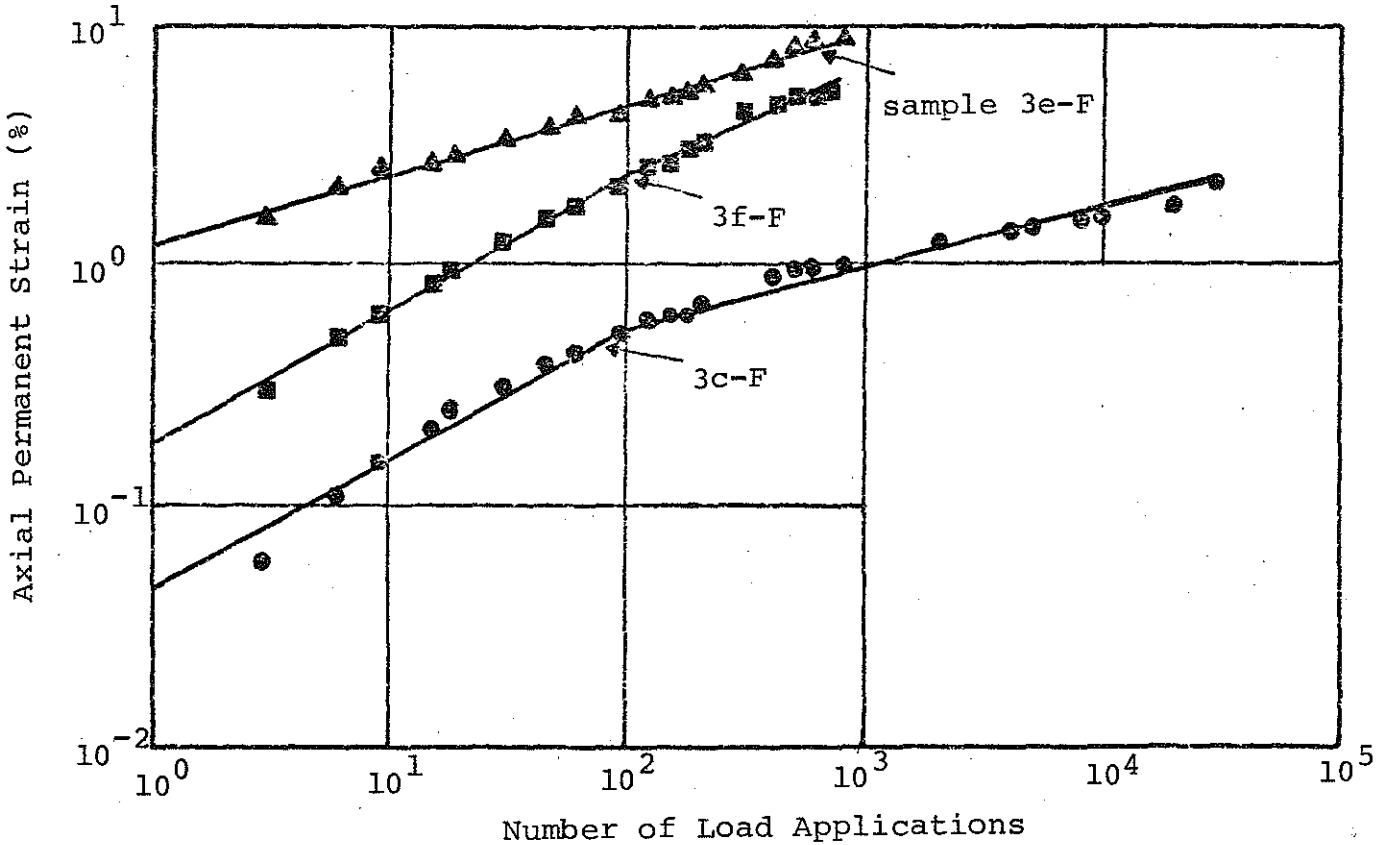

FIGURE 4.9 Typical Axial Permanent Strain versus Number of Load Applications for Samples Consolidated under a Confining Pressure of 25 psi and Tested using Different Cyclic Stress Ratio, Site 2, Lower Peninsula.

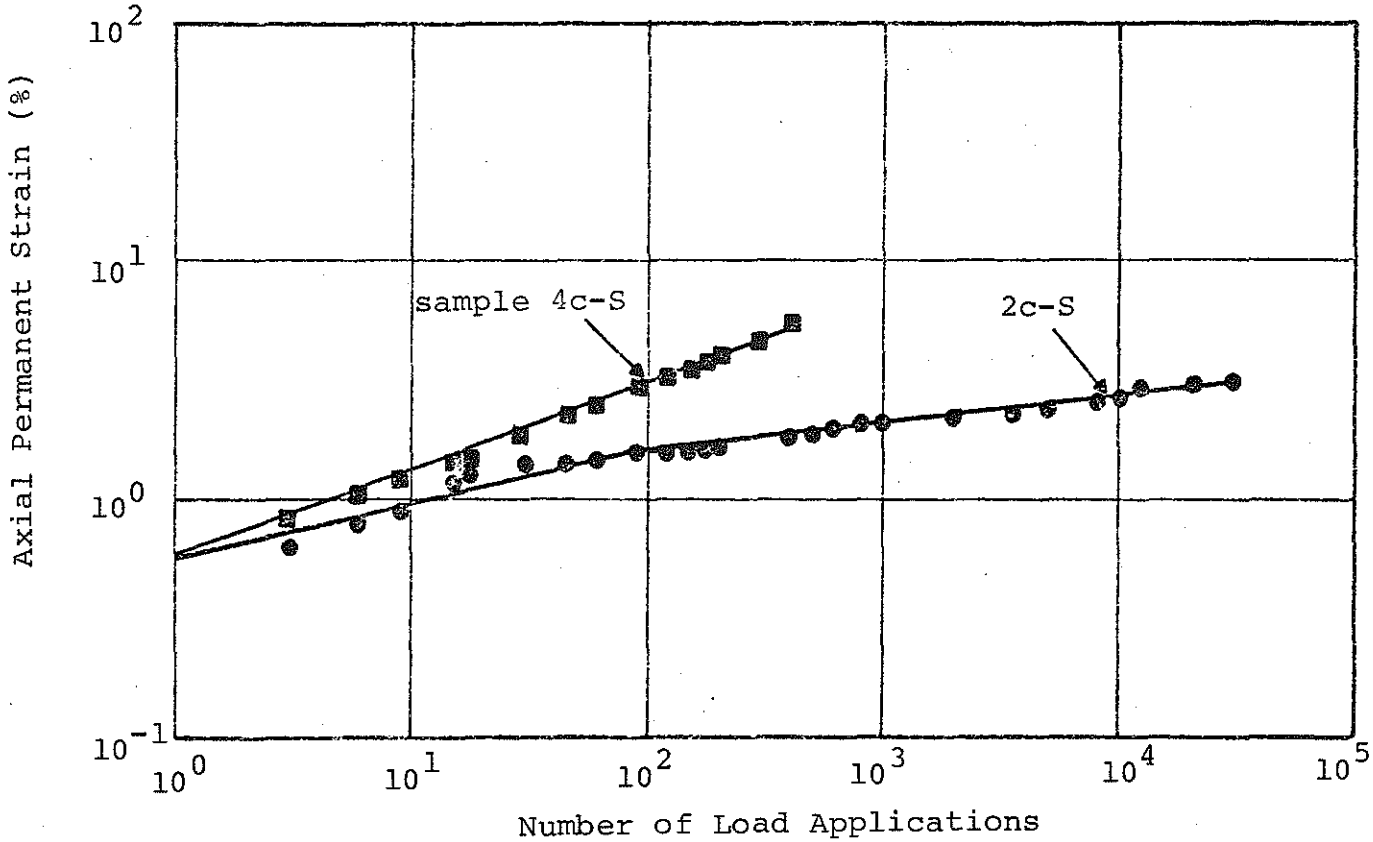

FIGURE 4.10 Typical Axial Permanent Strain versus Number of Load Applications for Samples Consolidated under a Confining Pressure of 50 psi and Tested using Different Cyclic Stress Ratio, Site 2, Lower Peninsula.

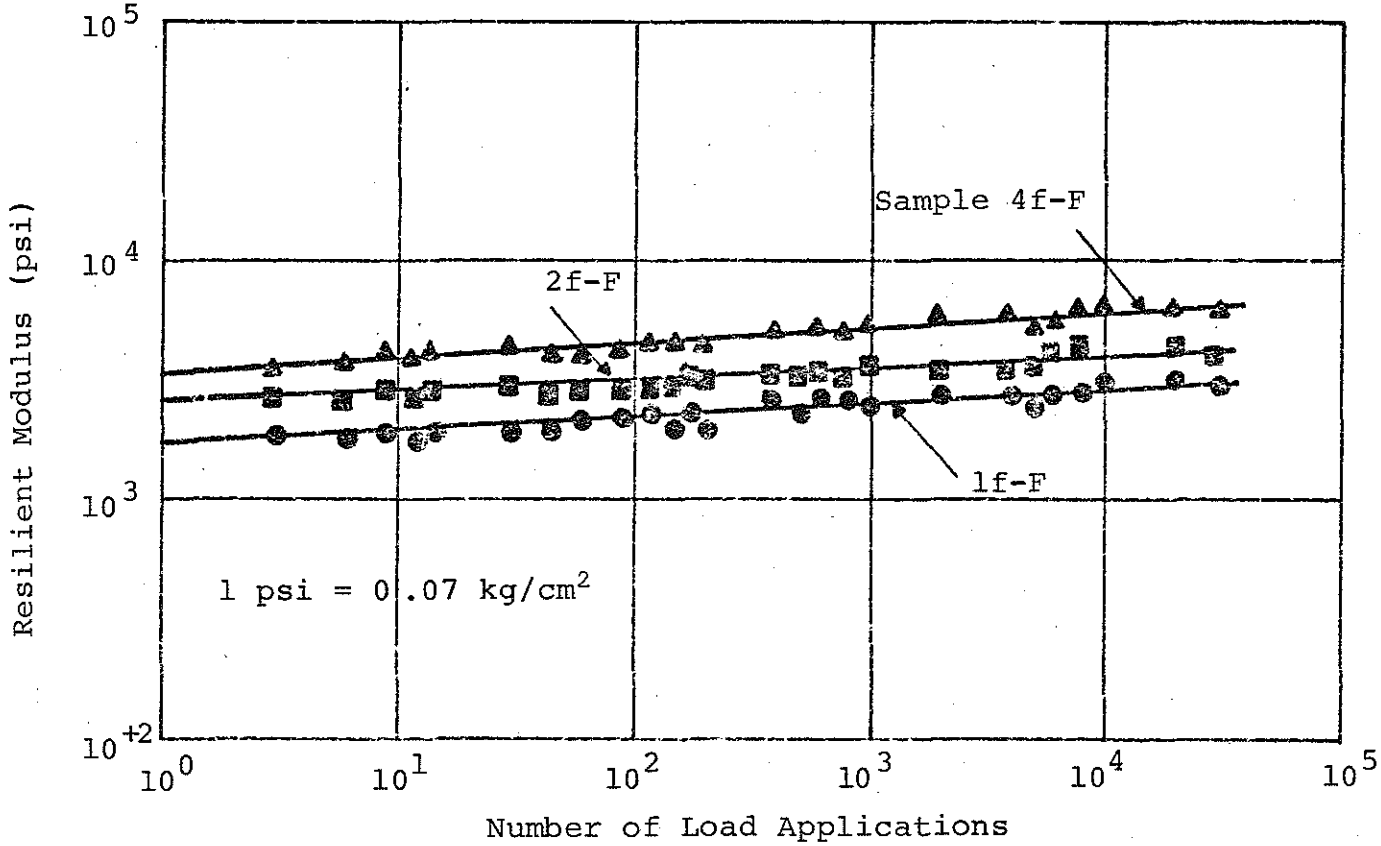

FIGURE 4.11 Typical Resilient Modulus versus Number of Load Applications for Samples Consolidated under a Confining Pressure of 5 psi and Tested using Different Cyclic Stress Ratio, Site 2, Lower Peninsula.

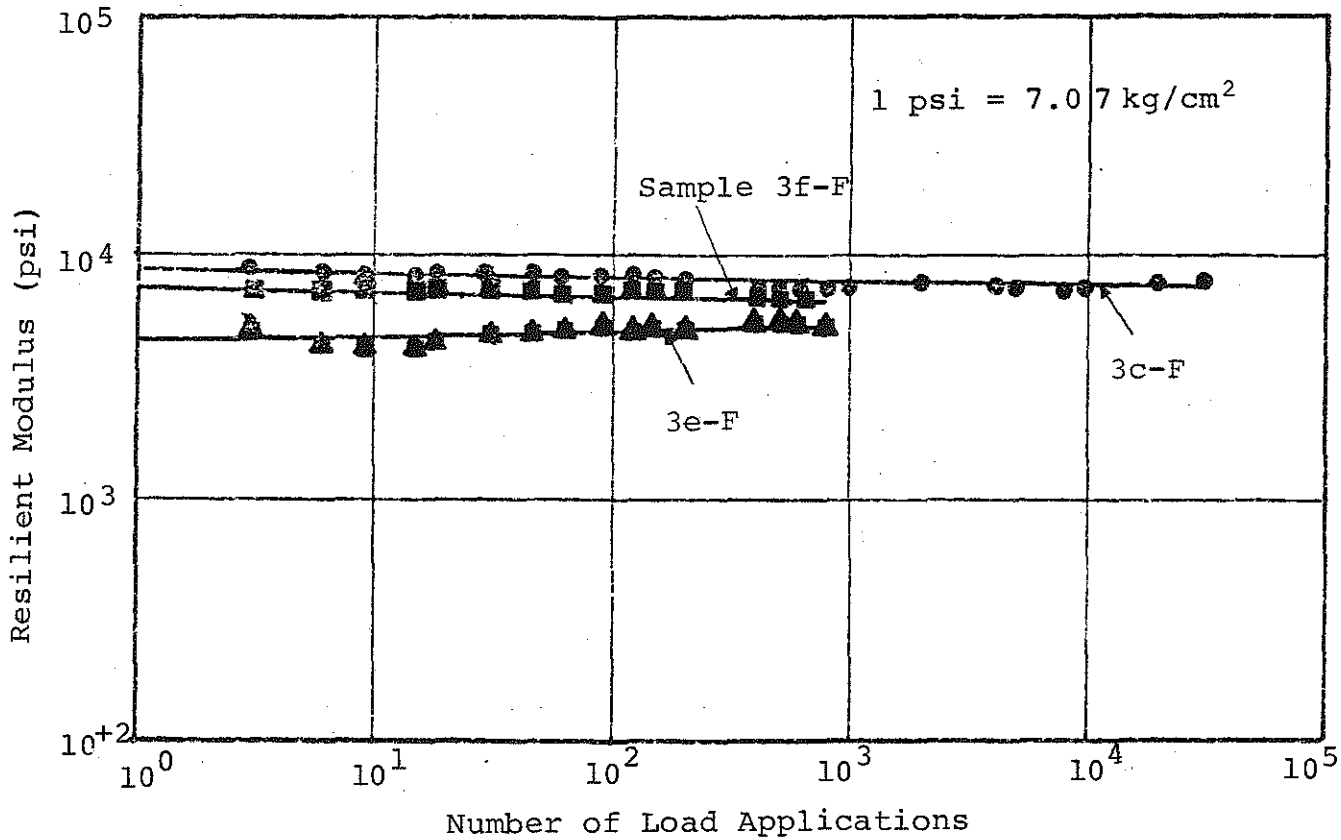

FIGURE 4.12 Typical Resilient Modulus versus Number of Load Applications for Samples Consolidated under a Confining Pressure of 25 psi and Tested Using Different Cyclic Stress Ratio, Site 2, Lower Peninsula.

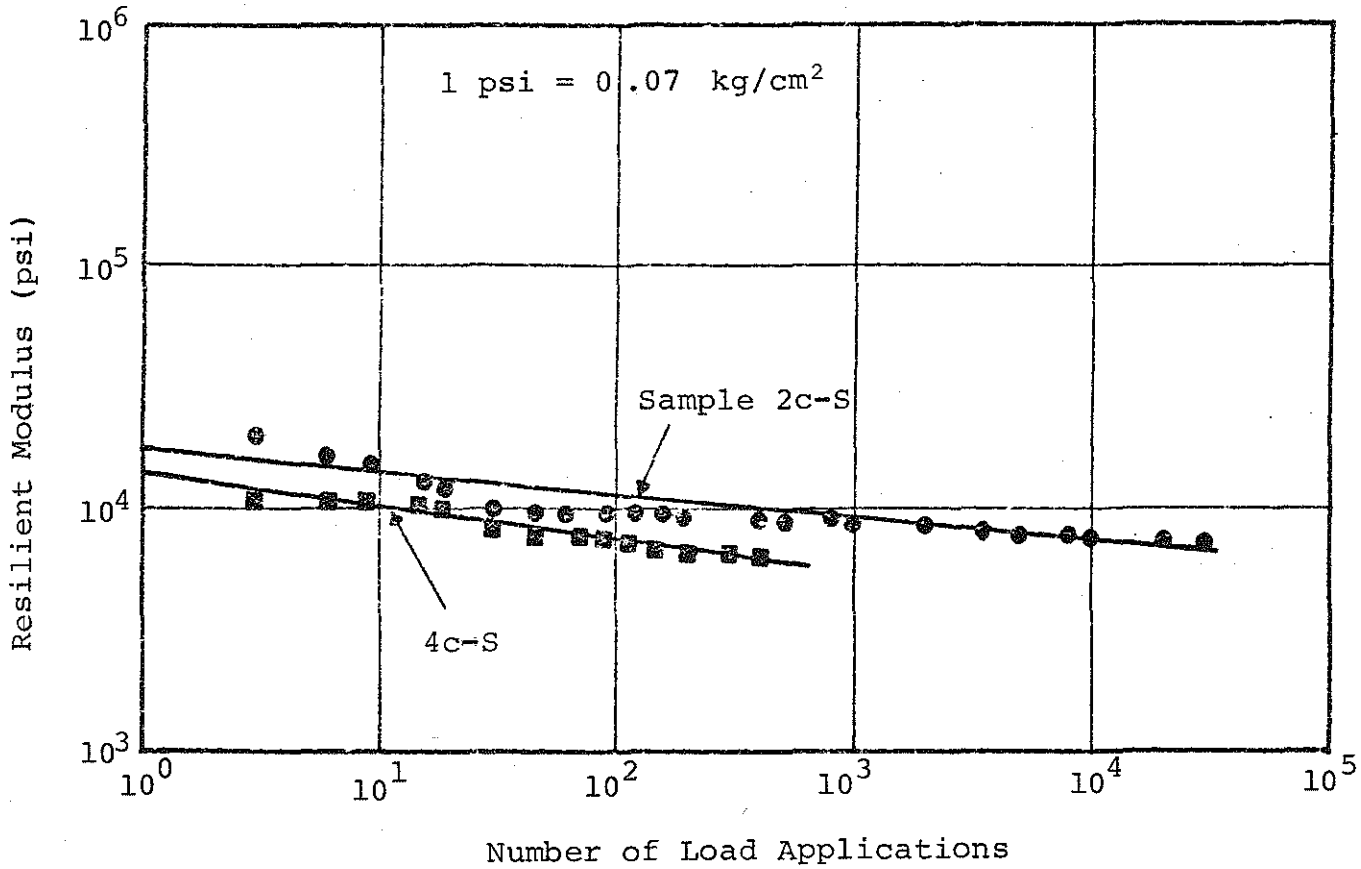

FIGURE 4.13 Typical Resilient Modulus versus Number of Load Applications for Samples Consolidated under a Confining Pressure of 50 psi and Tested Using Different Cyclic Stress Ratio, Site 2, Lower Peninsula.

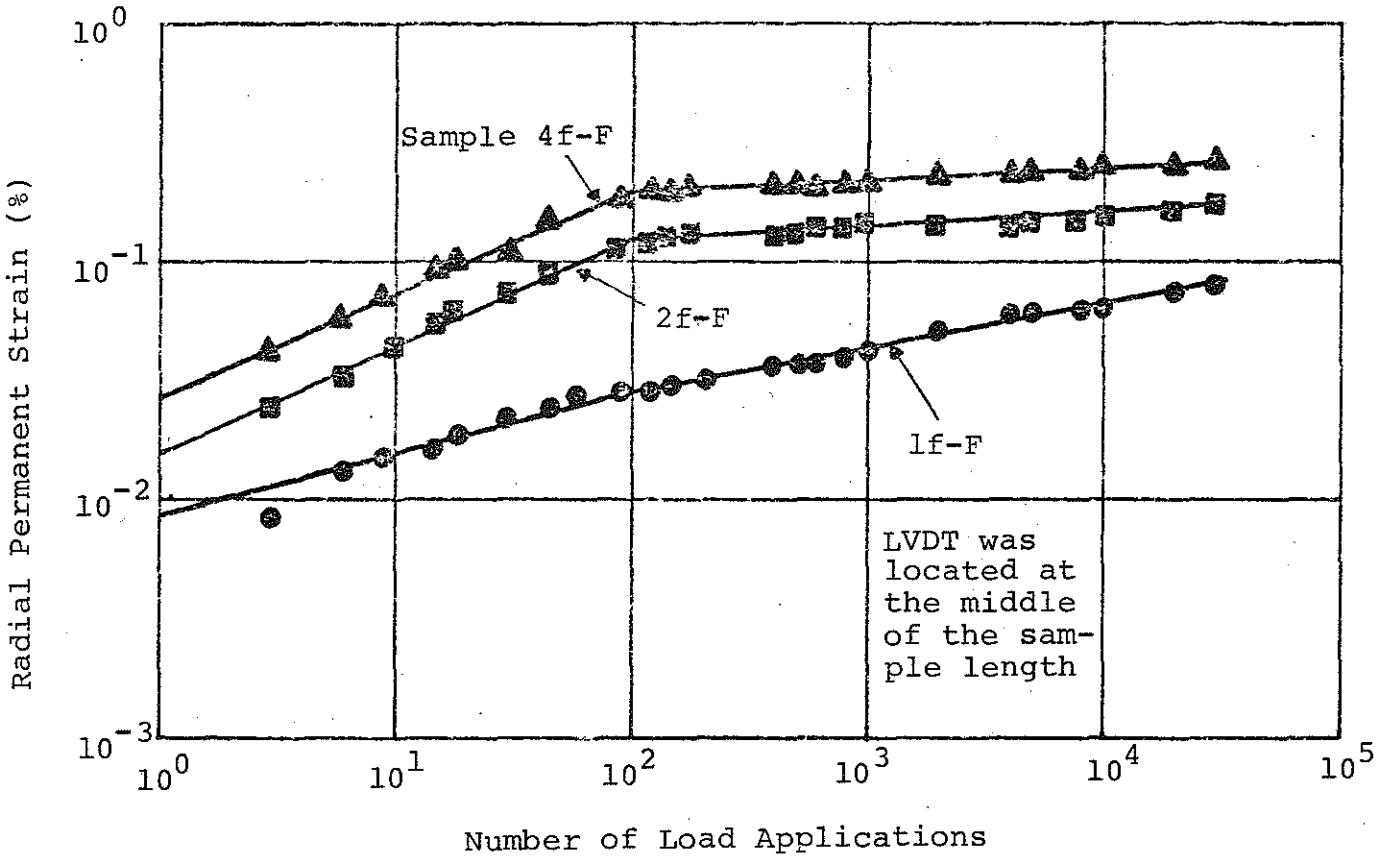

FIGURE 4.14 Typical Radial Permanent Strain versus Number of Load Applications for Samples Consolidated under Confining Pressure of 5 psi and Tested Using Different Cyclic Stress Ratio, Site 2, Lower Peninsula.

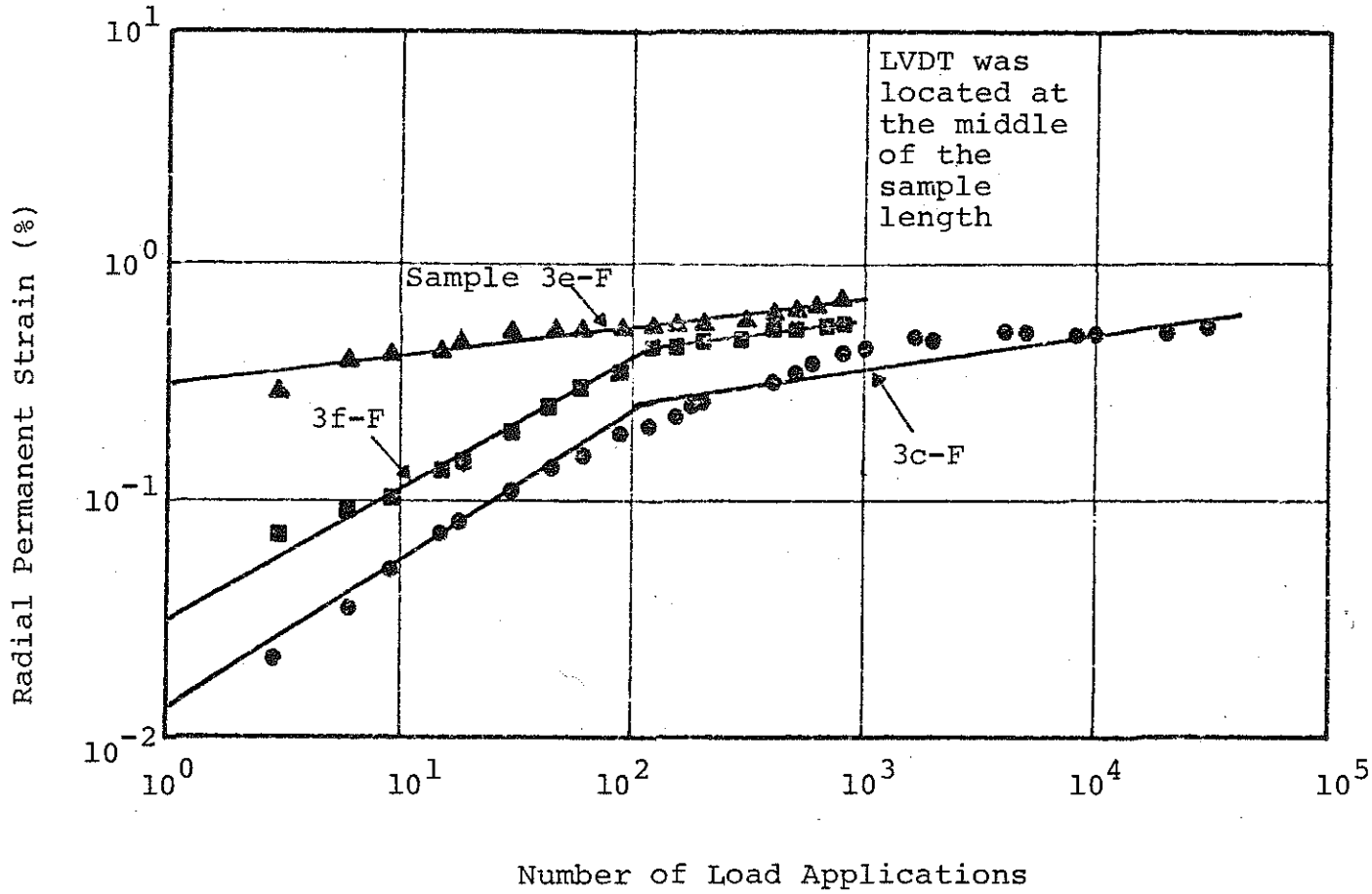

FIGURE 4.15 Typical Radial Permanent Strain versus Number of Load Applications for Samples Consolidated under a Confining Pressure of 25 psi and Tested under Different Cyclic Stress Ratio, Site 2, Lower Peninsula.

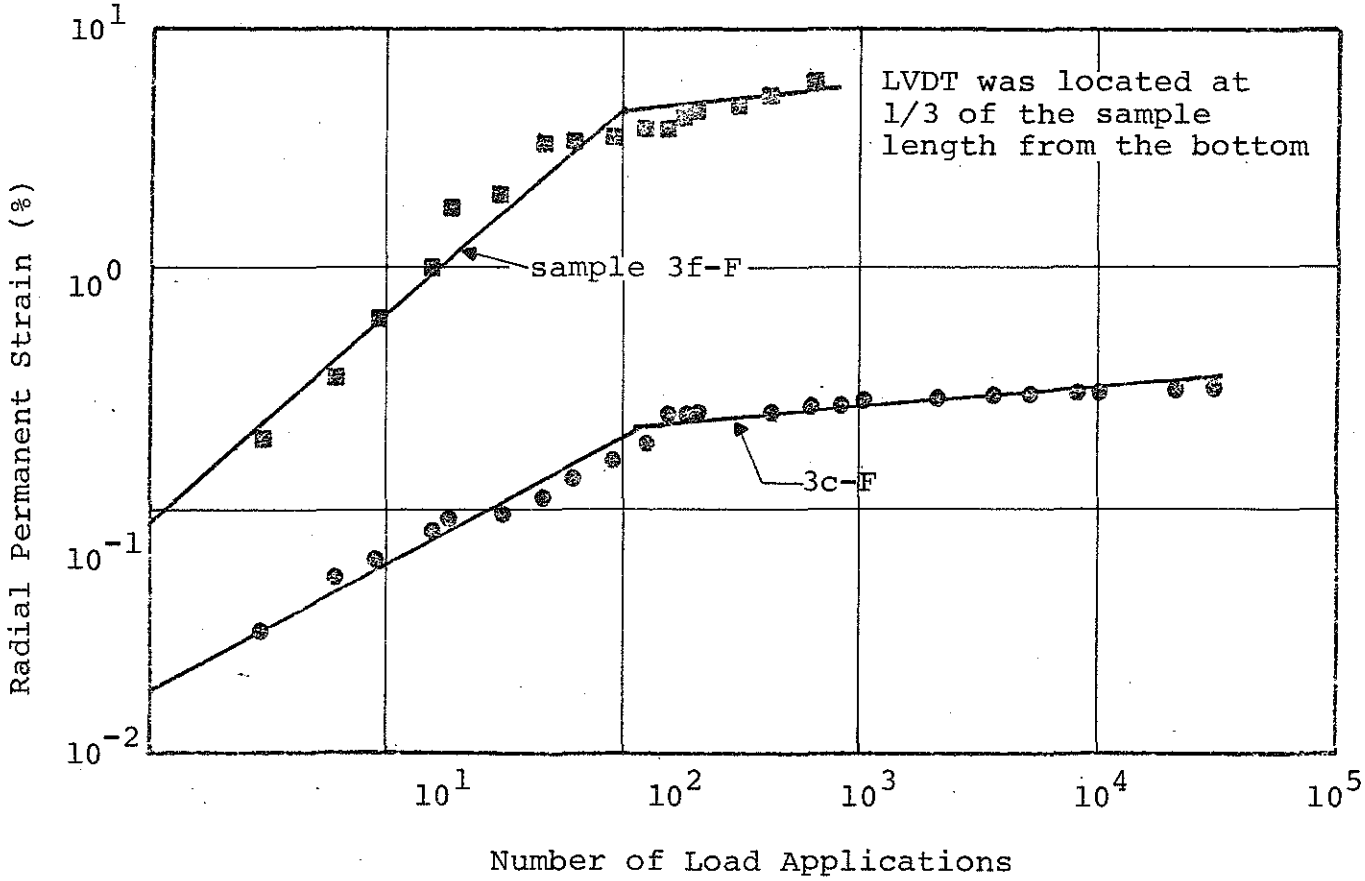

FIGURE 4.16 Typical Radial Permanent Strain versus Number of Load Applications for Samples Consolidated under a Confining Pressure of 25 psi and Tested under Different Cyclic Stress Ratio, Site 2, Lower Peninsula.

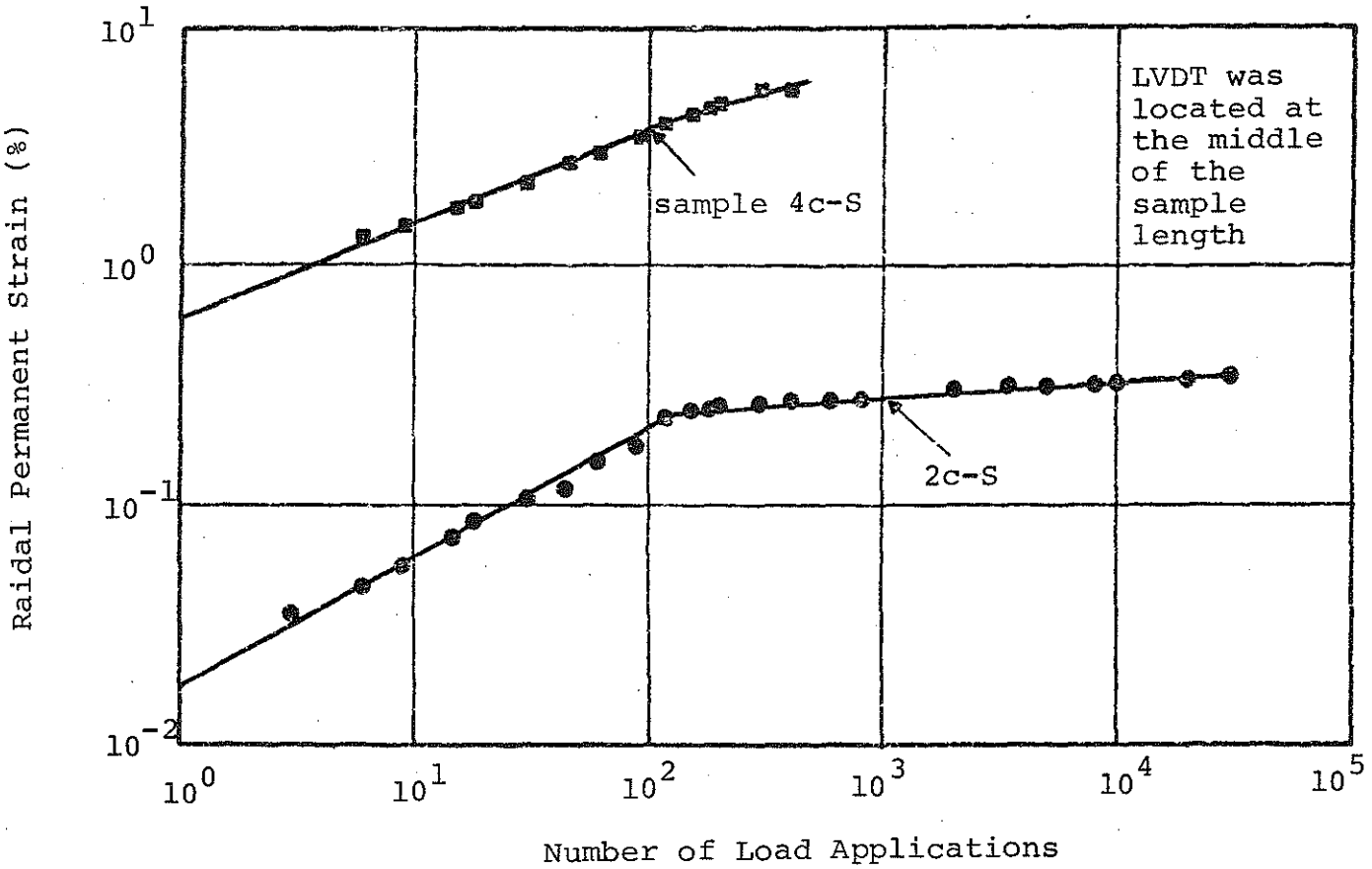

FIGURE 4.17 Typical Radial Permanent Strain versus Number of Load Applications for Samples Consolidated under a Confining Pressure of 50 psi and Tested under Different Cyclic Stress Ratio, Site 2, Lower Peninsula.

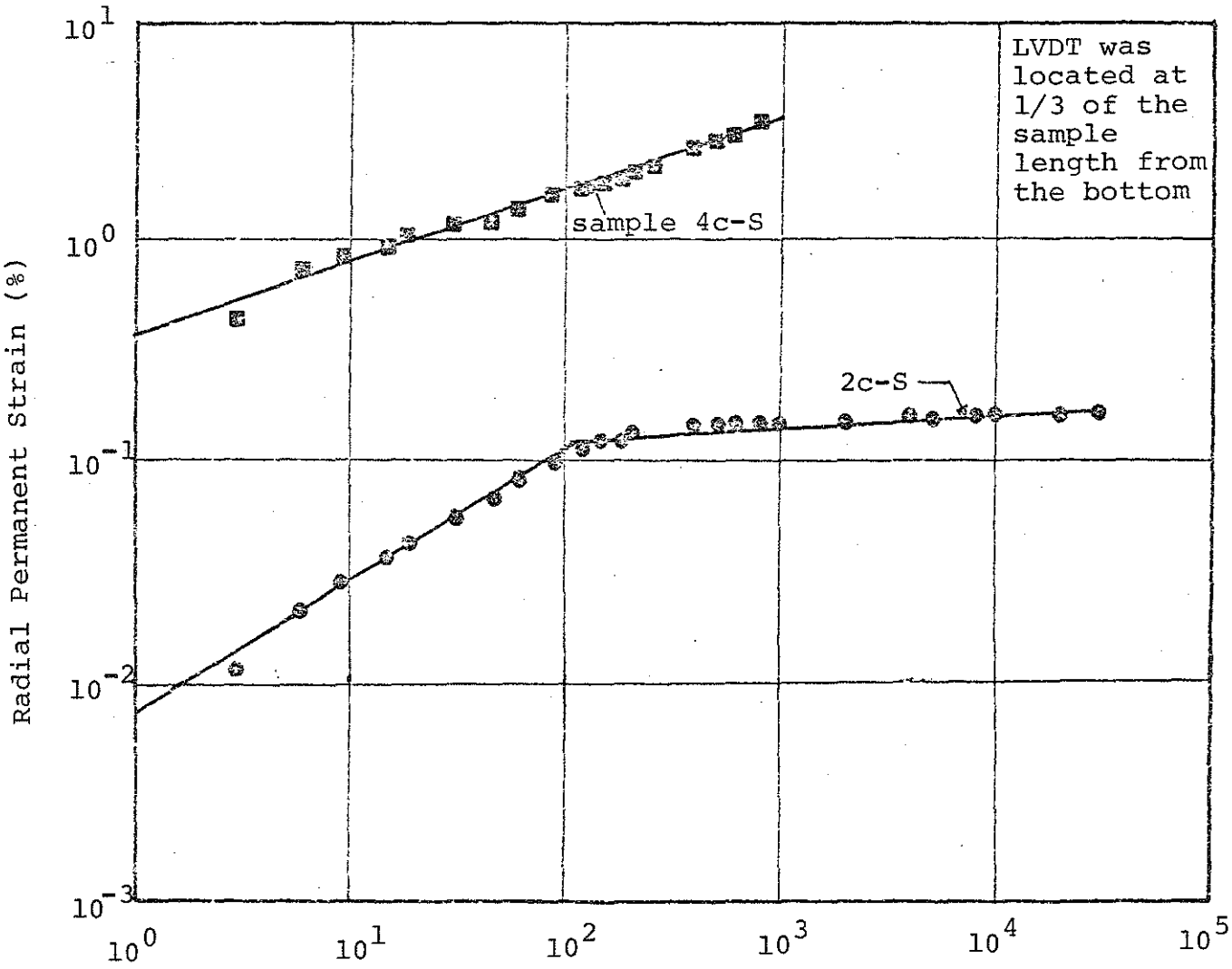

FIGURE 4.18 Typical Radial Permanent Strain versus Number of Load Applications for Samples Consolidated under a Confining Pressure of 50 psi and Tested under Different Cyclic Stress Ratio, Site 2, Lower Peninsula.

sustained axial stress of one psi (0.07 Kg/cm^2) was applied. The cyclic test was then started without giving a time for the sample to consolidate. The logarithm of the axial permanent strain, the logarithm of the resilient modulus and the logarithm of the radial permanent strain were all plotted against the logarithm of the number of load applications. These plots are shown in the following Figures 4.19 - 4.20, 4.21 - 4.22, and 4.23 through 4.26 respectively. As in the case of consolidated samples, the straight lines in the figures were obtained using least square fitting technique. The intercepts, slopes and the correlation coefficients are listed in Table 5.3.

4.3 Upper Peninsula Test Sites

4.3.1 Static Triaxial Tests

At least three unconsolidated static triaxial tests (ramp tests) were performed on three different samples from each test site using confining pressures of 0, 10 and 25 (0, 0.7 and 1.76 Kg/cm^2) or 0, 5 and 25 psi (0, 0.35, 1.76 Kg/cm^2). Figure 4.27 displays typical plots of stress-strain curves obtained from these tests for site number 4. The data for the other three sites are shown in Appendix D. Figures 4.28, 4.30 and 4.31 show Mohr circle diagrams and the resulting failure envelopes for sites 1, 2, 3 and 4 respectively.

4.3.2 Consolidated Cyclic Triaxial Tests

Few consolidated cyclic triaxial tests were executed on samples obtained from sites 1, 2 and 3 as shown in Table 4.2. The data from these tests are listed in Appendix D. It should be noted that the results obtained from the consolidation part of the tests were highly variable due to the nature of the samples. This is so because all test samples contained alternate layers of clays and sandy silts which made the test

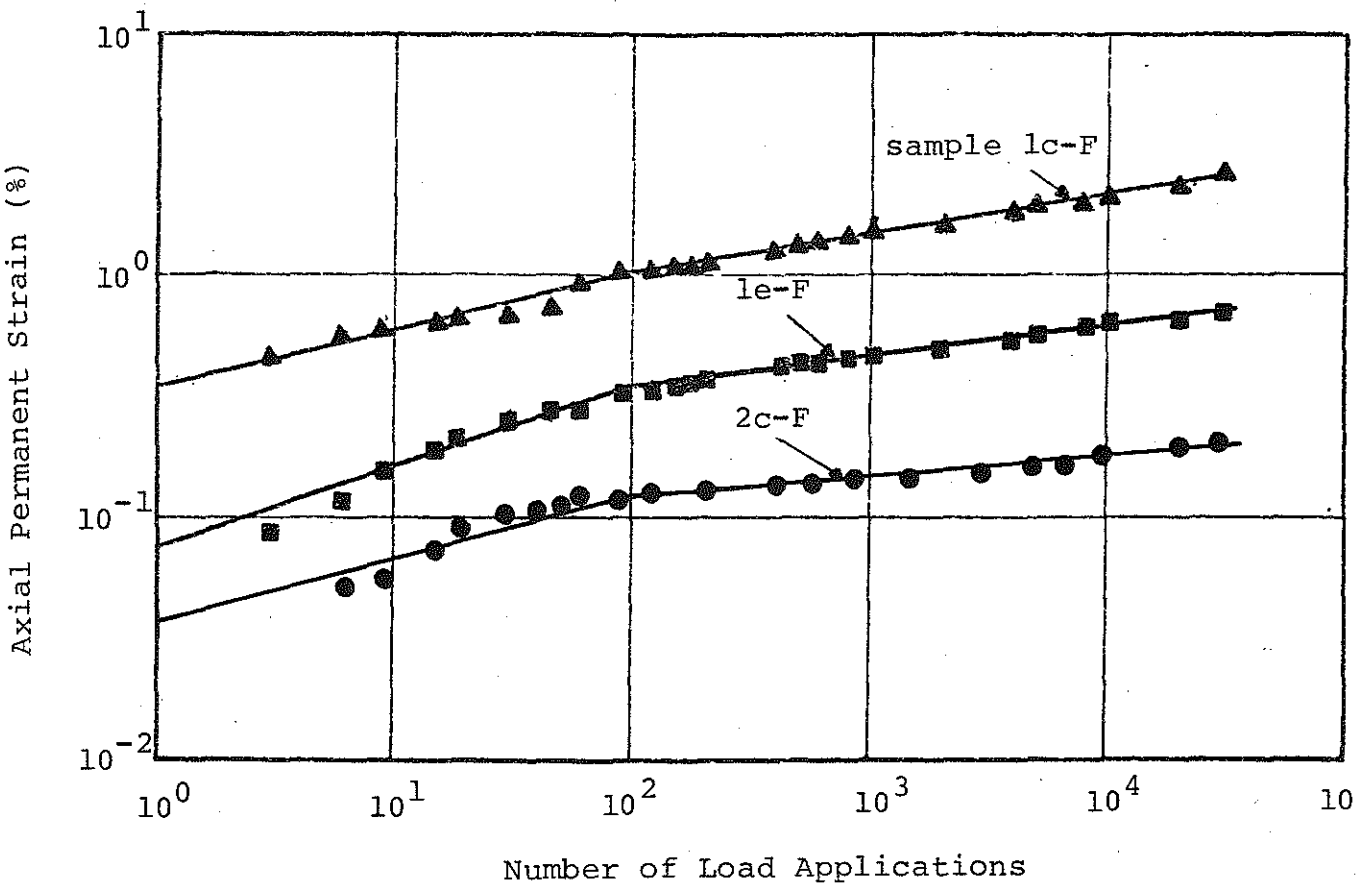

FIGURE 4.19 Typical Axial Permanent Strain versus Number of Load Applications for Unconsolidated Samples Tested under a Confining Pressure of 5 psi and Different Stress Ratio, Site 2, Lower Peninsula.

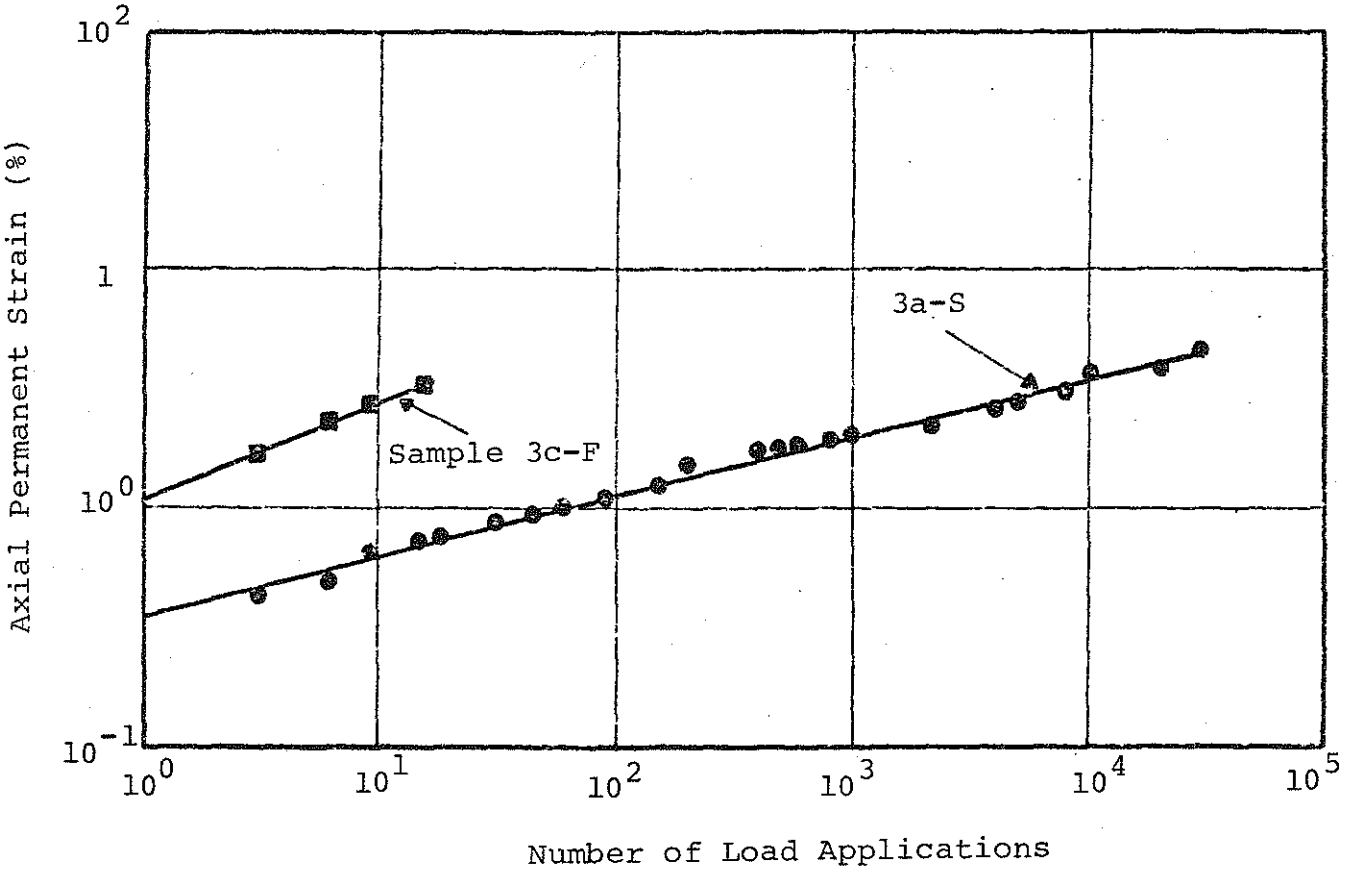

FIGURE 4.20 Typical Axial Permanent Strain versus Number of Load Applications for Unconsolidated Samples Tested under a Confining Pressure of 25 psi and Different Cyclic Stress Ratio, Site 2, Lower Peninsula.

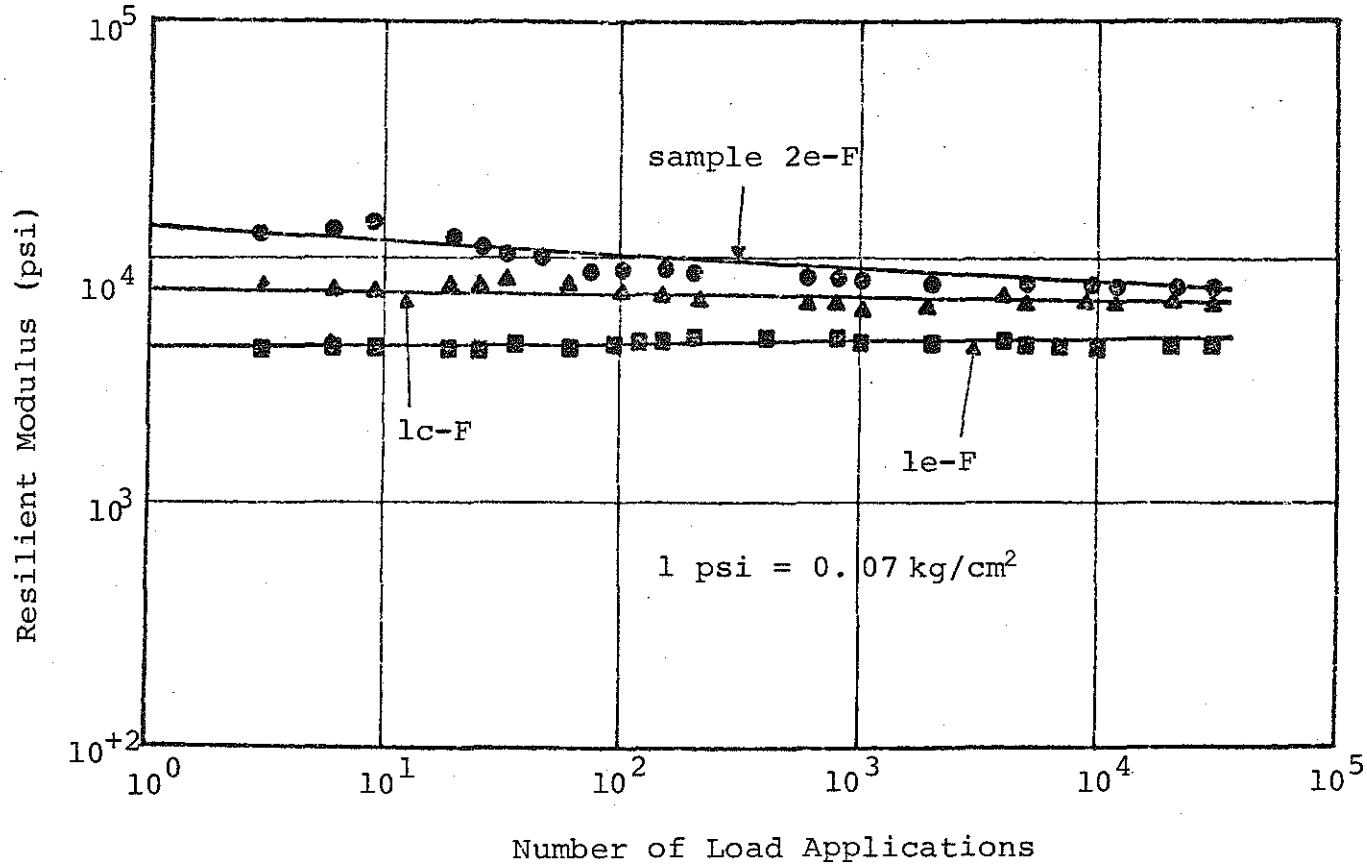

FIGURE 4.21 Typical Resilient Modulus versus Number of Load Applications for Unconsolidated Samples Tested Under a Confining Pressure of 5 psi and Different Cyclic Stress Ratio, Site 2, Lower Peninsula.

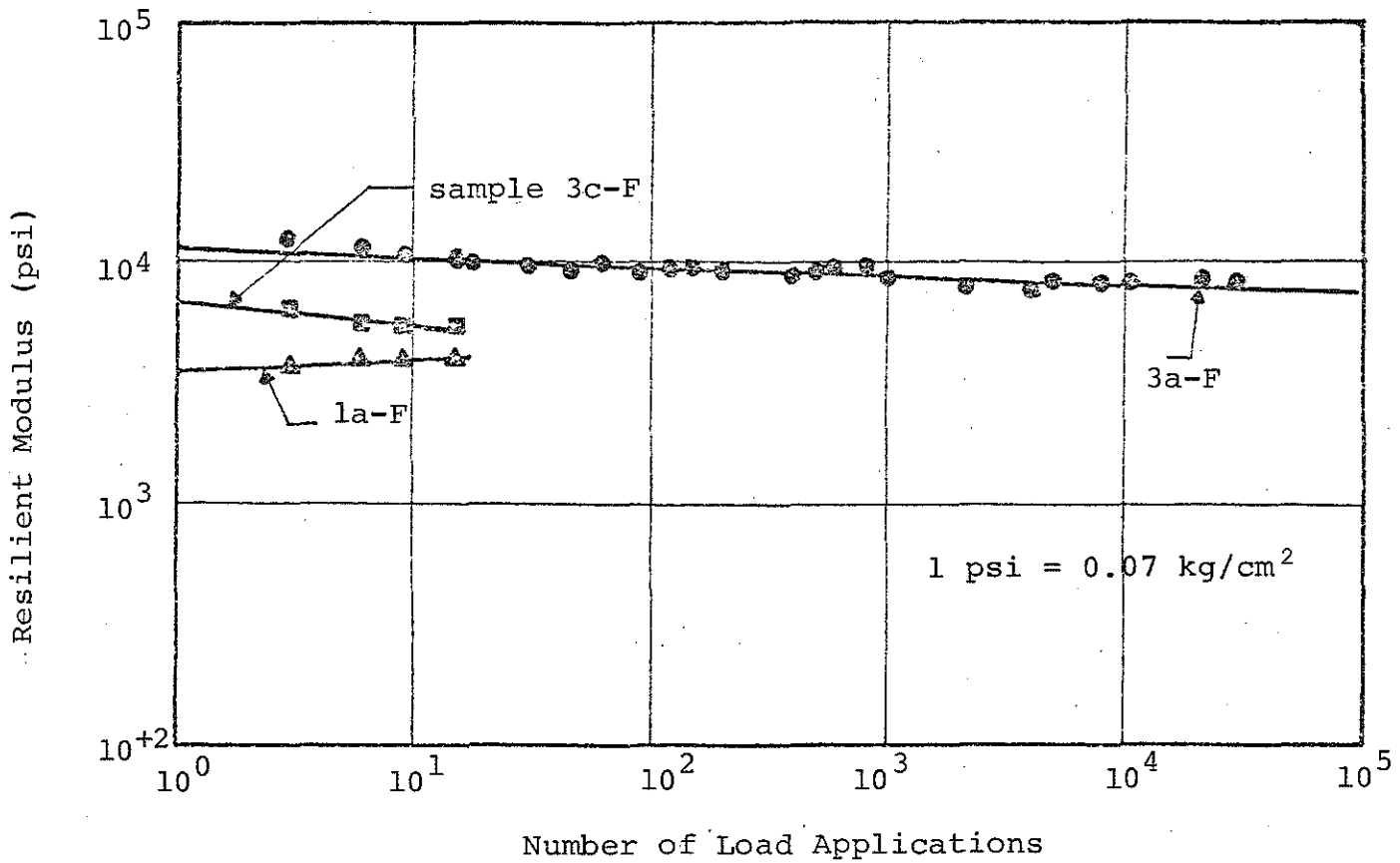

FIGURE 4.22 Typical Resilient Modulus versus Number of Load Applications for Unconsolidated Sample Tested under a Confining Pressure of 25 psi and Different Cyclic Stress Ratio, Site 2, Lower Peninsula.

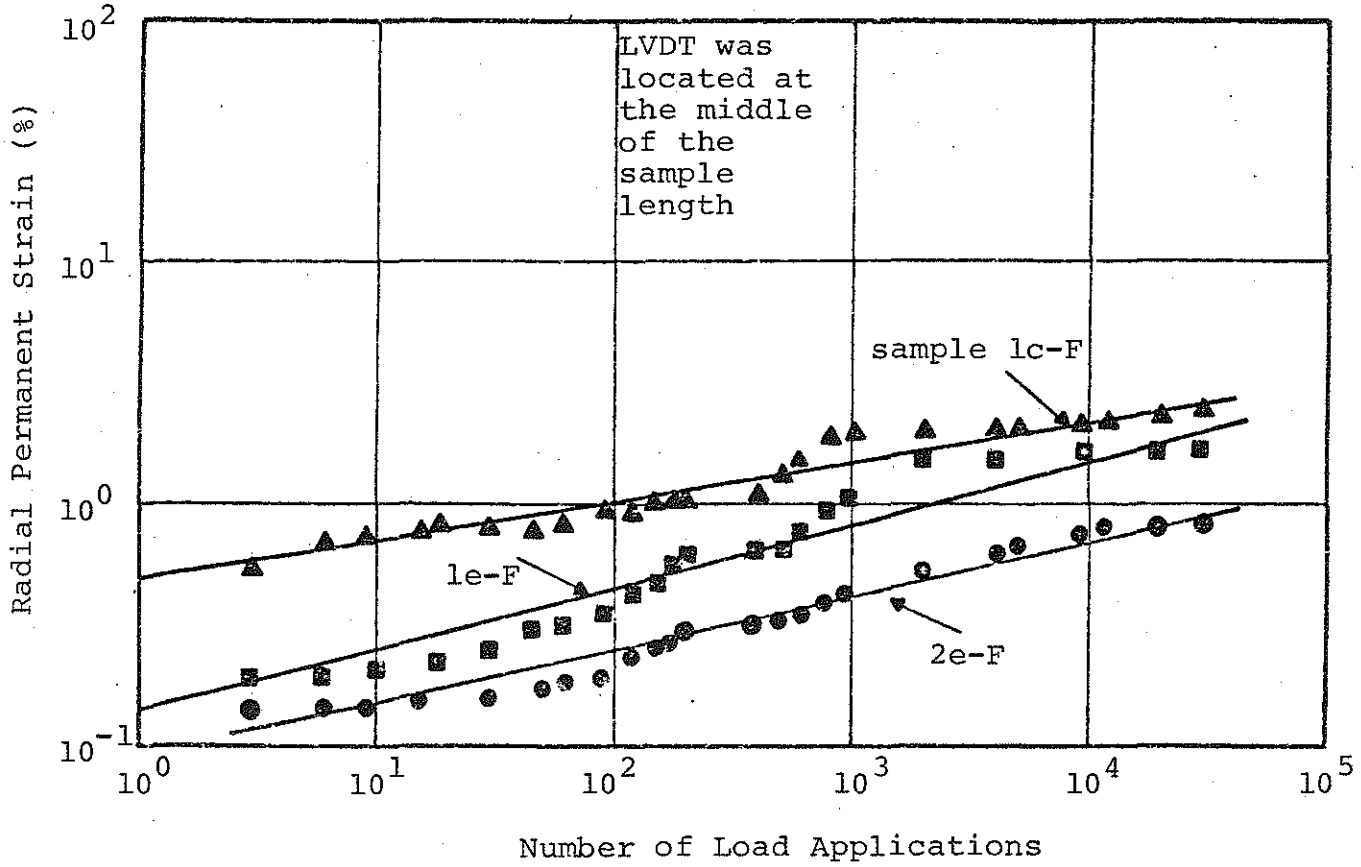

FIGURE 4.23 Typical Radial Permanent Strain versus Number of Load Applications for Unconsolidated Samples Tested under a Confining Pressure of 5 psi and Different Cyclic Stress Ratio, Site 2, Lower Peninsula.

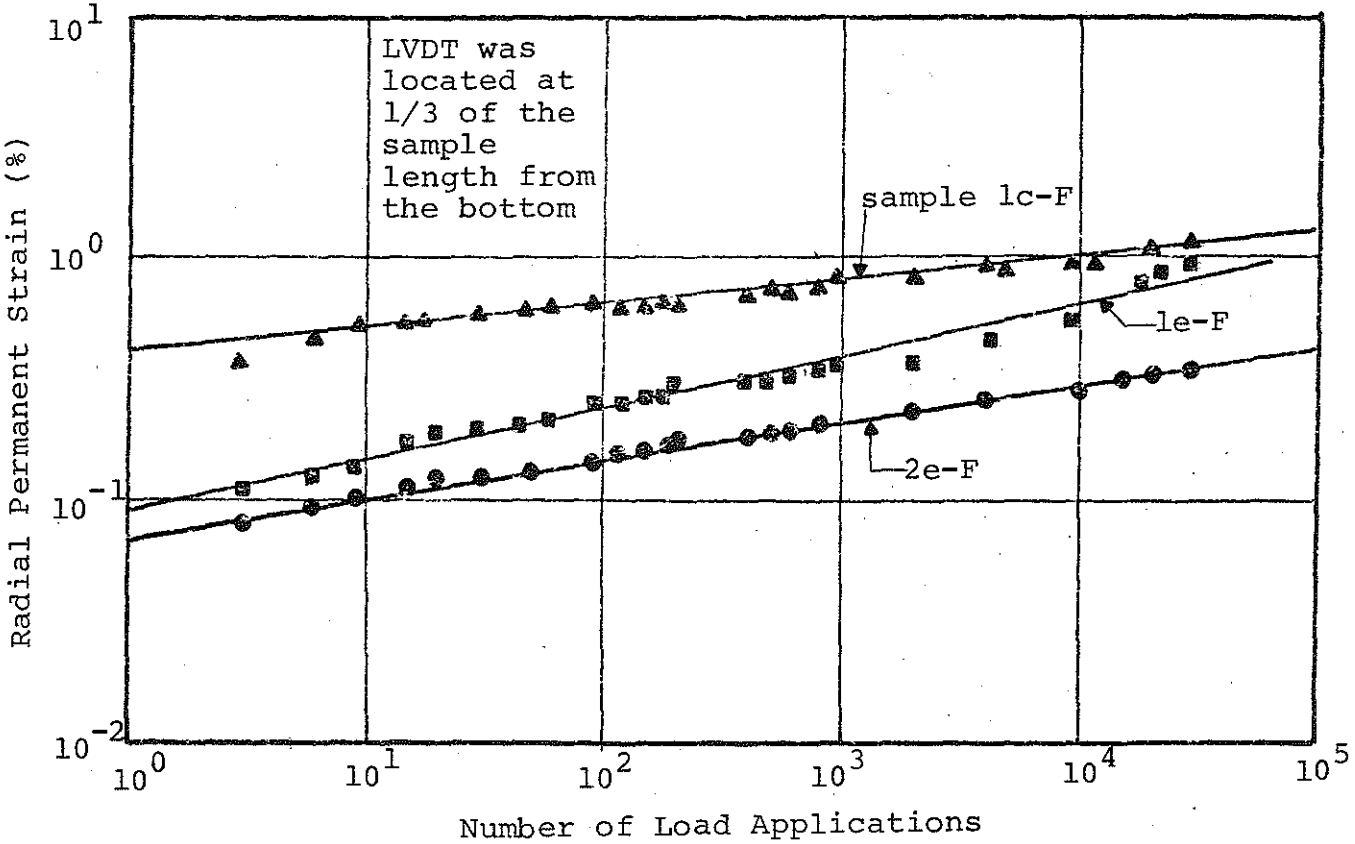

FIGURE 4.24 Typical Radial Permanent Strain versus Number of Load Applications for Unconsolidated Samples Tested under a Confining Pressure of 5 psi and Different Cyclic Stress Ratio, Site 2, Lower Peninsula.

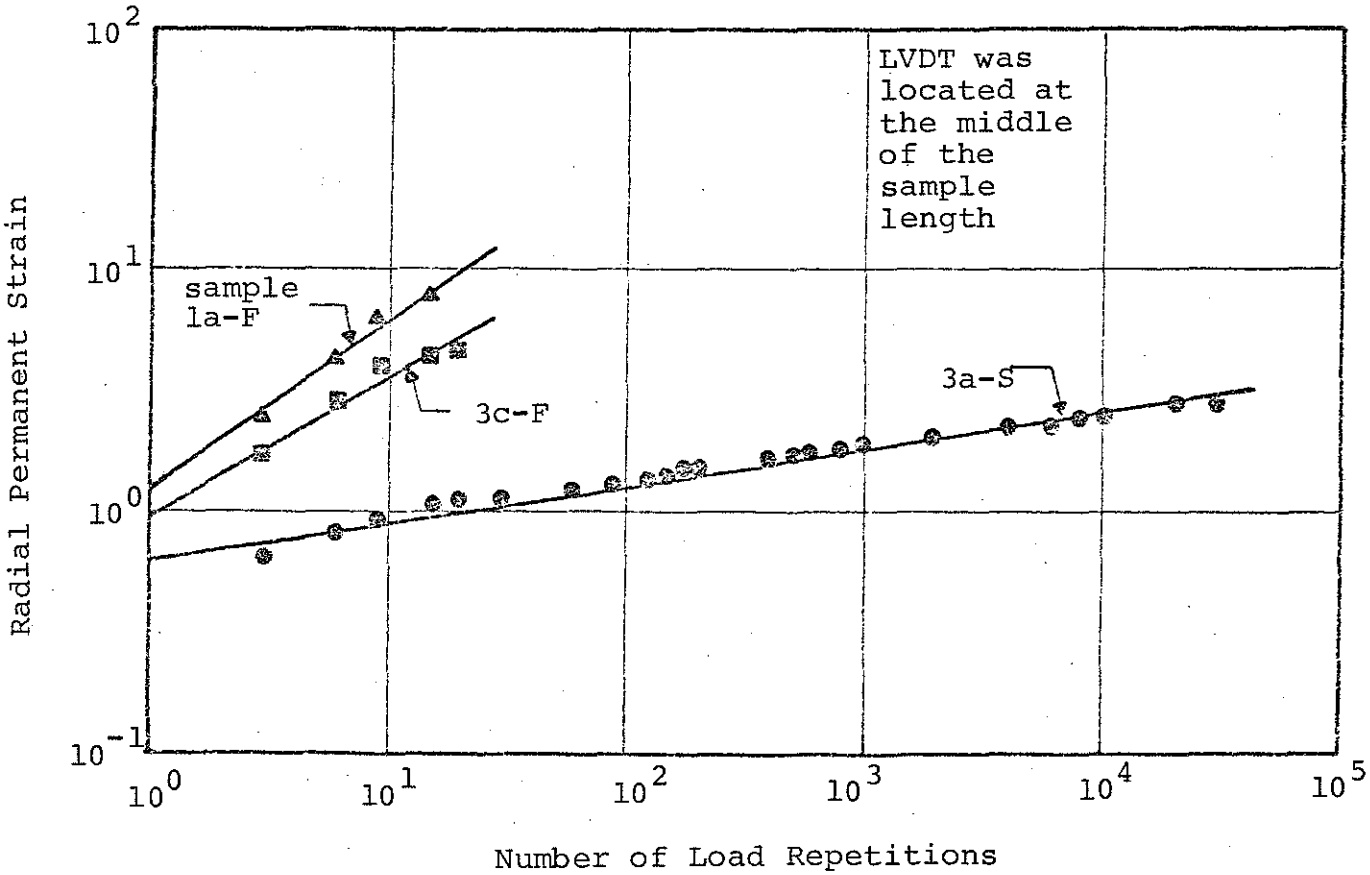

FIGURE 4.25 Typical Radial Permanent Strain versus Number of Load Applications for Unconsolidated Samples Tested under a Confing Pressure of 25 psi and Different Cyclic Stress Ratio, Site 2, Lower Peninsula.

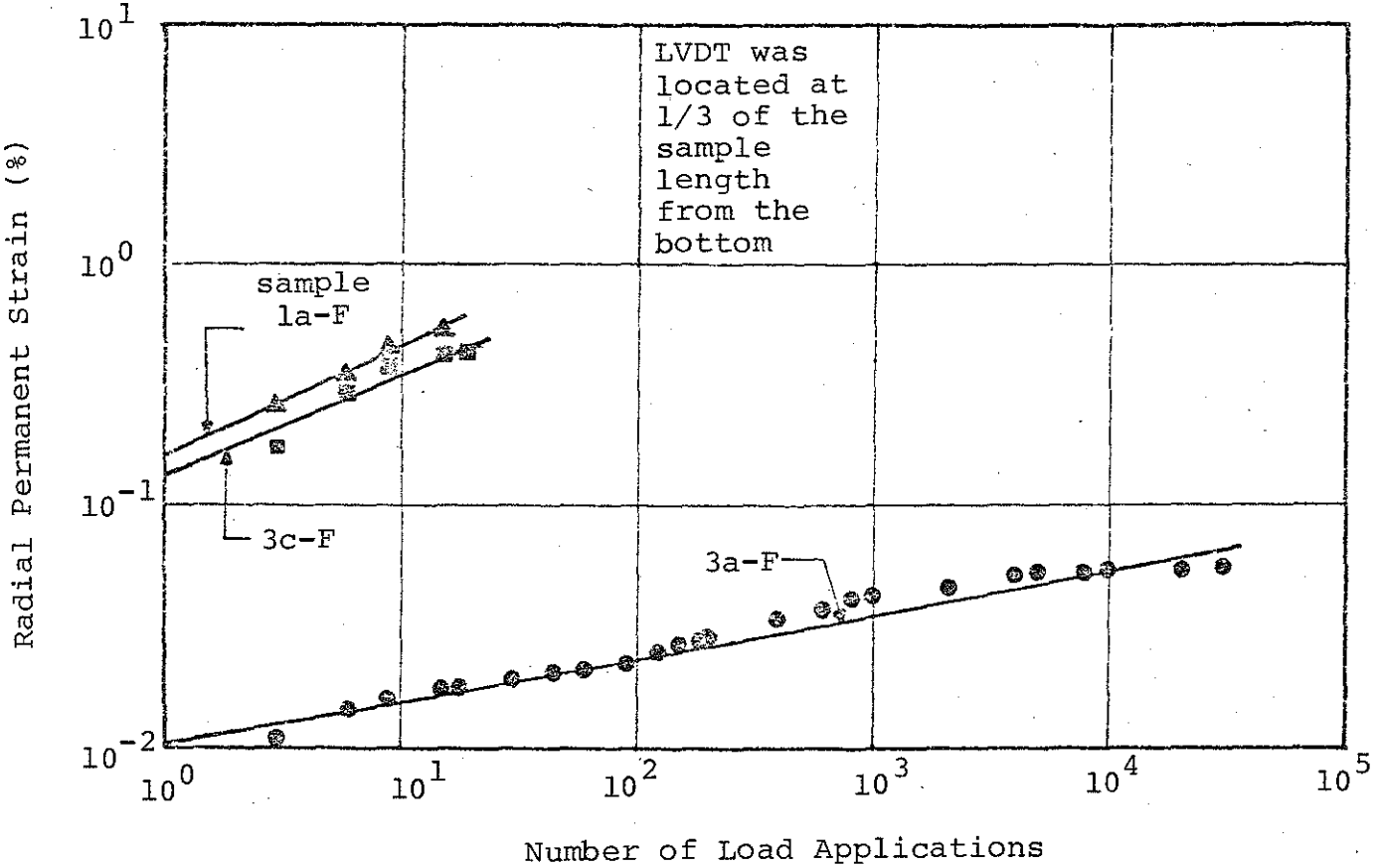

FIGURE 4.26 Typical Radial Permanent Strain versus Number of Load Applications Samples Tested under a Confining Pressure of 25 psi and Different Cyclic Stress Ratio, Site 2, Lower Peninsula.

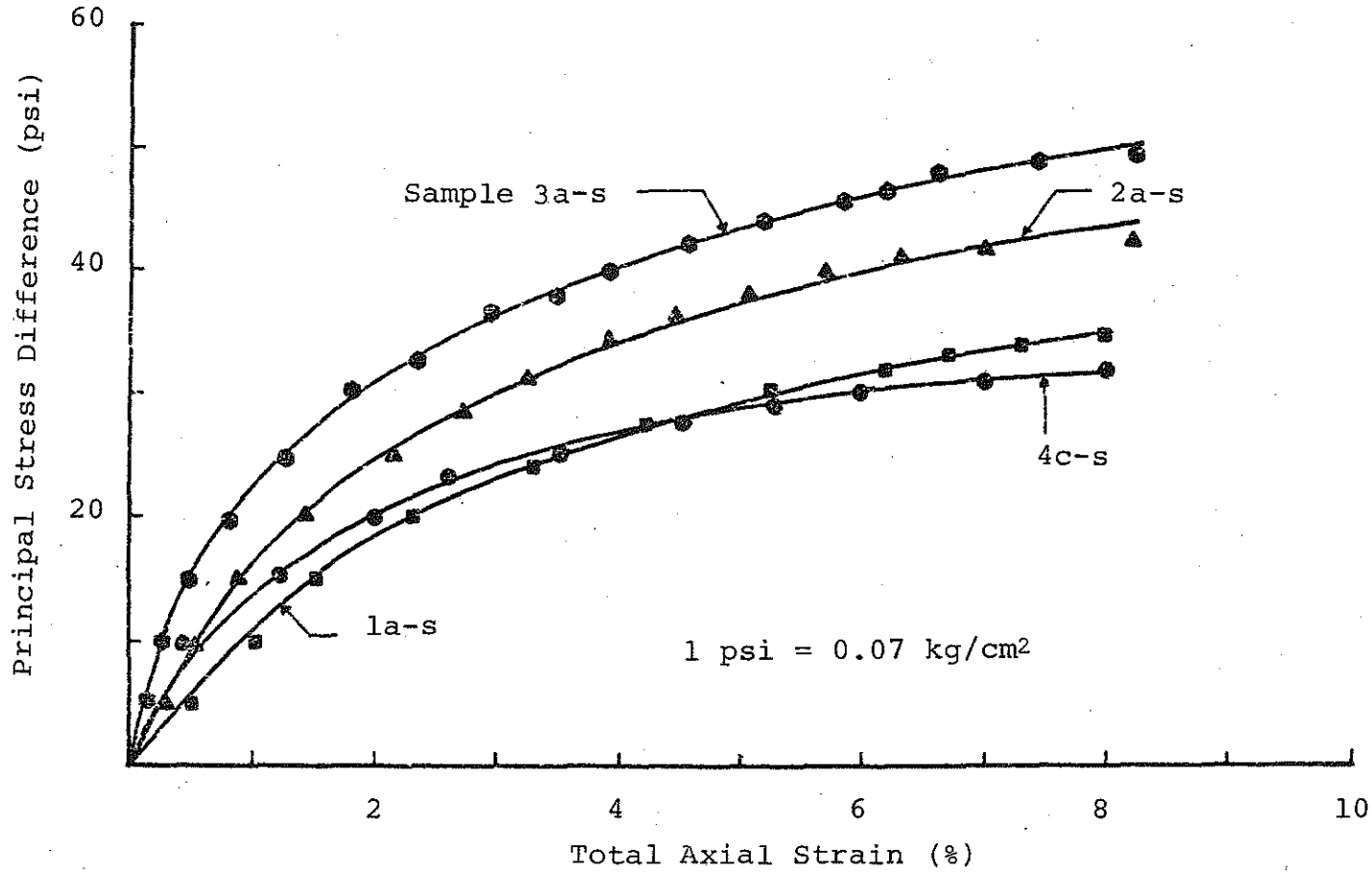

Figure 4.27 Principal Stress Difference versus Total Axial Strain from Ramp Tests, Site 4, Upper Peninsula.

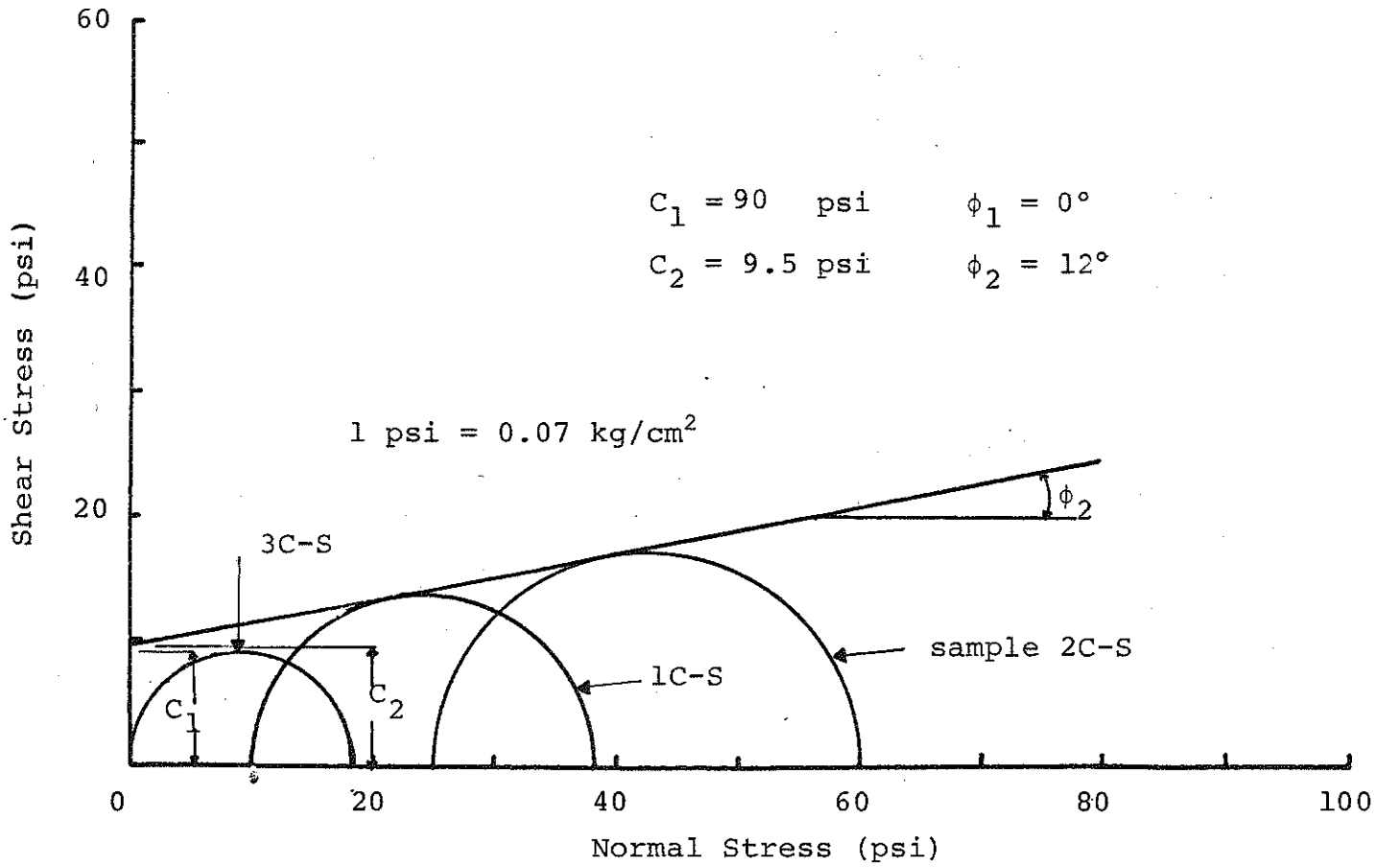

FIGURE 4.28 Mohr Circles and Failure Envelopes from Ramp Tests, Site I, Upper Peninsula.

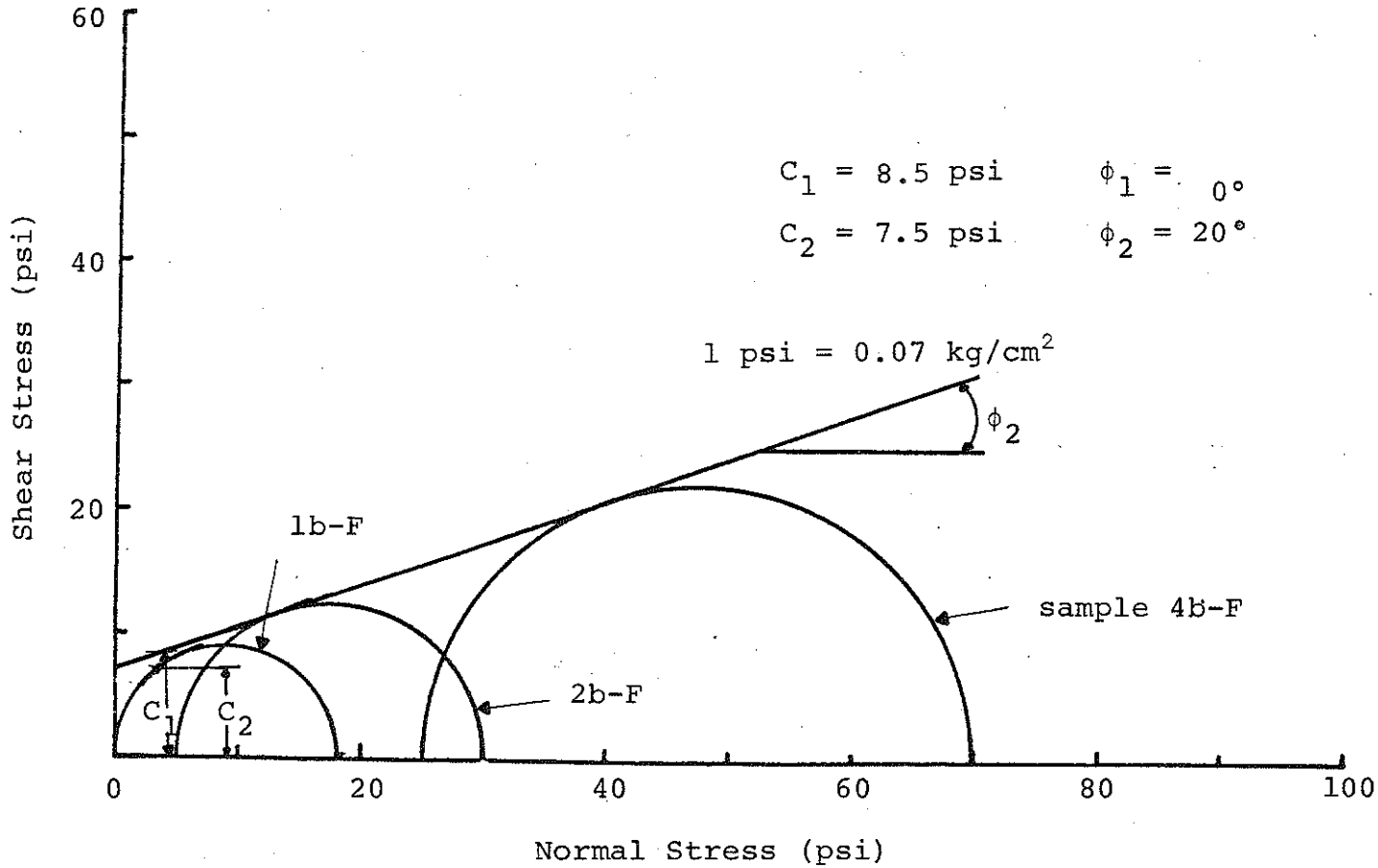

FIGURE 4.29 Mohr Circles and Failure Envelopes from Ramp Tests, Site 2, Upper Peninsula.

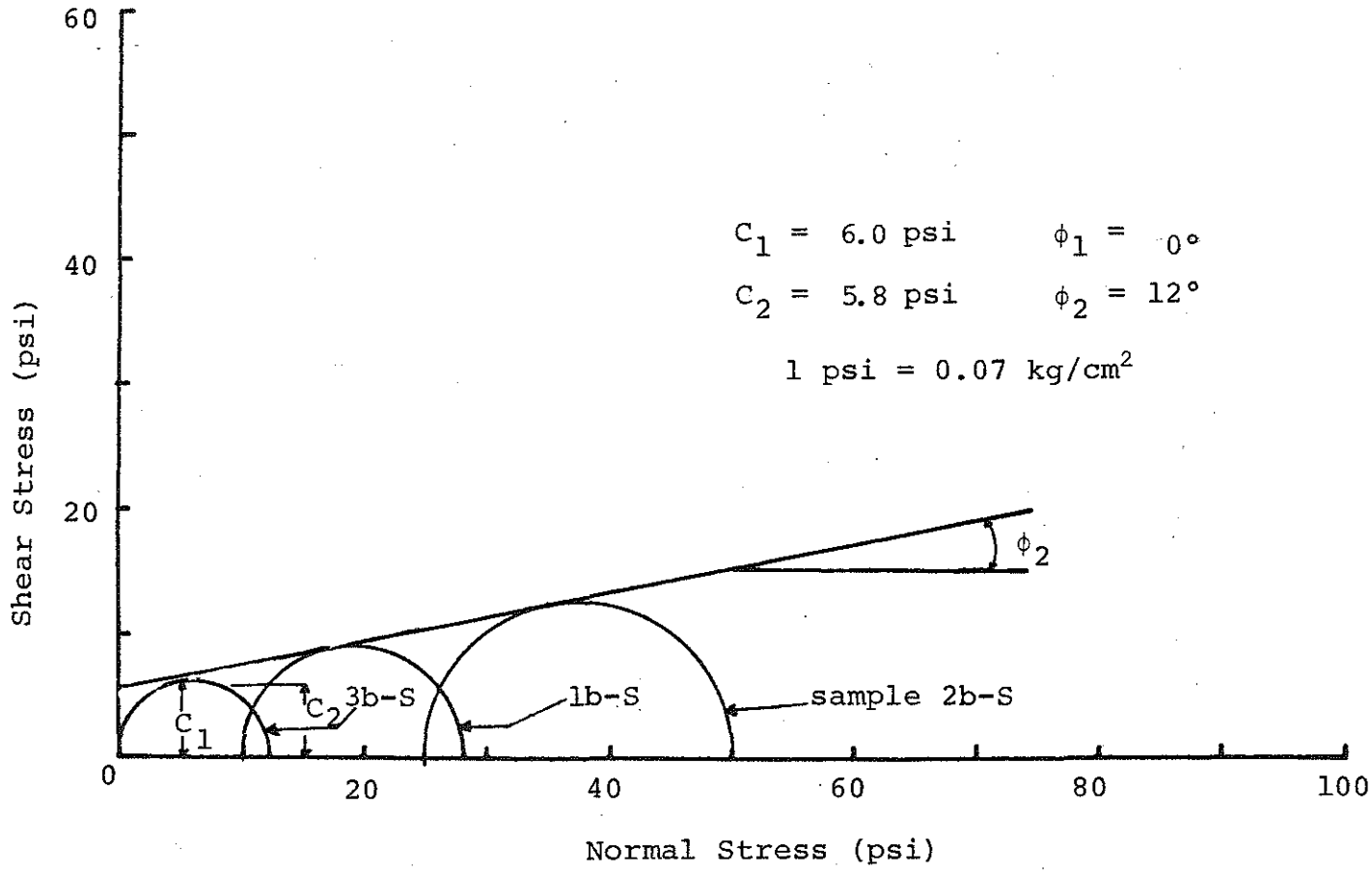

FIGURE 4.30 Mohr Circles and Failure Envelopes from Ramp Tests, Site 3, Upper Peninsula.

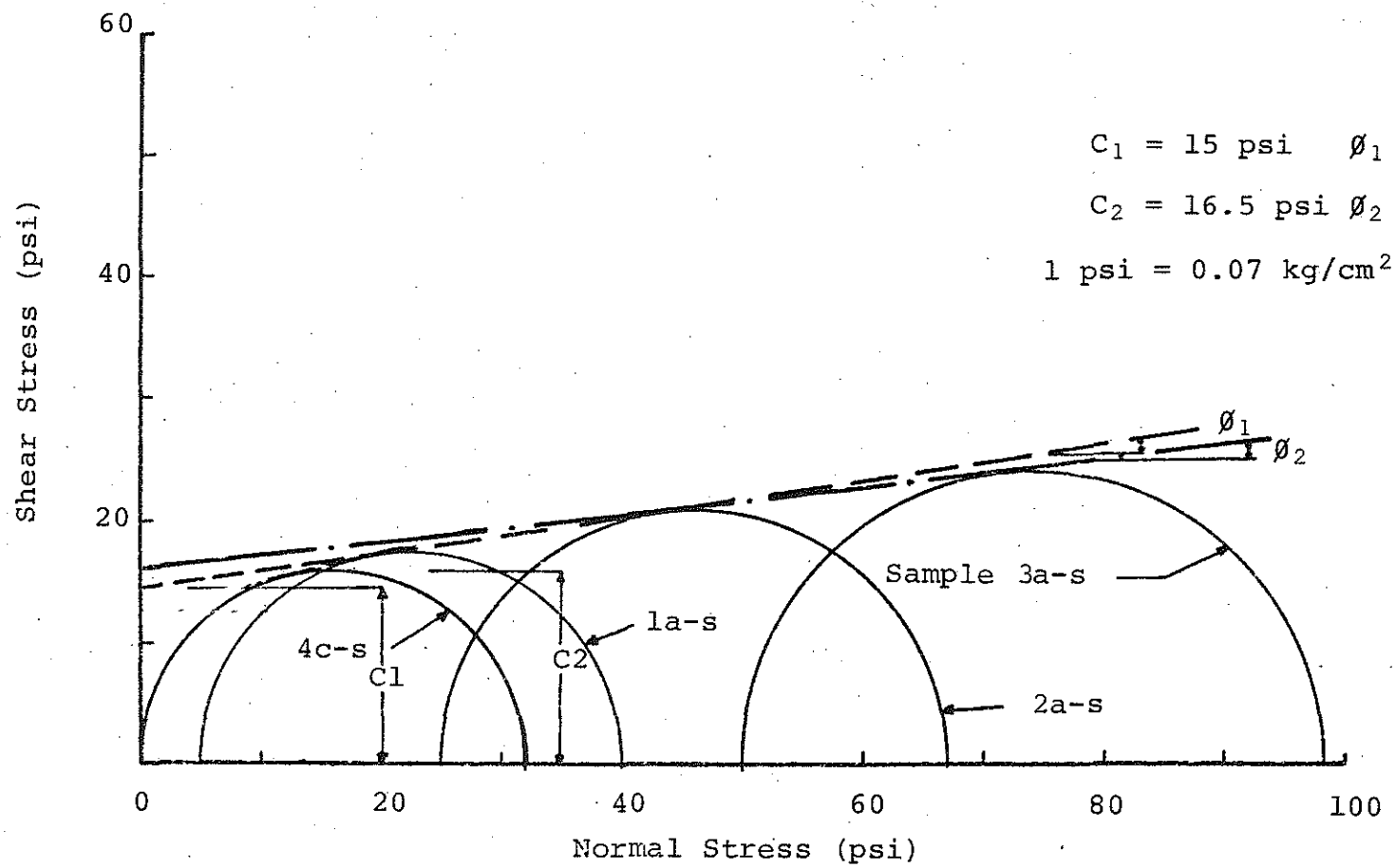

Figure 4.31 Mohr Circles and Failure Envelopes from Ramp Tests, Site 4, Upper Peninsula.

results highly variable and dependent upon the sequence and thickness of these layers. Consequently, the efforts in the testing program were shifted to unconsolidated samples and to the lower peninsula test sites.

4.3.3 Unconsolidated Cyclic Triaxial Tests

Figures 4.32, 4.33, 4.34 and 4.35 show plots of the axial permanent strain, the resilient modulus, the radial permanent strain measured at the middle of the sample and the radial permanent strain at 1/3 of the sample length from the bottom respectively, all plotted against the logarithm of the number of load applications for site number four. The data pertaining to the other test sites are listed in Appendix D.

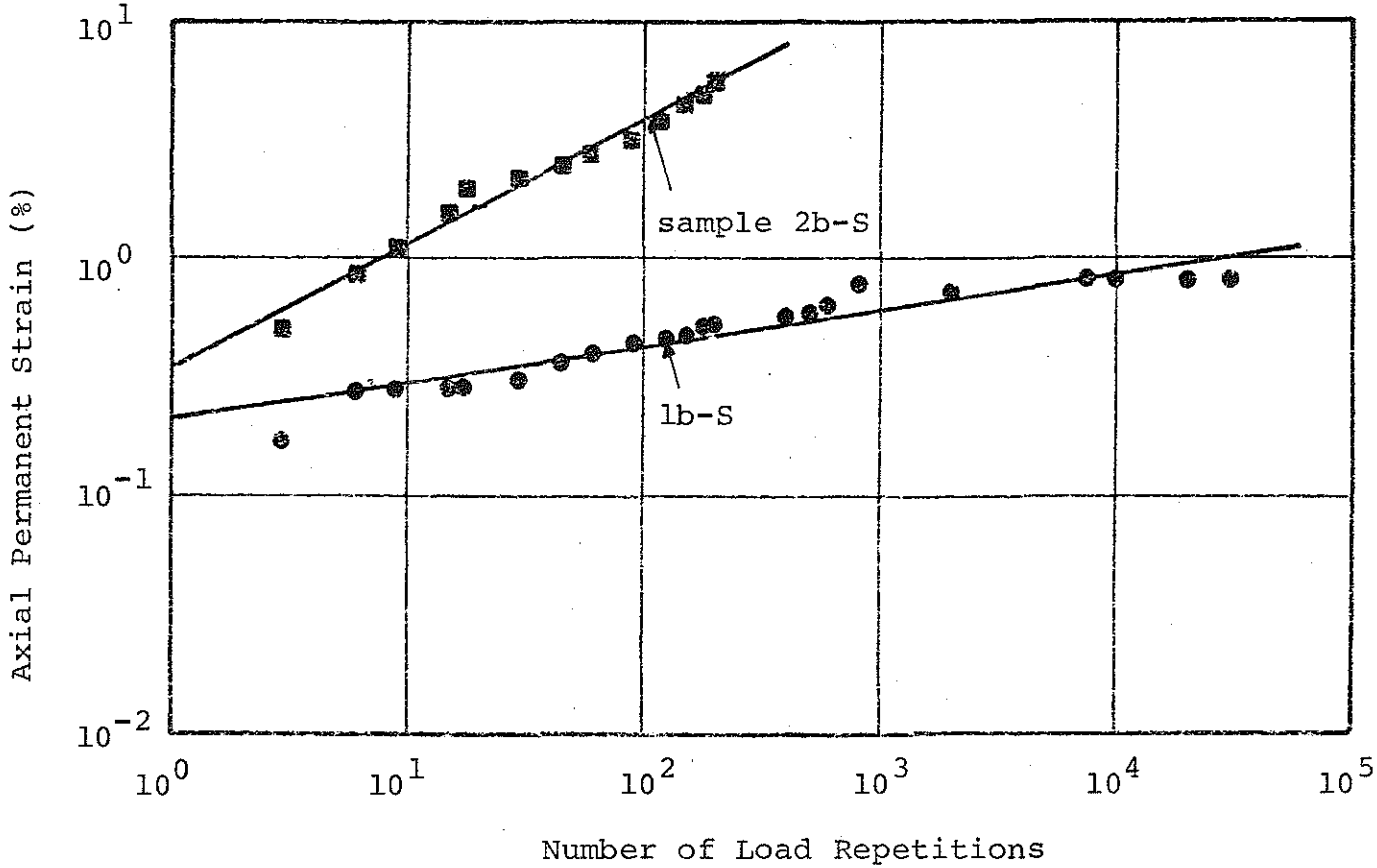

FIGURE 4.32 Typical Axial Permanent Strain versus Number of Load Applications for Unconsolidated Samples under a Confining Pressure of 5 psi and Different Cyclic Stress Tested Ratio, Site 4, Upper Peninsula.

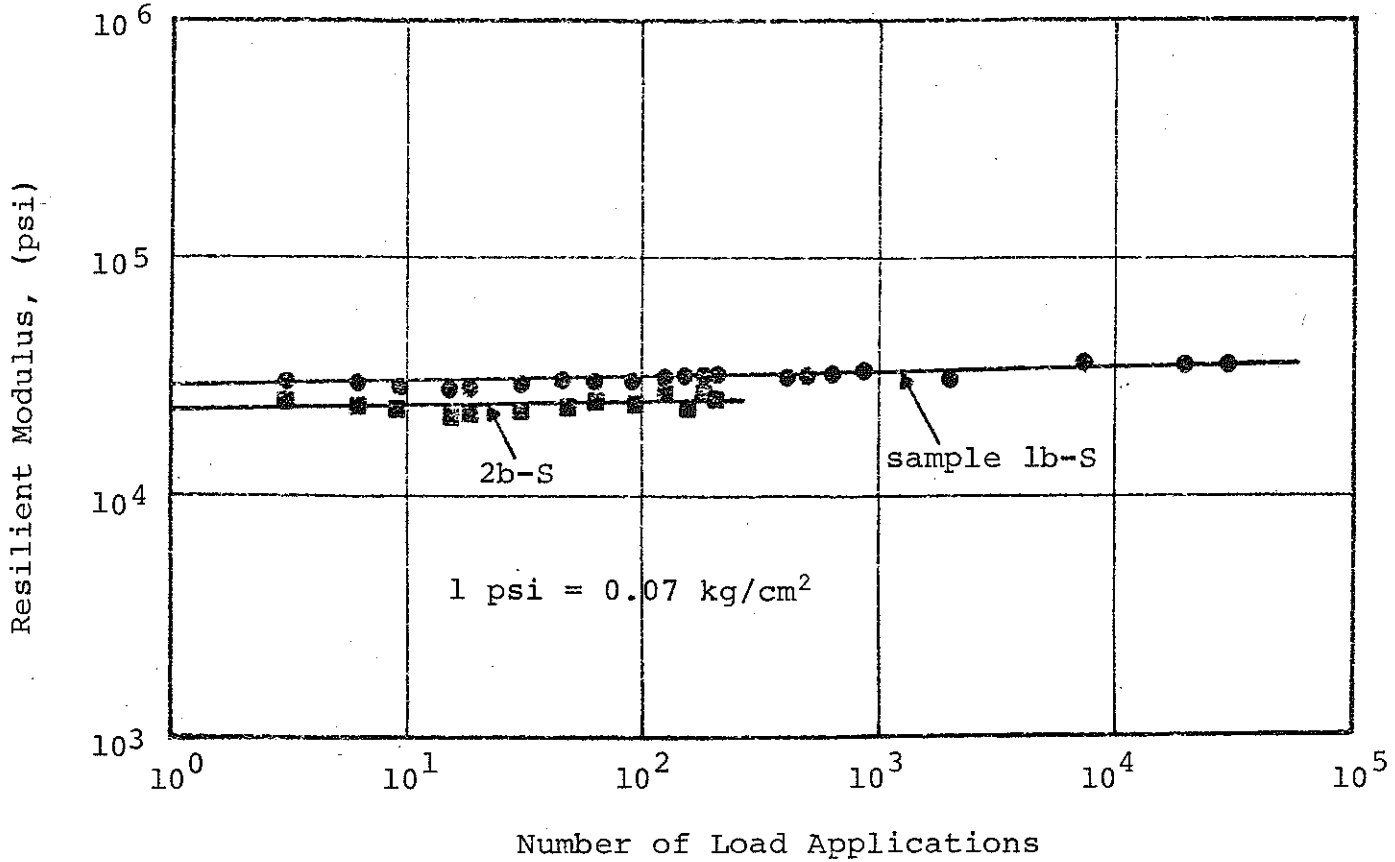

FIGURE 4.33 Typical Resilient Modulus versus Number of Load Applications for Unconsolidated Sample Tested under a Confining Pressure of 5 psi and Different Cyclic Stress Ratio, Site 4, Upper Peninsula.

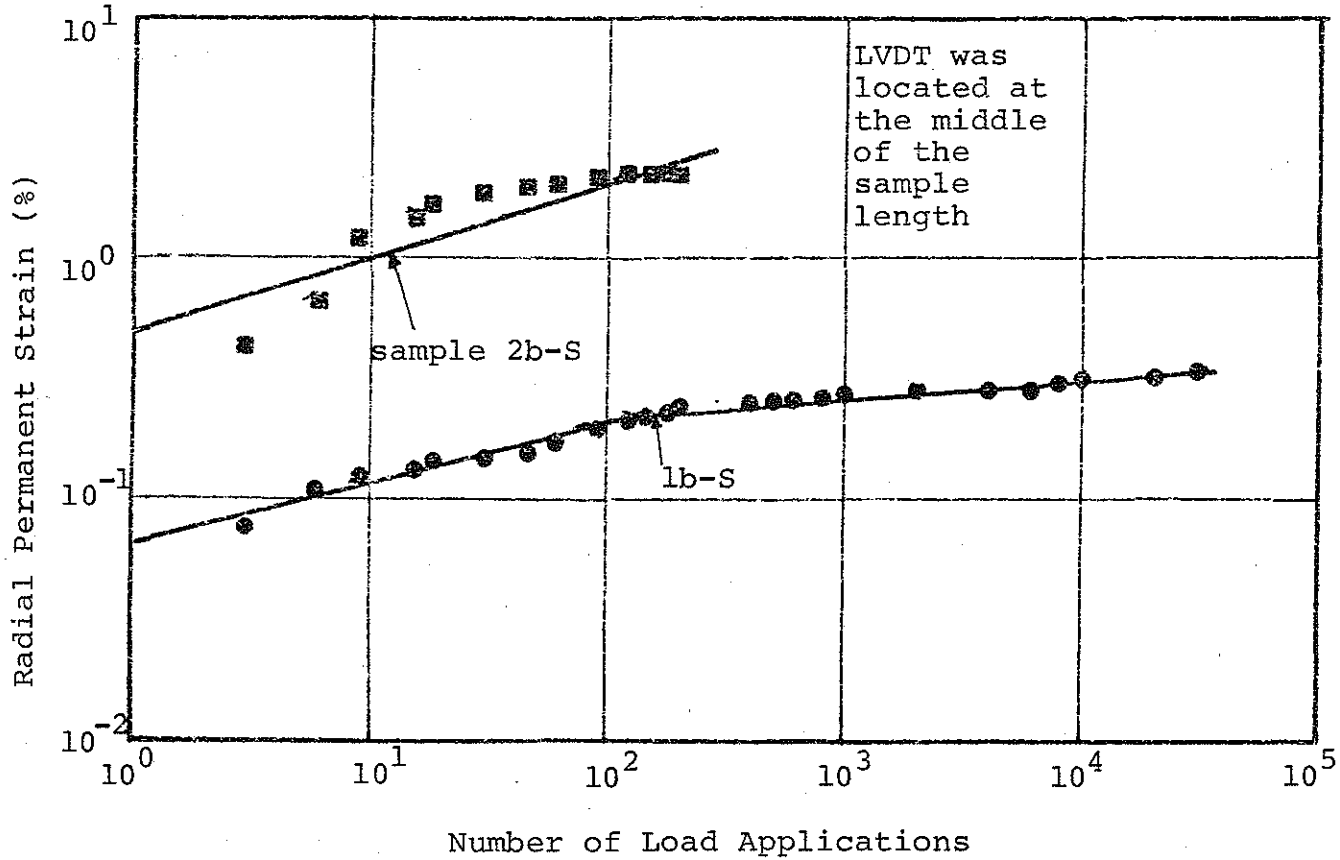

FIGURE 4.34 Typical Radial Permanent Strain versus Number of Load Applications for Unconsolidated Samples Tested under a Confining Pressure of 5 psi and Different Cyclic Stress Ratio, Site 4, Upper Peninsula.

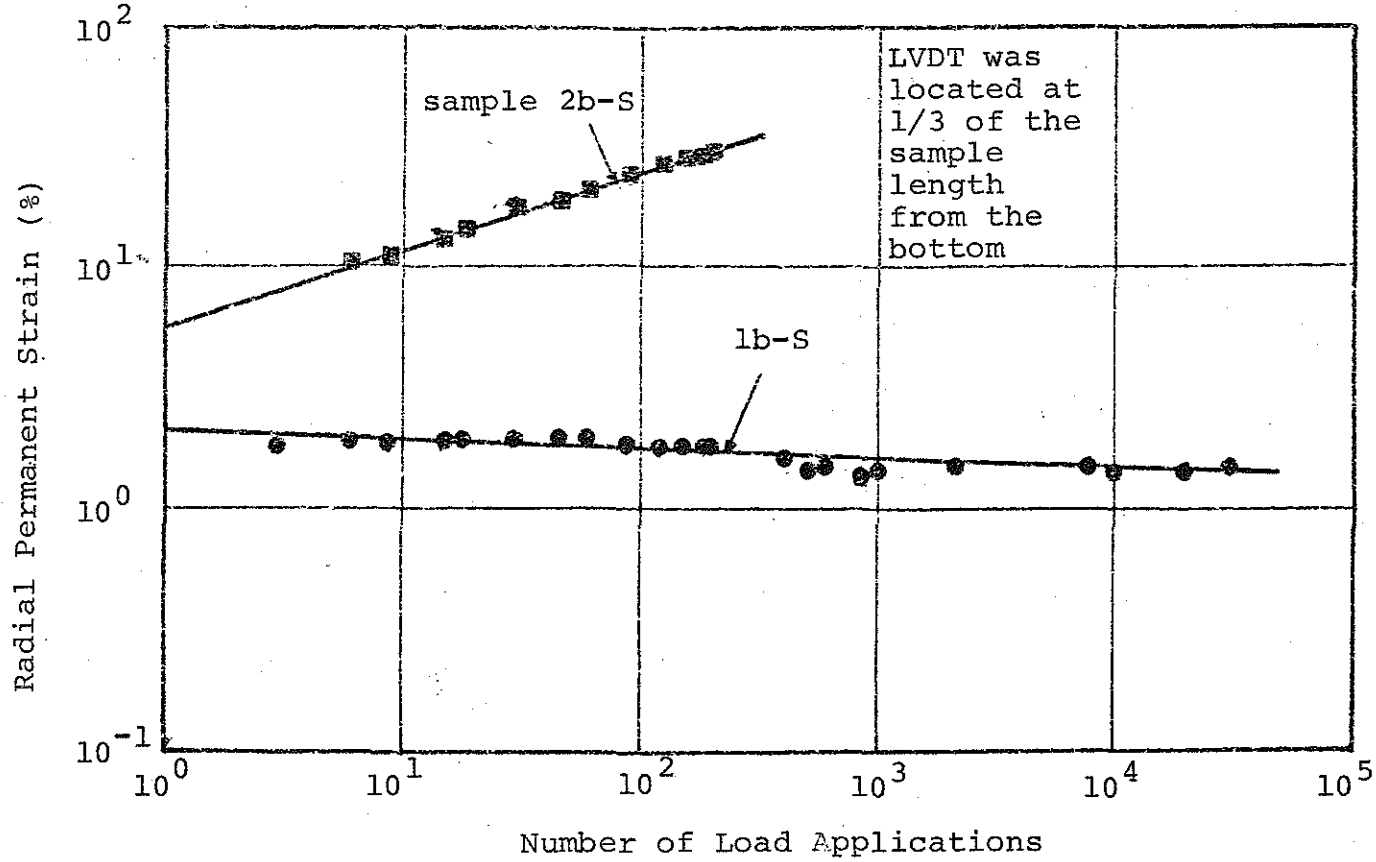

FIGURE 4.35 Typical Radial Permanent Strain versus Number of Load Applications for Unconsolidated Samples Tested under a Confining Pressure of 5 psi and Different Cyclic Stress Ratio, Site 4, Upper Peninsula.

CHAPTER V

DISCUSSION

5.1 General

It was hypothesized herein that there exists a relationship between the behavior of subgrade materials under traffic loadings and their characteristic values as measured in the repeated load cyclic tests. Further, it was assumed that the in-situ stresses induced by vehicular loadings could be approximated by a stress spectrum applied during the course of the cyclic test. These characteristic values could be used as follows:

01. As indicators of the performance and conditions of the subgrade soils and pavement system.
02. As measures of the elastic and plastic behavior of the test materials.
03. To study the effects of different stress conditions on the cumulative compressive permanent strain.
04. To establish a limiting design criterion whereby the cumulative damage could be minimized.

The test procedures for obtaining the sample characteristic values were outlined in Chapter III. Analyses of the data included:

01. Modeling the stress-strain characteristics of the test materials using a hyperbolic relationship.
02. Modeling the resilient and permanent characteristics at any number of load applications using exponential functions.
03. Convoluting the models in 1 and 2 above to yield a general predictive model whereby the plastic strain at any number of load repetitions could be predicted using typical triaxial test data.
04. Incorporating other investigators' data in 1, 2, and 3 above.
05. Correlating the material characteristics to the soil support values as defined by the AASHO interim guide for design of asphaltic pavements.

Item 1 was accomplished using the test data from the incremental creep tests and/or ramp tests (see Chapter III). The data from the triaxial cyclic tests were used in Item 2. Items 3, 4 and 5 were necessary to investigate the validity of the working hypothesis and to contribute to the state of the art.

Throughout the course of these investigations, the tests were designed and the analyses were performed to accomplish the following objectives.

01. Obtain disturbed and undisturbed clay samples from beneath existing Michigan highways.

02. Define a sample preparation technique whereby disturbed samples will be compacted so as to show similar behavior to the undisturbed samples when tested in a repeated load triaxial test.

03. Conduct repeated load triaxial tests on recompacted and undisturbed samples of the clay materials to evaluate the resilient stress-strain characteristics, and the cumulative compressive strain under different test conditions.

04. Establish a correlation equation between the material characteristics and the soil support values, and consequently generalize this correlation for sand and clay using data obtained from tests on both materials.

05. Use the cumulative permanent strain data to establish a limiting stress and/or strain criterion that could be used to minimize the cumulative damage due to a desired number of load applications.

To accomplish the above mentioned objectives, shelby tube and bag samples were collected from the test sites. However, only the shelby tube samples were used in the testing program due to the nature of the clay and varved clay soils encountered at the test sites. It was found, as expected, that the soil behavior and conditions did drastically change in the disturbed bag samples relative to those which existed in the field or in the shelby tube samples. This is so because the overburden and lateral pressures decrease during sampling causing the soil to expand. The tendency for expansion is resisted, to some extent, by the capillary pressure. Also, the shear stresses on the

samples are different than those which existed in the field and may vanish depending on the stress state. Although disturbed (bag samples) and relatively undisturbed (shelby tube samples) were subjected to the above mentioned behavior during sampling, the undisturbed samples, however, tend to retain the soil mass structure as it existed in the field. Bag samples on the other hand, are unlikely to preserve the structure. Generally speaking, soil samples inherit the same or similar strength characteristics that the soil structure had attained in the field. This behavior is known to be more pronounced in undisturbed samples of natural deposits than in compacted soils [93]. Further, the shear strength of a soil mass is highly dependent on the effective stress, the stress path, the soil type, and the soil structure and moisture that were attained either through natural deposition or compaction processes. Cohesive soil, in its natural state in the ground, may have single grained structure or compound structure. In the single grained structure, each particle is supported by contact with several of the grains. In the compound structure large voids are enclosed in a skeleton of arches of individual fine grains (honeycomb structure) or of aggregations of colloidal sized particles into chains or rings (flocculent structure) [94]. Casagrande [94] reported that the compound structure is the result of sedimentation of particles which are small enough to exhibit appreciable surface activity. Soils with compound structure are usually of low density, but may have developed considerable strength due to compression of the arches in the soil skeleton. When these soils are recompacted, their structure is changed [94] and consequently their strength characteristics may not reflect those which existed in the field. The cohesive soils at the test site are of these kind. Thus, it is extremely hard to impossible to recompact bag samples so as to achieve structural composition similar to those existing in the

field. Therefore, objective number 2, which calls to define a sample preparation technique whereby disturbed samples will be compacted so as to have similar soil structure to the undisturbed samples, was not feasible for this project (cohesive soils). This objective, however, was accomplished for sand materials in a previous research project [7,8,77].

5.2 Static Triaxial Tests

5.2.1 Incremental Creep Tests Versus Ramp Tests

As noted in Chapter III, conventional triaxial test equipment utilizing the same specimen size as that used in the MTS triaxial cell was not available. Thus, to provide the best possible correspondance between static and dynamic (cyclic) test conditions, the static tests were performed in the MTS triaxial cell using two different procedures: a) the load was incremented at ten percent of the estimated sample strength, the test was called an incremental creep test (ICT), and b) the load was applied at a constant rate, the test was called ramp test (RT). Both of the above tests (ICT and RT) are referred to herein as static triaxial tests to differentiate them from the cyclic tests. The purposes of the static triaxial tests include:

01. to model the static stress-strain relationship of the test materials, and
02. to provide a data base whereby the cyclic triaxial test data could be compared to and convoluted with, to yield a general predictive model of the plastic behavior of the materials.

Kholsa and Wu [95] were the first to use the incremental creep tests to study the stress-strain behavior of sand. Recently, Baladi and Lentz [23] used the ICT results to normalize the plastic behavior of sand subgrade materials and developed a permanent strain predictive model. They concluded that the model was successful and independent of the sample and test variables (water content, confining pressure, compaction efforts and stress level).

The main disadvantage of the ICT relative to the RT is that two independent investigators cannot duplicate the stress rate. The strain rate, however, is controlled by the soil type and sample behavior. In the ICT a new increment of loading is added when the strain rate due to the previous increment decreases to a certain level (see Chapter III). To alleviate this problem and after a brief discussion with the Federal Highway Administration personnel, Kenis [96] suggested that ramp tests (constant stress rate) be performed to check the ICT results and possibly to standardize the test. Figure 5.1 shows typical results of the ICT and RT for three different confining pressures. Examination of the figure indicated that at any strain level, the RT samples were subjected to a higher stress level than those of the ICT samples. This was expected because the stress rate of the ramp test was higher than that of the incremental creep test. The values of the strength parameters from both tests, however, showed very modest variations, as indicated in Figure 5.2. As it was expected, the stress-strain relationship and the strength parameters of sand subgrade materials, from both tests, showed very little to no variations. It should be noted herein that when the results from both tests were used to normalize and study the plastic behavior of the test materials the resulting model showed 1) a small variation for the clay materials and 2) no change at all for the sand subgrade materials. These observations along with the normalization process will be discussed in detail in Section 5.4 below.

5.2.2 Sample Failure and Failure Mode

Throughout the course of this study, sample failure was defined as follows: "the sample was considered to fail when the vertical deformations reached the maximum range of the vertical LVDT(s)". This corresponds

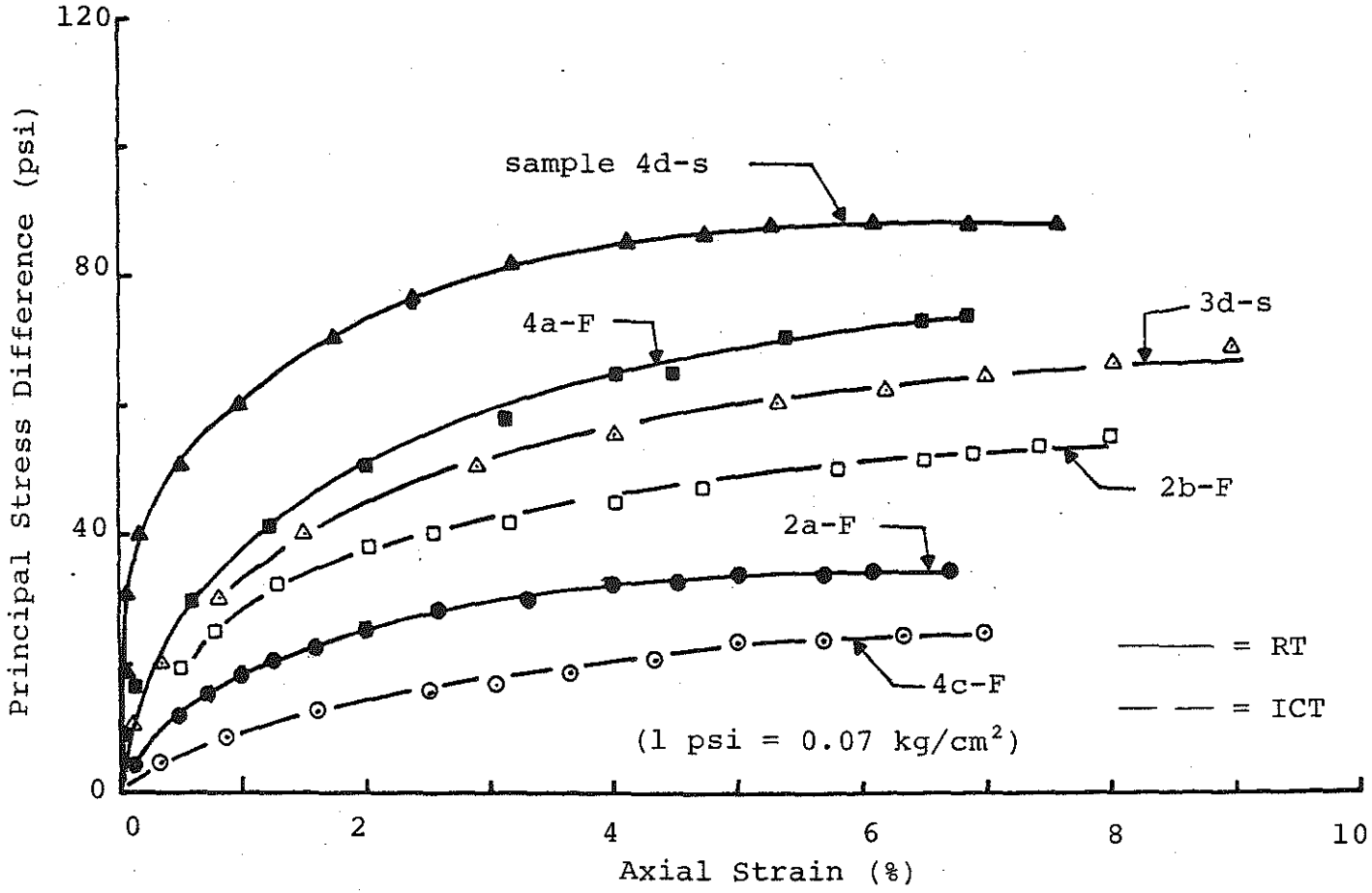

FIGURE 5.1 Principal Stress Difference Versus Total Axial Strain for Incremental Creep and Ramp Tests, Site 2, Lower Peninsula.

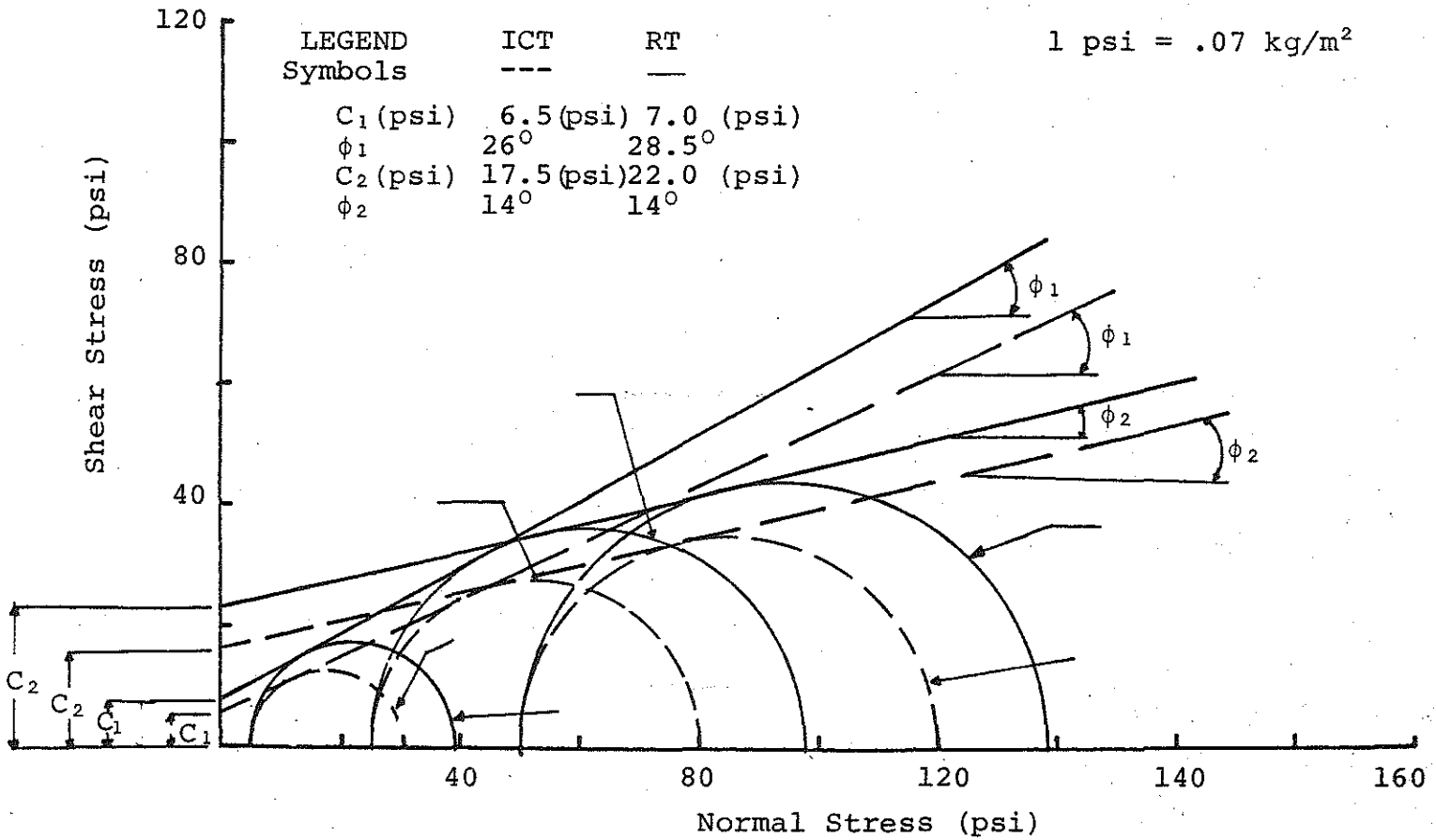

FIGURE 5.2 Mohr Circle Diagrams and Failure Envelopes for Incremental Creep and Ramp Tests, Site 2, Lower Peninsula.

to about 8 percent strain and it is dependent on the initial seating of the LVDT (datum). Also, all tests were performed using the stress controlled mode of the MTS system. This mode did not allow the load to drop after the peak sample strength was reached and consequently the sample continued to deform causing a system shut-off which was automatically activated when the maximum LVDT deflection range was reached. This could be restated as; the stress controlled mode of the MTS system did not allow the determination of the sample ultimate and/or residual strength. Rather, the vertical stress increased until shut-off. The shut-off mode was designed in the system as a safety precaution to prevent the MTS actuator from moving against some sensitive equipment parts inside the cell and eventually destroying them.

Observations of the test samples at failure revealed the following failure modes:

01. Michigan's Lower Peninsula test sites: Most of the cohesive soil samples obtained from the lower peninsula test sites characteristically exhibited general bulging failure rather than the formation of a distinct failure plane. This is so because of the high water content of the samples and the end effects of the upper and lower platens.

02. Michigan's Upper Peninsula test sites: Basically, three types of shear failure were noticed for soil samples obtained from the upper peninsula test sites. These failure types are:

    a) Bulging out of the clay layers, as shown schematically in Figure 5.3a,

    b) shear strength failure in the silt layer as shown in Figure 5.3b,

    c) squeezing out of the silt layers as shown in Figure 5.4.

The bulging out of the clay layers occurs when the samples were composed of a thick clay layer [greater than 1 inch (2.54 cm)] alternating with a relatively thin silt layer. This observation was also reported by Lo [97]. The squeezing out of the silt layers on the

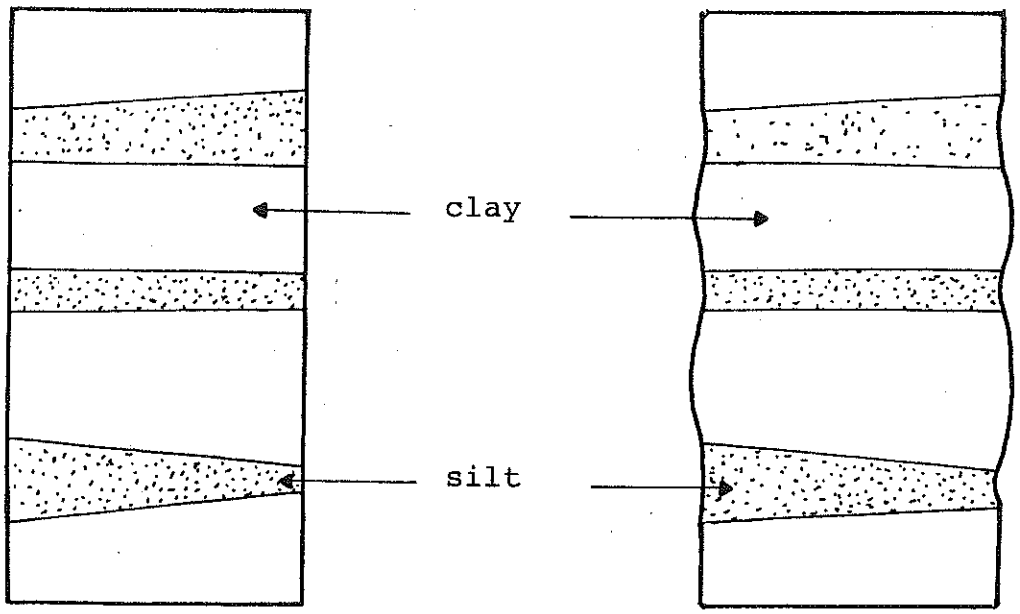

Sample Before Testing Sample After Testing

a) Bulging-Out of the Clay Layer

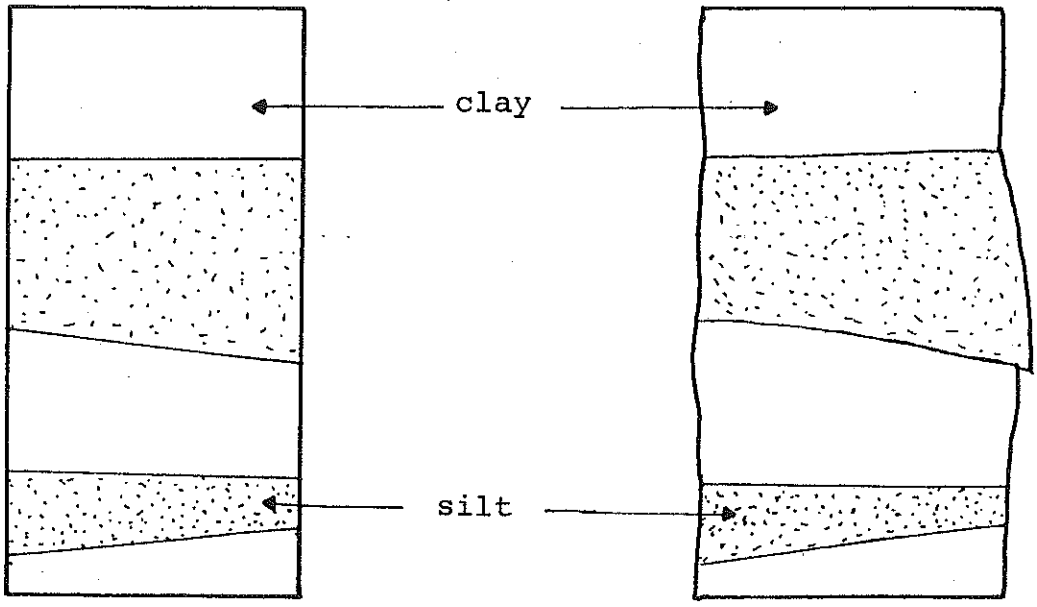

Sample Before Testing Sample After Testing

b) Shearing of the Silt Layer

FIGURE 5.3 Schematic Representation of Sample Failures

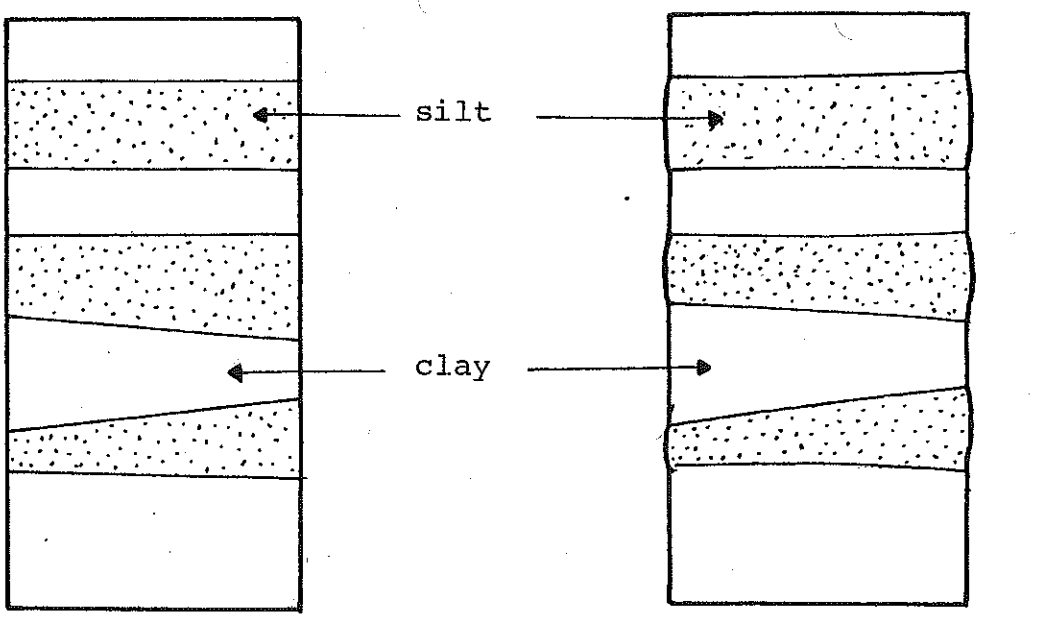

FIGURE 5.4 Schematic Representation of Sample Failure by Squeezing-Out of the Silt Layers.

other hand was found to be the dominating failure mode when the samples were composed of alternating thick horizontal layers of silt and clay. This is consistent with findings by Metcalf [98], Milligan [99] and Lo [97]. The third test failure mode was observed and reported when the samples were composed of: a) horizontal thin clay and silt layers, b) thick clay layers and thin inclined silt layers, or c) discontinuity in the layers.

5.2.3 Strength Parameters

In all tests (ICT, RT, and cyclic triaxial tests) the interior of the sample was connected to a saturated water line which in turn could be connected either to a pore pressure transducer (route 1) or to the atmosphere (route 2). For all samples, route 2 was used to check membrane leakage after the application of the confining pressure on the sample. Also, this route was used during the consolidation phase of the test for all samples consolidated under the confining pressure prior to shear or cyclic loading tests. The interior of the sample was connected to the pore pressure transducer, using route 1, and the pore water pressure was measured throughout the ICT, RT and cyclic triaxial tests. This measurement, as expected, showed very little development in the pore water pressure. Typical values were on the order of 0.1 to 0.3 psi (.007 to .021 Kg/cm^2) for confining pressures of 5 to 50 psi (.35 to 3.5 Kg/cm^2) respectively. These low values could be attributed to the unsaturated conditions of the test samples. Based on the pore pressure data, it was decided to use total stress analyses rather than effective stress analyses. The difference between the two analyses were negligible. It should be noted that the interested reader may obtain the data for the pore water pressure from the author upon request.

The data from the incremental creep tests and ramp tests were reduced and plotted as shown in Chapter IV and Appendix C. The peak sample strength data and the corresponding confining pressures were used to draw Mohr's circle diagrams from which the failure envelopes were constructed and the strength parameters were determined. These parameters are listed in Table 5.1 for the lower peninsula and Table 5.2 for the upper peninsula test sites.

As shown in Table 5.1, two sets of strength parameters are given (c_1, ϕ_1, and c_2, ϕ_2). The first set (c_1, ϕ_1) was obtained from tests using confining pressures of 5 and 25 psi (0.35 and 1.75 kg/cm^2). The second set (c_2, ϕ_2) was obtained from confining pressures of 25 and 50 psi (1.75 kg/cm^2 and 3.5 kg/cm^2). It is common practice to use a curved failure envelope to express the strength parameters of the soils. For this study, however, the induced lateral stresses in the subgrade materials due to a moving wheel load varies considerably and it is a function of tire pressure and pavement thickness. Consequently, it was felt that two sets of strength parameters may serve the user better than one single failure envelope. The strength parameters c_1 and ϕ_1 should be used for all pavements where the lateral stress in the subgrade materials is expected to be in between 5 and 25 psi (0.35 and 1.75 kg/m^2). The second set of strength parameters should be used for higher lateral stresses.

The soil samples from the upper peninsula test sites were tested using unconfined as well as confined ramp tests. All samples, except two from site 4, were obtained and tested (sheared) perpendicular to the varve orientation. The latter two samples were obtained at an angle to the varves using an inclined shelby tube during sampling. Figure 5.5 shows the stress-strain curves of two inclined and two vertical varved clay samples. Examination of the figure indicated that the vertical samples were subjected to higher stress at failure than

TABLE 5.1 Strength Parameters and Regression Constants of the Static Tests for the Lower Peninsula Test Sites.

Test-Site Number -Location	C_1 * (psi)	C_2 * (psi)	ϕ_1 *	ϕ_2 *	σ_3 * (psi)	n * ($X10^{-4}$)	m * ($X10^{-2}$)	r^2 *	Test -Mode
S1-LP	5	24	31^0	10^0	5 25 50	4.40 2.10 1.30	3.28 1.55 1.30	0.994 0.991 0.999	ICT-C
S1-LP	14.5	--	9.5^0	--	5 25	4.70 1.90	2.40 2.15	0.984 0.996	RT-U
S2-LP	6.5	17.5	26^0	14^0	5 25 50	7.80 4.70 1.80	2.85 1.02 1.29	0.988 0.987 0.995	ICT-C
S2-LP	7.0	22	28.5^0	14^0	5 25 50	-1.80 -0.006 -0.016	0.005 0.001 0.001	0.783 0.851 0.733	RT-C
S2-LP	10.5	--	15^0	--	5 25	3.30 1.20	0.06 0.03	0.940 0.892	RT-U
S3-LP	4	23	35^0	16^0	5 25 50	0.25 -2.86 -3.20	0.012 0.0021 0.0020	0.924 0.823 0.872	ICT-C
S3-LP	7.5	--	20^0	--	5 25	5.40 1.30	0.005 0.003	0.885 0.993	RT-U
S4-LP	3	--	15^0	--	5 25	0.40 -3.70	0.048 0.014	0.908 0.848	ICT-C

*See Table 5.2

TABLE 5.2 Strength Parameters and Regression Constants of the Static Tests for the Upper Peninsula Test Sites.

Test-Site Number -Location	C_1 (psi)	C_2 (psi)	ϕ_1	ϕ_2	σ_3 (psi)	n ($X10^{-4}$)	m ($X10^{-3}$)	r^2	Test -Mode
S1-UP	9.0*	9.5	0*	12^0	0 10 25	13.20 3.31 -2.36	0.190 0.101 0.064	0.976 0.976 0.904	RT-U
S2-UP	8.5*	7.5	0*	20^0	0 5 25	-30.45 -13.33 - 0.82	0.474 0.148 0.035	0.826 0.666 0.729	RT-U
S3-UP	6.0	5.8	0*	12^0	0 10 25	25.80 18.85 12.55	0.326 0.092 0.084	0.981 0.993 0.995	RT-U
S4-UP	16* 15	16.5	0* 9	7^0	0 5 25 50	-1.67 4.83 1.71 -0.54	0.071 0.044 0.032 0.028	0.880 0.859 0.847 0.836	RT-U
S4-UP	--	8.0	--	6^0	25 50	-9.7 -13.94	0.137 0.129	0.513 0.5663	

*unconfined compressive strength

C_1 and C_2 = cohesion

ϕ_1 and ϕ_2 = angle of internal friction

n and m = regression constants

σ_3 = confining pressure

r_2 = coefficient of correlation

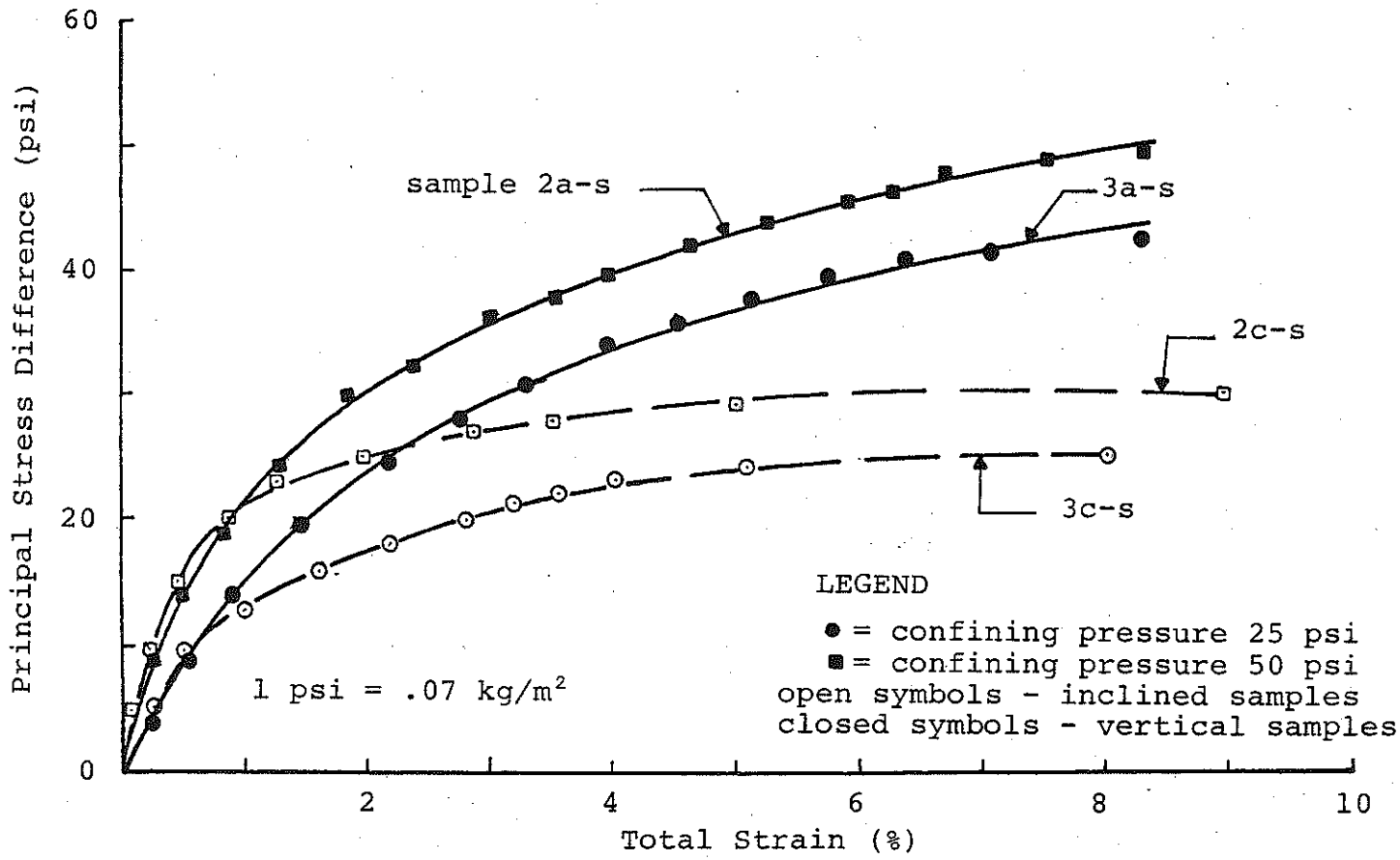

FIGURE 5.5 Stress-Strain Curves for Vertical and Inclined Varved Clay Samples Tested Under the Designated Confining Pressure.

the inclined samples. Figures 4.31 and 5.6 show Mohr's circle diagrams and the failure envelopes of the vertical and inclined samples respectively. The strength parameters of these and all the upper peninsular soil samples are listed in Table 5.2. It is apparent from the figures and the table that the strength of varved clay samples is highly dependent on the orientation of the soil layers. This finding was also reported by Murphy [100]. He concluded that varved clay had greater strength when sheared perpendicular to the varves. It should be noted that, due to limited resources, it was not possible in this project to model the strength of varved clay as a function of orientation.

5.2.4 Stress-Strain Relationship

One of the objectives of this research project was to establish a limiting stress and/or strain criterion that could be used to minimize the cumulative damage of a pavement system due to a desired number of load applications of a moving wheel load. This led first to study the stress-strain relationship of the subgrade materials when subjected to static loads (incremental creep tests or ramp tests). Such tests were performed on several samples from the lower and upper peninsula test sites. The stress-strain curves for these tests are shown in Appendix C and Appendix D for the lower and upper peninsula test sites respectively. Examination of these figures and previous reports by Konder [101], Konder and Zelasko [102, 103], and Duncan and Chan [104] indicated that the stress-strain data could be modeled using the following hyperbolic relationship

$$S_d = \frac{\varepsilon_t}{n+m\varepsilon_t} \qquad (5.1)$$

where S_d = principal stress difference,

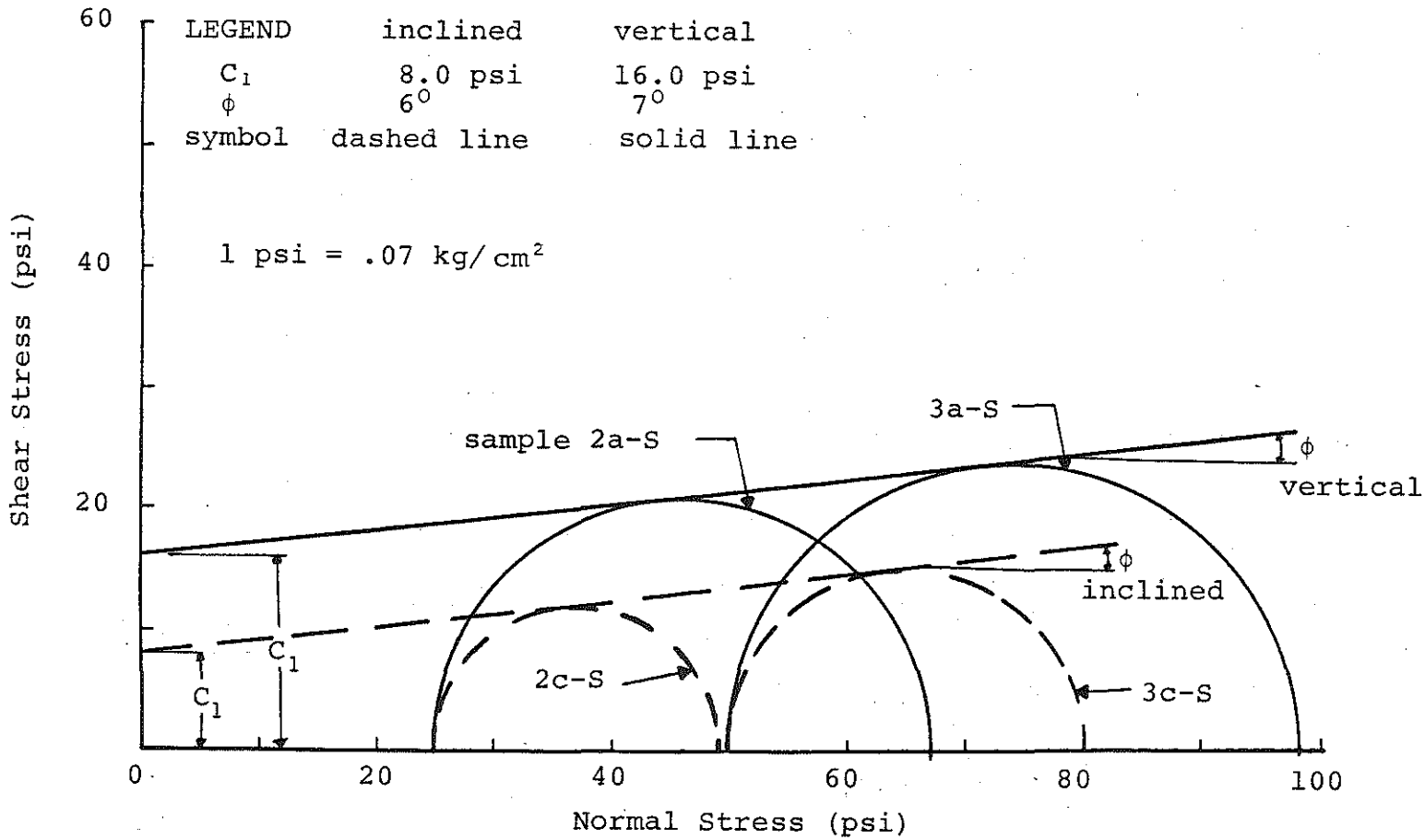

FIGURE 5.6 Mohr Circle Diagrams and Failure Envelopes for Vertical and Inclined Varved Clay Samples, Site 4, Upper Peninsula.

ε_t = total axial vertical strain, and

n, m = regression constants.

Rewriting equation 5.1 in a linear form yields:

$$\frac{\varepsilon_t}{S_d} = n + m\,\varepsilon_t \qquad (5.2)$$

This equation indicated that on a plot of (ε_t/S_d) versus (ε_t) the data will follow a straight line. The parameter n is the intercept, while m is the slope of the line. The stress-strain data were modeled using equation (5.1) and least square fitting technique. The regression constants n and m and the coefficient of correlation r^2 are listed in Tables 5.1 and 5.2 for the lower and upper peninsula test sites respectively. Examination of the stress-strain curves of Appendix C indicated that, in all tests, the higher the confining pressure the higher the principal stress difference at failure. This was expected and consistent with results reported in the literature. Study of the values of the regression constants (n and m) indicated that the higher the confining pressure the lower the values of n and m. This is shown in Figure 5.7 for site 1 of the lower peninsula. Attempts were made to model n and m as a function of the cell pressure and thereby be able to rewrite equation 5.1 in terms of confining pressure. These attempts, however, did not lead to conclusive results. The general consensus, however, indicated that, in general, for a constant principal stress difference the higher the confining pressure the lower the total axial vertical strain.

5.3 Cyclic Triaxial Tests

The application of stress to pavement materials by moving wheel loads is transient in nature. Consequently, any material characterization technique should be one in which the loads applied to specimens are also transient. The repeated load triaxial test is one such test in which

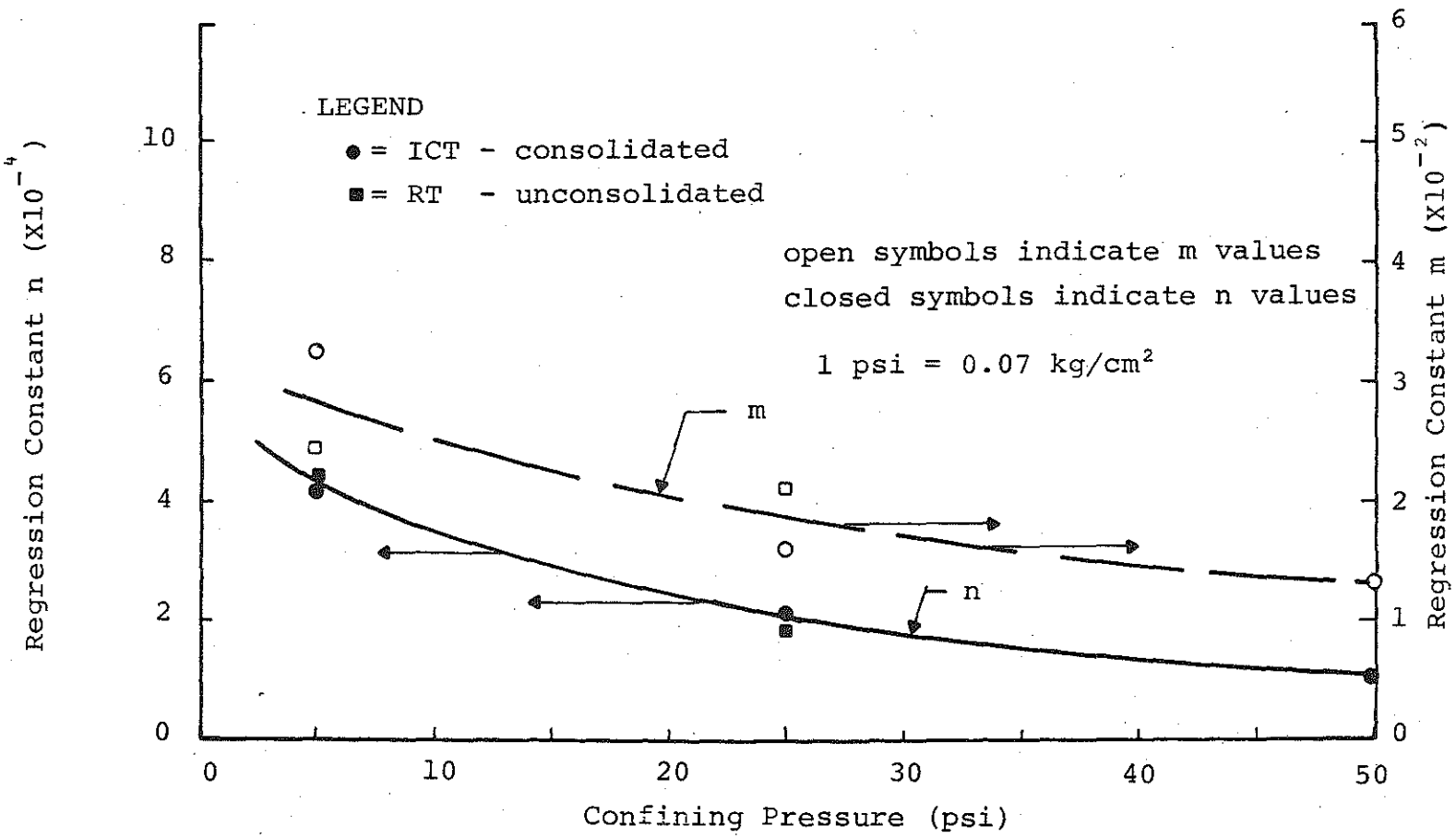

FIGURE 5.7 The Regression Constants m and n of Equation 5-1 Versus Confining Pressure, Site 1, Lower Peninsula.

samples of the soils or paving materials are placed in the cell and subjected to confining and axial stresses, just as in the static triaxial test. The difference, however, is that application of the axial stress to the sample in the cell is cycled or repeated. The repeated application of axial stress does not duplicate applied stresses in the field, but more realistically represent the form of stress applied to roadbed materials by moving traffic. In this research project, the cyclic loads were applied using a MTS closed loop electrohydraulic system (see Appendix A). Also, the sinusoidal wave form of the system was selected, which closely duplicates the applied stresses in the field [7, 23, 50]. The capability of the MTS system in simulating the transient nature of the traffic loading was recognized by several researchers [19, 23, 29, 30] who have been using the cyclic triaxial test for studying dynamic properties of pavement and subgrade materials. It should be noted that the MTS system did not produce exactly the same load input on every cycle; this characteristic was also reported by Lentz [23]. The variation in principal stress difference $(\sigma_1 - \sigma_3)d$ (especially in the first one hundred cycles) ranged from approximately two to five percent of the average principal stress difference. After the first one hundred cycles, the magnitude of the cyclic load was more consistent, although there was some variation from cycle to cycle throughout each test. These variations of the principal stress difference are mainly a function of the system's pump and fluid and the accuracy of the load cell.

The cyclic test program of this project calls for three cyclic triaxial tests to be performed on each test material and for each designated confining pressure. The purpose of these tests were 1) to provide information needed to study the cumulative nature of the axial and radial permanent deformations and the axial and radial resilient response of the subgrade soils, and 2) to study

the effects of stress level on item (1) above. In the next two sections, an investigation and study of the factors which affect the plastic and elastic responses of the test materials will be presented. These factors include:

a. number of load repetitions (N),
b. confining pressure (σ_3),
c. cyclic principal stress difference $(\sigma_1 - \sigma_3)_d$,
d. moisture content (w),
e. stress history,
f. consolidation.

5.3.1 Effect of Test and Sample Variables on the Axial Plastic Response

Examination of Figures 4.8 through 4.16 and C.7 through C.13 and analyses of the data listed in Tables C.2 have directed that the axial permanent strain is influenced by the following test variables.

5.3.1.1 Number of Load Repetitions

Before any attempt can be made to establish a limiting subgrade stress and/or strain criterion to be used in different pavement design methods, it is necessary to be able to predict the effect of number of load repetitions on permanent deformation. To accomplish this, the results from the cyclic triaxial tests were reduced. Typical data of permanent strain versus number of load applications plotted on arithmetic scales are shown in Figure 5.8. It should be noted that most of the cyclic tests were conducted up to thirty thousand cycles (unless failure occurs). In Figure 5.8, however, only the first one thousand cycles are plotted to show greater detail at low number of load repetitions. Examination of Figure 5.8 showed that the rate of accumulation of permanent strain is high in the first one hundred load applications and decreases as the number of load repetitions continue to increase. This observation can be explained by considering the general mechanisms of soils under

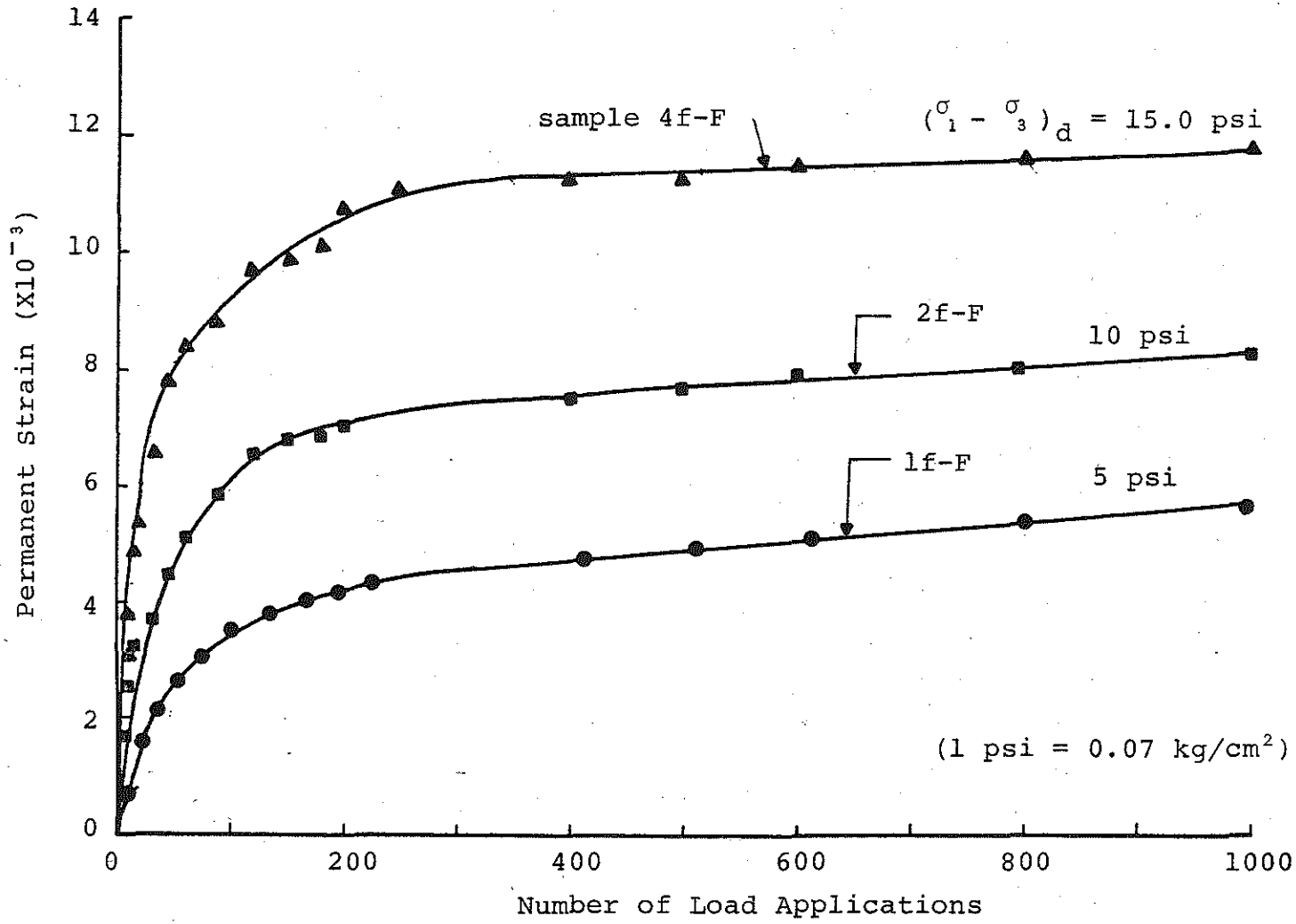

FIGURE 5.8 Typical Plot of Permanent Strain Versus Number of Load Cycles Under Confining Pressure of 5 psi, Site 2, Lower Peninsula.

dynamic loading. The energy applied to the sample during a loading cycle is partly stored as elastic strain energy and partly dissipated within the material causing plastic deformation, which is the result of crushing the grains at the particle contact points and intraparticle sliding. When the load is applied, the elastic and plastic components of the deformation will take place simultaneously until the rearrangement of particles results in a structural equilibrium. During unloading, the elastic strain energy stored during compression will be released, causing the soil skeleton to expand. This expansion will again cause some particles to slide over one another causing further particle rearrangements. It should be noted that a part of the energy input is lost as heat is generated by particle movements during loading and unloading. Also, during unloading, a part of the strain energy is not recovered, which results in a net permanent strain at the end of the load cycle. When the new particle arrangements are subjected to a second load cycle, elastic and plastic compression will again occur. This time the compression will commence from more stable conditions of the soil skeleton than existed during the first application of load. Thus, less crushing and sliding will occur to reach an equilibrium condition than took place during the first cycle. Therefore, the net permanent strain during the second cycle is less than that of the first cycle. Furthermore, each subsequent load cycle results in further rearrangement of particles into a more and more stable structure. This process is manifested by a large permanent strain during the first cycle of load followed by smaller increments of permanent strain due to each succeeding load cycle. Similar data were also reported by several investigators [7, 8, 23, 57, 101, 102].

Further examination of Figure 5.8 suggested that the relationship between permanent strain and the number of load repetitions can be described by some forms of logarithmic functions [23, 19]. Figure 5.9 shows typical

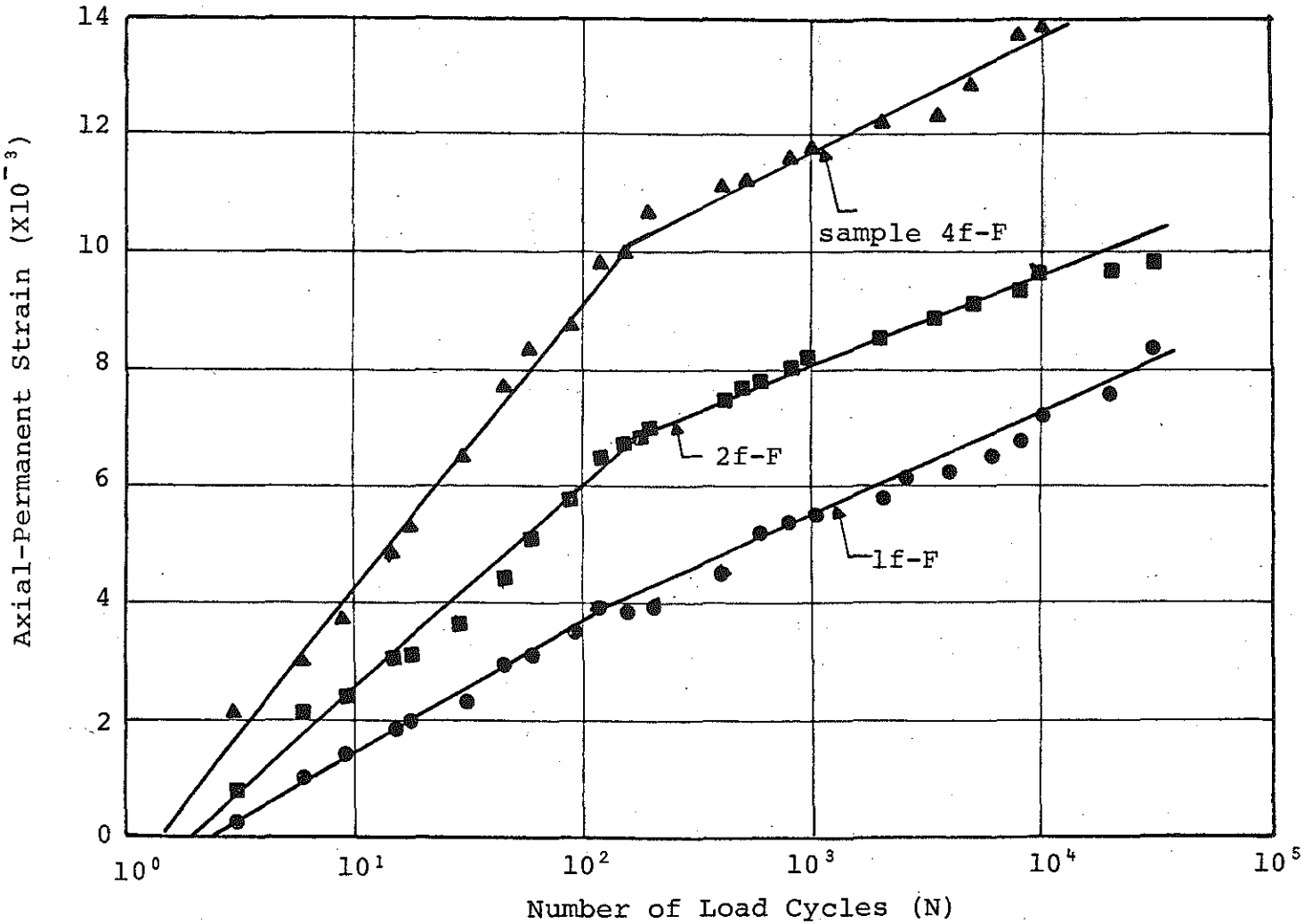

FIGURE 5.9 Typical Plots of Permanent Strain Versus Number of Load Cycles Under Confining Pressure of 5 psi, Site #2, Lower Peninsula.

permanent strain data plotted, on arithmetic scale, against the logarithm of the number of load repetitions. Figure 5.10, on the other hand, shows the same data plotted as the logarithm of permanent strain versus the logarithm of the number of load repetitions. Studies of Figures 5.9 and 5.10 revealed that both plots displayed certain characteristics. These include: 1) the relationship between permanent strain and the number of load applications can be expressed by logarithmic functions representing two discontinued straight lines, and 2) the two straight lines intersect around cycle number 100. Equations 5.3 and 5.4 were used to model the data in Figures 5.9 and 5.10 respectively.

$$\varepsilon_p = u(100-N)(A_1+B_1 \log N) + u(N-100)(A_{100}+B_{100}\log N) \quad (5.3)$$

$$\varepsilon_p = u(100-N)(a_1 N^{b_1}) + u(N-100)(a_{100} \cdot N^{b_{100}}) \quad (5.4)$$

where ε_p = cumulative permanent strain

N = number of load repetitions

A_1, A_{100} = the values of ε_p at N=1 and 100 respectively (semi-log plot)

B_1, B_{100} = the slopes of the straight lines between N=1 and 100 and N>100 respectively (semi-log plot)

a_1, a_{100} = the values of the logarithm of ε_p at N=1 and 100 respectively (log-log plot)

b_1, b_{100} = similar to B_1 and B_{100} but for the log-log plot

$u(100-N)$ = a step function the value of which is defined as $u(100-N) = \begin{cases} 0.0 \text{ for } (100-N)<0.0 \\ 1.0 \text{ for } (100-N)>0.0 \end{cases}$

$u(N-100)$ = a step function the value of which is defined as $u(N-100) = \begin{cases} 0.0 \text{ for } (N-100)<0.0 \\ 1.0 \text{ for } (N-100)>0.0. \end{cases}$

The straight lines in Figures 5.9 and 5.10 were determined using least square fitting technique. The regression parameters and the coefficient of correlation are

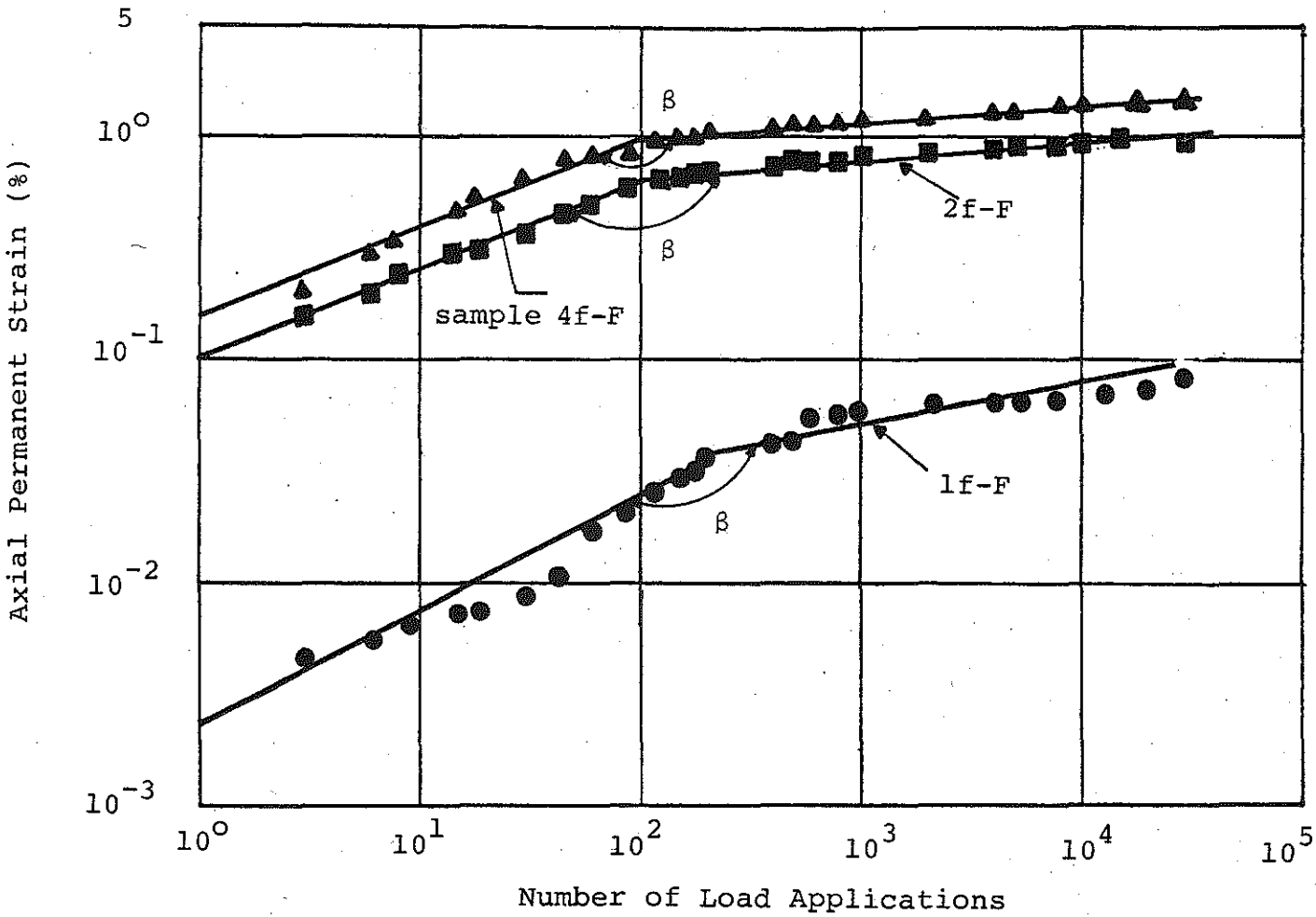

FIGURE 5.10 Typical Axial Permanent Strain versus Number of Load Applications for Samples Consolidated Under a Confining Pressure of 5 psi and Tested Using Different Cyclic Stress Ratio, Site 2, Lower Peninsula.

listed in the figures. Examination of the values of the regression parameters indicated that Equation (5.4) appears to model the data slightly better than Equation 5.3. This is due to a higher coefficient of correlation of Equation 5.4. These results were found to be consistent with those reported by Lentz [23] and Yoder and Witman [19]. Consequently, all other analyses in this study will be based on Equation 5.4.

Table 5.3 provides a summary of the values of the regression constants of all the test data for the lower peninsula test sites. The angle β in the table indicates the angle of intersection of the two straight lines as shown in Figure 5.10 and Appendix C. A study of the values of the angle β listed in Table 5.3 indicates that β decreases as the principal stress ratio increases. For a stress ratio of 1.0, β reaches its limiting value of 180^{o}. For this case, both slopes b_1 and b_{100} assume one limiting value which is proportional to the coefficient of consolidation of the sample. The significance of the angle β may be revealed by considering the cumulative rate of permanent strain during the first 100 load cycles ($\dot{\varepsilon}_{p1}$) relative to the rate beyond 100 cycles ($\dot{\varepsilon}_{p100}$). The lower the angle β, the higher the ratio of $\dot{\varepsilon}_{p1}/\dot{\varepsilon}_{p100}$ and the higher the damage delivered to the sample during its initial loading phase. One hundred cycles may not be significant when considering the life period of a pavement section which may be subjected to 100,000 or 1,000,000 load repetitions. However, for a pavement section newly opened to traffic, the first 100 load repetitions will set the initial border of the rut channel on the pavement surface. Consequently, the traffic distribution over the pavement will be narrowed and directed toward the rut channel which will accelerate pavement rutting.

The permanent strain data of the upper peninsula test sites are shown in Figures 4.32 through 4.35. The data show a behavior similar to that of the lower peninsula test sites; the cumulative axial permanent strain increases as the number of load repetitions increases. Due

TABLE 5.3 Regression - Parameters for Least Squares Fit of Equation 5.4

Site-Number Location	Sample Number	σ_3 (psi)	$\frac{(\sigma_1-\sigma_3)_d}{\sigma_3}$	a_1 ($X10^{-4}$)	a_{100} ($X10^{-4}$)	b_1 ($X10^{-1}$)	b_{100} ($X10^{-1}$)	r_i^2	r_{100}^2	β	Test Mode (CT)
	2a-F	5	2.0	10.90	32.25	3.8526	1.2319	0.9784	0.9806	165^0	C
	4a-S	50	0.5	189.15	--	3.9717	--	0.98423	--	**	C
	2b-F	5	1.0	6.450	25.910	4.1604	0.02591	0.9402	0.8953	163^0	C
	1c-F	5	3.0	57.90	124.13	2.9158	1.4318	0.9889	0.9365	172^0	C
	2d-F	25	1.0	25.026	137.494	4.3428	0.8224	0.91256	0.8989	163^0	C
S1-LP	3d-F	5	2.0	28.94	74.37	3.6355	1.4909	0.9709	0.9873	170^0	U
	4d-F	25	2.0	158325	--	7.523	--	0.99053	--	**	C
	1e-F	5	3.0	13.41	15.61	2.894	3.098	0.9459	0.9716	178^0	U
	2e-S	25	1.5	110.25	--	2.6704	--	0.97961	--		U
	1f-F	5	1.0	2.220	6.160	5.3192	2.4993	0.97537	0.9593	166^0	U
	2f-S	25	1.5	299.01	404.06	0.9057	0.1195	0.8100	0.9187	175^0	C
	3f-S	25	1.0	18.66	*	3.950	*	0.9957	*		U
	1a-F	25	2.0	183.0	*	9.3128	*	1.000	*	**	U
	3a-S	25	1.5	127.3	*	5.1379	*	0.9541	*	**	U
	1b-S	5	1.0	3.6708	5.715	3.025	1.939	0.9398	0.9954	169^0	C
	3b-S	25	1.0	3.790	26.326	6.0064	1.9292	0.9738	0.9488	167^0	C
	4b-S	5	1.0	3.0745	5.7145	3.41520	1.9393	0.9557	0.9954	170^0	C
	4b-F	25	1.5	122.02	*	2.9144	*	0.9796	*		C
	1c-F	5	3.0	3.694	48.640	2.0783	1.609	0.9321	0.9938	176^0	U
S2-LP	2c-F	5	1.0	3.0744	5.715	3.4152	1.9393	0.9557	0.9954	171^0	C
	3c-F	25	1.0	32.8	148.0	2.845	2.824	0.9660	0.9871	168^0	U
	4c-S	50	0.70	99.20	*	2.802	*	1.000	*		C
	2d-S	5	2.0	27.58	114.17	3.589	1.058	0.850	0.9882	165^0	C
	1e-F	5	2.0	5.744	19.064	4.1623	1.280	0.9382	0.9896	177^0	U
	2e-F	5	1.0	0.1528	8.501	5.963	6.592	0.8226	0.9656	168^0	U
	3e-F	25	2.0	183.01	*	0.9313	*	1.000	*		C

TABLE 5.3 Continued

Site-Number Location	Sample Number	σ_3 (psi)	$(\sigma_1-\sigma_3)_d/\sigma_3$	a_1 ($\times 10^{-4}$)	a_{100} ($\times 10^{-4}$)	b_1 ($\times 10^{-1}$)	b_{100} ($\times 10^{-1}$)	r_1^2	r_{100}^2	β	Test Mode (CT)
S2-LP	1f-F	5	1.0	1.990	21.41	5.1429	1.320	0.9384	0.8680	163°	C
	2f-F	5	2.0	10.506	46.843	3.796	0.7673	0.9966	0.9701	164°	C
	3f-F	25	1.5	18.341	*	9.534	*	0.9812	*		C
	4f-F	5	3.0	14.22	73.29	4.322	0.6647	0.9821	0.9632	165°	C
S3-LP	1a-F	5	3.0	55.2065	132.953	3.3236	1.6117	0.9774	0.9686	177°	C
	2a-F	25	1.5	90.001	279.323	3.0955	0.7032	0.9706	0.9877	173°	C
	3a-F	25	2.0	99.065	117.497	2.0699	1.8047	0.9954	0.9704	179°	C
	2b-F	5	2.0	27.2111	33.054	0.9636	0.6091	0.9550	0.9528	178°	C
	4b-F	25	1.0	78.012	92.05	4.3214	0.673	0.9816	0.9776	173°	C
	2c-F	5	1.0	2.810	6.075	2.039	1.068	0.9541	0.9771	172°	C
	2e-S	5	2.0	59.11	95.13	1.91203	0.86736	0.9724	0.9850	176°	U
S4-LP	1a-F	5	1.0	3.646	18.871	5.269	2.219	0.9951	0.9275	167°	C
	4a-F	5	1.162	3.460	3.460	4.859	2.075	0.9832	0.9463	168°	C
	2d-F	25	0.50	41.056	97.131	3.245	1.863	0.9947	0.9072	172°	C
	2e-F	25	1.0	64.401	162.552	4.353	2.551	0.9837	0.9914	170°	C
	3e-F	5	2.0	15.155	82.554	5.747	2.334	0.9589	0.8980	167°	C

* samples failed at less than 30,000 number of load applications

** samples failed at less than 100 number of load applications

to the nature and variability of the varved clay samples, however, two similar samples from the same test site did not show similar behavior when tested under the same confining pressure and cyclic load. Consequently, no further studies were performed and the test data were judged as erratic.

5.3.1.2 Confining Pressure

For the same cyclic stress ratio $(\sigma_1-\sigma_3)_d/\sigma_3$, the higher the confining pressure the higher the cumulative permanent strain. Figure 5.11 shows plots of the logarithm of permanent strain versus the logarithm of the number of load repetitions for two samples tested under the same cyclic stress ratio and different confining pressures. It can be seen that the higher the cell pressure the higher the permanent strain.

Recall that the results of incremental creep tests and/or ramp tests have indicated that the higher the confining pressure the lower is the ratio of sample strength to confining pressure. For example, if two samples were tested under confining pressures of 5 and 25 psi (.35 and 1.75 kg/m^2), then the strength ratio at failure $(\sigma_1-\sigma_3)_f/\sigma_3$ for the first sample is higher than that of the second sample. Further, if two identical samples were confined as above and then subjected to the same cyclic stress ratio $(\sigma_1-\sigma_3)_d/\sigma_3$ and if the cyclic principal stress difference $(\sigma_1-\sigma_3)_d$ is expressed as a percent of the sample strength, then this percentage will be lower for the sample with low confining pressure than that with high confining pressure. This is shown in Figure 5.12. The dashed curve in the figure is for samples tested under higher confining pressures than those represented by the solid curve. The cyclic stress ratio $(\sigma_1-\sigma_3)_d/\sigma_3$, however, is the same for both curves.

The above noted observations could also be seen by studying the permanent strain of the test samples after one single load application. This is represented by the values of the parameter a_1 in Table 5.3. Examination of

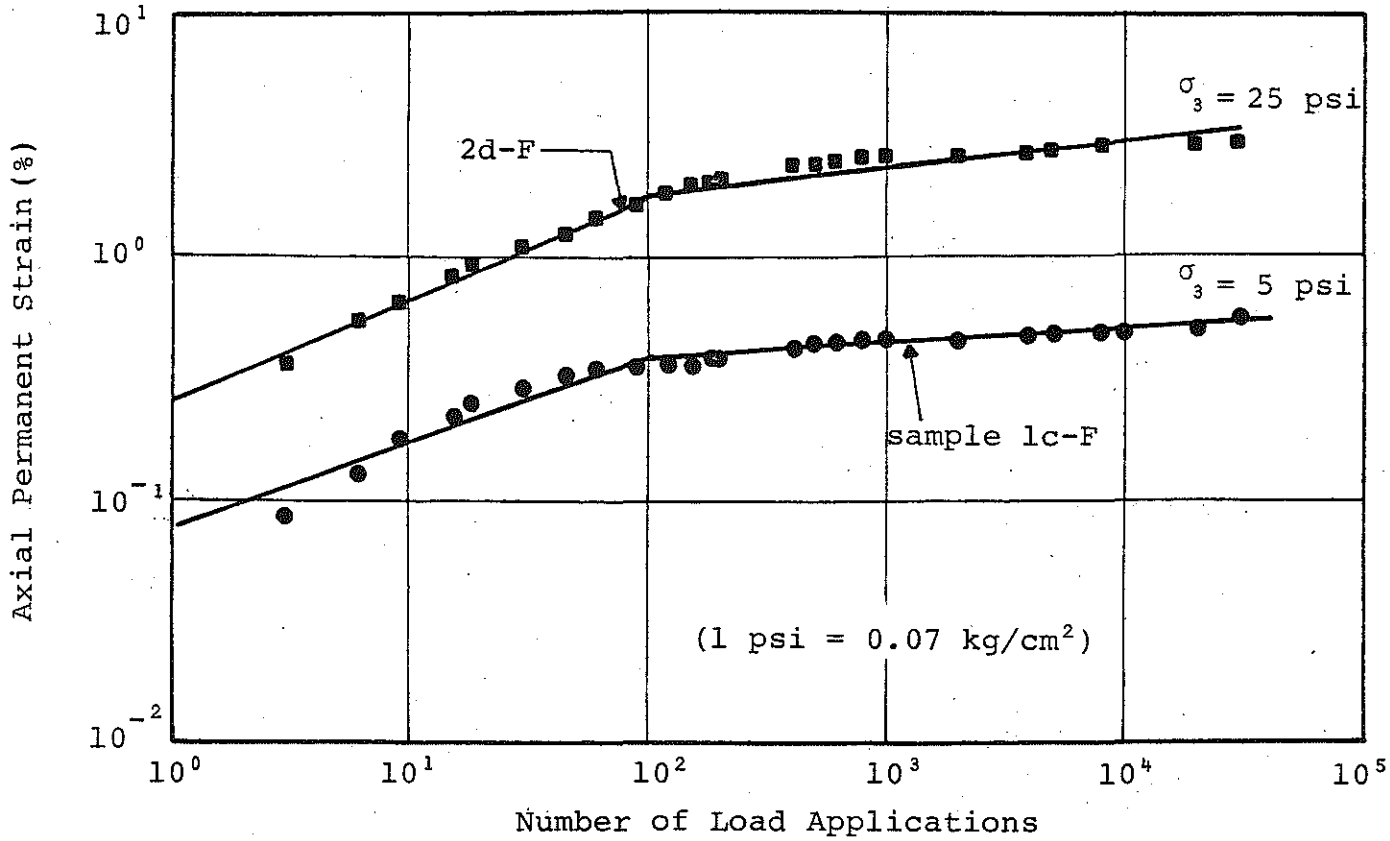

FIGURE 5.11 Axial Permanent Strain Versus Number of Load Applications for $(\sigma_1 - \sigma_3)_d/\sigma_3 = 1.0$ and Different Confining Pressures, Site 1, Lower Peninsula.

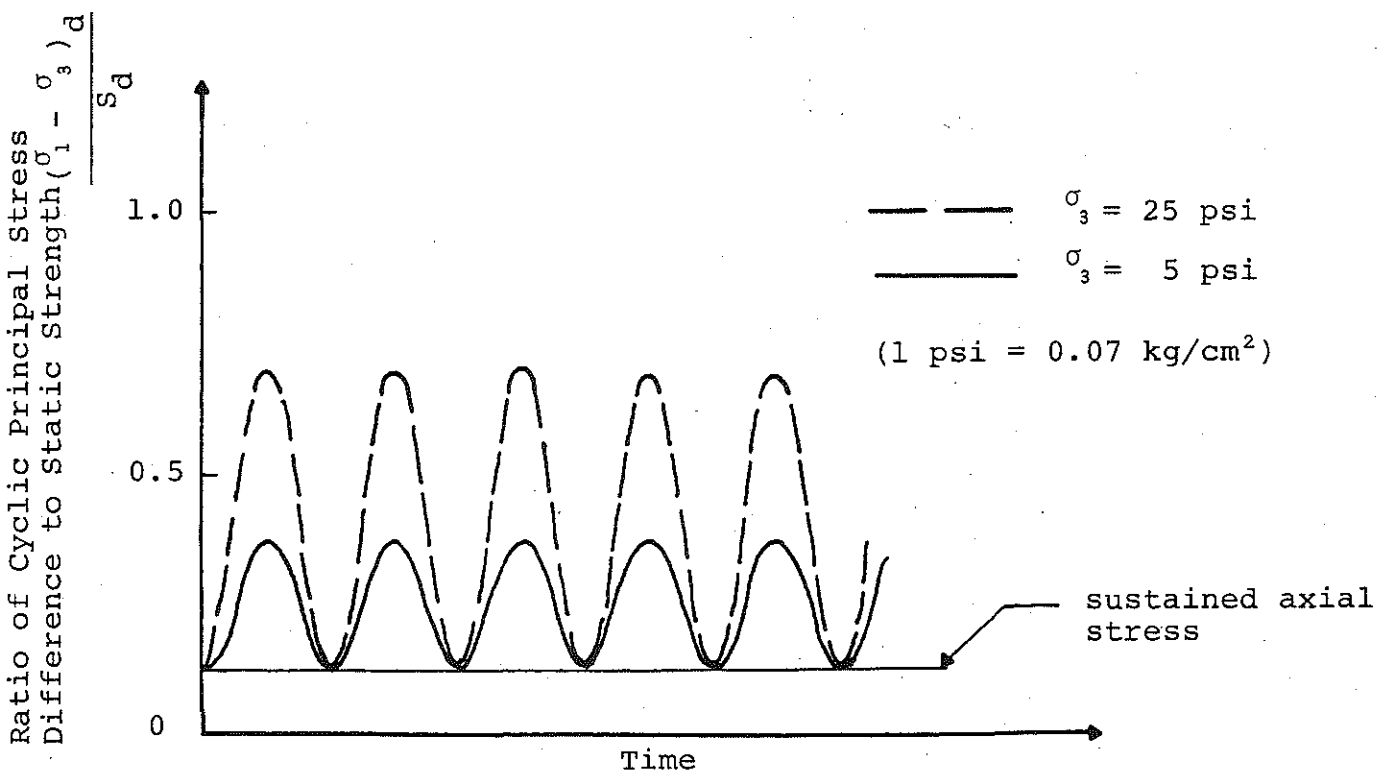

FIGURE 5.12 Cyclic Principal Stress Difference as Percent of Sample Strength Versus Time for Samples Tested at the Same Cyclic Stress Ratio and Different Confining Pressure.

Table 5.3 indicated that for a constant cyclic stress ratio the higher the cell pressure the higher the a_1 and consequently the higher the permanent strain after the first load repetitions. A similar conclusion was also made by several other investigators [23,101,105].

5.3.1.3 Stress Level

For a constant confining pressure, the higher the cyclic principal stress difference the higher the permanent strain after the first load cycle and the higher the rate of accumulation of permanent strain thereafter. Figure 5.13 displays the results of six different samples tested up to 30,000 load applications. For each sample, the cyclic principal stress difference was constant throughout the test. Three of these samples were tested under a confining pressure of 5 psi (.35 kg/cm^2). The cell pressure for the other three samples was 25 psi (1.75 kg/cm^2). It can be seen from the figure that the higher the stress level, the higher the permanent strain.

Recall that Equation 5.4 was used to model the permanent strain as a function of the number of load applications. The parameters a_1,b_1 and a_{100},b_{100} of the equation were calculated using a least square curve fitting technique and they are listed in Table 5.3. Figures 5.14 and 5.15 show the principal stress difference plotted against a_1,a_{100} and b_1,b_{100} respectively. Examination of the figures indicated that the higher the principal stress difference the higher the values of all four parameters and consequently the higher the permanent strain. This suggested that a relationship between principal stress difference and the regression constant could be developed and it may take an exponential function form. This relationship, when it is developed, will not be universal and it will not be useful for any other data. This is so because the permanent strain and ultimately the parameters of Equation 5.4 are dependent on several other variables. These include consolidation,

FIGURE 5.37 Normalized Cyclic Stress-Strain Ratio for Five Different Materials Subjected to 1,000,000 Load Repetitions.

ε_p = cumulative permanent axial strain @ desired No. load reps.

$\varepsilon_{0.95S_d}$ = axial strain @ 95% sample strength.

0.76 for the subballast materials,
0.85 for Michigan sand subgrade, and
0.98 for under-tie materials.

It should be noted that both the subballast and under-tie materials were classified as A-1-a according to the AASHTO soil classification (106). If the predesignated soil support value is superimposed on the above data (SSV=3.0 for A-6 and SSV≈10.0 for the under-tie), it follows that the SSV can be expressed using the following equation

$$SSV = 10 \frac{(\sigma_1-\sigma_3)_d}{S_d} \quad (f,\ N=10^6) \tag{5.7}$$

where the subscript (f, $N=10^6$) indicates failure at one million load applications. Equation (5.7) can be generalized as follows:

$$SSV = \alpha \frac{(\sigma_1-\sigma_3)_d}{S_d} \quad (f,\ N) \tag{5.8}$$

where α is constant depending on the number of load repetitions (N) and the subscript (f, N) indicates failure at N number of load applications.

Recall that (see section 5.4 above) the normalized model (equation 5.5) is a function of the number of load applications (N) and soil type. These observations suggested that (for each soil type) the parameters n and m of equation 5.5 can be expressed in terms of (N). Figure 5.38 shows a typical plot of the parameters n and m as function of (N). This functional relationship was found to be of the following form.

$$\begin{aligned} n &= a_n + b_n \ln N \\ m &= a_m + b_m \ln N \end{aligned} \tag{5.9}$$

The values of the regression constants a_n, b_n, a_m, and b_m are summarized in Table 5.4 for five different soil types.

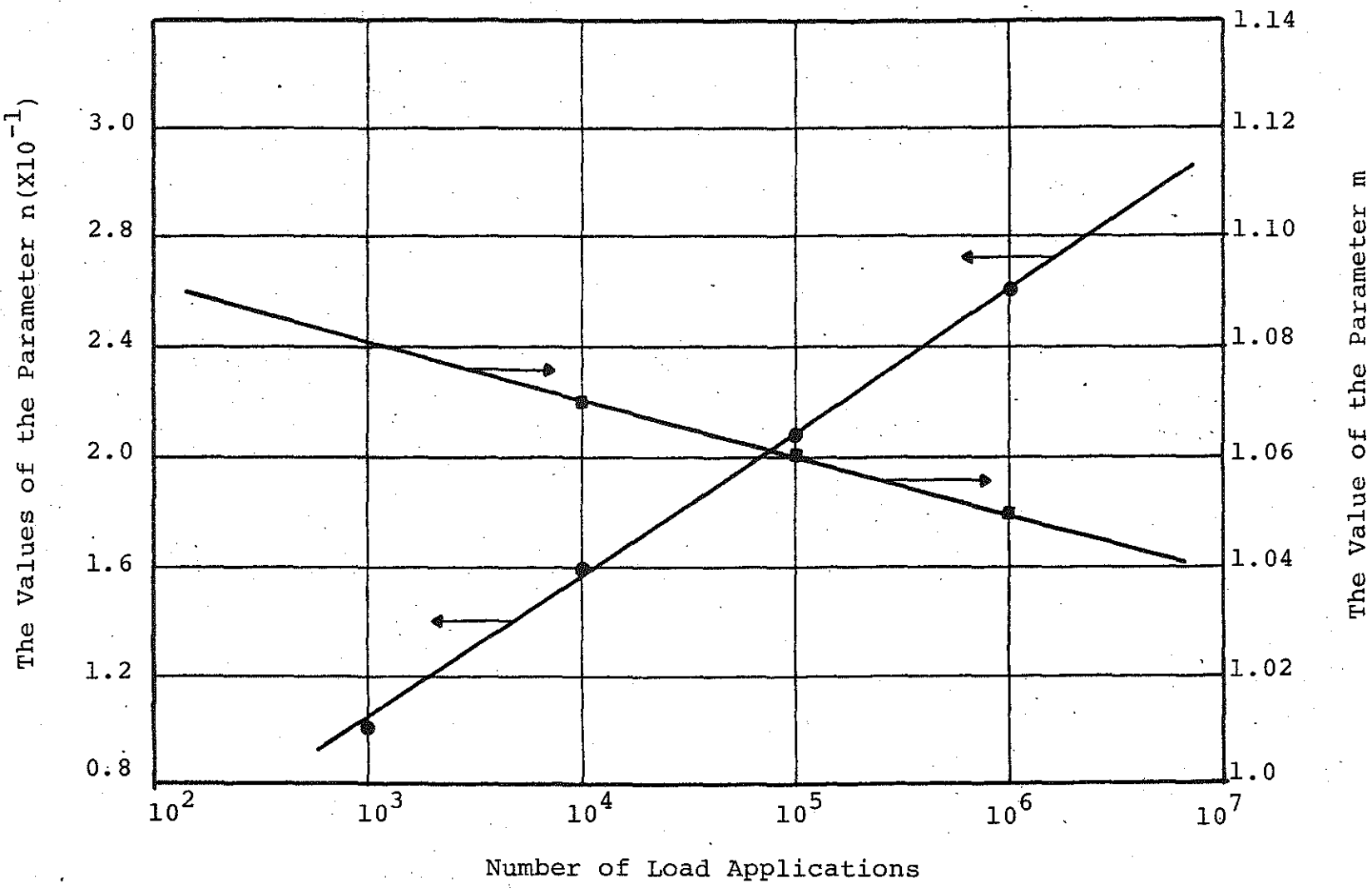

FIGURE 5.38 Typical Relationship Between Number of Load Applications and the Parameters n and m of Equation (5.5) for Subbalast Materials.

TABLE 5.4 The Values of the Regression Constants a_n, b_n, a_m and b_m for Five Different Materials

Soil	Soil Type	n		m	
		$a_n(X10^{-2}$	$b_n(X10^{-2})$	$a_m(X10^{-2})$	$b_m(X10^{-2})$
Undertie	1	-3.69700	1.74370	88.35894	-0.45769
Sand	2	-4.50225	2.26355	101.40517	-0.72966
Subballast	3	-4.82732	2.25408	111.57562	-0.46162
	4	No data available			
Clay	5	-12.66488	2.52718	283.89983	-7.44985
A-6	6	-13.05600	6.97645	331.63359	-7.91234

Substituting equations (5.9) into equation (5.5) yields

$$\frac{\varepsilon_p}{\varepsilon_{.95}S_d} = \frac{a_n + b_n \ln N}{\frac{S_d}{(\sigma_1-\sigma_3)_d} - (a_m + b_m \ln N)} \qquad (5.10)$$

which expresses the strain ratio as a function of the stress ratio and soil type. It should be noted that equation (5.10) is independent of confining pressure, water content and state of compaction.

5.6 Limiting Stress and Strain Criterion

The significance of the normalized model and the SSV correlation is that the model itself could be used for three different purposes. These purposes are:

01. To predict the cumulative permanent strain of the subgrade materials due to dynamic loadings once the static stress-strain characteristic is known.
02. To be able to calculate and better understand the soil support value of the materials.
03. To establish a limiting stress criteria that could be used in the pavement design.

Item 1 above was discussed in detail in references [8,23, 77]. Item 2 was discussed in Section 5.5. Item 3 could be accomplished using the normalized model. For example, assume that a pavement section is to be constructed using Michigan clay soils as subgrade materials and to be subjected to one million 18 kip equivalent single axle load. What are the limiting conditions, so that at the end of the life cycle the subgrade will experience rut depth (permanent strain) equal to 50% of the static strain at failure? The answer, using Figure 5.36, is that the limiting condition of the design should be that the traffic induced stress in the subgrade be no more than 40% of its static strength. This limiting condition could be related to the pavement thickness and consequently to the structural number.

The benefits of this limiting strain criteria could be maximized if it is incorporated into a pavement management system computer program. Such a program could then analyze current construction costs for the limiting condition versus future maintenance and rehabilitation costs.

5.7 Implementation

5.7.1 General

Assume that a pavement section is to be constructed on clay or sand subgrade soil. The highway engineer is inested to know the following information:

(a) estimate of the soil support value,
(b) estimate of the rut depth of the subgrade materials,
(c) the relative conditions of the subgrade at the end of the pavement life cycle, and
(d) alternative design options so as to maximize benefits at the lowest cost.

This information could be obtained by the highway engineer, prior to design and construction, using the following steps:

(1) Collect undisturbed as well as bag samples of the subgrade materials in question according to the AASHTO soil classifications using the bag samples.
(2) Classify the subgrade materials.
(3) Estimate the soil support value of the materials using Figure 5.36 and equation 5.7.
(4) Select the desired life cycle of the pavement.
(5) Conduct a conventional triaxial test using the undisturbed soil samples with the proper density and water content.
(6) Select a trial pavement section and the appropriate parameters of equation 5.6 if the AASHTO design procedure is to be used. Otherwise, select the proper parameters for the desired design procedure.
(7) Calculate, using any available computer program such as the Chevron program, the induced and sustained

stresses in the subgrade due to the 18 kips single axle load and the pavement weight respectively. These stresses shall include the vertical and lateral stresses.

(8) Calculate the stress ratio which is equal to the difference between the total vertical (σ_1) and lateral (σ_3) stresses divided by the sample strength (S_d) obtained in Step 5 above. The total vertical and lateral stresses herein include the traffic induced stresses as well as the stresses caused by the pavement section above the subgrade.

(9) Use the results of Steps 5 and 8 above and the appropriate parameters from table 5.4 as an input to equation 5.10 and calculate the strain ratio as well as the estimated rut depth of the subgrade materials.

(10) If the strain ratio (the ratio of permanent strain of the subgrade to the static strain obtained in Step 6 above) is high (close to 1.0) then select another trial section (thicker base and subbase) and go to Step 6. Otherwise, the subgrade is expected to fail at the end of the life cycle.

(11) Use the estimated SSV and the parameters of Step 6 above as input to the AASHTO design equation or charts to back calculate the life cycle of the pavement section in question.

(12) If the calculated life of the pavement section in question is not compatible to the estimated life then go to Step 5.

The above implementation steps are summarized in a flow-diagram that is presented in Figure 5.39.

5.7.2 Numerical Example

Assume that a clay soil classified as type 5 material is to be used as subgrade for a three feet thick flexible pavement section. The estimated applied vertical

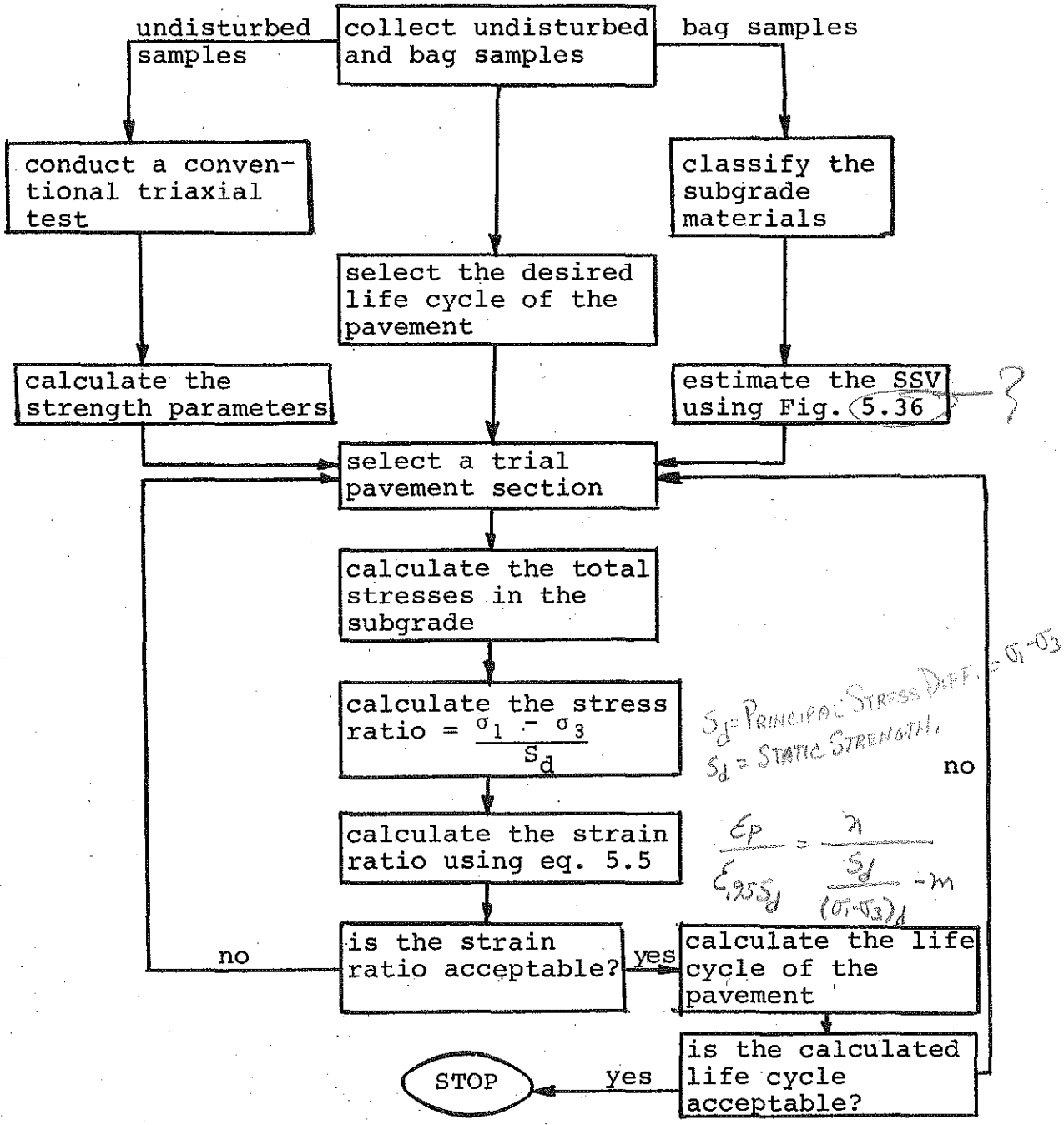

FIGURE 5.39 FLOW CHART OF THE IMPLEMENTATION.

Fig 5.36 = PP 189

and lateral stresses on the subgrade, due to the weight of the pavement section and an 18 kips equivalent single axle load, were found to be 7 and 3 psi respectively. A conventional triaxial test on representative sample of the compacted subgrade was conducted using a confining pressure of 3 psi (equal to the estimated lateral stress). The strength of the sample was found to be 13 psi and the strain at 95 percent strength was measured as 7.2%.

(a) The estimated soil support value of this material using Figure 5.36 is 4.92. This also could be calculated as $(\frac{10}{n+m})$ where n and m are the parameters of equation 5.10 calculated for N = 1,000,000 using the appropriate constants from Table 5.4.

PP189 ← Figure 5.36
PP195 ← equation 5.10
PP194 ← Table 5.4

(b) The stress ratio that the material will be subjected to in the field is

$$\frac{\sigma_1-\sigma_3}{S_d} = \frac{7-3}{13} = 0.308$$

(c) Calculate the strain ratio for different number of load applications using equation 5.10 with the proper parameters from Table 5.4 and a stress ratio of 0.308.

PP 194

N	Strain Ratio
100,000	.143
1,000,000	.174
10,000,000	.198

(d) Calculate the cumulative permanent strain (ε_p) of the subgrade. $\varepsilon_p = \varepsilon_{.95S_d}$ x (strain ratio)

N	ε_p(%)
100,000	1.03
1,000,000	1.25
10,000,000	1.43

(e) Calculate the rut depth (RD) of the subgrade assuming that the stressed zone is 3 feet deep. The depth of the stressed zone could be calculated using any available computer program such as the Chevron program.

N	RD (inch)
100,000	.371
1,000,000	.450
10,000,000	.515

(f) If the rut depth is high then select thicker pavement section and recalculate steps b, c, d, and e.

(g) Calculate the number of 18 kips equivalent of the pavement section using the AASHTO design equation, the SSV of step a above and the estimated structural number of the different pavement components. Assume the calculated 18 kips equivalent is 7,000,000. This means that at 7,000,000 load repetitions a rut depth of 0.5 inch should be expected. If this rut depth is high, then the rut model controls the pavement performance. Different distress mode controls the pavement section in question for low rut depth value.

CHAPTER VI

CONCLUSIONS AND RECOMMENDATIONS

6.1 Conclusions

On the basis of the test results of this study and in the range of the test and sample variables, the following conclusions were drawn:

(1) The cumulative permanent strain of Michigan cohesive subgrade materials was found to be a function of several variables. These include the stress level and stress path, moisture content, density and confining pressure.

(2) For a given set of sample and test variables, Equation 5.4 was found to model the cumulative permanent strain at any number of load applications.

(3) At any confining pressure and number of load repetitions, the relationship between the cyclic principal stress difference and the cumulative permanent strain of one sample was represented by a hyperbolic function.

(4) The effect of the test and sample variables, mentioned in conclusion 1 above, on the cumulative permanent strain was minimized or eliminated using a normalization procedure discussed in Section 5.4. This procedure calls for the normalization of the cyclic principal stress difference with respect to the static strength and of the cumulative permanent strain relative to the static strain at ninety-five percent of the static strength.

(5) The normalized procedure yielded a normalized predicted model which was found to be unaffected by the type of test (incremental creep or ramp test) from which the normalizing parameters were obtained.

(6) A general predictive model of the plastic behavior of the test materials was developed using the normalization procedure. The input parameters of the model consisted of the static strength and the corresponding total strain of the material in question.

(7) The normalized predictive model shown in Figure 5.36 was found to be a function of soil type and number of load applications only.

(8) A correlation between the soil support values and the normalized predictive model of the material was developed. This correlation was based on a single point related to the AASHTO A-6 material and its assigned soil support value of 3.

(9) It was demonstrated that the normalized predictive model could be used to establish a limiting stress and strain criterion of the pavement materials under consideration.

6.2 Recommendations

The results of this investigation has led to the development of a normalized predictive model of the plastic strain of pavement materials. The model has demonstrated its ability to evaluate and predict the plastic behavior of several materials subjected to cyclic loadings. The input parameters of the model consisted of the static strength and the corresponding total strain of the material in question. The model was tested and evaluated using five different materials ranging from gravel and sand to clay and clayey silt. Further, a correlation was developed between the soil support value and the normalized predictive model of the materials. It should be noted that no knowledge was available at the time of the soil support value of the test materials. Rather, the correlation was based on a singular point related to the AASHTO A-6 material and its assigned soil support value of 3. Consequently, it is recommended that studies be continued so that the singularity point of the correlation is eliminated and wider base is established.

The development of the normalized predictive model offers a new understanding of the plastic behavior of the test materials. This model is based on relatively rapid static tests and it eliminates the need for a long and time consuming cyclic tests. However, the model was not checked or validated against some variables. It is recommended that

efforts be expended to check the validity of the predictive model for soils subjected to freeze-thaw cycles and to verify its predicting capability using measured rut depth data in the field. The interaction mechanism between the different pavement layers and its effects on the plastic strain should be investigated and incorporated into the normalized predictive model.

BIBLIOGRAPHY

BIBLIOGRAPHY

1. Wen-Kuh-Luo, "The characteristics of soils subjected to repeated loads and their applications to engineering practice." Japanese Society of Soil Mechanics and Foundation Enginering, Vol. 13, No. 1, 1973.

2. Seed, H. B. and Chan, C. K., "Effect of Duration of Stress Application on Soil Deformation Under Repeated Loading." Proceedings of the 5th International Conference on Soil Mechanics and Foundation Engineering, Paris, 1961.

3. Monismith, C. L., Ogawa, N., and Freeme, C. R., "Permanent Deformation Characteristics of Subgrade Soils due to Repeated Loading," Transportation Research Record 537, 1975.

4. Peattie, K. R., "A Fundamental Approach to the Design of Flexible Pavements," Proceedings of the International Conference on Structural Design of Asphalt Pavements, Ann Arbor, Michigan, August, 1962.

5. Dorman, G. M., "The Extension to Practice of a Fundamental Procedure for the Design of Flexible Pavements," Proceedings of the International Conference on Structural Design of Asphalt Pavements, Ann Arbor, Michigan, 1962.

6. Whiffin, A. C. and Lister, N. W., "The Application of Elastic Theory to Flexible Pavements," Proceedings of the International Conference on Structural Design of Asphalt Pavements, Ann Arbor, Michigan, 1962.

7. Baladi, G. Y. and Boker, T. D., "Resilient Characteristics of Michigan Cohesionless Roadbed Soils in Correlation to the Soil Support Values," Final Report, Grant 75-1679, Division of Engineering Research, Michigan State University, 1978.

8. Lentz, R. W. and Baladi, G. Y., "Simplified procedure to characterize permanent strain in sand subjected to cyclic loading," International Symposium on Soil under Cyclic and Transient Loading, 1980.

9. Dorman, G. M. and Metcalf, C. T., "Design Curves for Flexible Pavements Based on Layered System Theory," HRB, Highway Research Record 71, pp. 69-84, 1965.

10. Barker, W. R. and Brabston, W. N., "Development of a Structural Design Procedure for Flexible Airport Pavements," U.S. Department of Transportation, Federal Aviation Administration, Rept. RD-74-199, 1975.

11. Witczak, M., "Design of Full-Depth Asphalt Airfield Pavements," Proceedings, 3rd International Conference on the Structural Design of Asphalt Pavements, 1972.

12. Chou, Y. T., and Hutchinson, R. L. and Ulery, H.H. Jr., "Design Method for Flexible Airfield Pavements," TRB, NAS, Transportation Research Record #421, 1974.

13. Yoder, E. J. and Witczak, M. W., "Principles of Pavement Design," John Wiley and Sons, Inc., New York, 1959.

14. AASHO Committee on Design, AASHO INTERIM GUIDE FOR DESIGN OF PAVEMENT STRUCTURES. 1972, American Association of State Highway Officials, Washington, D.C., 1972.

15. Barksdale, R. D., "Compressive Stress Pulse Times in Flexible Pavements for use in Dynamic Testing," HRB, Highway Research Record No. 345, 1971.

16. Finn, F. N., Nair, K., and Monismith, C. L., "Applications of Theory in the Design of Asphalt Pavements," Proceedings of the 3rd International Conference on the Structural Design of Asphalt Pavements, London, England, 1972.

17. AASHO Committee on Design, AASHO Interim Guide for Design of Pavement Structures 1962, American Association of State Highway Officials, Washington, D.C., 1962.

18. Kenis, William J., "Predictive Design Procedures - A Design Method for Flexible Pavements Using the VESYS Structural Subsystem," Proceedings of the 4th International Conference - Structural Design of Asphalt Pavements, Vol. I, Ann Arbor, Michigan, 1977.

19. Yoder, E. J., and Witczak, M. W., "PRINCIPLES OF PAVEMENT DESIGN," 2nd Edition, John Wiley and Sons, Inc., New York, 1975.

20. Monismith, C. L., and Finn, F. N., "Flexible Pavement Design: A State of the Art 1975." Proceedings, Pavement Design for Practicing Engineers, specialty conference, Georgia Institute of Technology, 1975.

21. Pell, P. S. and Brown, S. F., "The characteristics of Materials for the design of Flexible Pavement structures," Proceedings, 3rd International Conference, 1972.

22. Van Til, C. J., McCullough, B. F., Vallerga, B. A., and Hicks, R. G., "Evaluation of AASHO Interim Guides for Design of Pavement Structures," NCHRP 128, Washington, D.C., 1972.

23. Lentz, Rodney W., "Permanent Deformation of Cohesionless Subgrade Material under Cyclic Loading," Ph.D. Dissertation, Michigan State University, East Lansing, Michigan, 1979.

24. Skempton, A. W. and Northey, R. D., "The Sensitivity of Clays," Geotechnique, Vol. III, No. 1, 1952.

25. Chou, V. T., "Analysis of Subgrade Rutting in Flexible Airfield Pavements," Transportation Research Record 616, 1976.

26. Deen, R. C., Southgate, H. F. and Havens, J. H., "Structural Analysis of Bituminous Concrete Pavements," Research Report, Kentucky Department of Highways, KYP-SG HPR-1(6) Part III, Lexington, Kentucky, 1971.

27. Hufferd, William L. and Lai, James S., "Analysis of N-layered Viscoelastic Pavement Systems," Final report to Federal Highway Administration, Report No. FHWA-RD-78-22, 1978.

28. Brown, S. F. and Pell, P. S., "A Fundamental Structural Design Procedure for Flexible Pavements," Proceedings of the 3rd International Conference on the Structural Design of Asphalt Pavements, London, England, 1972.

29. Barksdale, R. O., "Laboratory Evaluation of Rutting in Base Course Materials," Proceedings of the 3rd International Conference Structural Design of Asphalt Pavements, London, England, 1972.

30. Brown, S. F., "Laboratory Testing for Use in the Prediction of Rutting in Asphalt Pavements," TRB, NAS, Transportation Research Record 616, 1976.

31. Monismith, C. L., "Rutting Prediction in Asphalt Concrete Pavements," TRB, NAS, Transportation Research Record 616, pp. 2-8, 1976.

32. Pell, P. S. and Brown, S. F., "The Characteristics of Materials for the Design of Flexible Pavement Structures," Proceedings of the 3rd International Conference on the Structural Design of Asphalt Pavements, London, England, 1972.

33. Nair, K., and Chang, C. Y., "Flexible Pavement Design and Management Materials Characterization," NCHRP 140, Washington, D.C., 1973.

34. Heukelom, W. and A. J. G. Klomp, "Consideration of Calculated Strains at Various Depths in Connection with the Stability of Asphalt Pavements," Proceedings, 2nd International Conference on the Structural Design of Asphalt Pavements, Ann Arbor, Michigan, 1967.

35. Monismith, C. L., "Permanent Deformation Studies of Pavement," FCP Research progress Review Report, San Francisco, California, 1973.

36. Timoshenko, L. P., "History of Strength of Materials," McGraw-Hill Book Co., Inc., New York, N.Y., 1953.

37. Thiers, Gerald R. and Seed, H. B., "Cyclic Stress-Strain Characteristics of Clay," Journal of Soil Mechanics and Foundation Div., SMZ, 1968.

38. Penzien, J. S. and Parmelee, R., "Seismic Analysis of Bridges on Long Pile," Journal of the Engineering Mechanics Division ASCE, Vol. 90, No. EM3, Proc. Paper 3953, pp. 223-254, 1964.

39. Parmelee, R. A., Penzien, J. S., Seed, H. B. and Thiers, G. R., "Seismic Effect on Structures Supported on Piles Extending through Deep Sensitive Clays," Reports to California State Div. of Highways, Inst. of Engr. Research, Univ. of California, Berkeley, California, 1964.

40. Crandall, S. H., Dahl, N. C. and Lardner, T. J., "An Introduction to the Mechanics of Solids," Second Edition, McGraw-Hill Book Co., Inc., New York, N.Y., 1972.

41. Mokhtar Annaki, A. M. and Kenneth, L. Lee, "Equivalent Uniform Cycle Concept for Soil Dynamics," Journal of the Geotechnical Engineering Division, Vol. 103, 1977.

42. Lee, K. L., and Focht, J. A. Jr., "Cyclic Testing of Soil for Ocean Wave Loading Problems," Proceedings of the 7th Annual Offshore Technology Conference, Houston, Texas, 1975.

43. Casagrande, A., "Characteristics of Cohesionless Soils Affecting the Stability of Slopes and Earth Fills," Journal of the Boston Society of Civil Engineers, 1936.

44. Izzat, M. Idriss, Ricardo Dobry and Ram D. Singth, "Non-linear Behavior of Soft Clays during Cyclic Loading, Journal of the Geotechnical Engineering Division, Vol. 104, 1978.

45. Richart, F. E., "Some Effects of Dynamic Soil Properties on Soil-Structure Interactions," Journal of the Geotechnical Engineering Division, 1975.

46. Rauhut, J. Brant, O'Quin, John C., Hudson, W. Ronald, "Sensitivity Analysis of FHWA Structural Model VESYS IIM," Proceedings 4th International Conference - Structural Design of Asphalt Pavements, Vol. I, Ann Arbor, Michigan, 1977.

47. Seed, H. B. and McNeil, R. L., "A Comparative Study of Soil Deformations in Normal Compression and Repeated Loading Tests," Highway Research Board, Bulletin 141, 1956.

48. Hveem, F. N., "Pavement Deflections and Fatigue Failures," Design and Testing of Flexible Pavement, Bulletin No. 114, Washington, D.C., Highway Research Board, 1956.

49. Raymond, G. P., Gaskin, P. N. and Addo-Abedi, "Repeated Compressive Loading of Leda Clay," Canadian Geotechnical Journal, Vol. 16, No. 1, 1979.

50. Seed, H. B., Chan, C. K., and Lee, C. E., "Resilience Characteristics of Subgrade Soils and Their Relation To Fatigue Failures in Asphalt Pavements," Proceedings of International Conference on Structural Design of Asphalt Pavements, University of Michigan, 1962.

51. Finn, F. N., Nair, K., and Monismith, C. L., "Applications of Theory in the Design of Asphalt Pavements," Proceedings of the 3rd International Conference on the Structural Design Asphalt Pavements, London, England, 1972.

52. Cannon, R. H. Jr., "Dynamic of Physical System," McGraw-Hill Book Company, 1967.

53. Chou, Vu T., "Engineering Behavior of Pavement Materials State of the Art," U.S. Army Engineer Waterways Experiment Station CE, Vicksburg, Miss, Technical Report S-77-9, 1977.

54. Monismith, C. L., Seed, H. B., Mitry, F. G., and Chan, C. K., "Prediction of Pavement Deflections from Laboratory Tests." Proceedings of the 2nd International Conference on Structural Design of Asphalt Pavements, U.M., 1967.

55. Seed, H. B., McNeill, R. L. and De Guenin, J., "Increased Resistance to Deformation of Clay caused by Repeated Loading," Journal, Soil Mechanics Division A.S.C.E. 84 SM2, 1958.

56. Seed, H. B., and Chan, C. K., "Effect of Stress History and Frequency of Stress Application on Deformation of Clay Subgrade under Repeated Loading," Proceedings HRB, Vol. 37, 1958.

57. Chou, Vu T., "Analysis of Permanent Deformation of Flexible Airport Pavements," U.S. Army Engineer Waterways Experiment Stateion, CE, Vicksburg, Miss., Technical Report S-77-8, 1977.

58. Mitchell, J. K., Shen, C. K., and Monismith, C. L., "Background equipment, preliminary investigation, repeated compression and flexure tests on cement treated silty clay". Report No. 1, University of California, Berkeley, December 1965.

59. Young, M. A. and Baladi, G. Y., "Repeated Load Triaxial Testing of the Art," Division of Engineering Research, Michigan State University, 1977.

60. Moretto, O., "Effect of Natural Hardening on the Unconfined Compression Strength of Remolded Clays," Proceedings, 2nd International Conference of Soil Mechanics, Vol. 1, 1948.

61. Seed, H. B. and Chan, C. K., "Thixotropic Characteristics of Compacted Clays," Journal, Soil Mechanics and Foundations Division, A.S.C.E. Vol. 83 SM4, 1957.

62. Humphries, W. K., and Wahls, H. E., "Stress History Effects on Dynamic Modulus of Clay," Journal of Soil Mechanics and Foundation Division, Proceedings ASCE, Vol. 94, No. SM2, 1968.

63. Seed, H. B., McNeil, R. L. and De Guenin, Jacques, "Clay Strength Increase caused by Repeated Loading," Journal, Soil Mechanics A.S.C.E. Transactions, 1958.

64. Barksdale, R. D., "Compressive Stress Pulse Times in Flexible Pavements for use in Dynamic Testing," HRB Record 345, 1971.

65. Allen J. and Thompson, M. R., "Resilient Response of Granular Materials Subjected to Time-Dependent Lateral Stresses," TRB, NAS, Transportation Research Record No. 510, 1974.

66. Hicks, R. G. and Monismith, C. L., "Prediction of the Resilient Response of Pavements Containing Granular Layers using Non-Linear Elastic Theory," Proceedings, 3rd International Conference on the Struct. Design of Asph. Pavement, London, England, 1972.

67. Seed, Mirty, Monismith, Chan, "Prediction of Flexible Pavement Deflections from Laboratory Repeated Load Tests," NCHRP Report No. 35, 1967.

68. Dehlen, "Test Procedures for Characterizing Dynamic Stress Strain Properties of Pavements Materials," Transportation Research Board, Special Report 162, Washington, D.C., 1975.

69. Tanimoto, K. and Nishi, M., "On Resilience Characteristics of Some Soils under Repeated Loading." Soil and Foundation Vol. 4, 1970.

70. Seed, H. B. and Monismith, C. L., "Some Relationships between Density and Stability of Subgrade Soils." HRB Highway Research Records, Bulleton No. 93, 1954.

71. Coffman, B. S., Kraft, D. C., and Tamayo, J., "A Comparison of Calculated and Measured Deflections for the AASHO Road Test," Proceedings, Association of Asphalt Paving Technologists, Vol. 33, 1934.

72. Seed, H. B., Mitry, F. G., Monismith, C. L., and Chan, C. K., "Factors Influencing the resilient deformations of untreated aggregate base in two-layer pavements subjected to repeated loading," HRB, Highway Research Record No. 190, Washington, D.C., 1967.

73. Finn, F. N., Nair, K., and Monismith, C. L., "Applications of Theory in the Design of Asphalt Pavements," Proceedings of the 3rd International Conference on the Structural Design of Asphalt Pavements, London, England, 1972.

74. Baladi, G. Y., et al, "Shear Strength of Cohesionless Soils, ASTM Special Publication STP 740, September 1981.

75. Highway Research Board "The AASHO Road Test" National Academy of Sciences - National Research Council Washington D.C. Publication 954 Special Report 61E 1962.

76. Hicks, R. G. and Monismith, C. L., "Factors Influencing the Resilient Response of Granular Materials," Highway Research Board, Highway Research Record No. 345, 1971.

77. Lentz, R. and Baladi, G. Y., "Permanent Deformation of Cohesionless Subgrade Material under Cyclic Loading." Proceedings of the International Symposium of Soil under Cyclic and Transient Loading, Swansea, 1980.

78. Casagrande and Fadum, R. E., "Notes on Soil Testing for Engineering Purposes," Harvard University Graduate School of Engineering Publication 268.

79. "Field Manual of Soil Engineering, Fifth Edition by Michigan Department of State Highways, Lansing, Michigan, 1970.

80. Tien-Hsing, Wu, "Properties of Soil Deposits," Soil Mechanics and Foundation Design, Second Edition, 1976.

81. Suzanne M. Lucasse and Charles Ladd, "Undrained Behavior of Embankments on New Liskeard Varved Clay," Canadian Geotechnique, January, Vol. 14, 1977.

82. Stermac, A. G. and Lo, K. Y., "The Performance of an Embankment on a Deep Deposit of Varved Clay," Canadian Geotechnical Journal, Vol. 4, No. 1.

83. Metcalf, J. B. and D. L. Townsend, "A Preliminary Study of the Geotechnical Properties of Varved Clay," as Reported in Canadian Engineering Case Records.

84. Milligan, V. M., ASCE, Soderman, L. G. and Rutka, A., "Experience with Canadian Varved Clays," Journal of the Soil Mechanics and Foundation Division Proceedings, of the A.S.C.E., 1962.

85. James D. Parsous, "New York Glacial Lake Foundation of Varved Silt and Clay," Journal of the Geotechnical Eng. Div., Vol. 103.

86. Bishop, A. W. and Henkel, D. J., "The Measurement of Soil Properties in the Triaxial Test," Second Edition, Edward Arnold (Publishers) Ltd., London, 1962.

87. Simons, N. E., "The effect of overconsolidation on the shear strength characteristics of an undisturbed Oslo clay," A.S.C.E. Research conference on shear strength of cohesive soils, 1960.

88. Peterson, R., et al., "Limitations of laboratory shear strength in evaluating stability of highly plastic clays," A.S.C.E. Research conference on shear strength of cohesive soils, 1960.

89. Barksdale, R. D. and Hicks, R. G., "Evaluation of Materials for Granular Base Courses," presented at the Third Interamerican Conference on Materials Technology, Rio de Janero, Brazil, August 14-17, 1972, pp. 134-143.

90. Wonder, C. H., Veatch, J. O. and Jones, L. R., "Soil Survey of Michigan Counties, Michigan," United State Department of Agriculture, Bureau of Chemistry and Soils (1919-1977).

91. Seed, H. B., Chan, C. K. and Monismith, C. L., Effects of Repeated Loading on the Strength and Deformation of Compacted Clay," Proceedings, Highway Research Vol. 34, 1955.

92. Seed, H. B., and McNeill, R. L., "Soil Deformation under Repeated Stress Applications, Conference on Soils for Engineering Purposes, Mexico City, A.S.T.M. Special Technical Publication 232, 1957.

93. Gibbs, H. J., and al, "Shear Strength of Cohesive Soils" ASCE Research Conference on Shear Strength of Cohesive Soils, 1980.

94. Casagrade, A., "The Structure of Clay and Its Importance in Foundation Engineering", Journal of the Boston Society of Civil Engineering, 1932.

95. Khosla, R. L., and Wu, T. H., "Stress-Strain Behavior of Sand", Journal of the Geotechnical Engineering Division, ASCE, Vol. 102, 1976.

96. Personal Communication with Mr. Ben Kenis, DOT, FHA.

97. Lo, K. Y., and Victor Milligan, "Shear Strength Properties of Two Stratified Clays", Journal of the Soil Mechanics and Foundation Division, ASCE, Vol. 93, No. SM1, 1967.

98. Metcalf, J. B., and D. L. Townsend, "A Preliminary Study of the Geotechnical Properties of Varved Clays as Reported in Canadian Engineering Case Records", Proceedings of the Fourteenth Canadian Soil Mechanics Conference, Associate Committee on Soil and Snow Mechanics, National Research Council of Canada, Ottawa, 1961.

99. Milligan, V., L. G. Soderman, and A. Rutka, "Experience with Canadian Varved Clays", Journal of the Soil Mechanics and Foundation Division, ASCE, Vol. 88, No. SM4, 1962.

100. Murphy, O. J., G. Wayne Clough, and Robert S. W. "Temporary Excavation in Varved Clay", Journal of the Geotechnical Engineering Division, ASCE, Vol. 101, NO GT3, 1975.

101. Konder, R. L., "Hyperbolic Stress Strain Response: Cohesive Soils", Journal of the Soil Mechanics and Foundation Division, ASCE, Vol. 89, No. SM1, Proceedings Paper 3429, 1963.

102. Konder, R. L., and Zelasko, J. S., "A Hyperbolic Stress Strain Formulation for Sands," Proceedings, Second International Pan-American Conference of Soil Mechanics and Foundation Engrg. Vol. 1, Brazil, 1963.

103. Konder, R. L., and Zelasko, J. S., "Void Ratio Effects on the Hyperbolic Stress Strain Response of a Sand", Laboratory Shear Testing of Soils, ASTM STP No. 361 Ohawa, 1963.

104. Duncan, James M., and Chan, Chin-Yung, "Nonlinear Analysis of Stress and Strain in Soils," Journal of the Soil Mechanics and Foundation Division, ASCE, Vol. 96, No. SMS, 1970.

105. Chan, Chin-Yung and Duncan, J. M., "Nonlinear Analysis of Stress and Strain in Soils," Journal of the Soil Mechanics and Foundation Division, ASCE, Vol. 96, No. SM5, 1970.

106. Thomas J. Siller, "Properties of Railroad Ballast and Subballast for Track Performance Prediction" University of Massachusetts, Project Report Concrete Tie Correlation Study, Amberst, Massachusetts, 1980.

107. AASHTO Interim Specifications and Methods of Sampling and Testing Adopted by the AASHTO subcommittee of materials, 1980.

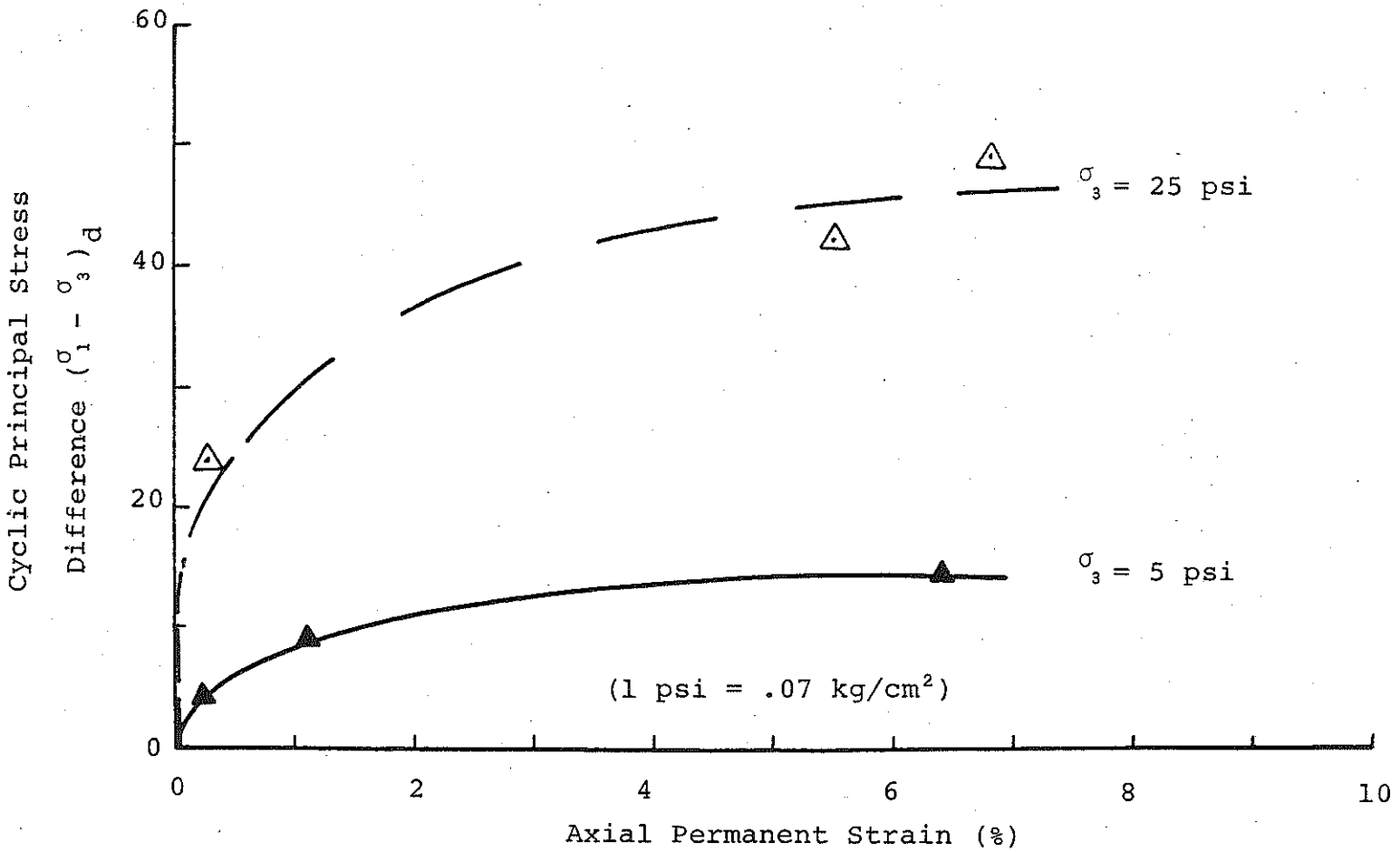

FIGURE 5.13 Effect of Stress Level on Permanent Strain for Samples Tested Up to 30,000 Load Applications, Site 3, Lower Peninsula.

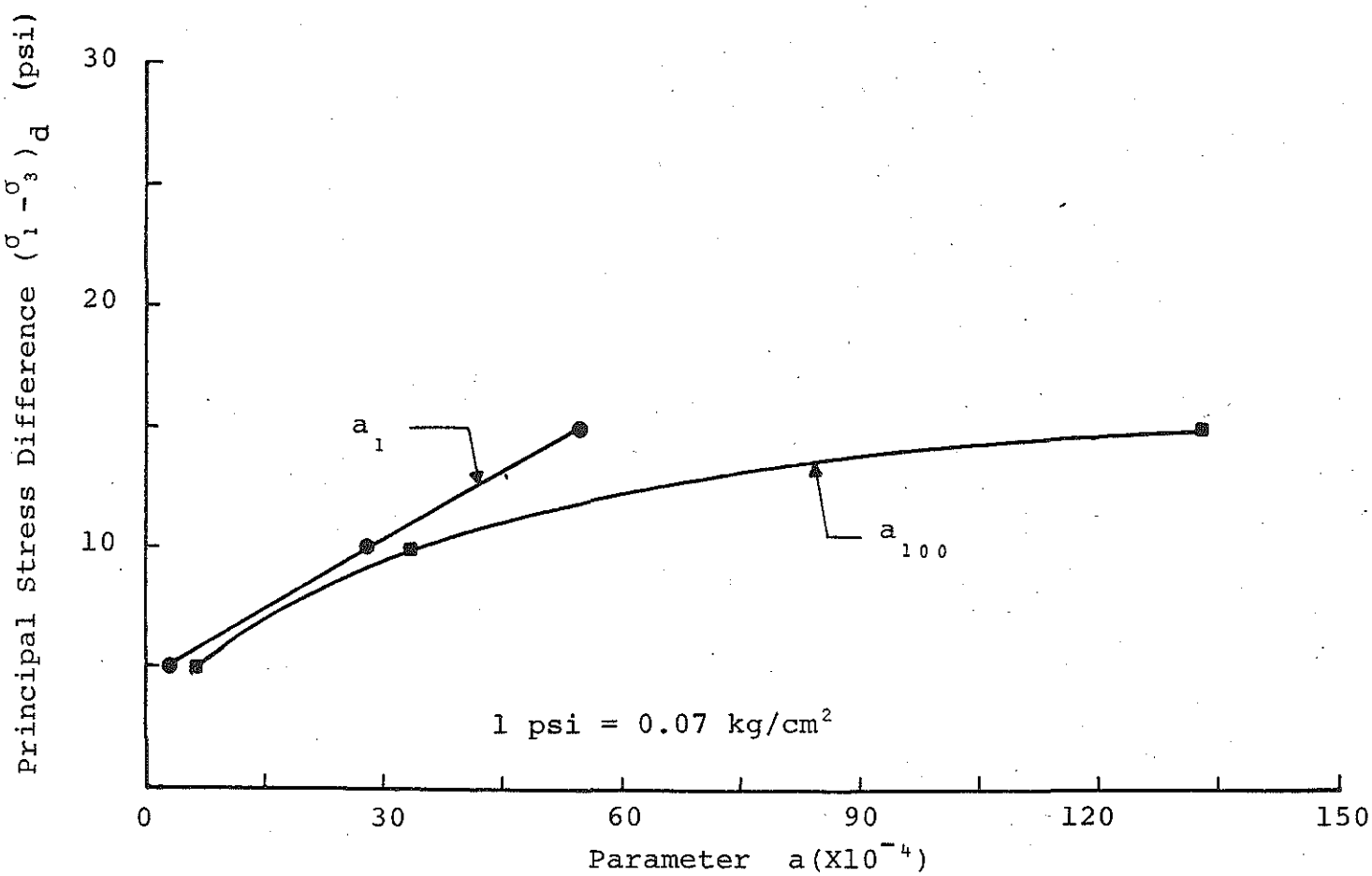

FIGURE 5.14 Principal Stress Difference Versus the Regression Constants a_1 and a_{100} of Equation 5.4, Site 3, Lower Peninsula.

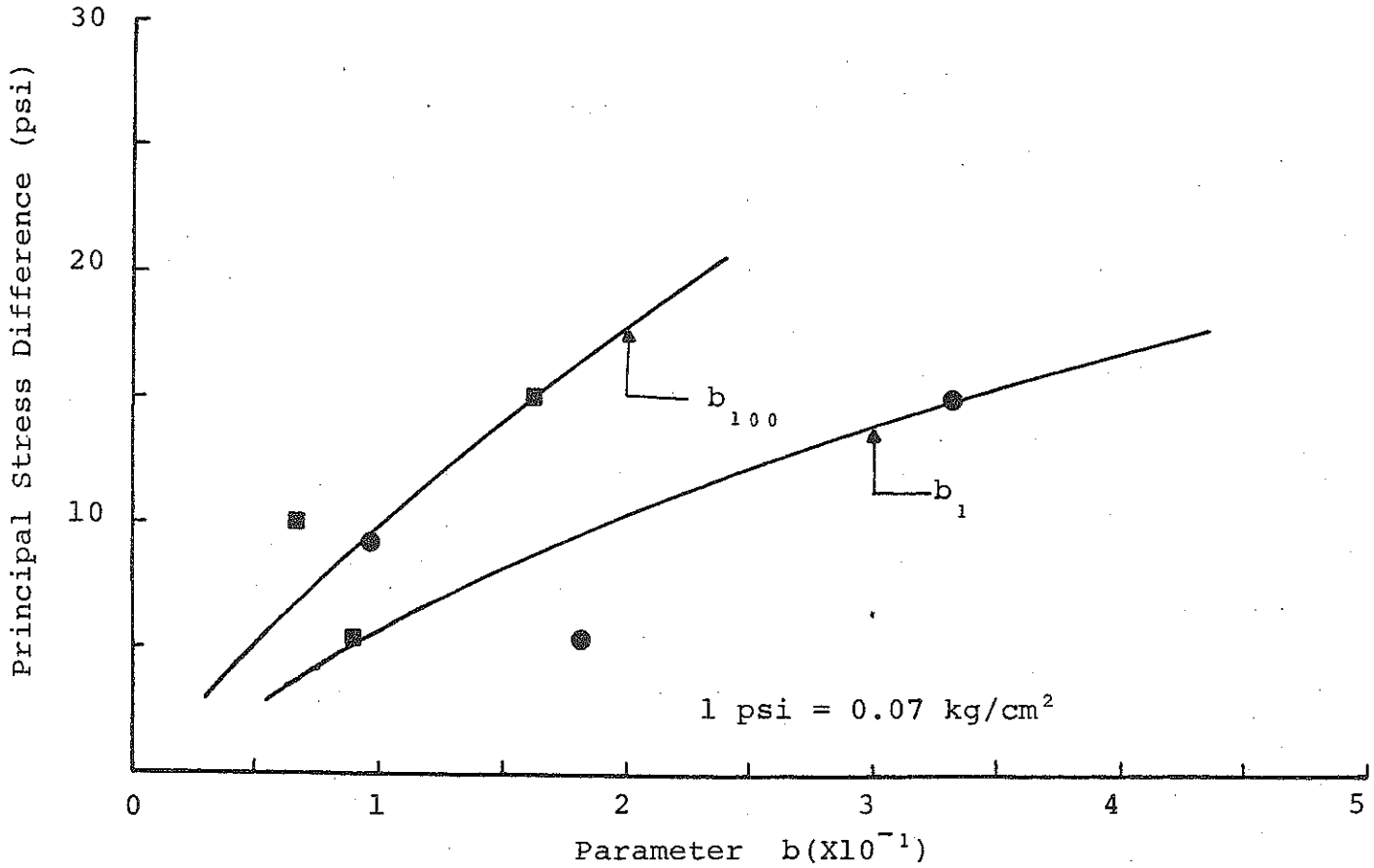

FIGURE 5.15 Principal Stress Difference Versus the Regression Constants b_1 and b_{100} of Equation 5.4, Site 3, Lower Peninsula.

load frequency, relaxation period, sample storage time, confining pressure, water content, sample disturbance, and several others. Consequently, such a relationship may be misleading and represent oversimplification of an otherwise very complicated function.

5.3.1.4 Stress History

Figure 5.16 shows plots of the logarithm of cumulative permanent strain versus the logarithm of the number of load repetitions for two different samples consolidated under a confining pressure of 5 psi (.35 kg/cm^2) and tested using two different stress paths. Sample 2d-s was tested up to 30,000 load repetitions using a constant cyclic stress ratio $(\sigma_1-\sigma_3)_d/\sigma_3$ of 2.0. The cyclic stress for sample 4b-s, on the other hand, was kept constant at 1.0 for 30,000 load repetition, after which it was increased to 1.5 for another 30,000 load repetitions and to 2.0 for the last 30,000 cycles. Figure 5.17 shows similar plots, but for unconsolidated samples where sample 2e-s was tested under a constant cyclic stress ratio. In both figures the permanent strains due to the first cycle of samples 4b-s and 4c-s were used as a datum for the other two samples. This eliminated any possible effects of the air gap (if any) between the sample and the top plate. Also, by using the datum as explained, the behavior of the samples between cycle number one and cycle number 90,000 can be analyzed.

Examination of Figures 5.16 and 5.17 indicated that, as expected, the samples which were subjected to increasing load experienced less permanent strain than the ones tested under constant load. Indeed, sample 4c-s experienced much less permanent strain (about .4%) at 90,000 load repetitions than did sample 2e-s, which showed plastic strain of about 2% after only 30,000 load repetitions. Similar results were reported by Seed [55,63], Lentz [23], and Lentz and Baladi [8,77].

The above observations gave rise to the question as to what load a pavement section, newly opened to traffic,

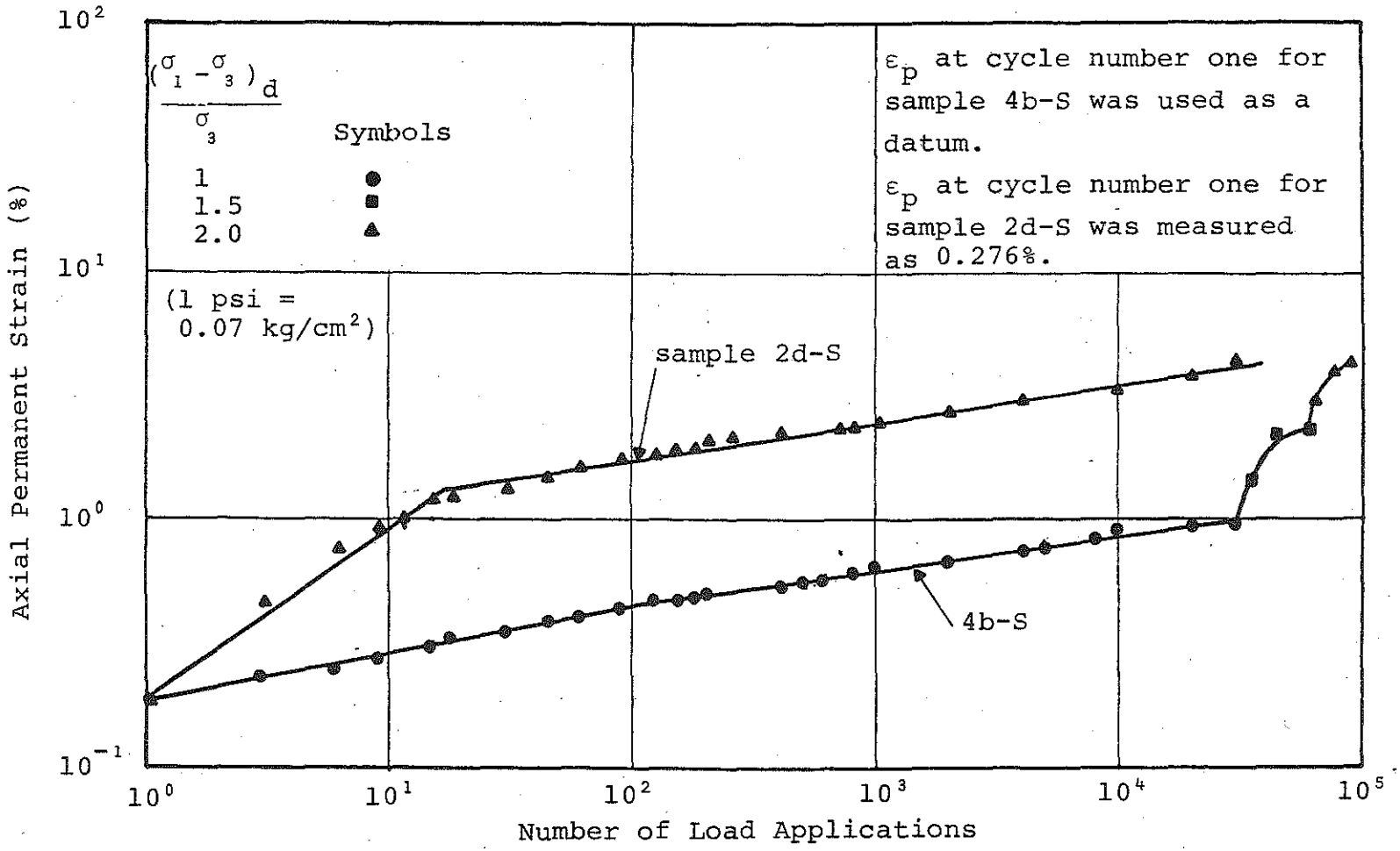

FIGURE 5.16 Axial Permanent Strain Versus Number of Load Applications for Consolidated Samples Tested Under Different Stress Path, Site 2, Lower Peninsula.

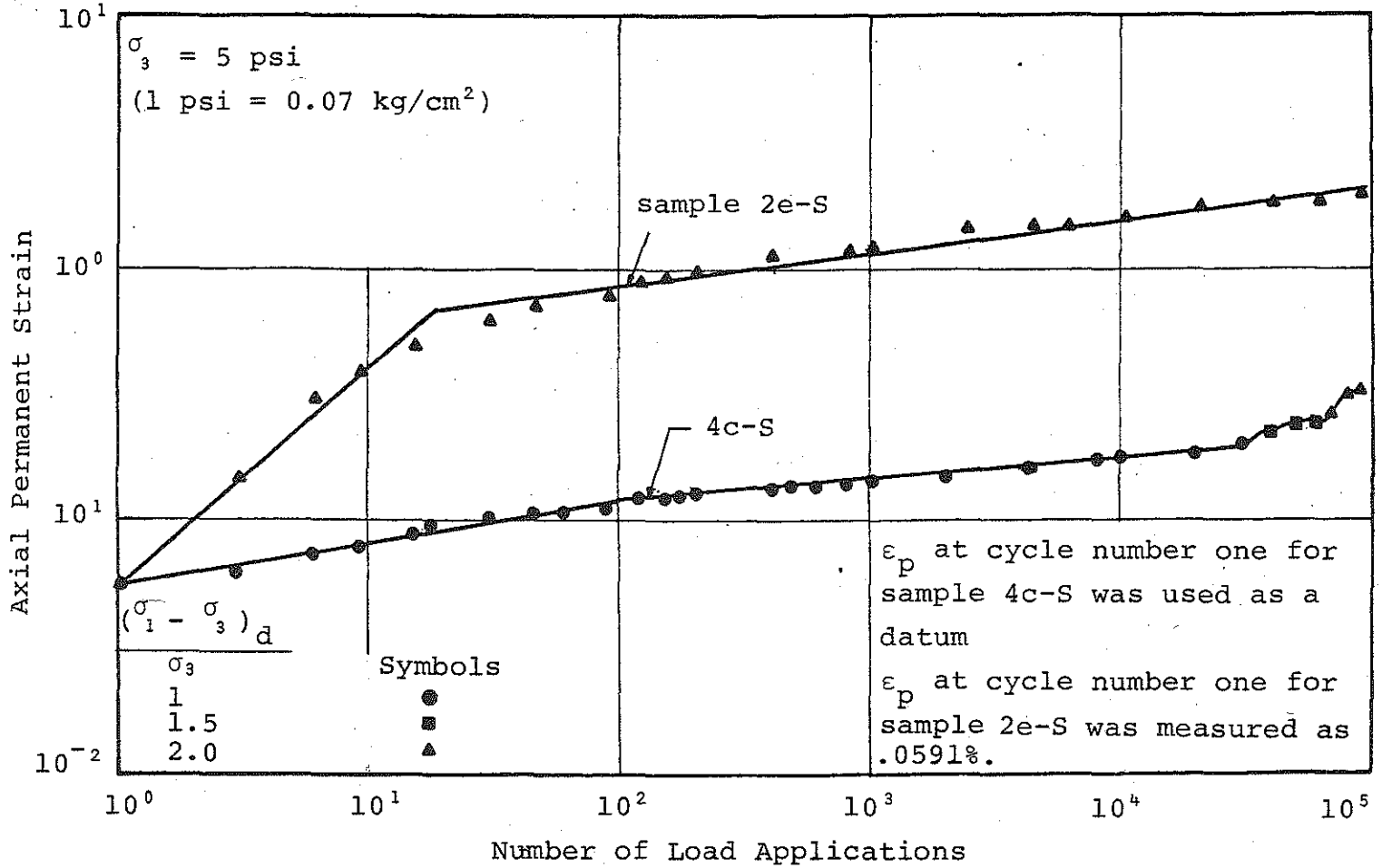

FIGURE 5.17 Axial Permanent Strain Versus Number of Load Applications for Unconsolidated Soil Samples Tested Under Two Different Stress Paths, Site 3, Lower Peninsula.

should be subjected to relative to the expected traffic load throughout the life cycle of the pavement. Study of the stress history of laboratory samples indicated that the damage (in form of permanent strain) could be minimized if the applied stresses were small and they increased gradually. Consequently, in the field, and as far as the pavement deformation is concerned, a newly constructed pavement should be opened to light traffic (light tire pressure) prior to trafficking the pavement indiscriminantly. This process, however, may prove to be either expensive or to cause higher user cost. Further, the lateral stress in a newly constructed pavement is a function of the pavement materials, thickness, and method of compaction. If, however, the lateral stress in a pavement section at the end of construction is taken as a datum, then the lateral stress at any time after opening the pavement to traffic is greater* than the datum. The increase in lateral stress is due mainly to the pavement section being seated by the action of traffic. Increasing the lateral stress will permit higher load and thus less damage. It should be noted that (see section 5.3.1.2) increase in the lateral stress should not be interpreted as unlimited license to substantially increase the axial load on the pavement.

5.3.1.5 Water Content and Consolidation

The variation of water contents of samples for the same site was not significant to influence the plastic characteristics of the sample. Consequently, this section will be restricted to the effect of consolidation.

Figure 5.18 shows plots of permanent strain versus the number of load repetitions for two samples. Sample 2b-f was consolidated under a confining pressure of 5 psi (.35 kg/cm^2), then subjected to cyclic principal stress difference of 5 psi (.35 kg/cm^2). Sample 1f-f was subjected to the

* Assuming that the pavement does not heave or deform radially.

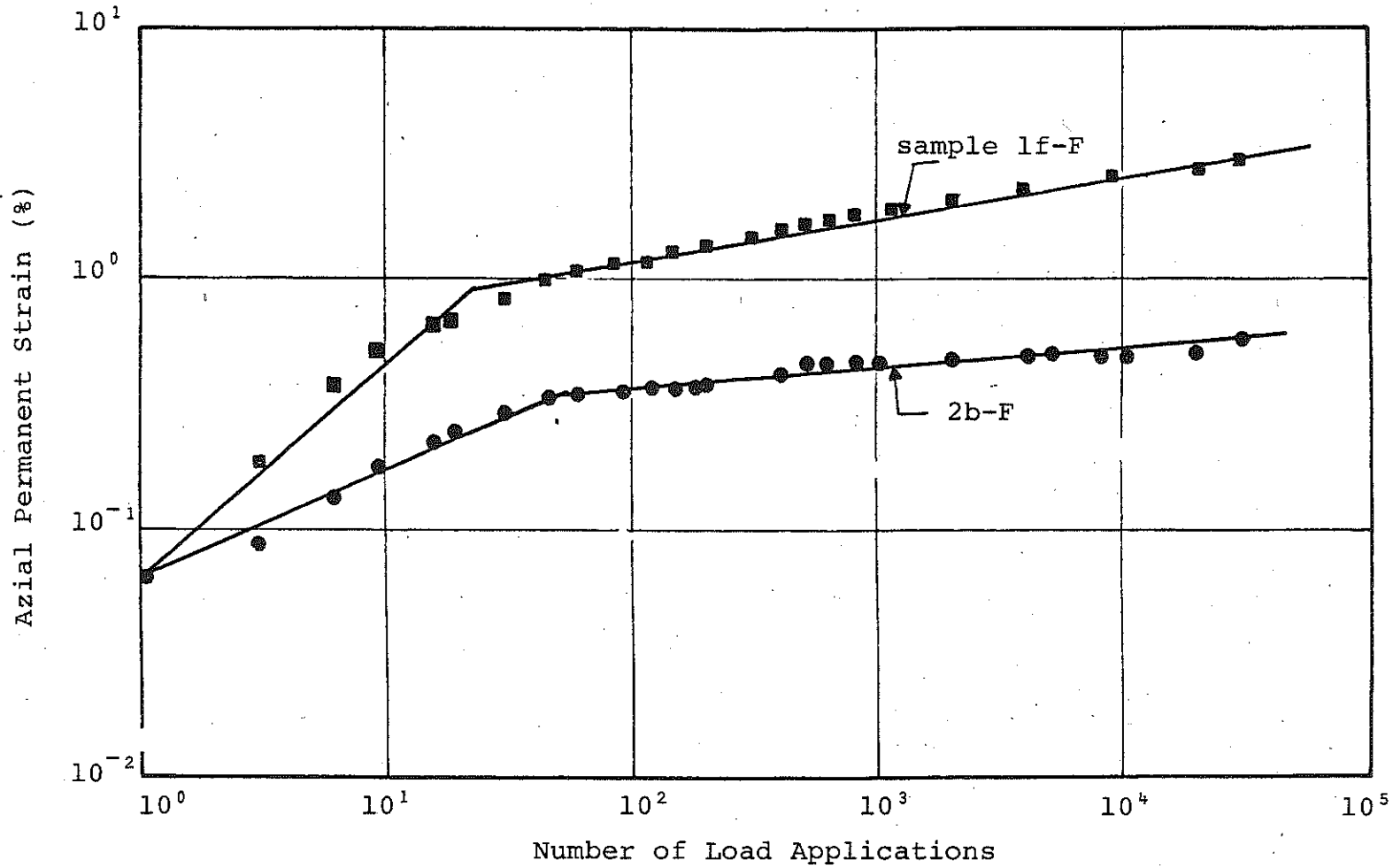

FIGURE 5.18 Axial Permanent Strain Versus Number of Load Applications for Unconsolidated and Consolidated Samples Under a Confining Pressure of 5 psi, Site 1, Lower Peninsula.

same confining pressure and principal stress difference with no consolidation allowed. From the figure, it is apparent that the unconsolidated sample experienced much higher permanent strain than the consolidated sample. Indeed, the permanent strain of sample 1f-f was in order of magnitude greater than that of sample 2b-f.

The effects of consolidation on the plastic behavior of the samples appears to decrease as the cyclic principal stress difference increases. This was expected because the sample, during the consolidation phase, did some particle reorientation which resulted in a more stable structure to resist the consolidation pressure. As the sample was subjected to a larger virgin load due to axial load that it had never experienced before, new particle reorientation and a higher order of stable structure are required. This will result in increased plastic deformation. This could be rewritten as follows: the higher the ratio of virgin pressure to the consolidation pressure of a sample, the lower the effects of consolidation on the sample deformation due to that virgin load.

5.4 Stress-Strain Relationship

Lentz [23] and Lentz and Baladi [8,77] provided the technical guidance for the early phase of this work. They reported that the plastic strain of sand subgrade materials could be predicted using triaxial test results. They concluded that the prediction model is dependent on the number of load applications and independent of the test variables (confining pressure, stress level) and sample variables (compaction effort and moisture content). They observed that the cyclic and static tests are highly dependent on the same test and sample variables. Consequently, they rationalized that the data from both tests could be normalized to minimize the effects of the sample and test variables. Their normalization process could be summarized as follows:

01. The cyclic principal stress difference $(\sigma_1-\sigma_3)_d$ was expressed in terms of the peak static strength (S_d)

of an identical soil sample tested under the same confining pressure using incremental creep tests. (It was shown later that the normalization results did not change when the incremental creep test was substituted by the ramp tests.)

02. The cumulative permanent strain at the desired number of load repetitions (ε_p) was normalized relative to the axial strain at 95% of the sample strength ($\varepsilon_{.95S_d}$) of an identical sample tested under the same confining pressure using incremental creep test. Figure 5.19 shows their normalized data for natural sand deposit as well as manufactured sand. For more information on their data and normalization procedure, the reader is referred to reference [23] in the bibliography.

The above normalization procedure was also used in this research project. The sample strength and the strain at 95% of sample strength were determined using the incremental creep test. Figure 5.20 displays typical stress-strain data of a sample tested under 5 psi (.35 kg/m^2) confining pressure using incremental creep test. As illustrated in the figure, the value of the strain at failure (peak strength) could not be determined because the stress-strain curve becomes asymptotic to the strain axis. Consequently, the strain at 95% strength was used as shown in the figure.

Figure 5.21 shows a plot of the normalized stress-strain data at 30,000 load repetitions for the four test sites of the lower peninsula. Examination of the figure indicated that the normalized data could be expressed in one single hyperbolic function that expresses the normalized strain ratio in terms of the normalized stress ratio or vice versa. This function (Equation 5.5) is independent of confining pressure, principal stress difference, density, and water content.

$$\frac{\varepsilon_p}{\varepsilon_{.95S_d}} = \frac{n}{\frac{S_d}{(\sigma_1-\sigma_3)_d} - m} \qquad (5.5)$$

where ε_p = cumulative permanent strain at the desired number of load repetitions,

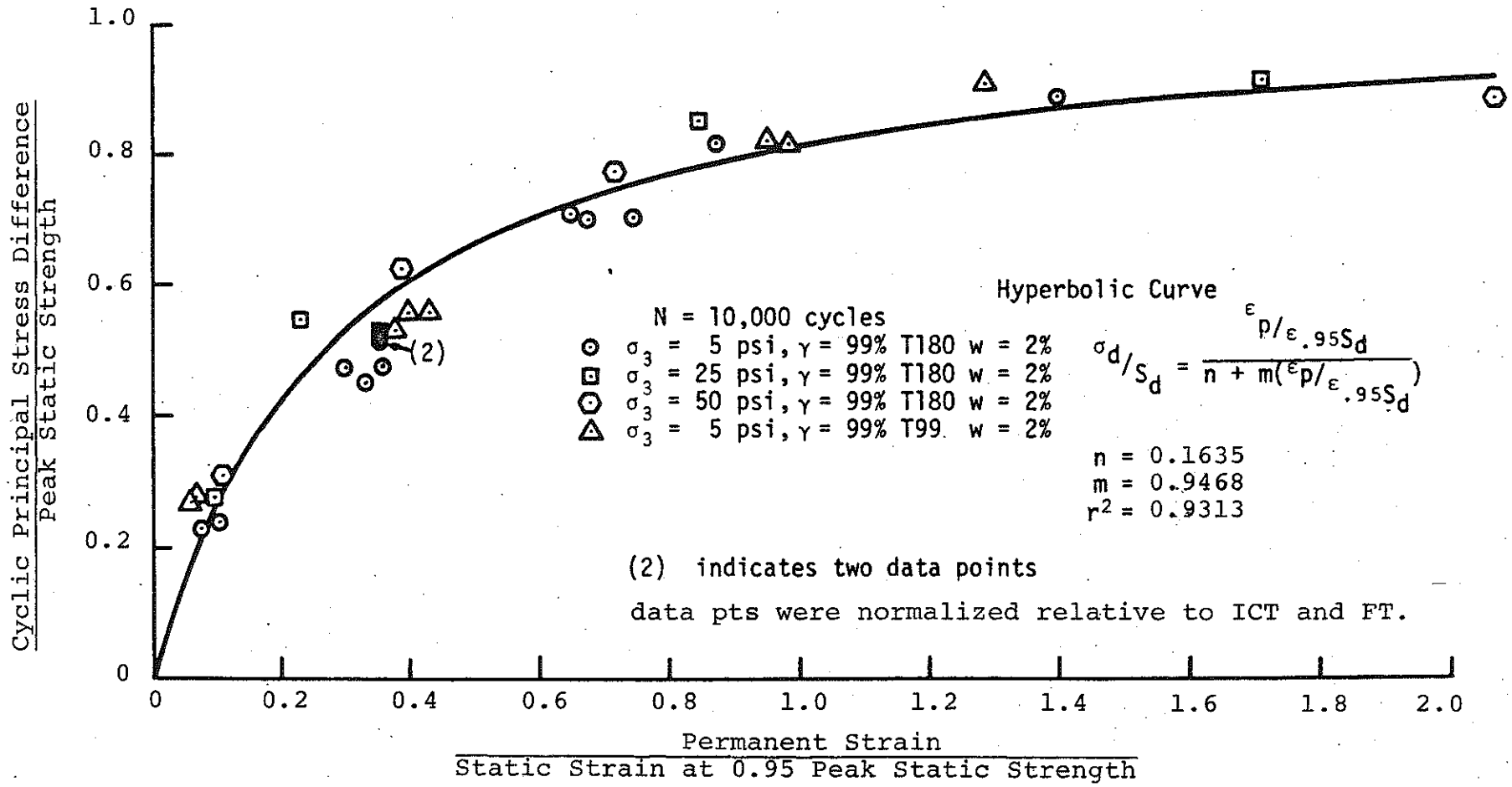

FIGURE 5.19 Normalized Cyclic Principal Stress Difference Versus Normalized Permanent Strain. (After 23).

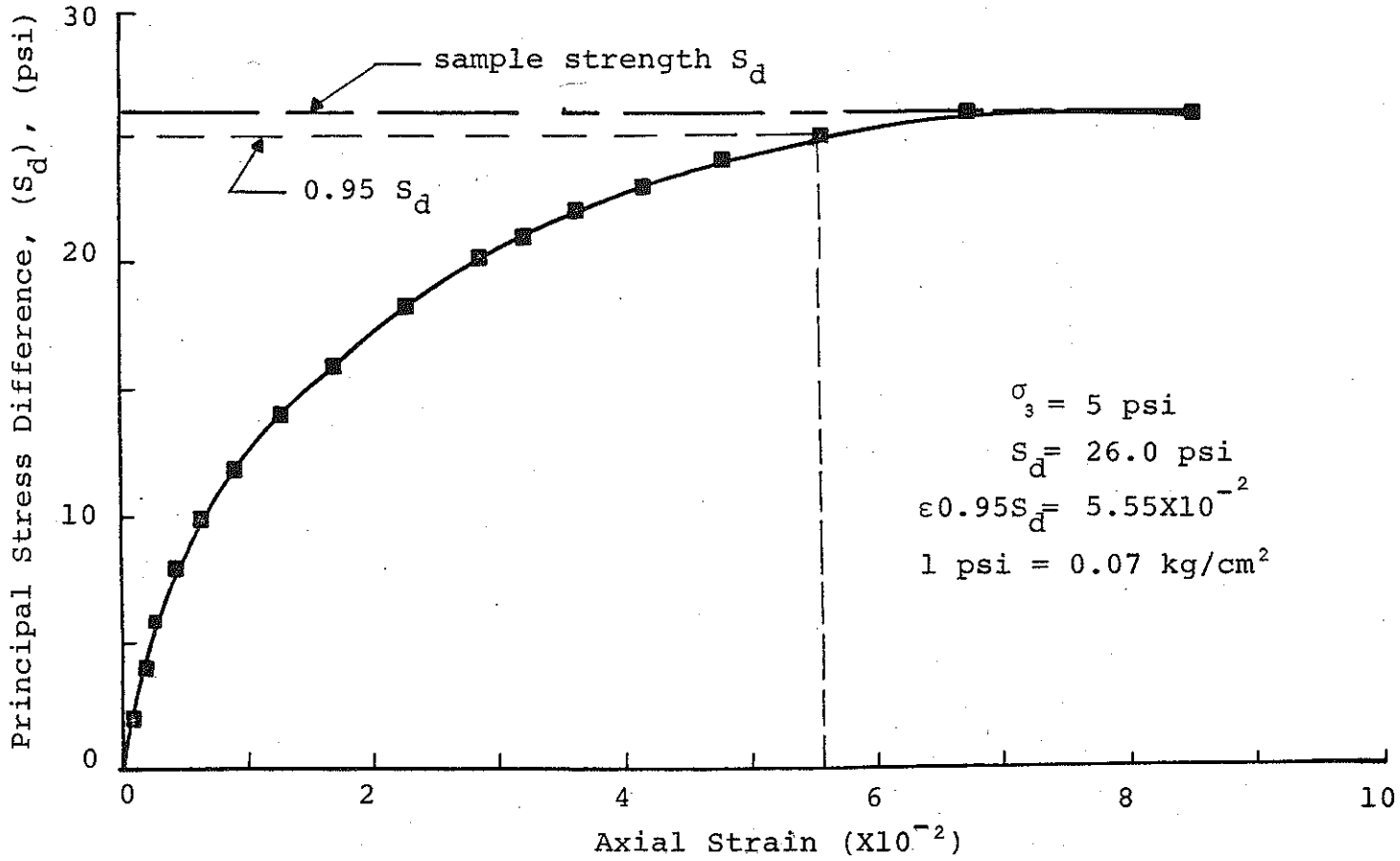

FIGURE 5.20 Typical Principal Stress Difference Versus Strain From Incremental Creep Test.

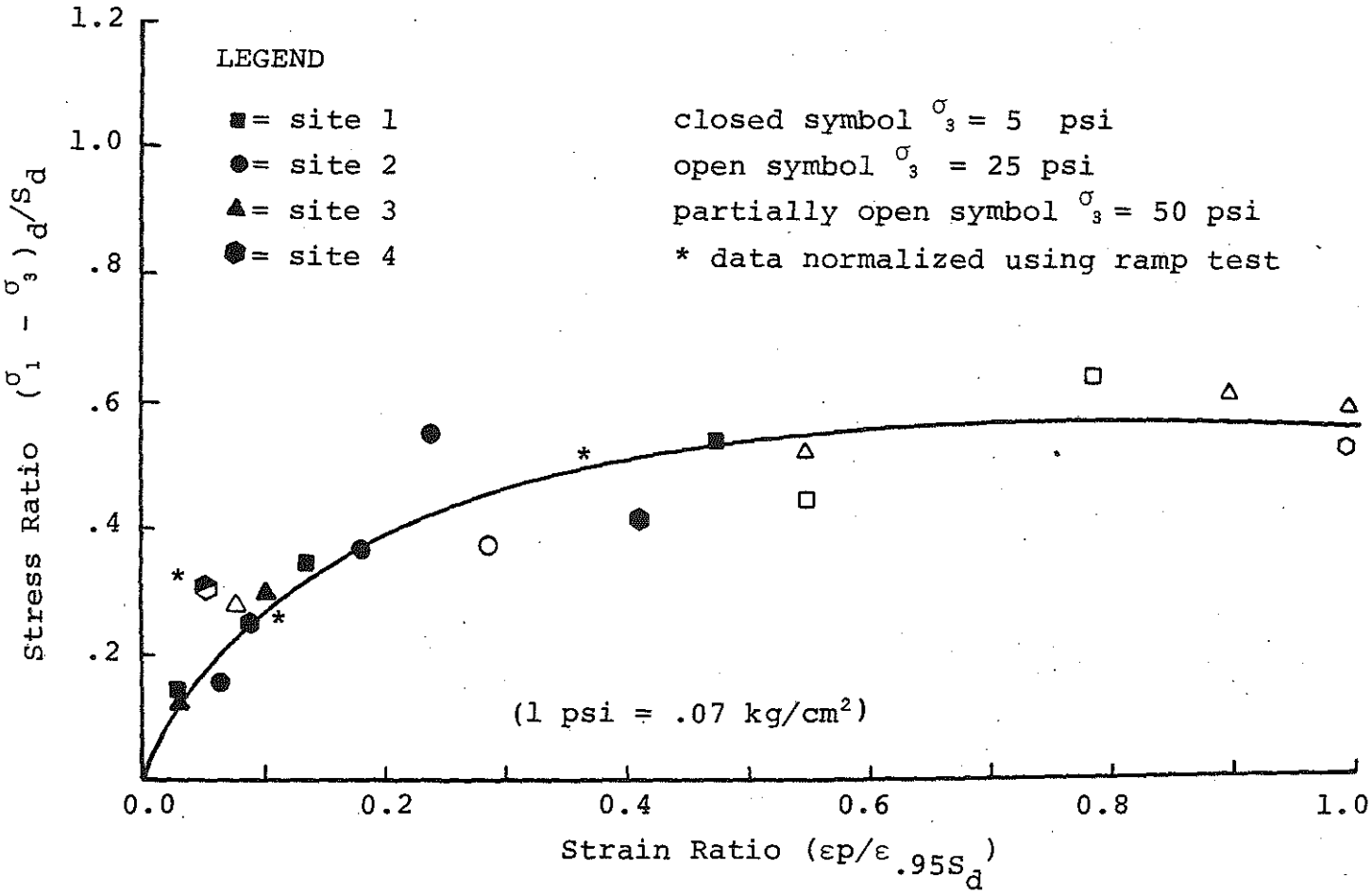

FIGURE 5.21 Normalized Stress Ratio Versus Normalized Strain Ratio at 30,000 Cycles

$\varepsilon_{.95S_d}$ = axial strain at 95% of the static strength,

S_d = static strength,

n,m = regression parameters,

$(\sigma_1-\sigma_3)_d$ = cyclic principal stress difference.

Indeed, the same hyperbolic function describes the data from test site 4 as well as test sites 1, 2, and 3, which are several hundred miles apart. Lentz [23] and Lentz and Baladi [8,77] found a similar function for natural sands as well as for manufactured sand. The differences between the sand and clay functions, however, are the values of the parameters n and m. These findings suggested that during the normalization procedure the effects of the test and sample variables are minimized or even eliminated. Consequently, it was thought that if soils, in general, could be classified into, say, six different types (silty clay, clay, sandy clay, sand, sandy gravel, and gravel) then a set of six different parameters could be found to be used in Equation 5.5.

It should be noted that ramp test data were also used to check the normalization process and the resulting general relationship. This is shown in Figure 5.21 by asterisks. It can be seen that the normalized data follow the same general relationship (curve) as that obtained using the incremental creep test as a base for normalization. At this time and in order to check the validity and generality of the normalization process, a call for data was initiated and mailed to several independent researchers. The call inquired static and dynamic data for all type soils. The response was overwhelming and encouraging. Unfortunately, a substantial part of the received data consisted of either dynamic or static stress-strain curve. As noted above, both cyclic and static data of some kind are required to initiate the normalization process. Figures 5.22 and 5.23 show the normalized data of subballast and under-tie materials respectively. The data were received from Dr. Sileg at the University of Massachusetts, Amherst [106]. The gradation curves

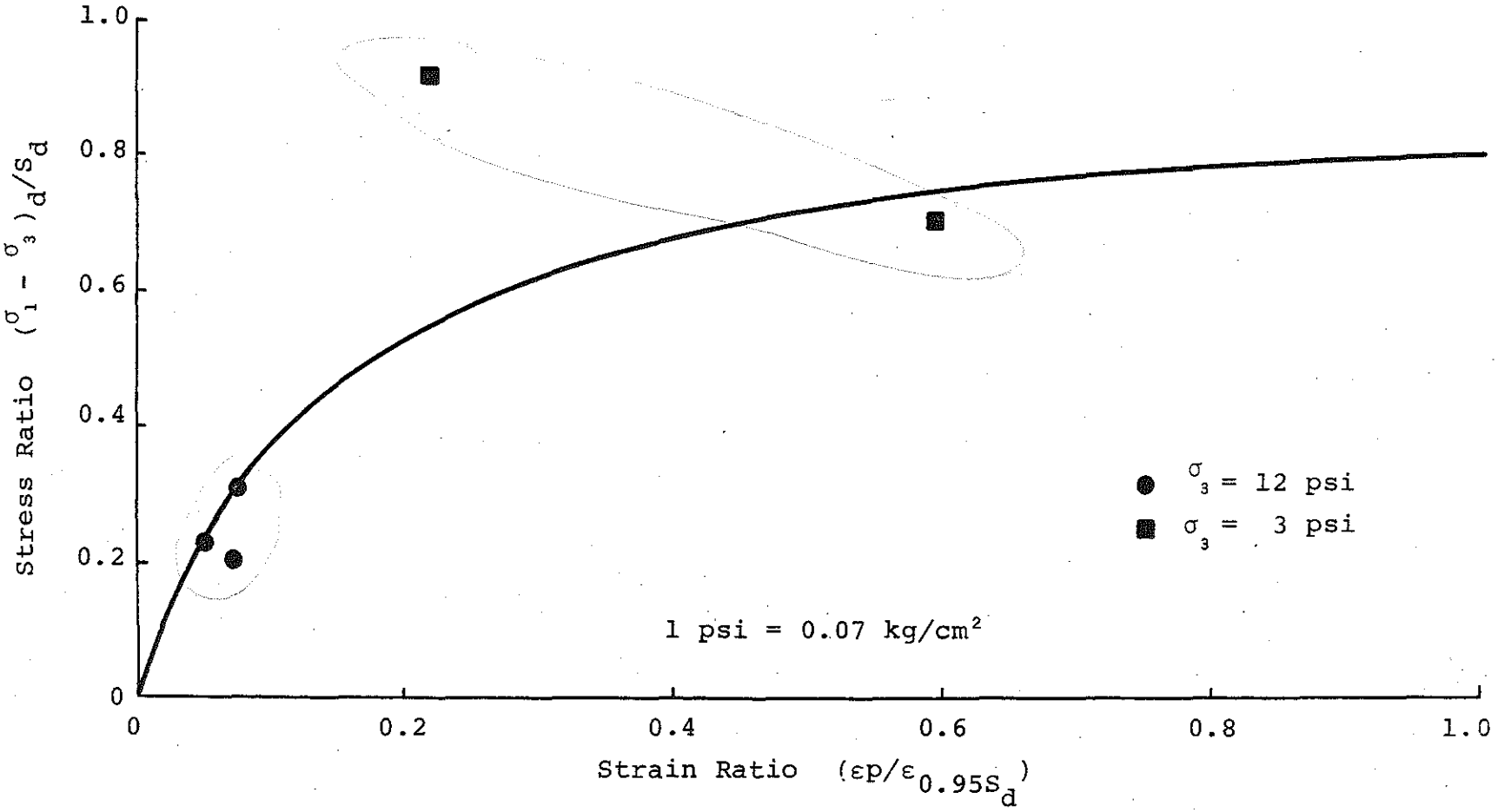

FIGURE 5.22 Normalized Cyclic Stress-Strain Data for Subbalast Materials Subjected to 10,000 Load Repetitions (After 106).

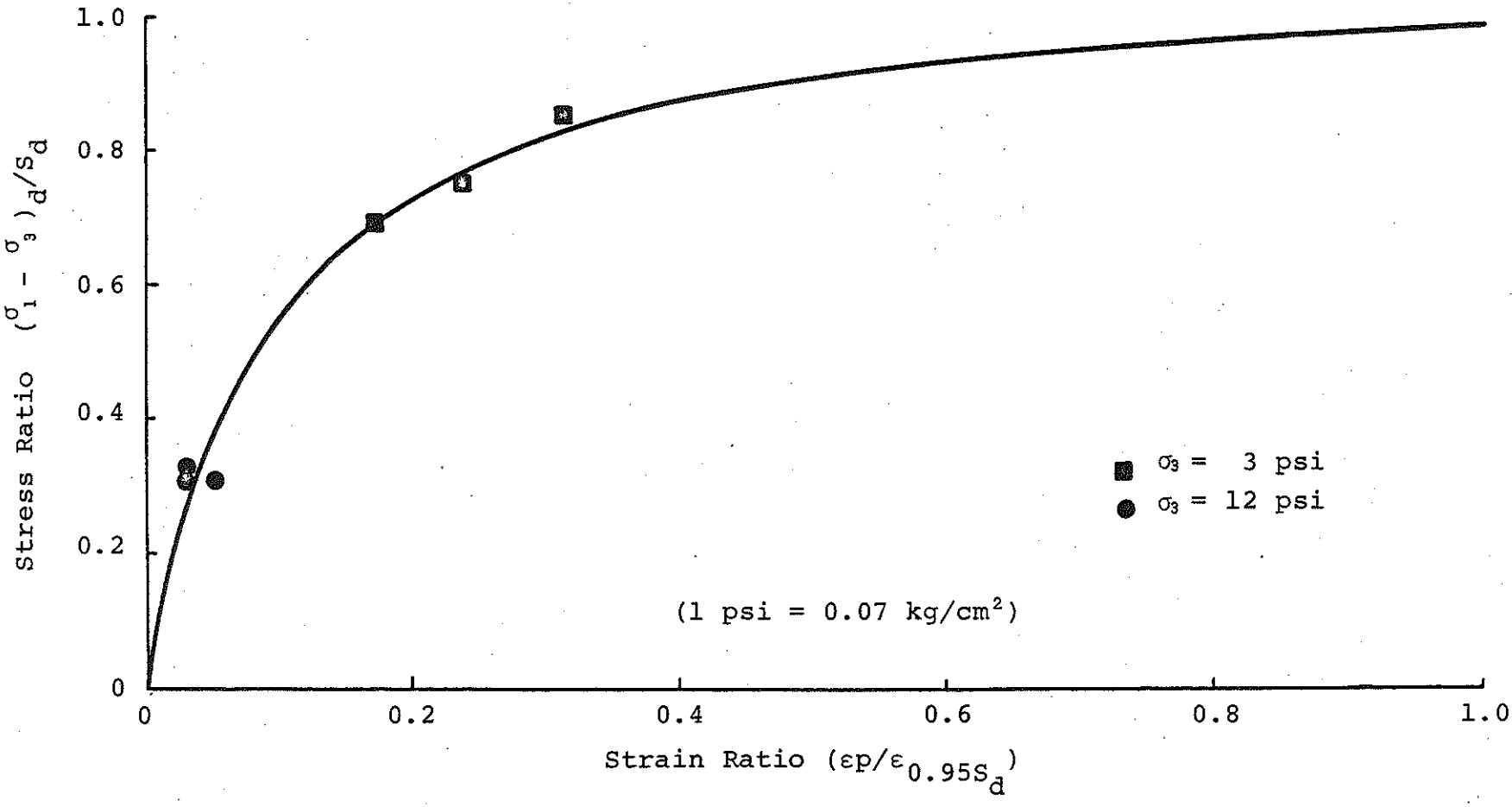

FIGURE 5.23 Normalized Cyclic Stress-Strain Data for Under Tie Materials Subjected to 10,000 Load Repetitions. (After 106).

of the subballast and under-tie materials are presented in Figure 5.24. Figure 5.25 shows the normalized data for the AASHTO A-6 materials; the tests were conducted under the direction of Dr. Baladi during the course of a previous research project sponsored by the Michigan Department of Transportation. Figure 5.26, on the other hand, shows the normalized data for the clay subgrade materials of the lower peninsula test sites. It should be noted that the data for the curves in Figures 5.19, 5.22, 5.23, 5.25, and 5.26 indicated that each type of soil could be represented by one single and unique curve. Finally, it is appropriate to note that other data received from Penn State, the National Crushed Stone Association, Rensselaer Polytechnic Institute, Japan, and the Federal Highway Administration showed similar normalized curves.

Recall that Equation 5.4 was used in this research to model the permanent strain as a function to the number of load repetitions. It was found that the same equation could be used to model all the received data. At this point in time it was suggested that the normalization process be repeated at a higher number of load repetitions. Consequently, the plastic strain at one million load cycles for each material was calculated and normalized relative to the corresponding static data. Figures 5.27 through 5.31 show plots of normalized curves at ten thousands and one million load applications for AASHTO A-6 subgrade soils, the clay subgrade soils, the subballast, the sand subgrade, and the under-tie materials respectively. Examination of the figures indicated that the values of the parameters m and n which control the position of the curve are dependent on soil type and number of load applications.

Figure 5.32 shows different plots of the normalized stress and strain ratio for different numbers of load repetitions. It can be observed that the curves tend to shift and rotate downward as the number of load repetitions increases. This shift in the curve is reflected in a change in the value of the parameters n and m of Equation 5.5.

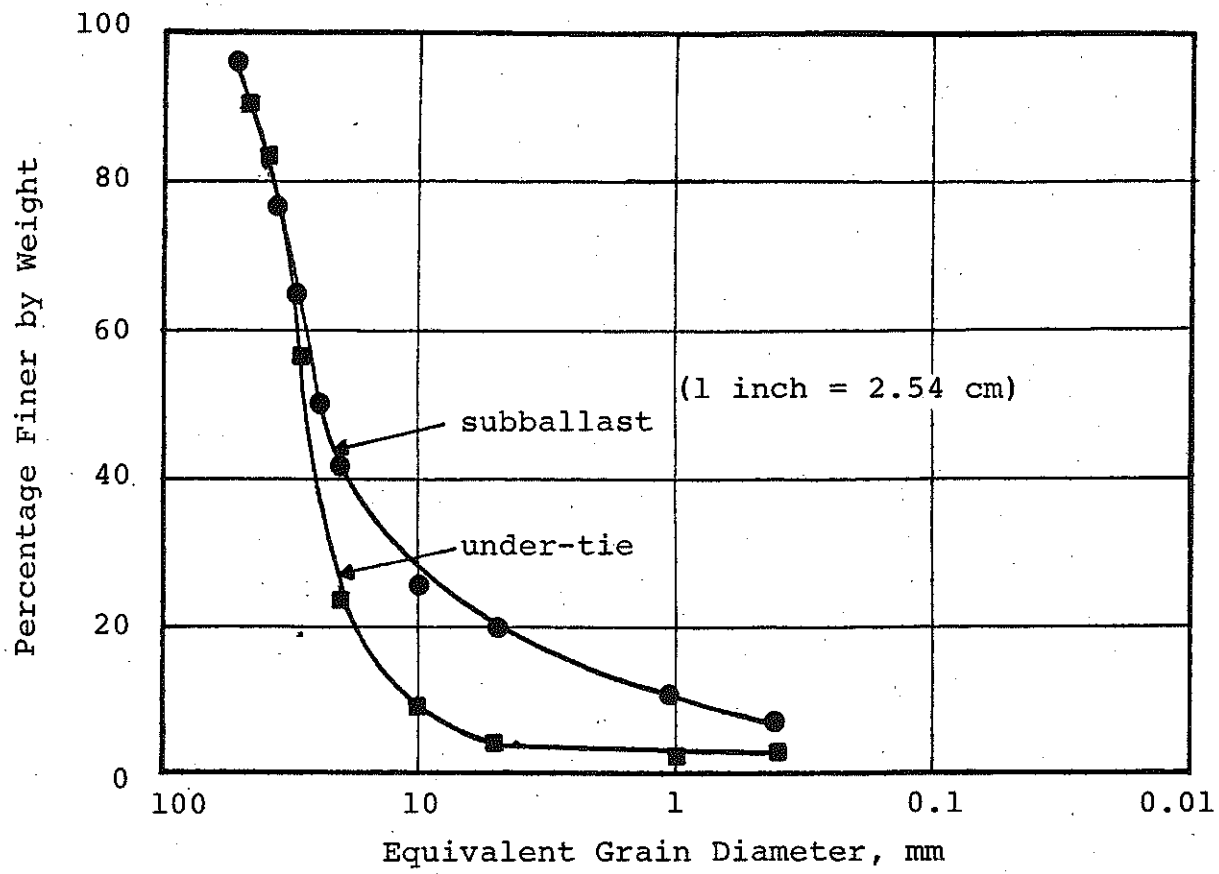

FIGURE 5.24 Average Grain Size Distribution Curves for Lorraine and Aberdeen Subballast and Under-Tie Materials (After 106).

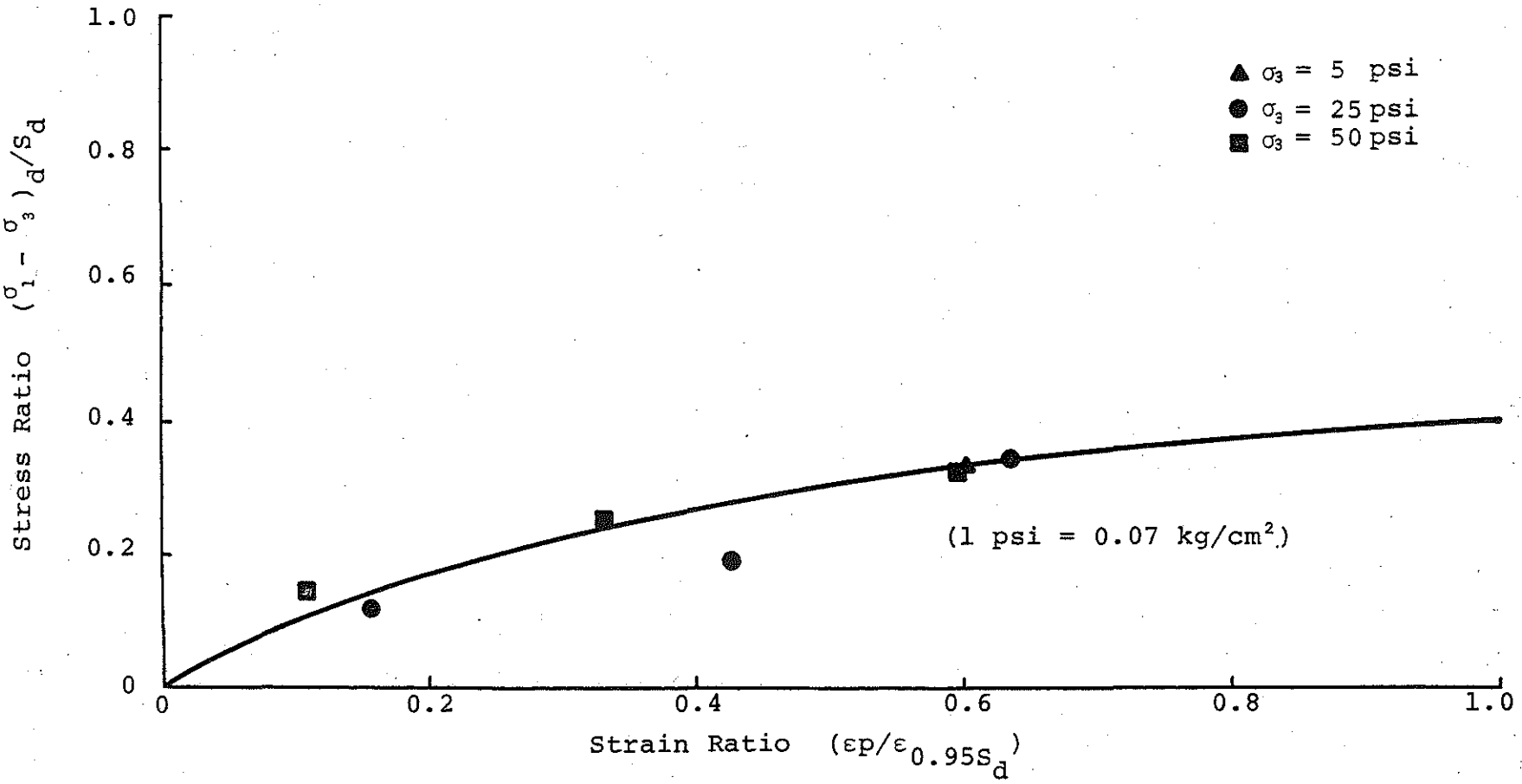

Figure 5.25 Normalized Cyclic Stress-Strain Data for A-6 AASHTO Subgrade Soils Subjected to 10,000 Load Repetitions. (After 23).

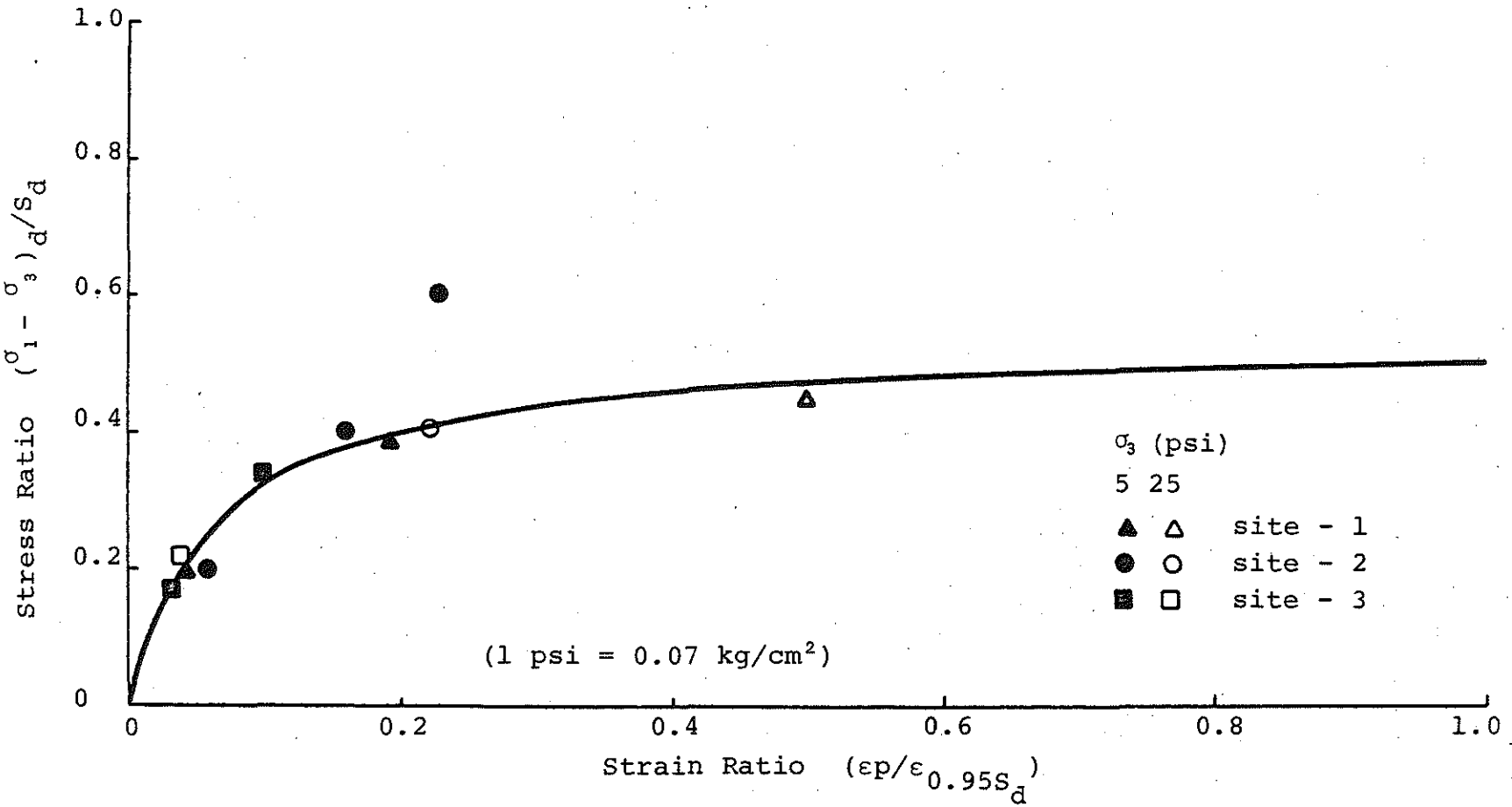

FIGURE 5.26 Normalized Stress-Strain Data for Clay Subgrade Materials from Four Different Test Sites Subjected to 10,000 Load Repetitions.

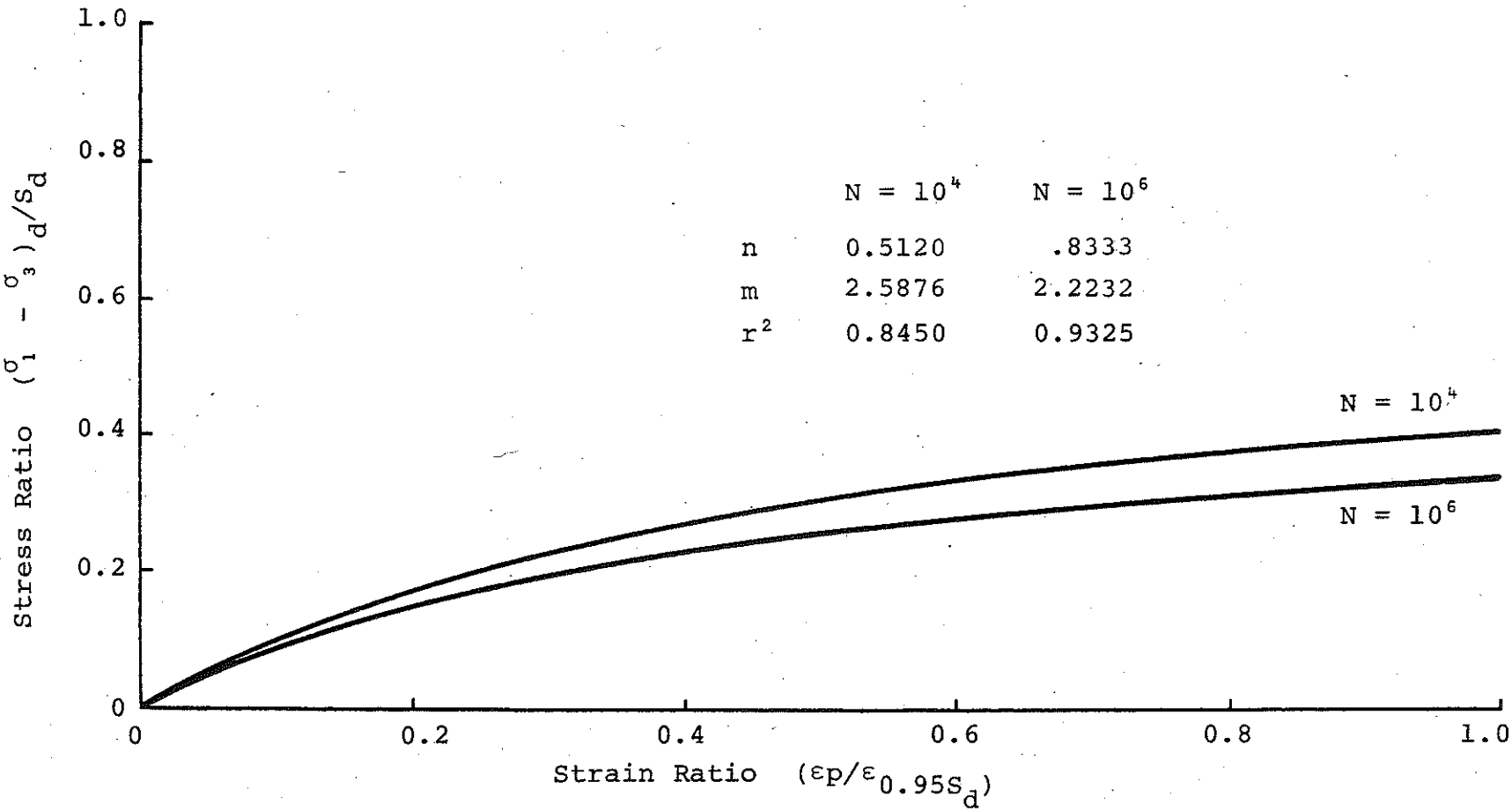

FIGURE 5.27 Normalized Cyclic Stress-Strain Data for A-6 AASHTO Subgrade Soils Subjected to 10,000 and 1,000,000 Load Repetitions

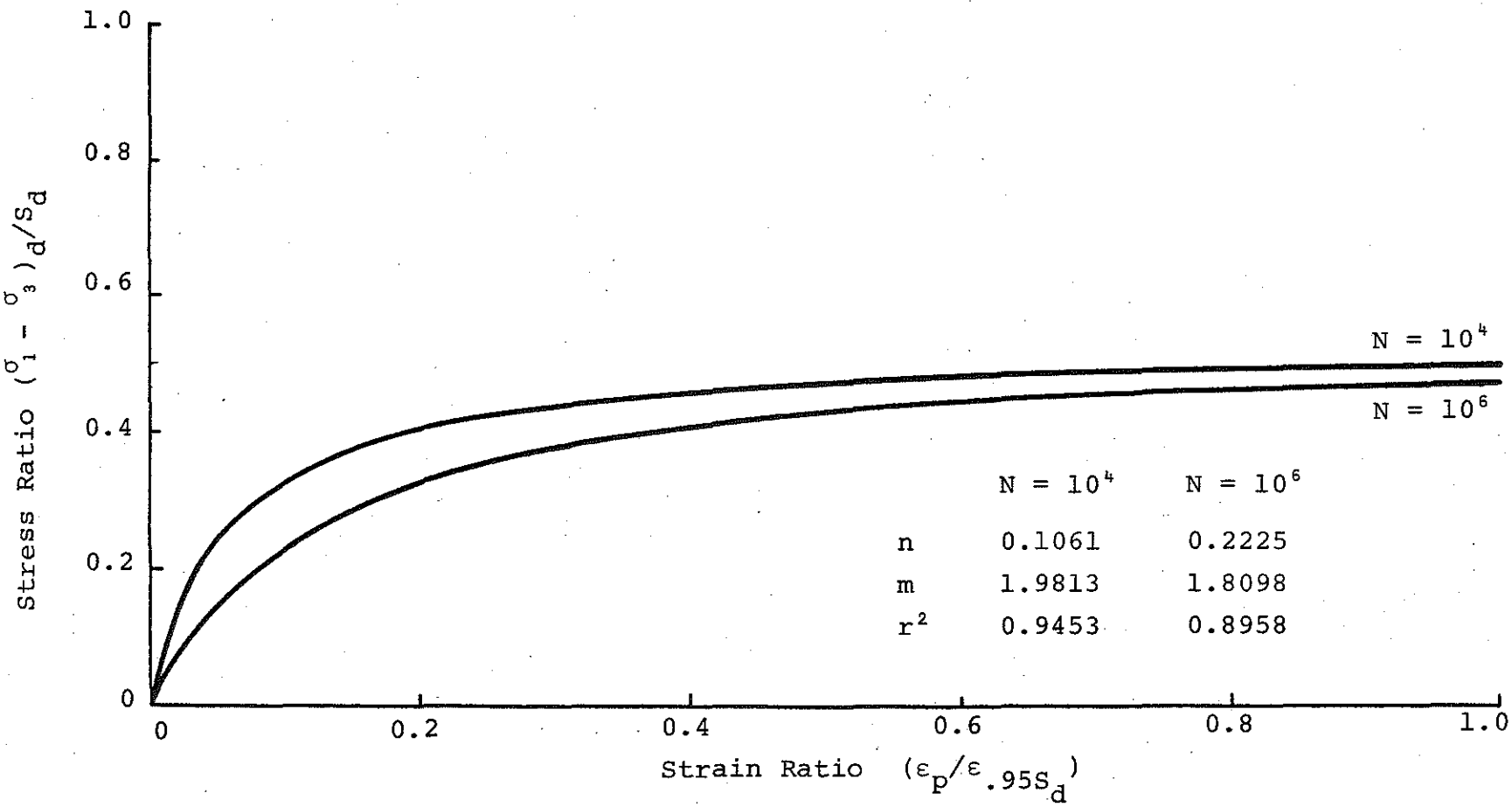

FIGURE 5.28 Normalized Stress-Strain Data for Clay Subgrade Materials from Four Different Test Sites Subjected to 10,000 and 1,000,000 Load Repetitions.

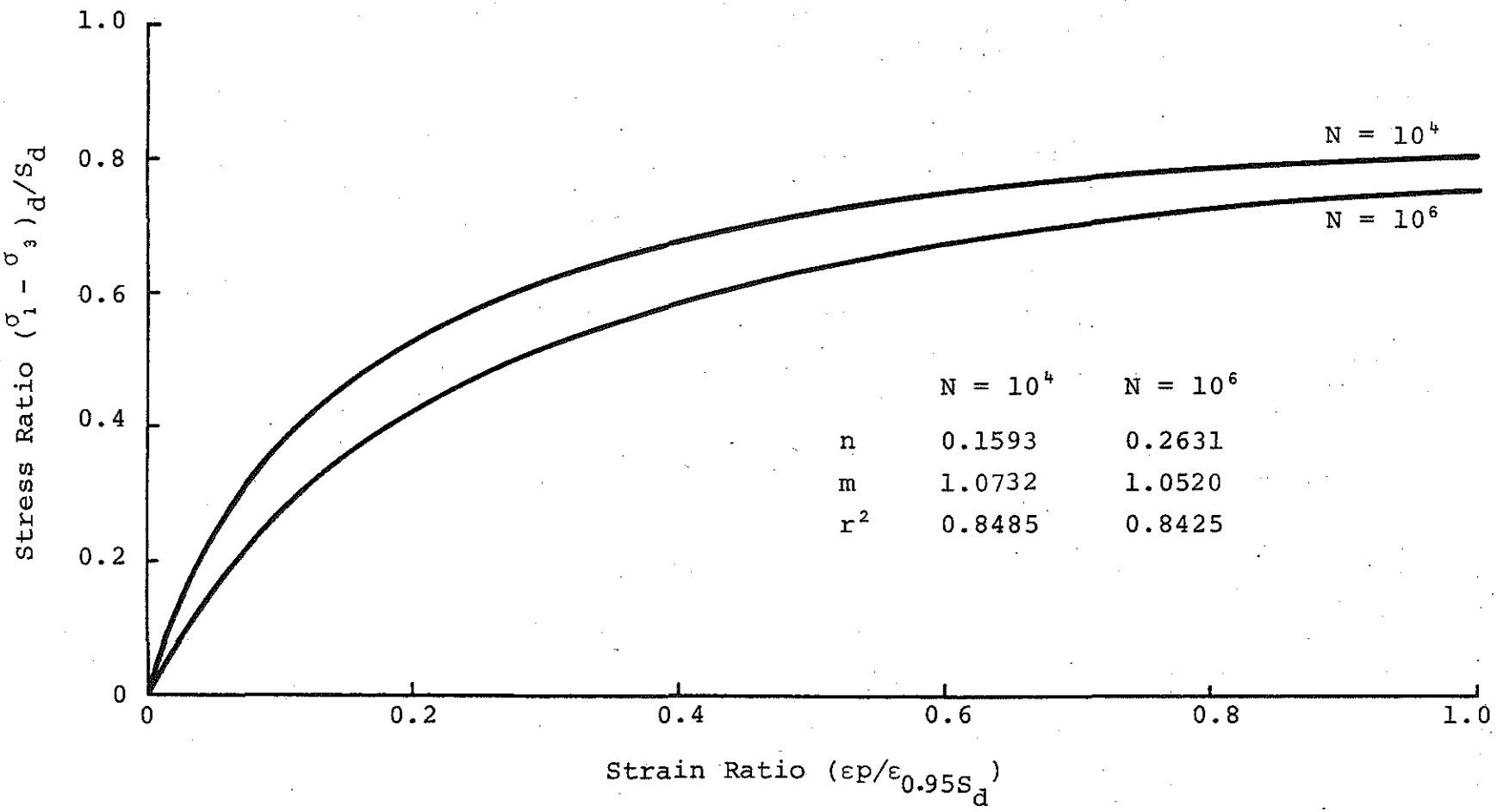

FIGURE 5.29 Normalized Cyclic Stress-Strain Data for Subballast Materials Subjected to 10,000 and 1,000,000 Load Repetitions.

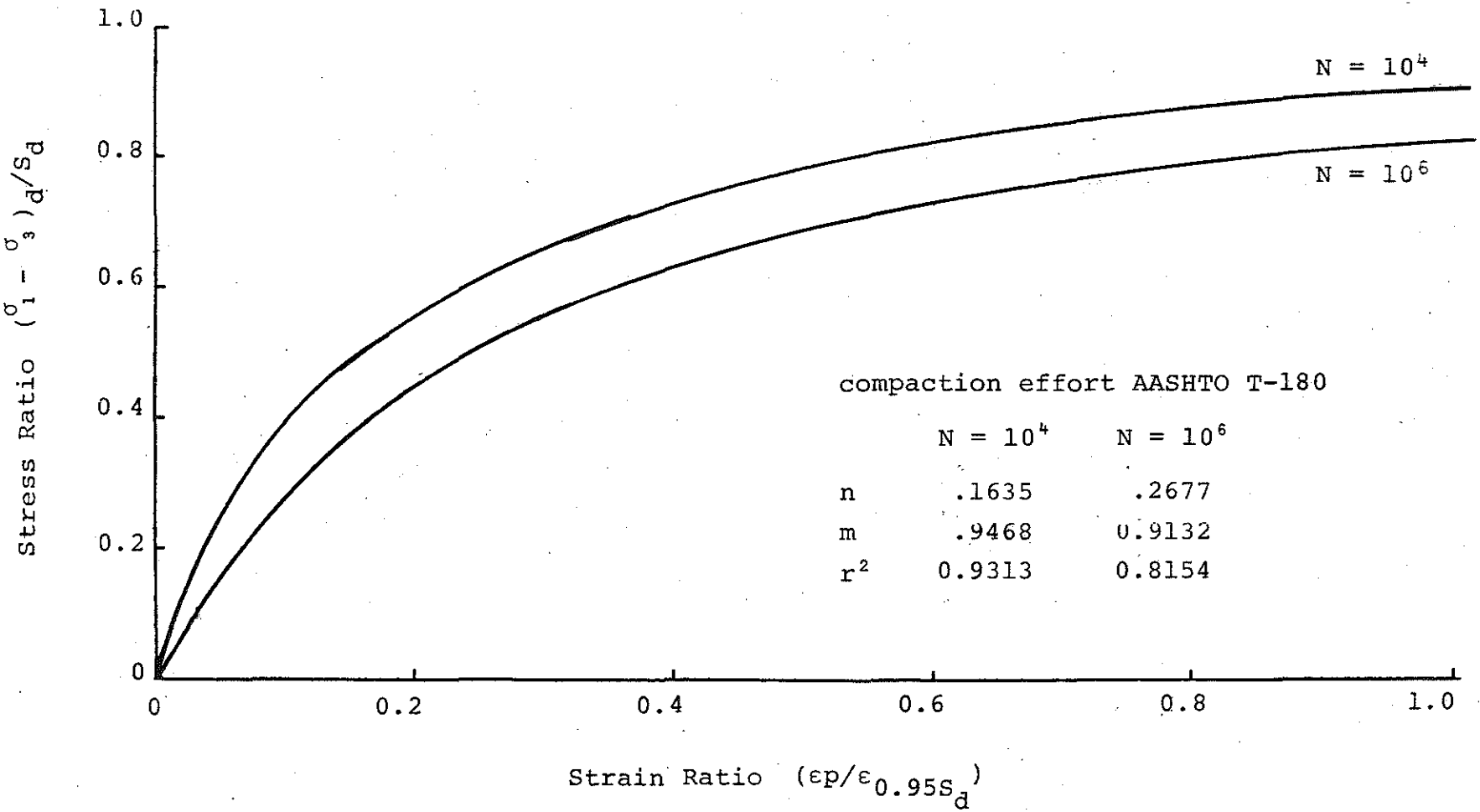

FIGURE 5.30 Normalized Cyclic Stress-Strain Data for Compacted Sand Subgrade Materials Subjected to 10,000 and 1,000,000 Load Repetitions.

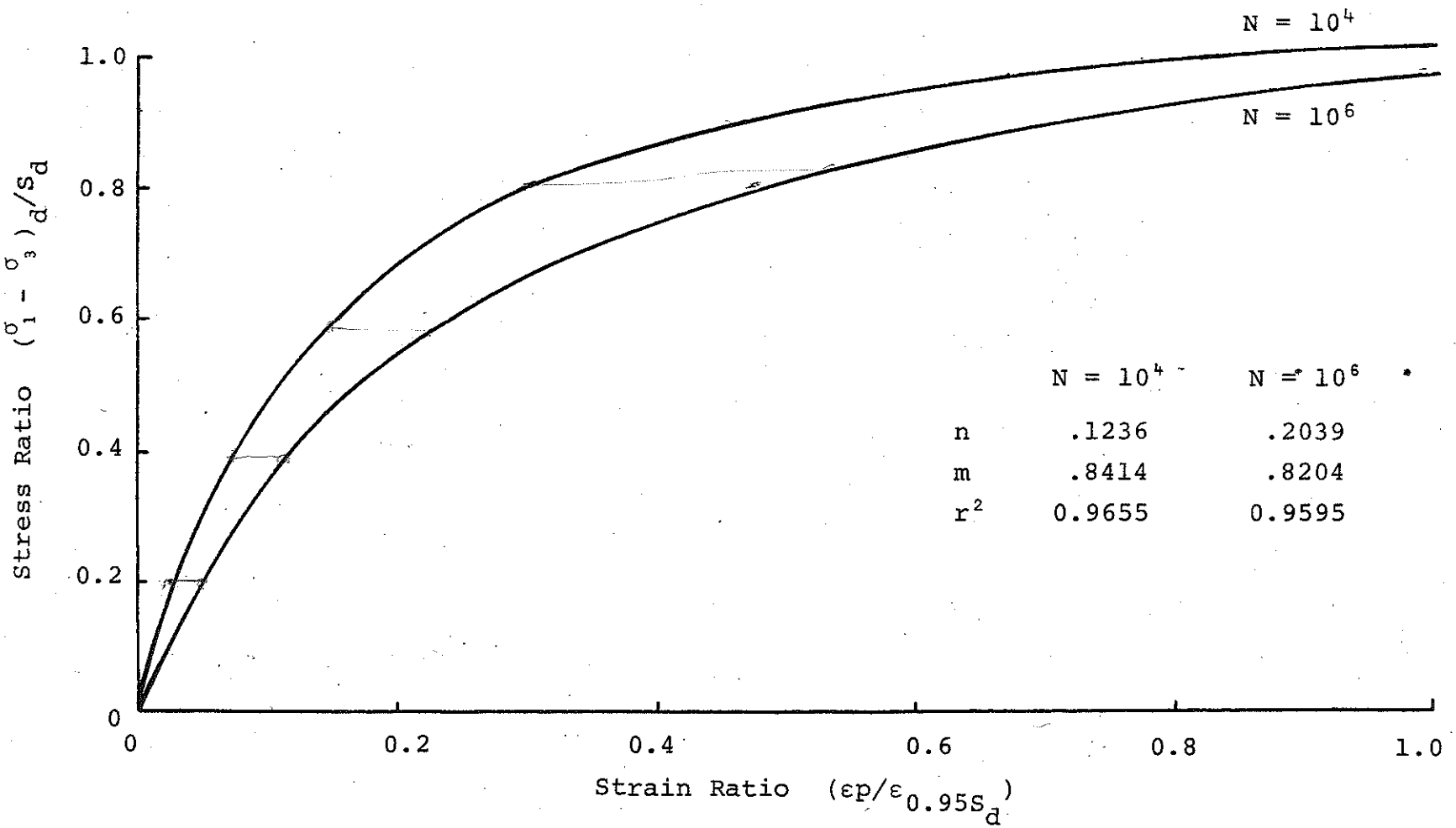

FIGURE 5.31 Normalized Cyclic Stress-Strain Data for Under Tie Materials Subjected to 10,000 and 1,000,000 Load Repetitions.

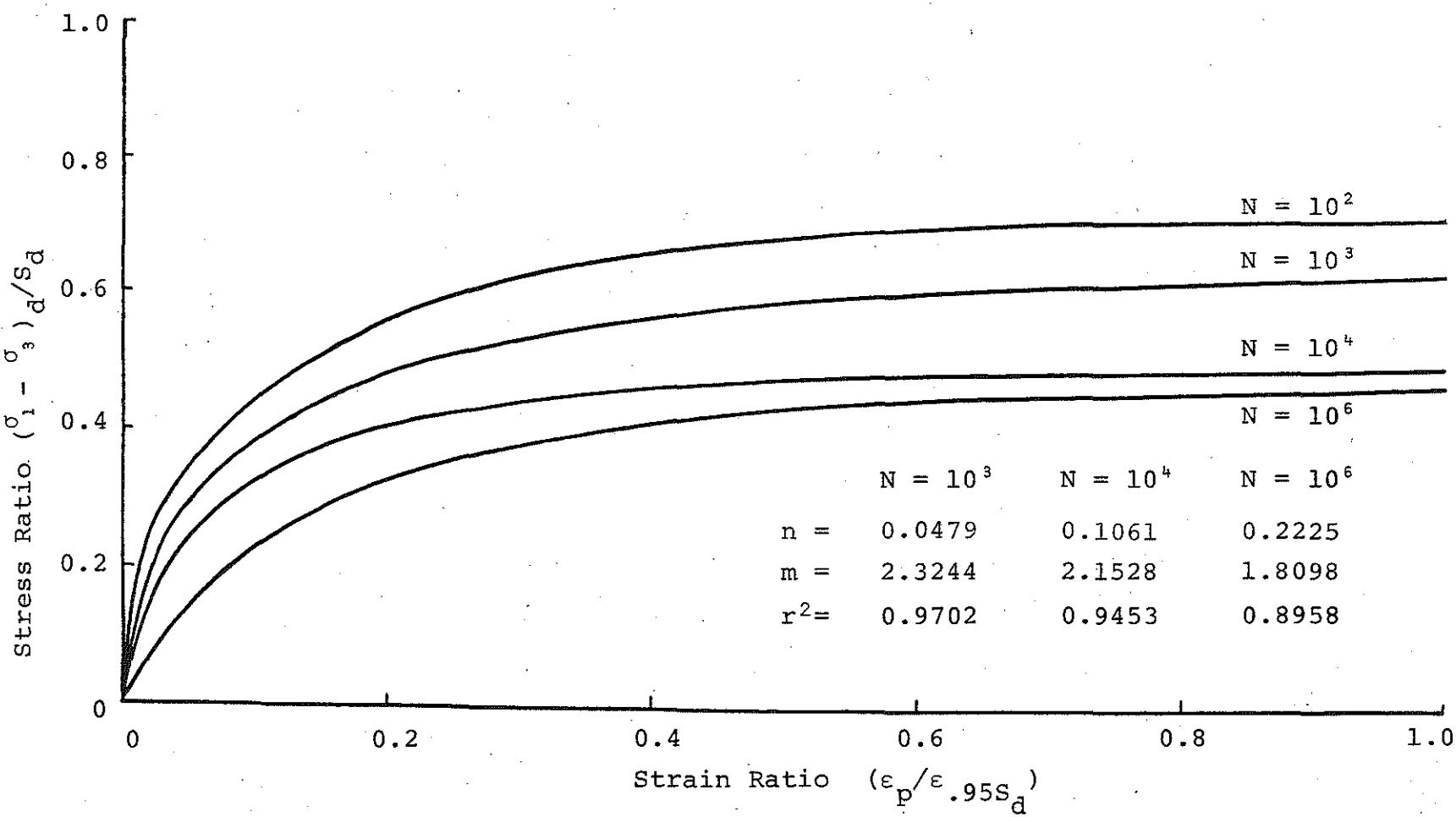

FIGURE 5.32 Normalized Stress-Strain Data for Clay Subgrade Materials from Four Different Test Sites Subjected to Different Load Repetitions.

This aspect of the parameters n and m and their influence over the normalized model will be discussed more in the next section.

5.5 Soil Support Value

Equation 5.6 is the AASHTO final flexible pavement design expression:

$$\log W_{t18} = 9.36 \log(\overline{SN} + 1) - 0.20 + \frac{\log[(4.2 - p_t)/(4.2 - 1.5)]}{0.40 + [1094/(\overline{SN} + 1)^{5.19}]} + \log \frac{1}{R} + 0.372(SSV - 3.0) \qquad (5.6)$$

where W_{t18} = total number of load applications for a given SSV and at the end of time t,

$\overline{SN}$ = structural number of pavement,

p_t = serviceability at end of time t (2.0 or 2.5),

R = regional factor,

SSV = soil support value.

In order to study the parameters of Equation 5.6 and to simulate them to the laboratory test and sample variables, the following comparisons were made:

01. W_{t18} could be simulated and compared to the number of load repetitions in the cyclic triaxial tests.

02. $\overline{SN}$ is the structural number and is related to the thickness of the pavement components. As far as the subgrade is concerned, the higher the structural nymber, the thicker is the pavement section above the subgrade and the less is the stress applied to the subgrade. Consequently, the structural number ($\overline{SN}$) in Equation 5.6 could be compared and related to the stress level or principal stress difference in the cyclic test.

03. p_t is the defined failure of the pavement section. It is called the terminal serviceability index, which could be related to or compared with the definition of failure of a laboratory test sample. Generally, the latter definition is based on a specified strain level. Thus, p_t could be related to the defined strain at failure.

04. SSV is the soil support value. The main objective of this project is to relate the SSV to some physical parameter of the subgrade materials.

Figure 5.33 shows the soil support value of Equation 5.5 plotted against the total number of load applications for a regional factor of 2.0, terminal serviceability index of 2.5, and several structural numbers. Examination of the figure indicated that for one particular subgrade soil (constant SSV), the higher the structural number the thicker the pavement section and the higher is the number of load repetition to failure. Using the previous simulation, the above statement could be rewritten for a laboratory sample as: the lower the stress level the higher the number of load applications to failure (see Section 5.3.1.3 above). Figure 5.34 shows the soil support value plotted against the structural number for a terminal serviceability index of 2.5 and regional factor of 2.0 and several number of load repetitions. It can be seen that for one particular value of W_{t18} the higher the structural number the lower the SSV required. Once again, this could be related to the laboratory soil sample as for the same number of load repetitions to failure the lower the stress level the lower the required sample strength. Figures 5.35 and 5.36 show similar features to those of Figures 5.33 and 5.34. It should be noted that all four figures were plotted using Equation 5.5.

Further examination of Figures 5.33 through 5.36 indicated that the SSV of one particular subgrade material is independent of lateral stress, stress level, water content, regional factor, and method of compaction. The SSV, however, is dependent only on the soil type. This could be restated as: the soil support value of one material is fixed and constant unless some stabilizing agent is introduced and thus the soil type is changed. Indeed, according to AASHTO classification the A-6 materials were assigned a soil support value of 3.0, and a soil support value of 10.0 was assigned for the A-1 materials. These observations suggested

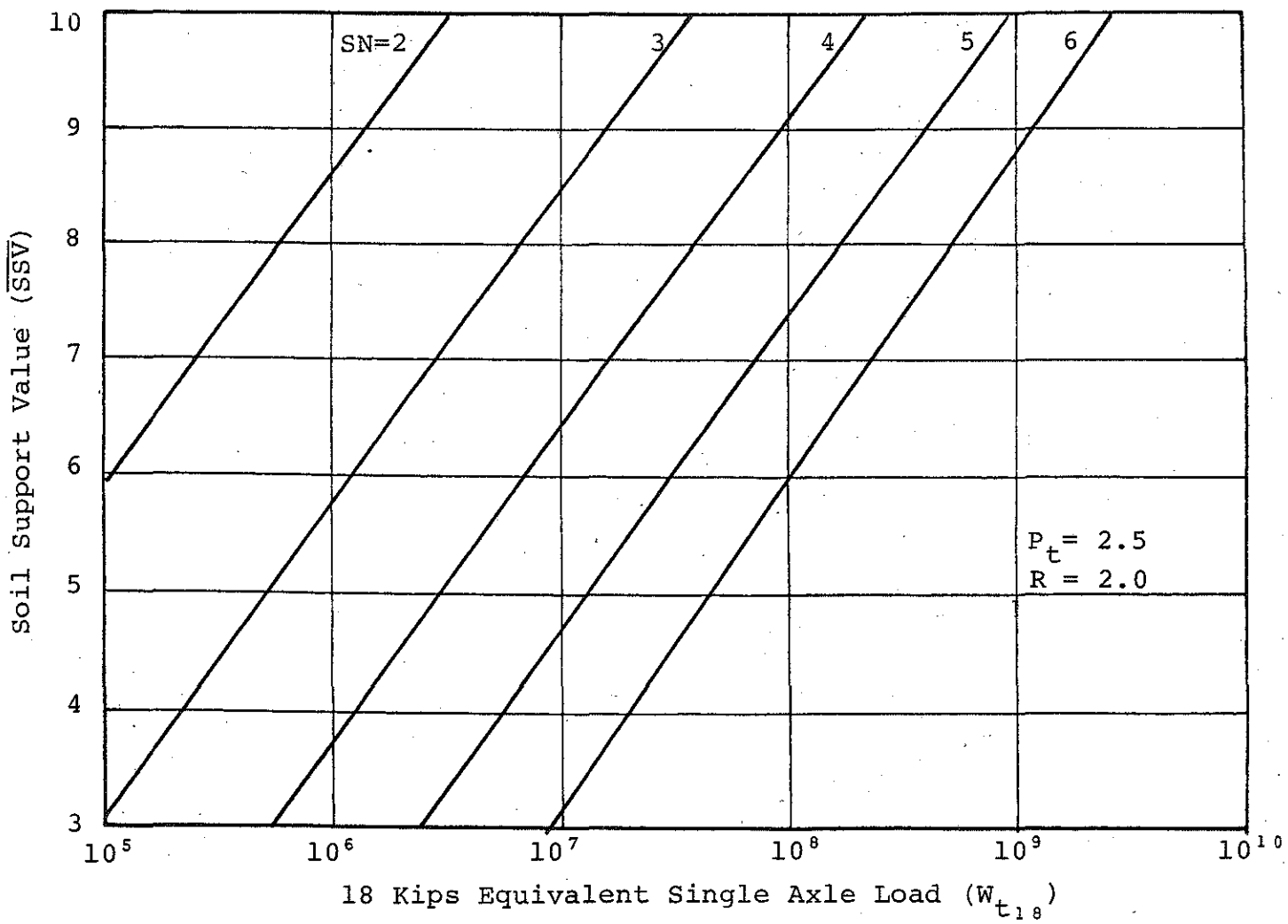

FIGURE 5.33 Soil Support Value Versus 18 Kips Equivalent Single Axle Load for Regional Factor of 2.0, Terminal Serviceability of 2.5 and Different Structural Numbers.

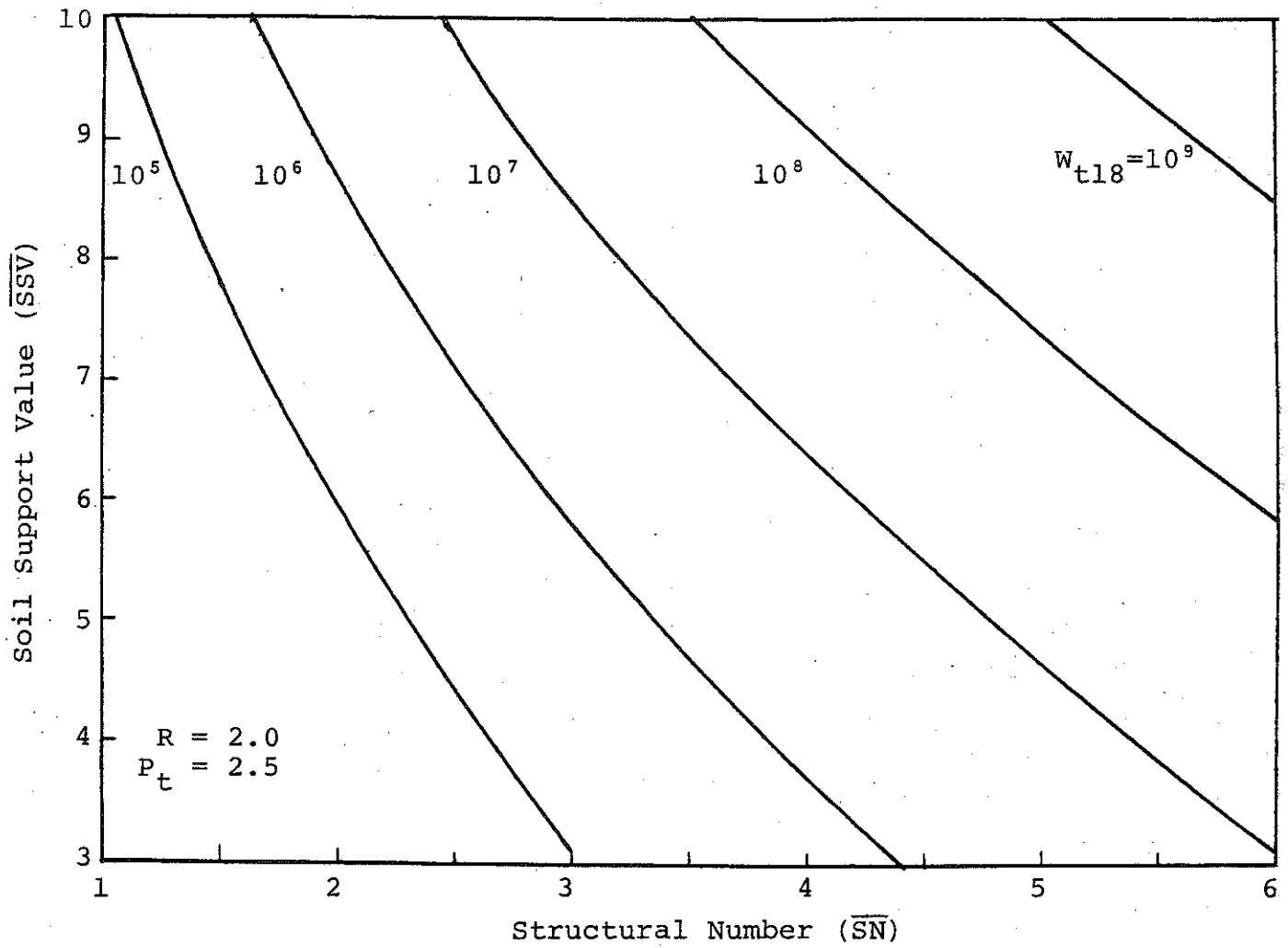

FIGURE 5.34 Soil Support Value Versus Structural Number for Regional Factor of 2.0, Terminal Serviceability of 2.5 and Different Numbers of 18 Kips Equivalent Single Axle Load.

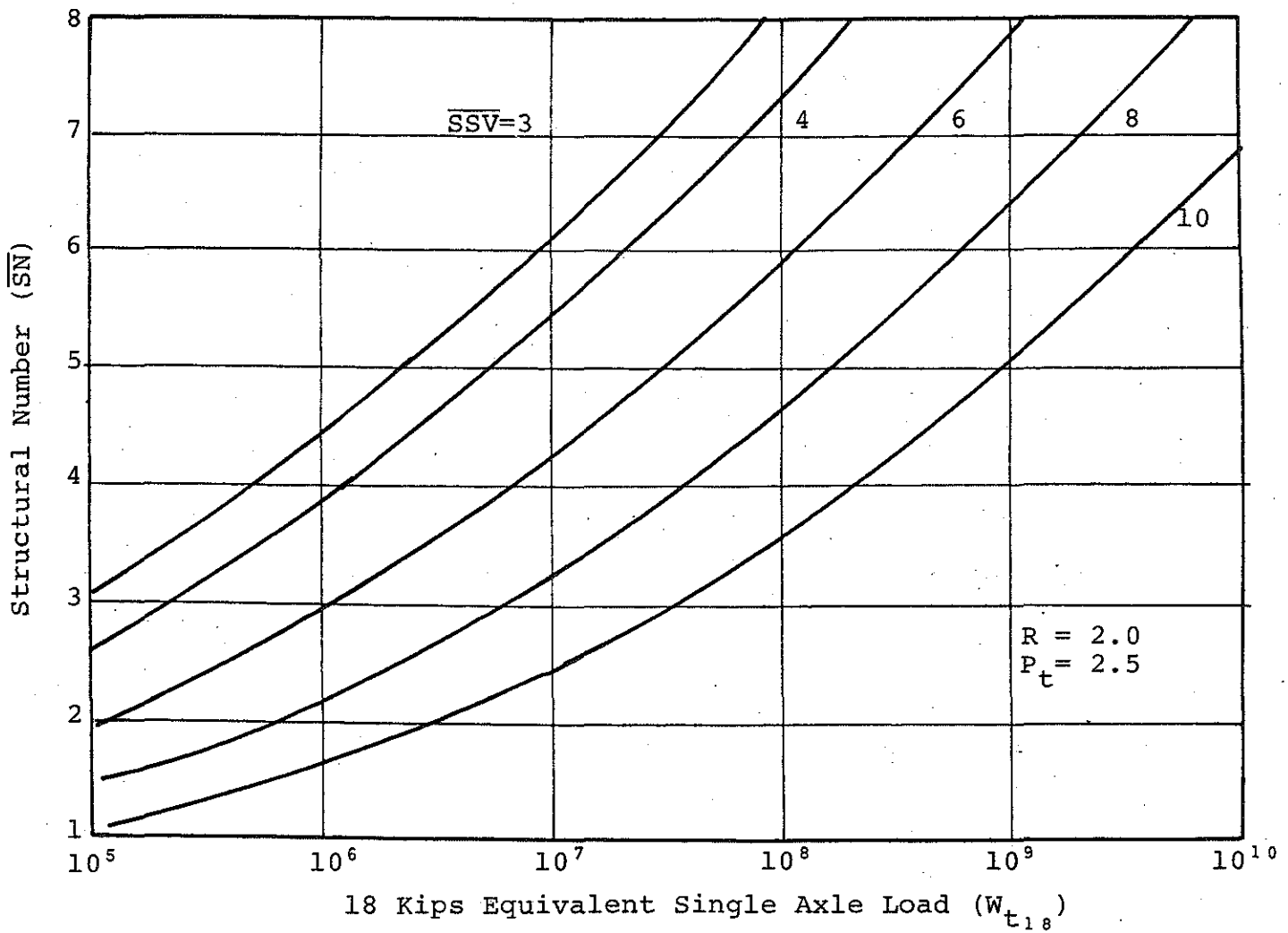

FIGURE 5.35 Structural Number Versus 18 Kips Equivalent Single Axle Load for Regional Factor of 2.0, Terminal Serviceability of 2.5 and Different Soil Support Values.

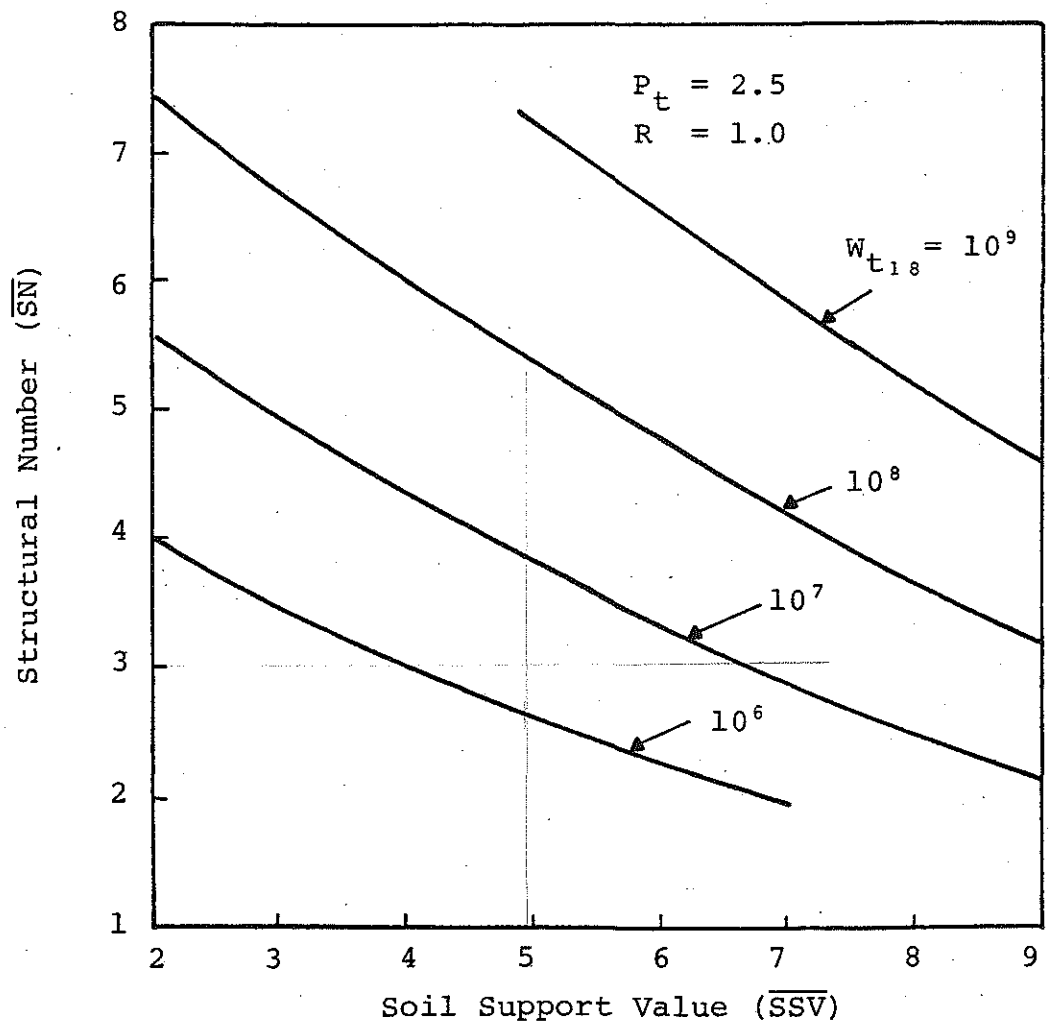

FIGURE 5.36 Structural Number Versus Soil Support Value for Regional Factor of 1.0, A Terminal Serviceability of 2.5 and Different Numbers of 18 Kips Equivalent Single Axle Load.

that the physical parameter of subgrade material to be related to the SSV should possess the following properties: 1) be independent of lateral stress, 2) be independent of stress level, 3) be independent of ambient and moisture conditions, 4) be independent of density, void ratio, and consolidation, and finally 5) be dependent only on soil type. To the best of the author's knowledge, such a physical parameter does not exist. Consequently, a new search to explain the SSV and relate it to a mathematical and/or physical model, rather than one single parameter, was initiated The requirements of the model should be the same as those of the physical parameter.

At this time, the normalization process discussed in Section 5.4 above was finalized and proven to be valid for a wide range of materials. Recall that the normalized curve (stress ratio versus strain ratio) was found to be independent of: 1) confining pressure, 2) stress level, 3) moisture content, 4) density, void ratio, and consolidation, and finally 5) dependent on soil type and the number of load applications. These requirements appeared to be adequate except for the dependency of the normalized model on the number of load applications. These observations suggest the idea that if the normalized model is fixed at a number of load repetitions, then it could be used to examine its relation to the SSV.

Figure 5.37 shows the normalized stress ratio plotted against the normalized strain for five different materials. It should be noted that each curve in the figure is dependent on the particular soil that it represents. If it is assumed that for each soil type, failure occurs when the strain ratio reaches 100%. It follows that, for the same number of load repetitions, a different stress ratio is required to fail different materials. These stress ratio for the five materials in Figure 5.36 are:

0.33 for A-6 subgrade soils,

0.49 for Michigan clay subgrade,

APPENDICES

APPENDIX A

APPENDIX A

EQUIPMENT

A.1 The Cyclic Triaxial Test (MTS) System

A schematic diagram of the cyclic triaxial test equipment is shown in Figure A.1. The test set up is shown in Figure A.2; it consisted of the following components:

01. An MTS electrohydraulic closed loop test system which consisted of the actuator, servovalve, hydraulic power supply, servo and hydraulic controllers. (These applied the cyclic axial stress to the sample.)
02. A triaxial cell which contained the sample, load cell, and LVDT's.
03. A control box for interfacing the MTS closed loop to the output recording equipment.
04. Output recording equipment which monitored the load (stress) and displacement (strain) during the tests.
05. Minicomputer (digital) system, which modified the loading system.

A.1.1 The MTS Electrohydraulics Closed Loop Test System

A schematic representation of the MTS electrohydraulic closed loop test system is shown in Figure A.3. The system consists of:

01. An MTS hydraulic power sypply, Model 506.02, 6.0 gal per minute at 3000 psi.
02. An MTS hydraulic control unit, Model 436.11, with a function generator.
03. An MTS servovalve controller, Model 406.11, with AC and DC feedback signal conditioning.
04. An MTS actuator, Model 204.52, capacity of 5.5 kips with a Model 252.23A-01 servovalve.
05. A Strainsert load cell, Model FL5U-2SGKT, maximum capacity 5000 pounds.

The system operates as follows:

01. A command signal (voltage) from the function generator in the 425.11 (see Figures A.2 and A.3) or other external source is input to the 406.11, where it is compared to the feedback signal (voltage) from a transducer (e.g., a load cell or LVDT) monitoring the response of the specimen in the closed loop.

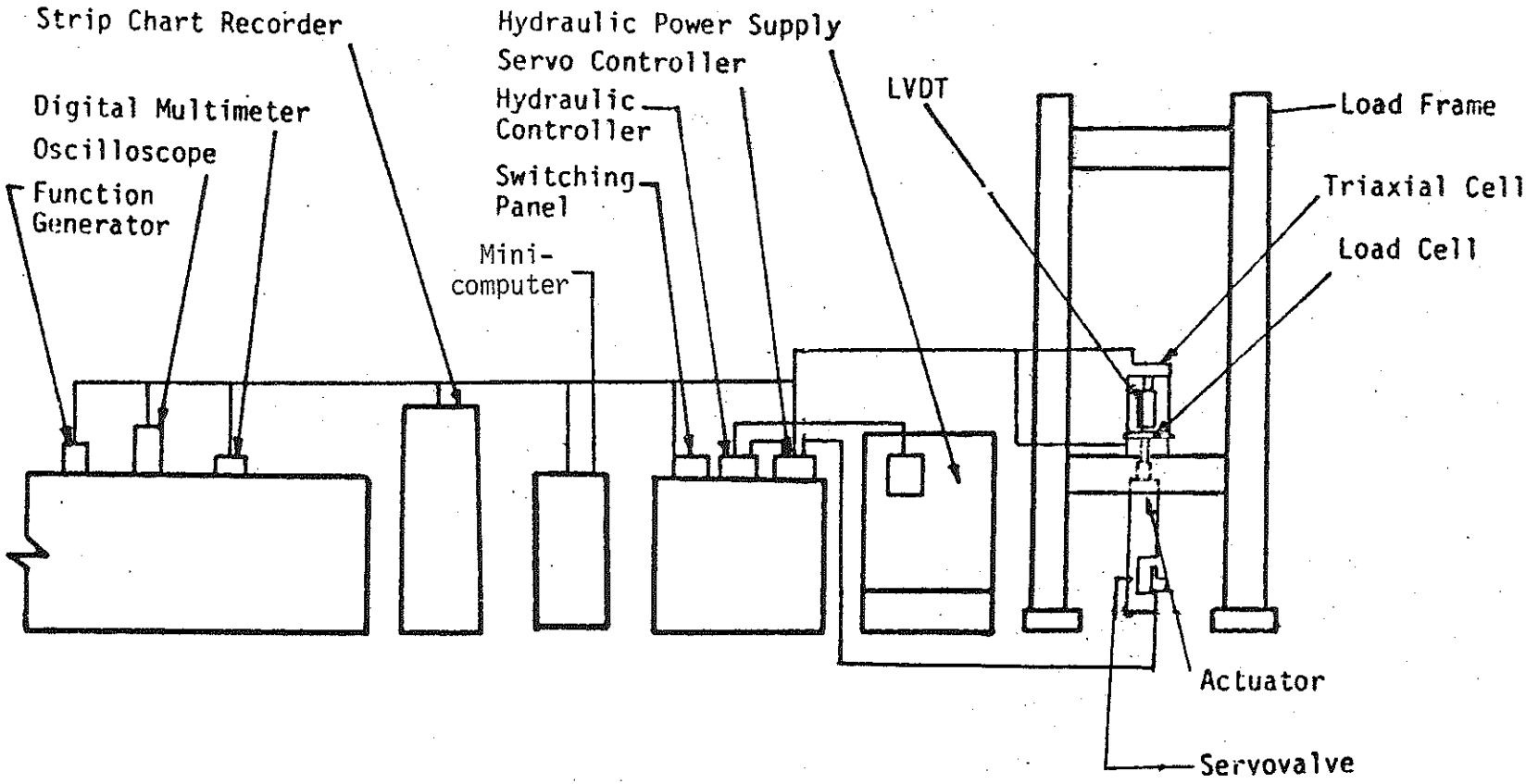

FIGURE A.1 Schematic of Cyclic Triaxial Test Equipment.

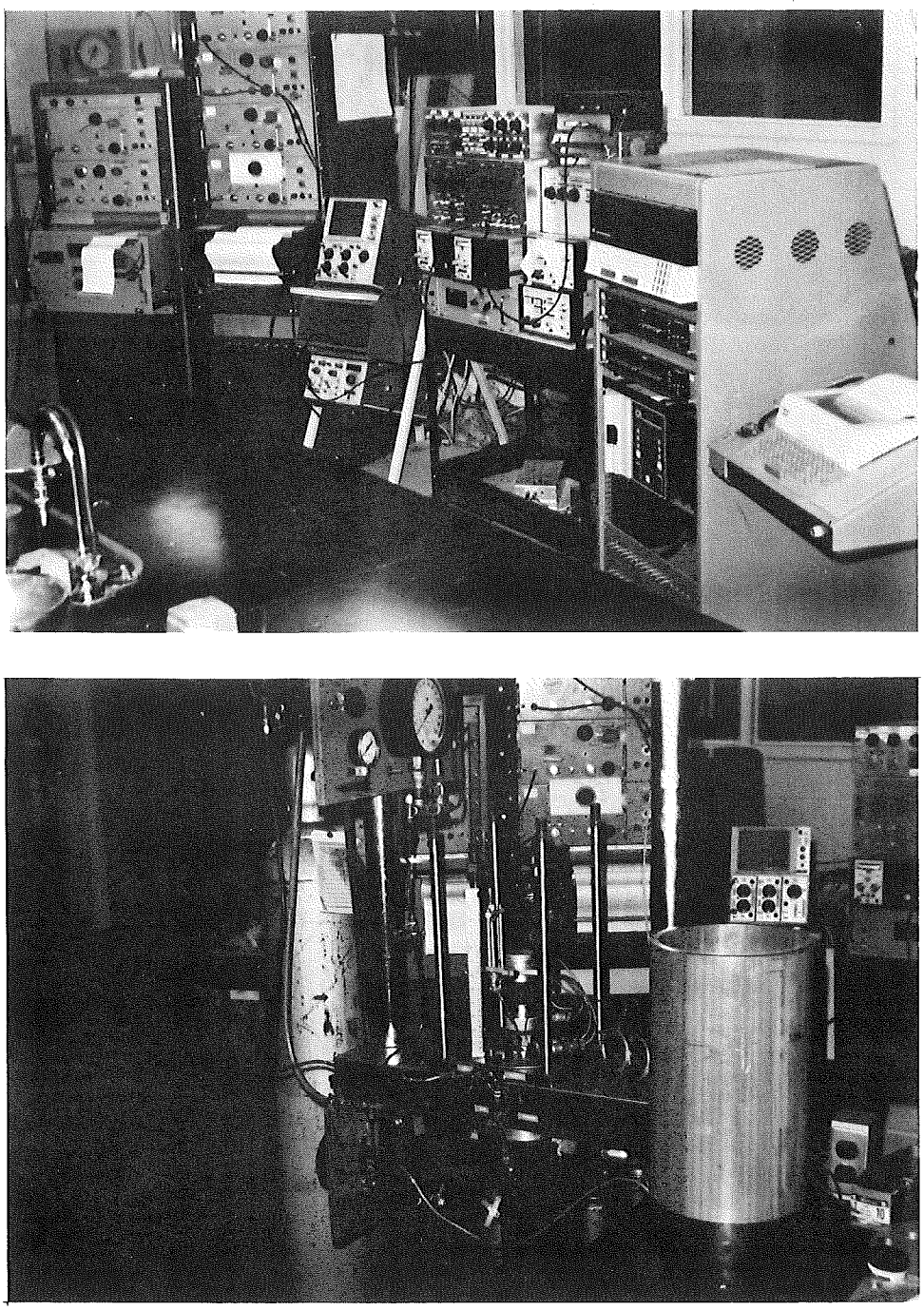

FIGURE A.2 Test Set-Up.

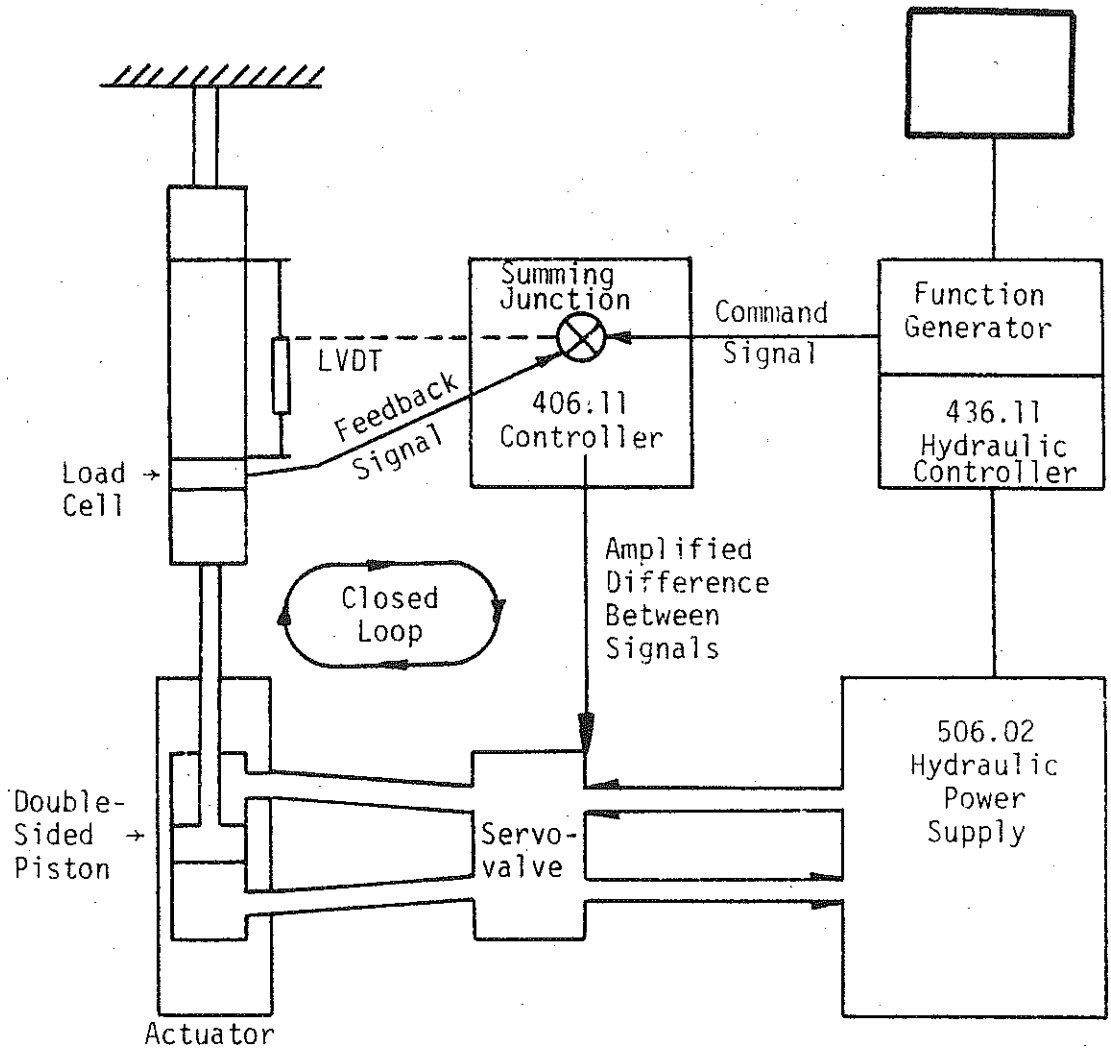

FIGURE A.3 Schematic of MTS Electrohydraulic Closed Loop Test System.

02. The difference error between the two signals is amplified and applied to the torque motor in the servovalve coupled to the actuator.

03. The torque motor drives a pilot stage which in turn drives a power stage of the servovalve which directs hydraulic fluid under pressure to one side or the other of the double-sided actuator piston to cause the actuator to move.

04. The movement of the actuator causes the specimen to respond in such a way that the transducer monitoring the specimen "feeds back" a signal which is equal to the command signal.

The speed at which these steps are executed causes the sample, for all practical purposes, to be subjected to a loading equal to the command signal. A more complete treatment of closed loop testing theory is given by Johnson [58].

A.1.2 The MTS Servovalve Controller Model 406.11

The front panel of the 406.11 controller is shown in Figure A.4. The controls indicated by the circled numbers are discussed in order below.

01. The panel voltmeter has two functions. First, it can be used to indicate the error between the command signal and the feedback transducer. Second, it can be used to indicate the voltage output of feedback transducer XDCR1, XDCR2, or the servovalve drive. (The servovalve regulates the flow of hydraulic pressure between the hydraulic power supply and the actuator.) For the cyclic triaxial tests a negative error means compression and positive error means tension to the specimen. The panel voltmeter was most often used to monitor the error between the command signal and the feedback transducer before applying the hydraulic pressure. To insure that the actuator does not move when hydraulic pressure is applied, the error signal must be zero.

02. The Set Point control provides a static command signal (voltage). There are 1000 divisions on the Set Point dial. Each division is equivalent to 20 mv. A positive command signal (Set Point between 500 and 000) produces actuator piston compression; a negative command signal (Set Point between 500 and 1000) produces actuator piston extension. When the feedback signal is from the LVDT in the actuator, Set Point is used to move the actuator up or down even with no specimen in the loop. When the feedback is from any other transducer, the Set Point control establishes a static level

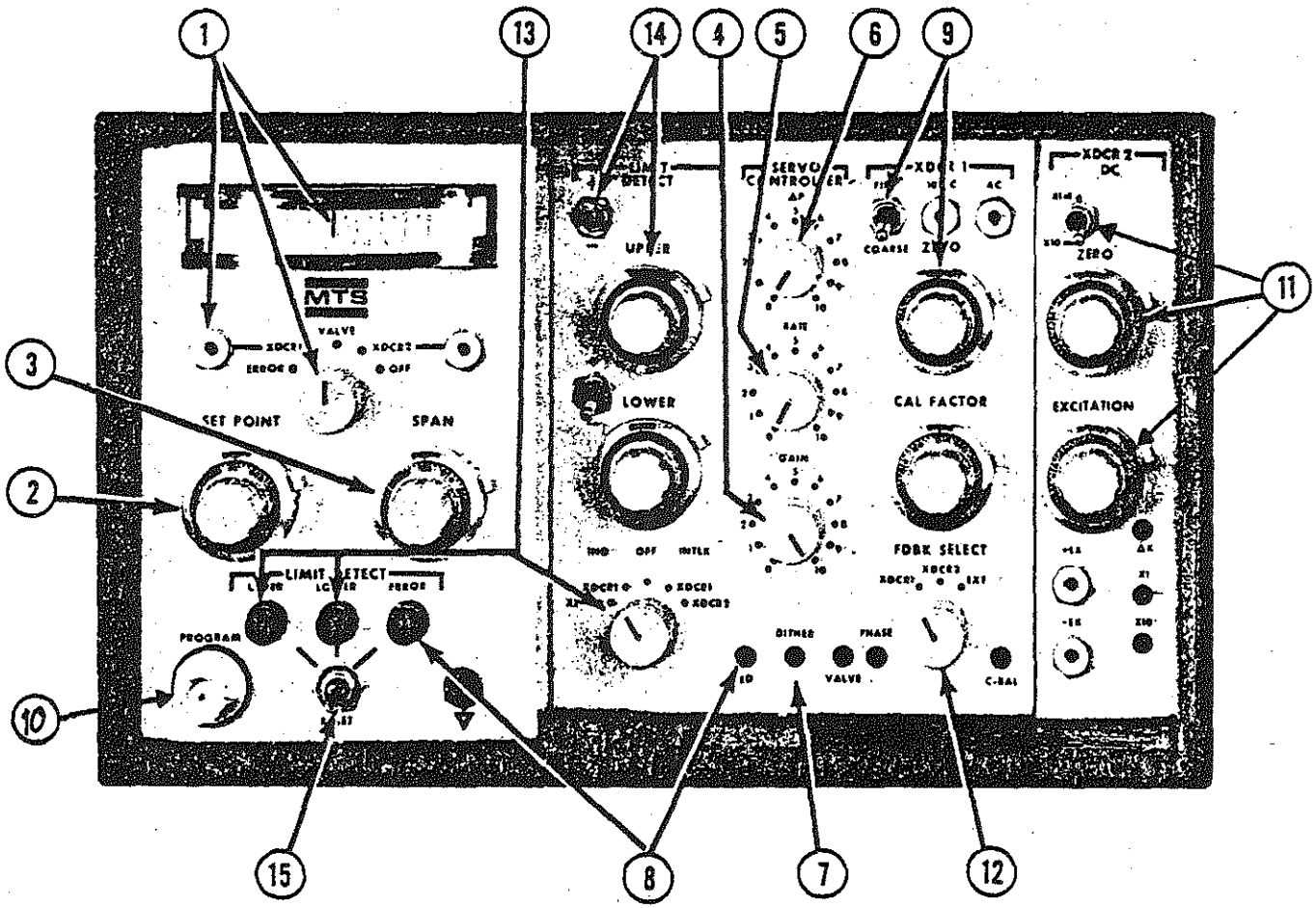

FIGURE A.4 MTS Servovalve CONTROLLER Model 406.11.

of response of the specimen. With feedback from the load cell, Set Point was used to apply static compressive loads for the static triaxial tests. Set Point was also used to apply static load of one-half σ_d for the cyclic triaxial tests.

03. The Span control established the amplitude of a command signal waveform during cyclic loading. The amplitude is about the Set Point level. There are 1000 divisions on the Span control dial. Each division is equivalent to an amplitude of 10 mv. The Span was used to set the load amplitude during cyclic triaxial testing.

04. The Gain control establishes the rate and accuracy of response of the actuator ram to the command signal. The Gain control is therefore used to improve the response of the closed loop test system, which includes the specimen. To set the system at optimum Gain, the sample was subjected to a low frequency, low amplitude square wave loading. The feedback signal was monitored with an oscilloscope. The Gain control was turned clockwise until small oscillations were observed at the peak of the square wave, as shown in Figure A.5b. At this point, the Gain was reduced until the oscillations stopped, as shown in Figure A.5c. The Rate (described below) was adjusted to eliminate "overshoot" at the corner of the peak of the square wave, as shown in Figure A.5c.

05. The Rate control helps prevent "overshoot" at high Gain settings. The Rate was adjusted after the Gain had been set as described above.

06. The ΔP control is operative only when the 406 is equipped with option B. Provides added stability in some systems by addition of the signal from a differential pressure (ΔP) transducer across the actuator cylinder.

07. The DITHER trimmer controls the amplitude of a small cyclic signal applied to the servovalve coil to prevent servovalve silting.

08. The Error Detector (ED) trimmer adjusts the percentage of error at which the Error Detector circuit sets, turning on the ERROR indicator and opening the fail-safe interlock. When ERROR lights, all other limit and error detecting circuits, including those on any other channels, automatically become inoperative.

09. The Cal factor, Zero, and Fine/Coarse controls provide adjustment of the signal for transducer XDCR1. In general, the transducer used with XDCR1 was an LVDT. Cal Factor was used to adjust the voltage output from the LVDT. The Cal Factor was adjusted to obtain ± 10 volts when the core of the LVDT moved 0.100 inch. The

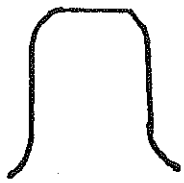

a) Overdamped, Gain too low

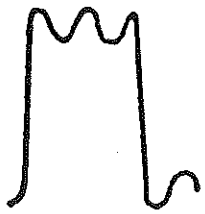

b) Underdamped, Gain to high

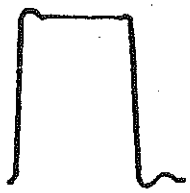

c) Optimum Gain

FIGURE A.5 Gain and Stability Adjustment.

Zero control introduces an electrical offset to the signal from the LVDT. It has 1000 divisions on the dial. A Zero control setting of 500 corresponds to zero voltage offset. The Zero control provides negative electrical offset when it is between (000) and (500) and positive offset when it is between (500) and (1000). The Fine/Coarse switch determines the operating range for the Zero control. When it is selected to Fine, the electrical offset from the Zero control per division is lower than when it is selected to Coarse. In this experiment, high electrical offset is necessary; therefore, the switch was selected to Coarse.

10. Program is used to input an external source of command signal.

11. The Excitation, Zero, and (x1/x10) switch provides adjustment of the signal for transducer XDCR2. In general, the transducer used with XDCR2 was a load cell. The Excitation was used to adjust the voltage output from the load cell. It has 1000 divisions on the dial. The Excitation was adjusted to obtain 20 mv per pound of loading using a 5 Kip load cell. The Zero control introduces an electrical offset to the signal from the load cell. It has (100) divisions on the dial. A Zero control setting of (500) corresponds to zero voltage offset. It provides positive electrical offset when it is between 500 and 1000. The x1/x10 switch determines the operating range for the signal from the load cell. When in the (x10) position, the signal from the load cell is amplified 10 times that of the x1 position. The x10 position was used in the laboratory investigations phase of this research program. By selecting the x10 position, the 5000 pound load cell functioned effectively as a 500 pound load cell. This was desirable because of the relatively small loads used in the testing program. High output signals could thus be obtained without the danger of the load cell being overstressed.

12. The Feedback Select position determines which feedback signal will be used in the closed loop test circuit. This may be the signal from Transducer Conditioner 1 (XDCR1), Transducer Conditioner 2 (XDCR2), or from an external transducer conditioner (EXT). For the current research it was desired to control the load amplitude. Therefore, Feedback Select was placed in position XDCR2 to feedback the signal from the load cell to use in the closed loop circuit.

13. The Limit Detector determines which transducer conditioner (XDCR1 or XDCR2) signal will be monitored in the "failsafe" circuit. If the switch is set on INTKL,

the failsafe interlock circuit will turn off the hydraulic power supply when the signal voltage is greater or lower than a selected range of voltage. If the switch is set on IND, the Limit Detector will indicate, by the upper or lower red light on the panel, when the signal voltage is greater or lower than a selected range of voltage.

14. The Upper and Lower limit controls are used to select the range of acceptable voltage. The Upper limit is set at the most positive or least negative limit. The Lower limit is set at the most negative or least positive limit. Each limit dial has 1000 divisions corresponding to 10 volts.

15. The Reset is used to extinguish the indicator light when the signal voltage level is within the selected voltage range. If the light for the Limit Detector is still lit with the failsafe interlock circuit in operation, the hydraulic power supply cannot be engaged. Therefore, before applying the hydraulic power supply, the light has to be extinguished with the Reset button. If the switch is in the off position, the failsafe circuit is inoperative.

A.1.3 The MTS Controller Model 436.11

The front panel of the 436.11 is shown in Figure A.6. The controls indicated by the circled number are discussed in order below.

01. The Power control applied AC operating voltage to the control unit.

02. The HYD Pressure Low or High or Hydraulic Off control is used to turn the hydraulic power supply on and off.

03. The Program Stop or Run control is used to start or stop generation of a command signal waveform.

04. The HYD INTLK (hydraulic interlock) switch indicator is associated with abnormal condition sensors, such as the failsafe circuits in the controller and the overtemperature and low fluid level conditions of the hydraulic power supply. The indicator will light when any such condition occurs. At the same time, the hydraulic pressure is automatically removed from the servovalve and the programmer stop. When the abnormal condition has been removed, the HYD INTLK should be extinguished by pushing it and holding it to allow the system to be restarted without removing the abnormal condition, unless that condition is related to the hydraulic fluid overheating (overtemperature) or is at low level.

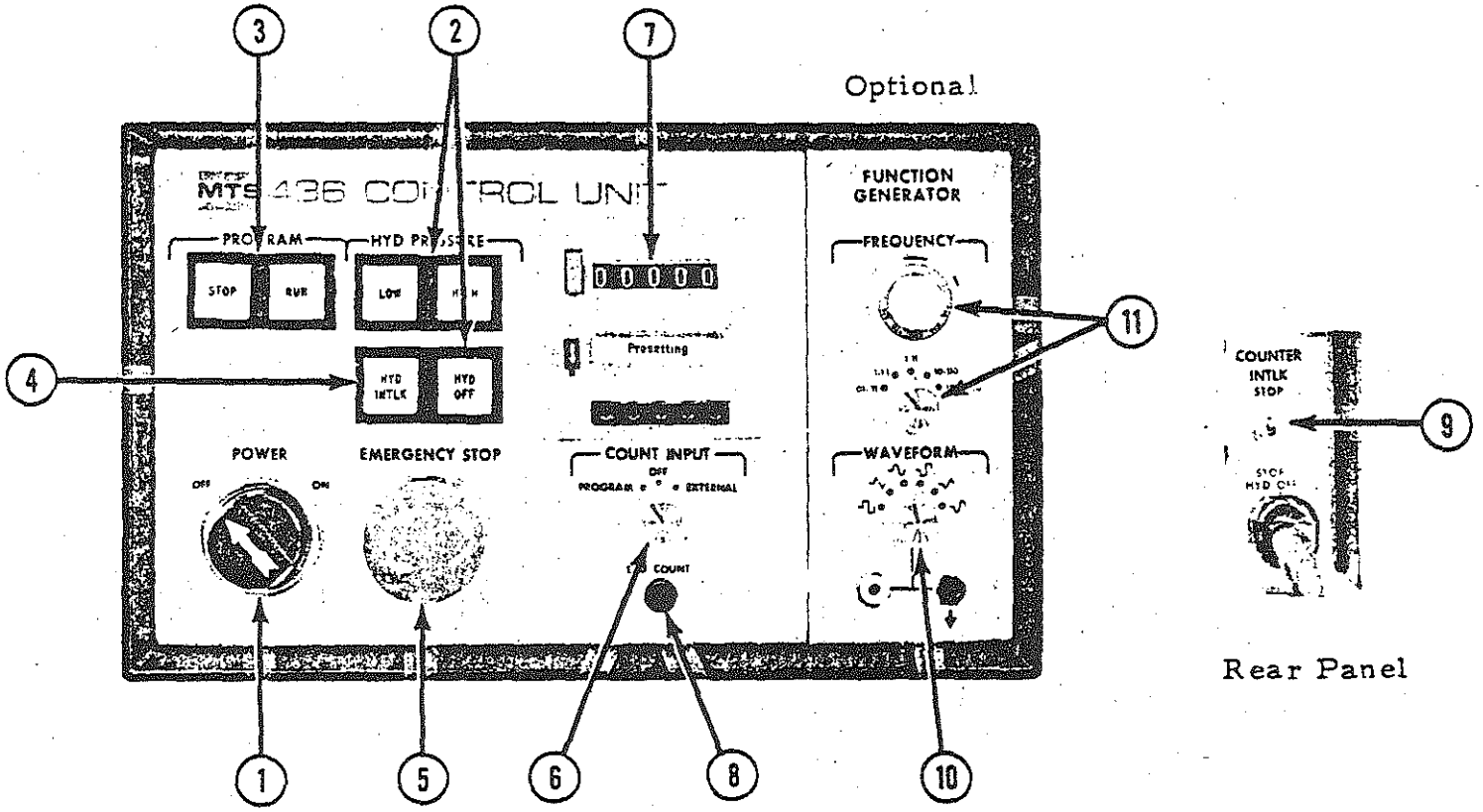

FIGURE A.6 The MTS Control Unit Model 436.11.

05. Emergency Stop is used to stop the hydraulic power supply and generation of the command signal waveform. Emergency Stop and Hyd Off have the same effect.

06. The Count Input control is used to select the method of controlling the number of cycles during a test. If Program is selected, the duration of the test must be present.

07. The Counter indicates the number of elapsed cycles in increments of ten.

08. The End Count indicator lights when the upper counter register reaches the preset count.

09. The Counter INTLK switch determines whether an END COUNT causes complete system shutdown, including removal of hydraulic pressure (STOP-HYD OFF position), or only program stop (STOP position) After the required number of cycles has been reached, the program will automatically stop and the End Count will light up. If the Off position is selected, the program will run either until the operator pushes Stop or until the Failsafe system is triggered.

A.1.4 Control Box

The control box was built at Michigan State University. The front panel of the box is shown in Figure A.7. The control box allows for switching between two complete MTS electrohydraulic closed loop systems so that output recording equipment can be shared. Also, electronic circuits are incorporated which can be used to offset and amplify output signals so that they are compatible with the input requirements of a minicomputer. Provision is also made for recording the unadultrated output signals. Voltage offsets are also provided to offset large constant voltages so that amplitudes of cyclic signals can be recorded with better resolution.

A.1.5 Output Recording Equipment

The following equipment was used to monitor the load cell and LVDT during the testing program (see Figure A.2).

01. A Sanborn Model 150 strip chart recorder with two DC Coupling Preamplifiers, Model 150-1300. Both load and deformation were recorded directly on the strip chart recorder.

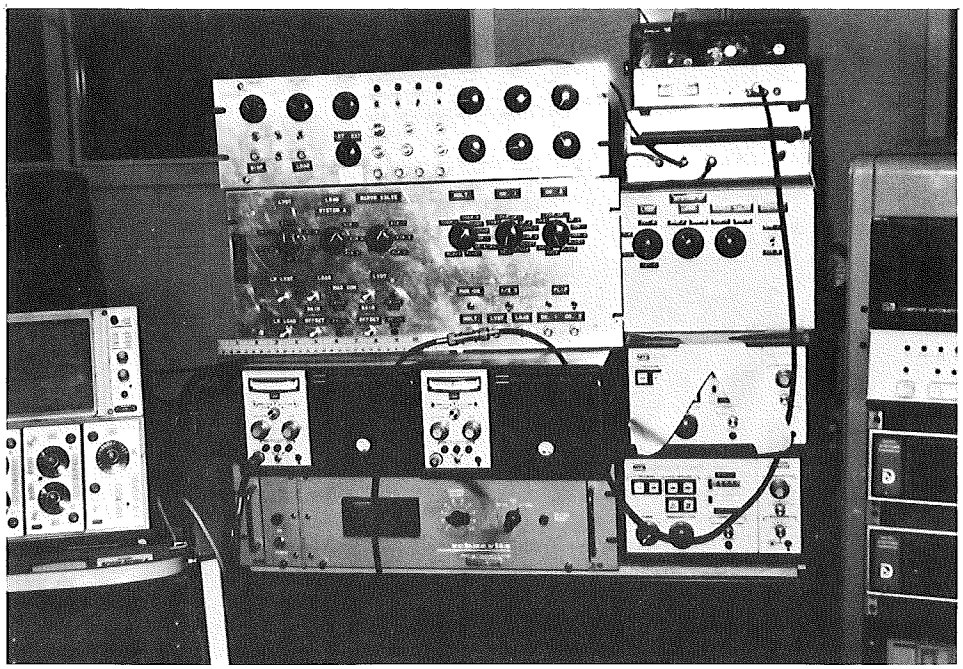

FIGURE A.7 Front Panel of the Control Box.

02. A Simpson Model 460 digital voltmeter. The voltmeter was used to monitor both load cell output and LVDT output during the experimental set up. The voltmeter was also used to monitor both load and deformation during the static triaxial tests and to monitor load as static load of one-half σ_d was being applied.

03. A Tektronic Model D13 dual beam storage oscilloscope with two 5A18N dual trace amplifiers.

A.2 Minicomputer System

The LSI-2 minicomputer system shown in Figure A.8 was used to control the signal and frequency output of the MTS controller. A detailed description of the system and program is discussed below.

A.2.1 Waveform Shaper Circuit

An interface between the LSI-2 minicomputer from Computer Automation and the MTS 436 Control Unit was designed to generate waveforms of the shape shown in Figure A.9. The frequency range of this signal varies from 0.01 Hz up to 20 Hz. The waveforms are generated by means of the generator associated with the control circuits of the MTS 436 Control Unit. This generator is triggered "on" and "off" by means of the minicomputer and under complete software control. All information required by the computer is typed on a teletype during an initialization phase.

A.2.1.a Characteristics of the MTS 436 Signal Generator

The signal generator delivers triangular, rectangular, or sinusoidal signals with peak amplitudes of 10V. No attenuation circuits are provided to adjust the amplitudes to different levels. Frequencies ranging from 2 KH2 down to 0.01 Hz are available. When triggering the "run" switch (either on the front panel or by means of the programmed input on the rear panel), the generator begins delivering a signal that starts at zero volt and stops at zero volt at the end of the last half-cycle during which the "stop" switch (either on the front panel or under program control on the rear panel) has been triggered. Figure A.10

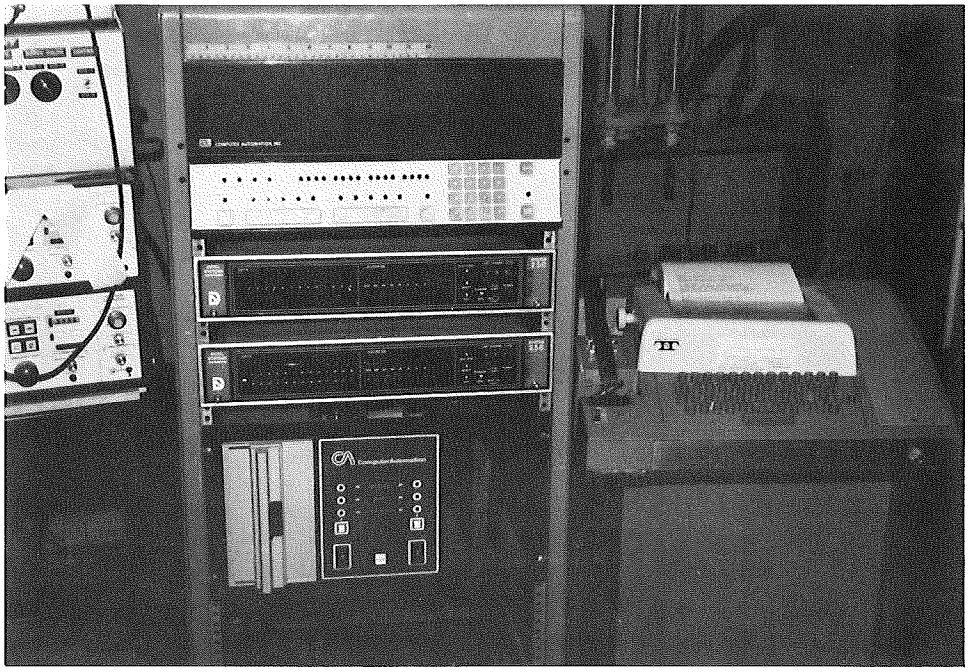

FIGURE A.8 Front Panel of the Minicomputer.

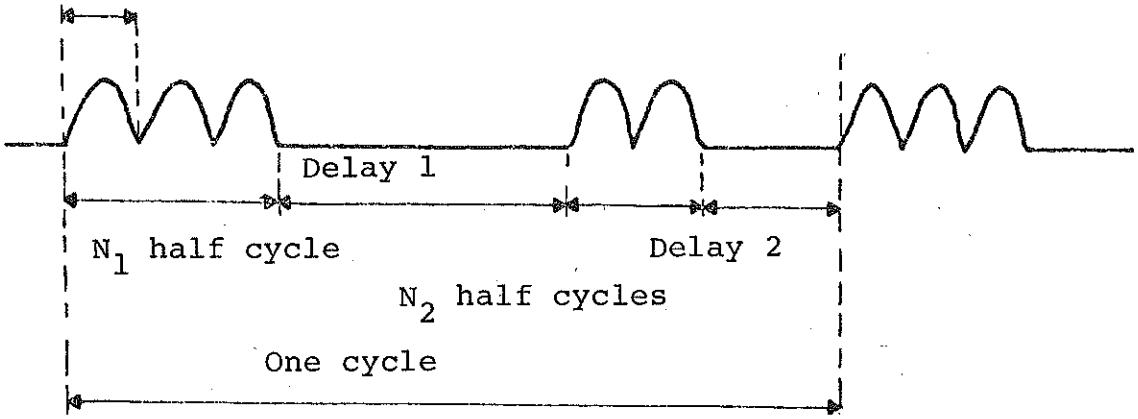

FIGURE A.9 Generated Waveforms.

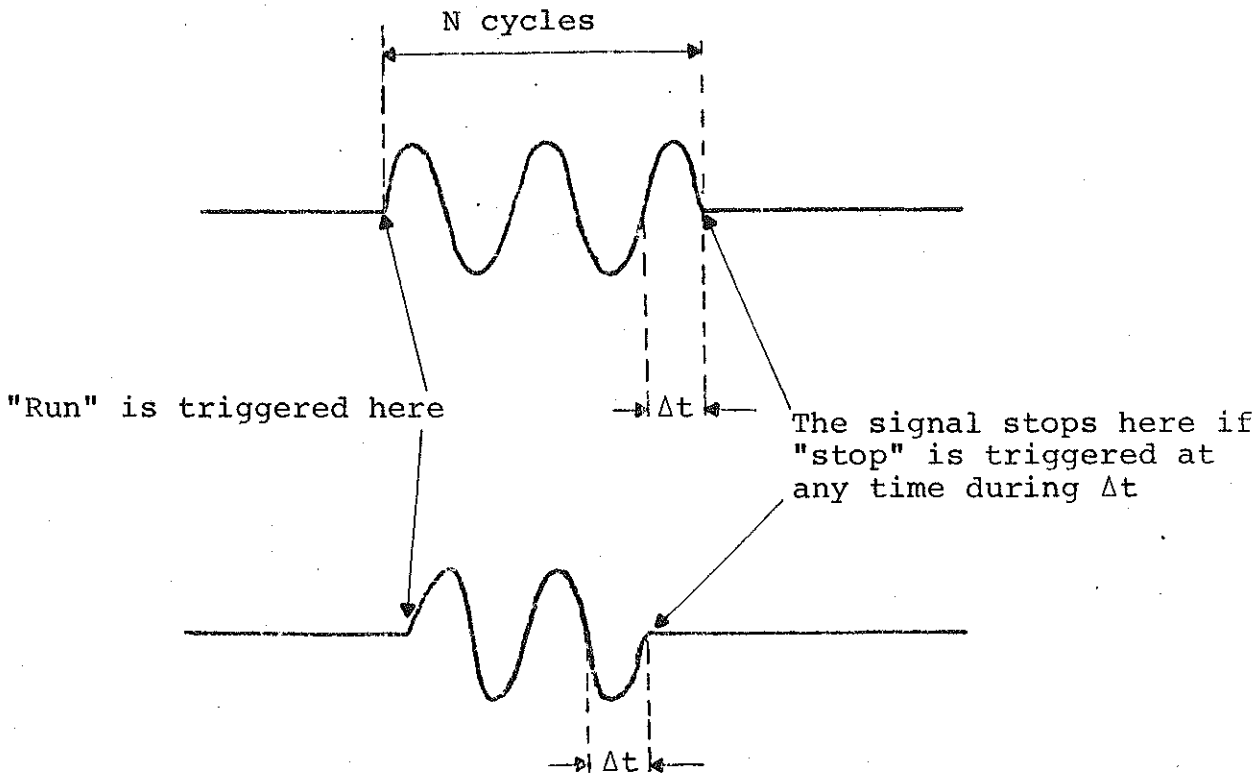

FIGURE A.10 Start and Stop Generator's Outputs.

illustrates this mode of operation. The same operation holds, whatever the shape of the signal, for the triangular and/or rectangular signals. A selector on the front panel allows the user to select positive-starting loading or negative-starting unloading signals.

To generate the type of signal represented in Figure A.11 from the previously mentioned considerations, it is obvious that a positive-starting signal (sinusoidal in this case) should be selected and that the generator's "Run" and "Stop" circuits should be triggered at the times indicated in Figure A.11.

It should be noted that: 1) if the stop is not triggered the generator goes on delivering a sinusoidal signal, the frequency of which, in this case, is that read on the frequency selector on the front panel; 2) the word "frequency" herein is referred to as the frequency of the equivalent sinusoidal periodic signal even if the generated signal is not periodic. Also, this frequency is equal to (1/T) where T is the period, as shown in Figure A.12. Further, this frequency should be distinguished from the "frequency of repetition," which is the rate at which the signal frames repeat in time.

The "Run" and "Stop" circuits in Figure A.11 will be triggered under program control.

A.2.1.b Triggering the Circuits on the MTS 436 Rear Panel

Figure A.13 shows the typical signals that should be applied to the triggering circuits. "Run" and "Stop" may be triggered as follows:

01. The user has access to the Run triggering circuit by means of connectors T15A, T15B, and T15C on the rear panel. On any of these connectors, plus C and F have to be used to trigger the "Run," i.e., start generating a half-cycle (see Figure A.14). It should be noted that pin F is ground (signal ground) and pin C is normally open, and so is the connection to the "Run" switch on the front panel. The voltage, when pin C is open, is around 11 volts (measured with a voltmeter). In order to trigger the "Run," one has to short-circuit

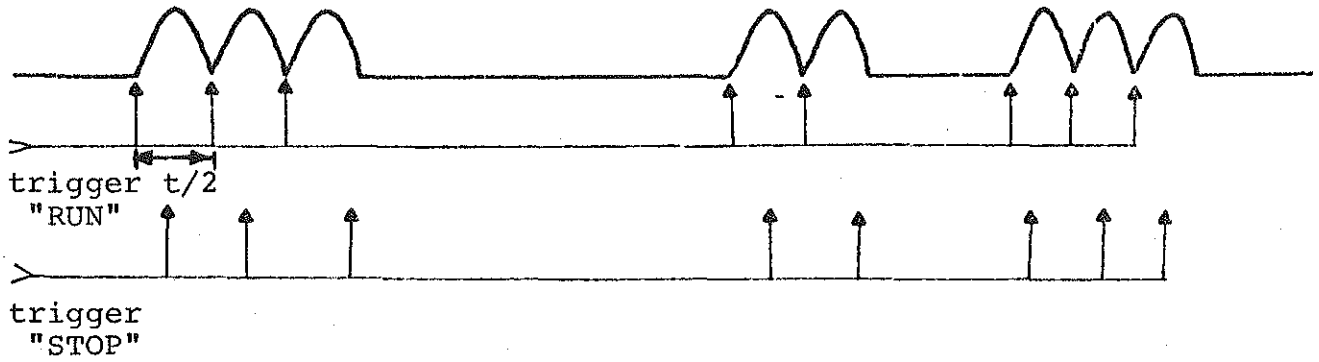

FIGURE A.11 Triggered Time.

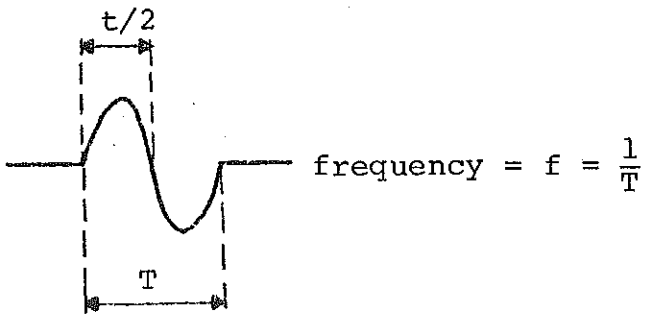

FIGURE A.12 General Signal Output from the MTS System.

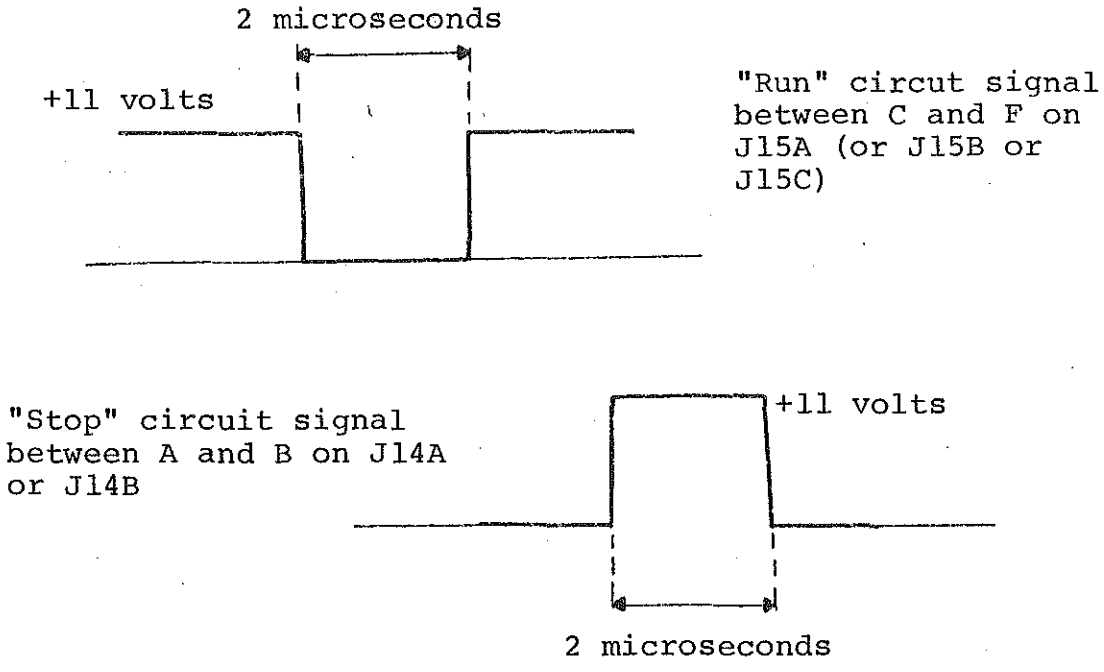

FIGURE A.13 Typical Signals for Triggering the Circuits.

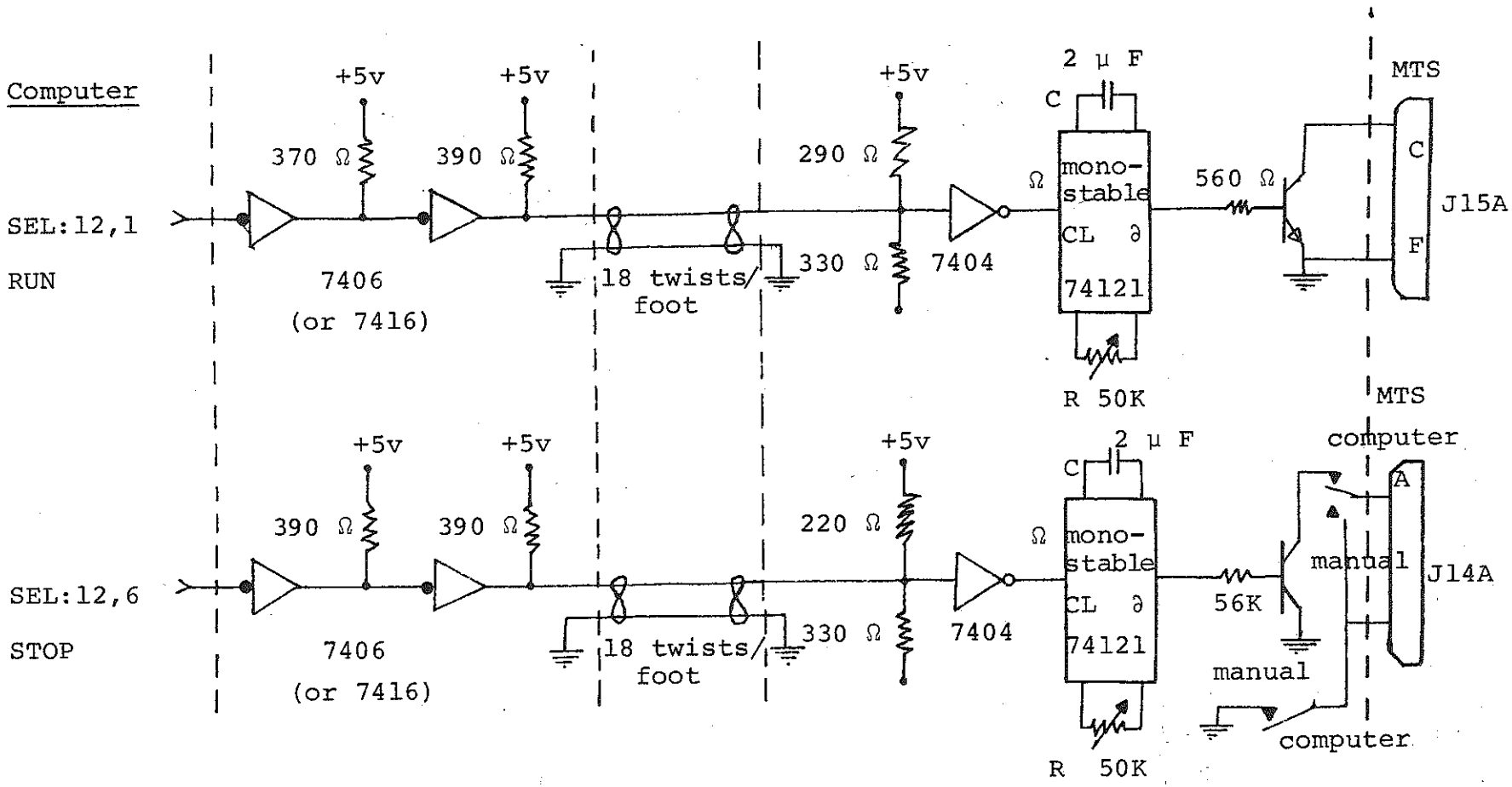

FIGURE A.14 Schematic Electrical Diagram of the Driving Circuit.

C and F during a time t_1 whose minimum value is only limited by the time-constant of the network (R17, C5, R16, C4). Experimental tests have proven that this time should not be less than 2 microseconds to ensure that triggering occurs.

02. The user has access to the "Stop" triggering circuit by means of connectors T14A and T14B on the rear panel of the MTS 436. As can be seen in Figure A.14 on both of these connectors, pins A and B are normally short-circuited and connected to ground through the front panel "Stop" switch. Pushing the front panel "Stop" switch, as well as breaking the short-circuits between A and B, will cause T14A and T14B connectors to trigger the "Stop" circuit. Due to the time-constant of the network (R11, C1, R12, C2), the circuit must be kept open for at least 2 μ'2 to ensure "Stop" triggering.

It should be noted that when triggering the "Run" and "Stop" citcuits under program control, the program must be written is such a way that the "Run" and "Stop" triggering signals never overlap. In other words, "Stop" should only be triggered after the "Run" signal has returned to 11 volts. This requires a software delay in the program.

A.2.1.c Circuits Used to Generate the Signals Previously Mentioned

The output stages of the driving circuits are made of 2N 222 transistors. These transistors are triggered by monostables with adjustable output pulse widths. As mentioned before, pulse widths of at least 2 μ's are needed to ensure that triggering always occurs. Here they have been adjusted to 5 μ's by means of the internal elements R and C. Figure A.15 gives the typical signals at the outputs of the monostables and the corresponding transistors. Figure A.15 gives the complete electrical diagram of the driving circuits. The two functions are driven at the SELECT lines of the computer, available on connector T1.

Figures A.16 and A.17 show the different connections between the apparatus. For all connections, 18 twists/foot cable is used. As can be seen on these figures, a DPDT switch is used to switch from Program-Control Mode (or Computer Mode) to MANUAL MODE. This allows the user to trigger

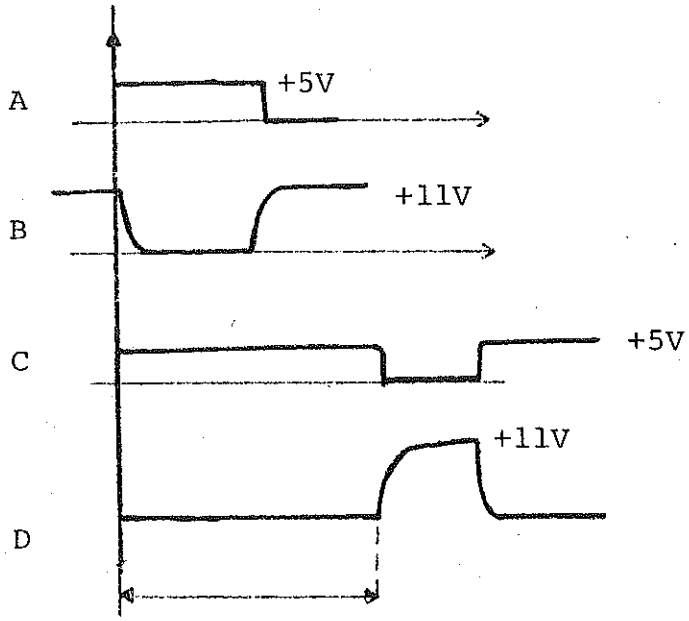

LEGEND

A Output of "RUN" Monostables

B Output of "RUN" transistor

C Output of "STOP" monostable

D Output of "STOP" transistor

FIGURE A.15 Typical Output of the Monostables and Transistors.

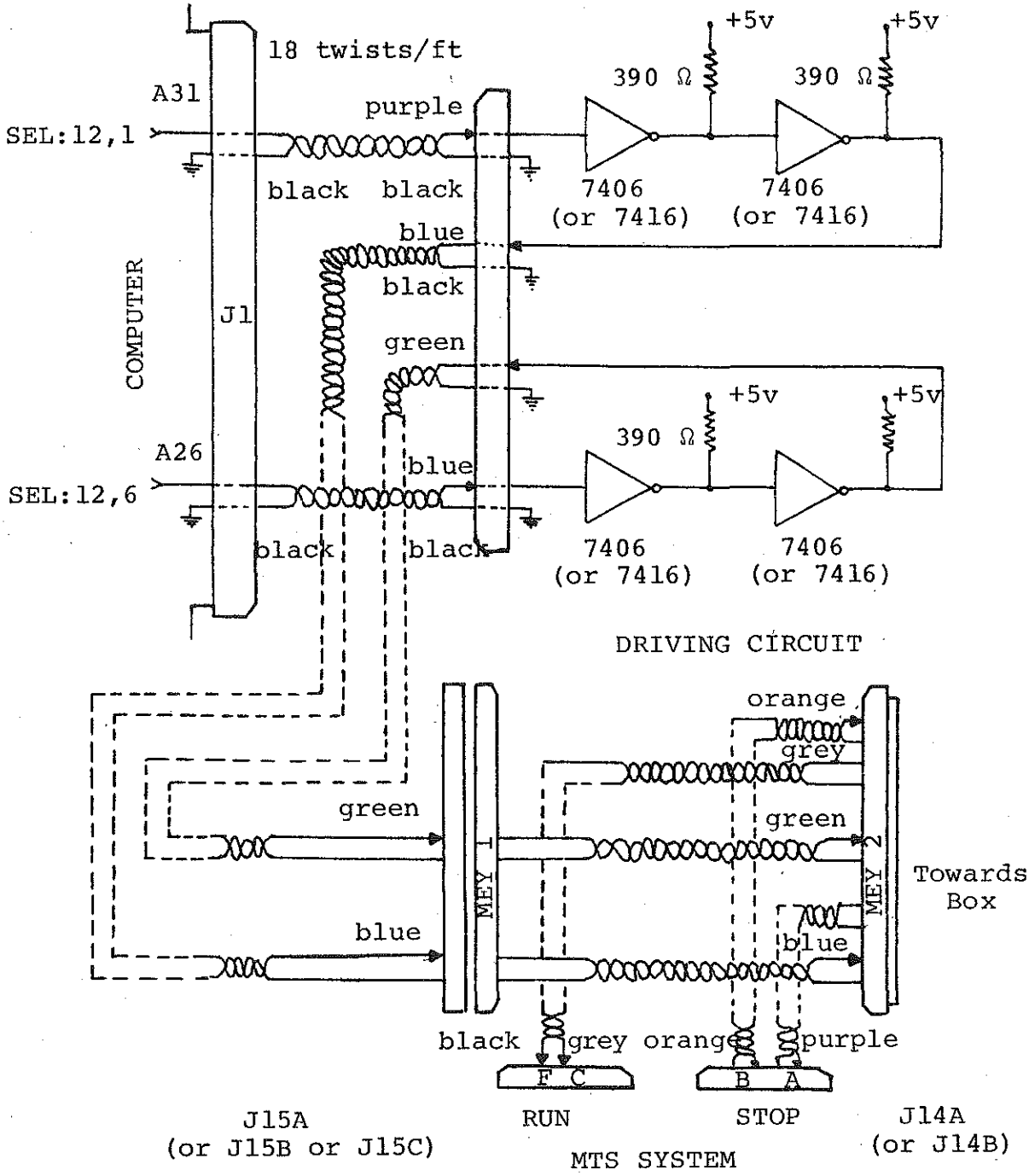

FIGURE A.16 Connection Diagram Between the Apparatus.

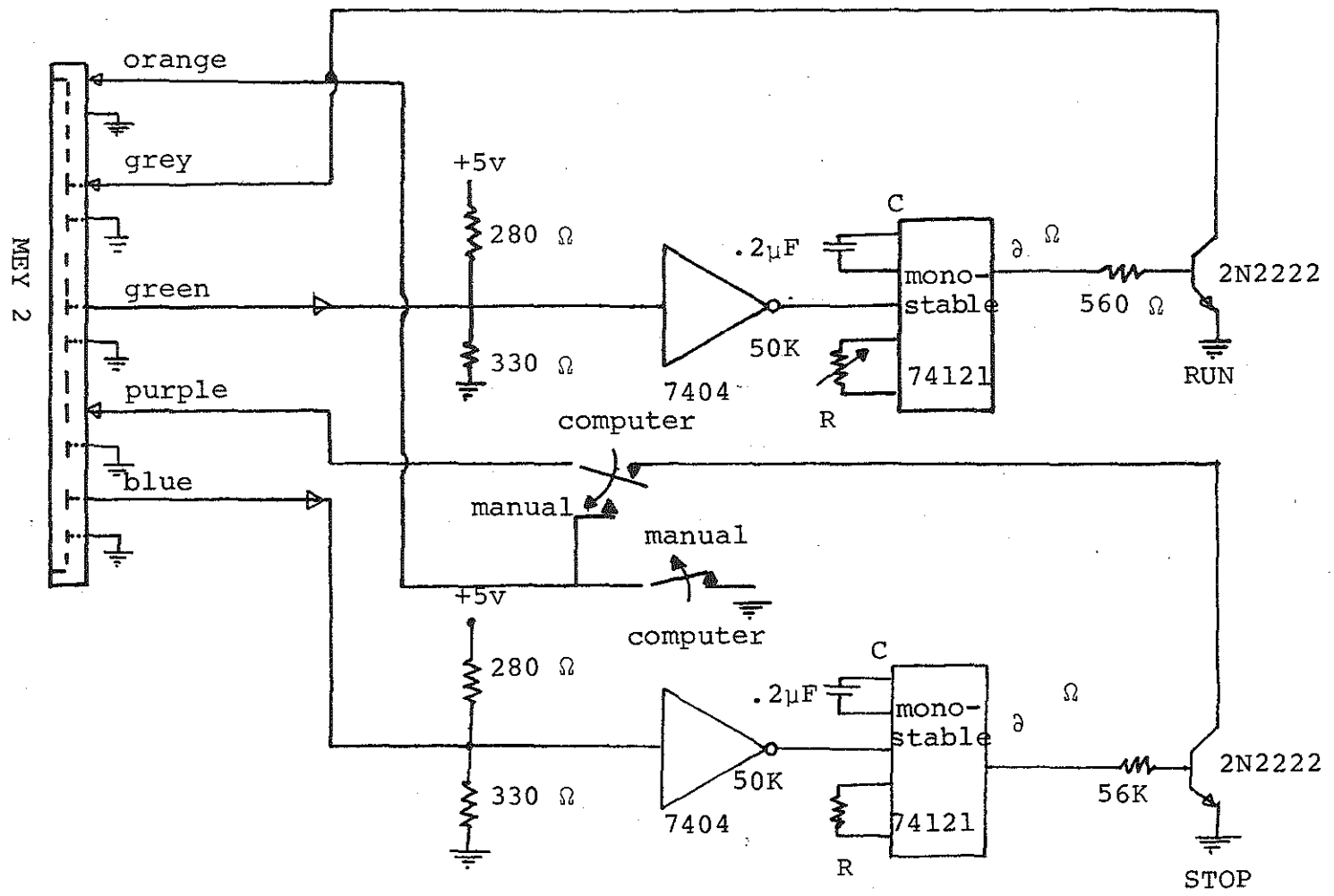

FIGURE A.17 Connection Diagram in the Waveshaper Box.

the "Run" and "Stop" on the front panel of the NTS 436, without disconnecting the computer from the T14A and T15A connectors.

A.2.1.d Software

The program has been written in the assembly language of the LSI-2. It has been stored on diskette by means of the SIGMA Loader. SIGMA is also on diskette and is loaded into the minicomputer by means of the "autoload" feature. The program has been called WVSHPR (standing for "waveform shaper").

After switching the computer on, to execute WVSHPR, SIGMA must be loaded from diskette into the minicomputer by means of autoload. Then SIGMA is used to load WVSHPR from diskette and to link it with TUP (the utility package). When the program is loaded, to begin the execution, one must input the starting address (normally taken as X'0200') by means of the console register into the P register. When putting the minicomputer into the "Run" mode, the initialization phase starts and the user has to input all the required values (N1, Delay 1, N2, Delay 2, frequency of the "equivalent periodic signal"). The program then computes the delay D corresponding to the given frequency by means of two different algorithms, one for the frequencies above 1000 mHz, the other for those under 1000 mHz. These algorithms are needed because no floating point routines are available. The execution then continues by giving the user a few instructions. The program then waits for the user to input a "Go" message. This message starts the triggering of the MTS system, i.e., the signal to be generated.

The execution can be stopped at any time by pushing the "Stop" switch on the console and then can be resumed by switching the computer from the "Stop" mode into the "Run" mode.

Figure A.18 shows a flow-chart of the program. A listing of the program is given hereafter.

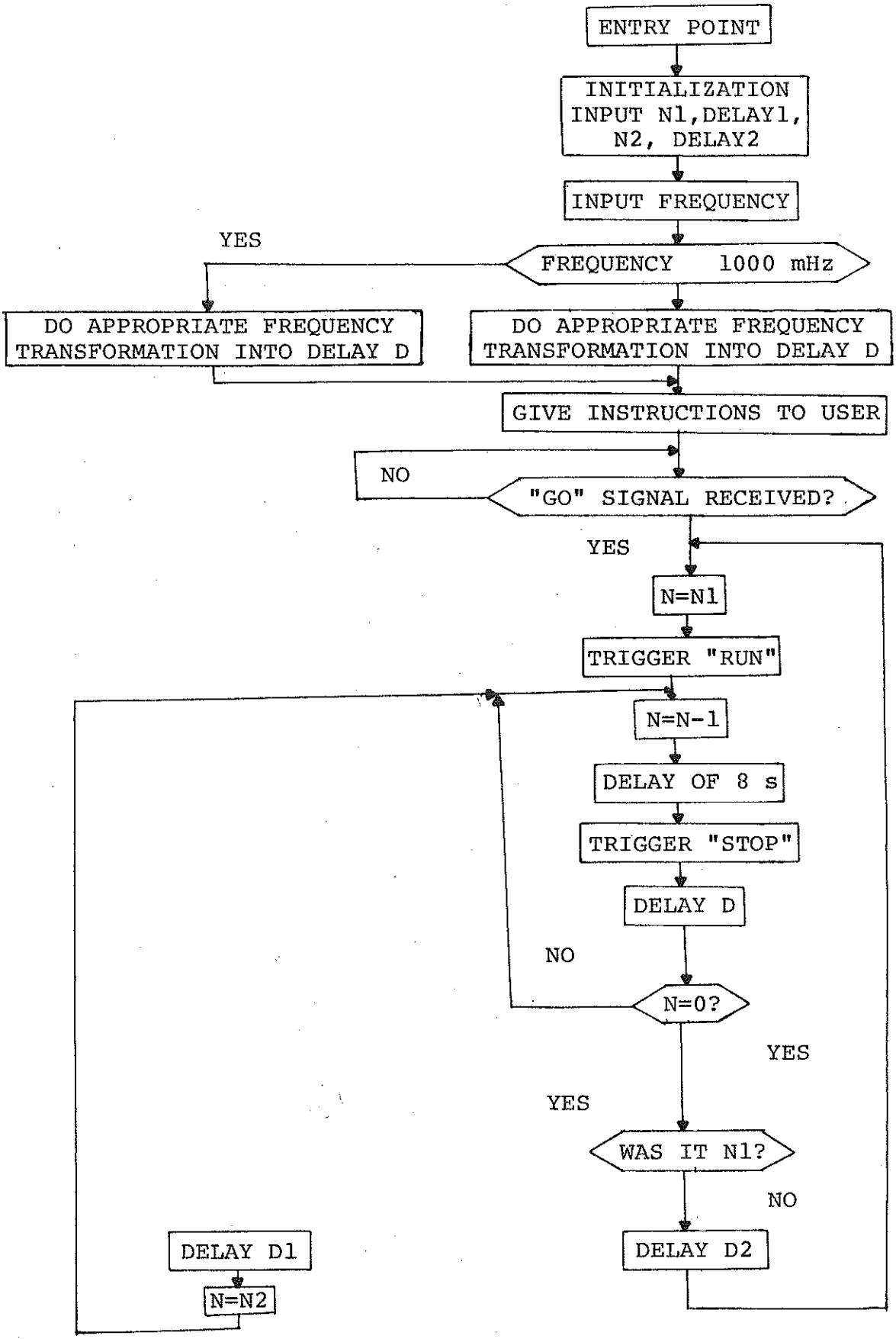

FIGURE A.18 Program Flow Chart.

```
0001                                NAM     WVSHPR
0002  0000                          REL     0
0003        0000  WVSHPR  EQU     $
0004  0000  4005  INIT    CIE
0005  0001  0A00          EIN
0006  0002  0118          ZAX
0007  0003  0F00          SWM
0008  0004  F900          JST     *CRLF
                81AD
0009  0005  C6BD          LAP     '='         ASK FOR N1
0010  0006  0F00          SWM
0011  0007  F900          JST     *OTL
                81A8
0012  0008  00FF          DATA    LOC1
0013  0009  0F00          SWM
0014  000A  F900          JST     *IDEC
                81AA
0015  000B  EADC          STX     N1
0016  000C  0F00          SWM
0017  000D  F900          JST     *CRLF
                81AD
0018  000E  0110          ZAR                 ASK FOR DELAY1
0019  000F  C6BD          LAP     '='
0020  0010  0F00          SWM
0021  0011  F900          JST     *OTL
                81A8
0022  0012  0101          DATA    LOC2
0023  0013  0F00          SWM
0024  0014  F900          JST     *IDEC
                81AA
0025  0015  EAD4          STX     DELAY1
0026  0016  0F00          SWM
0027  0017  F900          JST     *CRLF
                81AD
0028  0018  0110          ZAR                 ASK FOR N2
0029  0019  C6BD          LAP     '='
0030  001A  0F00          SWM
0031  001B  F900          JST     *OTL
                81A8
0032  001C  0112          DATA    LOC3
0033  001D  0F00          SWM
0034  001E  F900          JST     *IDEC
                81AA
0035  001F  EAC9          STX     N2
0036  0020  0F00          SWM
0037  0021  F900          JST     *CRLF
                81AD
0038  0022  0110          ZAR                 ASK FOR DELAY2
0039  0023  C6BD          LAP     '='
0040  0024  0F00          SWM
0041  0025  F900          JST     *OTL
                81A8
0042  0026  0114          DATA    LOC4
```

```
0043  0027  0FC0          SWM
0044  0028  F900          JST     *IDEC
                81AA
0045  0029  EAC1          STX     DELAY2
0046  002A  0F00          SWM
0047  002B  F900          JST     *CRLF
                81AD
0048  002C  0110          ZAR
0049  002D  C6BD          LAP     '='
0050  002E  0F00          SWM
0051  002F  F900          JST     *OTL
                81A8
0052  0030  019B          DATA    LOC9
0053  0031  0F00          SWM
0054  0032  F900          JST     *IDEC
                81AA
0055  0033  EABA          STX     FREQ
0056  0034  0030          TXA
0057  0035  D2C2          CMS     TH
0058  0036  F201          JMP     X2
0059  0037  F210          JMP     X1
0060  0038  0118  X2      ZAX
0061  0039  E2C0          LDX     TTH
0062  003A  1B00          LLL     1
0063  003B  1970          DVD     FREQ
                003C  00EE
0064  003D  0110          ZAR
0065  003E  1960          MPY     TEN
                003F  00F6
0066  0040  1B80          LLR     1
0067  0041  0030          TXA
0068  0042  92B2          SUB     EIGHT
0069  0043  9AAE          STA     TCNT
0070  0044  C719          LAM     25
0071  0045  9AAB          STA     TRTC
0072  0046  9AA9          STA     TRTC0
0073  0047  F216          JMP     A
0074  0048  0118  X1      ZAX
0075  0049  E2A4          LDX     FREQ
0076  004A  1B00          LLL     1
0077  004B  1970          DVD     HUN
                004C  00F7
0078  004D  EAA1          STX     NFR
0079  004E  0118          ZAX
0080  004F  E2A9          LDX     FTH
0081  0050  1B00          LLL     1
0082  0051  1970          DVD     NFR
                0052  00EF
0083  0053  0110          ZAR
0084  0054  1960          MPY     TEN
                0055  00F6
0085  0056  1B80          LLR     1
0086  0057  0030          TXA
```

```
0087  0058  92A2          SUB     RSDEL
0088  0059  0310          NAR
0089  005A  9A95          STA     TRTC0
0090  005B  9A95          STA     TRTC
0091  005C  B297          LDA     ONE
0092  005D  9A94          STA     TCNT
0093  005E  0F00    A     SWM
0094  005F  F900          JST     *CRLF
                81AD
0095  0060  0F00          SWM
0096  0061  F900          JST     *CRLF
                81AD
0097  0062  0110          ZAR
0098  0063  C6B5          LAP     ';'
0099  0064  0F00          SWM
0100  0065  F900          JST     *OTL
                81A8
0101  0066  0125          DATA    LOC5
0102  0067  0F00          SWM
0103  0068  F900          JST     *CRLF
                81AD
0104  0069  0110          ZAR
0105  006A  C6AE          LAP     '.'
0106  006B  0F00          SWM
0107  006C  F900          JST     *OTL
                81A8
0108  006D  013F          DATA    LOC6
0109  006E  0F00          SWM
0110  006F  F900          JST     *CRLF
                81AD
0111  0070  0110          ZAR
0112  0071  C6AE          LAP     '.'
0113  0072  0F00          SWM
0114  0073  F900          JST     *OTL
                81A8
0115  0074  0154          DATA    LOC7
0116  0075  0F00          SWM
0117  0076  F900          JST     *CRLF
                81AD
0118  0077  0110          ZAR
0119  0078  C6AE          LAP     '.'
0120  0079  0F00          SWM
0121  007A  F900          JST     *OTL
                81A8
0122  007B  016B          DATA    LOC7A
0123  007C  0F00          SWM
0124  007D  F900          JST     *CRLF
                81AD
0125  007E  0110          ZAR
0126  007F  C6AE          LAP     '.'
0127  0080  0F00          SWM
0128  0081  F900          JST     *OTL
                81A8
```

```
0129  0082  0184          DATA  LOC8
0130  0083  0F00          SWM
0131  0084  F900          JST   *CRLF
                81AD
0132  0085  C6AE          LAP   '.'       WAIT FOR INPUT
0133  0086  0F00          SWM
0134  0087  F900          JST   *IKL
                81AB
0135  0088  01AE          DATA  BFR1
0136  0089  4006          CID
0137  008A  B100          LDA   BFR1
                01AE
0138  008B  D271          CMS   GO        IS IT "GO"?
0139  008C  F62E          JMP   A         NO
0140  008D  F62F          JMP   A         NO
0141  008E  0F00    A0    SWM             YES
0142  008F  F900          JST   *CRLF
                81AD
0143  0090  B257    A1    LDA   N1
0144  0091  9A53          STA   N
0145  0092  B261          LDA   ONE
0146  0093  9A53          STA   N0
0147  0094  4091    B     SEL   :12,1
0148  0095  B24F          LDA   N
0149  0096  00D0          DAR
0150  0097  9A4D          STA   N
0151  0098  C750          LAM   80
0152  0099  9A52          STA   RTCCT
0153  009A  B261          LDA   BR0
0154  009B  9A4A          STA   NN
0155  009C  B257          LDA   ONE
0156  009D  F221          JMP   C2
0157  009E  4096    B1    SEL   :12,6
0158  009F  C750          LAM   80
0159  00A0  9A4B          STA   RTCCT
0160  00A1  B244          LDA   NN
0161  00A2  0150          IAR
0162  00A3  9A42          STA   NN
0163  00A4  B24F          LDA   ONE
0164  00A5  F219          JMP   C2
0165  00A6  B24A    B2    LDA   TRTC
0166  00A7  9A48          STA   TRTC0
0167  00A8  9A43          STA   RTCCT
0168  00A9  B23C          LDA   NN
0169  00AA  0150          IAR
0170  00AB  9A3A          STA   NN
0171  00AC  B245          LDA   TCNT
0172  00AD  F211          JMP   C2
0173  00AE  B236    B3    LDA   N
0174  00AF  D243          CMS   ZERO
0175  00B0  F61C          JMP   B         NO;CONTINUE
0176  00B1  F61D          JMP   B         NO;CONTINUE
0177  00B2  B233          LDA   NN
```

```
0178  00B3  0150          IAR
0179  00B4  9A31          STA     NN
0180  00B5  C764          LAM     100
0181  00B6  9A39          STA     TRTC0
0182  00B7  9A34          STA     RTCCT
0183  00B8  B22E          LDA     N0
0184  00B9  D239          CMS     ZERO
0185  00BA  F203          JMP     C1
0186  00BB  F202          JMP     C1
0187  00BC  B22E          LDA     DELAY2
0188  00BD  F201          JMP     C2
0189  00BE  B22B  C1      LDA     DELAY1
0190  00BF  9A2D  C2      STA     COUNT
0191  00C0  4006  D0      CID
0192  00C1  4044          SEL     8,4       INITIALIZE RTC
0193  00C2  4042          SEL     8,2
0194  00C3  4040          SEL     8,0
0195  00C4  0A00          EIN
0196  00C5  F600          WAIT
0197  00C6  F606          JMP     D0
0198  00C7  F31E          JMP     *NN
0199  00C8  F62A  BR      JMP     B1
0200  00C9  F623          JMP     B2
0201  00CA  F61C          JMP     B3
0202  00CB  B21B  D2      LDA     N0        WAS IT DELAY1?
0203  00CC  D226          CMS     ZERO
0204  00CD  F202          JMP     E
0205  00CE  F201          JMP     E
0206  00CF  F63F          JMP     A1
0207  00D0  00D0  E       DAR
0208  00D1  9A15          STA     N0
0209  00D2  B216          LDA     N2
0210  00D3  9A11          STA     N
0211  00D4  F640          JMP     B
0212  00D5  0800  CLK     ENT
0213  00D6  B219          LDA     TRTC0
0214  00D7  9A14          STA     RTCCT
0215  00D8  B214          LDA     COUNT
0216  00D9  00D0          DAR
0217  00DA  9A12          STA     COUNT
0218  00DB  D217          CMS     ZERO      IS COUNT=0?
0219  00DC  F204          JMP     CL1
0220  00DD  F203          JMP     CL1
0221  00DE  B609          LDA     CLK
0222  00DF  0150          IAR
0223  00E0  F201          JMP     CL2
0224  00E1  B60C  CL1     LDA     CLK
0225  00E2  0150  CL2     IAR
0226  00E3  9E0E          STA     CLK
0227  00E4  F70F          RTN     CLK
0228  00E5        N       RES     1
0229  00E6        NN      RES     1
0230  00E7        N0      RES     1
```

```
0231  00E8          N1      RES     1
0232  00E9          N2      RES     1
0233  00EA          DELAY1  RES     1
0234  00EB          DELAY2  RES     1
0235  00EC          RTCCT   RES     1
0236  00ED          COUNT   RES     1
0237  00EE          FREQ    RES     1
0238  00EF          NFR     RES     1
0239  00F0          TRTC0   RES     1
0240  00F1          TRTC    RES     1
0241  00F2          TCNT    RES     1
0242  00F3  0000    ZERO    DATA    0
0243  00F4  0001    ONE     DATA    1
0244  00F5  0008    EIGHT   DATA    8
0245  00F6  000A    TEN     DATA    10
0246  00F7  0064    HUN     DATA    100
0247  00F8  03E8    TH      DATA    1000
0248  00F9  1388    FTH     DATA    5000
0249  00FA  4E20    TTH     DATA    20000
0250  00FB  009E    RSDEL   DATA    :009E
0251  00FC  00C8    BR0     DATA    BR
0252  00FD  C7CF    GO      TEXT    'GO'
0253  00FE  C9CE    IN      TEXT    'IN'
0254  00FF  CEB1    LOC1    TEXT    'N1 ='
      0100  A0BD
0255  0101  C4C5    LOC2    TEXT
      0102  CCC1
      0103  D9B1
      0104  A0C9
      0105  CEA0
      0106  C8D5
      0107  CEC4
      0108  D2C5
      0109  C4D4
      010A  C8D3
      010B  A0CF
      010C  C6A0
      010D  C1A0
      010E  D3C5
      010F  C3CF
      0110  CEC4
      0111  A0BD
0256  0112  CEB2    LOC3    TEXT    'N2 ='
      0113  A0BD
0257  0114  C4C5    LOC4    TEXT
      0115  CCC1
      0116  D9B2
      0117  A0C9
      0118  CEA0
      0119  C6D5
      011A  CEC4
      011B  D2C5
      011C  C4D4
```

```
                0152  CCC5
                0153  A0AE
0261            0154  D4CF    LOC7    TEXT
                0155  A0D2
                0156  C5D3
                0157  D4C1
                0158  D2D4
                0159  ACA0
                015A  D0D5
                015B  D4A0
                015C  A2B0
                015D  B2B0
                015E  B0A2
                015F  A0C9
                0160  CED4
                0161  CFA0
                0162  C3CF
                0163  CED3
                0164  CFCC
                0165  C5A0
                0166  D2C5
                0167  C7C9
                0168  D3D4
                0169  C5D2
                016A  A0AE
0262            016E  D3D7    LOC7A   TEXT
                016C  C9D4
                016D  C3C8
                016E  A0AA
                016F  D7D2
                0170  C9D4
                0171  C5AA
                0172  A0CF
                0173  CEEB
                0174  A0D0
                0175  D2C5
                0176  D3D3
                0177  A0AA
                0178  D0AA
                0179  BBA0
                017A  D3D7
                017B  C9D4
                017C  C3C8
                017D  A0AA
                017E  D7D2
                017F  C9D4
                0180  C5AA
                0181  A0CF
                0182  C6C6
                0183  A0AE
0263            0184  D0D2    LOC8    TEXT
                0185  C5D3
                0186  D3A0
```

```
                0187   AAD2
                0188   C5D3
                0189   C5D4
                018A   AABB
                018B   D3D7
                018C   C9D4
                018D   C3C8
                018E   A0AA
                018F   D3D4
                0190   CFD0
                0191   AAA0
                0192   CFC6
                0193   C6EB
                0194   A0D0
                0195   D2C5
                0196   D3D3
                0197   A0AA
                0198   D2D5
                0199   CEAA
                019A   A0AE
0264            019E   C6D2   LOC9    TEXT
                019C   C5D1
                019D   D5C5
                019E   CEC3
                019F   D9A0
                01A0   C9CE
                01A1   A0CD
                01A2   C9CC
                01A3   CCC9
                01A4   ADC8
                01A5   C5D2
                01A6   D4DA
                01A7   A0BD
0265            01A8          OTL     REF
0266            01A9          OTT     REF
0267            01AA          IDEC    REF
0268            01AB          IKL     REF
0269            01AC          IKB     REF
0270            01AD          CRLF    REF
0271            01AE          BFR1    RES     50
0272            01E0          BFR2    RES     50
0273            001E                  ABS     :1E
0274            001E   F100           JMP     INIT
                       0000
0275            0018                  ABS     :18
0276            0018   D900           IMS     RTCCT
                       00EC
0277            001A                  ABS     :1A
0278            001A   F900           JST     CLK
                       00D5
0279                                  END
0000  ERRORS
```

A	00 5E		A0	00 8E		A1	00 90		BFR1	01 AE	
BFR2	01 E0		BR	00 C8		BR0	00 FC		B	00 94	
B1	00 9E		B2	00 A6		B3	00 AE		CLK	00 D5	
CL1	00 E1		CL2	00 E2		COUNT	00 ED		CRLF	01 AD	
C1	00 BE		C2	00 BF		DELAY1	00 EA		DELAY2	00 EB	
D0	00 C0		D2	00 CB		EIGHT	00 F5		E	00 D0	
FREQ	00 EE		FTH	00 F9		GO	00 FD		HUN	00 F7	
IDEC	01 AA		IKB	01 AC		IKL	01 AB		INIT	0000	
IN	00 FE		LOC1	00 FF		LOC2	0101		LOC3	0112	
LOC4	0114		LOC5A	012F		LOC5	0125		LOC6	013F	
LOC7A	0165		LOC7	0154		LOC8	0164		LOC9	0195	
NFR	00 EF		NN	00 E6		N	00 E5		N0	00 E7	
N1	00 E8		N2	00 E9		ONE	00 F4		OTL	01 A2	
OTT	01 A9		RSDEL	00 FB		RTCCT	00 EC		TCNT	00 F2	
TEN	00 F6		TH	00 F8		TRTC	00 F1		TRTC0	00 F0	
TTH	00 FA	X	WVSHPR	0000		X1	0048		X2	0038	
ZERO	00 F3										

A.2.1.e Procedures to Run the Program

01. Turn Main Power Switch on.

02. Turn MTS 436 on.

03. Press Stop switch on the computer's console to put the computer into the Stop mode. Make sure light indicator is on.

04. Load Waveshaper program from diskette into memory by doing the following steps:

    a. Make sure computer is still in Stop mode (i.e., Stop light indicator is on).

    b. Press SREG/DATA switch on the right of the console until the corresponding light indicator is on.

    c. Put "6" in the sense register. "0110" should appear in the four least significant bits of the console data register light indicators.

    d. Press SREG/DATA switch off (the light indicator should be off).

    e. Press SENSE switch on (on the left side of the computer).

    f. Press RESET switch momentarily.

    g. Press Stop switch off (light indicator should go off).

    h. Press AUTO switch on and wait. The teletype will then write: SIGMA CR (CR means push the Carriage Return).
    Note: Each time a line is drawn under a teletype message in this explanation note, it means that the message has been printed on the teletype independently from any user's action. If the line does not appear, it means the user has to type in these characters on the teletype's keyboard. The user must type in "L" after the previous message, which means that he wants to enter the load procedure. This complete operation can be summarized as:

    SIGMA CR loader

    L. CR link.

    The computer then performs a few Carriage Returns and the following message will appear on the teletype:

    REL ADR (AR) = 200. CR

    BASE PG (XR) = 0. CR

    MODE/PRN (SR) = 2. CR

```
                                CR
WYSHPR                          CR
TUP                             CR
                                CR
                                CR
WYSHPR 0200                     CR
E 00F5 0478                     CR
                                CR
                                CR
```

05. Start program execution by doing the following steps:

    a. Put computer into the Stop mode, i.e., press Stop switch on.

    b. Make sure SREG/DATA switch is off.

    c. Press WRITE/READ switch on.

    d. Put '0200' into the Console Data register.

    e. Press P switch momentarily.

    f. Press WRITE/READ switch off.

    g. Press RESET momentarily.

    h. Press STOP switch off.

    i. Press RUN switch on.

    j. Enter all data the computer asks, namely N1, DELAY 1, N2, DELAY 2, FREQUENCY.

    k. While the computer prints out the procedure message, adjust the frequency of the generator from the MTS system to the value you have given to the computer.

    l. Type GO; the whole procedure starts.

06. To stop at any time, put the computer into the Stop mode and repeat (5) to restart the process.

07. At the end, just put the computer into Stop mode and switch the Main Power Switch off.

A.3 Figure Conditioning Box

01. Two inverters have been installed into Signal Conditioning Box #2. Only one is needed, namely to invert the signal delivered by the generator. The reason for this is that in order to have a positive-going (upward-going) movement of the sample, one should take a negative-starting signal on the generator. But, by only using negative half-cycles, the internal counter is not incremented. Therefore, to have at the same-time

counter incrementing and upward-going movement of the sample, the signal which goes from the MTS-436 to the MTS-416 is inverted, as shown in Figure A.19.

02. Three offset circuits have also been installed (OFFSET 1, OFFSET 2, OFFSET 3) to apply an offset to the signals which come from the sample and arrive at the chart recorders. This is shown schematically in Figure A.20. The electric diagrams of the above circuits are shown in Figures A.21 and A.22, respectively.

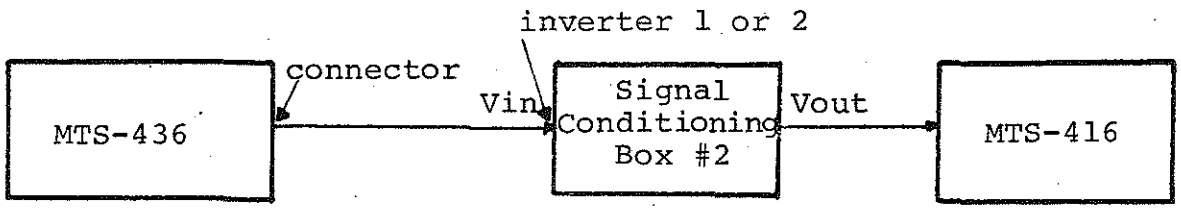

FIGURE A.19 Inverters Location.

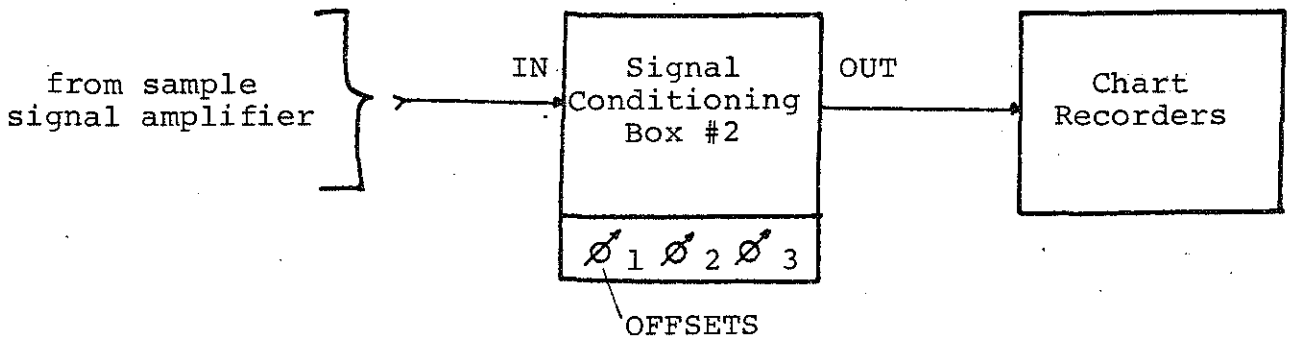

FIGURE A.20 Offsets Location.

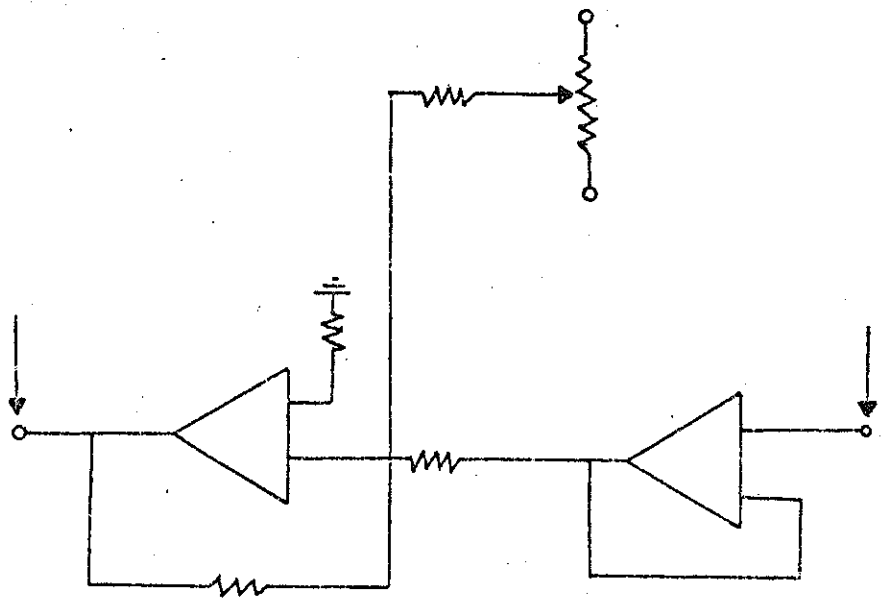

FIGURE A.21 Electrical Circuits of the inventers in the signal conditioning box.

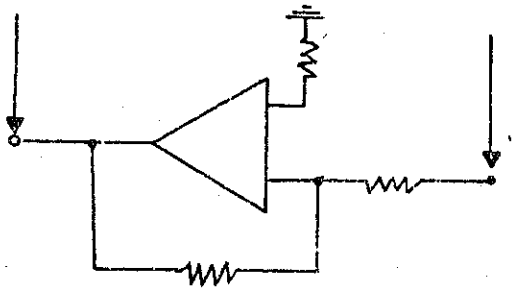

FIGURE A.22 Electrical circuits of the offset in the signal conditioning box.

APPENDIX B

APPENDIX B

CALIBRATION INFORMATION

B.1. Load Cell

In these investigations, a five kips maximum capacity load cell was used. The calibration of this load cell was accomplished by applying known loads to the cell and adjusting the excitation setting to produce the desired voltage outputs. The load was applied using lead bricks which had been previously weighed to the nearest one-hundredth of a pound. The excitation setting was adjusted to produce the desired calibration factor of twenty millivolts per pound. The switch on the MTS controller was set to X10 factor. This amplified the output signal so that the full output signal of ten volts corresponded to a load of five hundred pounds, or ten percent of the load cell capacity. This was chosen to permit higher resolution and accuracy and because the applied axial loads were less than five hundred pounds.

B.2 Linear Variable Differential Transducers (LVDT)

Axial and radial sample deformations were measured using two vertical and two radial LVDT's. The calibration of these LVDT's was performed using a micrometer which read to the nearest 0.0001 inch. The LVDT's were mounted in a bracket holding the micrometer. Movement of the LVDT core was measured with the micrometer, and the calibration factor of the different signal conditioners was adjusted to produce the desired voltage outputs. These calibration factors were:

01. The main axial LVDT, which was calibrated to produce ±10 volts output for a full range deflection of ± two tenths of an inch.
02. The second axial LVDT was calibrated to produce ±10.0 volts output for a full range deflection of ± twenty-five hundredths of an inch.

03. Both radial LVDT's were calibrated to produce ±10.0 volts output for a full range deflection of ± one tenth of an inch.

B.3 Strip Chart Recorder

The calibration of the strip chart recorder was checked before each test using the built-in cal button, which applies a one hundred millivolt input signal to produce an output movement of the stylus of .787 inch (20 mm). The static response was also checked by comparing the strip chart reading with the voltage reading on the Simpson 460 voltmeter for the same output signal. Lentz determined that the dynamic response of the strip chart recorder was unaffected by frequency up to fifty hertz. He used a function generator and a power supply to simultaneously apply and compare the signal to the strip chart recorder and to an oscilloscope. For each loading frequency the proper paper speed and stylus temperature of the strip chart recorder are marked on the recorder.

APPENDIX C

APPENDIX C

TEST RESULTS OF THE LOWER PENINSULA TEST SITES

This appendix summarizes all the test results in the form of figures and tables as follows:

01. The conventional consolidation curves of the lower peninsula test sites are presented in Figures C.1 through C.3.

02. The Incremental Creep Tests

    a. The results of the consolidation tests performed prior to the commencement of the incremental creep tests are presented in Figures C.4 through C.6.

    b. The incremental creep test results are shown in Figures C.7 through C.9.

03. Unconsolidated Ramp Tests

    a. The results of the ramp tests are plotted in Figures C.10 through C.12.

    b. Mohr's circle diagrams obtained from the ramp tests are shown in Figures C.13 through C.15.

04. Consolidated Cyclic Triaxial Tests

    a. The data of the consolidation tests performed prior to the commencement of the cyclic loading tests are plotted in Figures C.16 through C.24.

    b. The axial permanent strain curves are shown in Figures C.25 through C.31.

    c. The resilient Modulus data are plotted in Figures C.32 through C.38.

    d. The radial permanent strain data are listed in Table C.1.

05. Unconsolidated Cyclic Triaxial Tests

    a. The axial permanent strain and the resilient modulus data are tabulated in Table C.2.

    b. Table C.3 provides a list of the radial permanent strain data.

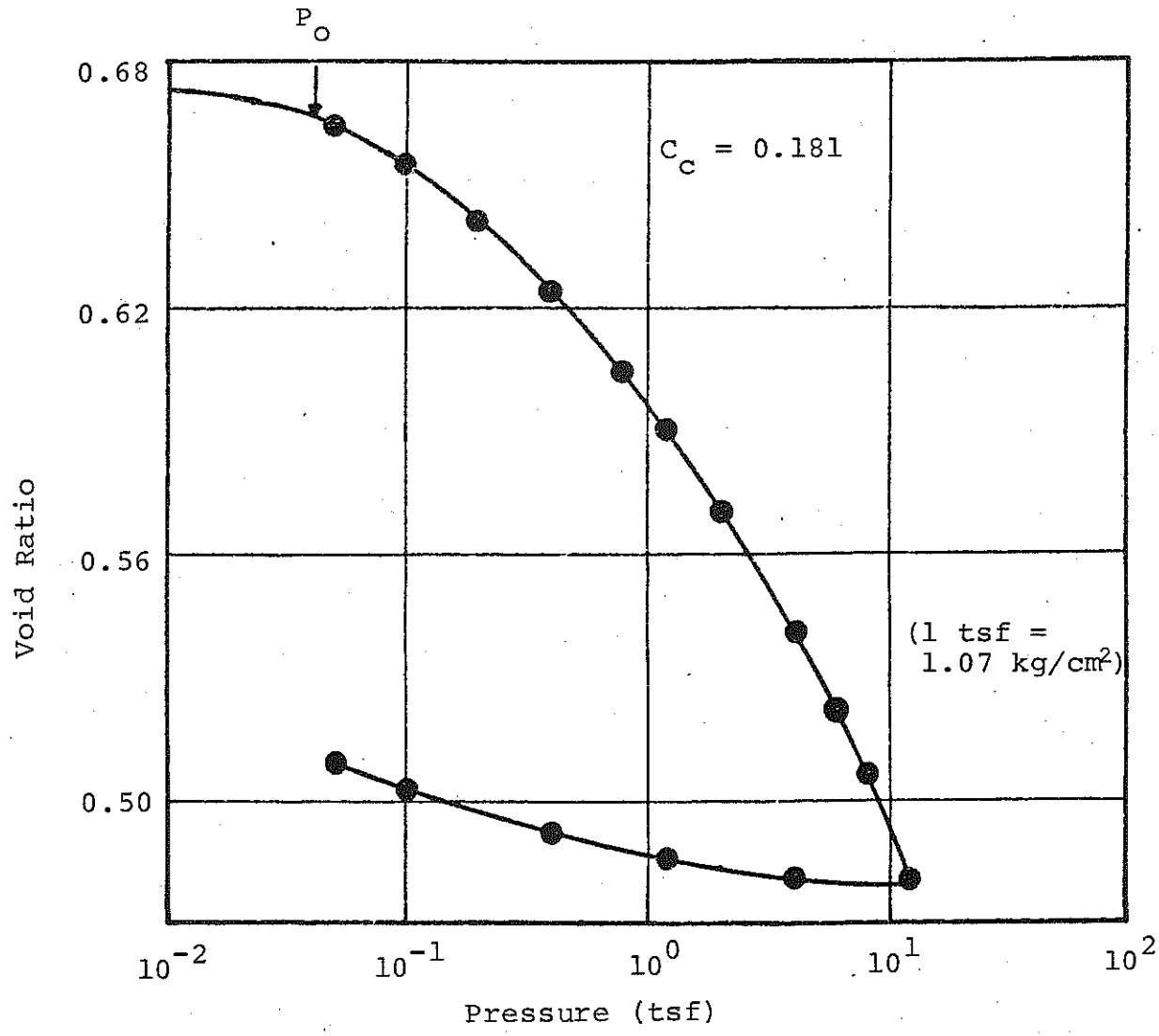

FIGURE C.1 Consolidation Curve, Void Ratio versus Logarithm of Pressure, Site 1, Lower Peninsula.

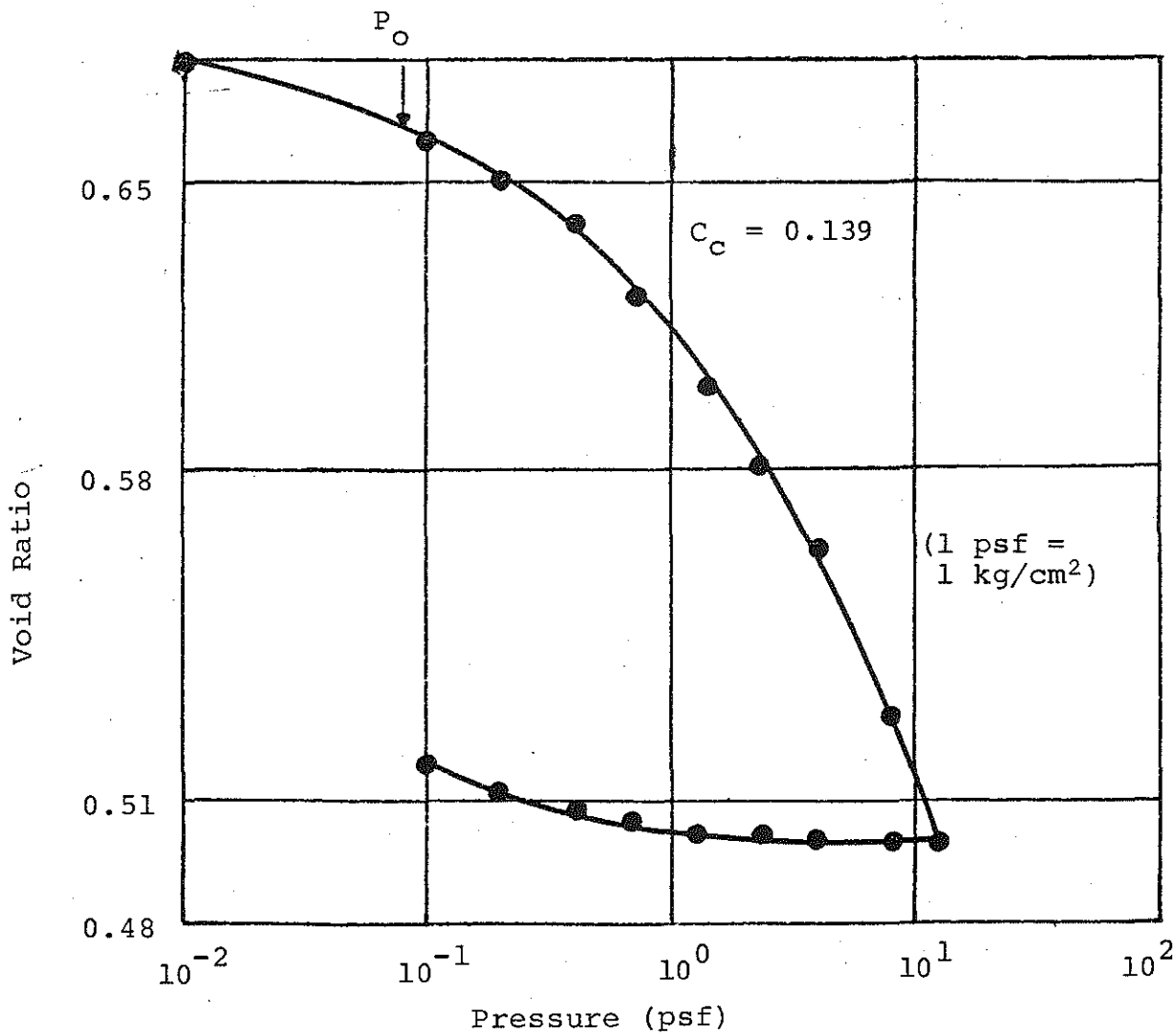

FIGURE C.2 Consolidation Curve, Void Ratio versus Logarithm of Pressure, Site 2, Lower Peninsula.

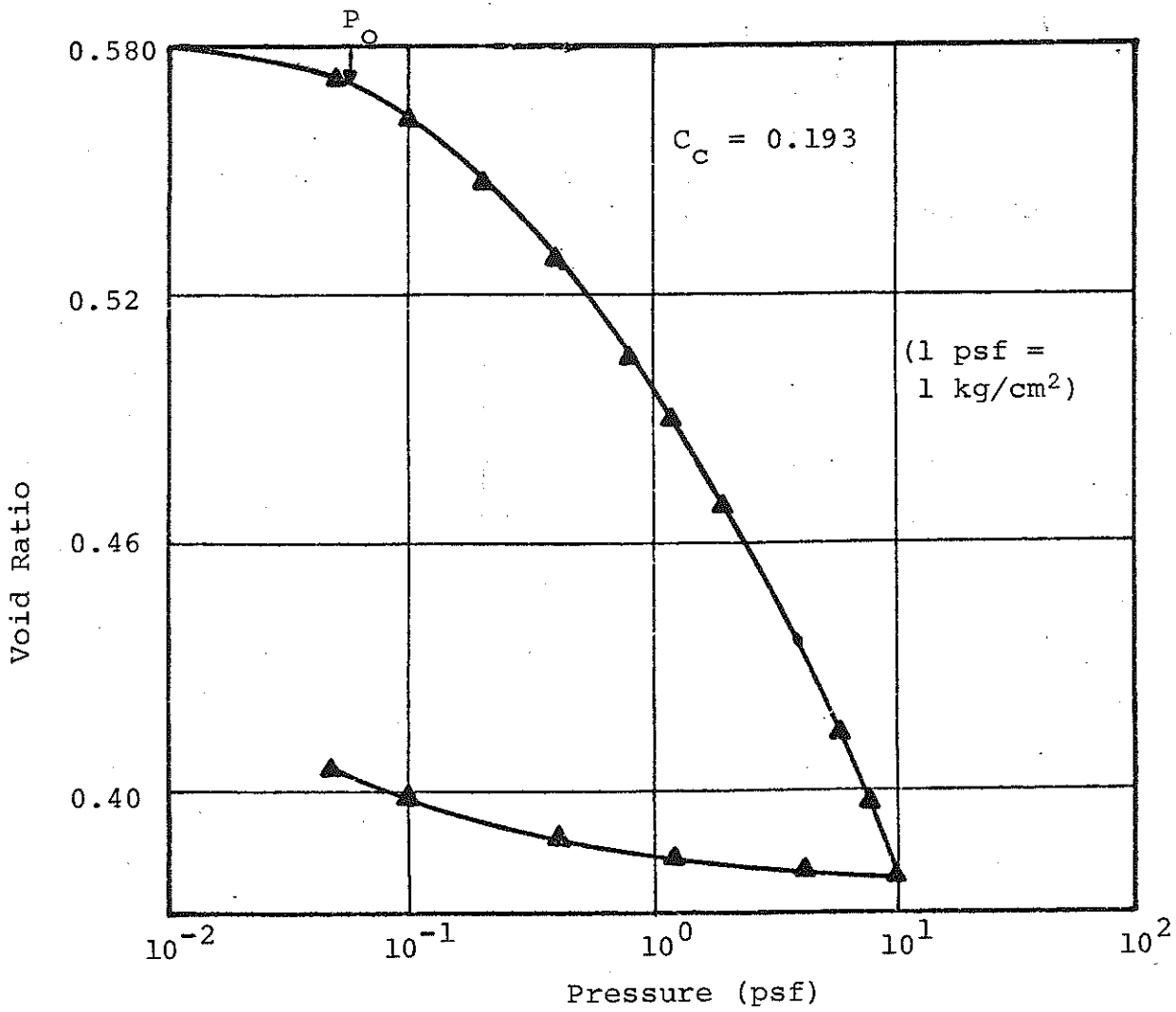

FIGURE C.3 Consolidation Curve, Void Ratio versus Logarithm of Pressure, Site 4, Lower Peninsula.

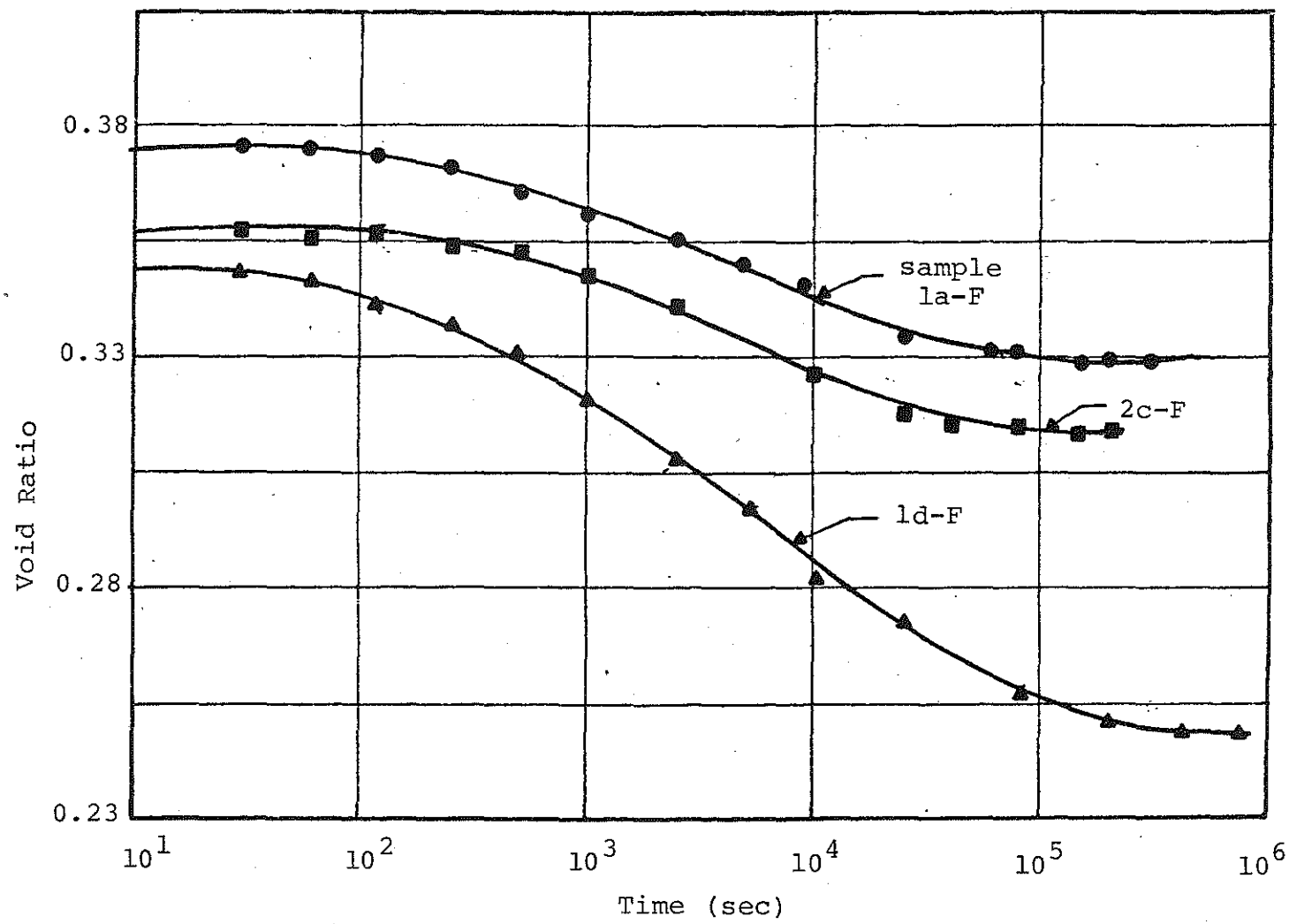

FIGURE C.4 Void-Ratio versus the Logarithm of Time for Samples Consolidated under the Designated Confining Pressure Prior to the Commencement of the Incremental Creep Tests, Site 1, Lower Peninsula.

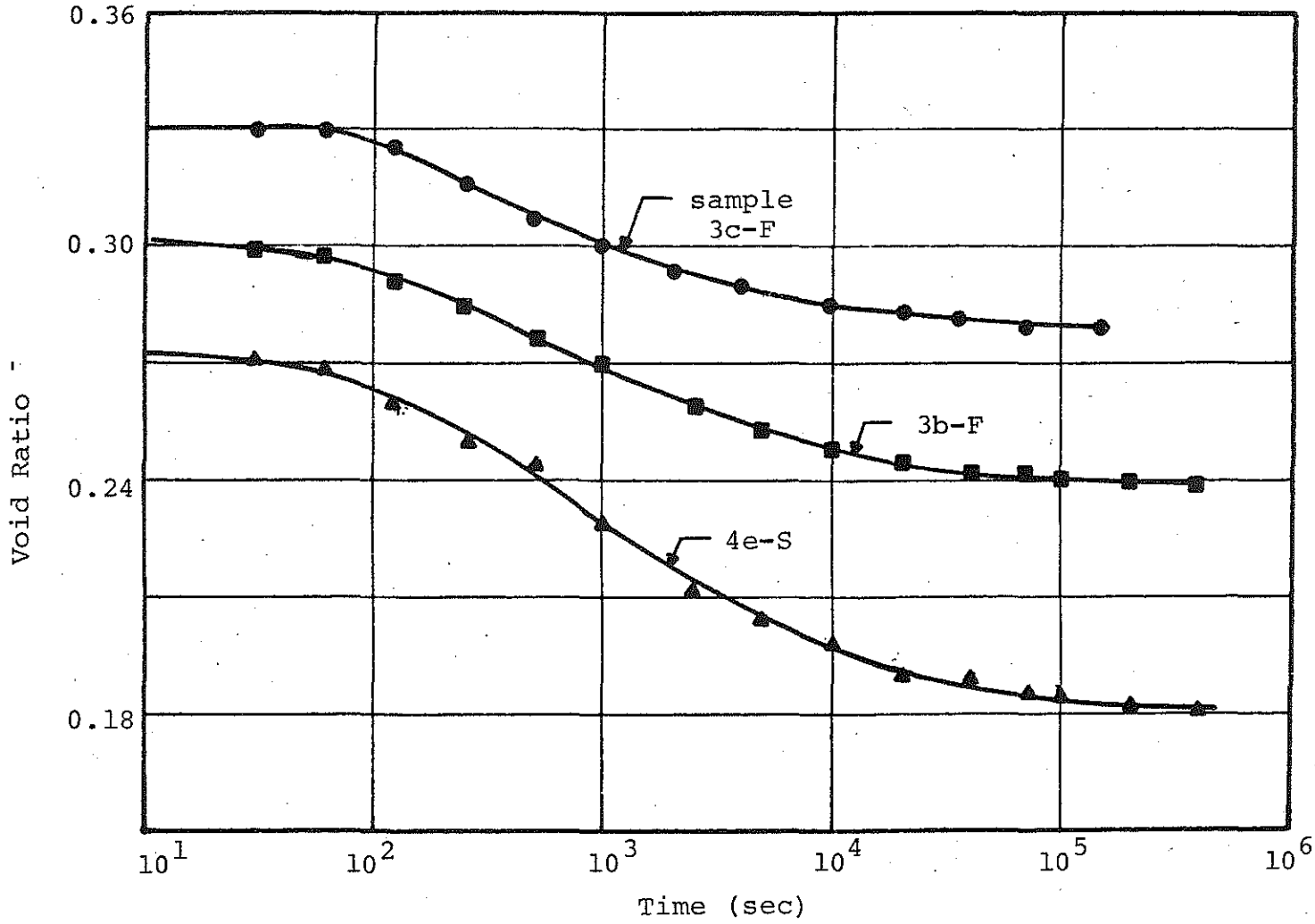

FIGURE C.5 Void Ratio versus Logarithm of Time for Sample Consolidated under the Designated Confining Pressure Prior to the Commencement of the Incremental Creep Tests, Site 3, Lower Peninsula.

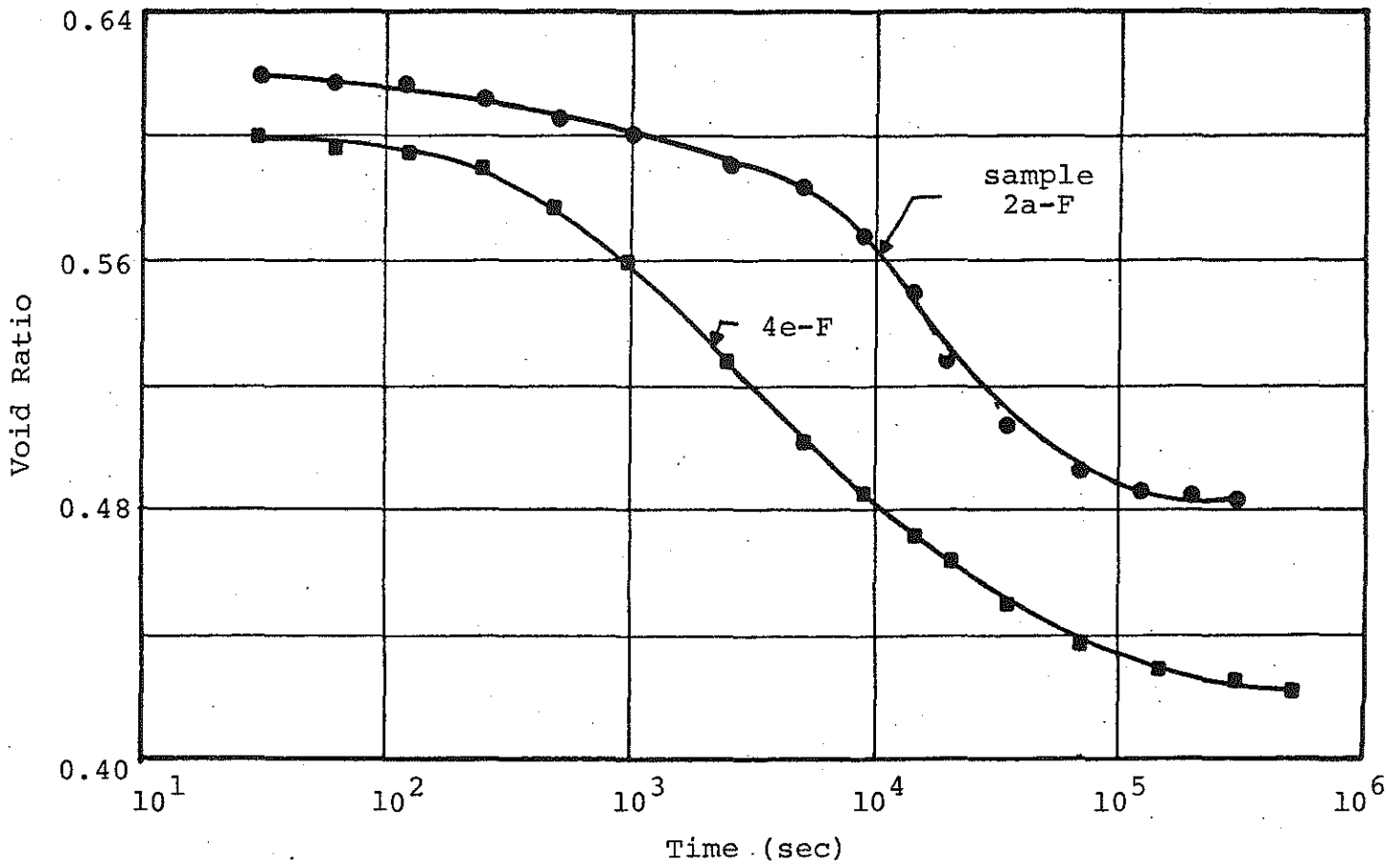

FIGURE C.6 Void Ratio versus the Logarithm of Time for Samples Consolidated under the Designated Confining Pressure Prior to the Commencement of the Incremental Creep Tests, Site 4, Lower Peninsula

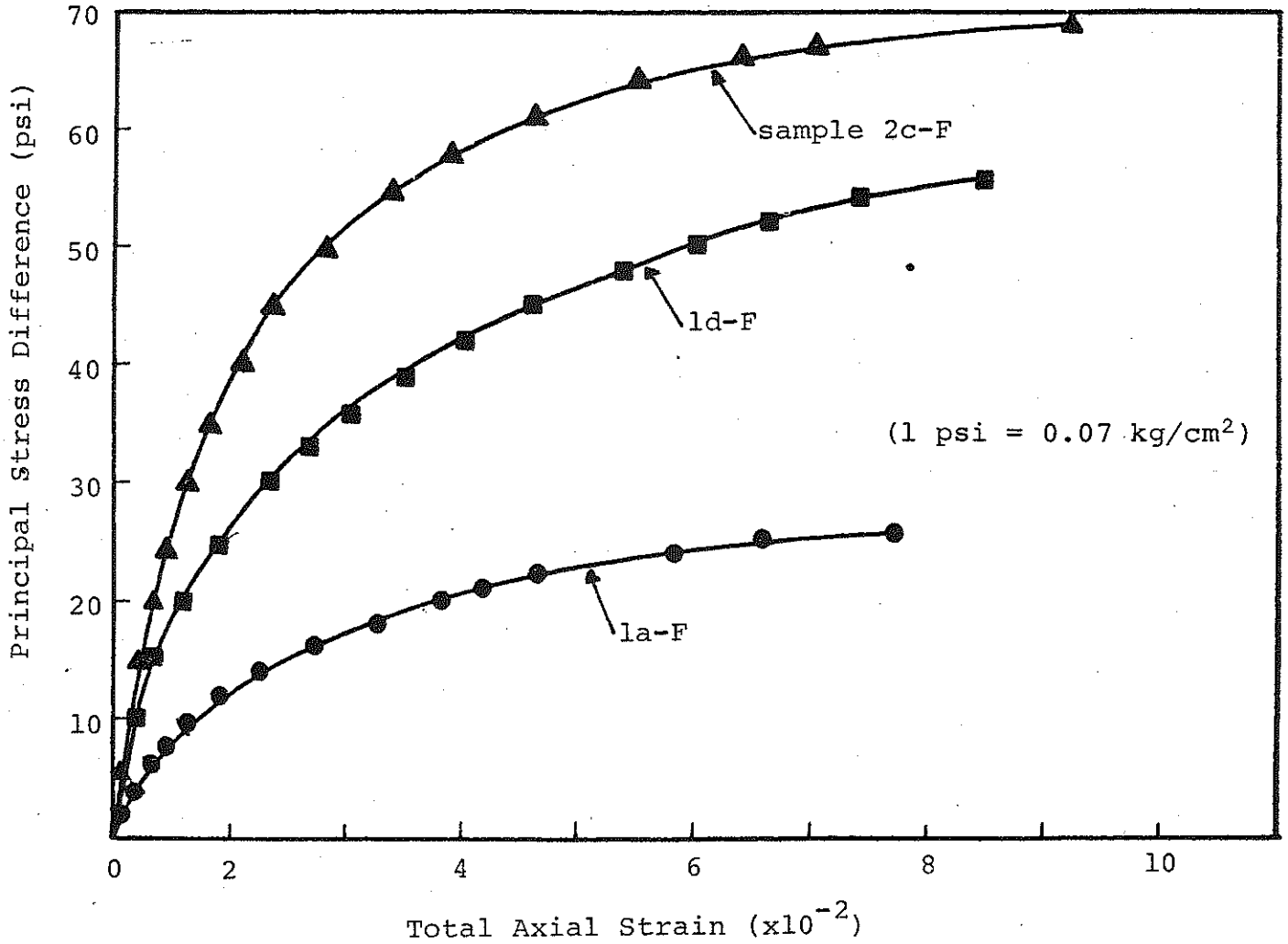

FIGURE C.7 Principal Stress Difference versus Total Axial Strain from Incremental Creep Tests, Site 1, Lower Peninsula.

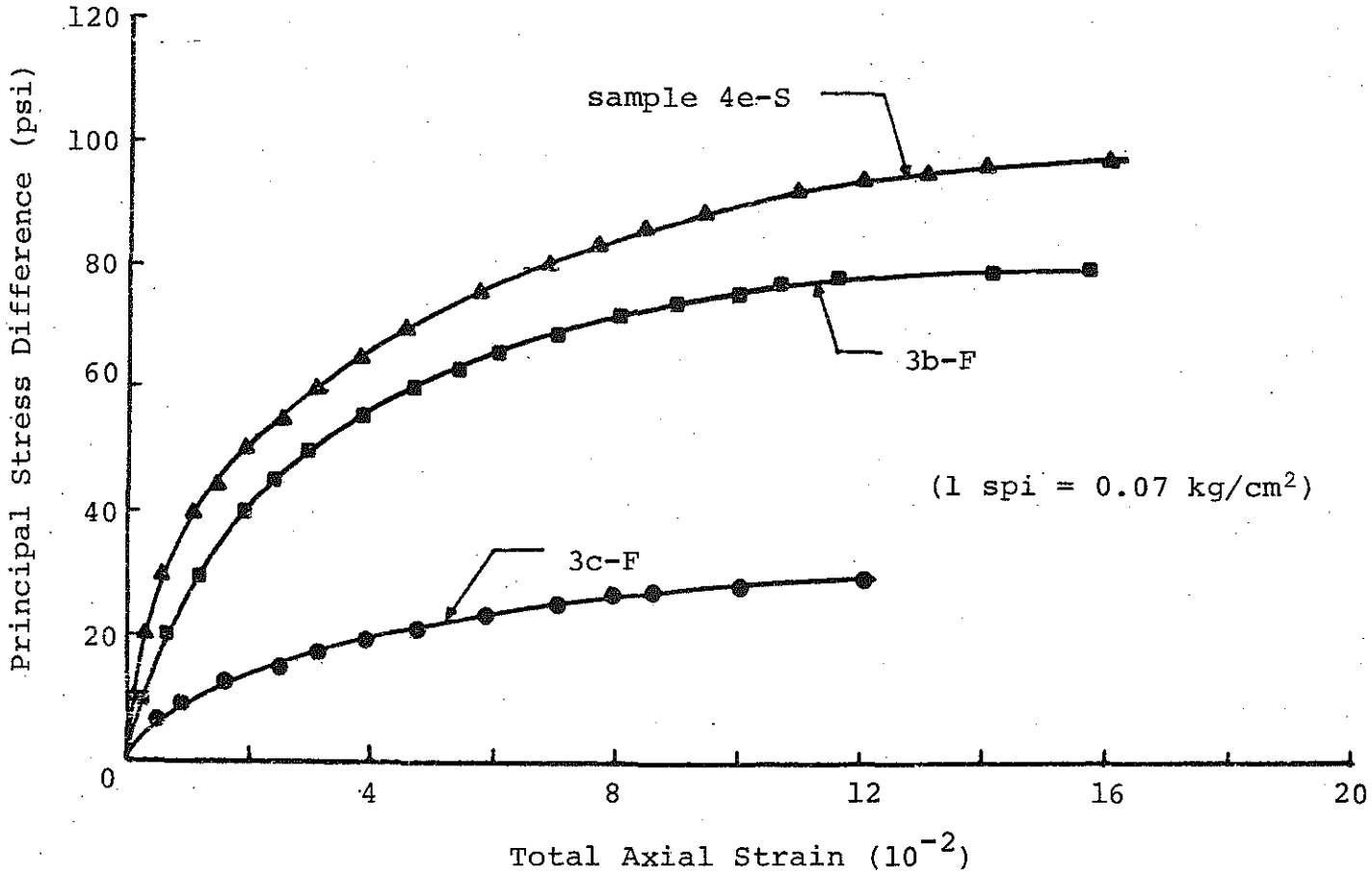

FIGURE C.8 Principal Stress Difference versus Total Axial Strain from Incremental Creep Tests, Site 3, Lower Peninsula.

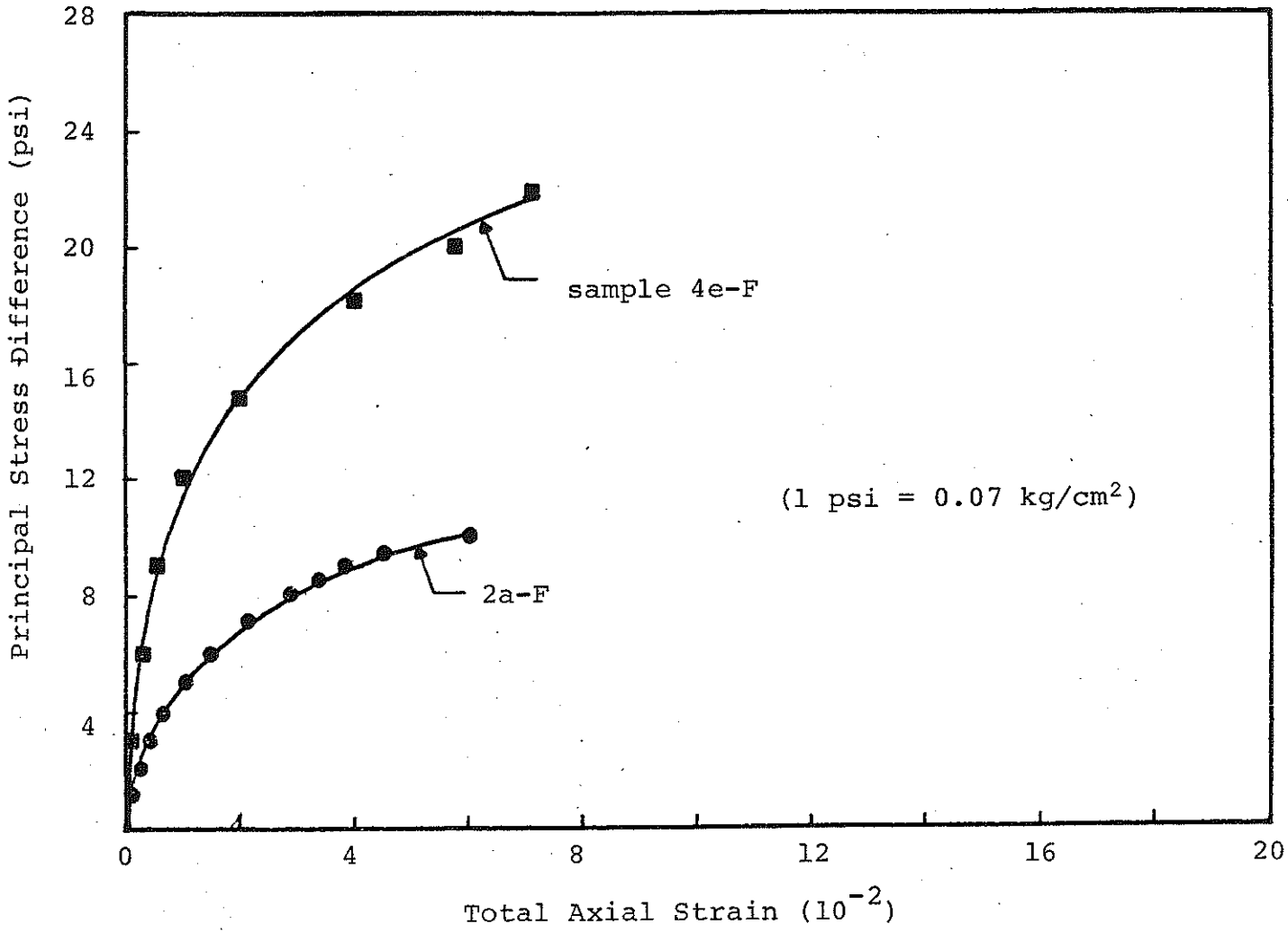

FIGURE C.9 Principal Stress Difference versus Total Axial Strain from Incremental Creep Tests, Site 4, Lower Peninsula.

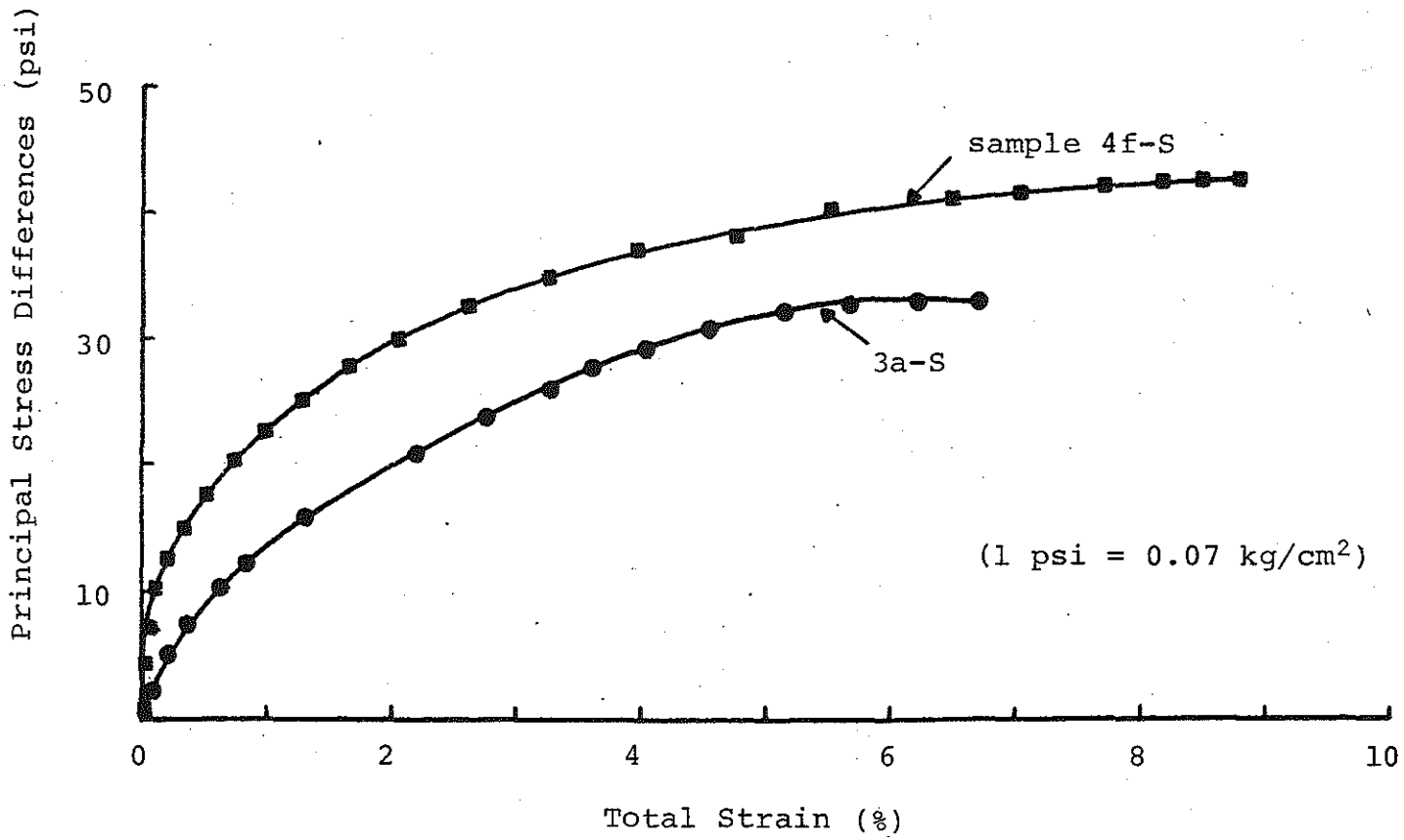

FIGURE C.10 Principal Stress Difference versus Total Axial Strain from Ramp Test, Site 1, Lower Peninsula.

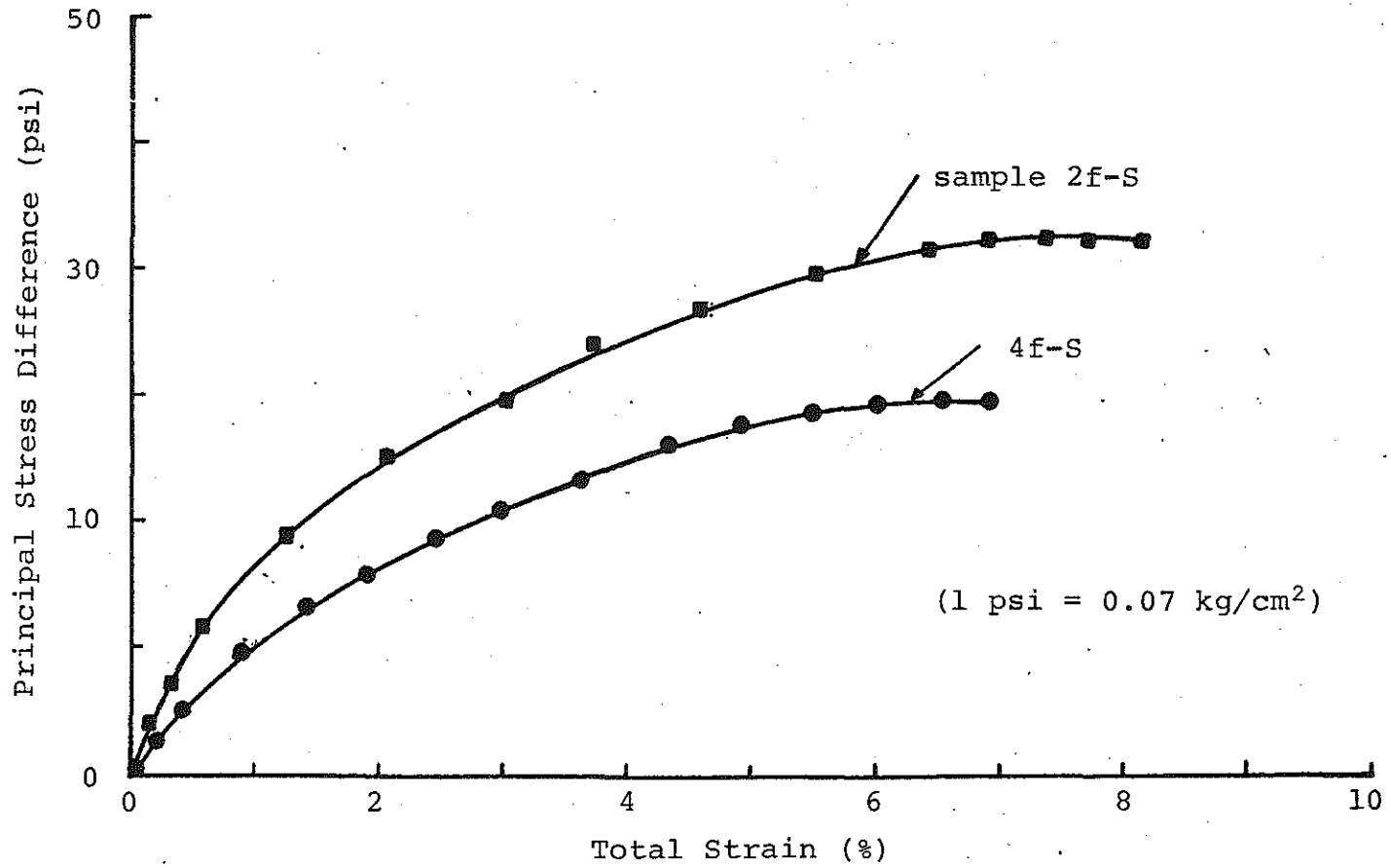

FIGURE C.11 Principal Stress Difference versus Total Axial Strain from Ramp Tests, Site 2, Lower Peninsula.

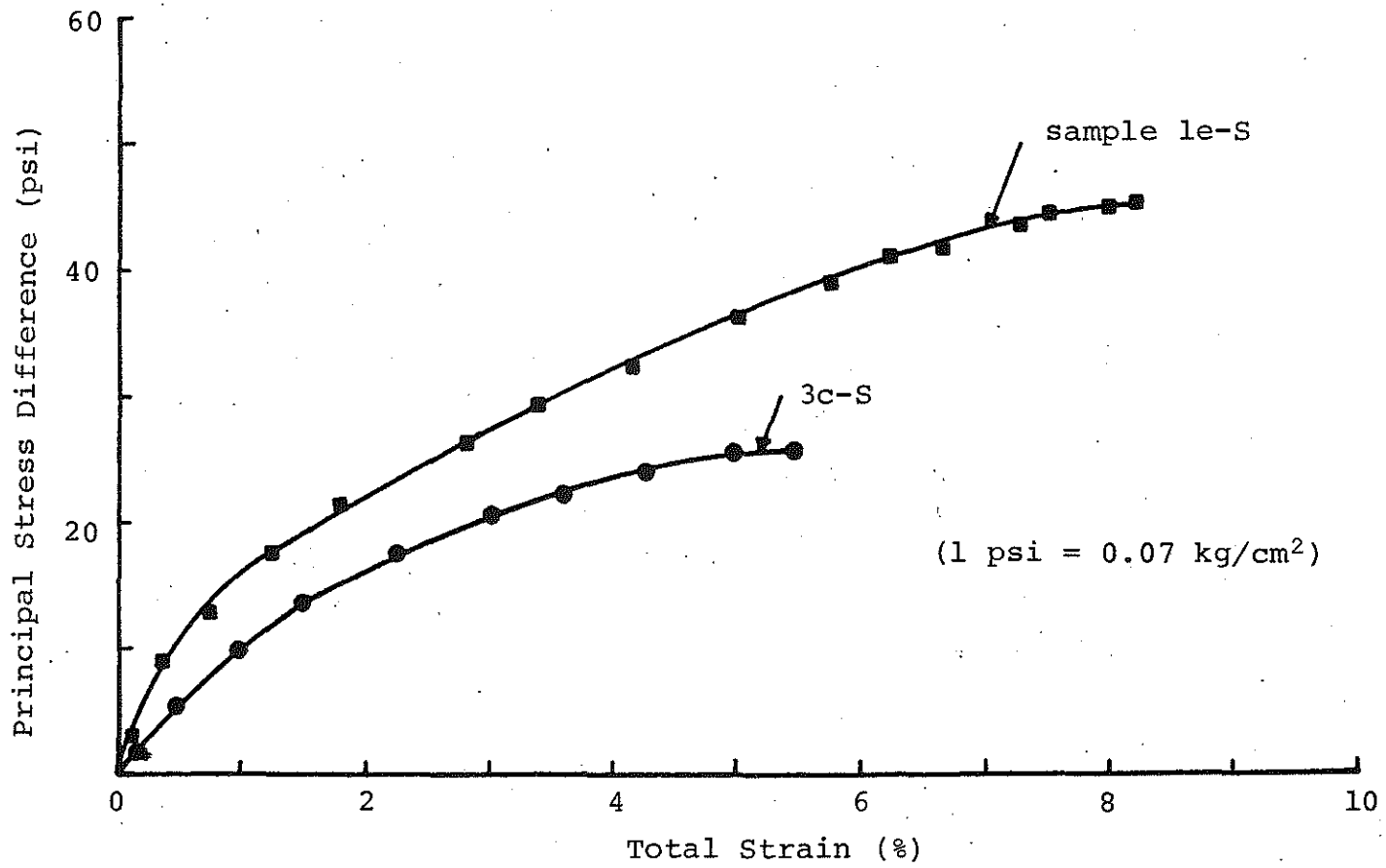

FIGURE C.12 Principal Stress Difference versus Total Axial Strain from Ramp Tests, Site 3, Lower Peninsula.

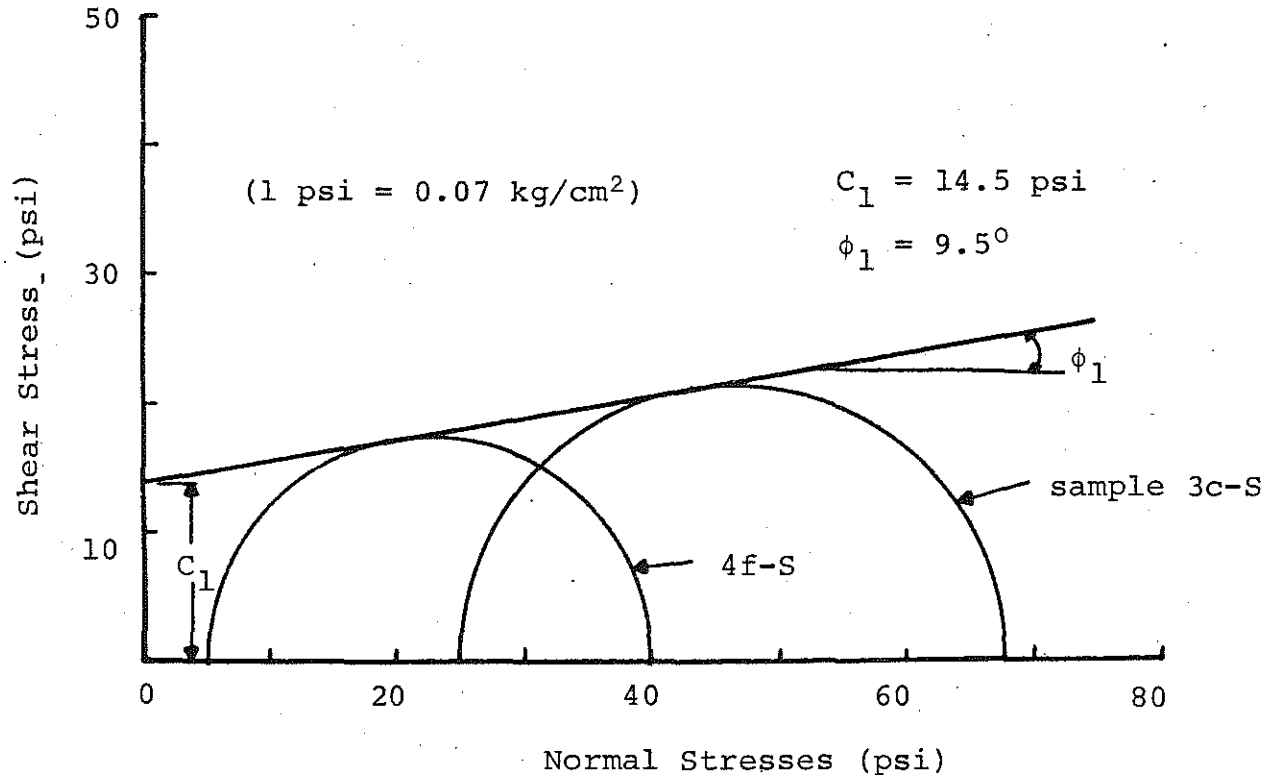

FIGURE C.13 Mohr Circles and Failure Envelopes from Ramp Test, Site 1, Lower Peninsula.

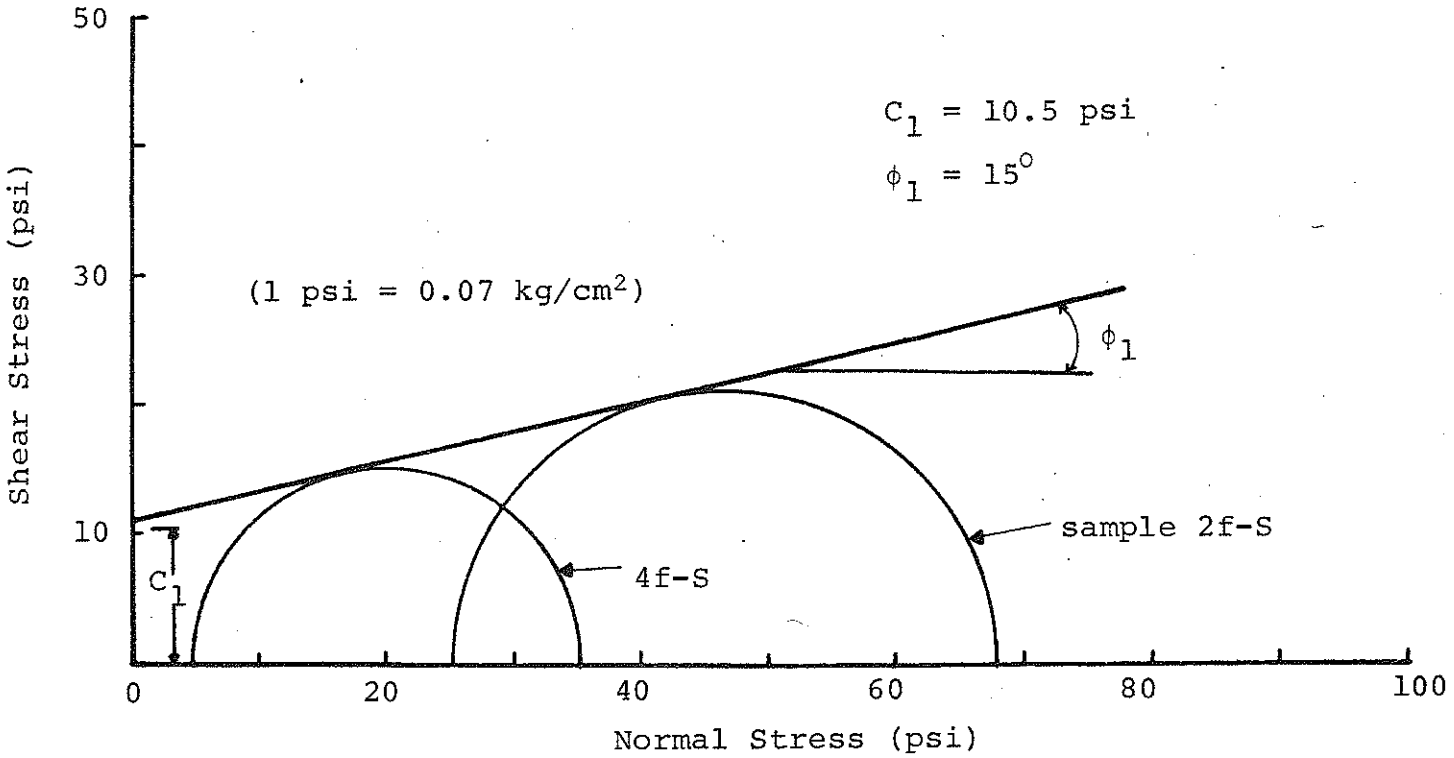

FIGURE C.14 Mohr Circles and Failure Envelopes from Ramp Test, Site 2, Lower Peninsula.

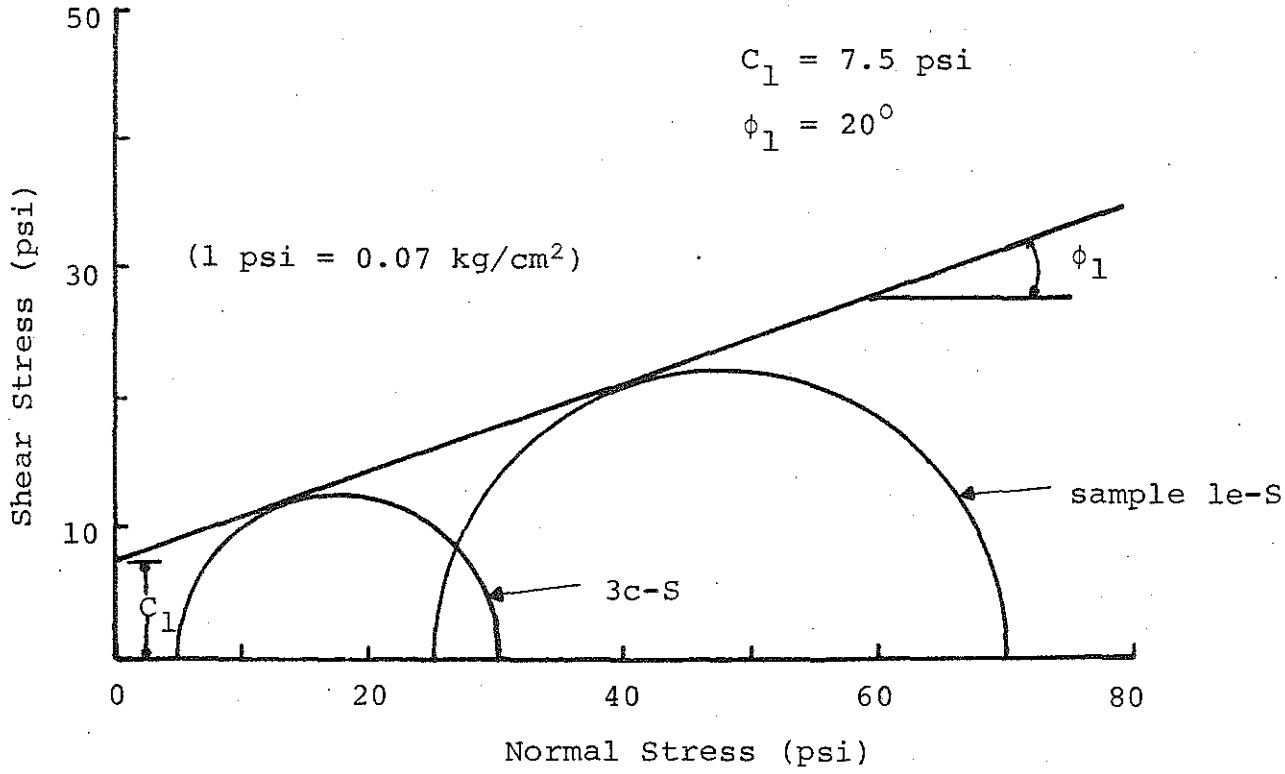

FIGURE C.15 Mohr Circles and Failure Envelopes from Ramp Test, Site 3, Lower Peninsula.

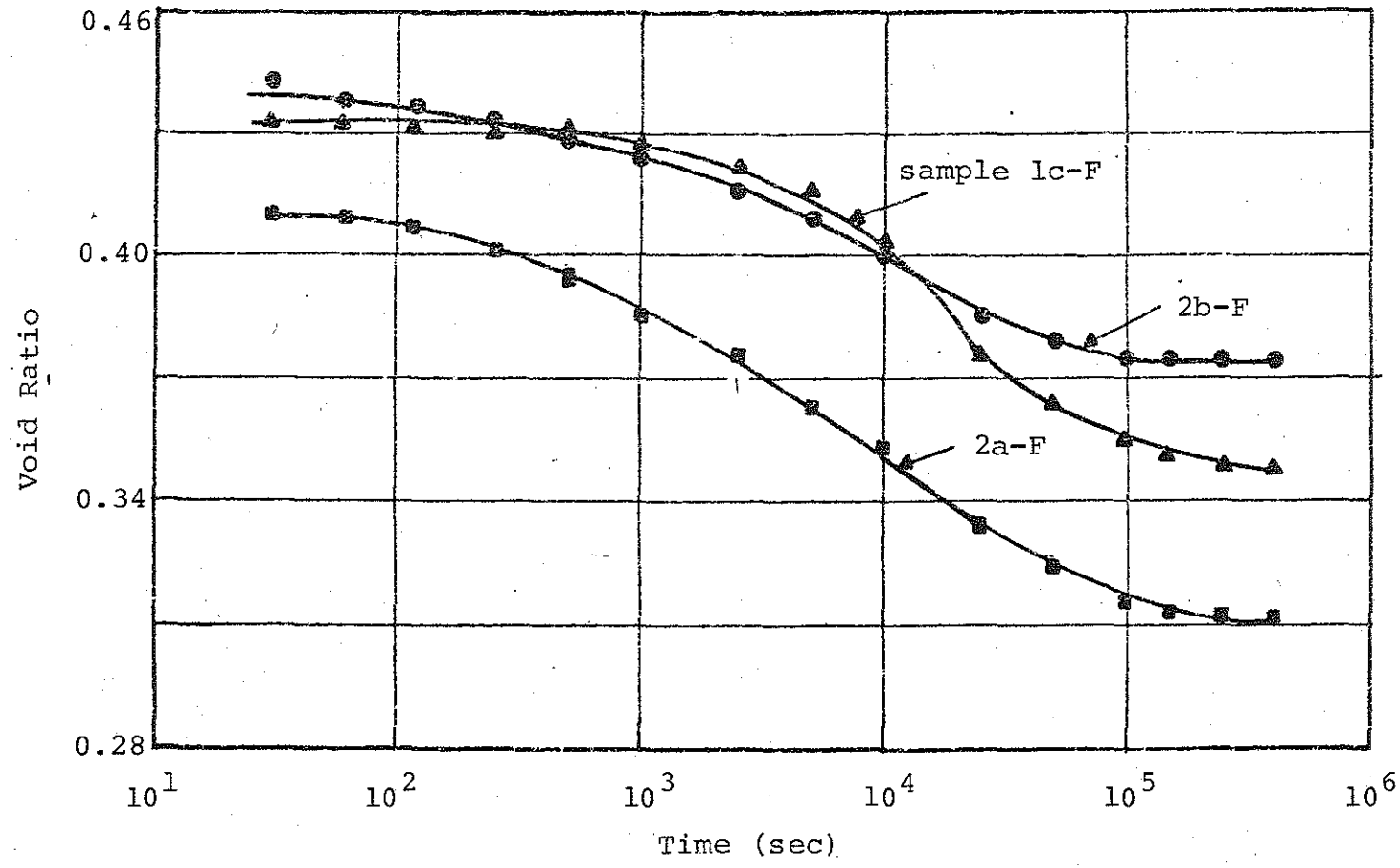

FIGURE C.16 Void Ratio versus the Logarithm of Time for Samples Consolidated under a Confining Pressure of 5 psi Prior to the Commencement of the Triaxial Cyclic Load, Site 1, Lower Peninsula.

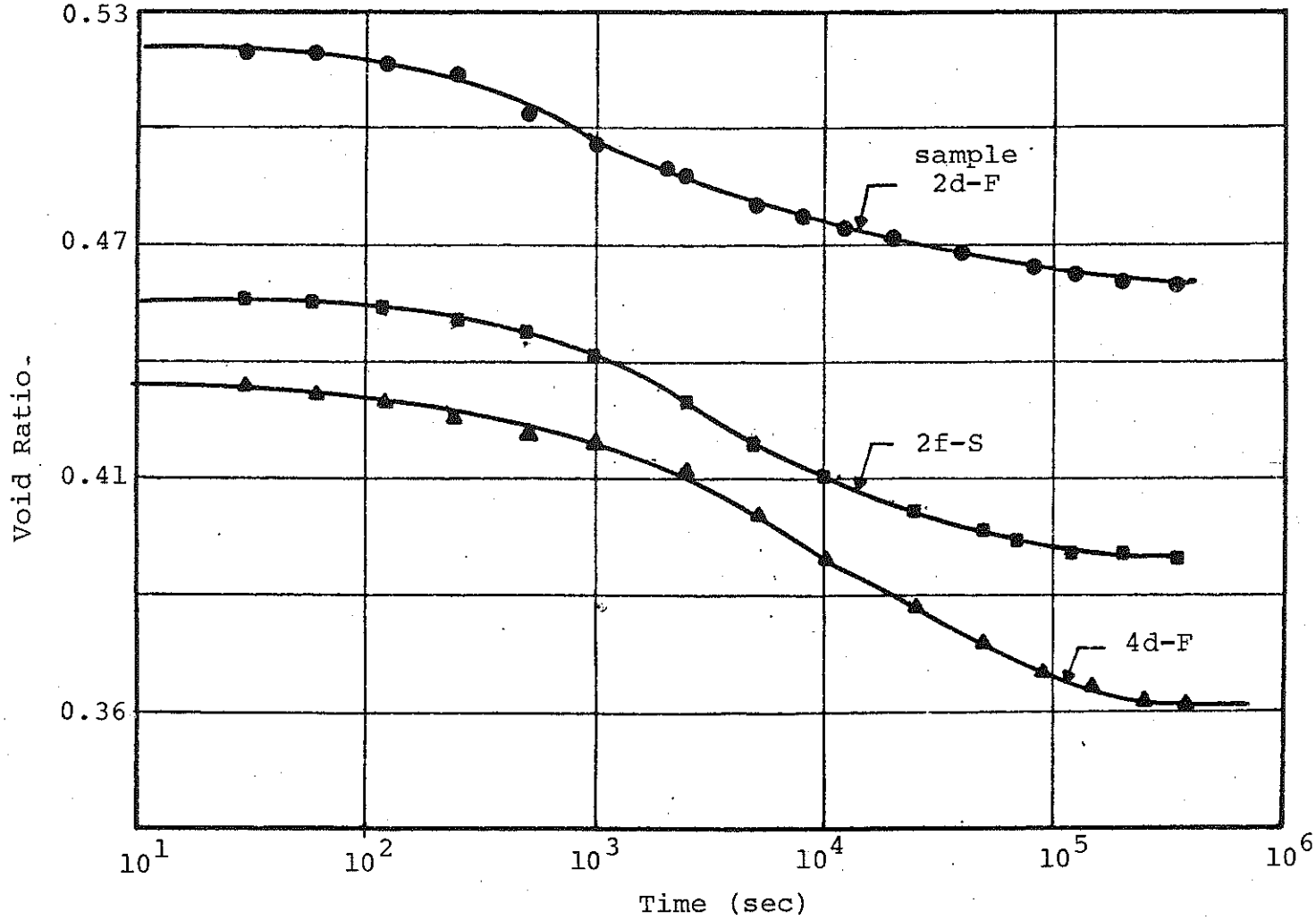

FIGURE C.17 Void Ratio versus the Logarithm of Time for Three Samples Consolidated under a Confining Pressure of 25 psi Prior to the Commencement of the Triaxial Cyclic Load, Site 1, Lower Peninsula.

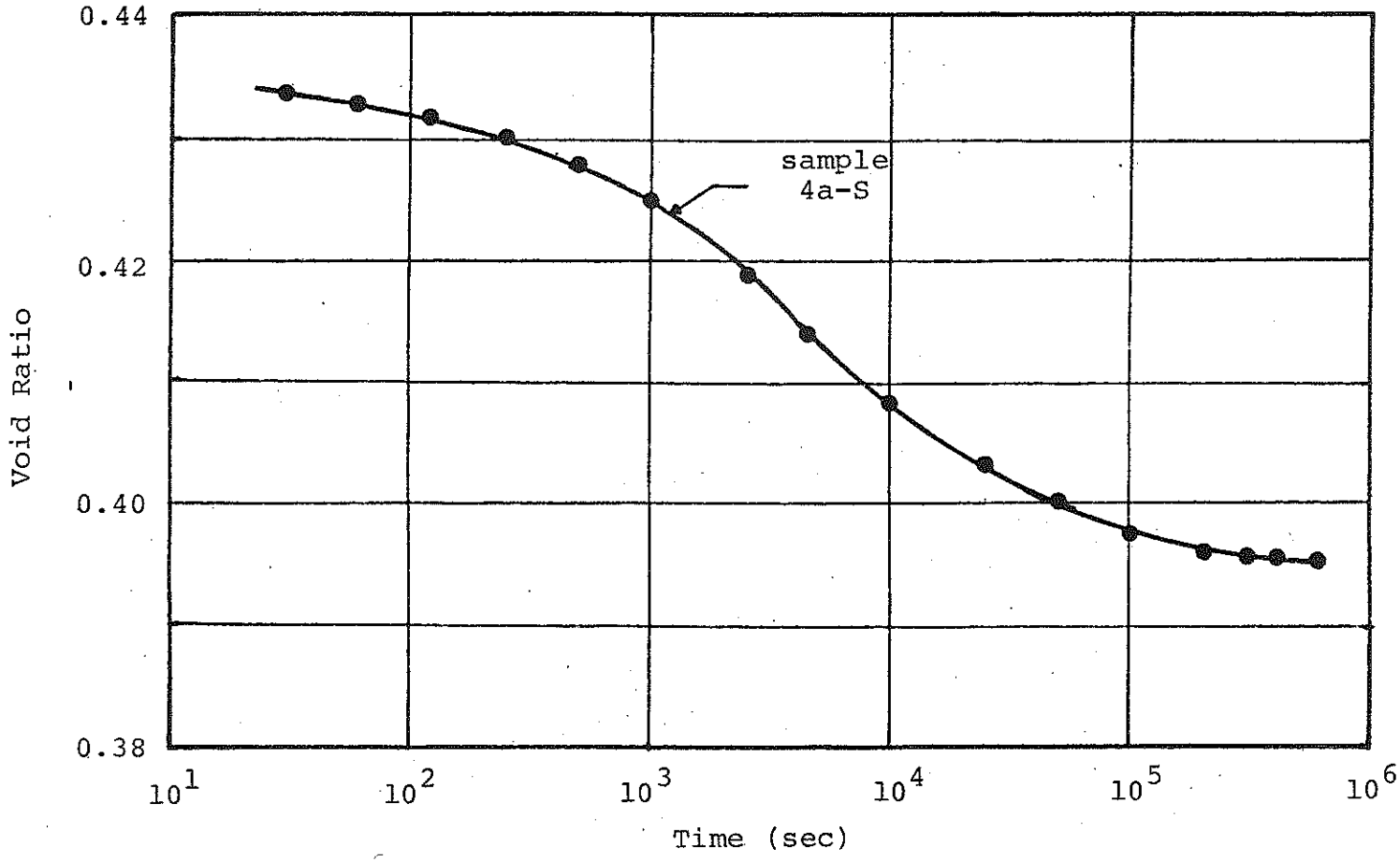

FIGURE C.18 Void Ratio versus the Logarithm of Time for Three Samples Consolidated under a Confining Pressure of 50 psi Prior to the Commencements of the Triaxial Cyclic Load, Site 1, Lower Peninsula.

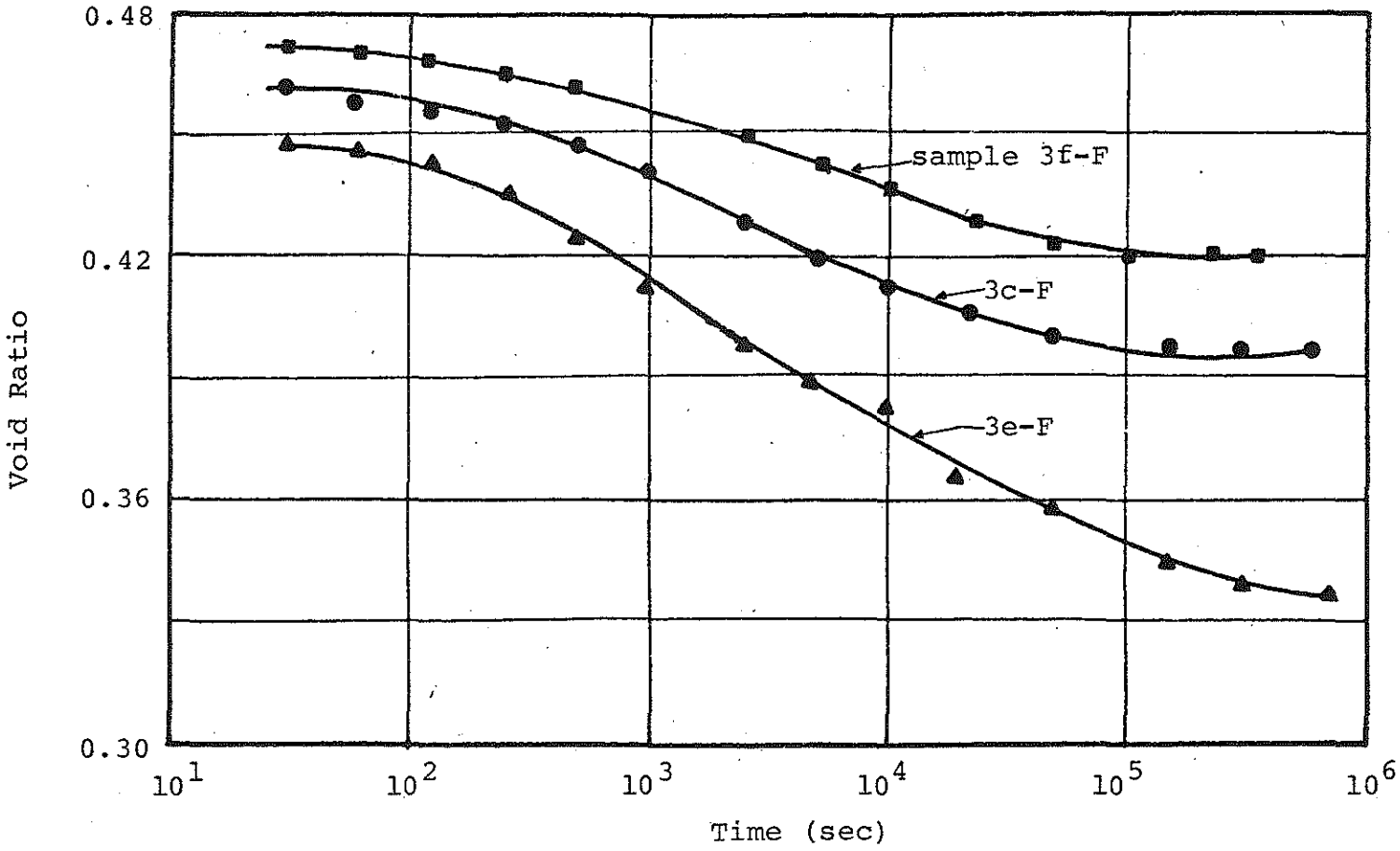

FIGURE C.19 Void Ratio versus Logarithm of Time for Three Samples Consolidated under a Confining Pressure of 25 psi Prior to the Commencement of the Triaxial Cyclic Load, Site 2, Lower Peninsula.

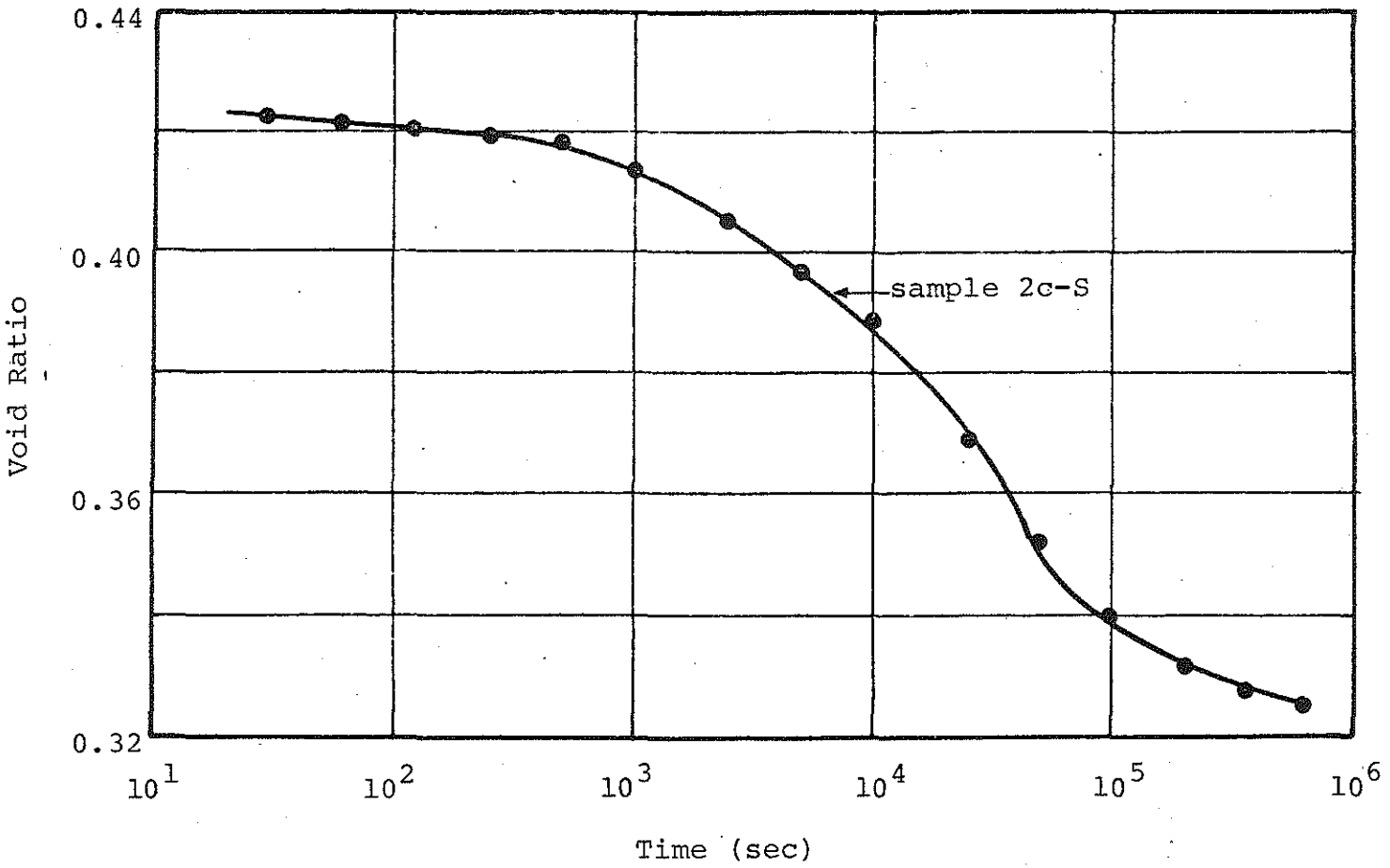

FIGURE C.20 Void Ratio versus the Logarithm of Time for Three Samples Consolidated under a Confining Pressure of 50 psi Prior to the Commencement of the Triaxial Cyclic Load, Site 2, Lower Peninsula.

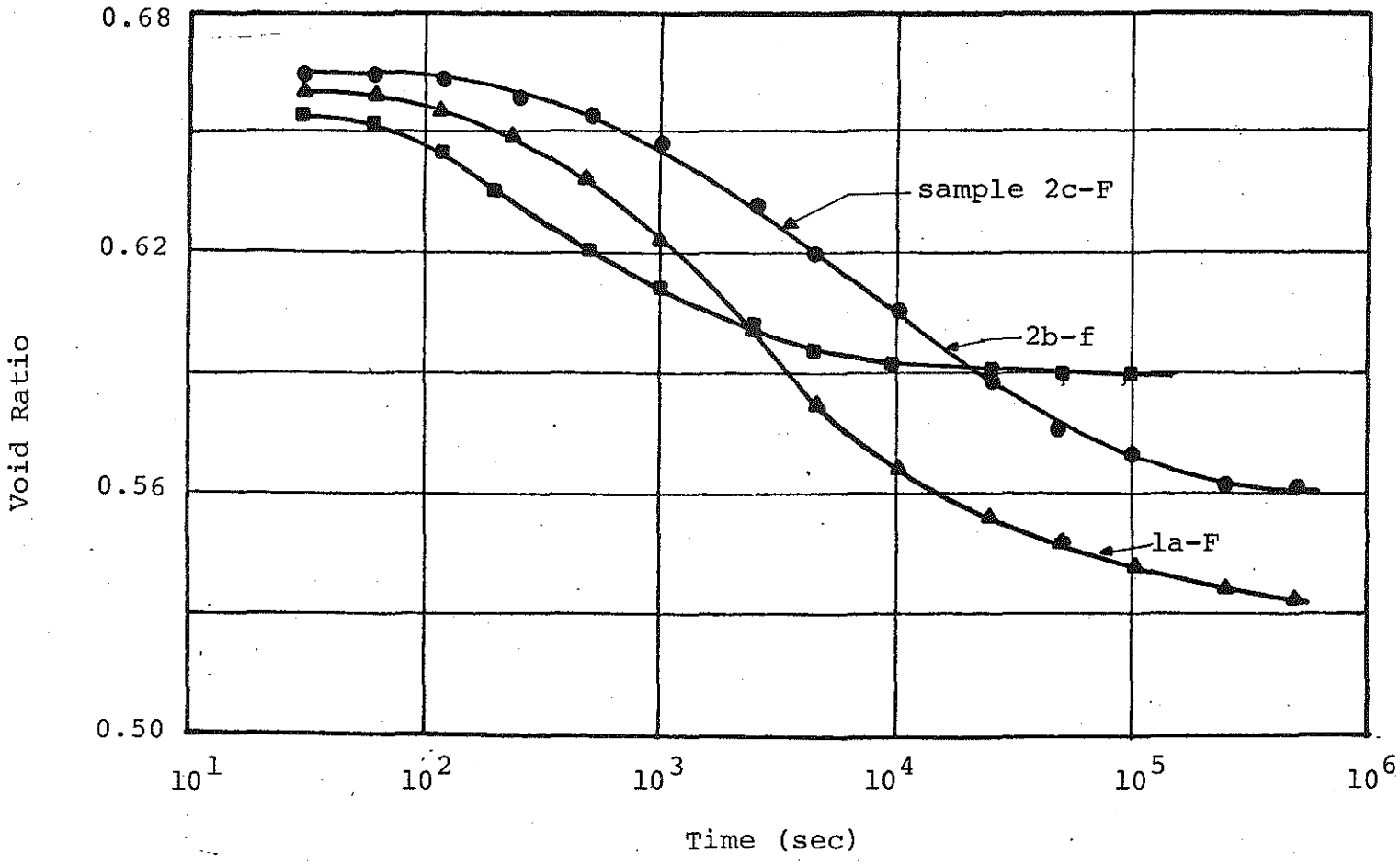

FIGURE C.21 Void Ratio versus Logarithm of Time for Three Samples Consolidated under a Confining Pressure of 5 psi Prior to the Commencement of the Triaxial Cyclic Load, Site 3, Lower Peninsula.

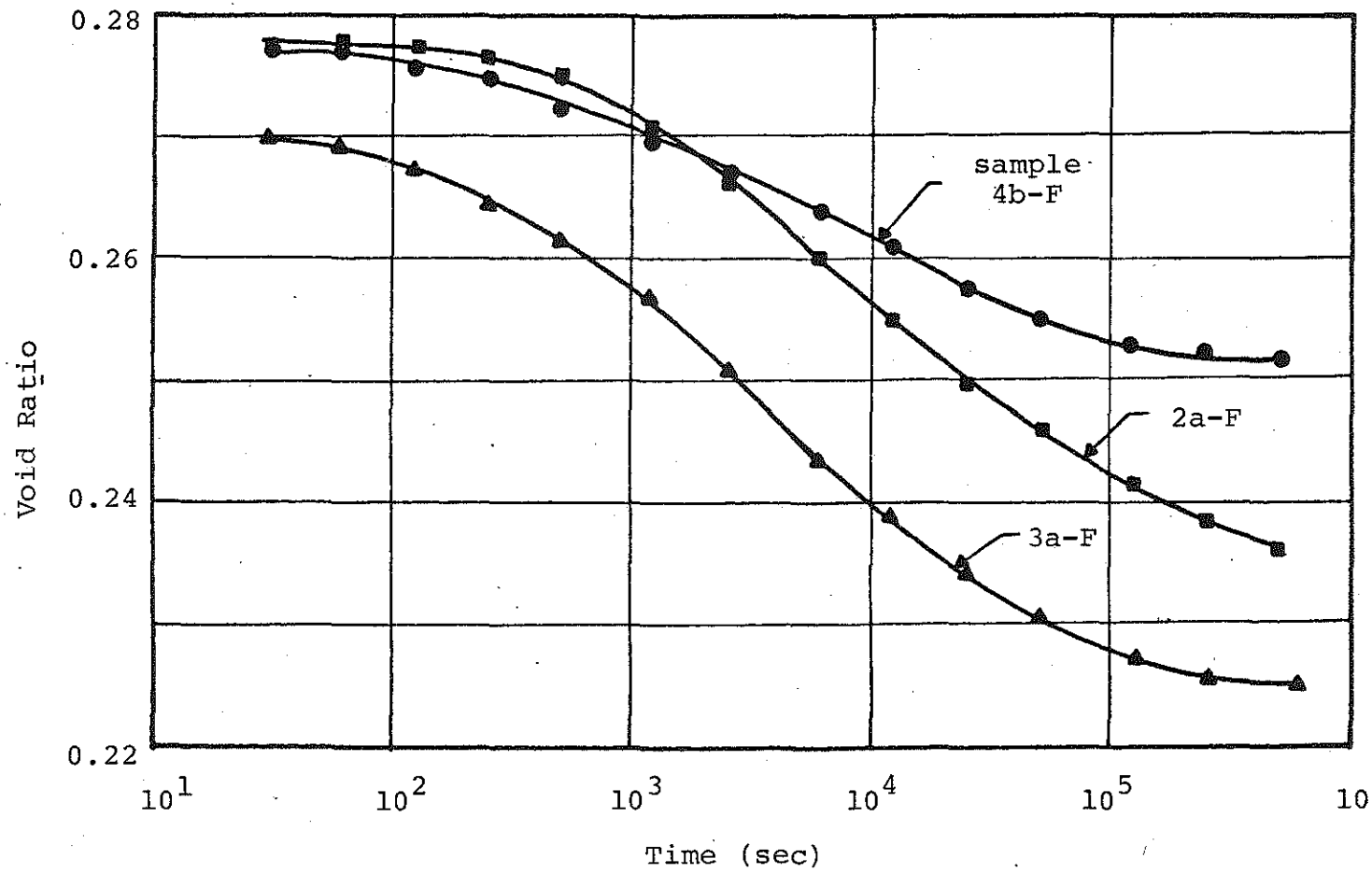

FIGURE C.22 Void Ratio versus Logarithm of Time for Three Samples Consolidated under a Confining Pressure of 25 psi Prior to the Commencement of the Triaxial Cyclic Load, Site 3, Lower Peninsula.

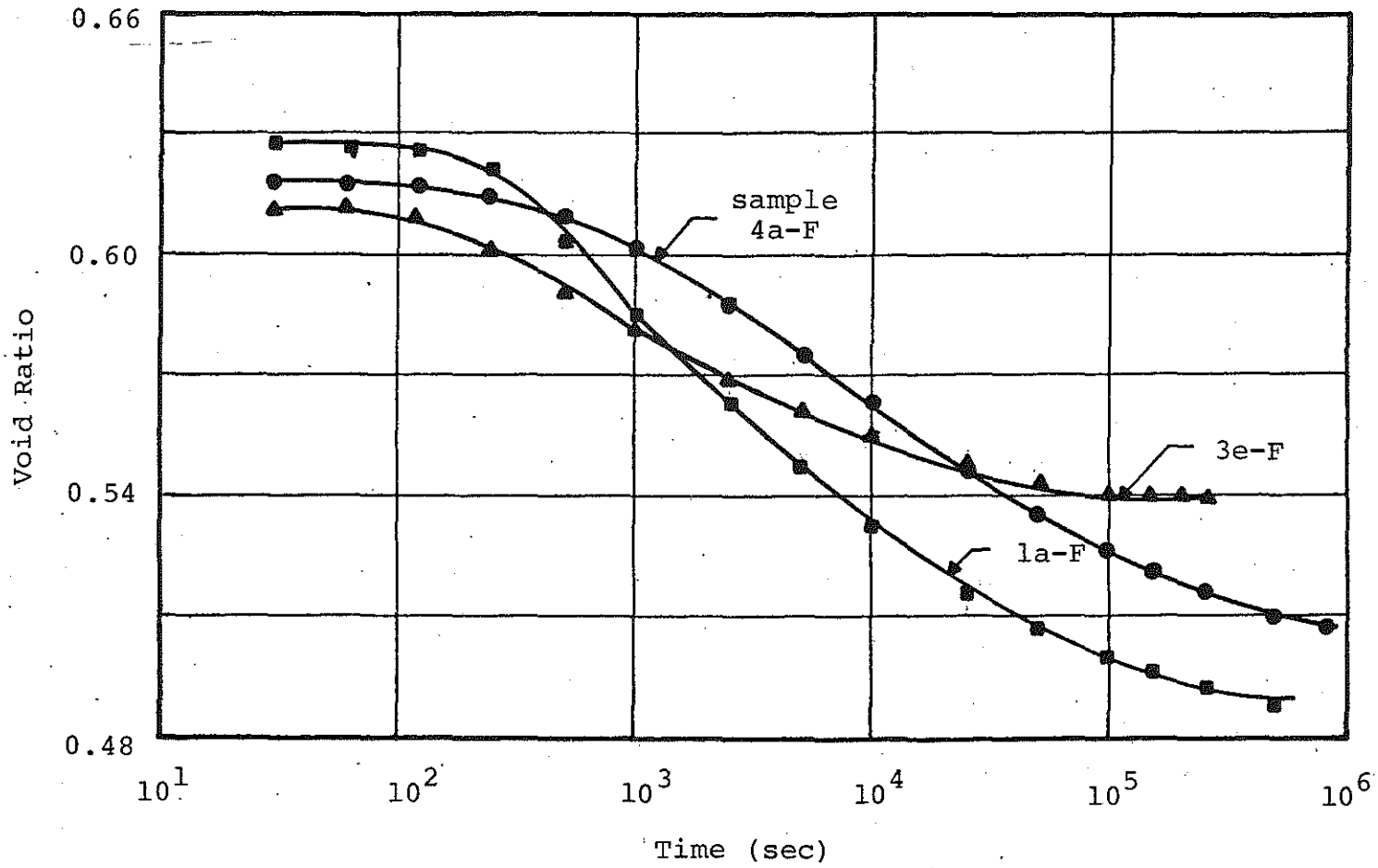

FIGURE C.23 Void Ratio versus Logarithm of Time for Three Samples Consolidated under a Confining Pressure of 5 psi Prior to the Commencement of the Triaxial Cyclic Load, Site 4, Lower Peninsula.

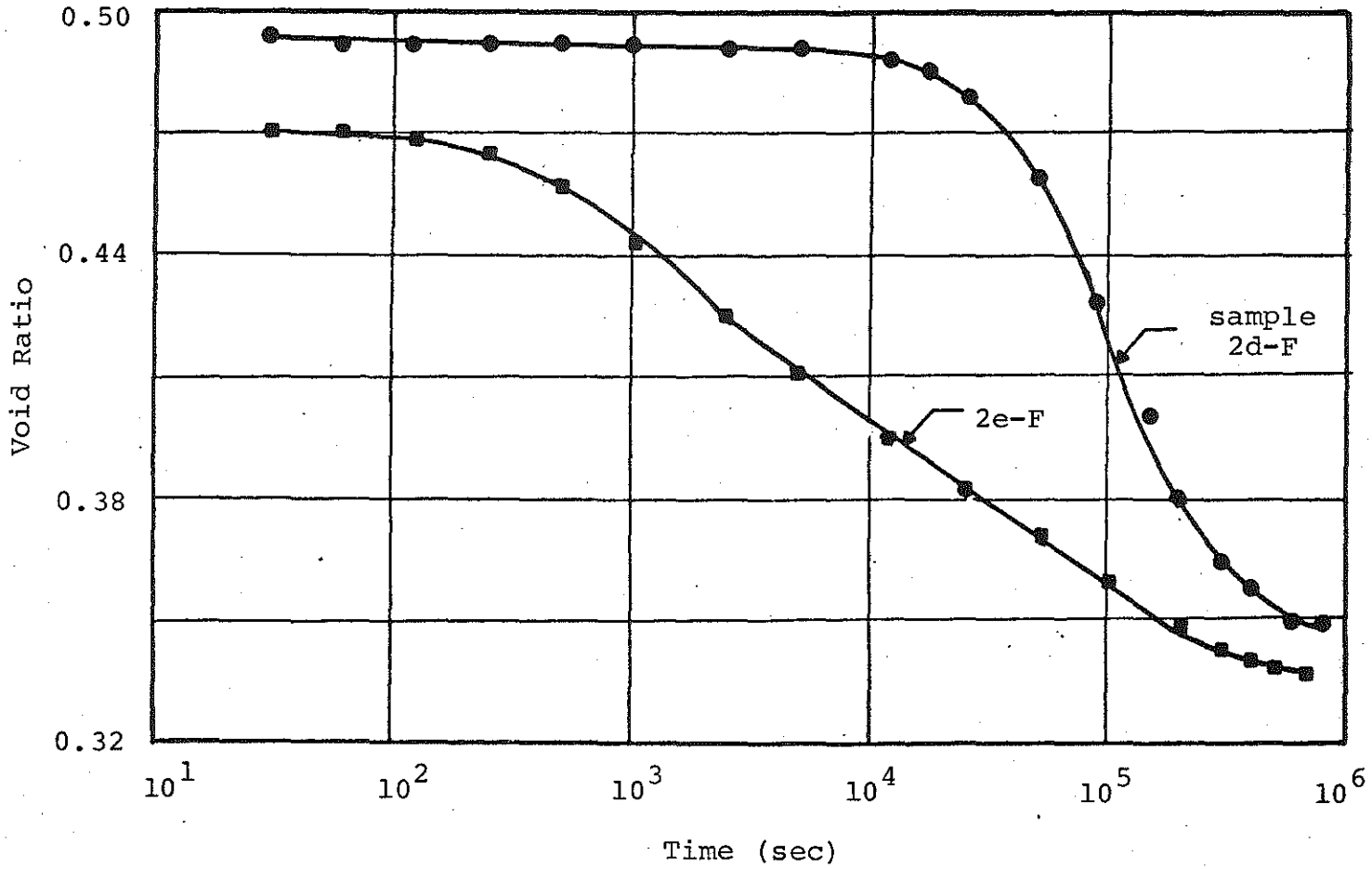

FIGURE C.24 Void Ratio versus Logarithm of Time for Three Samples Consolidated under a Confining Pressure of 25 psi Prior to the Commencement of the Triaxial Cyclic Load, Site 4, Lower Peninsula.

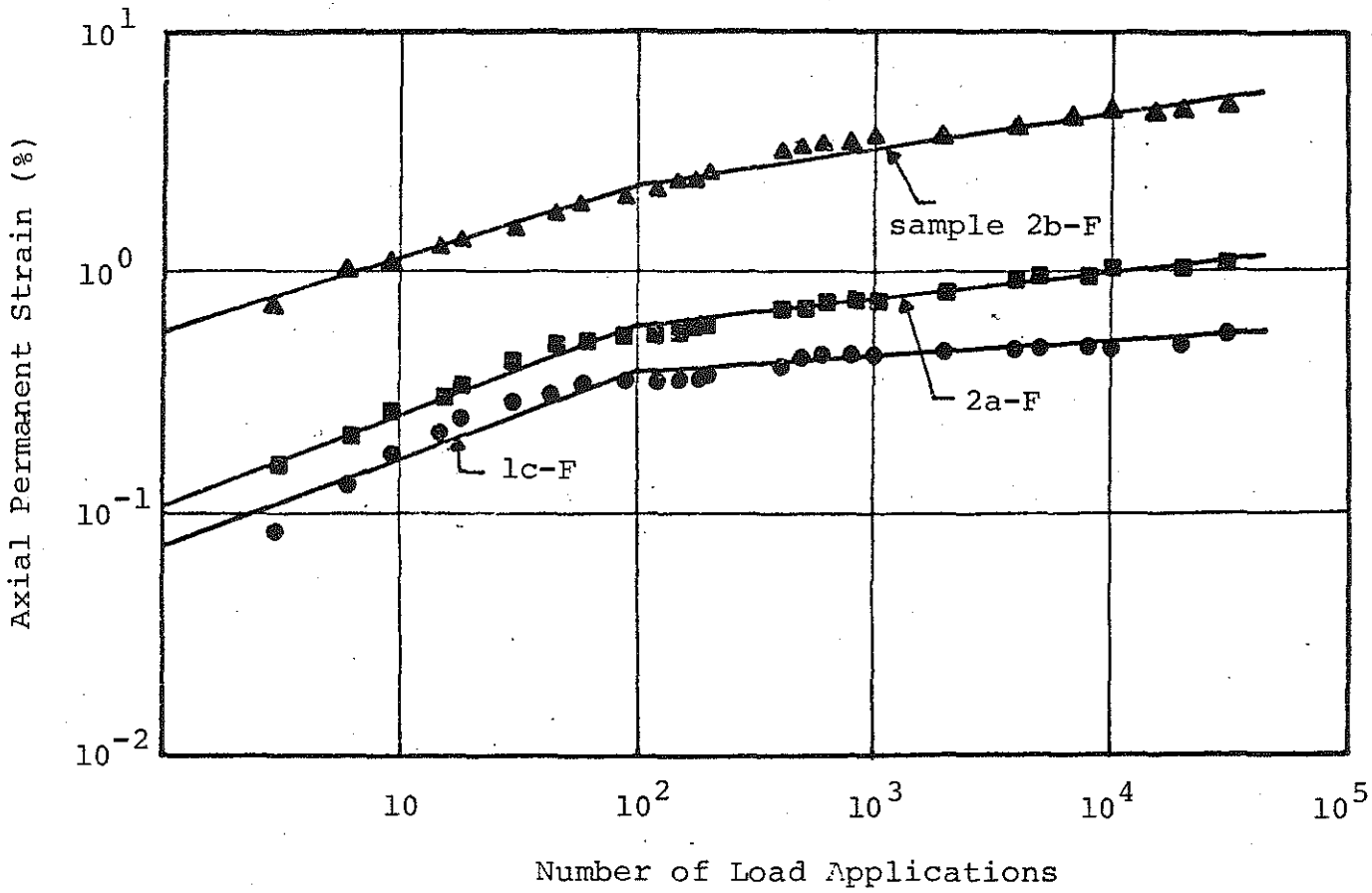

FIGURE C.25 Axial Permanent Strain versus Number of Load Applications for Samples Consolidated under a Confining Pressure of 5 psi and Tested Using Different Cyclic Stress Ratio, Site 1, Lower Peninsula.

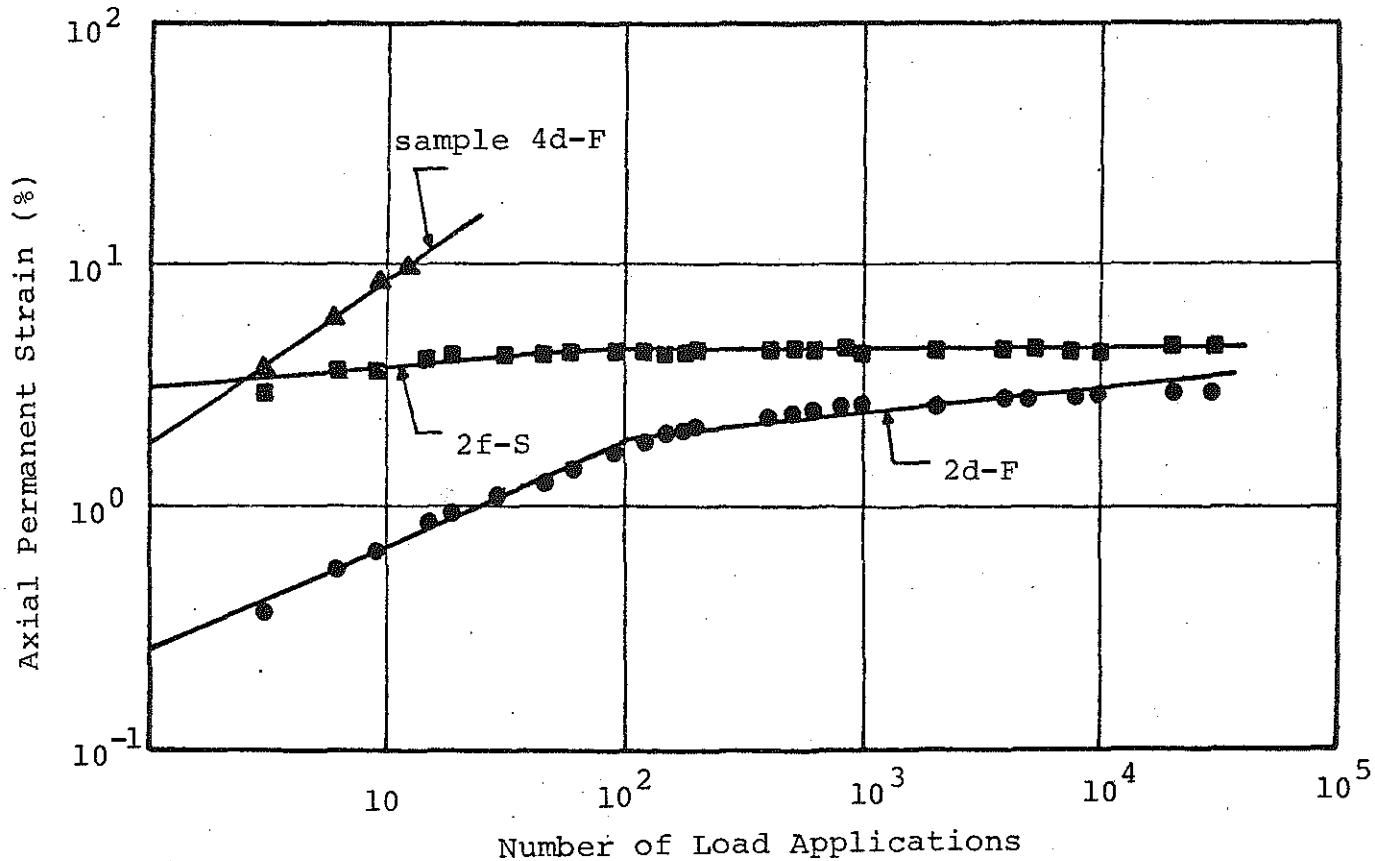

FIGURE C.26 Axial Permanent Strain versus Number of Load Applications for Samples Consolidated under a Confining Pressure of 25 psi and Tested Using Different Cyclic Stress Ratio, Site 1, Lower Peninsula.

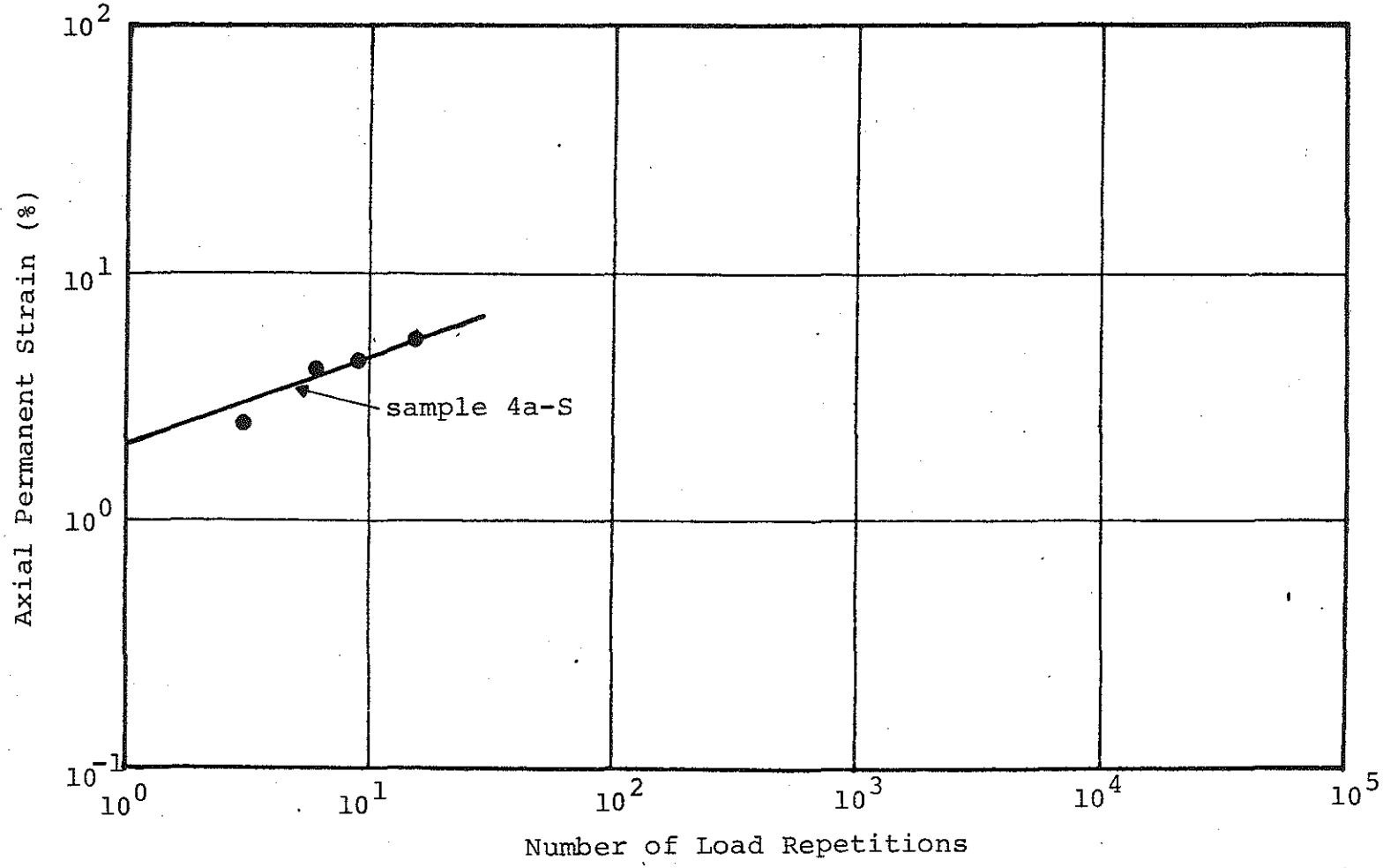

FIGURE C.27 Axial Permanent Strain versus Number of Load Cycles for Samples Consolidated under a confining Pressure of 50 psi and Tested using Different Cyclic Stress Ratio, Site 1, Lower Peninsula.

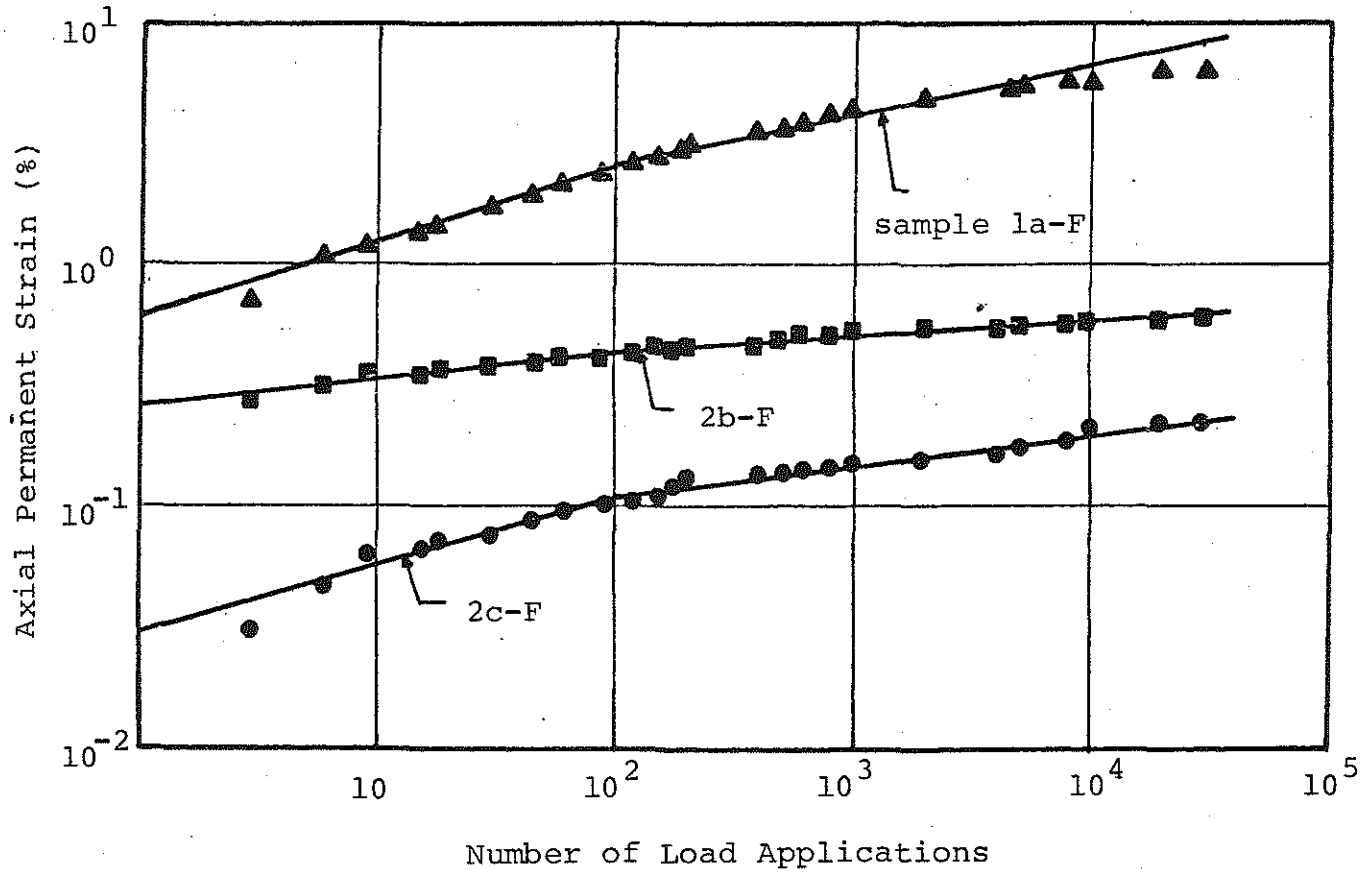

FIGURE C.28 Axial Permanent Strain versus Number of Load Applications for Samples under a Confining Pressure of 5 psi and Tested Using Different Cyclic Stress Ratio, Site 3, Lower Peninsula.

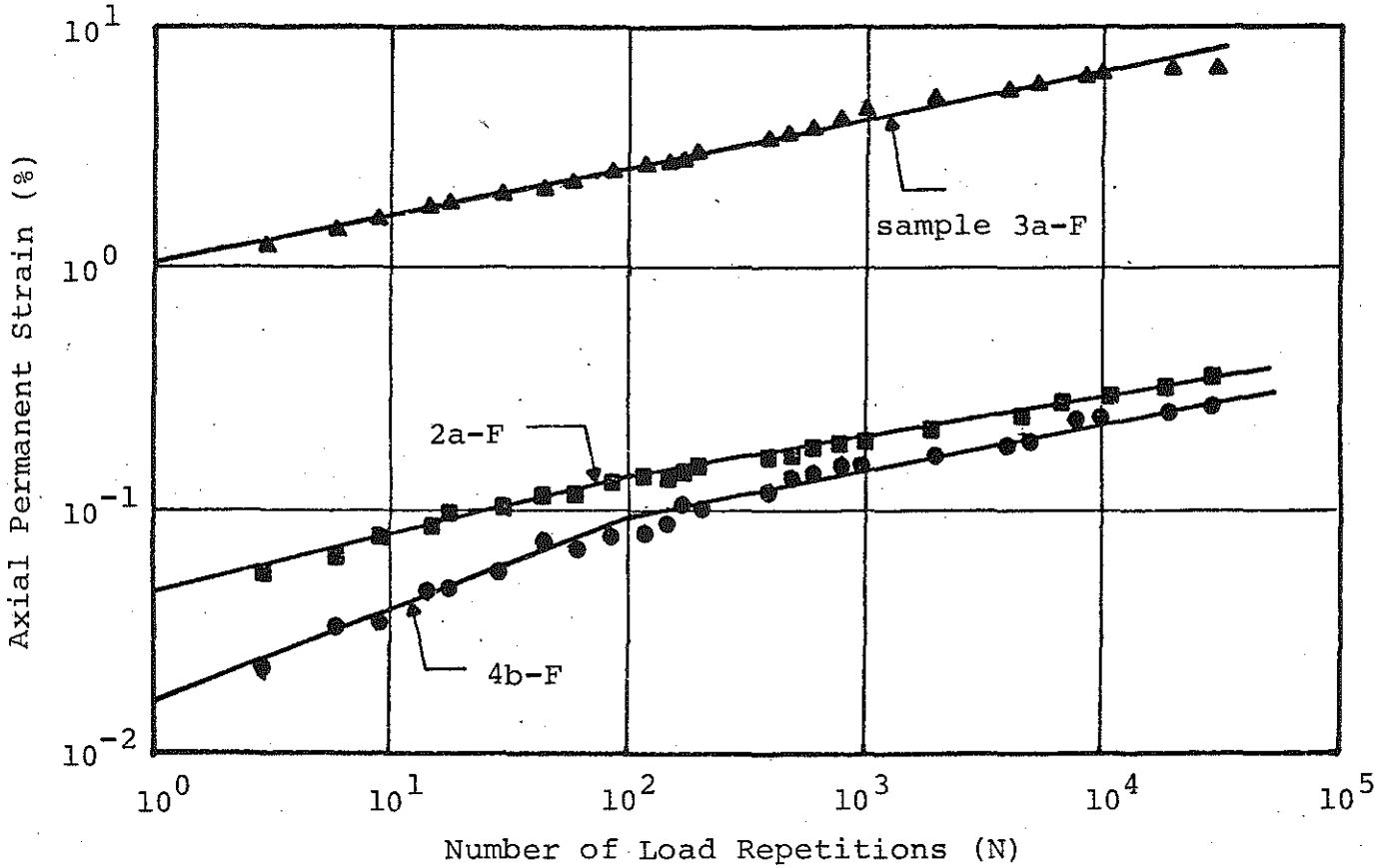

FIGURE C.29 Axial Permanent Strain Versus Number of Load Cycles for Samples Consolidated under a Confining Pressure of 25 psi and Tested Using Different Cyclic Stress Ratio, Site 3, Lower Peninsula.

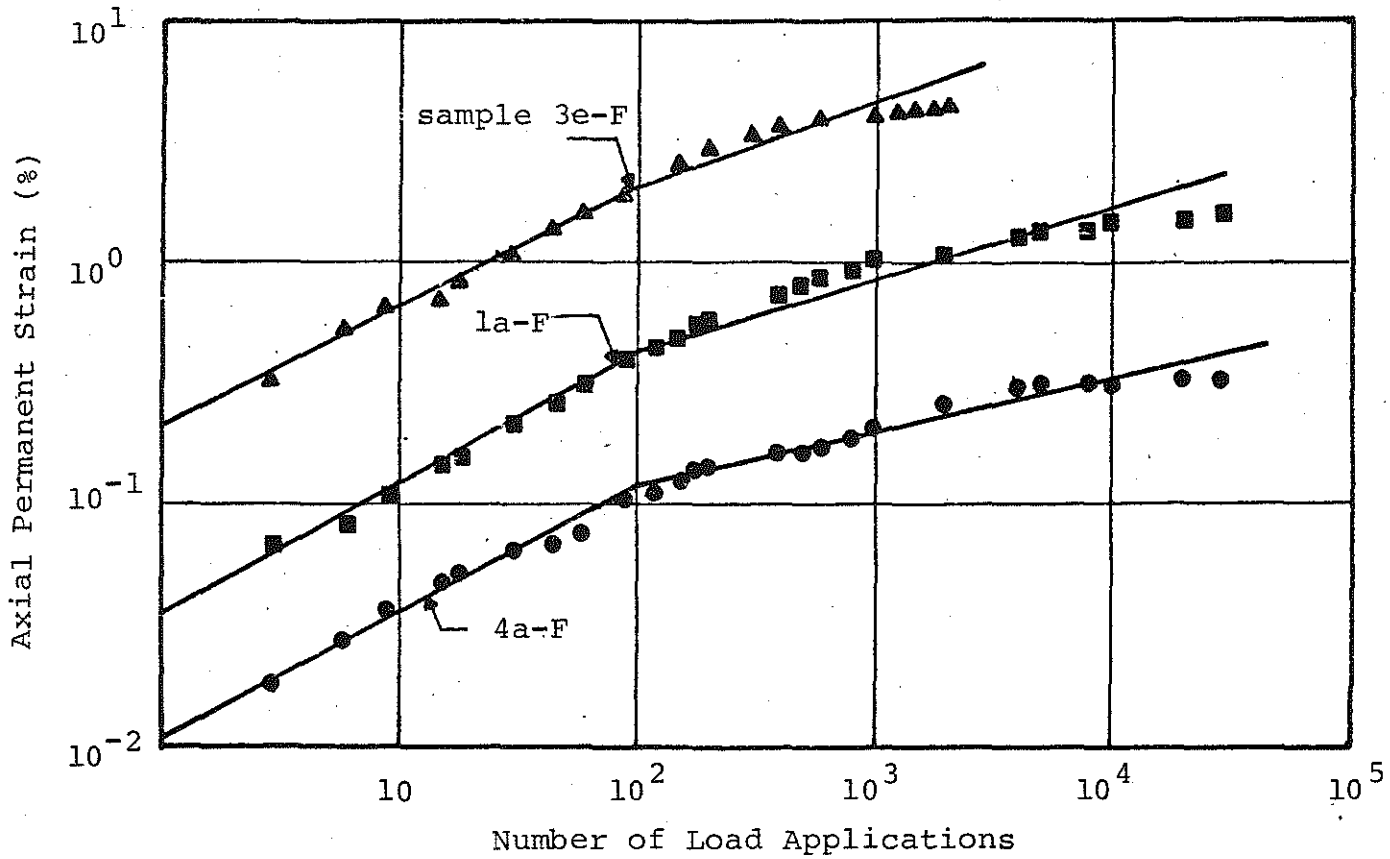

FIGURE C.30 Axial Permanent Strain versus Number of Load Applications for Samples Consolidated under a Confining Pressure of 5 psi and Tested Using Different Cyclic Stress Ratio, Site 4, Lower Peninsula.

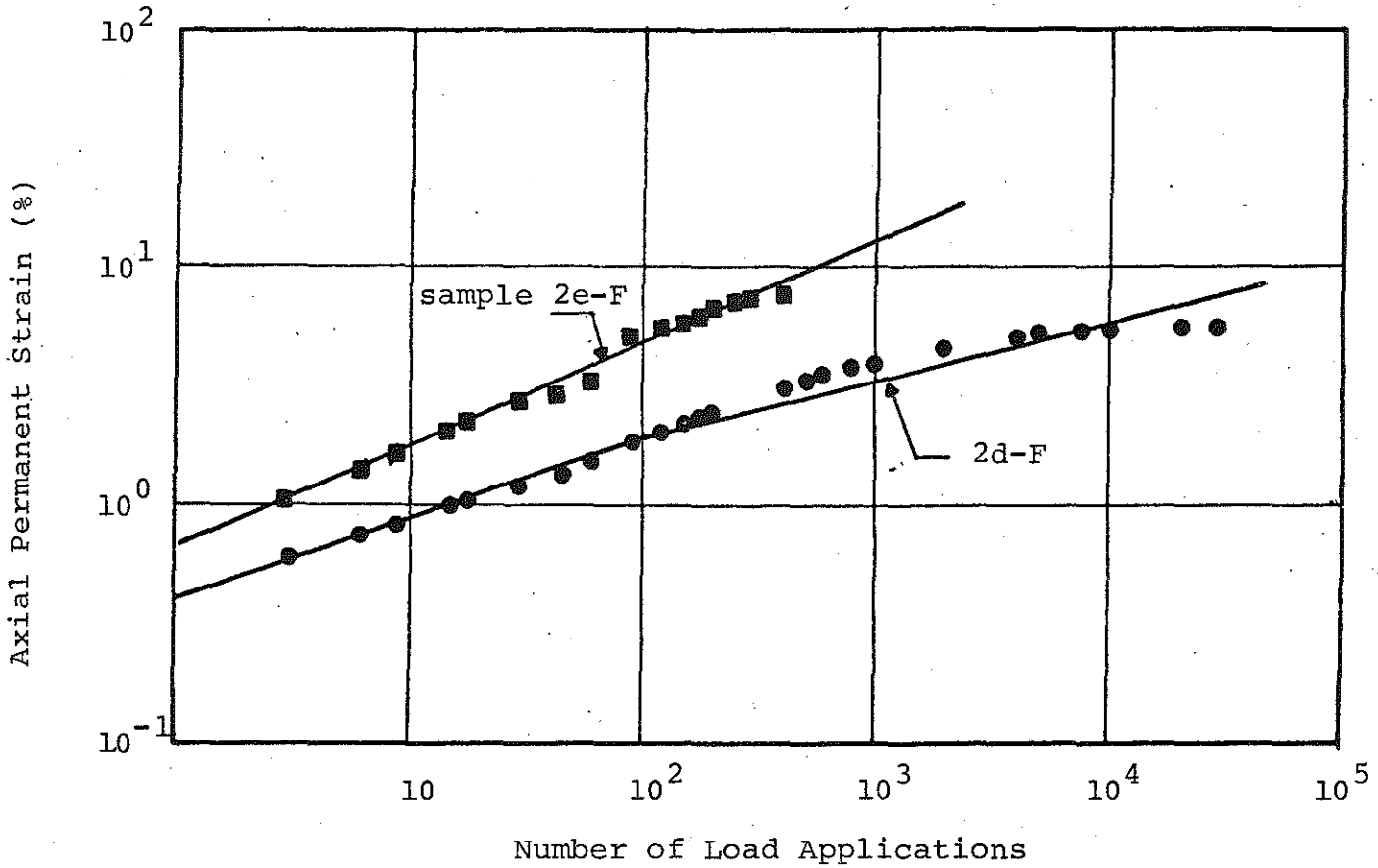

FIGURE C.31 Axial Permanent Strain versus Number of Load Applications for Samples Consolidated under a Confining Pressure of 25 psi and Tested Using Different Cyclic Stress Ratio, Site 4, Lower Peninsula.

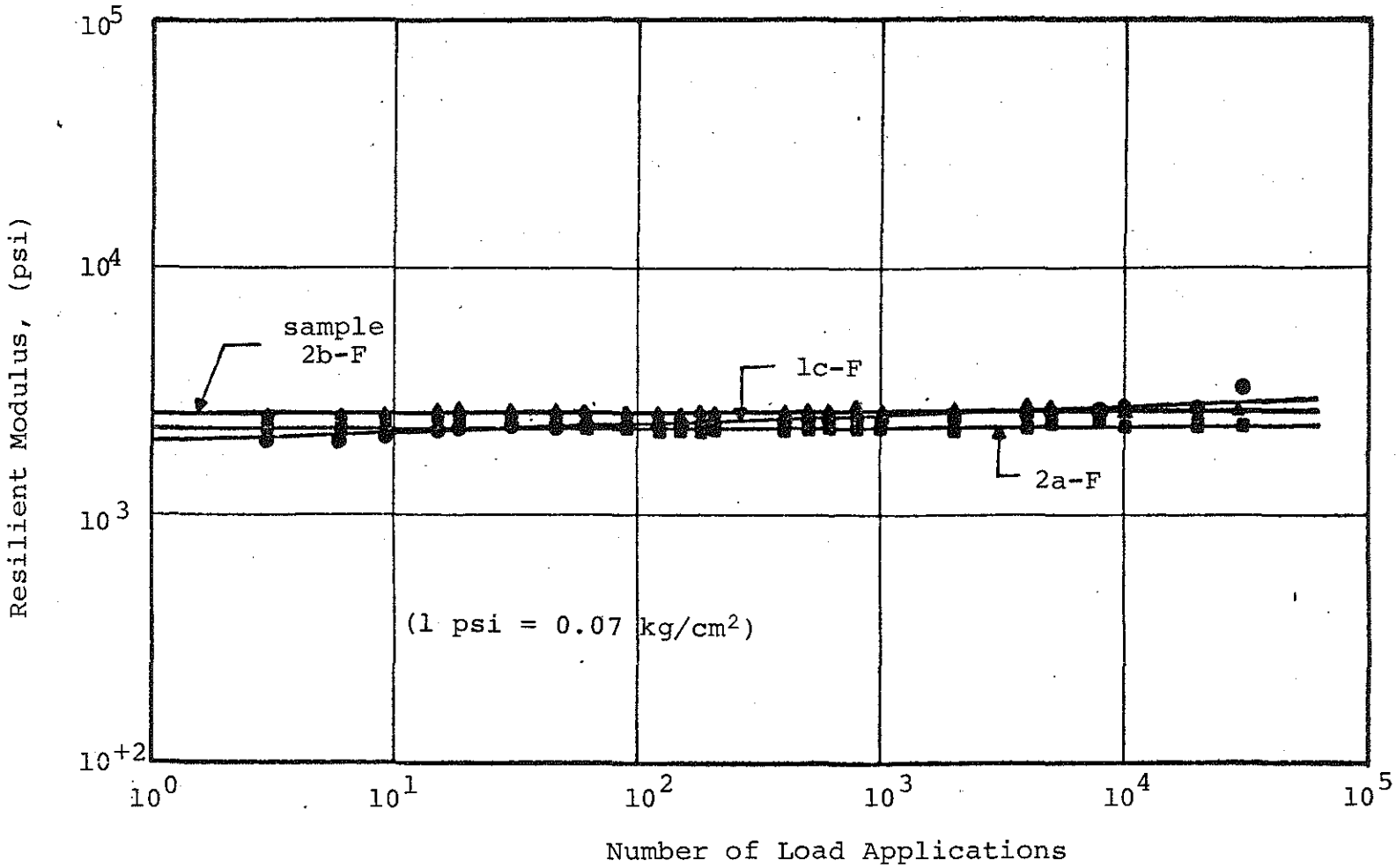

FIGURE C.32 Resilient Modulus versus Number of Load Applications for Samples Consolidated under a Confining Pressure of 5 psi and Tested using Different Cyclic Stress Ratio, Site 1, Lower Peninsula.

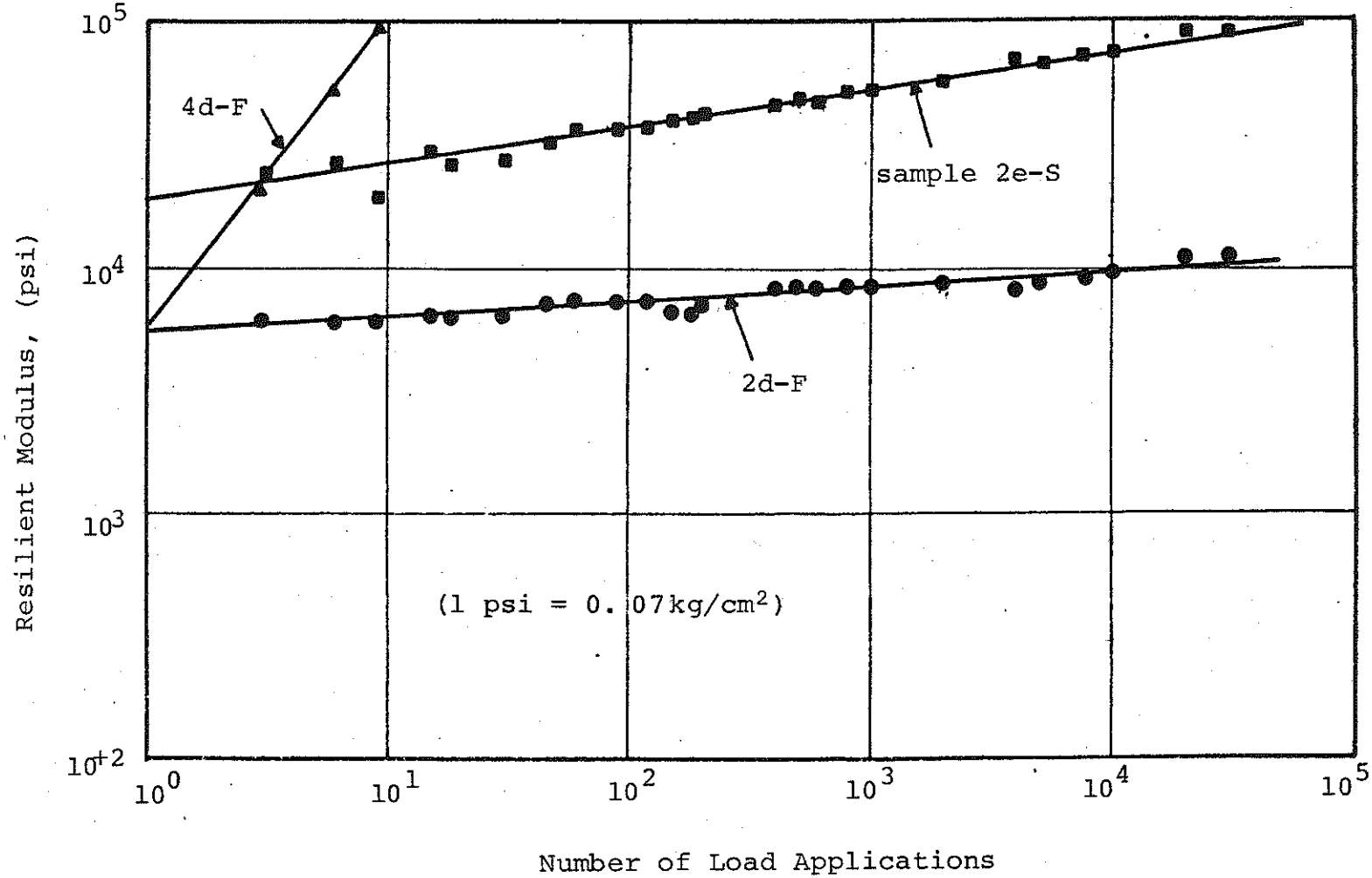

FIGURE C.33 Resilient Modulus versus Number of Load Applications for Samples Consolidated under a Confining Pressure of 25 psi and Tested using Different Cyclic Stress Ratio, Site 1, Lower Peninsula.

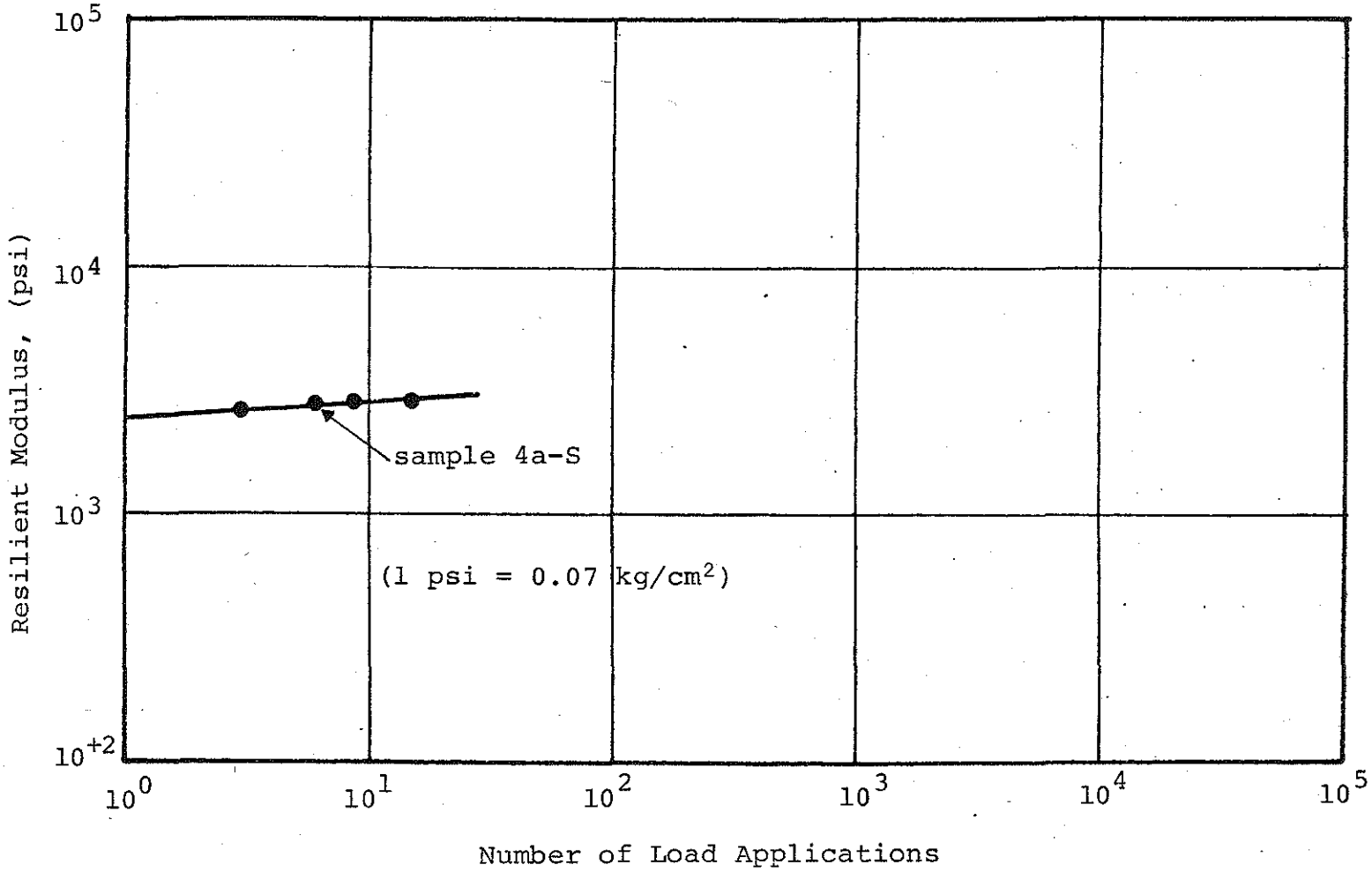

FIGURE C.34 Resilient Modulus versus Number of Load Applications for Samples Consolidated under a Confining Pressure of 50 psi and Tested using Different Cyclic Stress Ratio, Site 1, Lower Peninsula.

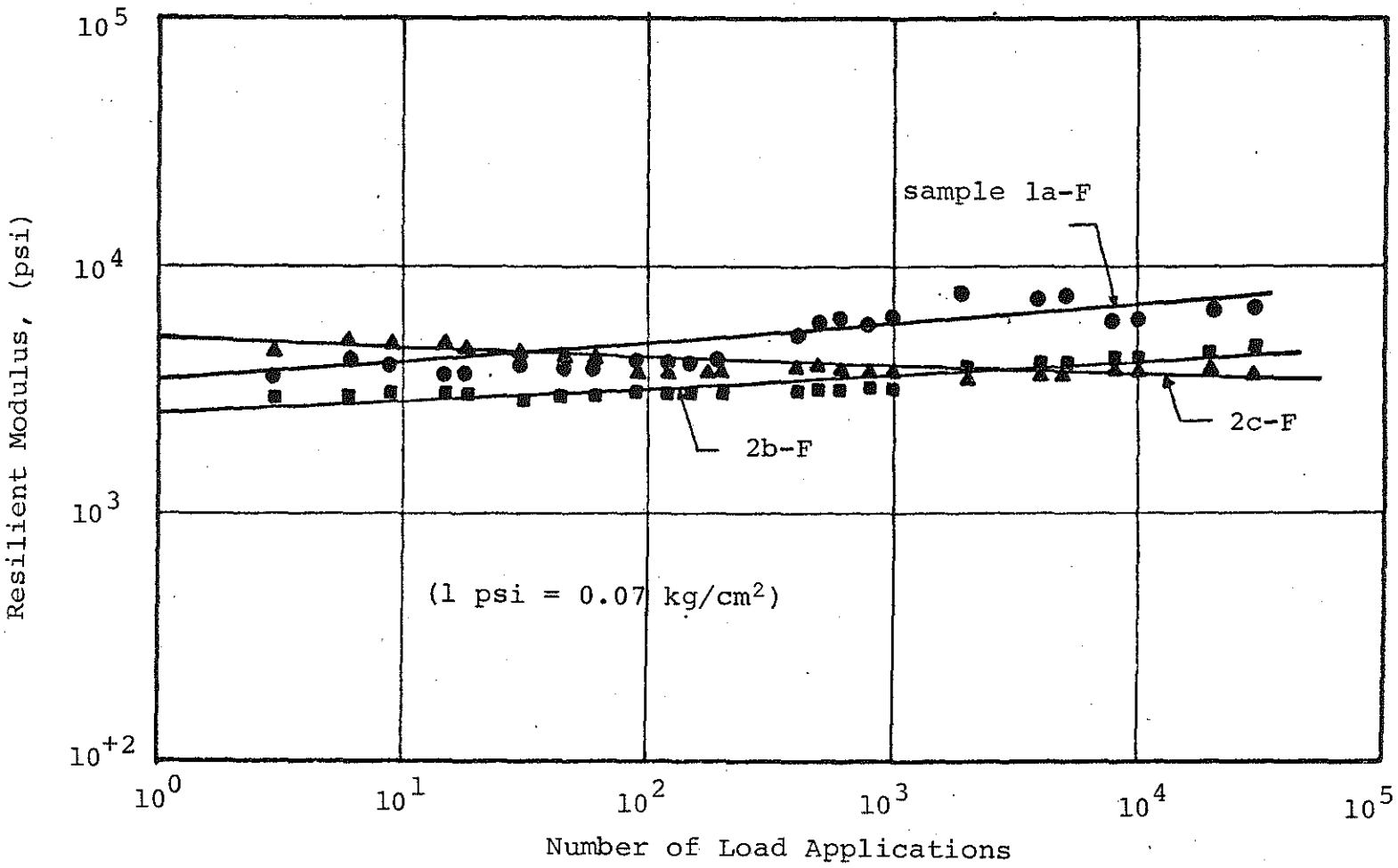

FIGURE C.35 Resilient Modulus (M_R) versus Number of Load Applications for Consolidated Samples Consolidated Under a Confining Pressure of 5 psi and Tested Using Different Cyclic Stress Ratio, Site 3, Lower Peninsula.

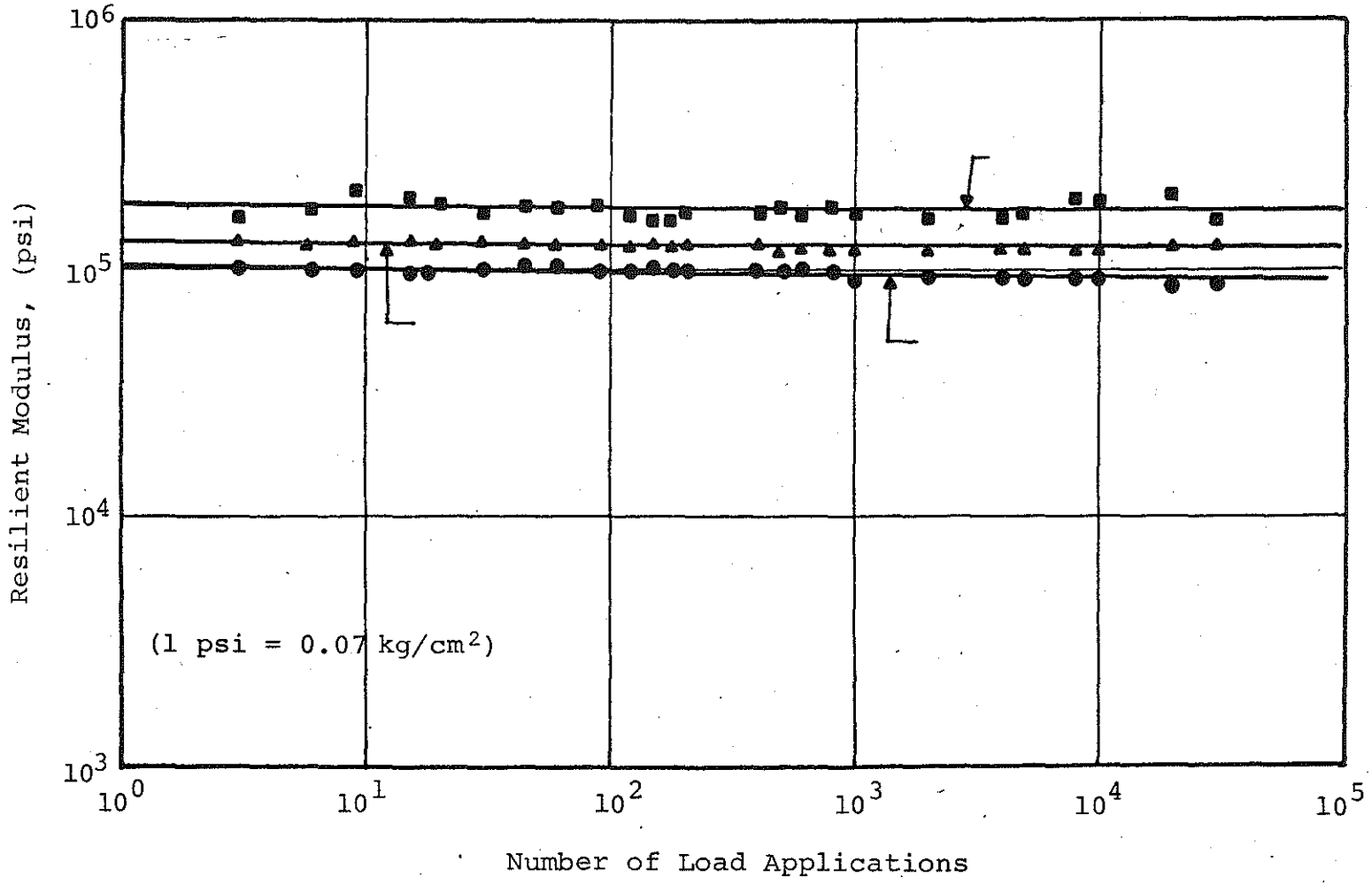

FIGURE C.36 Resilient Modulus versus Number of Load Applications for Samples Consolidated under a Confining Pressure of 25 psi and Tested using Different Cyclic Stress Ratio, Site 3, Lower Peninsula.

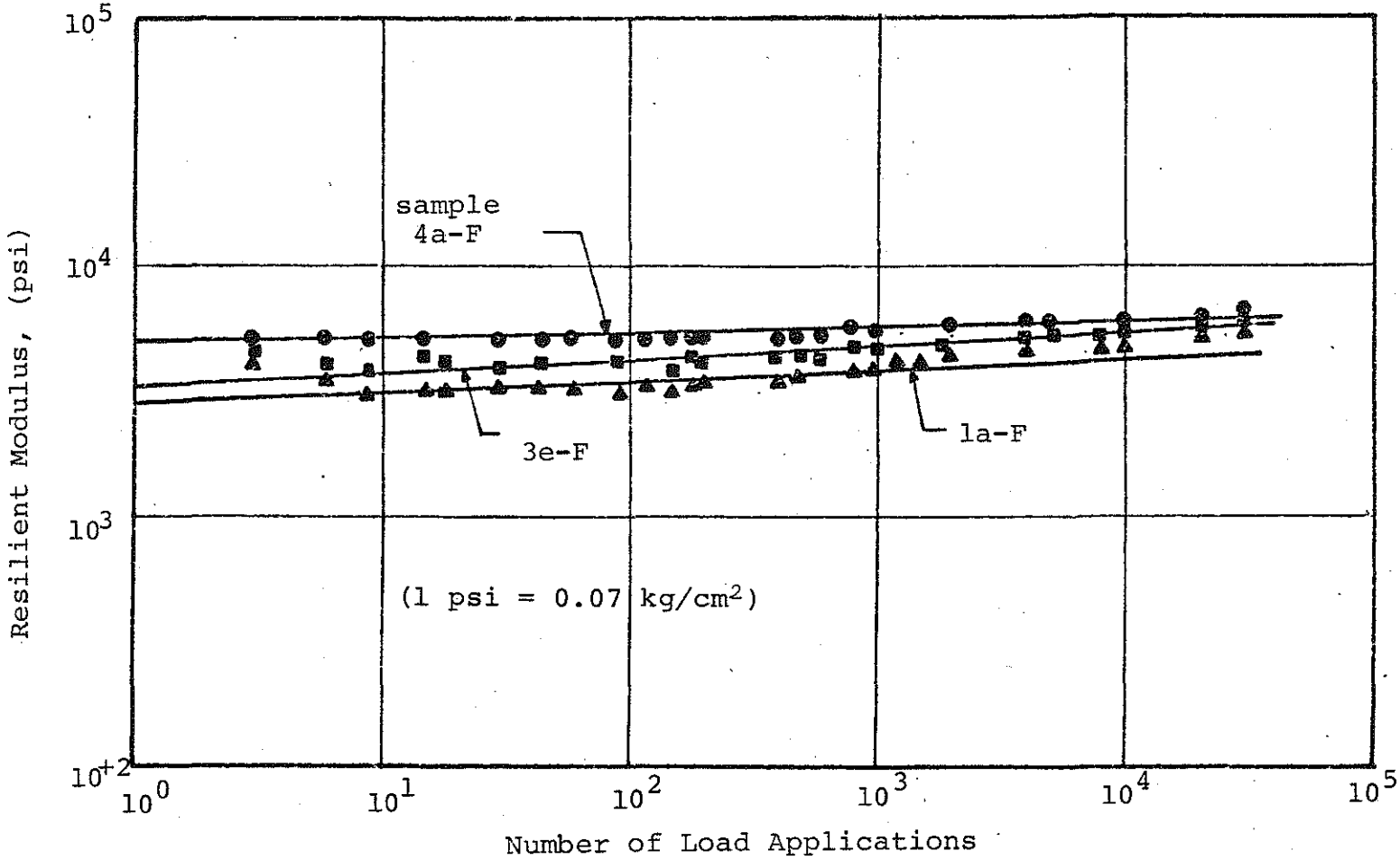

FIGURE C.37 Resilient Modulus versus Number of Load Applications for Samples Consolidated under a Confining Pressure of 5 psi and Tested Using Different Cyclic Stress Ratio, Site 4, Lower Peninsula.

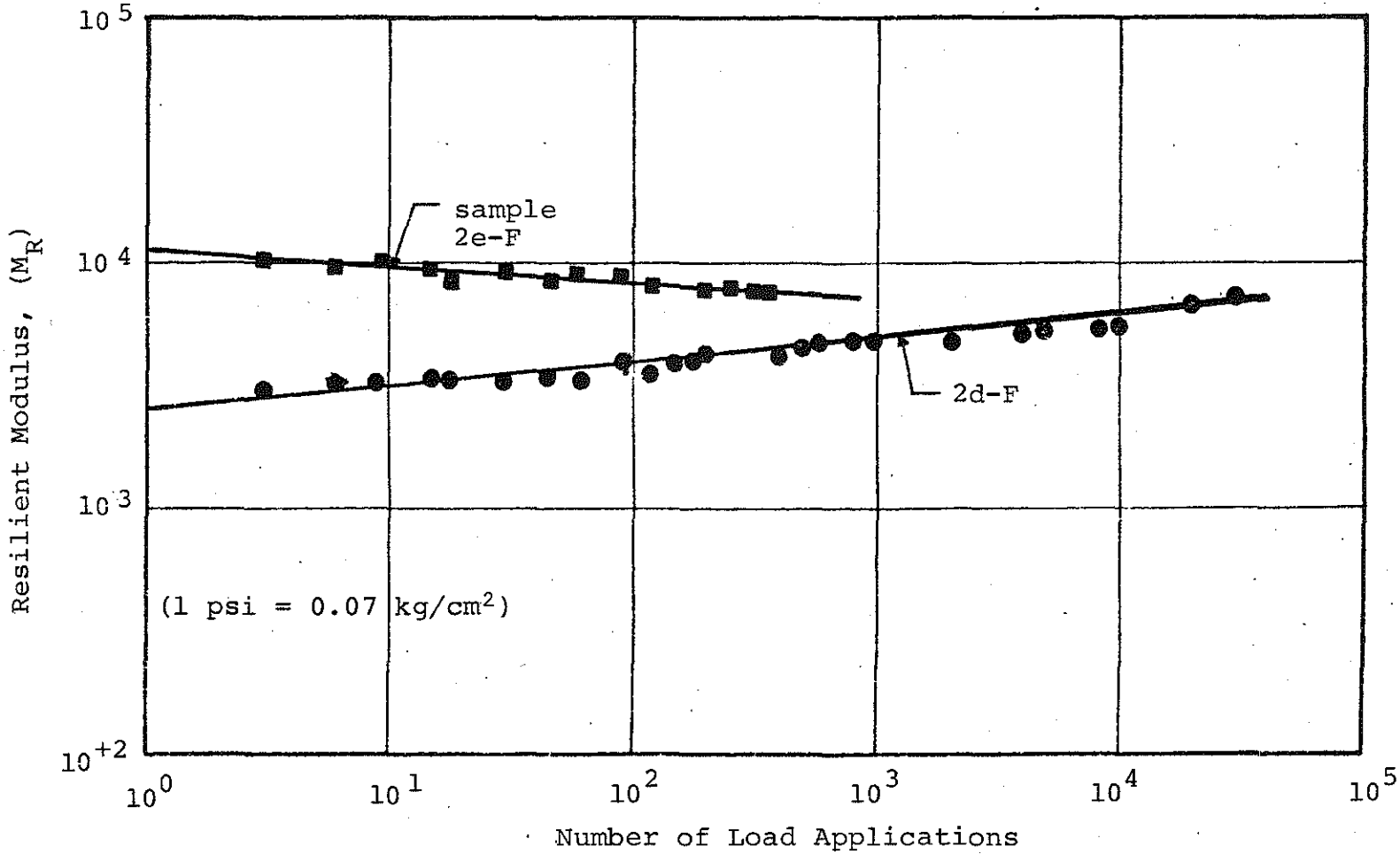

FIGURE C.38 Resilient Modulus versus Number of Load Applications for Samples Consolidated under a Confining Pressure of 25 psi and Tested using Different Cyclic Stress Ratio, Site 4, Lower Peninsula.

TABLE C.1 List of the Radial Permanent Strain for Consolidated Samples, Sites 1, 3 and 4, Lower Peninsula.

SITE	σ_3	SAMPLE NUMBER	$\frac{(\sigma_1-\sigma_3)d}{\sigma_3}$	RADIAL PERMANENT STRAIN AT MIDDLE OF SAMPLE ($x10^{-4}$) / RADIAL PERMANENT STRAIN AT 1/3 FROM THE SAMPLE BOTTOM ($x10^{-4}$)					
				N=1	10	100	1,000	10,000	30,000
1	5	2b-F	1	3.72 / *	4.00 / *	8.07 / 1.02	12.1 / 7.02	15.2 / 10.3	19.6 / 15.2
		2a-F	2	1.89 / 1.01	3.50 / 1.29	19.6 / 13.7	21.7 / 20.1	23.1 / 21.8	25.3 / 22.1
		1c-F	3	9.28 / 4.03	10.2 / 7.29	48.3 / 31.8	67.9 / 41.4	87.2 / 60.8	102. / 87.2
	25	2d-F	1.0	10.8 / 8.85	20.0 / 17.0	47.6 / 43.3	76.3 / 58.2	84.8 / 60.2	85.1 / 61.2
		2e-S	1.5	109. / 41.7	142. / 44.8	154. / 46.6	155. / 47.2	155. / 48.1	157. / 48.4
		4d-F	2.0	4.37 / 1.13	7.30 / 3.13				
	50	4a-S	0.5	6.17 / 37.8	84.2 / 51.8				

TABLE C.1 (Continued)

SITE	σ_3	SAMPLE NUMBER	$\frac{(\sigma_1-\sigma_3)d}{\sigma_3}$	RADIAL PERMANENT STRAIN AT MIDDLE OF SAMPLE ($x10^{-4}$) / RADIAL PERMANENT STRAIN AT 1/3 FROM THE SAMPLE BOTTOM ($x10^{-4}$)					
				N=1	10	100	1,000	10,000	30,000
3	5	2c-F	1.0	5.13 / *	6.75 / 1.08	8.19 / 1.81	9.13 / 7.05	10.2 / 9.15	31.4 / 21.2
		2b-F	2.0	9.18 / *	10.5 / 2.78	21.3 / 8.34	51.6 / 12.1	81.2 / 50.7	111. / 90.1
		1a-F	3.0	15.7 / 4.72	26.1 / 6.19	86.9 / 25.6	180. / 65.7	170. / 125.	181. / 140.
	25	4b-F	1.0	6.84 / 1.02	9.02 / 3.18	12.3 / 8.69	54.3 / 13.2	78.2 / 28.1	103. / 87.2
		2a-F	1.5	19.1 / 12.8	40.8 / 27.8	65.6 / 28.8	86.8 / 29.9	102. / 30.5	105. / 32.2
		3a-F	2.0	10.2 / 6.83	25.2 / 10.8	88.3 / 12.2	164.6 / 17.8	174.0 / 34.0	183.4 / 35.8

TABLE C.1 (Continued)

SITE	σ_3	SAMPLE NUMBER	$\frac{(\sigma_1-\sigma_3)d}{\sigma_3}$	RADIAL PERMANENT STRAIN AT MIDDLE OF SAMPLE ($x10^{-4}$) / RADIAL PERMANENT STRAIN AT 1/3 FROM THE SAMPLE BOTTOM ($x10^{-4}$)					
				N=1	10	100	1,000	10,000	30,000
4	5	4a-F	0.7	1.08 / *	1.24 / *	1.69 / 1.39	2.85 / 1.84	4.40 / 2.10	4.82 / 3.10
		1a-F	1.0	2.01 / *	2.21 / 1.16	5.74 / 5.24	37.8 / 11.8	41.6 / 16.5	48.7 / 17.7
		3e-F	2.0	8.73 / 1.82	10.4 / 2.38	7.29 / 21.2	112. / 52.5		
	25	2d-F	0.5	9.82 / 8.41	30.9 / 14.3	58.9 / 29.7	115. / 31.5	147. / 32.1	159. / 33.3
		2e-F	1.0	13.8 / 9.79	22.6 / 15.0	51.8 / 46.2			

* Measurements were less than the accuracy of the LVTD.

Blank space indicates sample failed before the designated number of load repetitions was reached

TABLE C.2 List of Axial Permanent Strain for Unconsolidated Samples

SITE	σ_3	SAMPLE NUMBER	$\frac{(\sigma_1-\sigma_3)d}{\sigma_3}$	AXIAL PERMANENT STRAIN ($\times 10^{-4}$) / RESILIENT MODULUS ($\times 10^3$) (psi)					
				N=1	10	100	1,000	10,000	30,000
1	5	1f-F	1.0	3.37 / 2.60	8.16 / 2.98	21.8 / 3.73	31.1 / 4.27	64.1 / 3.47	91.4 / 2.96
		3d-F	2.0	37.6 / 3.02	69.6 / 2.71	140. / 2.71	219. / 2.98	296. / 2.73	325. / 2.58
		1e-F	3.0	19.1 / 3.09	26.0 / 3.36	57.0 / 3.77	149. / 4.63	321. / 4.35	330. / 4.02
	25	3f-S	1.0	13.9 / 2.53	21.1 / 2.48	37.8 / 2.51	54.0 / 2.40		
		2e-S	1.5	21.2 / 2.44	35.2 / 2.45	78.0 / 2.42			
3	5	4c-S	1.0	51.0 / 1.74	70.5 / 1.89	120. / 2.37	150. / 3.09	178. / 3.04	200. / 2.57
		2e-S	2.0	68.4 / 5.11	93.3 / 5.42	132. / 4.98	176. / 5.79	210. / 5.63	235. / 5.39
	25	3e-S	1.5	9.8 / 13.7	9.5 / 14.3	14.5 / 13.4	28.4 / 13.6	50.1 / 12.2	55.4 / 11.8

TABLE C.3 List of Radial Permanent Strain for Unconsolidated Samples

SITE	σ_3	SAMPLE NUMBER	$\frac{(\sigma_1-\sigma_3)d}{\sigma_3}$	RADIAL PERMANENT STRAIN AT MIDDLE OF SAMPLE ($\times 10^{-4}$) / RADIAL PERMANENT STRAIN AT 1/3 FROM THE SAMPLE BOTTOM ($\times 10^{-4}$)					
				N=1	10	100	1,000	10,000	30,000
1	5	3d-F	1.0	7.56 / *	11.8 / 1.81	23.7 / 7.13	40.2 / 21.0	61.5 / 32.0	92.0 / 58.0
		1f-F	2.0	12.6 / 1.28	24.8 / 3.84	94.3 / 15.2	107. / 71.4	161. / 98.2	187. / 132.
		1e-F	3.0	21.0 / 3.27	31.5 / 6.54	73.5 / 9.81	147. / 52.3	172. / 114.	210. / 144.
	25	3f-S	1.0	27.8 / 19.8	88.4 / 53.0	112. / 67.0	137. / 72.0		
		2e-S	1.5	138. / 84.0	274. / 117.	312. / 191.			
3	5	4c-S	1.0	21.0 / *	56.1 / 9.34	80.6 / 13.8	85.9 / 26.4	87.6 / 38.9	94.6 / 54.8
		2e-S	2.0	42.1 / 31.0	70.1 / 38.4	119. / 112.	189. / 140.	217. / 172.	231. / 189.
	25	3e-S	1.5	10.8 / 2.07	37.3 / 10.3	58.4 / 19.2	90.9 / 51.6	135. / 37.2	154. / 48.4

*Measurements were less than the accuracy of the LVTD.

APPENDIX D

APPENDIX D

TEST RESULTS OF THE UPPER PENINSULA TEST SITES

This appendix summarizes all the laboratory and field test results of the Upper Peninsula test sites in forms of figures and tables as follows:

(1) The pavement deflection curves that were measured using a highway truck and a Benkelman beam of all the Upper Peninsula test sites are presented in Figure D.1.

(2) The standard deviation of the pavement deflection curves of all the Upper Peninsula sites are shown in Figure D.2.

(3) The conventional consolidation curves of the Upper Peninsula test sites are presented in Figure D.3 through D.6.

(4) Consolidated Incremental Creep Tests
   (a) The results of a consolidation test performed prior to the commencement of the incremental creep test is presented in Figure D.7.
   (b) The incremental creep test results are shown in Figure D.8.

(5) Consolidated Ramp Tests
   (a) The results of the consolidation test performed prior to the commencement of the ramp test is presented in Figure D.9.
   (b) The ramp test results are shown in Figure D.10.

(6) Unconsolidated Ramp Test
   (a) The results of the unconsolidated ramp tests are plotted in Figures D.11 through D.13.

(7) Consolidated Cyclic Triaxial Tests
   (a) The time dependent consolidation curves of the consolidation tests performed prior to the commencement of the cyclic loading tests are plotted in Figures D.14 through D.16.
   (b) The axial permanent strain curves are shown in Figures D.17 through D.19 as a function of the number of load repetitions.

(c) The resilient modulus of the Upper Peninsula test sites data are plotted in Figures D.20 through D.22 as a function of the number of load repetitions.

(d) The radial permanent strain data are listed in Table D.1.

(8) Unconsolidated Cyclic Triaxial Tests

(a) The axial permanent strain from the unconsolidated cyclic triaxial tests data are shown in Figure D.23.

(b) The resilient Modulus data are plotted and shown in Figure D.24.

(c) The radial permanent strain data are listed in Table D.1.

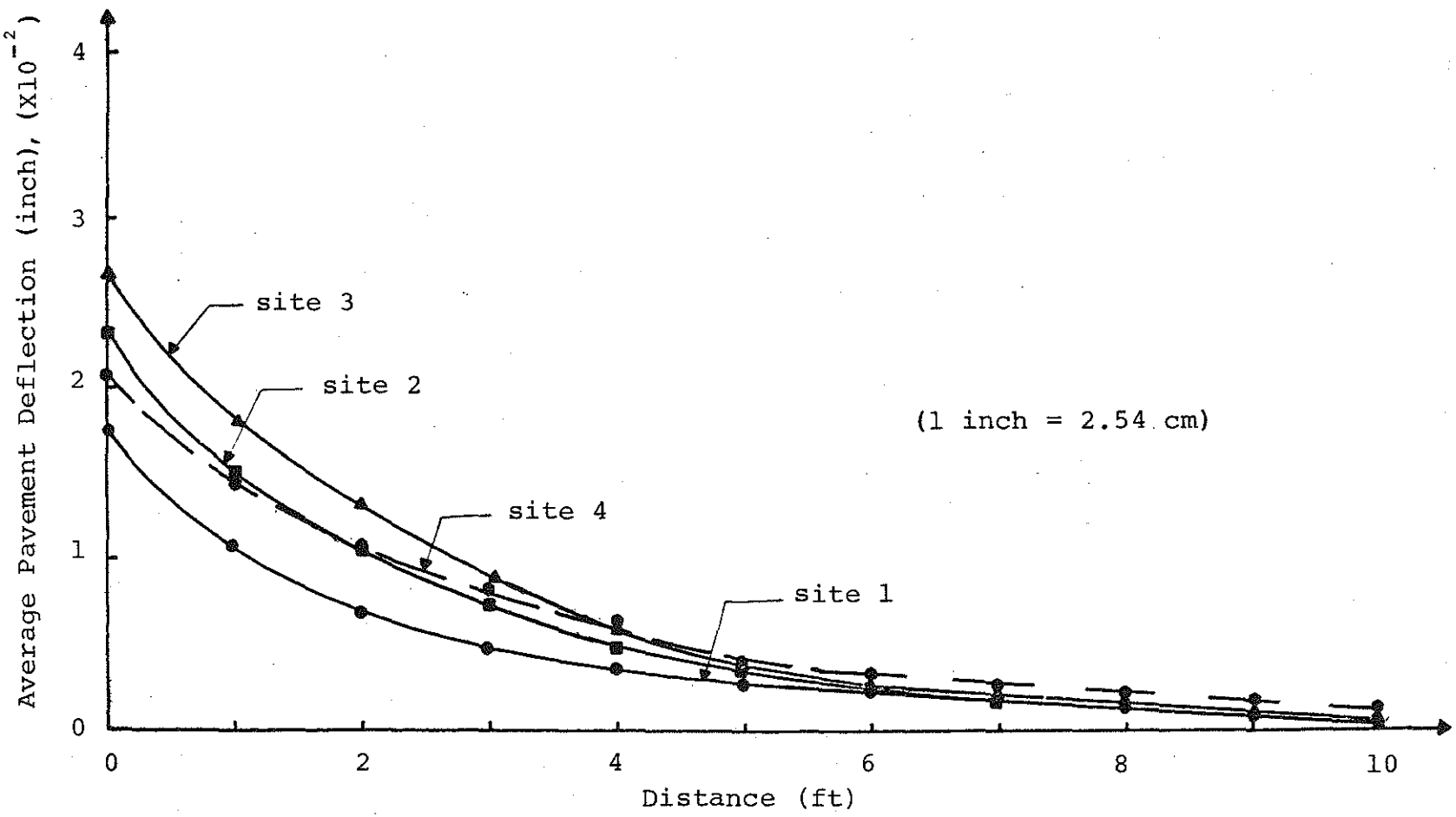

FIGURE D.1 Average Pavement Deflection Versus Distance from Wheel Load, Upper Peninsula.

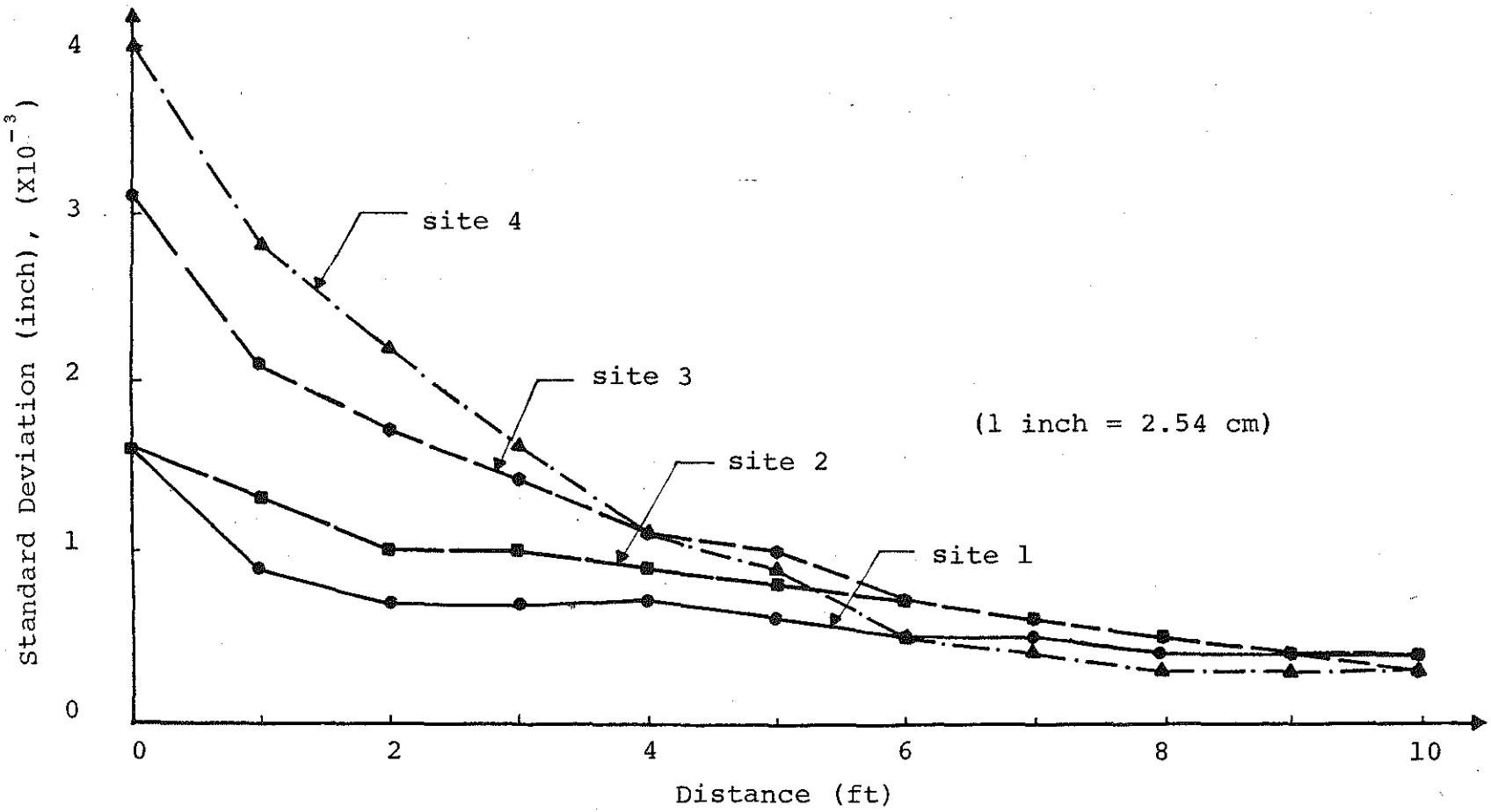

FIGURE D.2 Standard Deviation Versus Distance from the Wheel Load, Upper Peninsula.

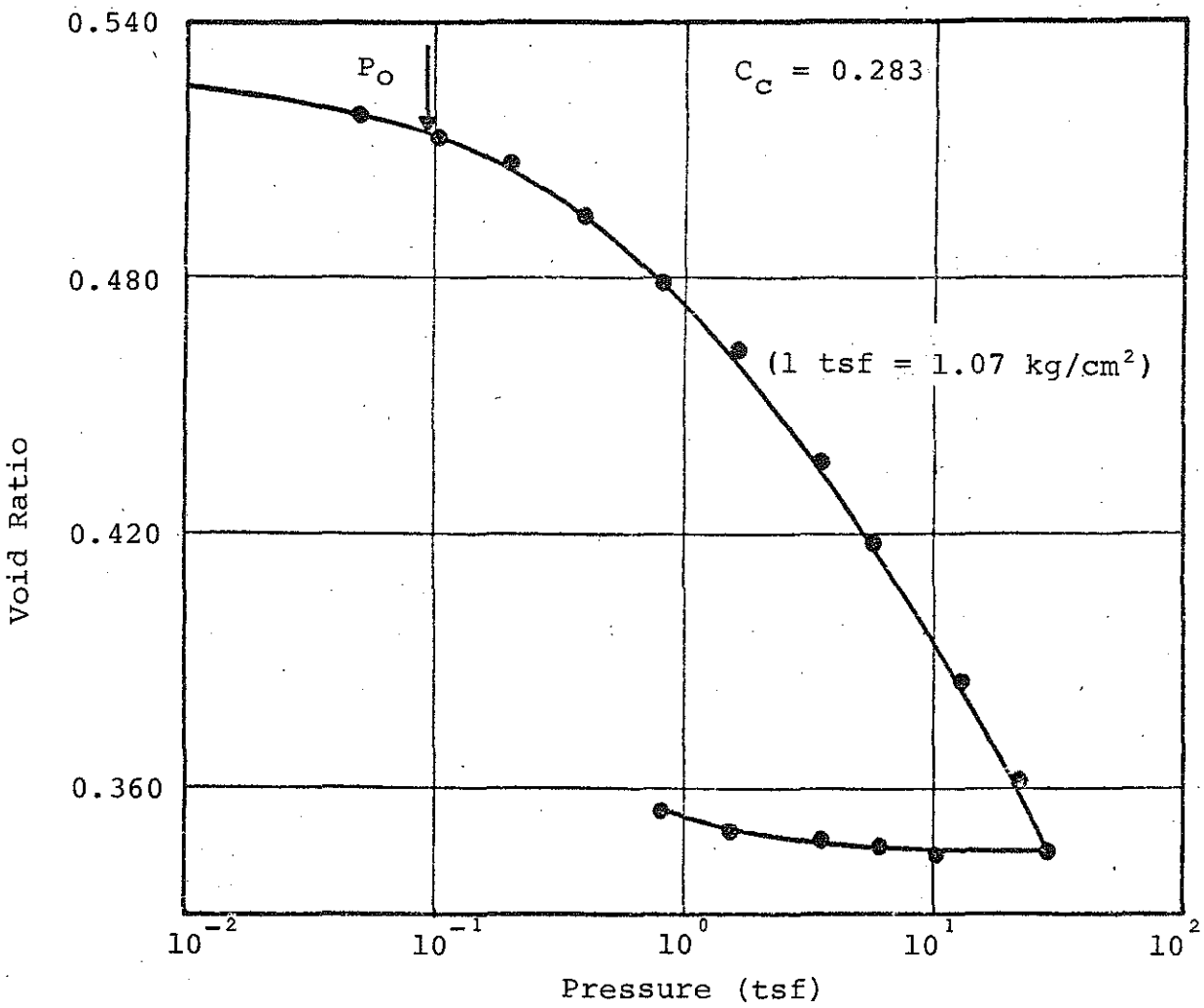

FIGURE D.3 Consolidation Curve, Void Ratio Versus Logarithm of Pressure, Site 1, Upper Peninsula

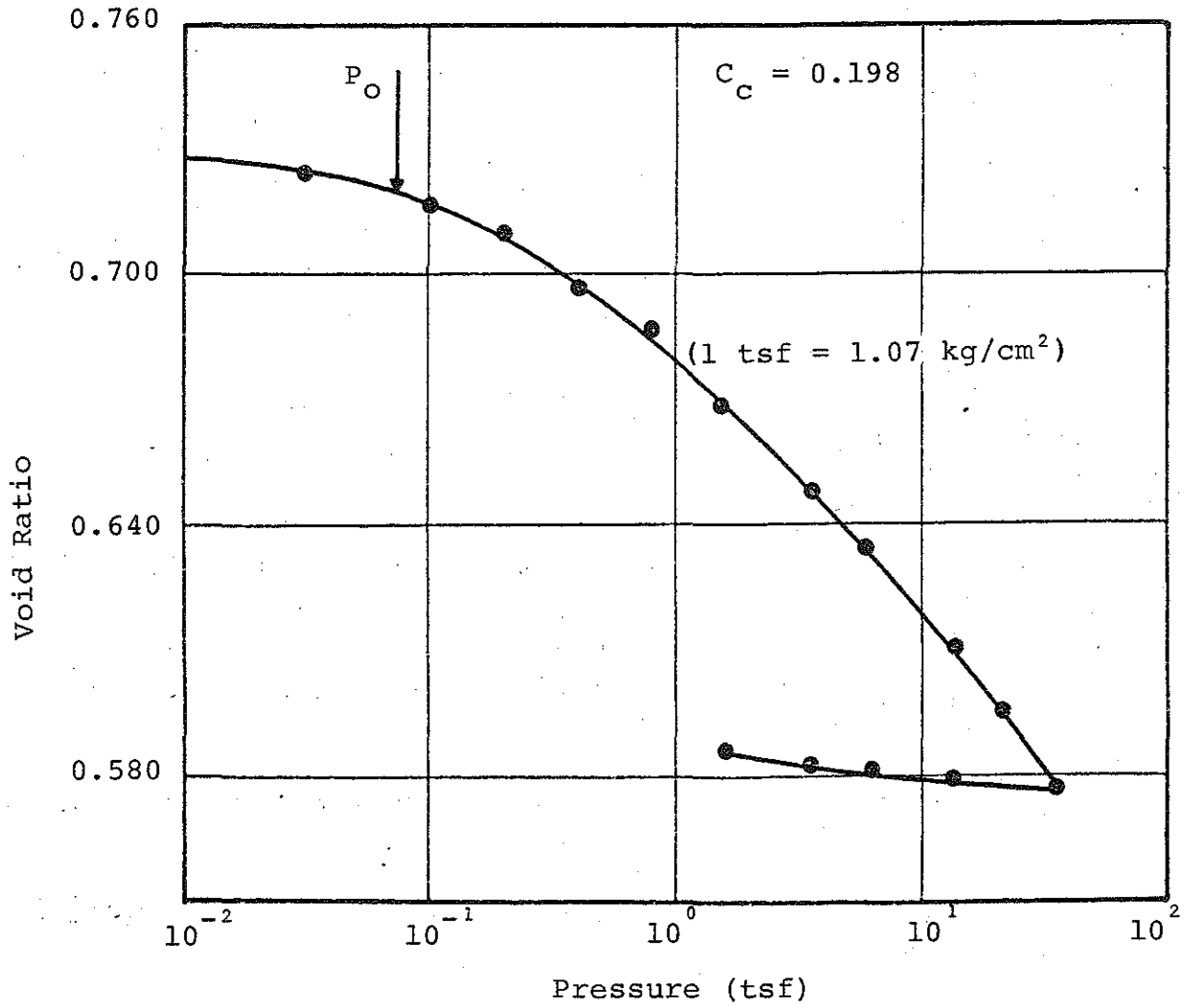

FIGURE D.4 Consolidation Curve, Void Ratio Versus Logarithm of Pressure, Site 2, Upper Peninsula

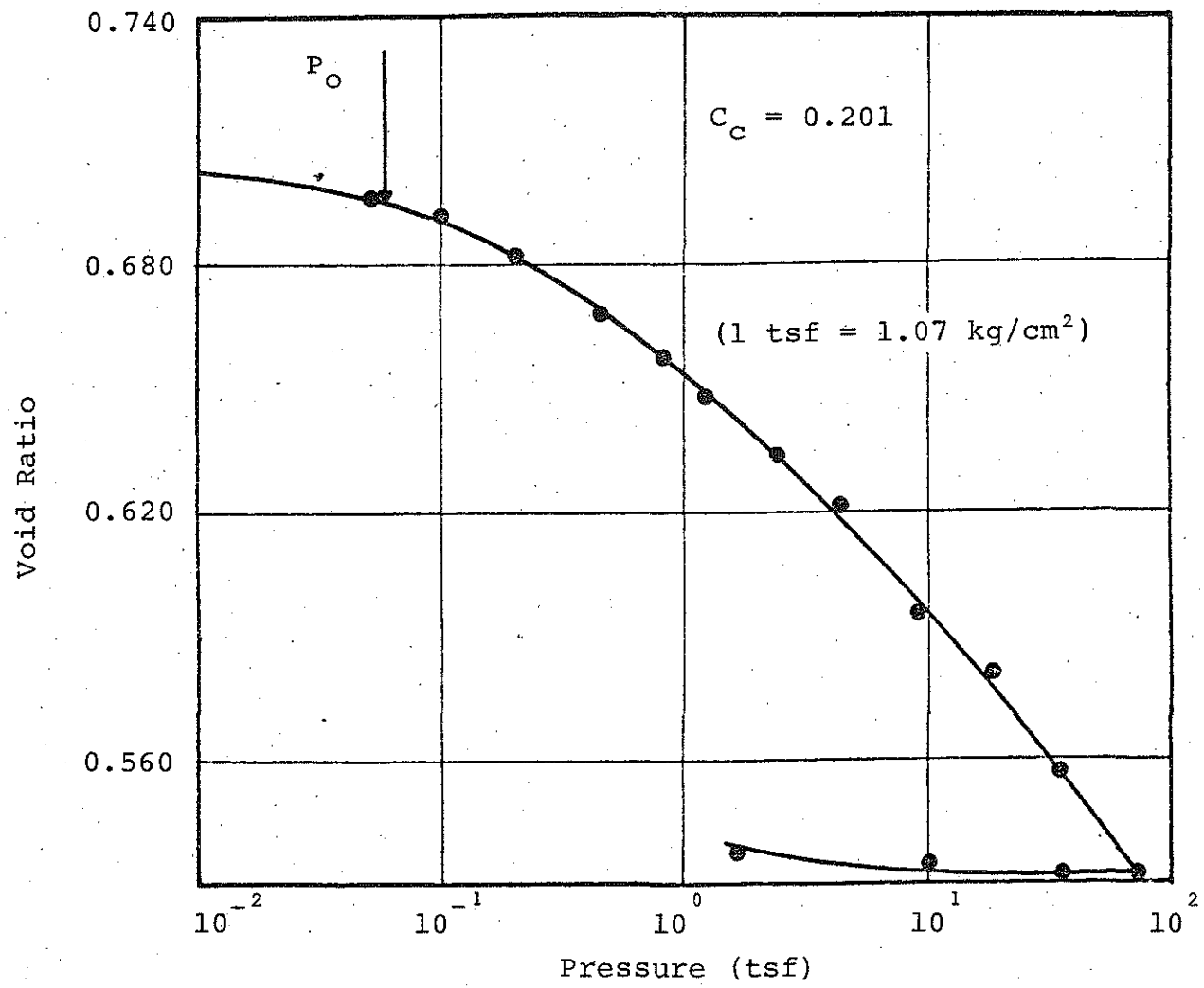

FIGURE D.5 Consolidation Curve, Void Ratio Versus Logarithm of Pressure, Site 3, Upper Peninsula

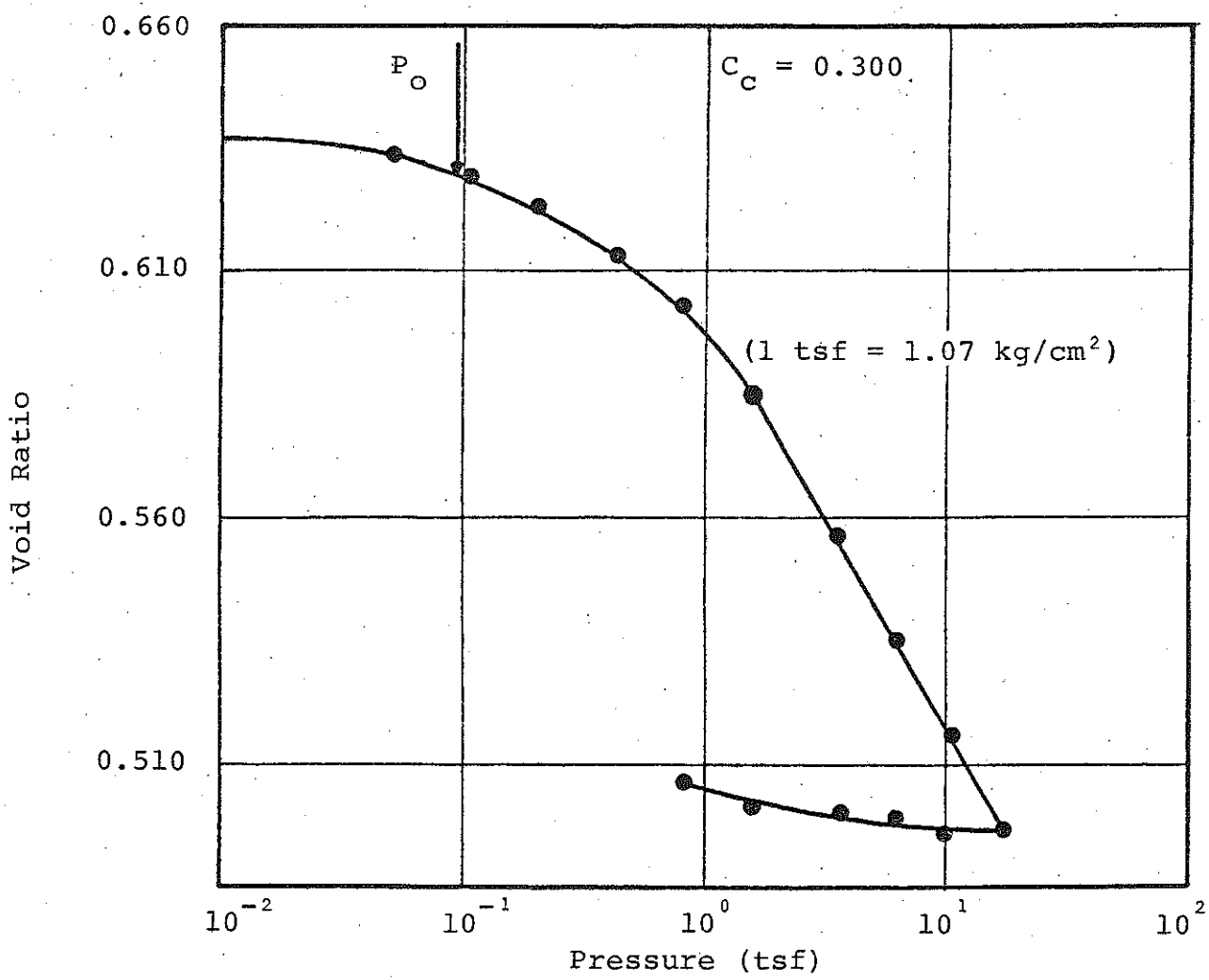

FIGURE D.6 Consolidation Curve, Void Ratio Versus Logarithm of Pressure, Site 4, Upper Peninsula

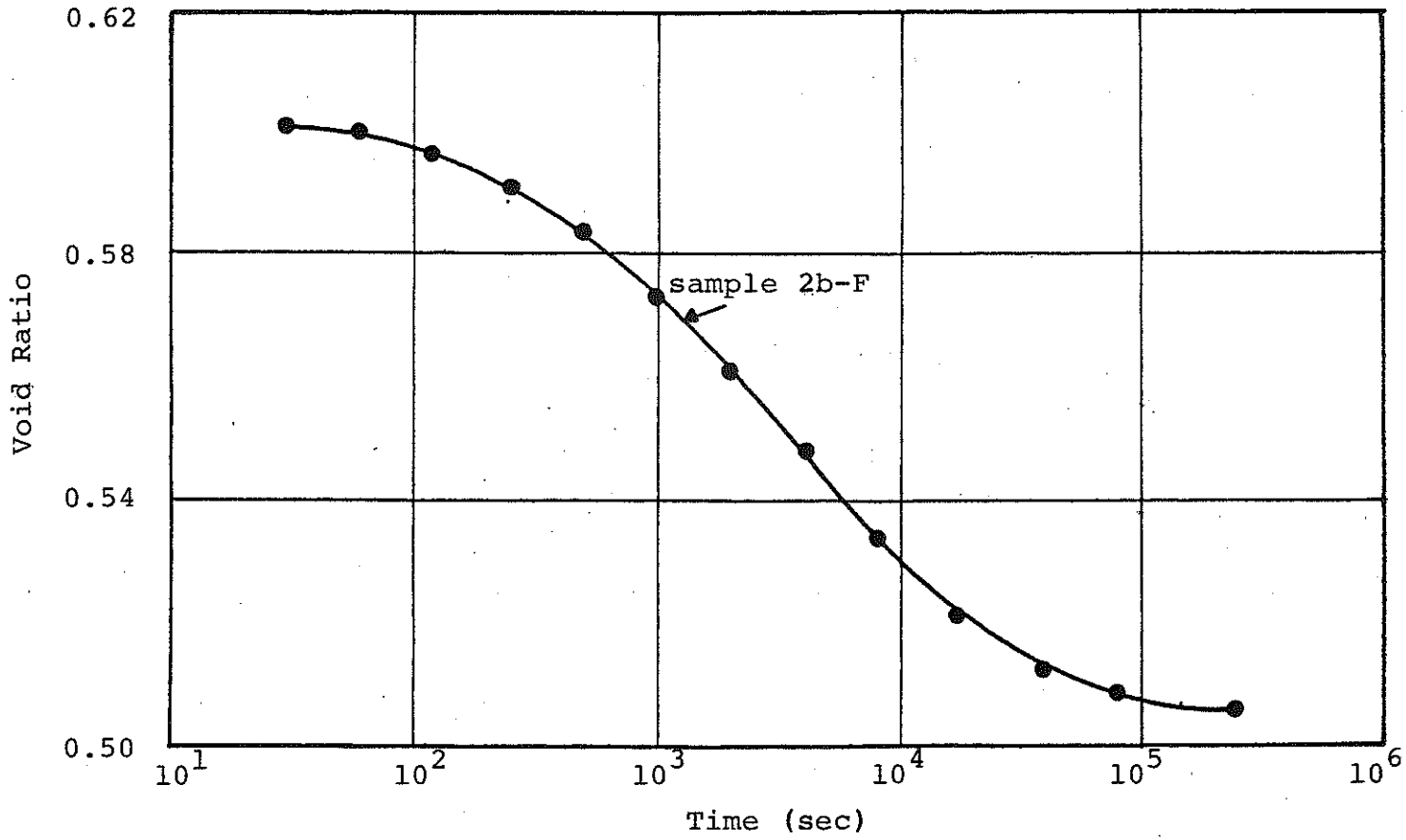

FIGURE D.7 Void Ratio Versus Logarithm of Time for Sample Consolidated Under Confining Pressure of 25 psi Prior to the Commencement of the Incremental Creep Test, Site 1, Upper Peninsula.

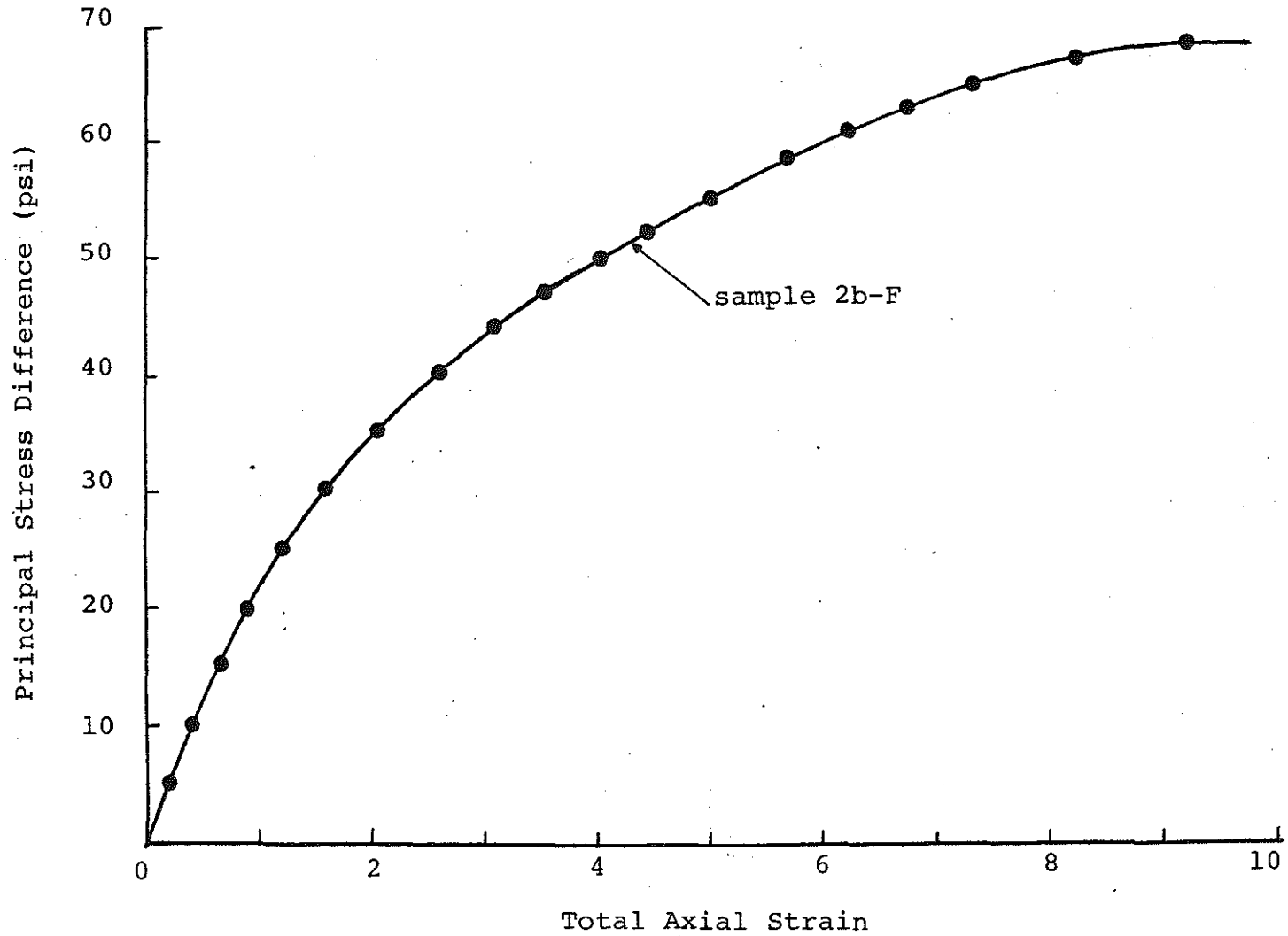

FIGURE D.8 Principal Stress Difference Versus Total Axial Strain Consolidated Sample Under 25 psi, Prior to Incremental Creep Test, Site 1, Upper Peninsula

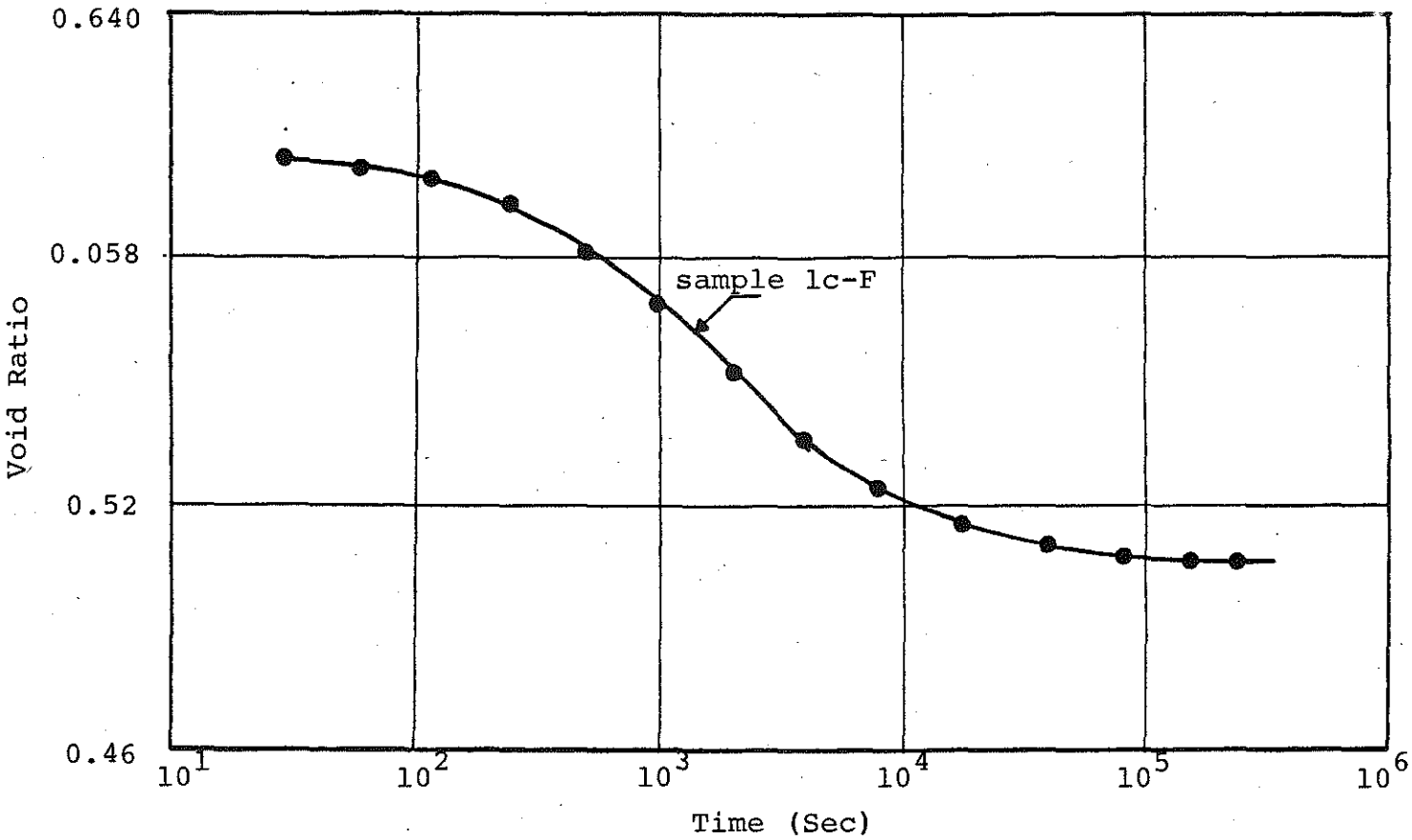

FIGURE D. 9 Void Ratio Versus Logarithm of Time for Sample Consolidated Under Confining Pressure of 10 psi Prior to the Commencement of the Ramp Tests, Site 2, Upper Peninsula.

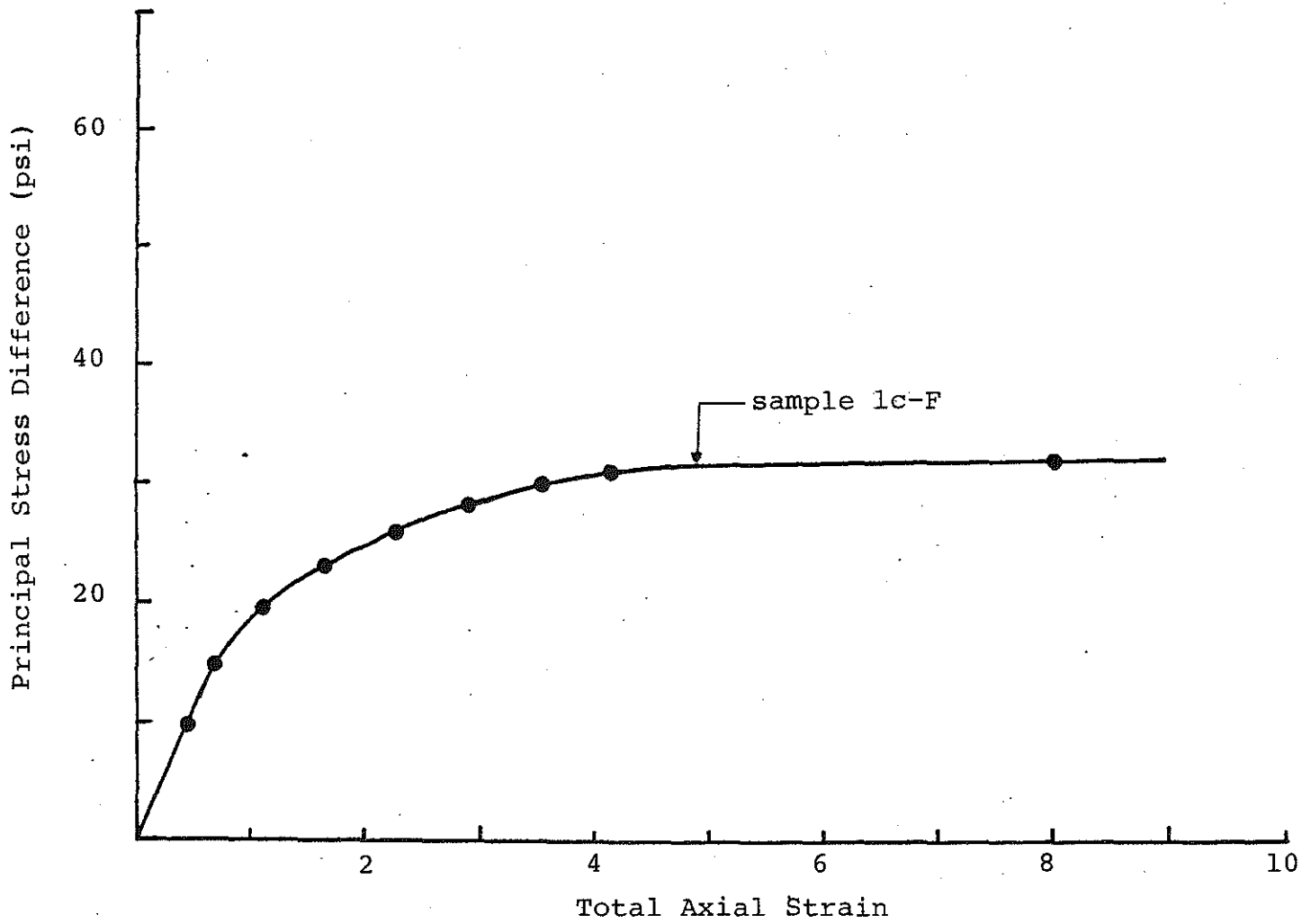

FIGURE D.10 Principal Stress Difference Versus Total Axial Strain Consolidated Sample Under 10 psi, Prior to Ramp Test, Site 2, Upper Peninsula

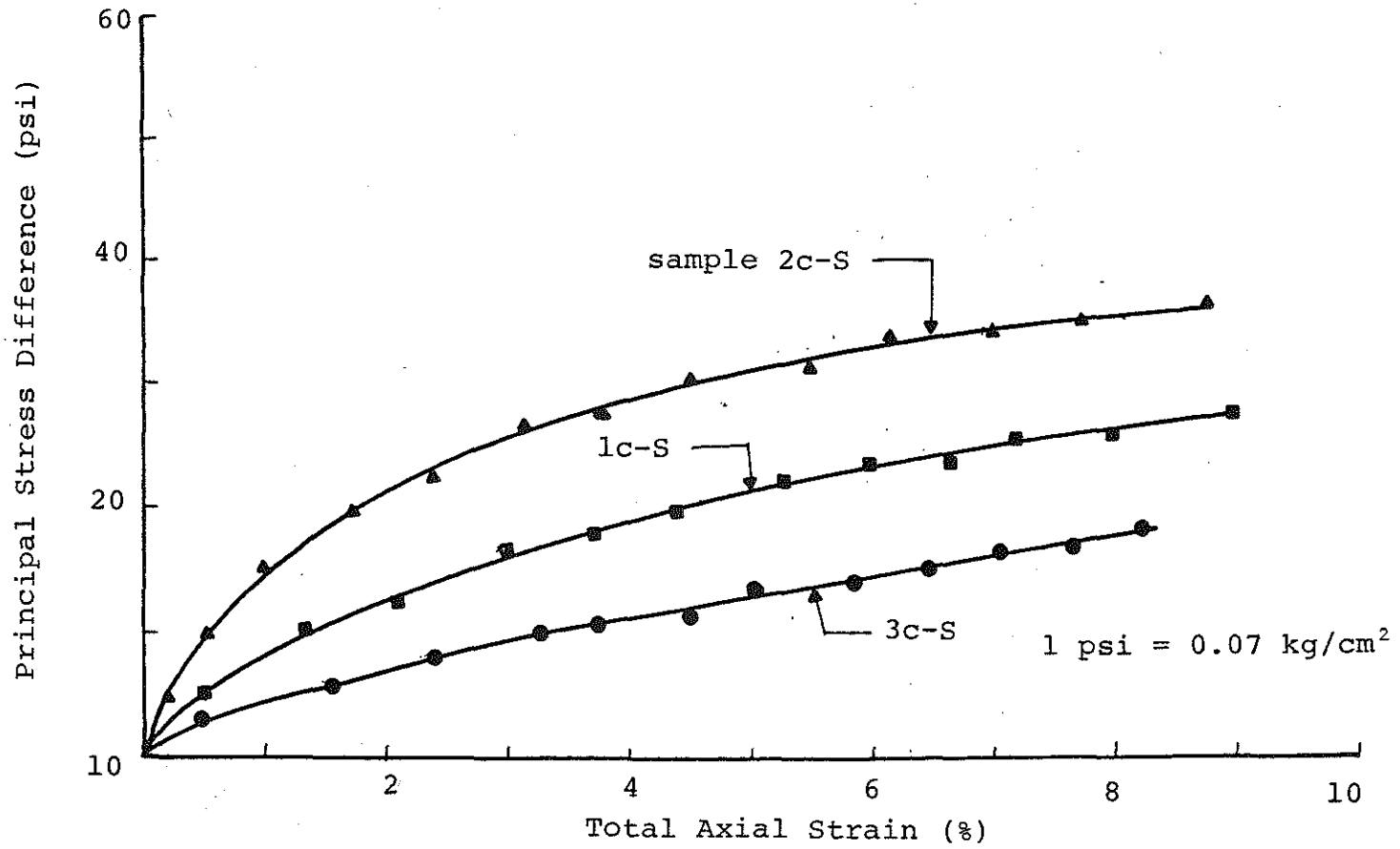

FIGURE D.11 Principal Stress Difference Versus Total Axial Strain from Ramp Tests, Site 1, Upper Peninsula

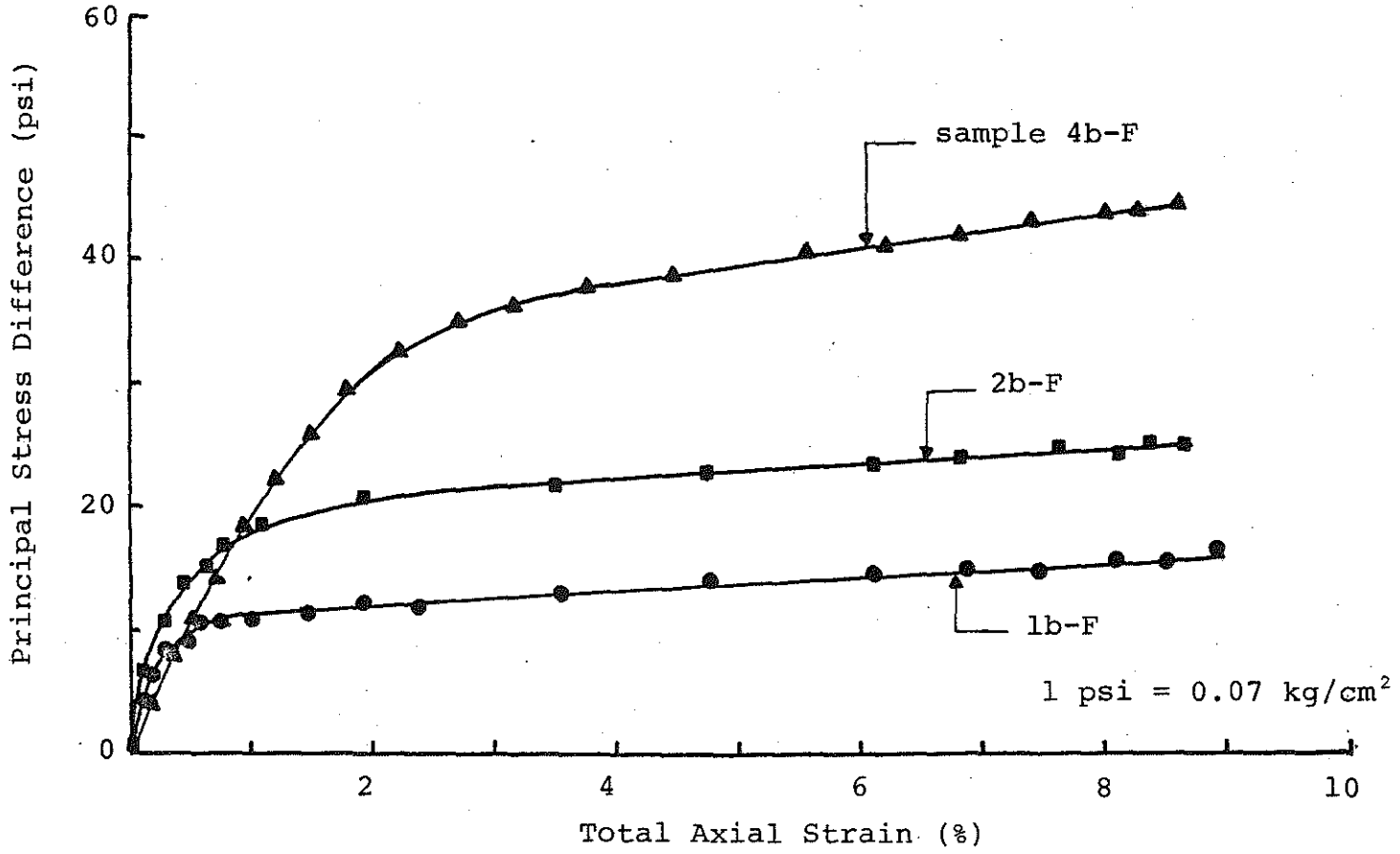

FIGURE D.12 Principal Stress Difference Versus Total Axial Strain from Ramp Tests, Site 2, Upper Peninsula

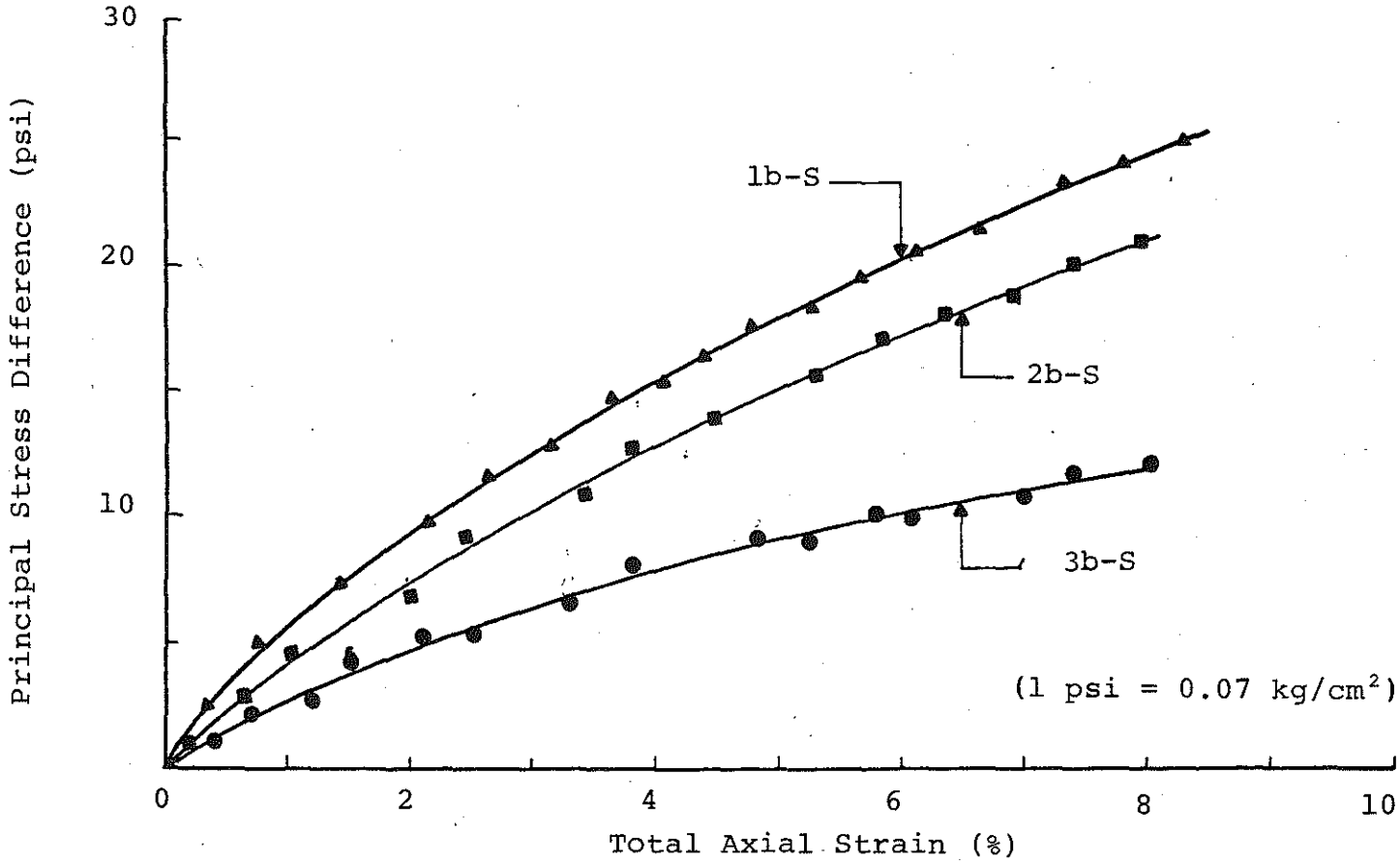

FIGURE D.13 Principal Stress Difference Versus Total Axial Strain from Ramp Tests, Site 3, Upper Peninsula.

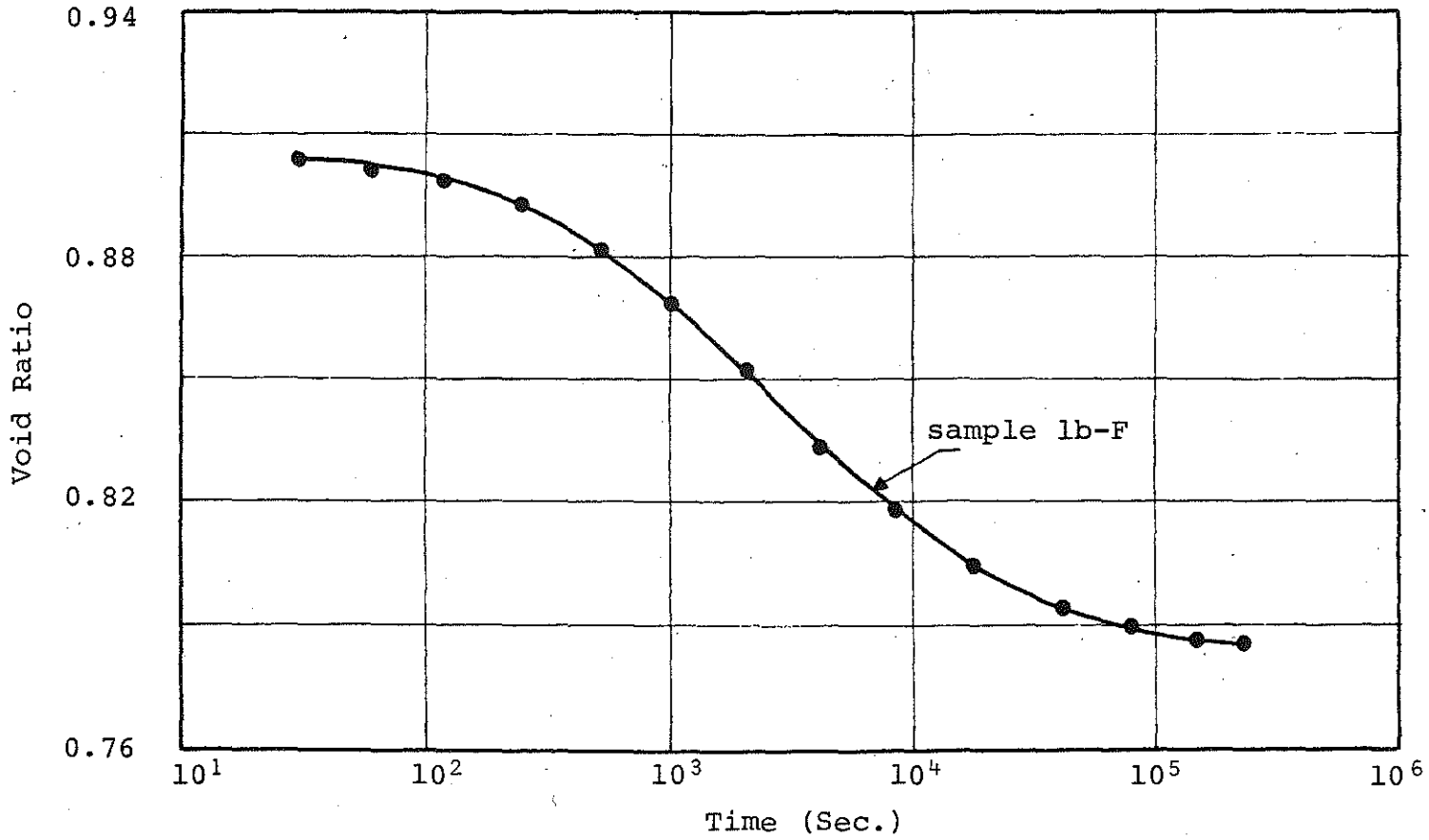

FIGURE D.14 Void Ratio Versus the Logarithm of Time for a Sample Consolidated Under a Confining Pressure of 10 psi Prior to the Commencement of the Triaxial Cyclic Load, Site 1, Upper Peninsula.

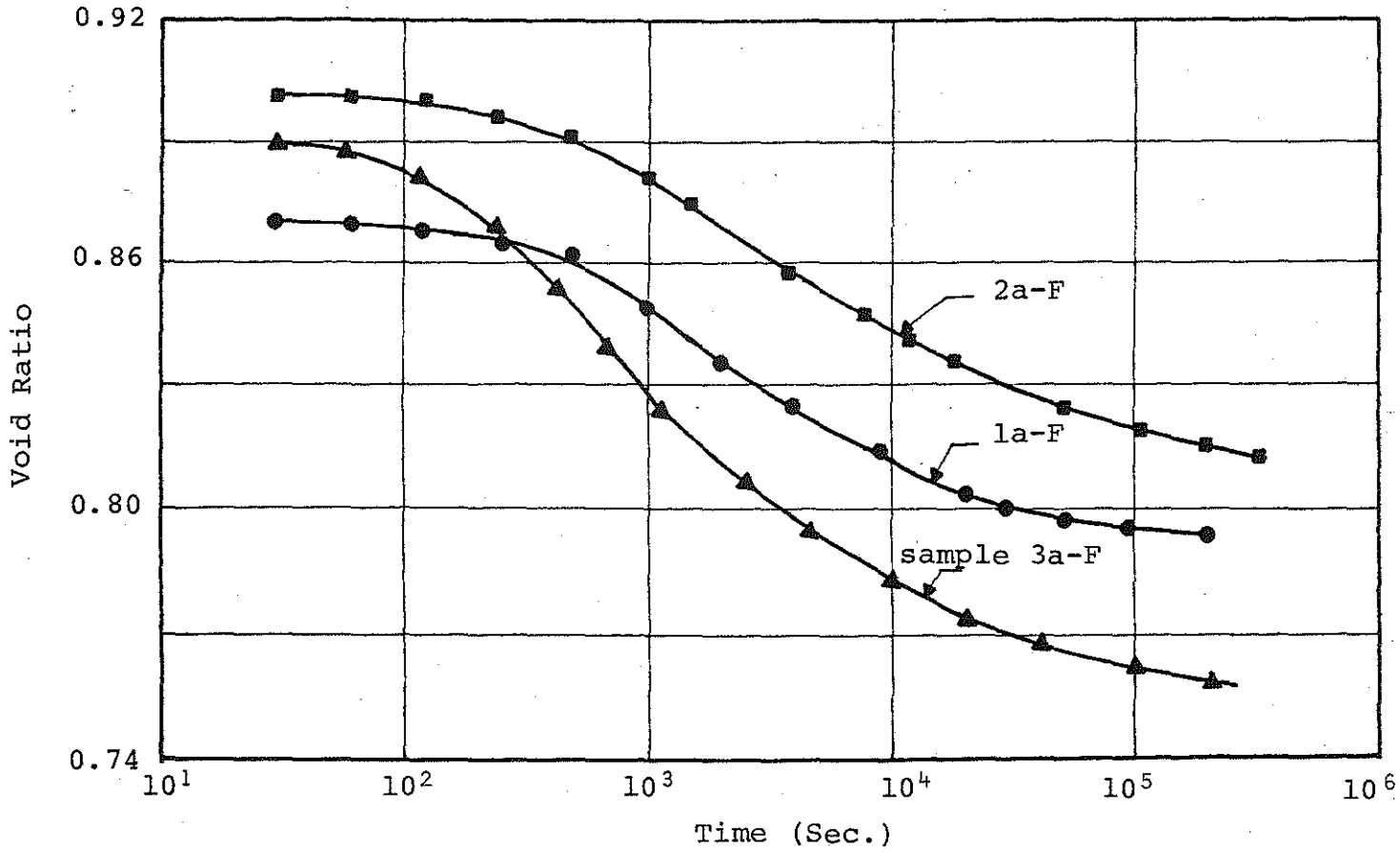

FIGURE D.15 Void Ratio Versus the Logarithm of Time for Three Samples Consolidated Under a Confining Pressure of 10 psi Prior to the Commencement of the Triaxial Cyclic Load, Site 2, Upper Peninsula.

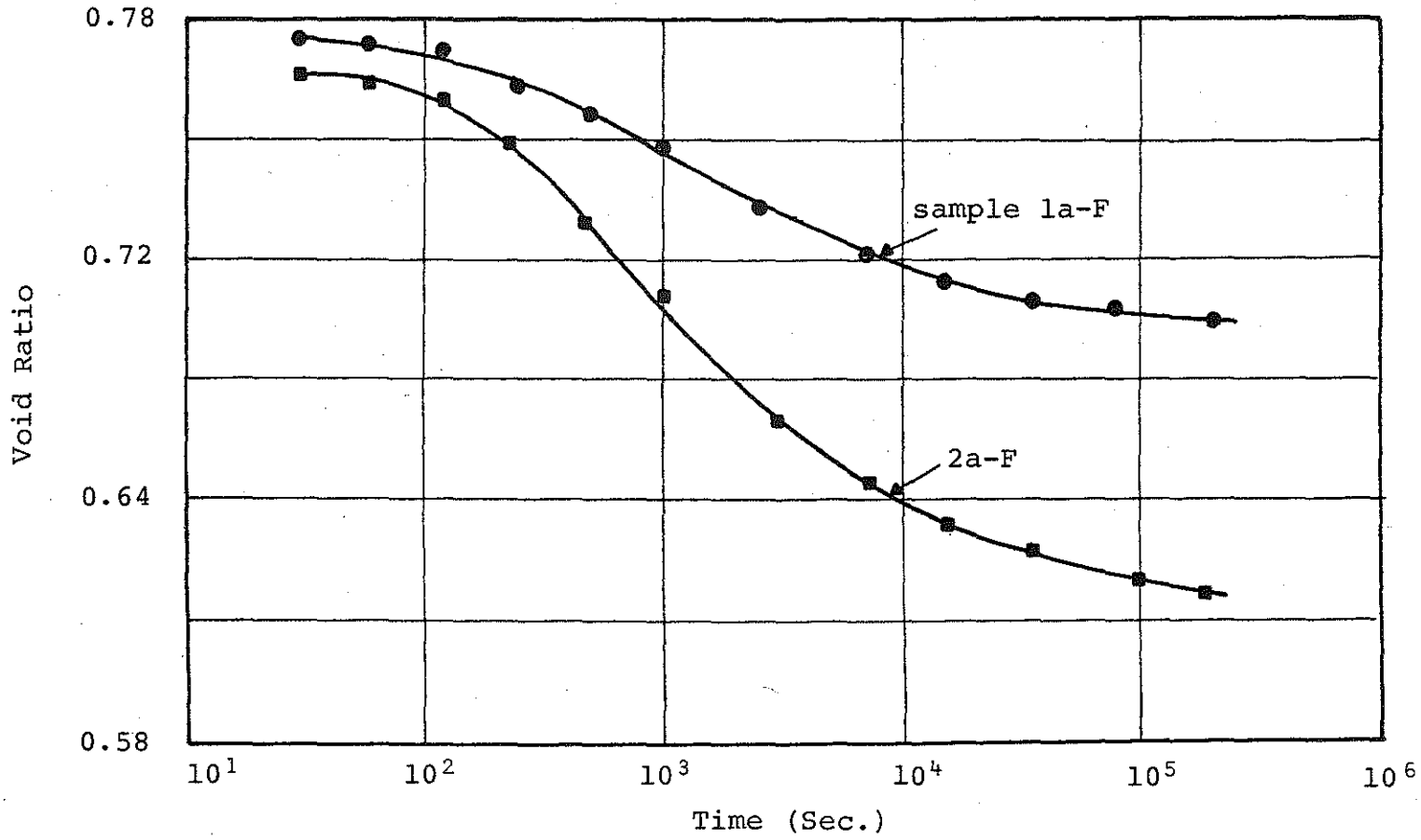

FIGURE D.16 Void Ratio Versus the Logarithm of Time for Two Samples Consolidated Under a Confining Pressure of 10 psi, Prior to the Commencement of the Triaxial Cyclic Load, Site 3, Upper Peninsula.

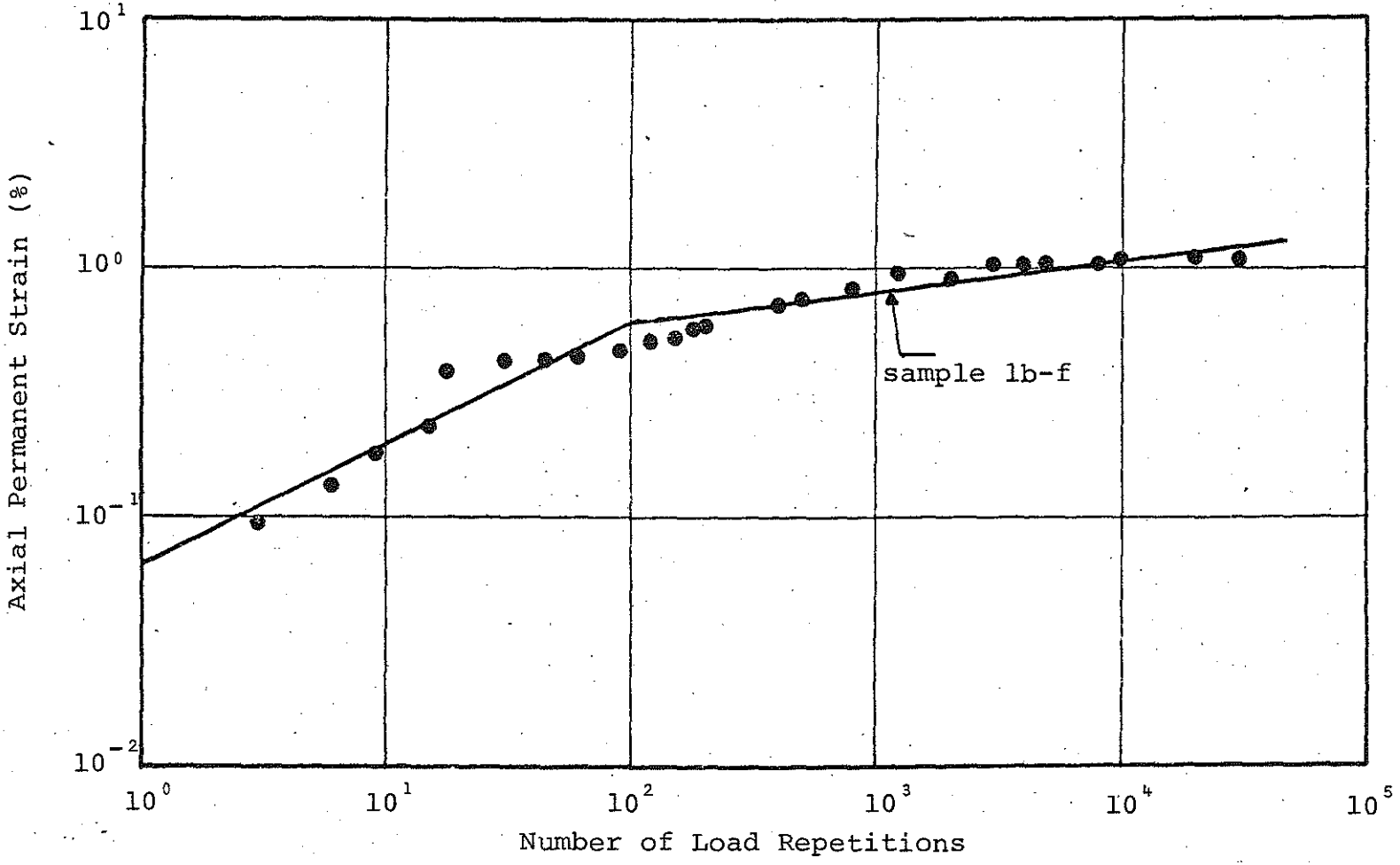

FIGURE D.17 Axial Permanent Strain Versus Number of Load Applications for Consolidated Samples Tested Under a Confining Pressure of 10 psi and at Cyclic Stress Ratio of 1.0, Site 1, Upper Peninsula

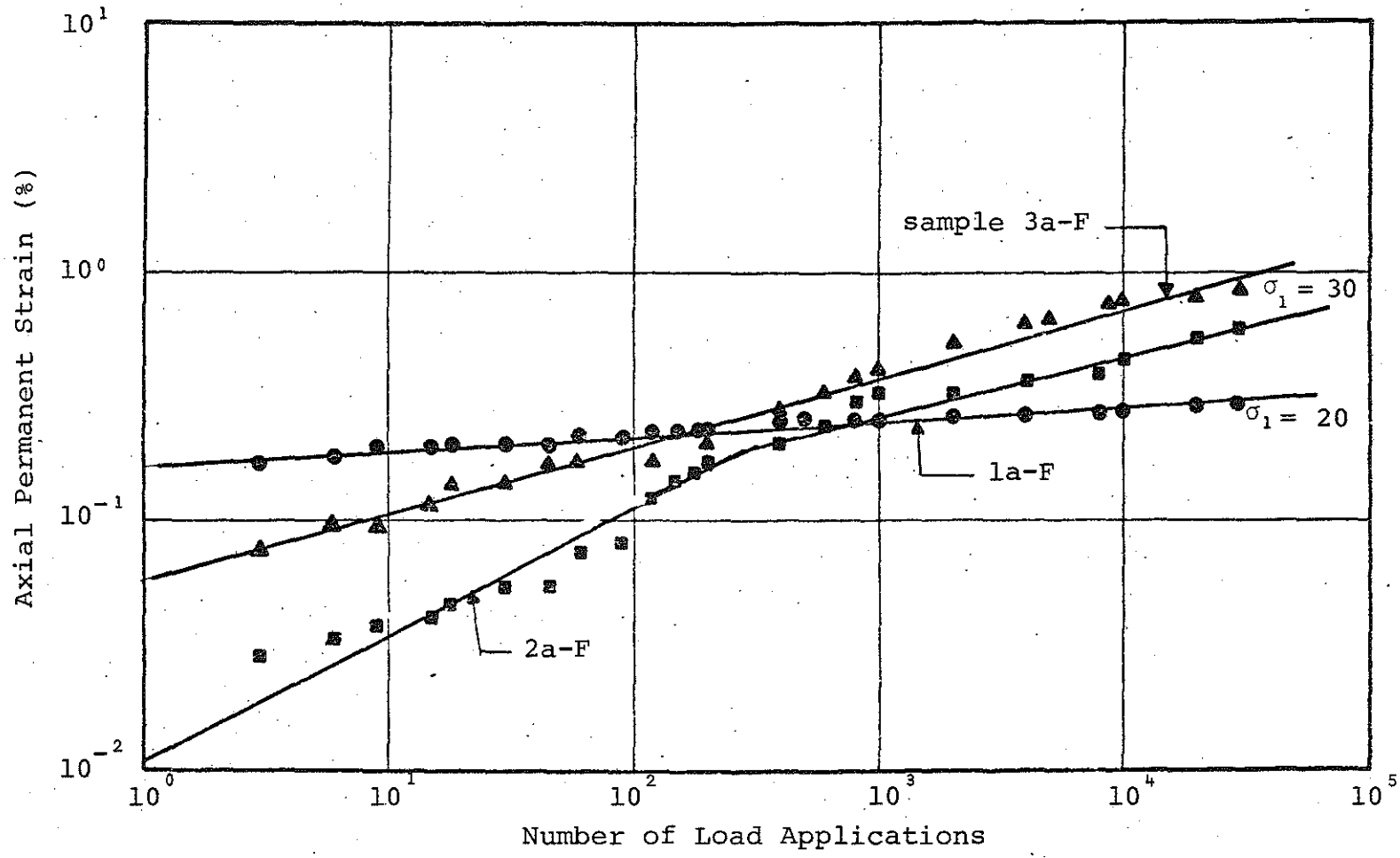

FIGURE D.18 Axial Permanent Strain Versus Number of Load Applications for Consolidated Samples Tested Under a Confining Pressure of 10 psi and Different Cyclic Stress Ratio, Site 2, Upper Peninsula

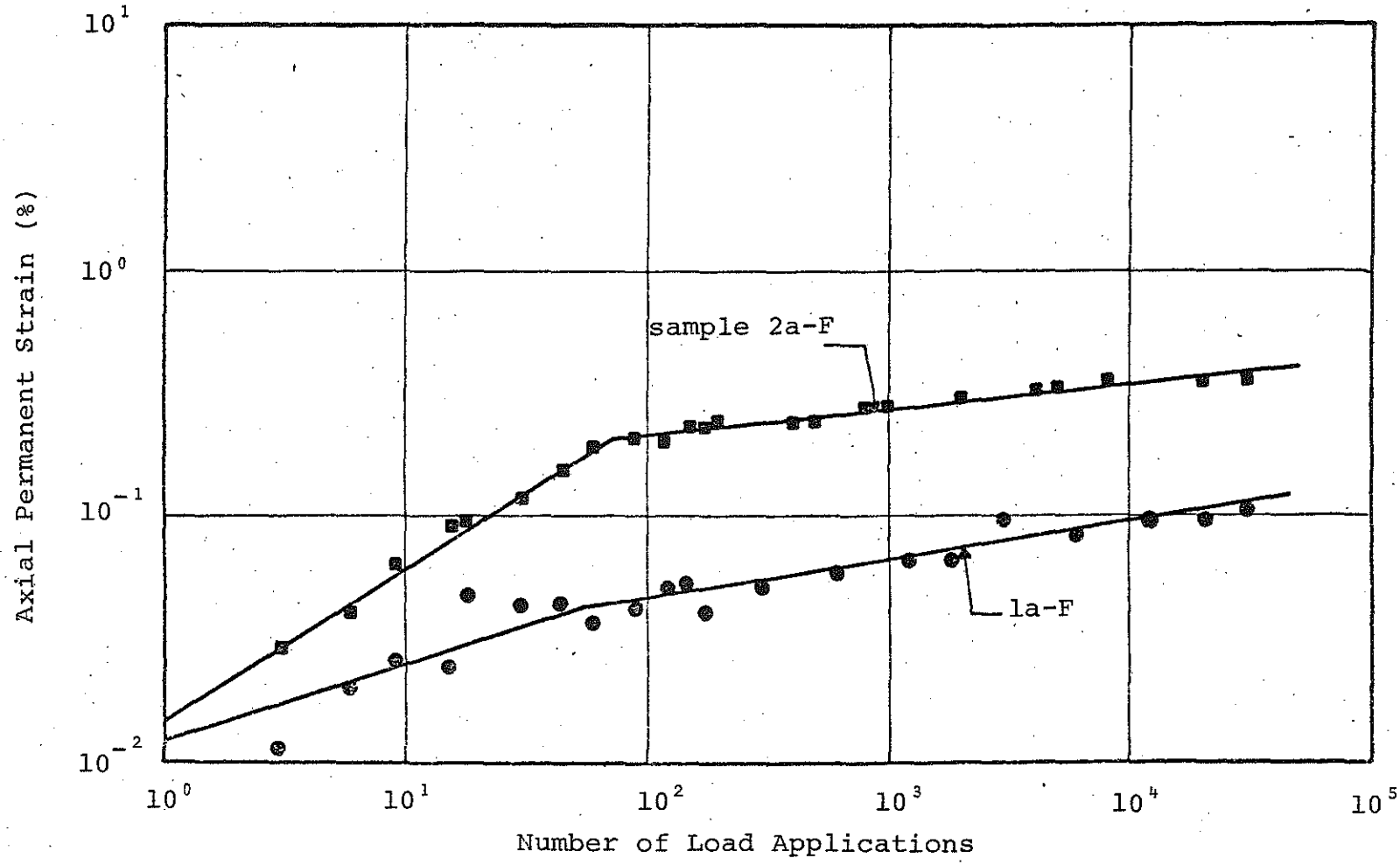

FIGURE D.19 Axial Permanent Strain Versus Number of Load Applications for Consolidated Samples Tested Under a Confining Pressure of 10 psi and Different Cyclic Stress Ratio, Site 3, Upper Peninsula.

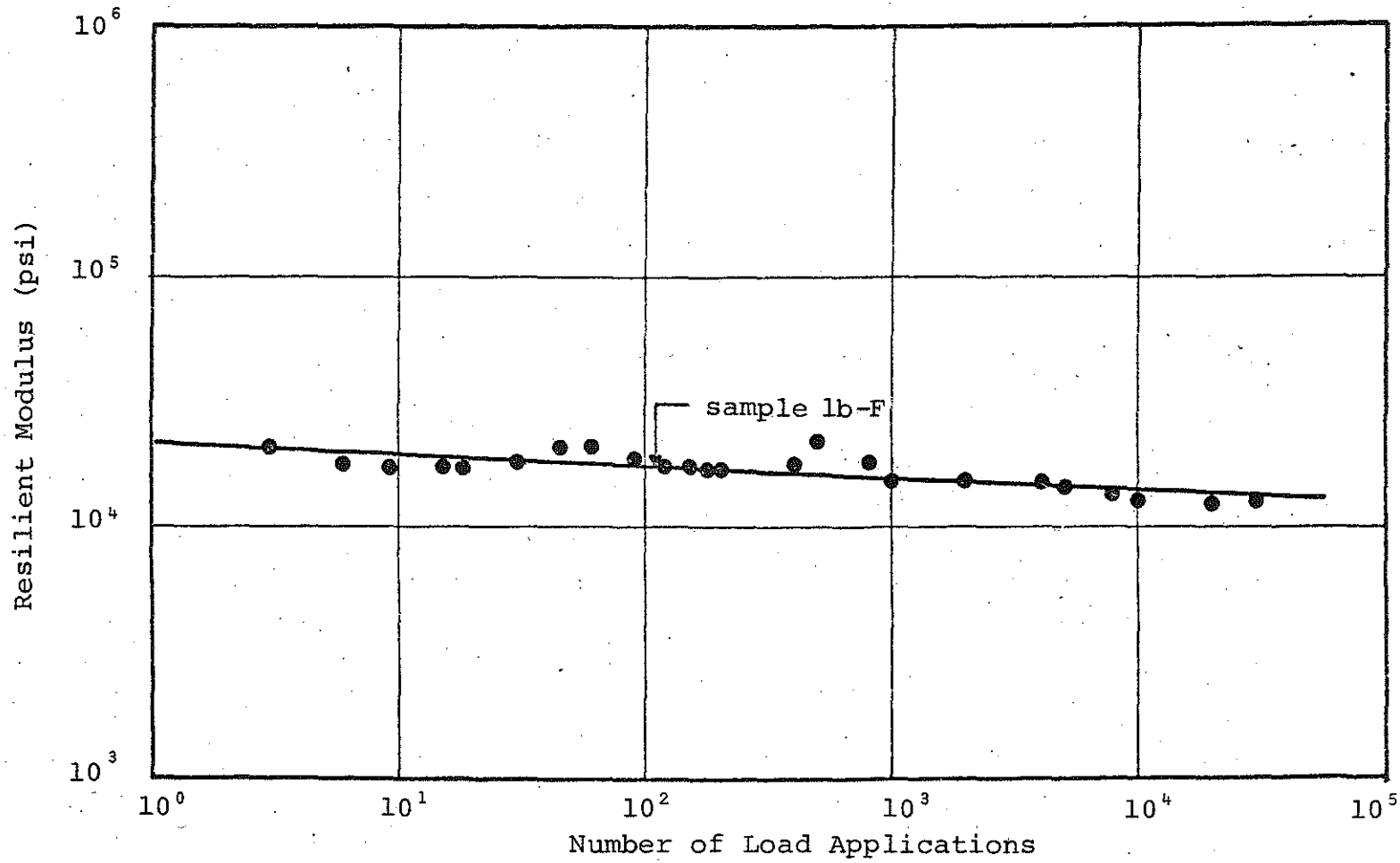

FIGURE D.20 Resilient Modulus Versus Number of Load Applications for Consolidated Sample Tested Under a Confining Pressure of 10 psi and Cyclic Stress Ratio of 1.0, Site 1, Upper Peninsula

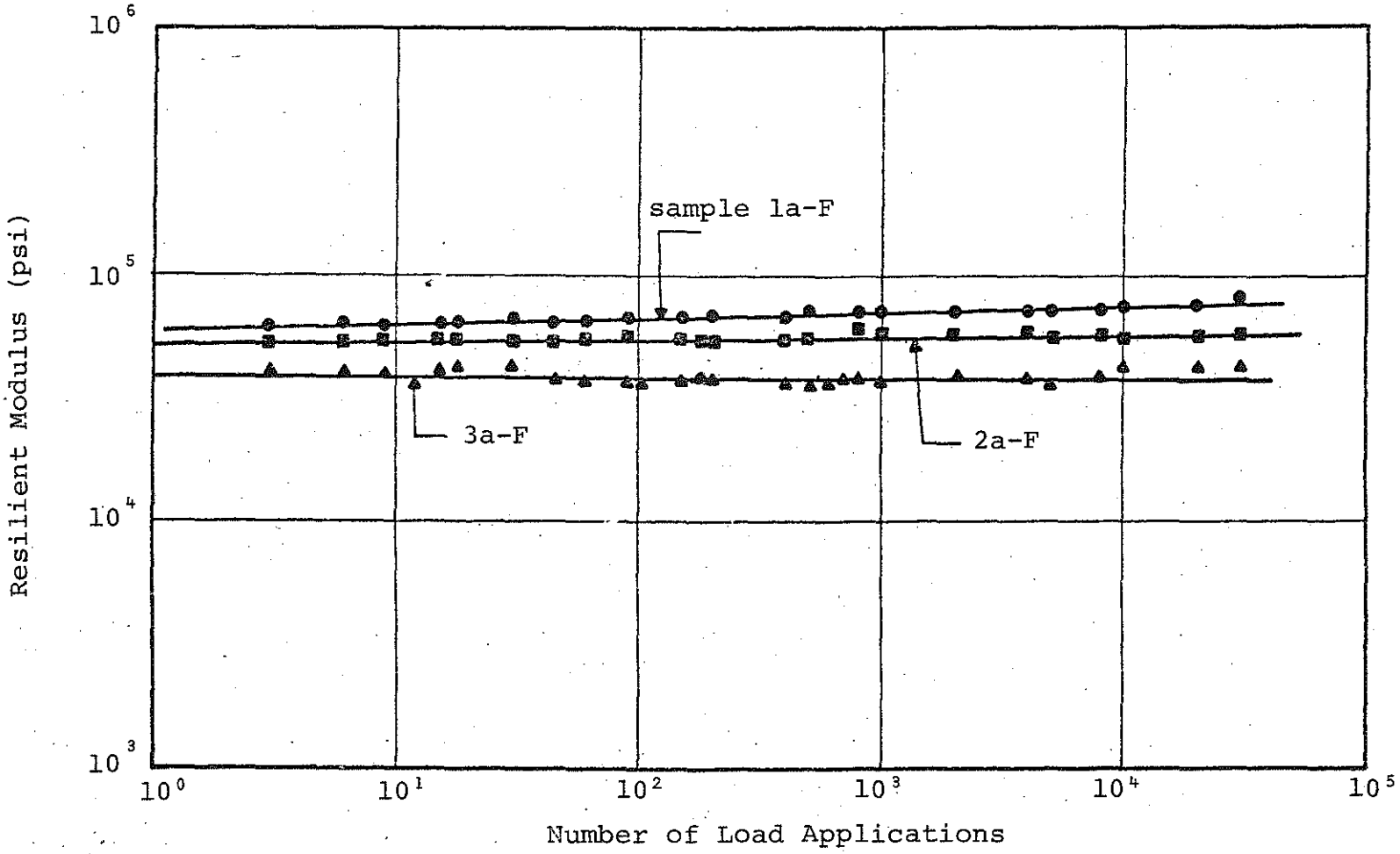

FIGURE D.21 Resilient Modulus Versus Number of Load Applications for Consolidated Samples Tested Under a Confining Pressure of 10 psi and Different Cyclic Stress Ratio, Site 2, Upper Peninsula

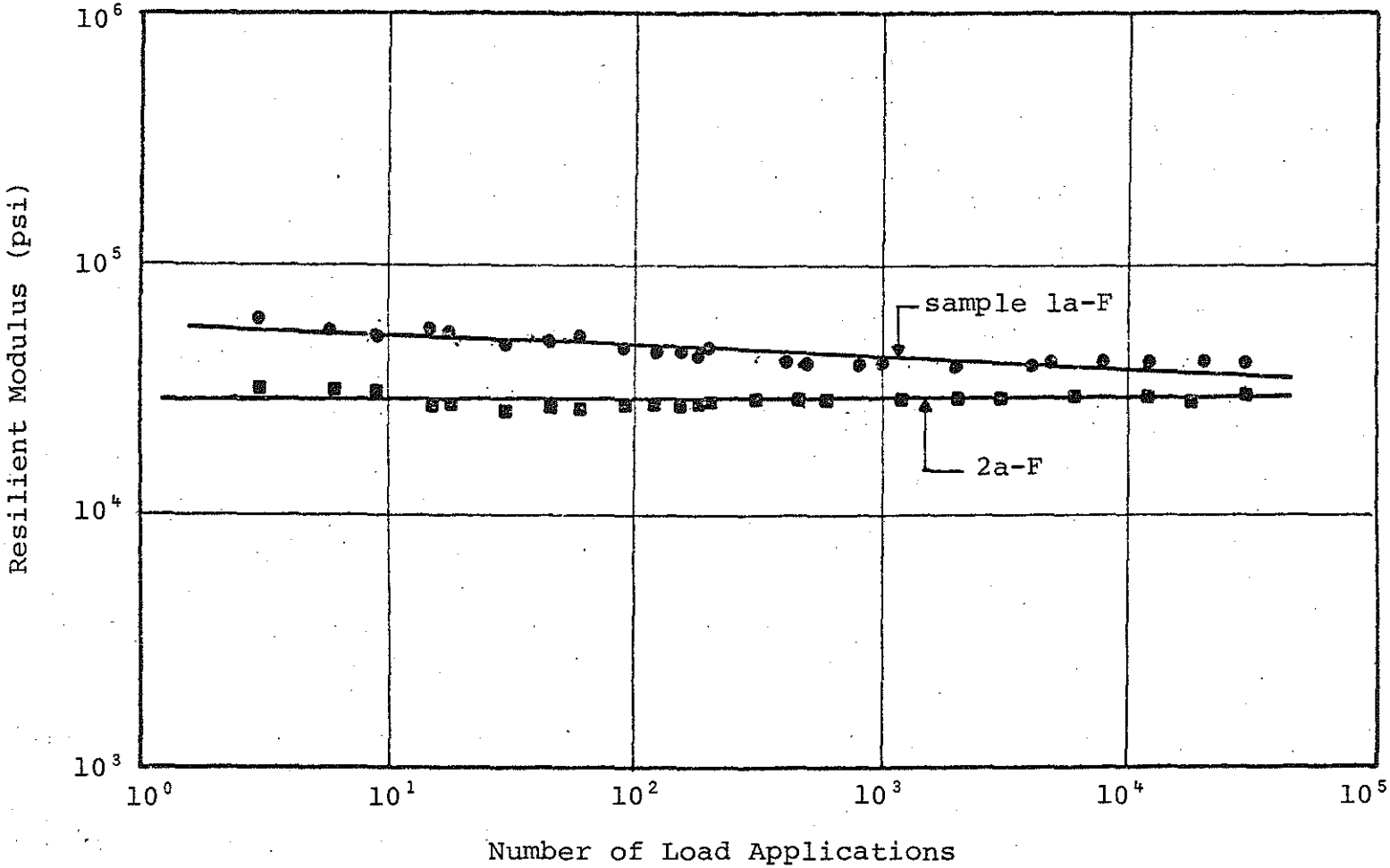

FIGURE D.22 Resilient-Modulus Versus Number of Load Applications for Consolidated Samples Tested Under a Confining Pressure of 10 psi and Different Cyclic Stress Ratio, Site 3, Upper Peninsula.

TABLE D.1 List of the Radial Permanent Strain for Test Sites 1, 2, 3 Upper Peninsula

Site	σ_3	Sample Number	$\frac{(\sigma_1-\sigma_3)d}{\sigma_3}$	Radial Permanent Strain at Middle of Sample ($X10^{-4}$)			Radial Permanent Strain at 1/3 From the Sample Bottom ($X10^{-4}$)			Test Mode
				N=1	10	100	1000	10000	30000	
S1-UP	10	1b-F	1.0	2.46	3.33	4.23	5.19	6.44	6.49	C
				*	*	*	*	1.61	1.82	
	10	3b-S	1.0	3.58	4.36	5.82	7.12	9.43	10.4	U
				*	1.04	2.01	3.43	3.51	3.61	
S2-UP	10	1a-F	1.0	1.37	3.60	5.60	7.49	8.19	8.87	C
				*	*	1.42	1.81	1.93	2.05	
	10	2a-F	2.0	1.42	5.46	6.96	10.90	18.5	20.5	C
				*	1.09	1.24	1.68	1.94	2.08	
	10	3a-F	3.0	2.37	4.23	6.91	15.7	19.8	22.4	C
				1.01	1.15	1.32	1.61	1.83	1.94	
S3-UP	10	1a-F	1.0	2.18	2.59	5.04	6.63	6.63	6.67	C
				*	*	*	*	1.15	1.43	
	10	2a-F	2.0	3.55	5.46	5.68	9.56	15.7	18.2	C
				*	*	1.81	1.97	2.17	2.35	

*Readings are smaller than 10^{-5}

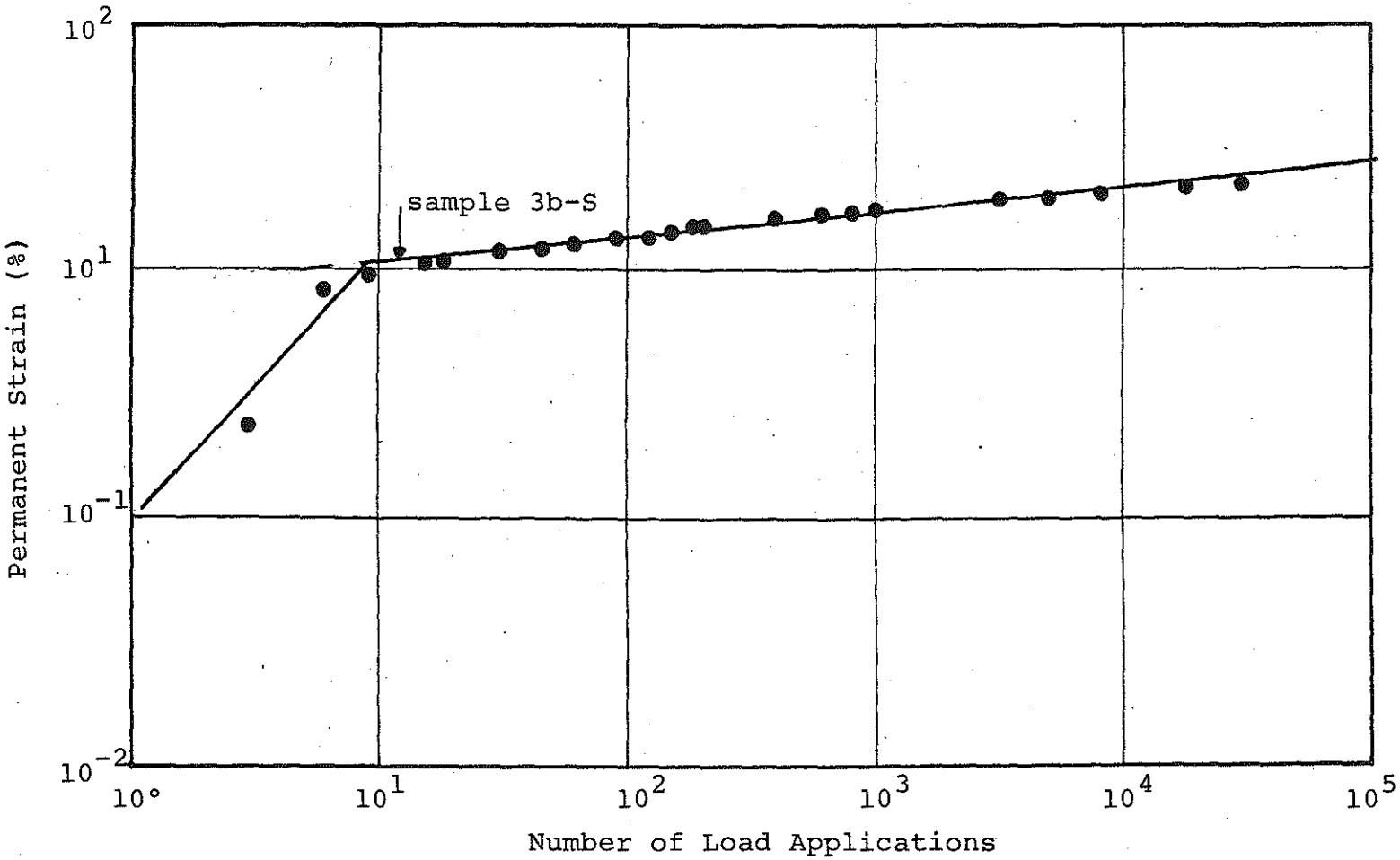

FIGURE D.23 Axial Permanent Strain Versus Number of Load Applications for Unconsolidated Samples Tested Under a Confining Pressure of 10 psi, Site 1, Upper Peninsula

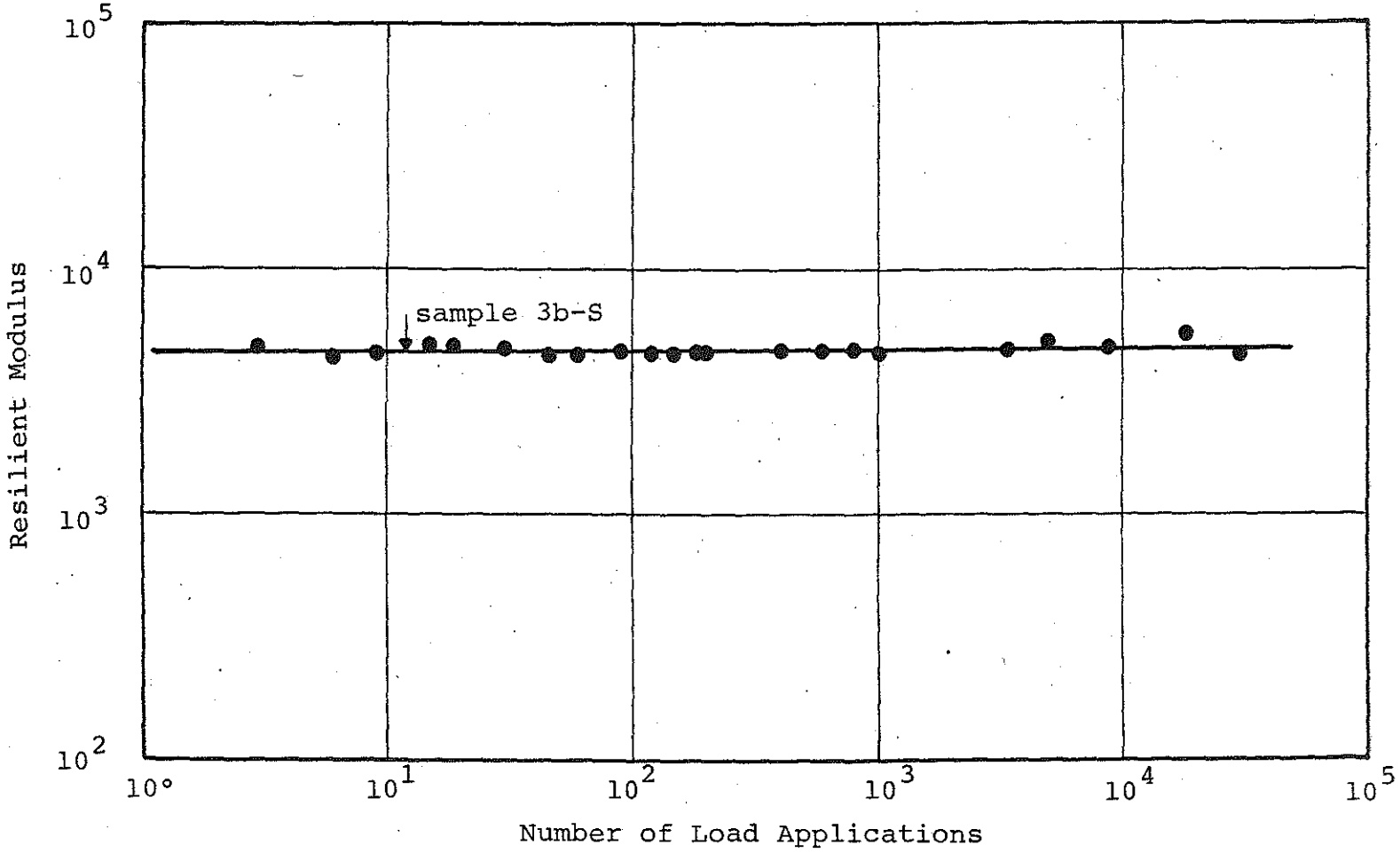

FIGURE D.24 Resilient Modulus Versus Number of Load Applications for Unconsolidated Sample Tested Under a Confining Pressure of 10 psi, Site 1, Upper Peninsula